NASACR-152,373

NASA-CR-152373
19810002506

A Reproduced Copy

OF

N81-11014 #

Reproduced for NASA

by the

NASA Scientific and Technical Information Facility

NASA Contractor Report 3437

Full Scale Wind Tunnel Investigation of a Bearingless Main Rotor

Final Report

Boeing Vertol Company
Philadelphia, Pennsylvania 19142

Contract NAS2-10333

October 1980

NASA

Ames Research Center

NASA CR 152373

NASA

Full Scale Wind Tunnel Investigation of a Bearingless Main Helicopter Rotor Final Report

Marc Sheffler — Project Manager

James Staley — Dynamics

James Hoover — Loads

Cheryl Savjak — Performance

Fred White — Flying Qualities

October 1980

Prepared Under Contract No. NAS2-10333

for

National Aeronautics and Space Administration

Ames Research Center

by

BOEING VERTOL COMPANY

A DIVISION OF THE BOEING COMPANY

PHILADELPHIA, PENNSYLVANIA 19142

D210-11659-1

TABLE OF CONTENTS

LIST OF TABLES

NOMENCLATURE

SYMBOL	DEFINITION	UNITS
A_1	Lateral Cyclic Pitch	rad. (deg.)
b	Number of Blades	ND
B_1	Longitudinal Cyclic Pitch	rad. (deg.)
c	Blade Chord	m (ft.)
CB	Chord Bending Moment	Nm (in.-lb)
C_{De}/σ	Effective Drag Coefficient $\frac{De}{\rho \pi R^2 (\Omega R)^2 \sigma}$	ND
C_{LR}/σ	Rotor Lift Coefficient $\frac{L}{\rho \pi R^2 (\Omega R)^2 \sigma}$	ND
C_P/σ	Power Coefficient $\frac{550\ RHP}{\rho \pi R^2 (\Omega R)^3 \sigma}$	ND
C_{PM}/σ	Pitching Moment Coefficient $\frac{PM}{\rho \pi R^3 (\Omega R)^2 \sigma}$	ND
C_{XR}/σ	Propulsive Force Coefficient $\frac{X}{\rho \pi R^2 (\Omega R)^2 \sigma}$	ND
D_e	Effective Drag $\frac{RHP}{V} - X$	N (lb)
FB	Flap Bending Moment	Nm (in.-lb)
F_e	Equivalent Flat Plate Drag Area	m^2 (ft^2)
L	Lift	N (lb)
L/De	Lift/Equivalent Drag Ratio	ND
L/q	Lift/Dynamic Pressure	m^2 ($ft.^2$)
PM	Pitching Moment	NM (ft-lb)
q	Dynamic Pressure	N/m^2 ($lb/ft.^2$)

NOMENCLATURE

SYMBOL	DEFINITION	UNITS
R	Rotor Radius	m (ft)
RHP	Rotor Horsepower	Nm/sec (lb-ft/sec)
S_E	Endurance Limit	N (lb) or Nm (in.-lb)
S_L	Li it Load	N (lb) or Nm (in.-lb)
TB	Torsion Bending Moment	Nm (in.-lb)
V	Tunnel Velocity	m/sec (ft/sec)
X	Propulsive Force	N (lb)
α_s	Shaft Angle of Attack	rad. (deg.)
η	Fixed System Damping (% Critical)	ND
η_ζ	Structural Damping Ratio	ND
σ	Solidity ($bc/\pi R$)	ND
$\theta_{.7}$	Collective Pitch Angle at 70% Span	rad. (deg.)
ρ	Density	Kg/m^3 ($lb\text{-}sec^2/ft^4$)
Ω	Rotor Speed	rad./sec (rpm)
ω_ζ	Lag Natural Frequency	rad./sec (Hz)
μ	Advance Ratio (V/V_{TIP})	ND

1.0 SUMMARY

A full scale wind tunnel test of the Bearingless Main Rotor was conducted in the NASA-Ames 40-by 80-foot wind tunnel. The preparation and test activities were performed under the supervision of the Large Scale Aerodynamics Branch at NASA-Ames and with the co-operation of the 40-by-80 test crew. The test was primarily a stability test program, a consideration which guided the formulation of the test plan. The effects of airspeed, collective pitch, rotor speed and shaft angle on stability and loads were determined at speeds beyond that attained in the BMR/BO-105 flight test program. Loads and performance data were gathered at forward speeds up to 165 knots. The effect of cyclic pitch perturbations on rotor response was investigated at simulated level flight conditions. Two configuration variations were tested for their effect on stability. One variable was the control system stiffness. An axially softer pitch link was installed in place of the standard BO-105 pitch link. The second variation was the addition of elastomeric damper strips to increase the structural damping.

The Bearingless Main Rotor system as installed on the BO-105 helicopter was used in this wind tunnel test. Minor modifications included the extension of the pitch link barrel length to adapt to the Rotor Test Apparatus (RTA) swashplate location, and the fabrication of some new adapter equipment to mate with the RTA. Following hub tares and track and balance runs, the

remainder of the test was primarily devoted to obtaining stability, loads and performance data for a wide range of test conditions. The basic testing sequence was to set the desired rotor speed, collective, shaft angle and tunnel speed, maintaining zero one/rev flapping using lateral and longitudinal cyclic pitch. Loads and performance steady-state data were taken. The rotor was then excited using the Dynamic Control System (DCS), the excitation stopped, and the decay of a chord bending gage signal analyzed to compute the fixed system damping. Additional testing included loads and performance testing at simulated level flight conditions, and perturbations on lateral and longitudinal cyclic inputs to determine the fixed system response to a transient.

The BMR was stable at all conditions tested. At fixed collective pitch, shaft angle and rotor speed, damping generally increased between hover and 60 knots, remained relatively constant from 60 to 90 knots, then decreased above 90 knots. Analytical predictions are in good agreement with test data up to 90 knots, but the trend of decreasing damping above 90 knots is contrary to the theory. For both hover and forward flight, fixed system damping increases with increasing collective pitch at fixed rotor speed and shaft angle. Damping decreases with increasing rotor speed at constant collective and shaft angle. The effects of shaft angle are small. The analysis predicts the trends with collective and rotor speed very well. The correlation is good in hover and at low collectives in forward

flight. At collectives of 6° and above, the analysis begins to overpredict the damping level.

The BMR/RTA test results compare favorably with BMR whirl tower and BMR/BO-105 ground resonance and air resonance testing. The one exception is the ground resonance test results where a coupled rotor/body mode is present. The effects of the BO-105 fuselage coupling with the rotor cannot be duplicated on the RTA.

The effect of adding structural damping by bonding elastomeric damper strips to the flexbeams was to increase fixed system damping by about 2-3% critical in hover for all rotor speeds and collectives tested. Similar results were found at 90 knots. The correlation of the measured and predicted effects of the elastomeric damper strips is good.

The soft pitch links produced lower damping levels in hover below 425 rpm, and no change at 425 rpm. There was little or no effect in forward flight.

There was no effect on stability seen when the eight tunnel balance dampers were removed. The effects on stability of excitation amplitude and trim values of cyclic pitch were explored, with no effects indicated. The data base is small however, so more testing is recommended.

The testing was restricted to some extent by loads. For stability testing, peak torque tube chord bending restricted the minimum collective which could be achieved, since steady torque tube chord bending increased directly with decreasing collective. Outboard blade and flexbeam steady flap bending was increasingly flap down with airspeed and restricted the airspeed range, as did blade root torsion. During cyclic excitations for stability testing, vibratory chord bending was critical.

Vibratory flap bending generally increases with airspeed, while chord bending is greatest between 40 and 80 knots. Steady flap bending is increasingly flap down, while steady chord bending is virtually independent of airspeed. Vibratory and steady flap bending, vibratory chord, and vibratory and steady torsion increase with collective at constant rotor speed and shaft angle. No single trend for the effect of collective on steady chord could be defined. Vibratory loads generally increased with more positive shaft angles, at least to some extent, while steady loads were essentially independent of shaft angle.

The steady chord bending moments in the flexbeams were not distributed evenly between leading and trailing beams, while vibratory chord bending was divided evenly.

Flight test loads and loads measured in the BMR/RTA test are in good agreement, with differences attributable to variations in trim between the wind tunnel and flight test. The correlation of analysis with measured loads is good for flap bending and fair to poor for chord bending.

Analysis of the BMR performance data acquired during this test shows good agreement with theoretical predictions. Since the primary objective of the test was to determine rotor stability the testing was done at the lowest damping levels, hence lowest collective pitch angles, possible. The shaft angles selected for testing were chosen without regard to matching a specific F_e for every test point. For this reason, most of the test data was at simultaneous lift and propulsive force levels not representative of BO-105/BMR flight.

An estimate of the BMR hub drag was made based on test data and compared to pre-test predictions. At 120 knots (μ = .28) and a trimmed shaft angle of -2.3° the measured drag level of 4.75 ft^2 compares favorably with the pre-test estimate of 4.41 ft^2.

The hover data obtained during the test showed that the measured power was 4.3% higher than the theoretical estimates at 5000 pounds of thrust, which corresponds to the take-off gross weight of the BO-105/BMR.

The forward flight data showed generally good agreement with the theoretical predictions in the speed range tested.

The rotor responded to both lateral and longitudinal cyclic control inputs within two rotor revolutions after the input was initiated. The response was precise and of the first order, with little or no overshoot. The cross axis response showed no long term coupling. Responses to positive and negative cyclic inputs for lateral or longitudinal perturbations showed symmetry about trim.

2.0 INTRODUCTION

2.1 HISTORY OF THE BMR

The Bearingless Main Rotor (BMR) is the product of a contract effort undertaken by the Boeing Vertol Company, which was funded by the Applied Technology Laboratory at Ft. Eustis, Virginia, to design, fabricate and test a prototype bearingless rotor system. Awarded in June, 1976, the BMR development proceeded from an extensive analytical design phase through a series of fatigue tests, small-scale wind tunnel and whirl tower tests, culminating in a flight test program which began on October 26, 1978.

Boeing Vertol's involvement in the development of the Bearingless Main Rotor predates the Eustis contract. As early as 1964, Boeing teamed with MBB in the development of the hingeless, soft-inplane BO-105 rotor. In the 1970's Boeing Vertol gained significant experience in the analysis and testing of hingeless rotors with the YUH-61A (UTTAS) program. Analytical programs such as C-45 were written to predict aeroelastic stability, C-60 to predict loads and Y-71 to predict frequencies and mode shapes. The bearingless tail rotor was a key element in the development of the YUH-61A helicopter. This rotor system utilized fiberglass composite flexstraps for blade retention and collective pitch input. The testing of this stiff in-plane rotor provided a wealth of data towards the understanding of several types of aeroelastic stability phenomena. In addition, the sensitivity of stability to chord fre-

quency, flap frequency, torsion frequency, blade-to-strap pre-pitch, tip weights, chordwise center of gravity, sweep, and airfoil section was examined. Several alternative designs were tested, which added to the understanding of design requirements for bearingless rotors.

In 1974 Boeing Vertol submitted a proposal to the Applied Technology Laboratories at Ft. Eustis (at that time USAAMRDL) for an Improved Rotor Hub Concept (Reference 1). In that document the application of a lag-torsion-flap flexure to a hingeless rotor was discussed. Following that proposal, an analytical effort was initiated to apply bearingless rotor technology to the BO-105 helicopter. The results of the design study were utilized in preparing a response to an RFP issued by the ATL at Ft. Eustis, Virginia in 1975 (Reference 2). This led to the June 1976 contract award to Boeing.

The development of the BMR was divided into several phases. The preliminary design phase (June - December 1976) involved many iterations of the basic design concept to achieve the best tradeoff between dynamic characteristics and aeroelastic stability, structural integrity, flying qualities, control system requirements, and minimum modification to the BO-105 blade and control system.

The detail design phase (December 1976 - May 1977) consisted of both analysis and testing to refine the BMR design. Analytically, computer programs were developed which predict the loads and deflected shape of the highly contoured beams when subjected to chordwise and torsional loadings. These programs were used to better define the geometry of the fiberglass beams required to satisfy the design criteria. Static strain surveys and deflection tests were performed on beam specimens to verify that the final design met the design requirements. In addition, a wind tunnel test was conducted on a 1/5.86 Froude-scaled air resonance model shown in Figure 2.1. The model, free to pitch and roll about a two-axis gimbal system, was flown through the entire envelope of the BO-105 to verify the BMR stability. Over 400 hours of testing were accumulated on the model, including nineteen different configuration variations to identify the design with the optimum stability characteristics. Examples of parameters which were investigated include beam-to-hub prepitch angle, blade-to-beam pitch angle, beam-to-hub coning, blade-to-beam coning and first chord frequency. Data in hover were developed in terms of damping versus rpm at 1.0g thrust, and damping versus thrust at normal rotor speed. In forward flight the data were generated as damping versus airspeed at 1.0g thrust and normal rpm, and damping versus rotor speed at fixed thrust and airspeed. Simulated climbs and descents were also performed. The results of this testing, described in Reference 3, defined the final configuration for the detail design phase.

Following the detail design phase, full scale test specimens were fabricated to prove the manufacturing process and to perform static and dynamic bench testing. Static testing included stiffness verification and deflection tests. Particularly notable was the investigation of the control system requirements with simulated centrifugal force applied. Testing verified that the BMR required no modifications to the BO-105 controls. Limit load testing to a 3.5g maneuver condition verified the structural integrity of the BMR system. Non-rotating frequency and mode shape tests were performed to verify the Y-71 and NASTRAN analysis, since the modal properties are important inputs to the dynamic stability analysis.

Fatigue testing was performed using the test set-up shown in Figure 2.2. The purpose of these tests was to establish endurance limits for whirl and flight testing and to verify that the design criterion of a fatigue life greater than 3600 hours was achieved. A combined flap-chord-torsion loading with a simulated centrifugal force load was applied to the beam assembly to simulate a 2g load factor at 112 knots. Over 2.5 million cycles were applied to the BMR system with no failure. Similar fatigue testing was performed on the isolated torque tube assembly, the blades and the hub. The results of the fatigue tests (Reference 4) cleared the BMR for a minimum of 500 hours of flight. Based on the loadings in the fatigue test and the flight loading spectrum, a very conservative minimum fatigue

life of 1200 hours was established. It is felt that additional testing would verify the 3600 hour fatigue life criterion.

In July 1978, the BMR was installed on the Boeing 2B Whirl Tower (Figure 2.3). The 24 hours of testing included a thorough load and strain survey, determination of modal frequencies, an investigation of aeroelastic stability characteristics, and an endurance run. The load and strain survey consisted of cyclic sweeps at fixed values of thrust, up to shaft torque or shaft bending limits, at 425 rpm and 468 rpm (110% overspeed condition). Data recorded included blade and beam total strains, flap, chord, and torsion bending moments, pitch link loads, torque tube bending, shaft torque, shaft bending, and cyclic actuator loads. The results were compared to structural limits established during fatigue testing and to analytical results. The modal frequencies were found by spectral analysis of the gage output from the beams and blades. The full frequency spectrum from 0 rpm to 475 rpm was determined and the effect of collective pitch on modal frequencies was evaluated. Aeroelastic stability was investigated by harmonically exciting the swashplate at the appropriate frequency, stopping the excitation, and measuring the decay of the blade motion as indicated by the strain gages. Damping was measured at five distinct rotor speeds for several values of collective pitch. This information was also compared to predictions, with favorable results. Finally, an endurance run was performed at

468 rpm with loads and control settings data recorded periodically. The whirl tower test results are documented in Reference 5.

The BMR flight test program commenced with the first hovering flight on October 26, 1978. Figure 2.4 shows the aircraft at Boeing Vertol's Flight Test facility in Wilmington, Delaware during this flight. The more than 40 hours of testing included ground and air resonance damping investigations, vibration testing, loads surveys and flying qualities evaluations. References 6, 7 and 8 describe fully the flight test program and results. The aircraft was tested for ground resonance on both concrete and turf for a range of collective positions at rotor speeds from 75% to 102% normal rotor speed. The results indicated a somewhat lower damping level than the baseline BO-105, but with adequate stability margins throughout the range of conditions tested. It was found that the damping levels could easily be increased with longitudinal stiffening of the landing gear.

Air resonance damping was investigated at conditions which were expected to be critical. This included level flight speeds from hover to 106 knots at 3000 feet density altitude, and maximum power dives at speeds to 127 knots. Testing was also performed for climbs and descents from 20 to 100 knots, for autorotation at 60, 90 and 100 knots for rotor speeds from 85% to 108% normal rpm, and for pull-ups, push-overs and banked turns

at 2.5g's. The BMR demonstrated an acceptable stability margin at all flight conditions tested, with damping levels similar to the BO-105 for most of the flight regime.

A detailed loads survey was performed with the aircraft tested at load factors between zero and 2.3g's and forward speeds of -20 to 127 knots (Vne) were demonstrated. Maneuvers included left and right sideward flight up to 25 knots, stabilized banked turns up to 60°, descents up to Vne, including autorotation, and maximum power climbs. Flight testing was performed at 3,000 feet altitude and one (1) nominal center of gravity location due to the high gross weight of the instrumented aircraft. This demonstration was not limited by structural restrictions; however, higher than expected torque tube bending loads were experienced. The loads survey provided a wealth of information on the structural characteristics of this bearingless rotor design.

Three flights were devoted entirely to gathering flying qualities data such as stick positions, roll and pitch angles and rates, sideslip, and angle of attack versus CG position. This data was collected in order to predict stability derivatives of the BMR.

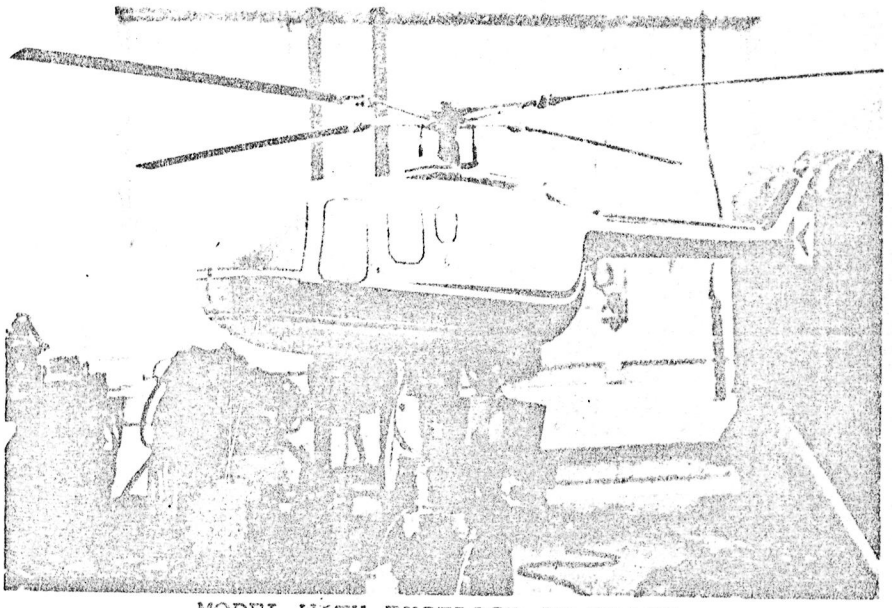

MODEL WITH FUSELAGE IN PLACE

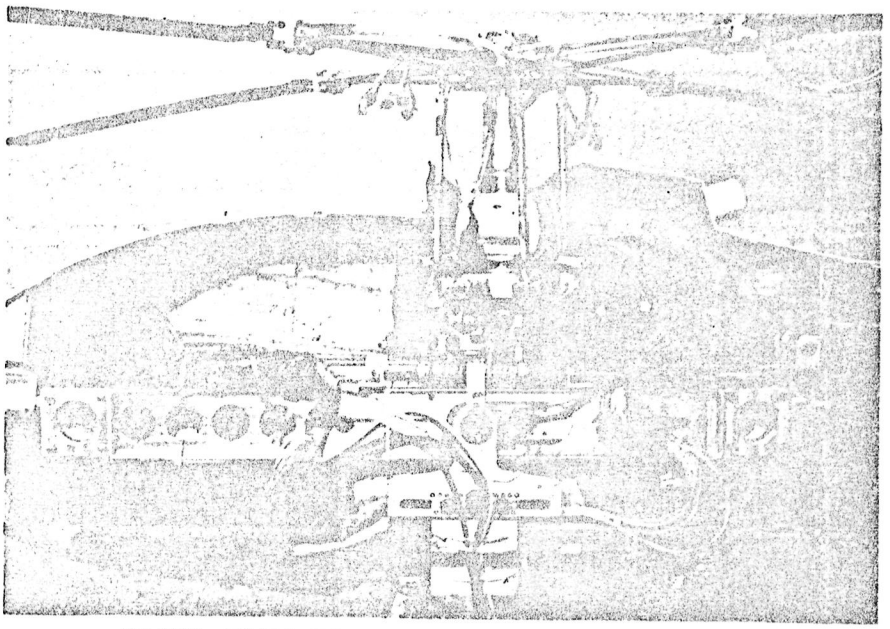

MODEL OPEN TO SHOW DYNAMIC COMPONENTS

FIGURE 2.1 1/5.86 FROUDE SCALED BMR AIR RESONANCE MODEL

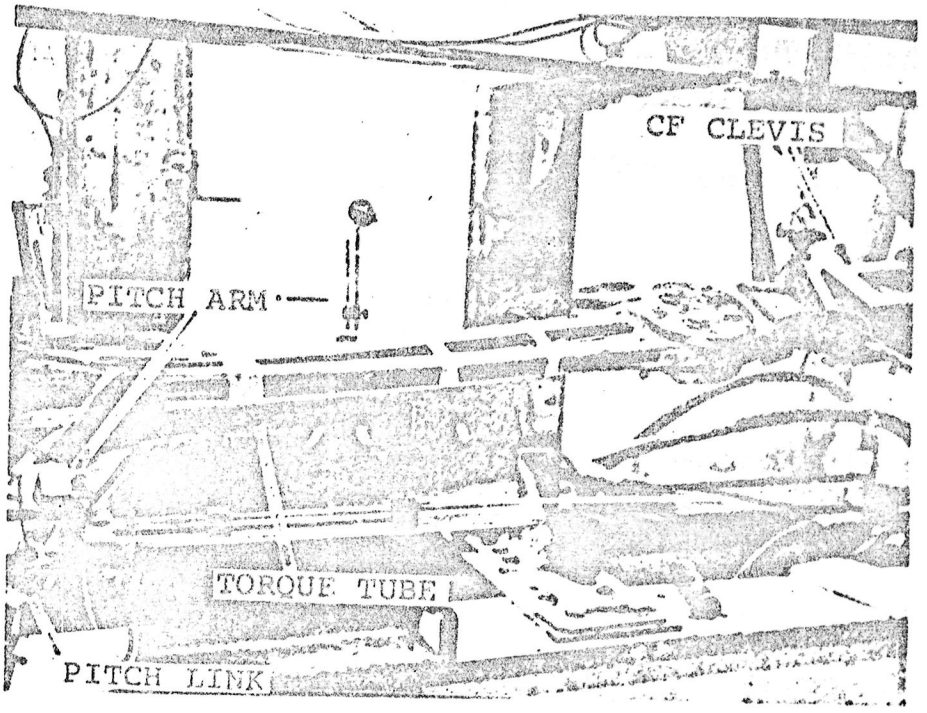

FIGURE 2.2 FATIGUE TEST SET-UP

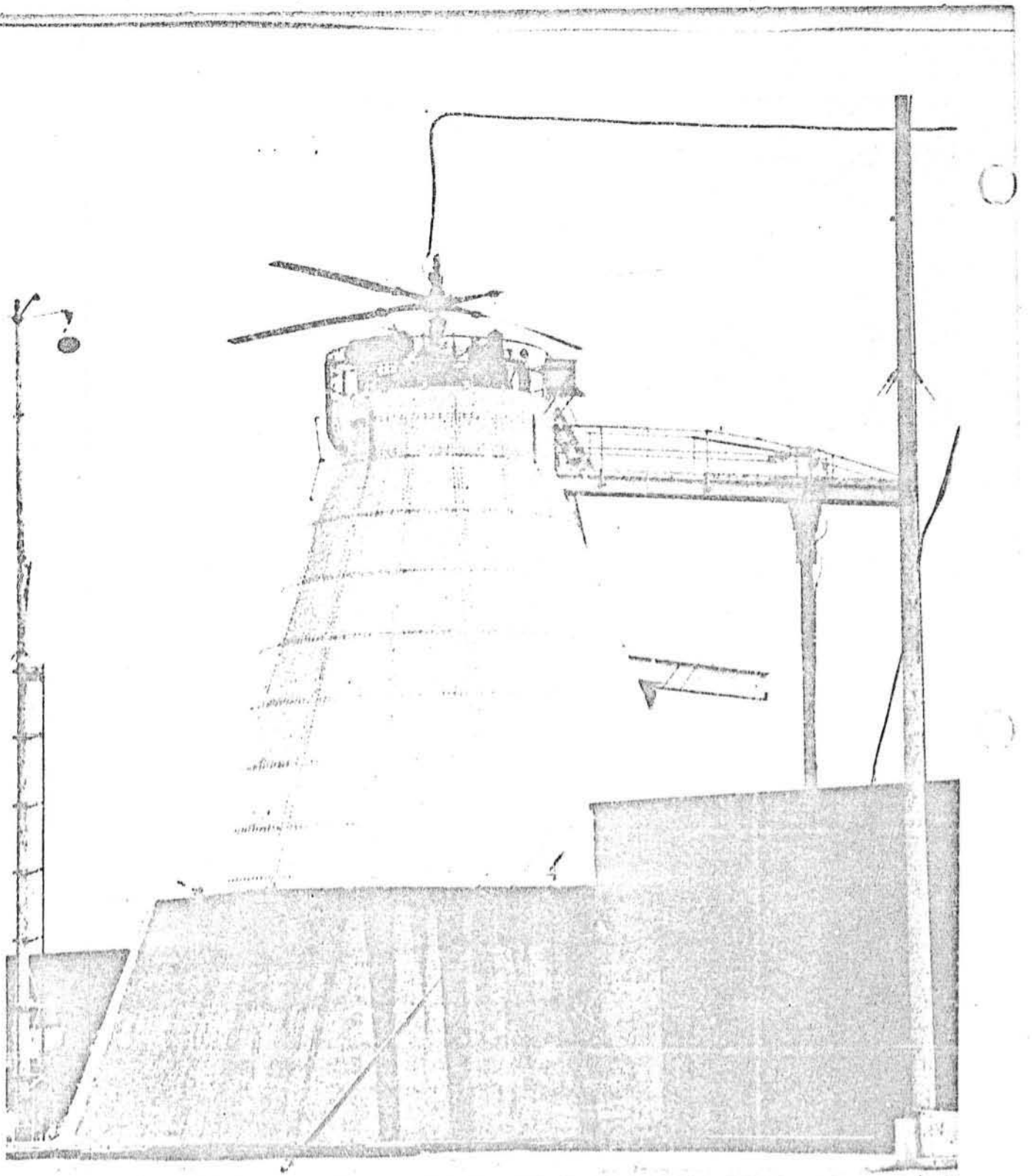

FIGURE 2.3 BMR ON THE BOEING VERTOL WHIRL TOWER

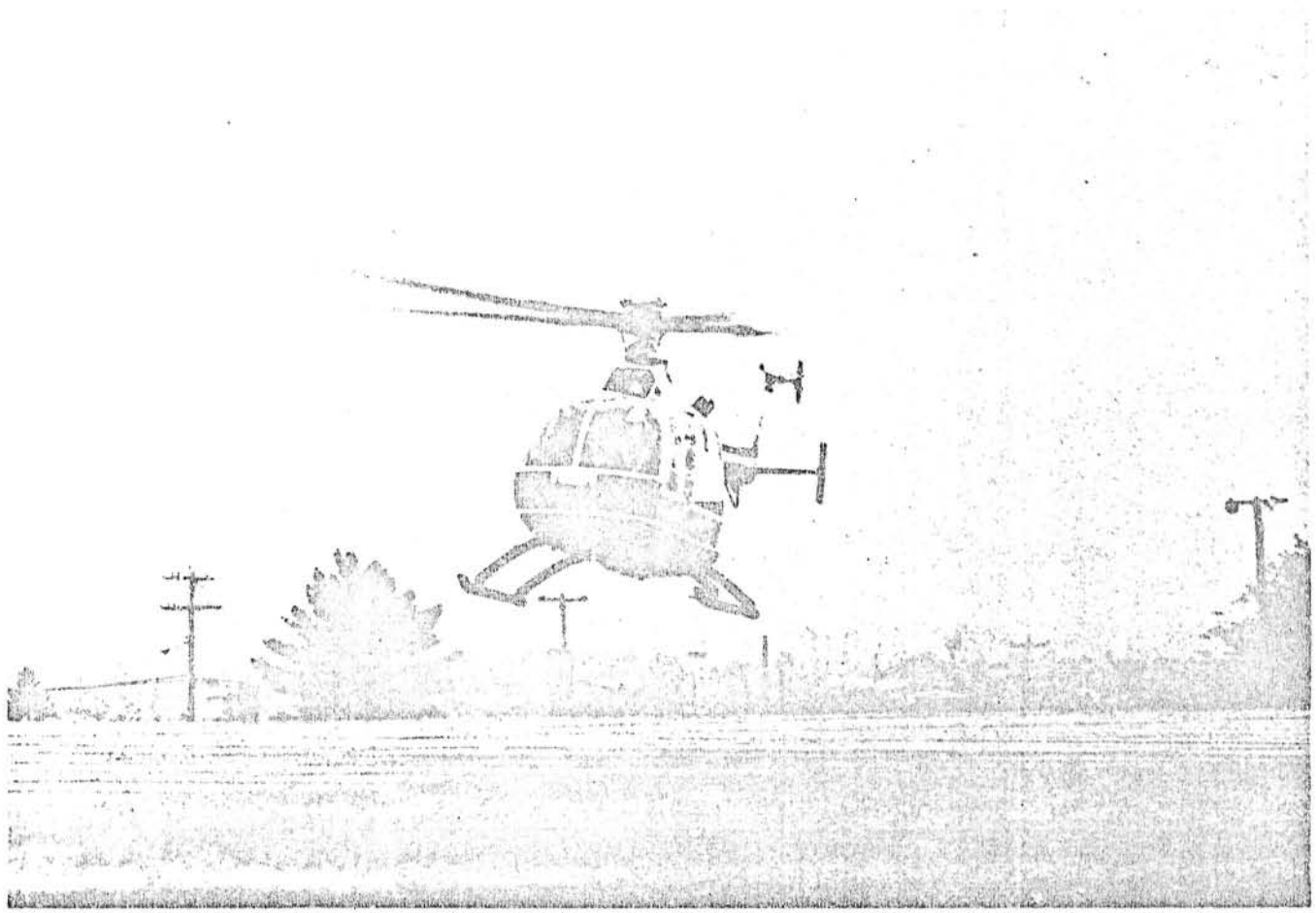

FIGURE 2.4 FIRST FLIGHT OF THE BMR ON OCTOBER 26, 1978

2.2 BACKGROUND FOR TESTING THE BMR IN THE 40-by-80 TUNNEL

Before the BMR flight test program had even started, the potential of this advanced rotor system was recognized by many in the helicopter industry. It was realized that while the flight test program could demonstrate the feasibility of this system and provide some information on loads and stability, a more thorough understanding of the dynamic and structural characteristics of the BMR would be possible in the controlled environment of a full scale wind tunnel test. Discussions were initiated with the personnel at the NASA-Ames 40-by-80 foot wind tunnel to plan a test of the BMR at that facility. The original concept of the test was a direct comparison of two configurations; the one built under the Eustis contract and a second generation BMR with a reduced effective flapping hinge offset. Due to budget and time constraints the scope of the program was reduced to testing the prototype BMR with several parameter variations.

2.3 TEST OBJECTIVES

The primary objective of the BMR test in the Ames 40-by-80 wind tunnel was to obtain a thorough evaluation of the aeroelastic stability characteristics of the Bearingless Main Rotor up to the maximum attainable forward speed. This was to include an investigation of system modal damping as a function of collective pitch, rotor speed, shaft angle, and if time permitted, rates of climb and descent.

The stability characteristics of the BMR defined from this program were to be compared to dynamic Froude-scale model test data, full-scale whirl tower data and flight test data where appropriate to establish the validity of the test results and contribute to the understanding of these results. It was intended that correlation work would be performed with theoretical data to validate and improve the mathematical models used to predict the stability of this type of hingeless rotor. One objective of the test program was to investigate whether the stability data is much different from flight test data when obtained in the wind tunnel where more precise control of trim conditions is possible.

Several configuration variations were to be tested to determine their effect on stability. Should the configuration changes prove to be beneficial for stability characteristics, potential improvements to the existing design could be realized such as reduced structural and design complexities. The planned configuration changes were softer pitch links, the addition of elastomeric damper strips and sweep variation.

In addition to the stability investigation, an extensive amount of loads data were to be recorded. The rotor was to be tested to forward speeds well beyond the capability of the BO-105 helicopter. Variations in thrust, rpm and shaft angle (propulsive force) were to be performed to further the understanding of the structural characteristics of the BMR components.

The measured loads data were to be compared to both whirl tower and flight test data so that the results obtained during this wind tunnel program could be better understood. Of particular significance were the torque tube loads, since flight testing produced some unexpected results. The transmitted vibration was measured so that the contribution of the BMR to vibration could be defined.

One purpose for monitoring the loads during the test was that the loads data obtained during the wind tunnel testing at Ames could be correlated with analytical predictions. The goal was to validate, and improve where necessary, the mathematical model used to predict the BMR loads. A specific area of interest was the multiple load path consisting of the dual beams and torque tube. Consequently one flexbeam/torque tube assembly was heavily instrumented to provide further insight into the nature of the elastic deformations.

A secondary objective was to measure the BMR configuration rotor performance. Parameters such as the lift/drag ratio, rotor power coefficient and rotor drag coefficient were recorded to provide a data base for understanding of the BMR performance characteristics. The measured data were to be compared to the analysis to establish correlation.

Flying qualities data were to be obtained subject to the limitations of the testing schedule. Step inputs of longitudinal and lateral cyclic were to be put in through the dynamic control system, and the time history of the rotor flapping response was to be recorded. This information could be translated into the response of the rotor disc to a transient input, providing data on the phasing and amplitude of the response to control inputs.

Acoustic data were recorded during testing and will be processed by NASA-Ames.

3.0 DESCRIPTION OF HARDWARE

3.1 BEARINGLESS MAIN ROTOR CONFIGURATION

3.1.1 Design Criteria

The selection of the BO-105 as the flight test vehicle influenced the formulation of a number of the design criteria. The BO-105 was chosen for several reasons. The development of a bearingless rotor proceeds easiest and most logically from a hingeless rather than an articulated rotor. The Boeing Company has conducted many research flight test programs using the BO-105, so we were very familiar with its characteristics and had a great deal of baseline data to draw upon. Additionally, the BO-105 is a soft in-plane rotor, which is significant in a design program where aeroelastic stability is of prime concern.

The stiff in-plane rotor system is not subjected to the air and ground resonance stability phenomena of the soft in-plane rotor, yet is susceptible to blade and rotor instabilities such as the flap-lag instability which can be equally disasterous. The soft in-plane rotor is free of the typical flap-lag instability, and by utilizing beneficial blade elastic couplings a rotor free of air and ground resonance instabilities can be designed.

The consideration of blade elastic couplings in the BMR design along with strength requirements dictated the geometric properties of the BMR system, particularly the fiberglass flexbeams. This arises from the fact that aeroelastic stability depends

on coupled natural frequencies and mode shapes, which are dependent on the spanwise variation of mass and stiffness. In addition, loads and stresses depend on the spanwise distributions of mass and stiffness, the material selected and the major cross-section dimensions. Finally, the control system requirements depend on the spanwise distribution of torsional rigidity of the flexbeams, as well as the inertia and aerodynamic pitching moment of the blade.

These factors led to the following design criteria for the BMR:

a. The BMR was to have no pitch bearings, no flap hinge and no lag hinge.

b. The aeromechanical stability of the baseline BO-105 aircraft system was to be retained.

c. Chordwise, flapwise and torsion stiffness and mass distributions would be selected to yield current BO-105 frequencies at 425 rpm:

1st flap	=	1.12 per rev
1st chord	=	.70 per rev
2nd flap	=	2.76 per rev
1st torsion	=	Greater than 3.2 per rev when coupled with the drive system.

d. All BMR components were to be designed to a minimum fatigue life goal of 3600 hours based on the flight profile specified in the contract Statement of Work.

e. The BMR would require no modification to the BO-105 control system, actuators or drive system components.

f. No degradation of the BO-105 flying qualities or performance would occur.

g. No modification to the BO-105 rotor shaft, meaning hub moments could not exceed the 60,000 inch-pound endurance limit.

3.1.2 General Description

The Bearingless Main Rotor system is shown in an isometric view in Figure 3.1, and a photograph of the flexbeam and hub area is presented in Figure 3.2. Everything above the conventional BO-105 rotor shaft is included as part of the BMR rotor system. Conventional BO-105 rotor blades have been modified at the inboard end to attach by means of an eight inch diameter titanium clevis to a set of dual fiberglass beams. The fiberglass beams are made of 3M-1002SF1 pre-impregnated material, and are basically a C-channel cross section. The beams permit flapwise and chordwise bending and full torsional travel. The root end of the beams are rigidly bolted to a metal hub assembly. Blade pitch is controlled by a filament wound torque tube which is solidly cantilevered at the blade-to-beam joint. At the inboard end it is supported by a rod end bearing of the type used in helicopter upper control assemblies. The pitch arm is connected to the torque tube just outboard of the rod end. Thus motion of the pitch link imparts a torsion moment to the torque tube, which in turn pitches the blades.

3.1.3 Stiffness and Geometry

All the geometric parameters of the fiberglass flexbeams, such as width, height, flange and web thickness, and spacing between the beams vary along the 52 inch nominal length. A typical cross section of the dual beam assembly is depicted in Figure 3.3, and the variation of the section geometry with span is shown in the same figure. Table 3.1 presents the same informa-

tion in tabular form, along with stiffness and mass properties. The root end connection of the flexbeams to the hub is at 2.38% radius station and the outboard bolted connection to the clevis is at 25.5% radius (49.3 inches).

The spanwise distribution of flap stiffness is presented in Figure 3.4. In Figure 3.5 the spanwise distribution of chord stiffness for an individual beam element about its local neutral axis is shown, along with the equivalent single beam representation of the total beam assembly chord stiffness. The torsional stiffness of the beam assembly is represented in Figure 3.6 as the spanwise twist distribution resulting from a 1000 inch-pound applied torsion moment. It can be seen that there is a significant stiffening effect due to centrifugal force. The equivalent torsional stiffness at normal rpm is $.32 \times 10^6$ lb.-in.^{2} All of the aforementioned properties, along with several other parameters, are tabulated in Table 3.1. Included is the EC_w term, which is the warping constraint that resists a component of the applied twisting moment.

The BMR maintains the 193.37 inches radius of the BO-105. The blade attachment pins are located at 27.1% radius (52.36 inches) resulting in a modified BO-105 blade as shown in Figure 3.7. With the beam flexure untwisted, and attached to the hub at an inclination of 12.5 degrees nose up, the blade chord line at 70% radius station has an incidence of 9.55 degrees (the theoretical cruise collective). The blade has a built in 2.5

degrees tip up predroop at the clevis attachment. Table 3.2 presents the mass and stiffness distributions of the blade and clevis.

3.1.4 Natural Frequencies

The BMR fully coupled natural frequency spectrum is given in Figure 3.8. These modal frequencies were identified during static shake testing and from spectral analysis of rotating strain gage data during whirl tower testing. The first flapwise and chordwise frequencies are nearly identical to those specified in the design criteria. The second flap mode is slightly under the desired frequency at 425 rpm, but is well placed with respect to the integer harmonics and the second chord frequency. The first torsion mode placement satisfies the criterion of exceeding 3.2 per rev when the rotor is coupled to the drive system. The second chord frequency is of particular interest. During the design phase, the second chord mode was predicted to be above 4 per rev. Nonrotating bang tests demonstrated a frequency closer to 3 per rev. This is a result of the chordwise shear mode coupled with a single beam bending mode. Fortunately, when coupled with the drive system the second chord mode falls safely below 3 per rev (2.72 per rev).

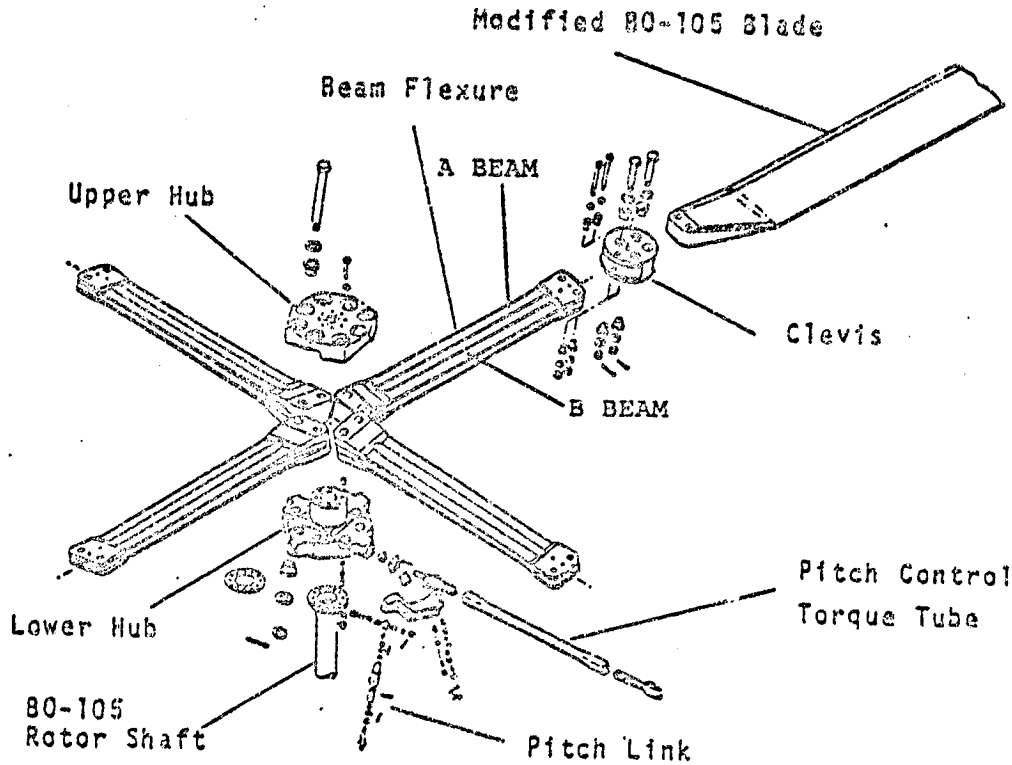

FIGURE 3.1 THE BEARINGLESS MAIN ROTOR SYSTEM

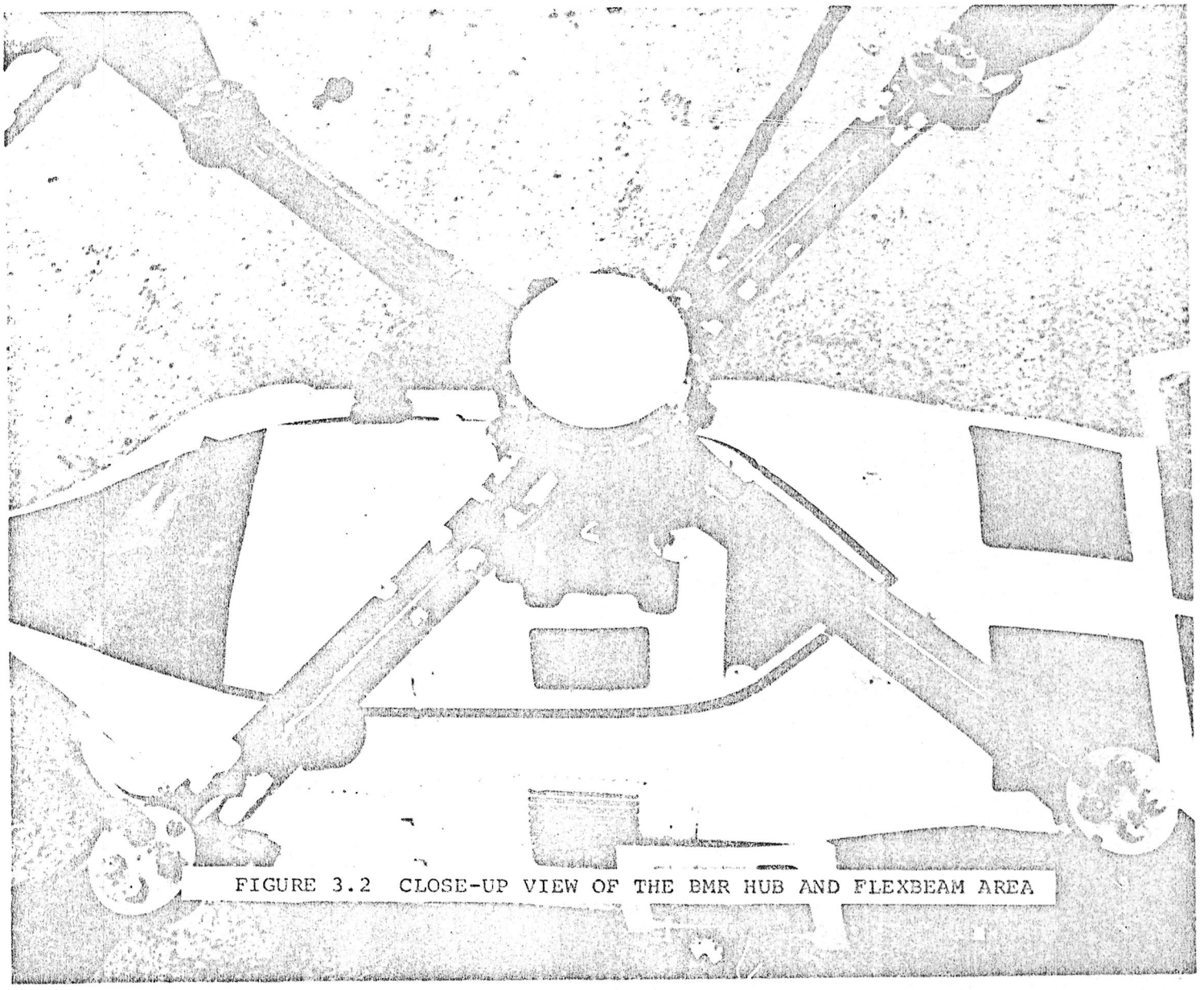

FIGURE 3.2 CLOSE-UP VIEW OF THE BMR HUB AND FLEXBEAM AREA

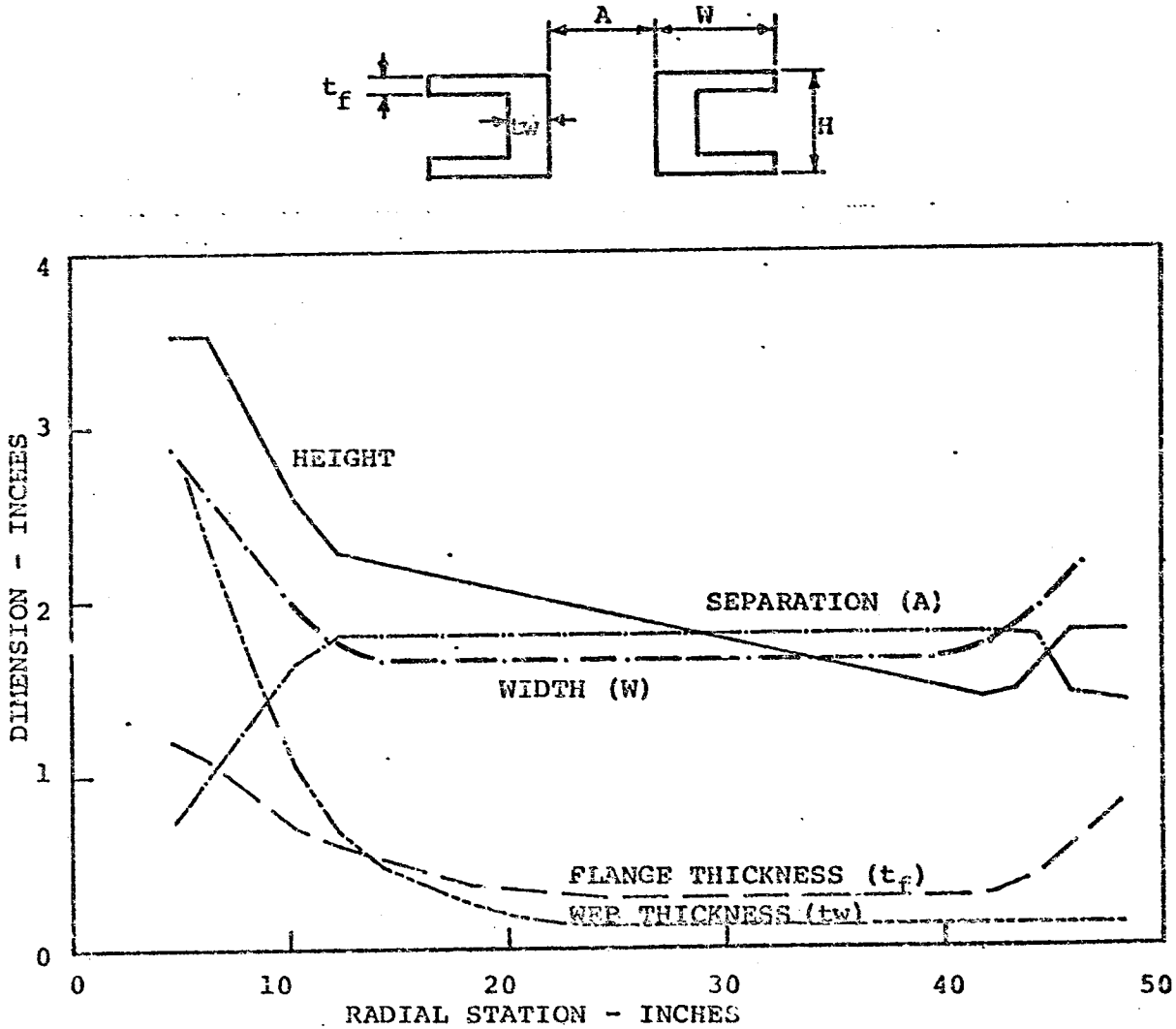

FIGURE 3.3 FLEXBEAM SECTION GEOMETRY

TABLE 3.1. TABULATION OF BMR PHYSICAL PROPERTIES
(Page 1 of 2)

RADIAL STN. (INS.)	WIDTH W (INS.)	HEIGHT H (INS.)	t_{FLANGE} t_f (INS.)	t_{WEB} t_w (INS.)	EI_f x 10^{-4} (LB-IN^2)	I_f (LB-IN^2)	EI_o x 10^{-4} (LB-IN^2)	I_o (LB-IN^2)
4.6	2.875	3.526	1.201	1.250	58.1600	15.992	330.8900	44.351
5.3	2.770	3.526	1.156	2.718	96.8550	20.223	392.3630	74.521
6.3	2.600	3.526	1.092	2.336	92.0356	18.593	350.1850	63.489
8.3	2.280	3.055	.895	1.651	60.0551	10.617	235.5785	40.144
10.3	1.960	2.583	.699	1.056	30.9167	5.379	151.0927	24.290
12.3	1.720	2.2756	.593	.676	19.5626	3.1545	104.713	15.958
14.3	1.650	2.2182	.516	.469	16.6151	2.673	79.639	12.358
16.3	1.650	2.1608	.439	.359	14.2379	2.320	66.083	10.361
18.3	1.650	2.1034	.362	.256	11.7275	1.949	52.548	8.401
20.3	1.650	2.0460	.337	.182	10.2690	1.723	46.903	7.614
22.3	1.650	1.9886	.311	.140	8.9609	1.520	42.021	6.934
24.3	1.650	1.9312	.286	.126	7.6857	1.313	39.041	6.358
26.3	1.650	1.8738	.286	.126	7.2890	1.249	38.014	6.349
28.3	1.650	1.8164	.286	.126	6.7715	1.159	37.975	6.336
30.3	1.650	1.7590	.286	.126	6.2735	1.072	37.935	6.322
32.3	1.650	1.7017	.286	.126	5.7959	.989	37.896	6.309
34.3	1.650	1.6443	.286	.126	5.3369	.909	37.857	6.296
36.3	1.650	1.5869	.286	.126	4.8974	.833	37.818	6.282
38.3	1.650	1.5295	.286	.126	4.4774	.761	37.778	6.269
40.8	1.650	1.4577	.286	.126	3.9793	.675	37.729	6.252
42.3	1.740	1.6647	.304	.126	5.979	1.009	43.986	7.241
44.3	1.920	1.6970	.410	.126	7.7065	1.362	71.2332	11.276
46.3	2.150	1.8500	.575	2.130	12.8540	2.269	135.6900	20.659

TABLE 3.1. TABULATION OF BMR PHYSICAL PROPERTIES
(Page 2 of 2)

RADIAL STN. (INS.)	EI_{co} x 10^{-6} (LB-IN.^{2})	EA x 10^{-6} (LB)	A (INS.^{2})	GK x 10^{-6} (LB-IN.^{2})	WT/IN. (LB/IN.)	I_θ (LB-IN.^{2}/IN.)	SEPARATION OF N. A.'s (INS.)	EC_w x 10^{-4} (LB-IN.^{4})
4.8	45.135	64.253	9.830	25.560	.688	4.224	3.600	419.78
5.3	36.241	81.247	19.408	26.215	1.359	[illegible]	3.550	404.43
6.3	31.728	76.810	17.627	15.747	1.233	5.746	3.488	157.90
8.3	13.087	61.355	12.338	6.425	.864	3.553	3.499	65.85
10.3	6.908	43.929	7.903	1.627	.559	2.077	3.378	25.68
12.3	3.905	33.485	5.554	.52145	.389	1.338	3.289	11.94
14.3	3.197	27.440	4.518	.3096	.316	1.052	3.224	7.73
16.3	2.767	22.657	3.818	.1936	.267	.888	3.221	5.75
18.3	2.235	17.716	3.095	.1134	.217	.725	3.245	4.18
20.3	1.885	15.228	2.724	.0931	.191	.654	3.328	3.28
22.3	1.587	13.307	2.435	.0756	.170	.592	3.391	2.73
24.3	1.399	11.944	2.226	.0611	.156	.537	3.414	2.40
26.3	1.394	11.926	2.216	.0610	.155	.532	3.416	2.26
28.3	1.387	11.900	2.201	.0609	.154	.525	3.419	2.12
30.3	1.379	11.874	2.187	.0607	.153	.518	3.423	1.98
32.3	1.372	11.847	2.172	.0606	.152	.511	3.426	1.85
34.3	1.364	11.821	2.158	.0605	.151	.504	3.429	1.72
36.3	1.357	11.795	2.143	.0603	.150	.498	3.433	1.60
38.3	1.349	11.768	2.129	.0602	.149	.492	3.436	1.48
40.8	1.340	11.735	2.111	.0601	.148	.485	3.440	1.34
42.3	1.630	13.127	2.358	.0734	.165	.578	3.504	1.91
44.3	2.0520	10.456	3.370	.1673	.236	.885	3.656	2.47
46.3	8.2719	21.577	7.955	9.7500	.557	2.165	3.681	45.34

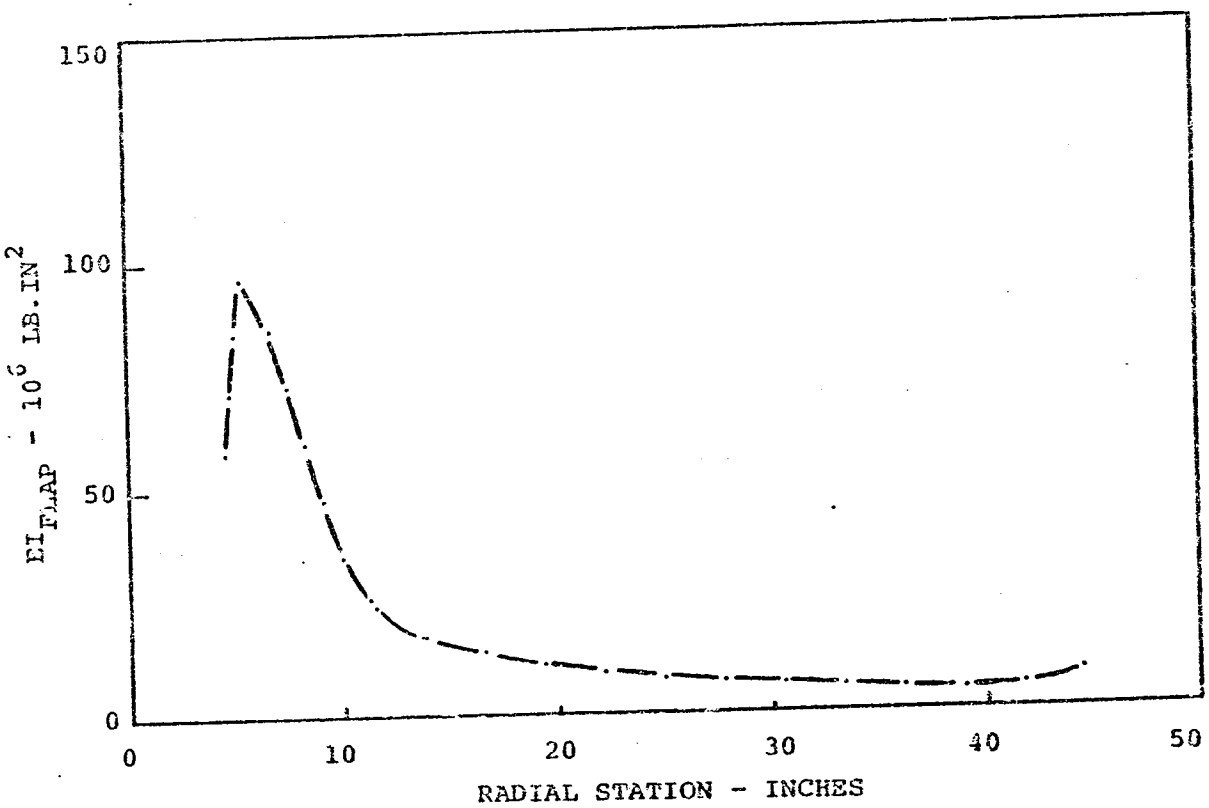

FIGURE 3.4 FLEXBEAM FLAP STIFFNESS DISTRIBUTION

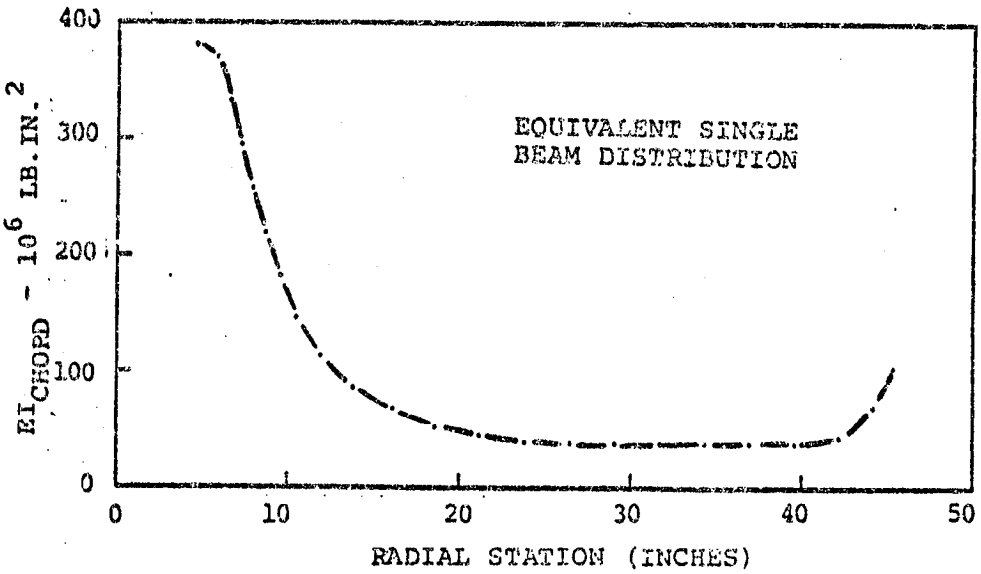

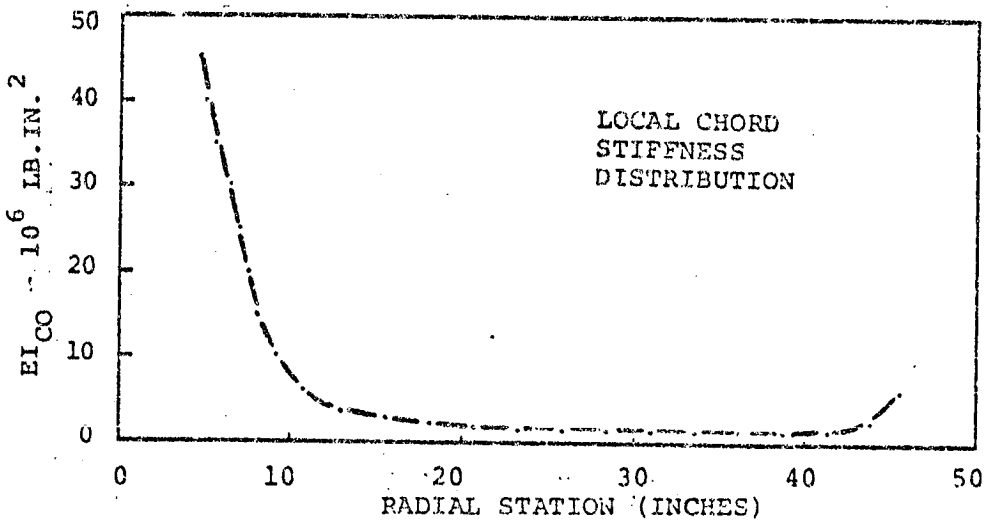

FIGURE 3.5 FLEXBEAM CHORD STIFFNESS DISTRIBUTION

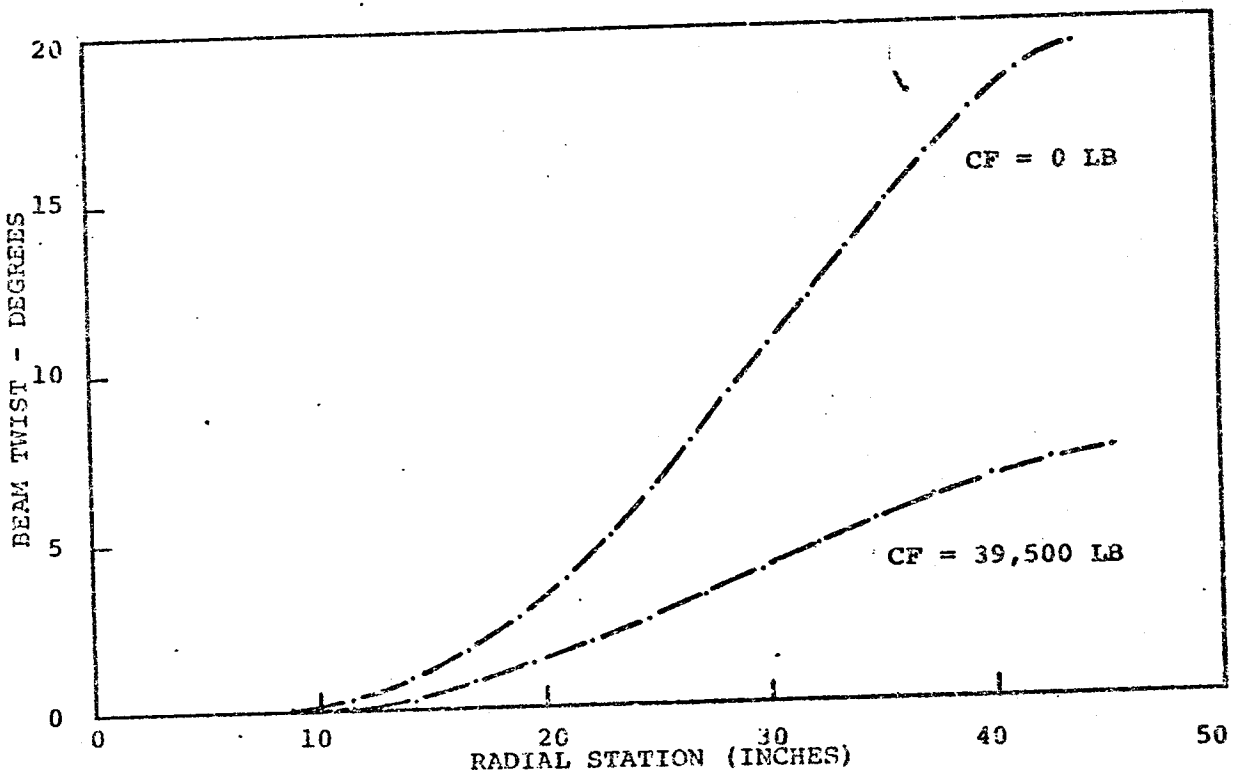

FIGURE 3.6 FLEXBEAM TWIST UNDER APPLIED TORQUE OF 1000 IN.-LB

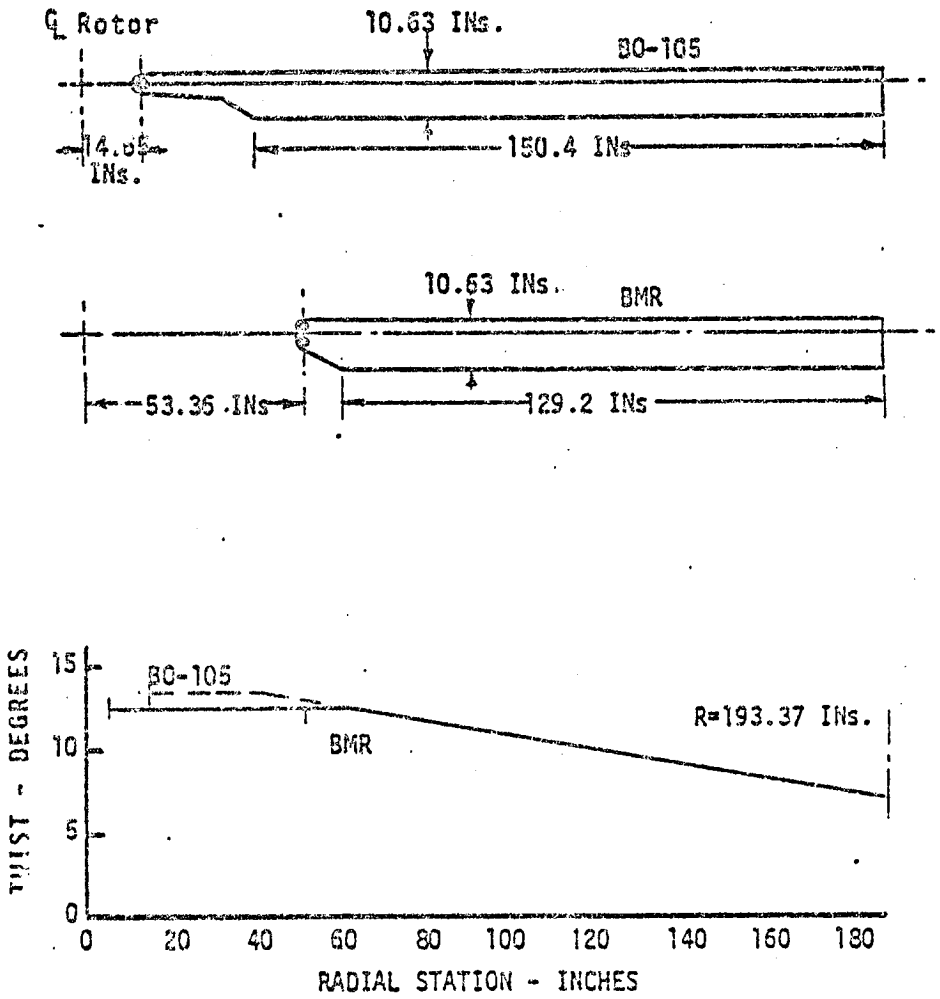

FIGURE 3.7 BMR AND BO-105 ROTOR BLADE - GEOMETRIC TWIST

TABLE 3.2. MODIFIED BO-105 BLADE PROPERTIES

R (INCHES)	r/R & RADIUS	WT./IN. (LBS/IN.)	EI-FLAP (10^6 LB-IN.^{2}) EI_F	EI-CHORD (10^6 LB-IN.^{2}) EI_C	TORSIONAL STIFFNESS (10^6 LB-IN.^{2}) GK
193.37	1.0	.71	2.38	59.4	1.36
192.02	.993	.71			
192.02	.993	.511			
188.92	.997	.511			
186.99	.967	.32			
153.92	.796	.32			
153.92	.796	.309			
97.65	.505	.309			
97.65	.505	1.447			
95.72	.495	1.447			
95.72	.495	.309			
87.79	.454	.309			
81.99	.424	.309	2.38	59.4	1.36
76.19	.394	.372	3.39	56.71	1.55
66.52	.344	.4762	5.084	52.21	1.74
62.85	.325	.5159	5.725	50.51	3.02
59.94	.304	.5474	6.234	49.16	3.00
53.95	.279	.6121	7.281	46.375	4.07
53.95	.279	2.573	82.20	68.375	4.10
52.	.269	2.573	157.28	266.375	5.19
50.4	.2607	2.573	164.4	291.38	5.77
50.4	.2607	1.3725	164.4	521.38	6.32
49.75	.2573	1.359	167.28	566.95	41.13
					41.13

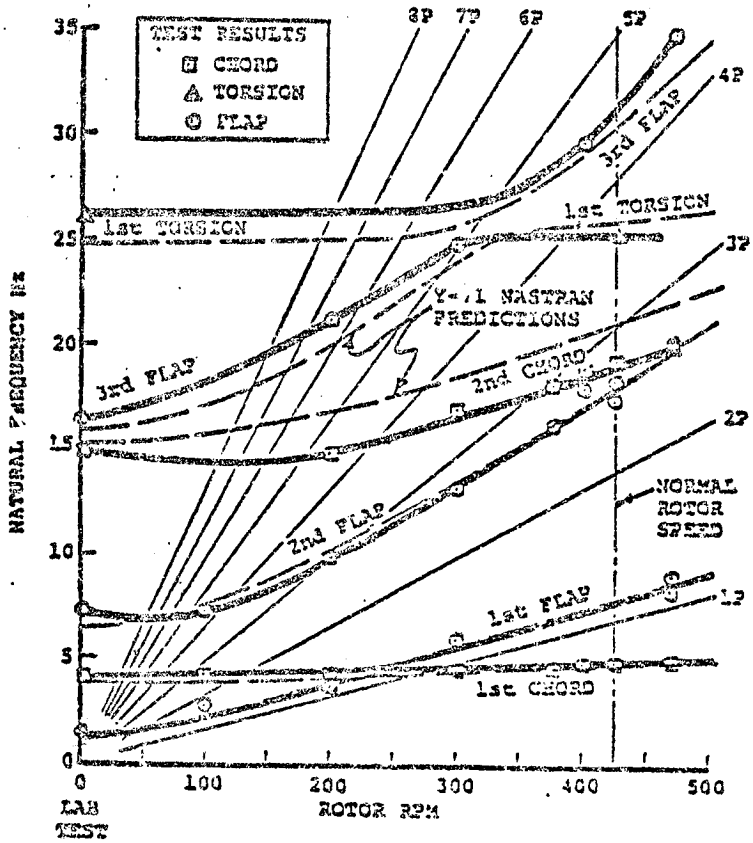

NATURAL FREQUENCIES (PER REV) AT N_{NORM} = 425 RPM

MODE	WHIRL TEST	GOAL	ANALYSIS
FIRST FLAP	1.12	1.12	1.12
SECOND FLAP	2.58	2.76	2.58
THIRD FLAP	4.45		4.34
FIRST CHORD	0.69	.70	.67
SECOND CHORD	2.72		3.01
FIRST TORSION	3.56	>3.2	3.70

FIGURE 3.8 BHR NATURAL FREQUENCIES ESTABLISHED BY WHIRL TOWER TESTING

3.1.5 Configuration Changes

The capability to vary three separate structural dynamic characteristics of the rotor system was incorporated into the basic BMR design. New pitch links were manufactured with axial flexibility to create a softer control springrate, which lowers the first torsional frequency. The ability to vary sweep was included, which alters the flap-lag-torsion coupling. Elastomeric damping material was purchased which changed the system structural damping level.

In addition to the conventional pitch links which characterized those used on the BO-105, an alternate design was fabricated. The barrel consisted of a 4130 steel upper and lower sleeve attached by lock bolts. The lower sleeve incorporated bellville spring washers on an end plug to provide axial flexibility. Oil impregnated guide bushings were used to accomodate the movement of the end plug within the bellville washers. The same rod end fittings as the baseline pitch links were used. A photo of the soft pitch links is shown in Figure 3.9. After the wind tunnel test a static deflection check was performed to determine the pitch link stiffnesses. The results are given in Figure 3.10.

A relatively simple change to the titanium clevis provided the ability to vary the sweep angle about station 52.36 inches from zero degrees to 2.5 degrees aft. At both blade bolt holes in the clevis, the holes were enlarged slightly and new eccentric

bushings were installed. When the bushings are rotated 182.5°, aft blade sweep of 2.5° results. The details of the hardware are presented in Figure 3.11. This parameter change was not tested during this program due to time constraints.

The final configuration change was the addition of elastomeric damper strips to the fiberglass flexbeams. The resulting additional structural damping produced a significant increase in modal damping during the wind tunnel test program. Each damper strip consists of a .02 inch thick layer of Lord Kinematic BTR VI elastomeric damping material sandwiched between a .01 inch thick layer of fiberglass cloth reinforced epoxy and a .08 inch thick constraining layer of graphite reinforced epoxy laminate. One each of these strips is adhesive bonded to the inner surface (upper and lower) of each flexbeam flange, for a total of 16 strips installed. This is illustrated in Figure 3.12. The change in stiffness as it affected modal frequencies is discussed in the stability results section of this report. Due to the uncontrolled curing environment, some portions of the damping material debonded during subsequent testing. However, this is not considered to have invalidated the data obtained.

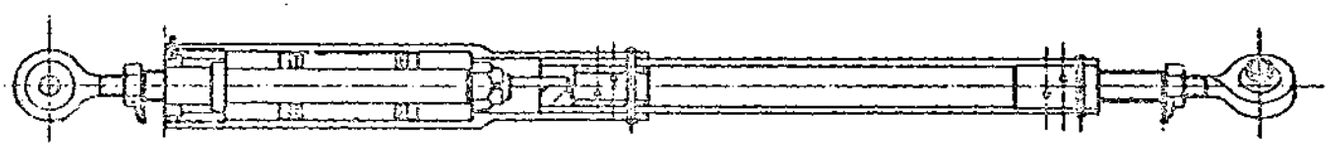

ASSEMBLY VIEW

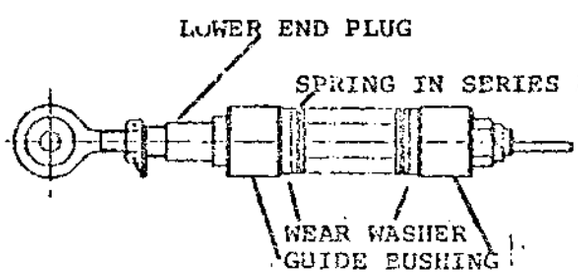

SPRING ASSEMBLY

FIGURE 3.9 REDUCED STIFFNESS PITCH LINKS

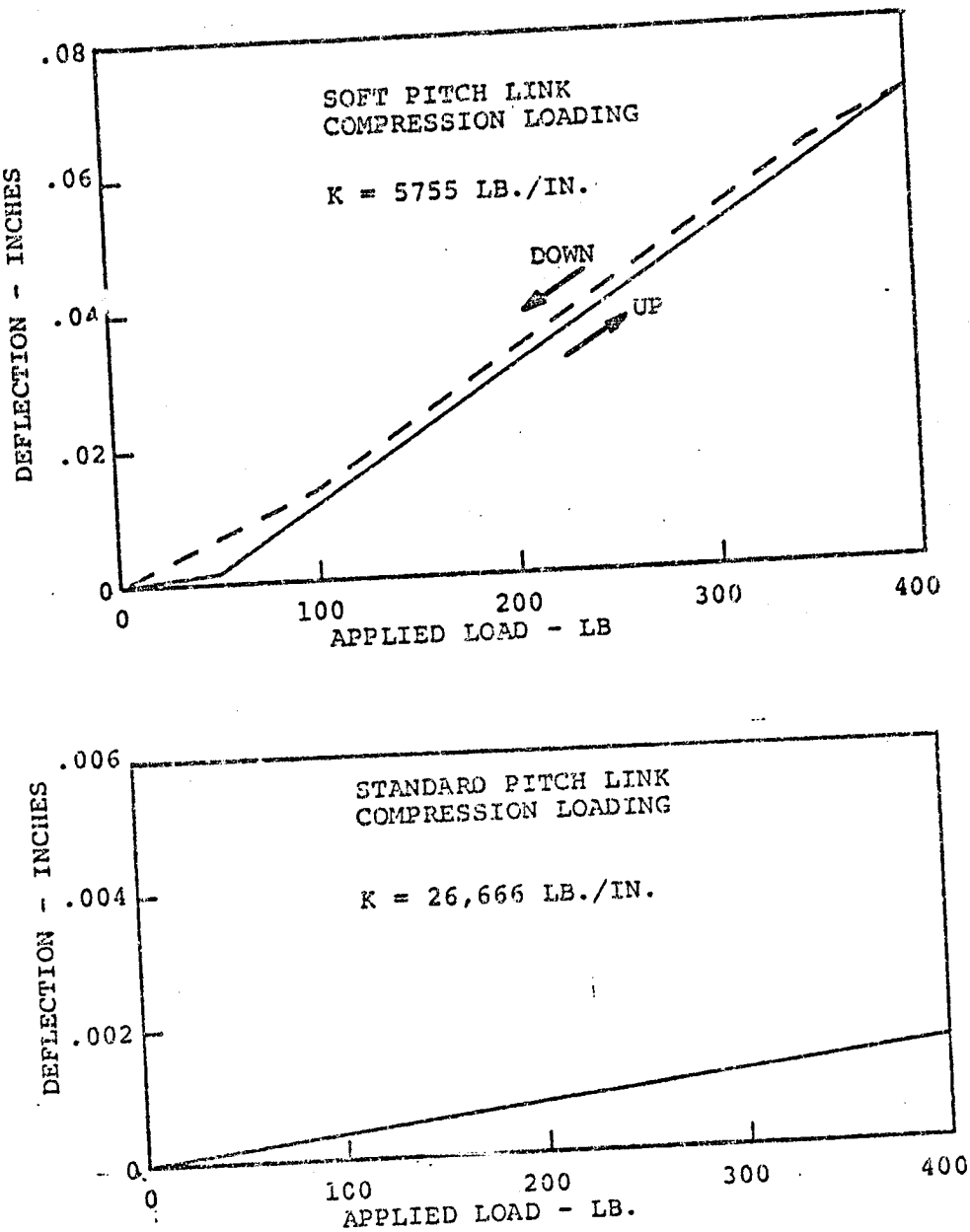

FIGURE 3.10 STATIC STIFFNESS DETERMINATION FOR STANDARD AND SOFT PITCH LINKS

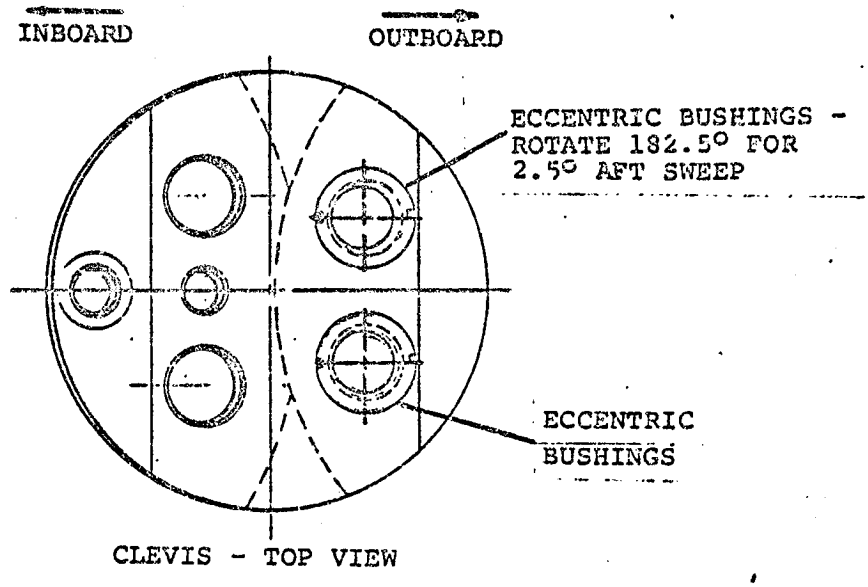

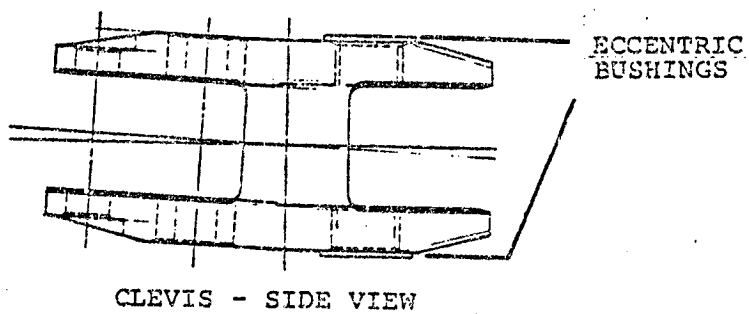

FIGURE 3.11 DETAILS OF SWEEP VARIATION HARDWARE

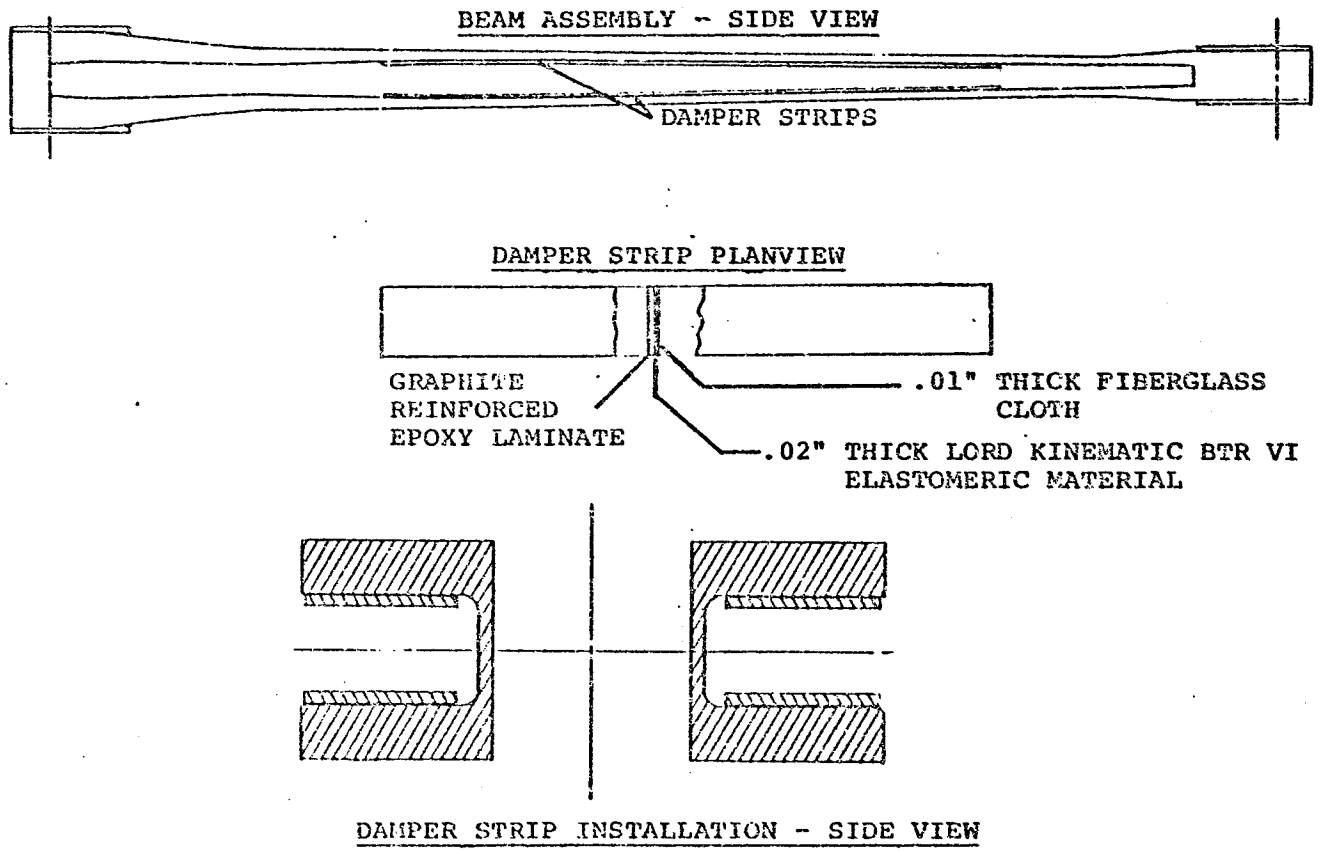

FIGURE 3.12 DAMPER STRIP INSTALLATION

3.2 MATING HARDWARE AND UPPER CONTROLS

3.2.1 Hub Adapter and Splined Collar

Some interface hardware was required to mate the BMR hub to the Rotor Test Apparatus (RTA) rotor shaft. The mating hardware consists of the hub adapter and splined collar, as pictured in Figure 3.13. On the upper surface the hub adapter (Part SK28259-1) contains holes with metric threads which accept the BMR hub studs. These hub studs attach directly to the flanged end of the BO-105 rotor shaft on the aircraft. On the lower surface, similar metric studs were used to attach to the splined collar. This collar (Part SK28258-1) has flanges which accept the metric studs from the hub adapter. At the lower end of the collar, lugs are provided to connect with the rotating scissors links. The collar has an internal spline to fit the external spline of the RTA rotor shaft. It is secured to the shaft with a collar retaining nut and lock washer. Rotation with respect to the shaft is further prevented by means of a lock key (Part SK28267-1) which picks up a slot in the collar and has teeth which mesh with the teeth in the collar retaining nut. The collar assembly is located with respect to the shaft by means of the existing RTA cone seats.

3.2.2 New Upper Controls Hardware

In order to accomodate the required BMR control motions and phasing, a new swashplate assembly was needed. The completed swashplate assembly as installed on the RTA (Part SK28260-1) is

shown in Figure 3.14. The assembly consists of the following items: stationary and rotating rings, bearing retainer, ball slider retainer, swashplate bearing, spacer spring and ball and socket assembly. The swashplate was designed to provide 42.1 degrees of total blade pitch using the available RTA actuator stroke. The rotating swashplate ring was designed to accept the RTA ball and socket assembly and spacer spring, made available for use during the test by NASA-Ames. The stationary and rotating rings were fabricated of 7075 aluminum alloy. The ball slider retainer was fabricated to capture the RTA ball and socket assembly, and a bearing retainer holds the purchased BO-105 swashplate bearing in place.

The rotating swashplate ring is driven by means of new rotating scissors, which attach to the splined collar (See Figure 3.14) and transmit rotor shaft torque to the swashplate. These drive links (Part SK28264-1) are comprised of an upper and lower scissors link made from 4340 steel. The stationary ring is restrained from rotation with respect to the shaft by a stationary link assembly (Part SK28263-1) which connects with the RTA attachment link. There are stationary scissors lugs on the RTA transmission upper bearing cap and on the stationary swashplate ring.

The swashplate design resulted in the need for new rod end assemblies (Part SK28266-1) to connect the RTA control input rods to the stationary swashplate ring. The various combinations of actuator motion provide tilting of the swashplate

about its horizontal plane (cyclic motion) as well as pure vertical motion (collective motion). The rotating swashplate ring is attached to the pitch arm by pitch links (Part SK28268-1). Because of the differences between the RTA and BO-105 installations, much longer pitch links were required for this program. The same design features as used on the BO-105 pitch links were duplicated for this test.

3.2.3 RTA Controls

The RTA controls are operated from a remote control console. The primary control system consists of three hydraulic servo-mechanisms, an electromechanical actuator tied to each servo, and a "walking beam" control rod linkage. Inputs originating at the remote control console may be sent to the actuators in one of two modes. Separate commands may be given to each actuator individually. A second option is for an electrically mixed signal resolved into collective and cyclic commands to be sent to the three actuators simultaneously. The signals position the hydraulic servo outputs, which drive the walking beams to locate the final stationary swashplate ring position. Any desired precession angle may be set so that cyclic motion will be about the desired control axes.

A modification to the control system allows for discrete pitch changes about the nominal blade angle position established by

the primary control system. At the pivot point of the lever arms which connect the primary servos and the stationary control rods, an eccentric mechanism driven by rotary actuators perturbates the nominal central position to provide ramp or oscillatory pitch inputs at a selected frequency. The oscillatory input may be swept-sine, from a function generator or random noise input. The input may be through collective pitch, longitudinal cyclic or lateral cyclic. An additional option is to command a dynamic input through the nutation control system. The longitudinal and lateral cyclic inputs are electrically combined to produce a signal which wobbles the swashplate to simulate stick whirl by the pilot at a specified frequency.

3.2.4 Description of the RTA

The Rotor Test Apparatus (RTA) is shown in Figure 3.15 mounted in the NASA-Ames 40-by-80 foot wind tunnel with the 32.23 foot diameter BMR system installed. The RTA fuselage is an A-frame structure, enclosed within a sheet aluminum aerodynamic fairing. The structural steel I-beam framework provides a rigid base for mounting the transmission and drive motors, and securing to the wind tunnel main and tail strut attachments. The non-structural fairing is supported by forms from the A-frame. Work platforms in the form of "clamshell" doors are provided on either side of the transmission, hinged at the fuselage sides and latched at the top.

The RTA is powered by two constant-torque, variable frequency electric motors rated at 1500 horsepower each. The motor operating speed range is 0 to 3000 rpm, and the motor is water cooled. A drive shaft connects the two motors, which transmits the power of the aft motor. Flexible couplings allow for misalignment. A second drive shaft connects the forward motor to the transmission, and transmits the power of both motors when in use. Flexible couplings are also used for misalignment on this drive shaft.

The transmission is a spiral bevel-helical gear speed reducer. The transmission gear ratio is 6.9:1, and at the maximum input rpm the tandem motor installation provides 3000 horsepower at 437 output rpm. The one piece rotor shaft has a three inch diameter hole for carrying instrumentation leads from the rotor hub to the slip ring unit mounted below the transmission. The transmission is lubricated by a forced oil lubrication system with electric motors driving oil pressure and scavenge pumps. Hydraulic pressure to the controls is maintained by electrically driven on-board pumps. All hydraulics have independent double stages.

The RTA is mounted on three struts mounted on a turntable. The model pitch angle is varied by changing the height of the tail strut. The two forward struts remain fixed throughout the

test. Yaw angle is achieved by rotating the turntable. Each strut is fitted with an aerodynamic fairing. Model power cables and hydraulics are routed through the struts to the RTA.

3.2.5 40-by-80 Tunnel Description

The NASA-Ames 40-by-80 foot wind tunnel is a closed circuit air return type tunnel. A cross-section at the test section is presented in Figure 3.16. The air is driven by six 40-foot diameter fans which are each driven by a 6000 horsepower electric motor. The tunnel can operate at any speed up to approximately 200 knots and at Reynold's numbers up to $2x10^6$ per foot at standard atmospheric conditions. When the test section overhead doors are open, a clear opening 78.5 feet by 49 feet is available for model entry. A 35 ton hoist is available for lifting models into the tunnel. A floating frame balance is used to measure the six components of forces and moments on the model. The balance frame may be locked (fore and aft and laterally) using a hydraulic snubbing system to protect the balance during large oscillatory load conditions. In addition, eight balance dampers may be added (or removed) to alter the system's dynamic response characteristics.

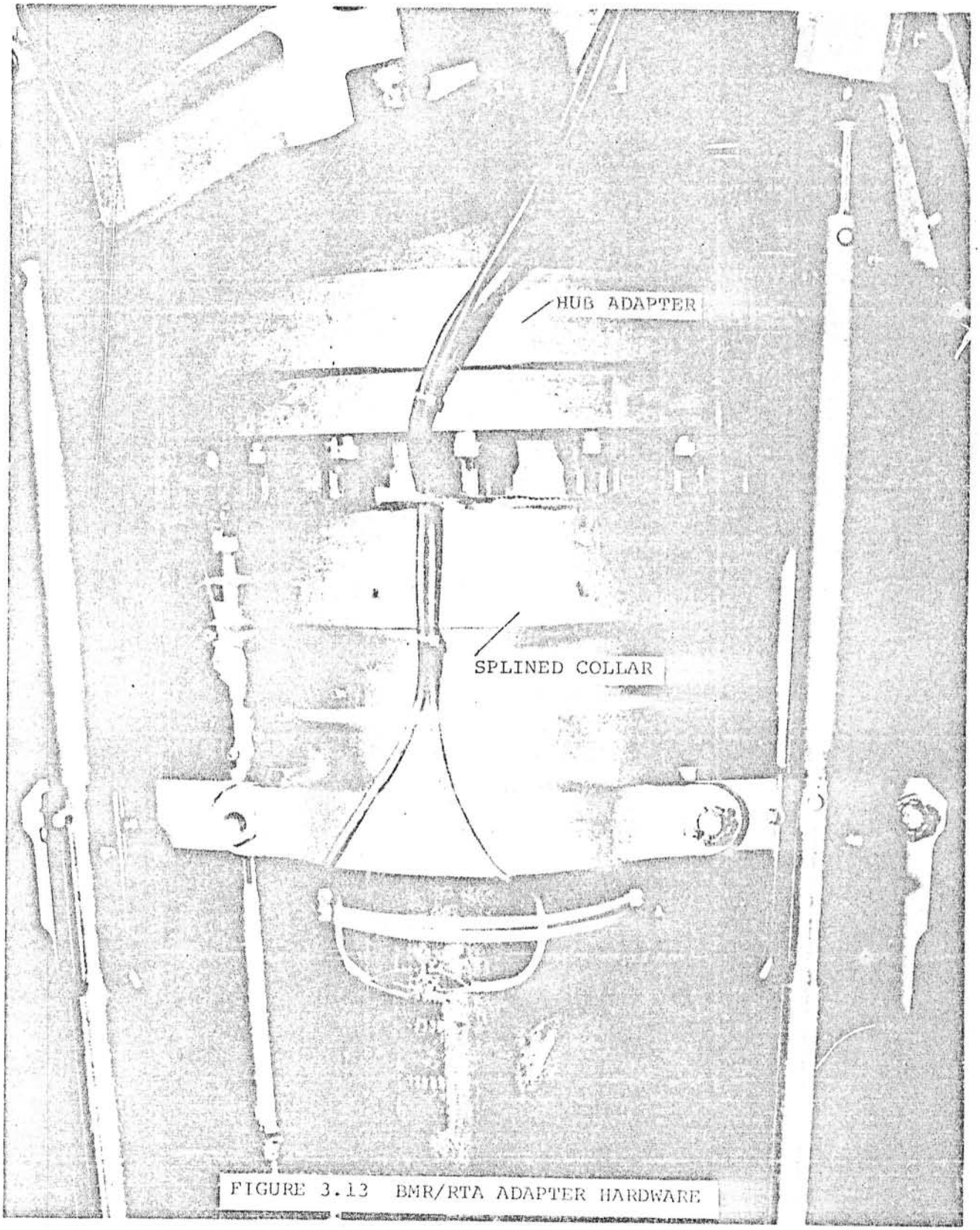

FIGURE 3.13 BMR/RTA ADAPTER HARDWARE

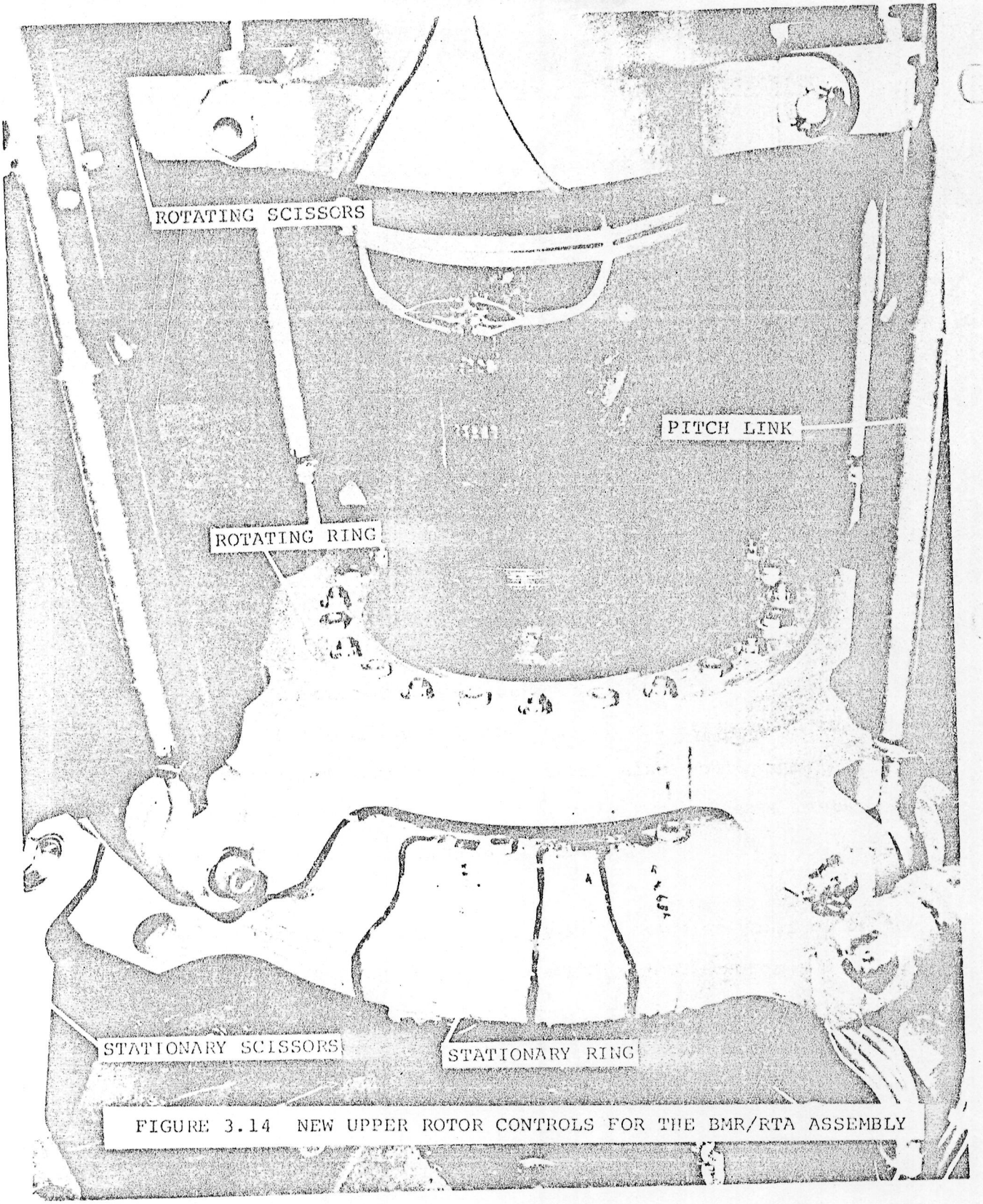

FIGURE 3.14 NEW UPPER ROTOR CONTROLS FOR THE BMR/RTA ASSEMBLY

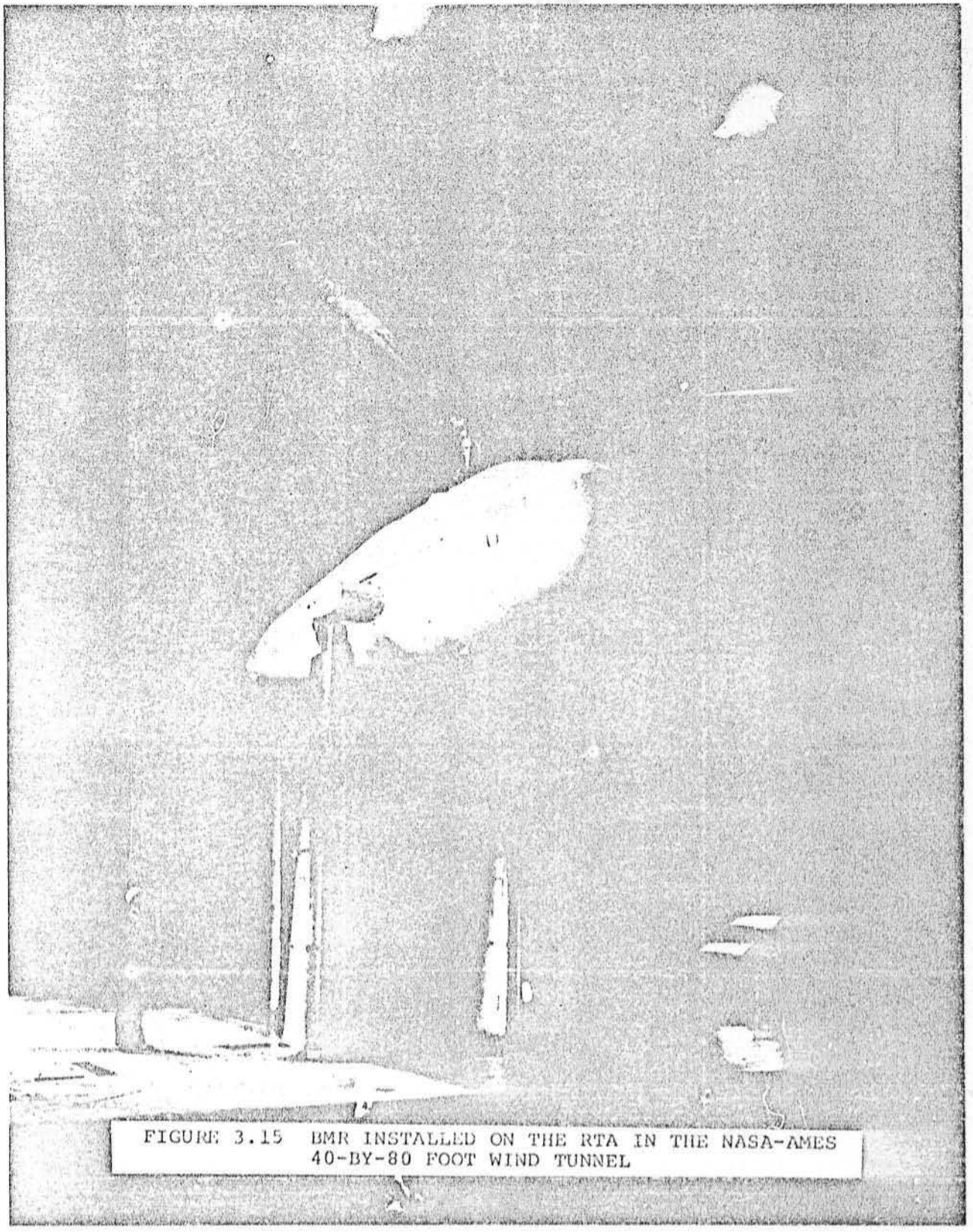

FIGURE 3.15 BMR INSTALLED ON THE RTA IN THE NASA-AMES 40-BY-80 FOOT WIND TUNNEL

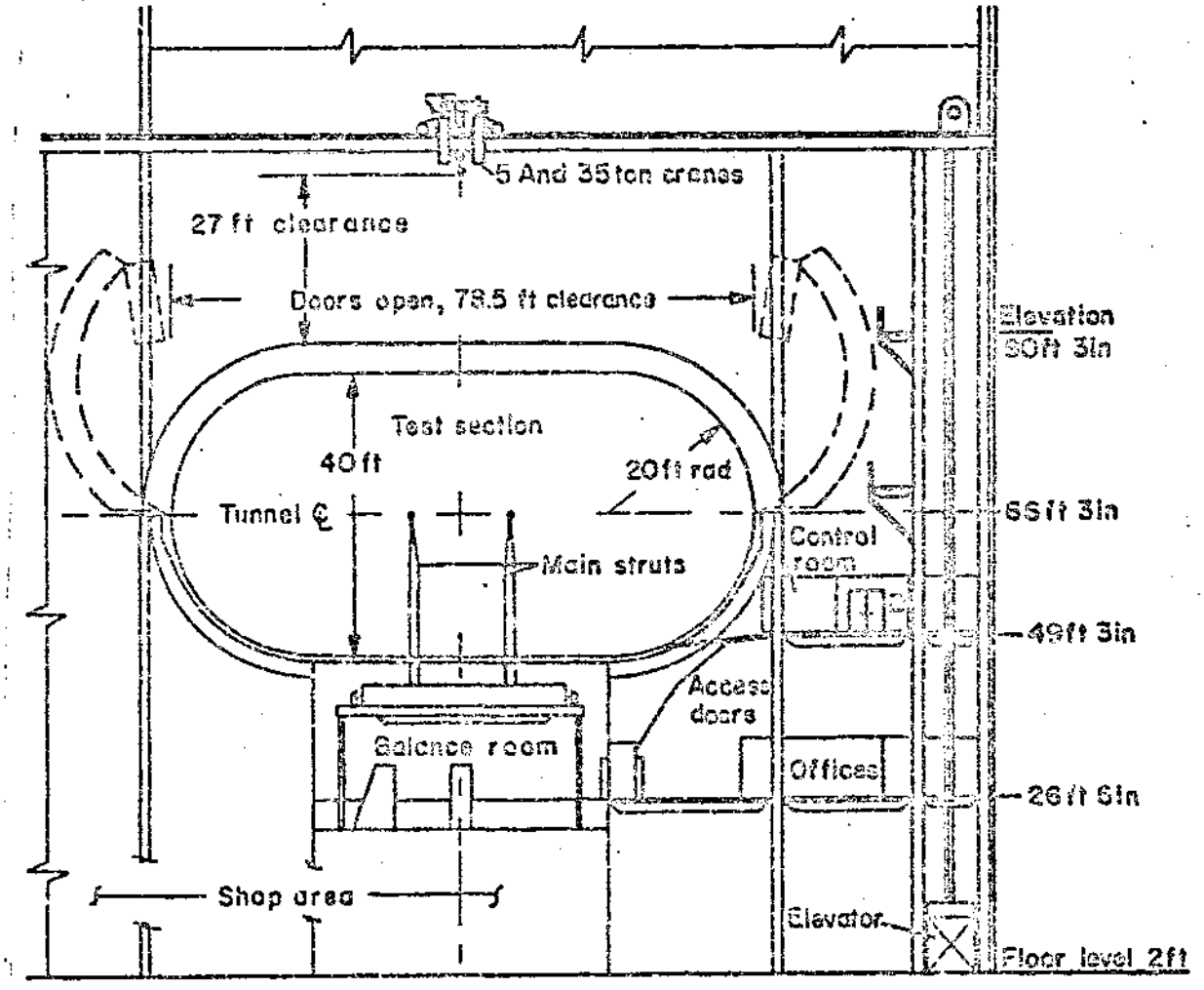

FIGURE 3.16 CROSS-SECTION OF NASA-AMES 40-BY-80 FOOT WIND TUNNEL

4.0 HARDWARE DESIGN AND ANALYSIS - STRUCTURAL INTEGRITY

4.1 BMR HARDWARE

The structural integrity of the BMR was demonstrated by analysis, bench fatigue testing and whirl testing. Positive margins in fatigue, limit and ultimate loading conditions were obtained in the analysis. The fatigue design condition was a 1.6g steady turn at 100 knots for normal gross weight. A fatigue life greater than 3600 hours was projected for all BMR components.

Bench fatigue, limit and ultimate tests were conducted as reported in Reference 4. All components were subjected to at least 2.55×10^6 cycles of fatigue loading. Run-outs were achieved in all cases, and the demonstrated fatigue lives based on a specified flight spectrum are given in Figure 4.1. Budget and time constraints precluded a demonstration of 3600 hours life for the beams and torque tubes, but it is felt that for higher applied loadings these items also would show fatigue lives greater than 3600 hours. Limit and ultimate tests were conducted without failures.

The BMR hardware structural integrity was also verified on the whirl tower. A thorough loads survey on the rotor and BO-105 control system was conducted over a thrust range from zero up to limits defined by rotor torque requirements. At normal (425 rpm) rotor speed and at 110 percent overspeed, loads were mea-

sured at positive and negative cyclic pitch settings until rotor shaft, beam flexure or torque tube bending limits were reached. Extensive strain gage instrumentation provided loads data.

To assess the integrity of the system under prolonged loading conditions, the rotor was whirled for 6.5 hours with loads in the most critical components at their endurance limits. At its uneventful conclusion, an overspeed test to 125 percent of normal operating rpm was conducted.

A subsequent teardown inspection, in which extensive non-destructive methods were used (e.g., X-ray, magnaflux and visual), revealed only minor fretting in the metal hardware which required minimum refurbishment prior to flight testing.

4.2 ADAPTER HARDWARE AND UPPER ROTOR CONTROLS

The structural integrity of the new hardware fabricated for this test program was verified strictly by analysis. The primary strength criterion for fatigue was to compute operating margins of safety using conservative loads predictions and conservative design allowables. In computing the operating margin of safety, 75% of the analytical endurance limit was used as an additional conservatism. Positive fatigue margins were found in all cases except for the basic ring section of the rotating swashplate ring, and for the bearing retainer. However, when the maximum loads actually encountered in the

test program are used in place of the very conservative loads used for these two items, the fatigue margins would be positive for both parts. For limit strengths, 2/3 of ultimate strength was used with no plasticity considered. All components demonstrated limit strengths at least three times greater than maximum expected loads except the pitch link (both the standard and "soft" links), which was twice the expected load.

During the test program, the actual loads as a percentage of endurance and limit loads were monitored to insure safe operation and inspections were performed before and after each run. Following the completion of the program, a thorough inspection verified that no damage was incurred by the adapter hardware or upper rotor controls.

4.3 ROTOR TEST APPARATUS

No formal analysis was performed of the impact of the BMR loads on the RTA strength. A comparison of the BMR loads with those of some much bigger rotors tested on the RTA, such as the H-34, indicated that the loads transmitted to the RTA would be considerably lower than those it was designed to handle.

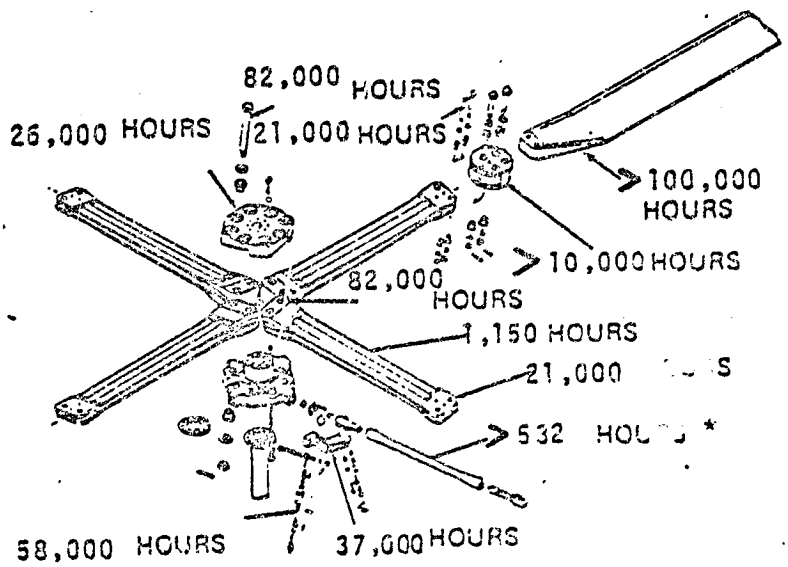

*CONSERVATIVE LIFE ESTIMATE FROM RUNOUT OBTAINED FROM UNCOMPLETED TEST

FIGURE 4.1 FATIGUE LIVES OF THE COMPONENTS DEMONSTRATED BY BENCH TESTING

5.0 DATA ACQUISITION SYSTEM

5.1 INSTRUMENTATION

To obtain loads, stress and dynamic data, the four beams, two blades and other significant rotating components were strain gaged. In addition to the instrumentation on the rotating hardware; data acquired included stationary control loads, RTA accelerations, steady balance loads, control positions and tunnel operating conditions.

An adapter plate located at the top of the rotor head, a slip ring assembly, terminal strips, lead wires and connectors provide the necessary links between the transducers and data acquisition equipment for each channel of measurement.

5.1.1 Rotor Instrumentation

Two blades and the four fiberglass beam assemblies were instrumented with strain gages of 1000 ohms resistance. Use of the 1000 ohm gages permits a higher bridge voltage to be applied, thereby improving channel sensitivity and compensating for the reduction due to the poor heat dissipation characteristics of fiberglass. Bridge completion networks for absolute strain measurements were installed close to the active strain gage with 3 wires from the gage to eliminate any lead-wire effect. Since all strain measurements were made into a completed 4-arm bridge at the gage location, the signal conditioning equipment did not require bridge completion capability.

The rotor instrumentation for two flexbeam assemblies consisted of flap and chord bending bridges on the individual beams at several span locations, as well as flap and chord bending bridges at two span locations on the blades and one torsion bridge. Instrumentation on the leading beam of a flexbeam assembly is referred to as on Beam A and on a trailing beam as Beam B. In addition, total beam flap, chord and torsion bridges were located at one span station for all four flexbeam assemblies. The torque tube was instrumented to monitor flapwise and chordwise bending, as well as torsion in the torque tube. Two of the pitch links were instrumented to measure control system loads. The rotor shaft was instrumented in the area above the swashplate to measure the torque in the rotor head assembly. Appendix A presents a complete list of the rotor instrumentation, including gage locations, engineering units, positive signal direction, calibration data and filter settings.

5.1.2 Additional Measurements

Instrumentation in the fixed system consisted of six stationary swashplate ring absolute gages, stationary control rod and actuator loads, and nine RTA accelerometers. In addition, the six components of model aerodynamic forces and moments were recorded using the "floating frame" system of balances comprising the Static Force System. (More complete information on the Static Force System is found in Reference 10.)

The rotor control positions, including collective pitch, longitudinal cyclic and lateral cyclic, were monitored at the rotor control console using feedback signals from the actuator servos. Other data included rotor speed (measured using the phototach signal) and shaft angle. Tunnel conditions such as velocity and temperature were also monitored continuously and recorded.

5.1.3 Wiring Connectors and Slip Ring

The strain gages were connected to the slip ring directly through wire bundles with connectors provided at the top of the BMR hub. The adapter plate formerly used to mount the BMR instrumentation canister was modified to provide mounting brackets for the connectors which mate the strain gage and slip ring wiring.

The slip ring provided a method whereby electrical power was supplied for excitation of the transducers, and low level signals were returned to the data recorders while the instrumented components were in a rotating operational mode. A one to one correspondence existed between the input and output connectors. The slip ring was located at the bottom of the gear box and driven by the rotor shaft. The "Rota-Switch" and the 256/rev generator were located at and driven by the lower part of the slip ring assembly. Consisting of 192 stacked brush and ring assemblies, the design of this unit was such that electrical noise from brush and ring contact was minimized.

5.2 ON-LINE MONITORING AND DATA ANALYSIS

The 40-by-80 data system is a computer based system which can be operated in either an on-line mode, or a stand alone with batch processing mode. It consists of the following major subsystems:

Dual Dec 11/70 Computers (Data Gathering Processor-DGP and Realtime Executive Processor - REP)

Static force system

Control console

Special instrument system (SI)

Dynamic recording system (DRS)

Dynamic analysis system (DAS)

Transducer conditioning system (TCS)

High speed data acquisition system (HSDAS)

Display system

Closed circuit television system

Acoustic recording system

On board multiplexing system

Reference Pressure system

The instrument subsystems in the control room are connected to the model via a general patch panel, permanently installed cables to junction boxes on the tunnel balance frame, and from there to the model. A schematic of the 40-by-80 data system is presented in Figure 5.1. A detailed description of the 40-by-80 data system is contained in Reference 10.

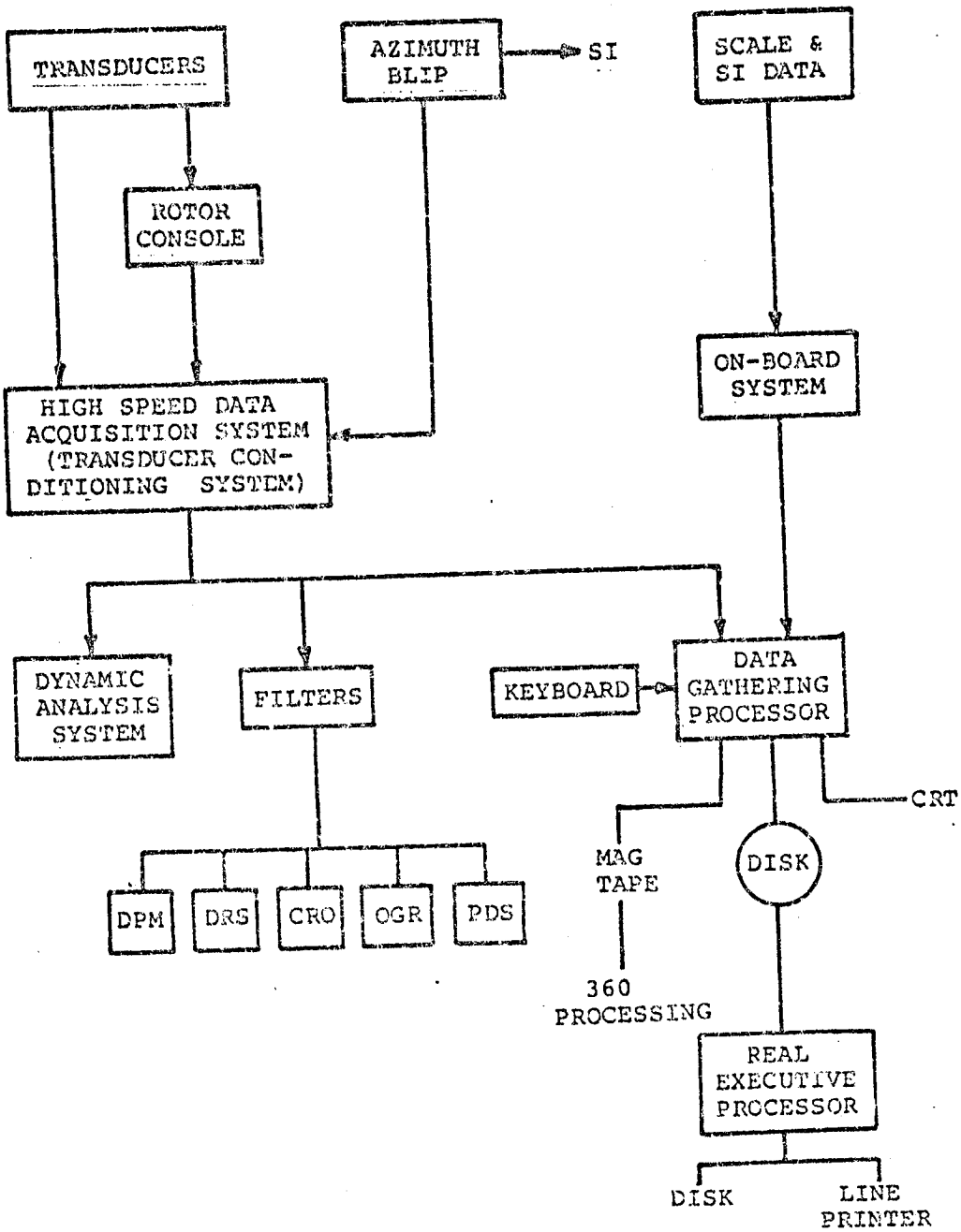

FIGURE 5.1 SCHEMATIC OF THE 40-BY-80 WIND TUNNEL DATA SYSTEM

Signals from the rotor transducers are first transmitted from the slip ring and RTA patch panel to the High Speed Data Acquisition System (HSDAS) and Transducer Conditioning System (TCS). The TCS supplies DC excitation, bridge completion when required, bridge balancing, shunt resistor calibration (RCAL) and external excitation. The transducers are connected to this system through the system patch panel. The HSDAS consists of sixty Newport 70A-4 amplifiers, a Xerox Data Systems sample and hold amplifier per channel, XDS 64 channel multiplexer and XDS ±14 bit analog to digital converter. This system is interfaced to the computer and cannot operate in a stand alone mode.

From the HSDAS the signal from each transducer channel may be routed to one or more of three possible sources. The signal may be directed to the Dynamic Analysis System (DAS). The system is primarily used in a stand alone mode for data acquisition/analysis and test conductance. It consists of a 32 channel analog conditioning element which can be sampled at rates up to 200 KHz. The primary use of the DAS is to perform one or more of the following operations on selected channels: Fourier or Inverse Fourier transforms, auto power spectrum, auto or cross correlation, histograms, transfer or characteristic functions, or any special programmed function such as moving block analysis.

Additionally, any signal from the HSDAS may be routed through filters to other on-line monitoring equipment. This consists of a Cathode Ray Oscilloscope (CRO) with the capability to display continuous time histories of up to 8 channels, two Oscillograph Recorders (OGR) with a capacity to provide a permanent record of the time history traces of up to 18 channels each, and a Peak Detection System (PDS) which displays up to 50 channels of data as a percentage of a prescribed limit value either in the peak or one-half peak-to-peak mode. The PDS can provide a paper tape record of the values at any time and has an alarm mode when a prescribed limit is reached on any channel. There are also ten digital panel meters (DPM) which display the signals from ten channels in counts or volts, and the information from these channels may be directed to the CRT for display. All the channels are also recorded on the Dynamic Recording System (DRS). This system provides for the recording of 56 channels of analog data, one channel of time code, two channels of PCM data, two channels of timing data and one channel of miscellaneous data on a 14 track magnetic tape. These signals are conditioned by amplifiers in the HSDAS. The DRS tapes may be processed following the test as an additional method of data analysis.

The third route of signals from the HSDAS is to the Data Gathering Processor (DGP). Scale data and special instrument data (data from the digital panel meters, the dangelometer, yaw readout and barometer) which has been processed by the data

management unit portion of the On-Board System (OBS) joins the selected dynamic data from the HSDAS at the DGP. Operated from a keyboard at the control console, the DGP is centered around a DEC 11/70 unit, magnetic tape units and a CRT display. The data which has been gathered may be displayed on the CRT for test conductance, written onto magnetic tape for post-test processing by the NASA-Ames IBM 360 computer, or put on disk storage for use by the Realtime Executive Processor (REP). The REP is used to process important high speed channels and static data following each run to provide a quick look at the data. This is useful for evaluating data quality and test results and for decision making in conducting the test.

5.3 POST-TEST DATA REDUCTION

At the conclusion of the test, the final reduced test data is produced. The tare runs are reviewed and the selection of appropriate hub tares for each run is made. A final listing of all static data for each run is produced. This consists of aerodynamic coefficients and loads obtained from the scale data, tunnel condition information, and model conditions such as shaft angle, yaw angle, collective pitch and cyclic angles, and rotor speed.

For each channel of dynamic data, the inputs required to compute engineering units from the raw signals are reviewed. These include static tare values, RCAL data, gains and filter

settings. Those runs or test points where a particular signal was bad are identified. When all the inputs have been verified, the dynamic data is processed to give the final listing of high speed data. For each run and test point for every channel, this consists of a harmonic analysis (10 harmonics), smoothed and averaged mean, RMS and half peak-to-peak data, magnitude versus frequency plots, and time histories for 3 revolutions plus an average waveform adjusted for filter settings.

6.0 TEST PROCEDURES

6.1 GENERAL APPROACH

The basic procedure used throughout this test program was to set a particular trim condition, record steady-state loads and performance data, then excite the rotor through the Dynamic Control System and compute the modal damping at that condition. To insure that no aeroelastic instability or excessive load condition was encountered, careful utilization of pretest predictions and on-line monitoring of data was employed. The critical safety instrumentation was monitored at all times, and a continuous log was made of the growth of specific parameters as test conditions were changed. In this manner it was possible to predict at what point limits would be reached or exceeded and prevent severe damaging conditions.

The test plan was structured so that for each series of stability data points, the test proceeded in the direction of decreasing stability. As each stability data point was taken, the modal damping was computed and plotted against predicted values so that the trend could be seen and an evaluation of the stability at the next planned test condition could be made. If indications were that the next point would have damping less than 1% fixed system critical damping, a new test condition could be selected.

6.2 LOADS AND PERFORMANCE TESTING

After the initial hub tare runs and track and balance verification, the procedures described here were followed for loads and performance testing. A detailed pre-run series of inspections and checklists were performed on the BMR rotor and controls hardware, the RTA, the rotor console and control system, tunnel motor operation, data monitoring equipment and instrumentation. When the model and tunnel were secured, a zero point was taken with zero shaft angle, 9.6° collective pitch and zero cyclic input.

To start the rotor, the controls were set for a shaft angle of -10 degrees and a moderate collective pitch angle, usually 4° or 8°. Then the rotor was brought up to the desired rpm, going rapidly through the 240 rpm to 325 rpm region where the first chord mode crosses both the one per rev and the first flap mode. As this is being done the rotor console operator is continuously adjusting cyclic pitch to maintain zero one per rev flapping. The flap bending moment at station 14.25 inches was used as the measure of one per rev flapping. The signal from one flexbeam was fed through electronics in the rotor control console which resolved the flap moment into its steady, one per rev sine and one per rev cosine components. The signal was not calibrated for the actual value of flapping, but since station 14.25 inches is inboard of the effective flap hinge zero flap moment was assumed to indicate minimum flapping. Once the rotor reached the desired rotor speed, adjustments

were made to the shaft angle and collective settings to minimize loads as the tunnel was brought to the desired velocity. When the desired tunnel speed was attained, the rpm, shaft angle and collective were adjusted to reach the first test point, and a steady-state loads and performance data point was taken.

Specific procedures were established to insure safe operation away from both loads and stability problems. Figure 6.1 shows the test boundaries which were established due to model control limits, clearances, power limits and stability requirements. Reference 11 presents the vibratory and vibratory plus steady load limits, as well as actions which were to be taken if any limit was exceeded. Careful attention to these procedures in the areas of damage count analysis and visual inspections during the test permitted operation at various load levels with confidence that the structural integrity of the system was not being compromised. Finally, procedures for changing tunnel speed, rpm, collective pitch angle and shaft angle were defined as to the proper order for varying each item so that safe load levels and stability margins could be maintained.

One type of loads and performance testing used a slightly different procedure. This was the 1g flight testing. To simulate level flight in the BO-105 aircraft, the rotor was brought to 425 rpm and the tunnel set to the desired forward speed. Then

TEST RPM	335 TO 437
VELOCITY (KNOTS)	0 TO 165
COLLECTIVE PITCH (DEGREES)	-.2 TO 15.8
SWEEP (DEGREES)	0 TO 2.5 AFT

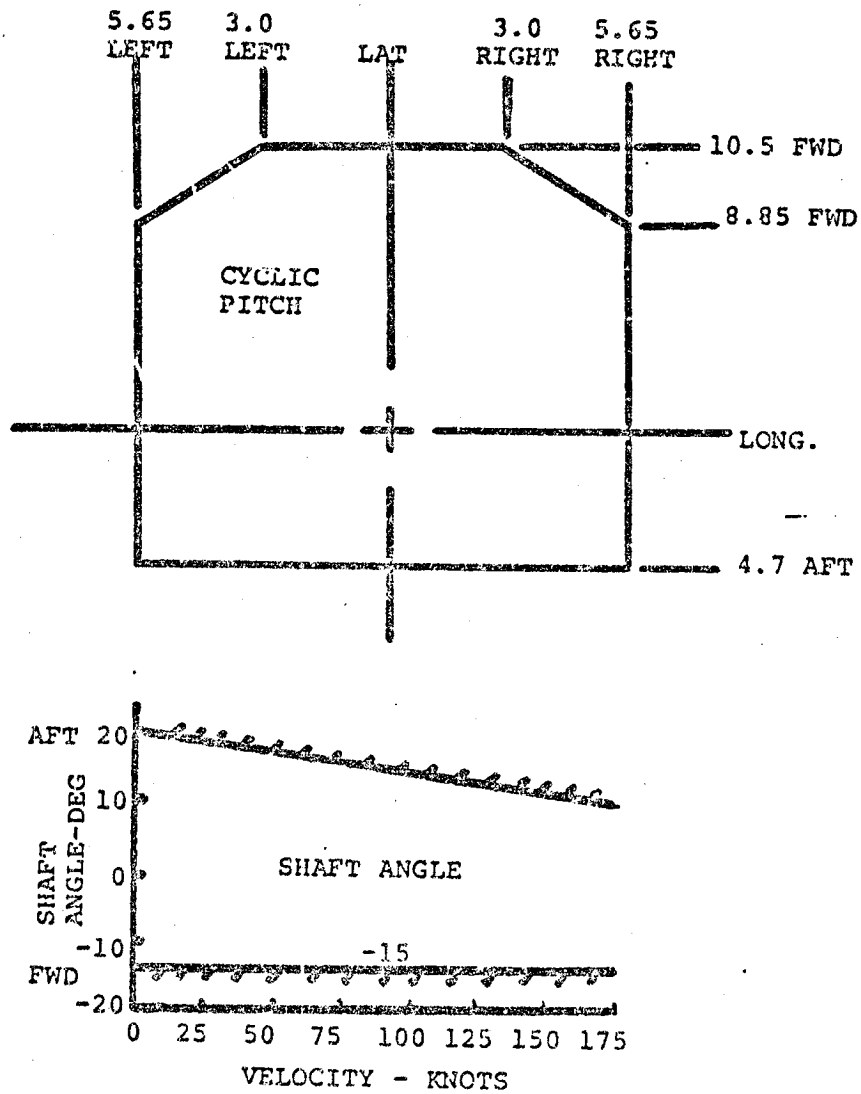

FIGURE 6.1 TESTING BOUNDARIES

collective pitch was adjusted to maintain C_L/σ = .072. Next the shaft angle was varied until the rate of descent was zero, based on a nominal rotor effective flat plate drag area (F_E) of 14.5 square feet. Longitudinal and lateral cyclic were adjusted to attain the predicted aircraft pitch and roll moments necessary to trim the BO-105/BMR. Finally, collective pitch, shaft angle and cyclic pitch were fine tuned since there is cross-coupling among the trim requirements. When trim was established, a steady-state data point was taken.

6.3 STABILITY TESTING

6.3.1 Dynamic Characteristics of the BMR/RTA

The potential for reduced damping or even instabilities exists when the lead-lag regressing rotor mode frequency coalesces with a body mode frequency of the RTA. Figure 6.2 shows the variation of the BMR lead-lag regressing mode frequency with rotor speed. This figure shows the RTA mode frequencies of interest for configurations with wind tunnel balance dampers installed and removed. RTA body mode frequencies are from Reference 10. With the balance dampers installed, a potential for instability exists at about 420 rpm and at about 455 rpm. RTA body mode frequencies change when balance dampers are removed, and rotor speeds for potential instability are expected at about 400 and 430 rpm.

6.3.2 Stability Predictions for the BMR/RTA

6.3.2.1 Predicted Stability

The BMR/RTA was modeled analytically using Boeing Vertol's C-90 aeroelastic stability analysis program; this program is discussed in more detail in Sections 7.1.1 and 7.2.1. The specific prediction results determined prior to testing in the NASA Ames 40-by-80 foot wind tunnel are shown in Figures 6.3 through 6.14. Figure 6.3 shows the expected damping level versus rotor speed for a startup at zero thrust (approximately zero collective pitch at 70 percent radius); this is expected to be the collective pitch for lowest damping. The stability level is shown in terms of time to half amplitude, amplitude decay rate, and fixed system critical damping ratio. In this report, aeroelastic stability mode damping ratios will be expressed in terms of fixed system damping ratio, i.e., the damping at the lead-lag regressing frequency. Results in Figure 6.3 are for 8 balance dampers installed and for long struts (these were the struts used to support the RTA during BMR/RTA testing). All analytical predictions are based on the assumption of no blade structural damping. As rotor speed increases, damping is expected to increase until about 200 rpm. Damping is then expected to decrease gradually until above 500 rpm except for a predicted damping reduction at about 470 rpm due to a body mode/lead-lag regressing mode coalescence. However, the maximum possible test rotor speed is 437 rpm so that this reduction in damping at about 470 rpm could not occur during BMR/RTA testing. The rotor speed test range where BMR/RTA damping was obtained was 335 to 437 rpm.

Figure 6.4 shows the predicted effect of removing wind tunnel balance dampers; predicted damping is shown versus rotor speed in hover (zero wind tunnel speed). Without balance dampers, damping is predicted to be reduced to about 0.4 percent critical at 428 rpm and to -1 percent critical at 468 rpm. These are rotor speeds where coalescences of the RTA body mode frequencies and the BMR lead-lag regressing mode frequency occurs. At other rotor speeds, damping is expected to be identical with and without balance dampers.

Figures 6.5 through 6.9 show predicted effects of airspeed, rotor speed, collective pitch and shaft angles on damping. Predictions are generally for all balance dampers installed, rotor speeds from 340 to 437 rpm, collective pitch from 0 to 12 degrees, airspeeds from 0 to 180 knots, and shaft angles from 0 to -6 degrees. Predictions generally indicate increasing damping with increasing collective pitch (with maximum values near 10 degrees), and decreasing damping with increasing rotor speed. Damping was not expected to be sensitive to shaft angle at constant wind tunnel velocity, rotor speed, and collective pitch. With other variables constant, damping was expected to increase with airspeed from hover to 60 knots, then decrease at 100 knots, and then increase for airspeeds up to 180 knots. Predicted damping levels in Figures 6.5 through 6.9 were interpolated to obtain predicted damping levels at planned test conditions (Ref. 11). A typical result is shown in Figure 6.10.

Figures 6.11 and 6.12 show predicted damping versus airspeed and shaft angle at zero and 4500 pounds thrust, respectively. Results in these two figures are for 425 rpm rotor speed.

Figures 6.13 and 6.14 show predicted effects of varying blade structural damping and blade sweep. Testing was conducted for a blade chord mode structural damping variation. Hardware was available for conducting a blade sweep variation, but due to time limitation in the wind tunnel, the sweep variation was not tested.

6.3.2.2 Use of Stability Predictions During Testing

Prior to conducting a particular test sequence, predicted stability data were plotted for the specific planned test conditions. As the test sequence progressed, test values of damping data were computed and plotted on the same graph with expected (predicted) damping to determine whether magnitudes and trends of damping levels were as expected. Figure 6.15 shows test and expected damping results for the first run made with the BMR/RTA with rotor blades installed.

6.3.3 Stability Test Procedures

Two general methods were considered for determining BMR/RTA aeroelastic stability levels. One was the moving block method (Reference 13) and the other was the instrumental variable method (Reference 14). The first method (discussed in more detail below) determines damping levels from a decaying signal.

- BALANCE DAMPERS ON

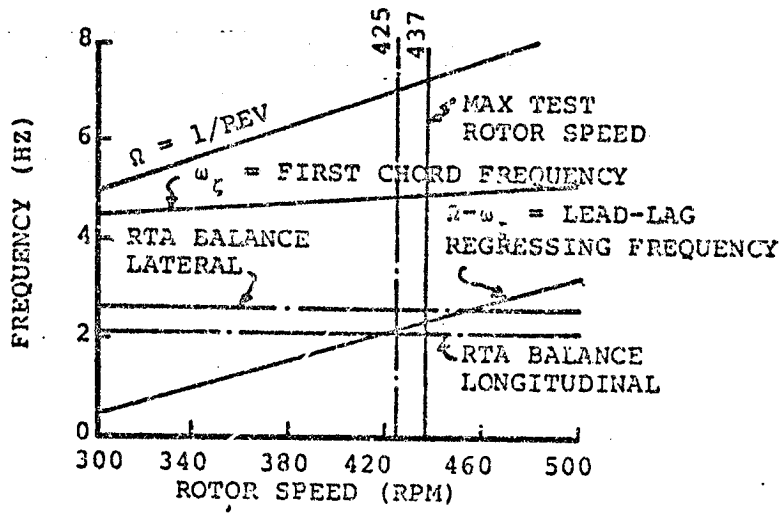

- BALANCE DAMPERS OFF

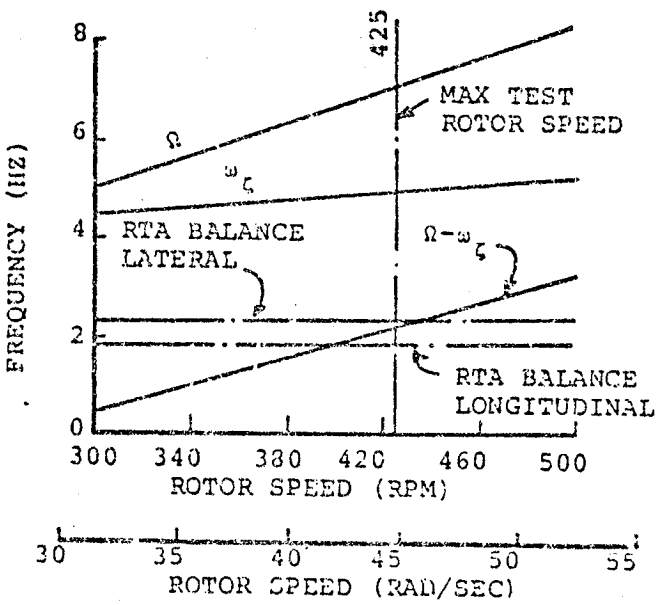

FIGURE 6.2 BMR LEAD-LAG REGRESSING MODE AND RTA BALANCE MODE FREQUENCIES VS ROTOR SPEED

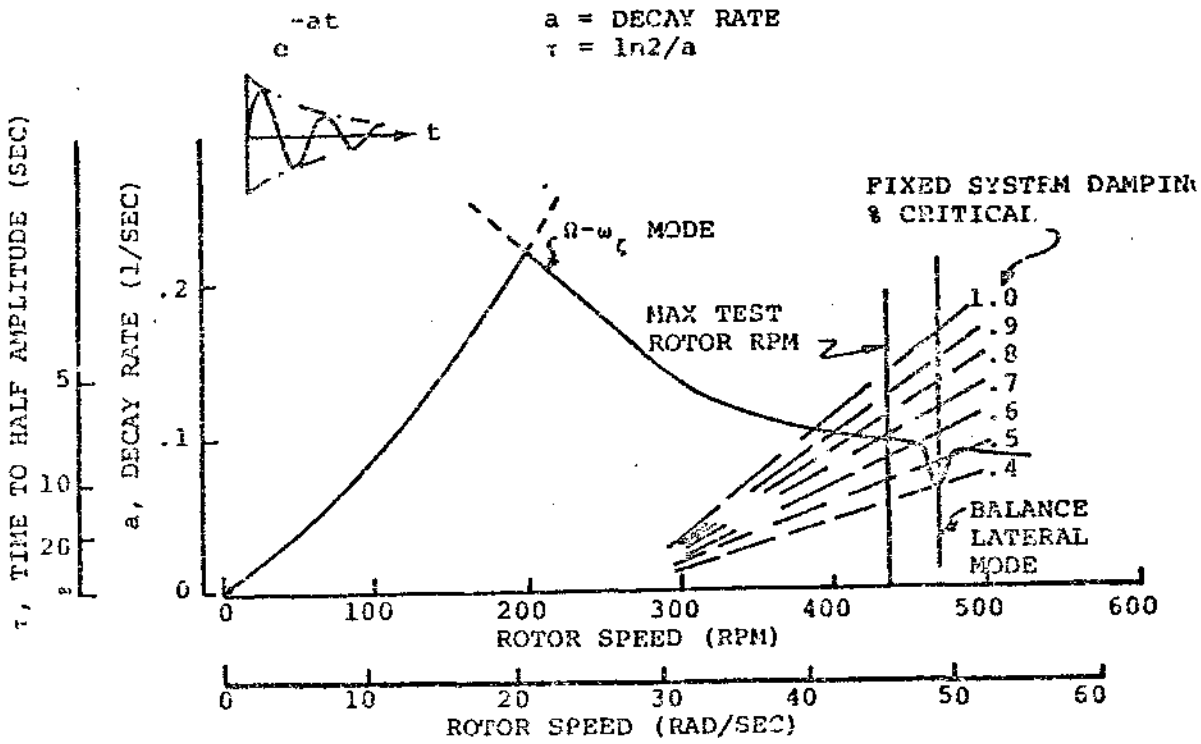

FIGURE 6.3 PREDICTED BMR/RTA STABILITY DURING START-UP AT ZERO AIRSPEED AND ZERO THRUST

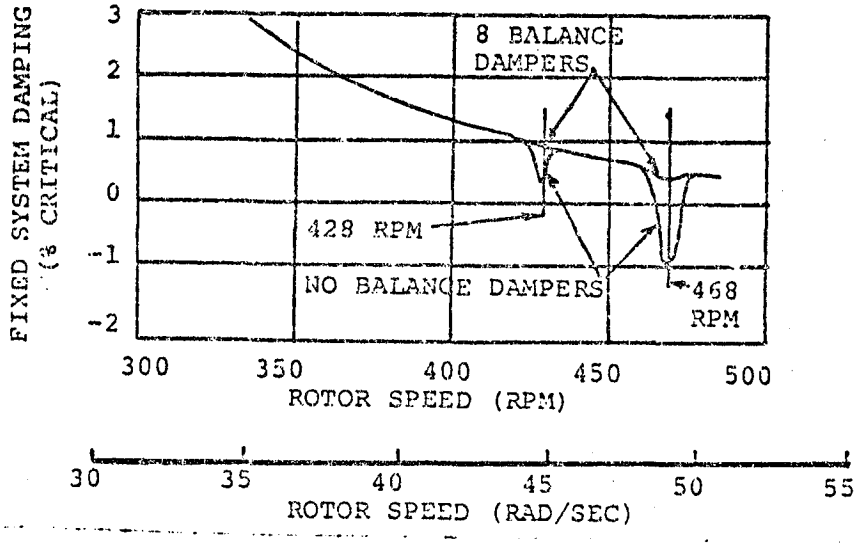

FIGURE 6.4 PREDICTED EFFECTS OF BALANCE DAMPERS ON BMR/RTA STABILITY AT ZERO THRUST AND ZERO AIRSPEED

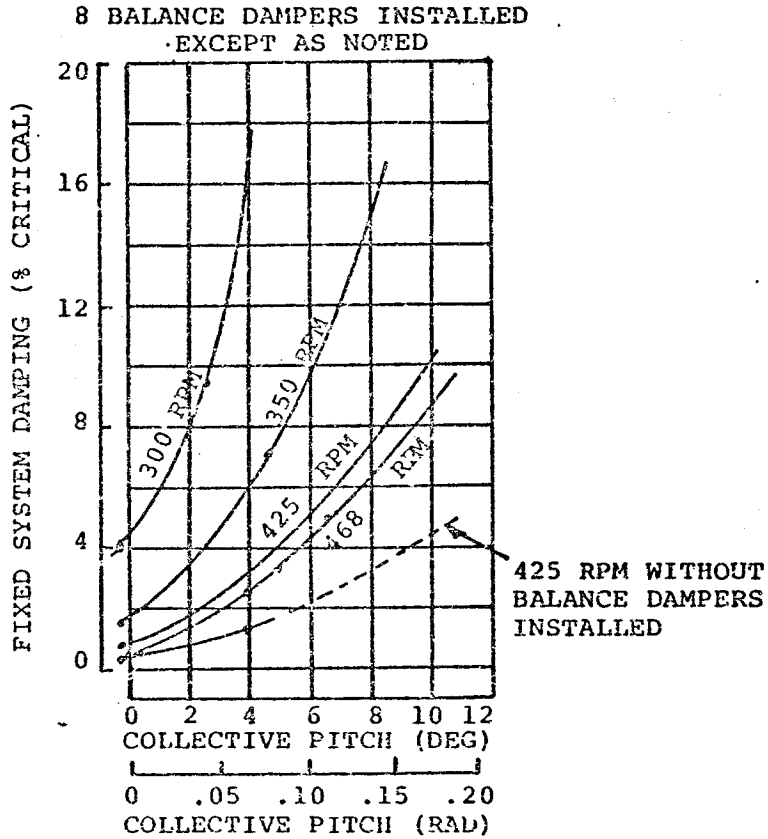

FIGURE 6.5 PREDICTED EFFECT OF ROTOR SPEED AND COLLECTIVE PITCH ON STABILITY FOR HOVER

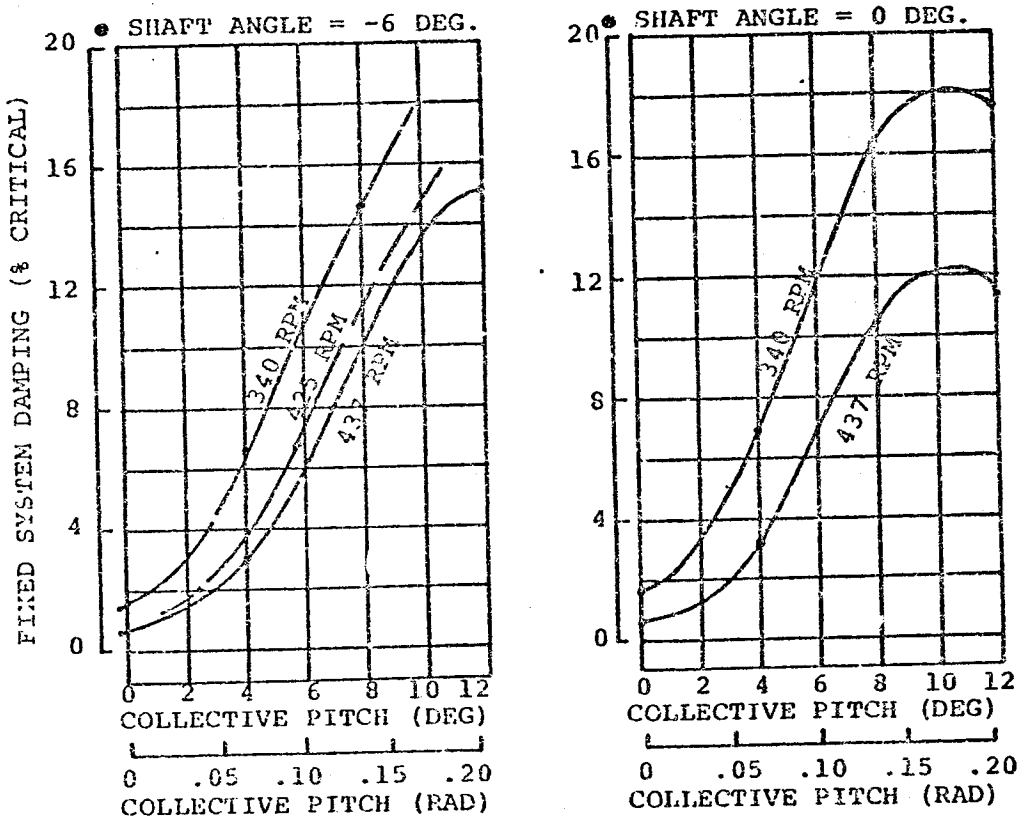

FIGURE 6.6 , PREDICTED EFFECTS OF ROTOR SPEED AND COLLECTIVE PITCH ON STABILITY AT 60 KNOTS FOR 0 AND -6 DEGREE SHAFT ANGLES

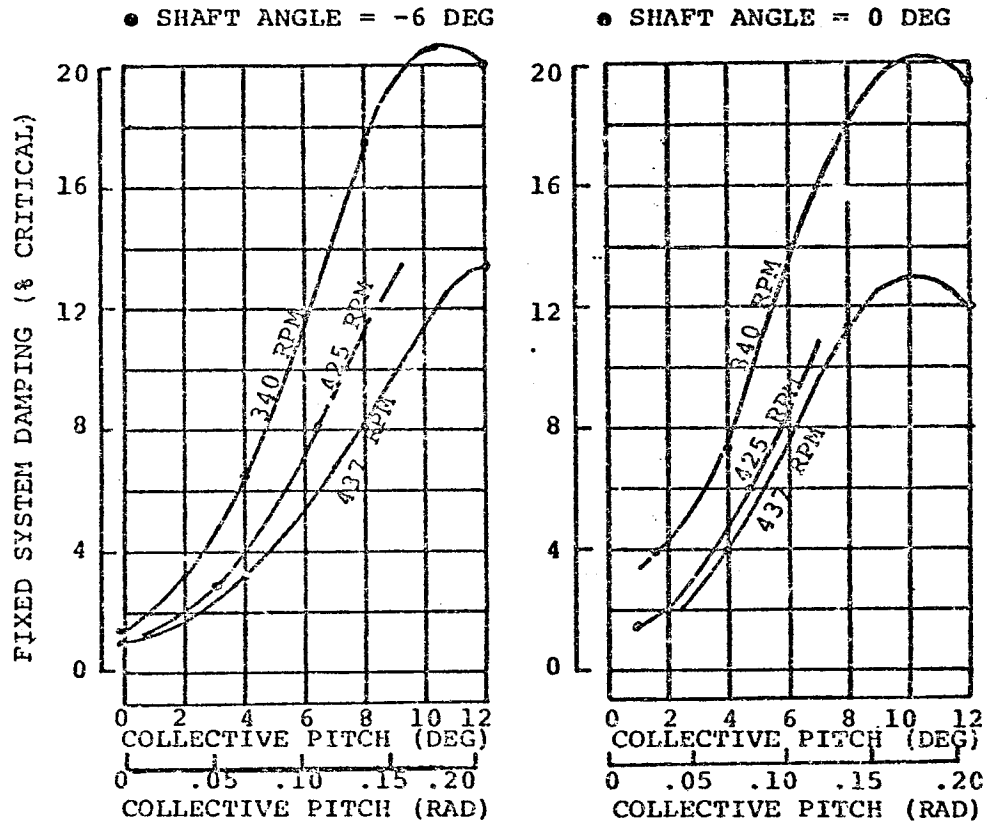

FIGURE 6.7 PREDICTED EFFECTS OF ROTOR SPEED AND COLLECTIVE PITCH ON STABILITY AT 100 KNOTS FOR 0 AND -6 DEGREE SHAFT ANGLES

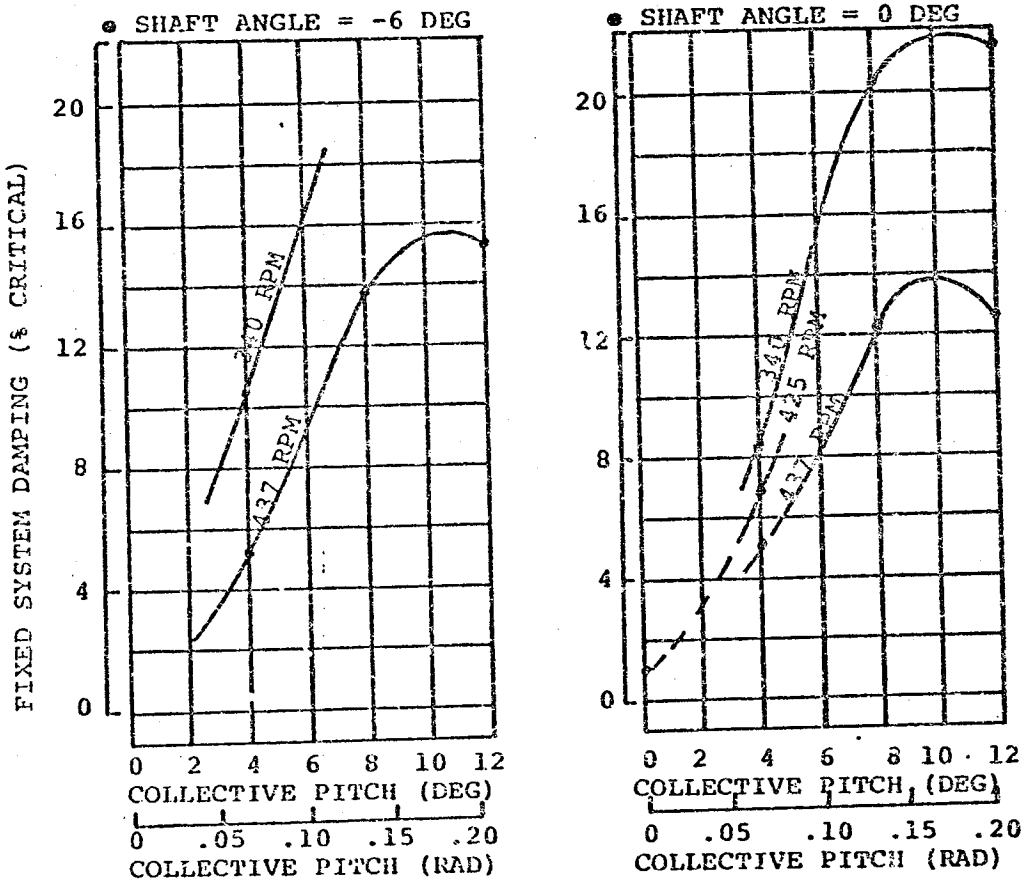

FIGURE 6.8 PREDICTED EFFECTS OF ROTOR SPEED AND COLLECTIVE PITCH ON STABILITY AT 140 KNOTS FOR 0 AND -6 DEGREE SHAFT ANGLES

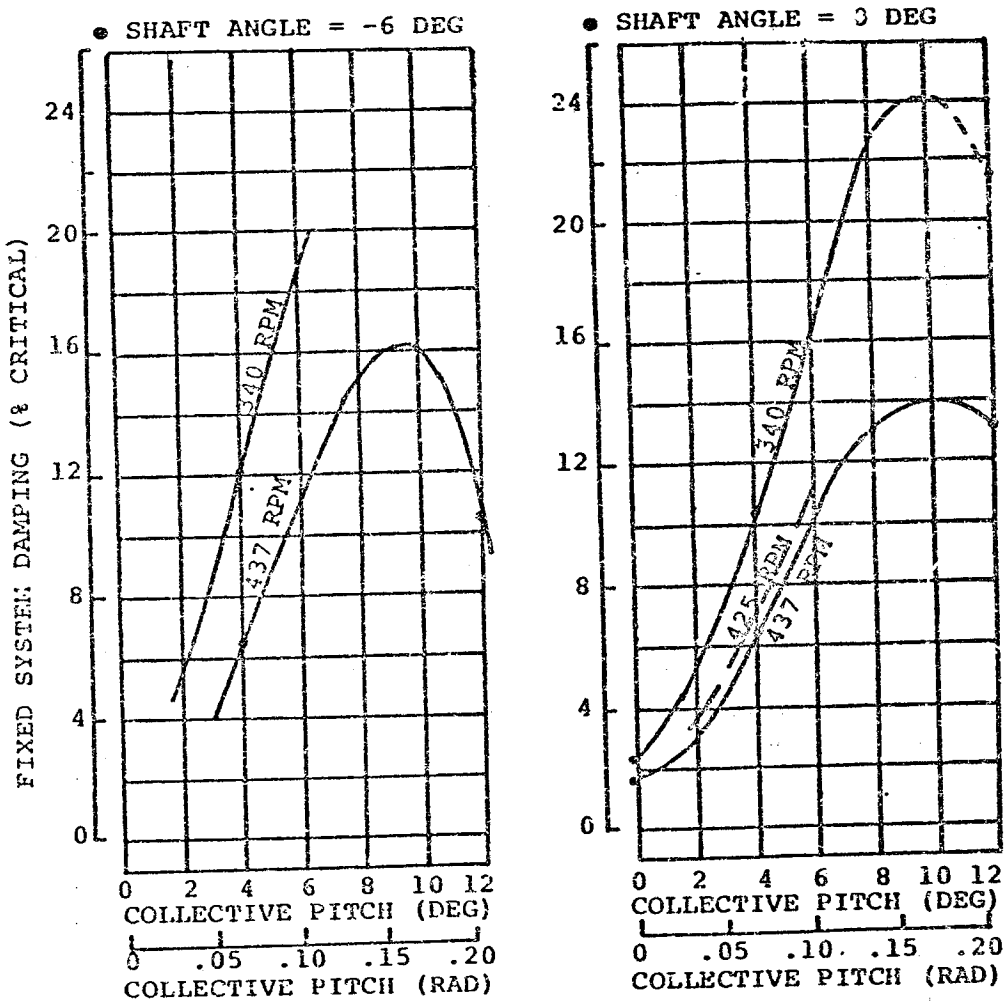

FIGURE 6.9 PREDICTED EFFECTS OF ROTOR SPEED AND COLLECTIVE PITCH ON STABILITY AT 180 KNOTS FOR 0 AND -6 DEGREE SHAFT ANGLES

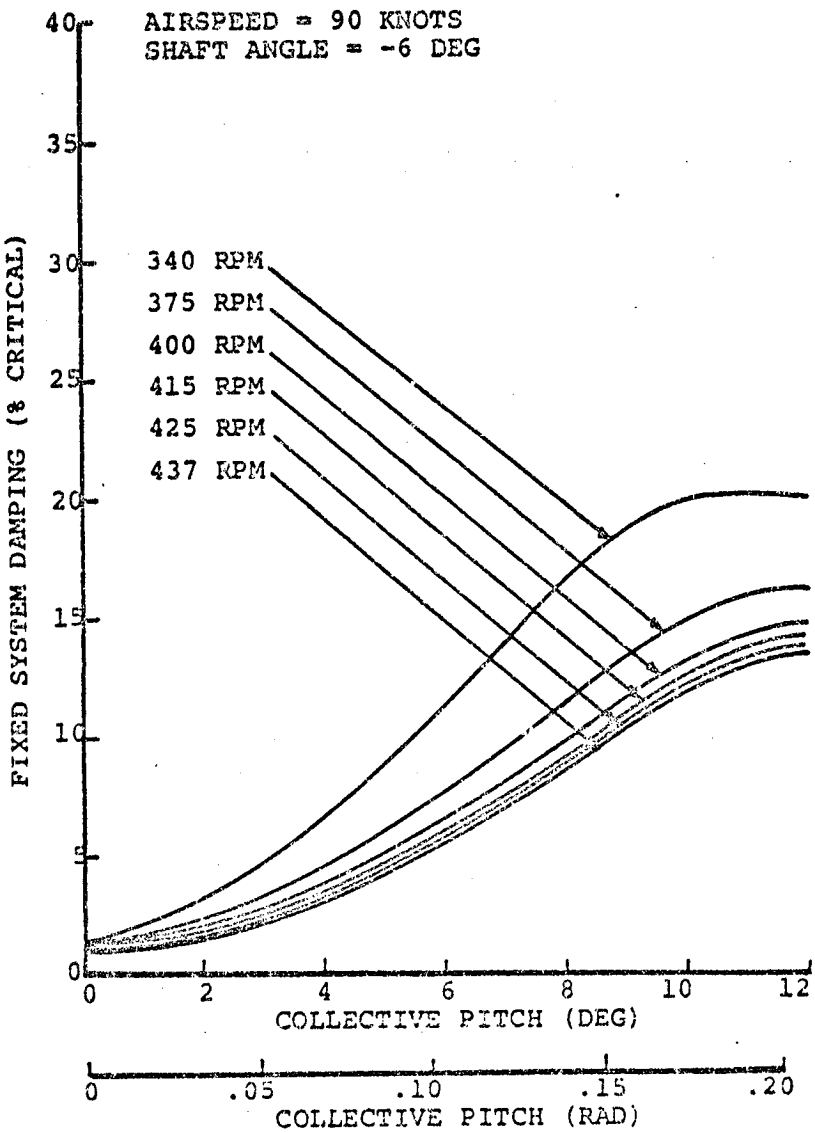

FIGURE 6.10 EXAMPLE OF PREDICTED BMR/RTA DAMPING DATA IN A FORMAT FOR TEST MONITORING (SHEET 1 OF 2)

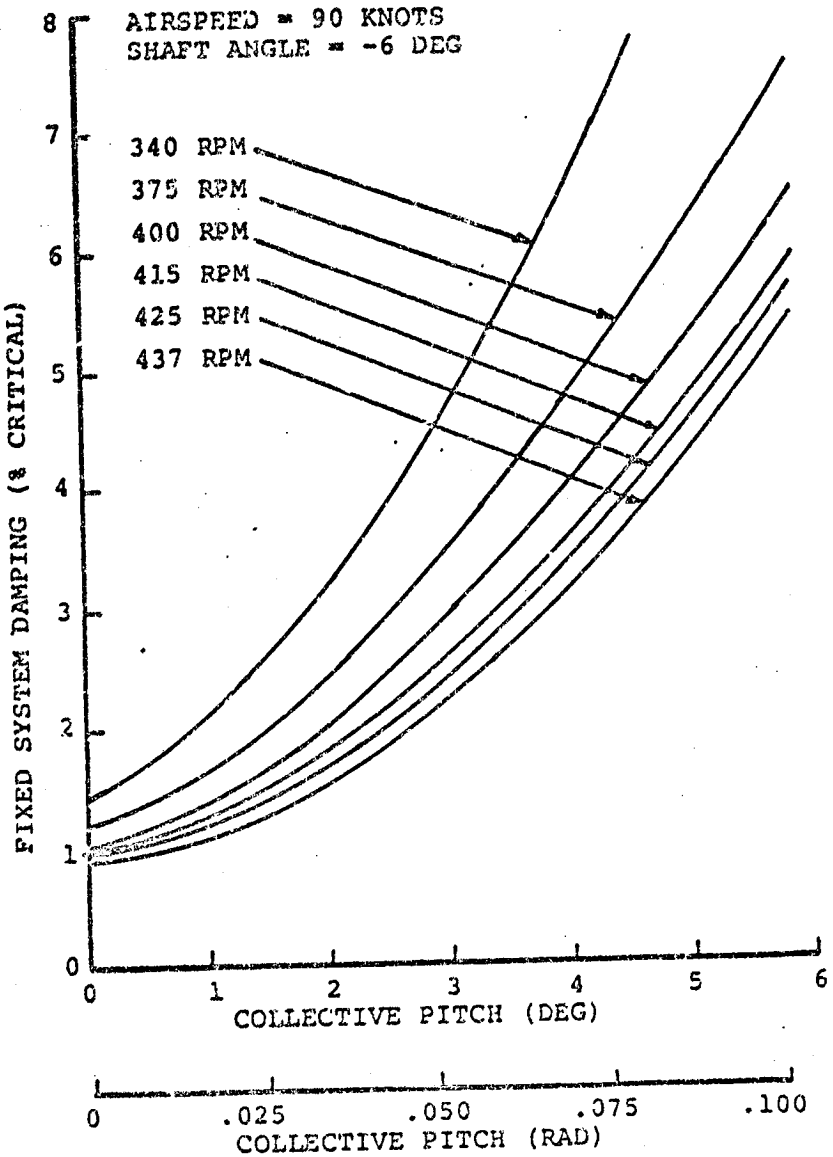

FIGURE 6.10 EXAMPLE OF PREDICTED BMR/RTA DAMPING DATA IN A FORMAT FOR TEST MONITORING (SHEET 2 OF 2)

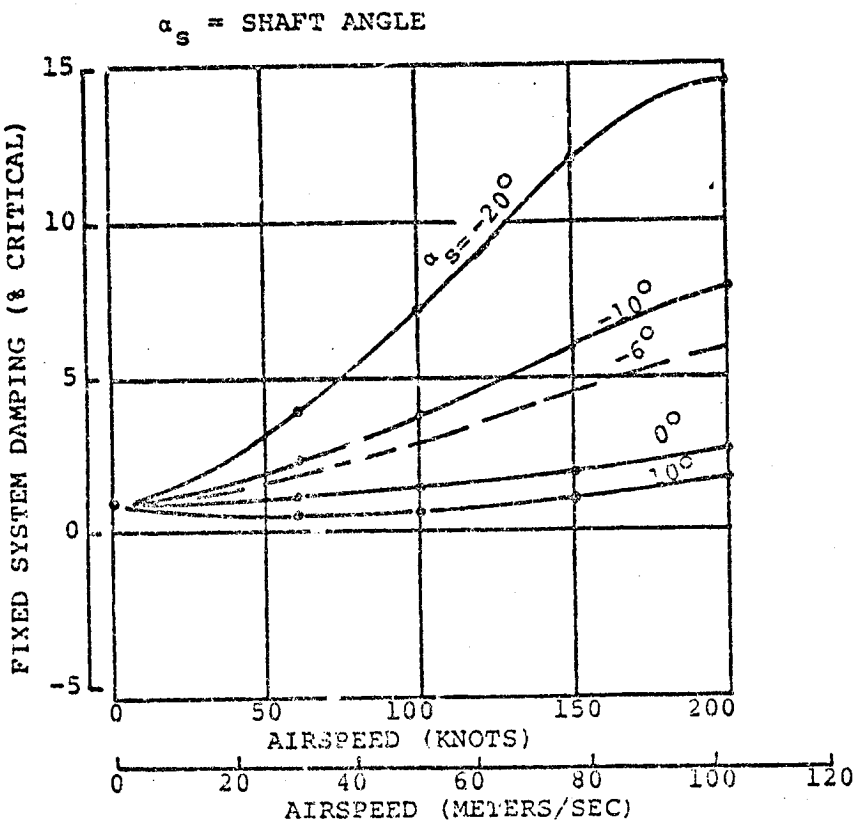

FIGURE 6.11 PREDICTED EFFECTS OF SHAFT ANGLE AND AIRSPEED ON DAMPING AT ZERO THRUST AND 425 RPM ROTOR SPEED (SHEET 1 OF 2)

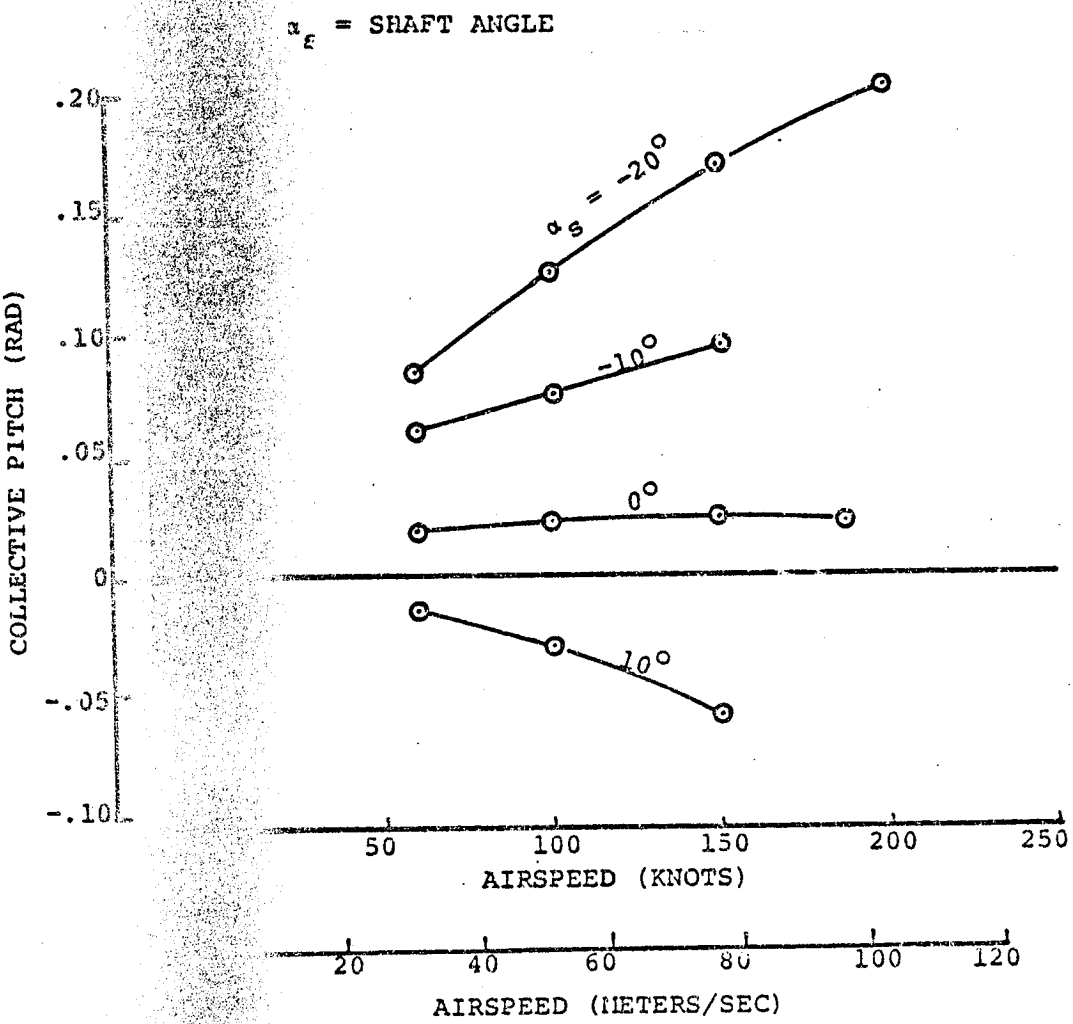

FIGURE 11 COLLECTIVE PITCH VALUES CORRESPONDING TO SHAFT ANGLES AND AIRSPEED FOR STABILITY PREDICTIONS AT ZERO THRUST AND 425 RPM (SHEET 2 OF 2)

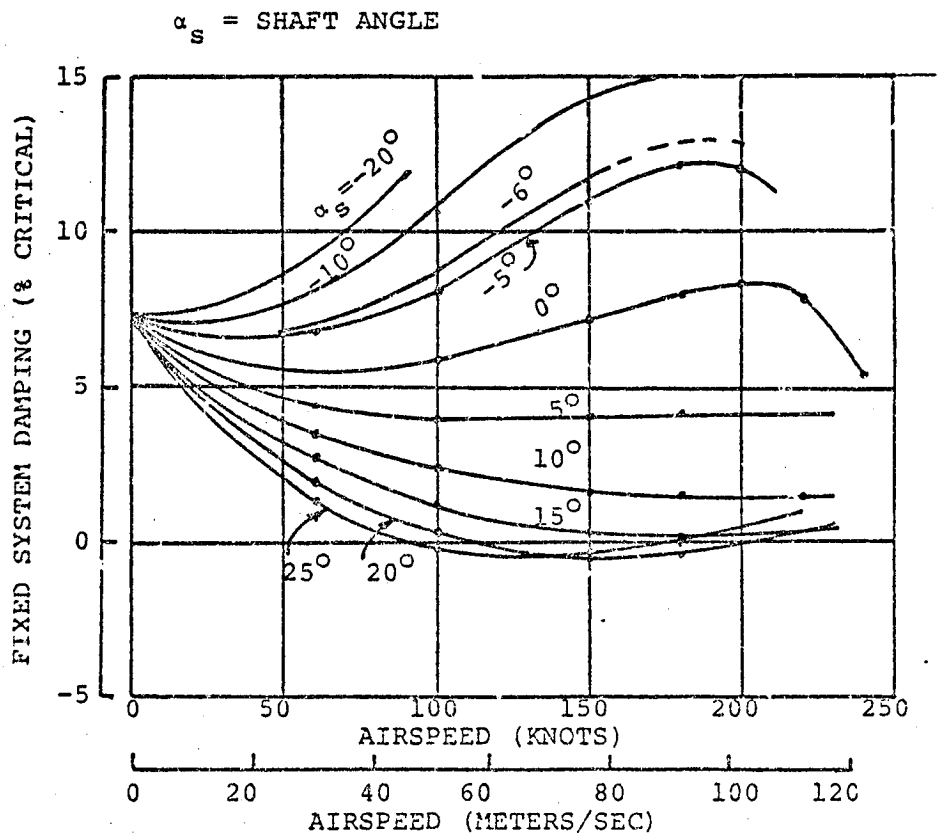

FIGURE 6.12 PREDICTED EFFECTS OF SHAFT ANGLE AND AIRSPEED ON DAMPING AT 4500 LB THRUST AND 425 RPM ROTOR SPEED (SHEET 1 OF 2)

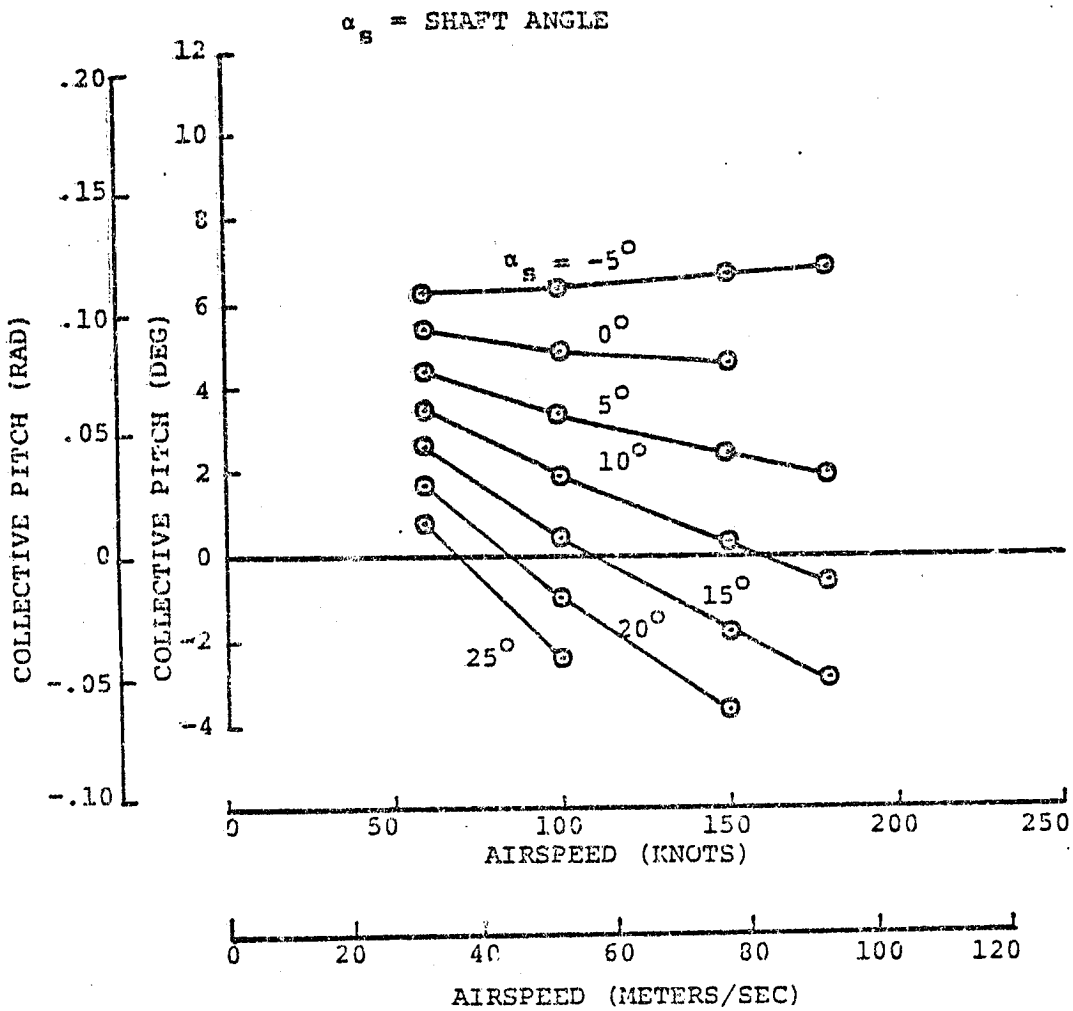

FIGURE 6.12 COLLECTIVE PITCH VALUES CORRESPONDING TO SHAFT ANGLES AND AIRSPEEDS FOR STABILITY PREDICTIONS AT 4500 LB THRUST AND 425 RPM (SHEET 2 OF 2)

C-2

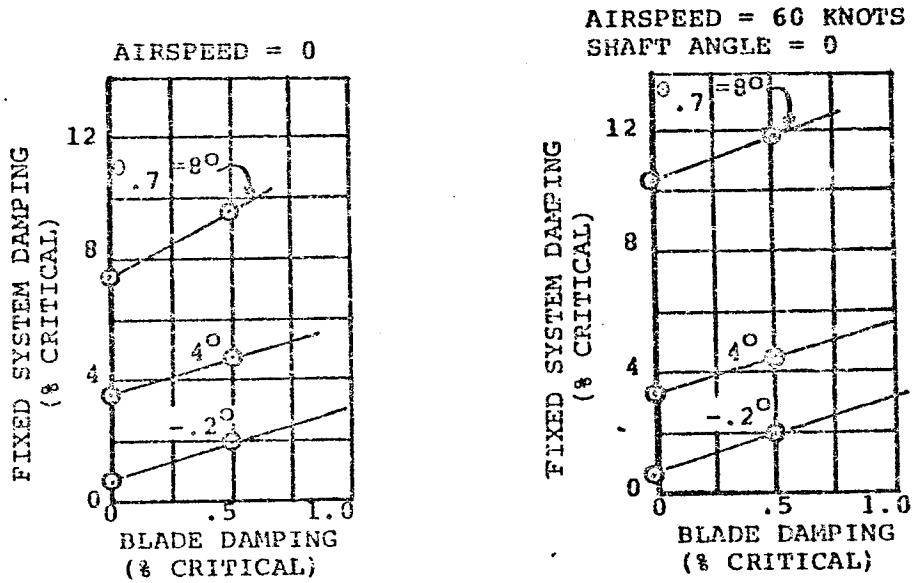

FIGURE 6.13 PREDICTED EFFECT OF BLADE CHORD MODE DAMPING ON BMR/RTA FIXED SYSTEM DAMPING AT ZERO AND 60 KNOTS AIRSPEED

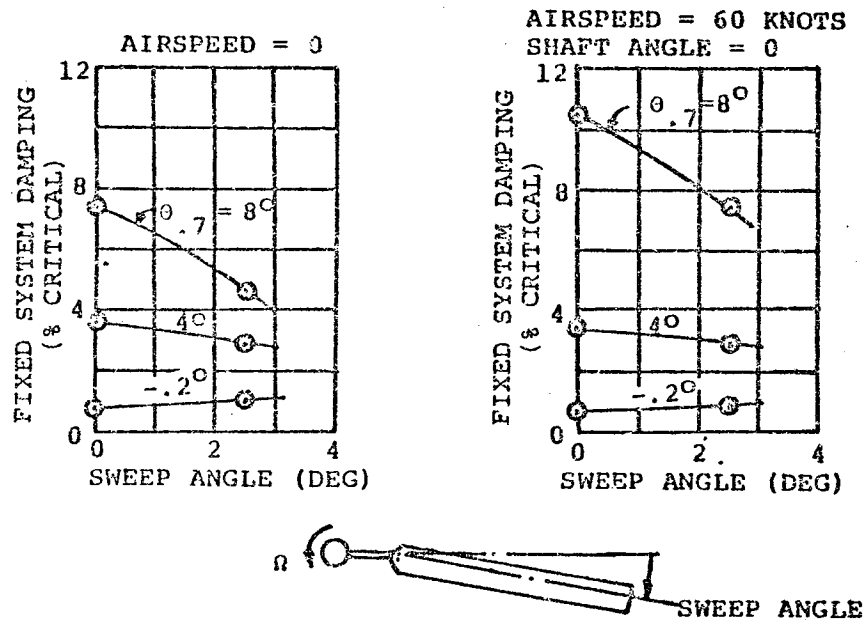

FIGURE 6.14 PREDICTED EFFECT OF BLADE SWEEP ANGLE ON DAMPING AT ZERO AND 60 KNOTS AIRSPEED

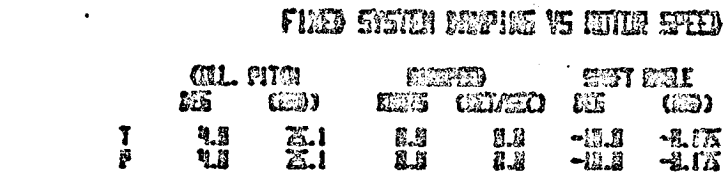

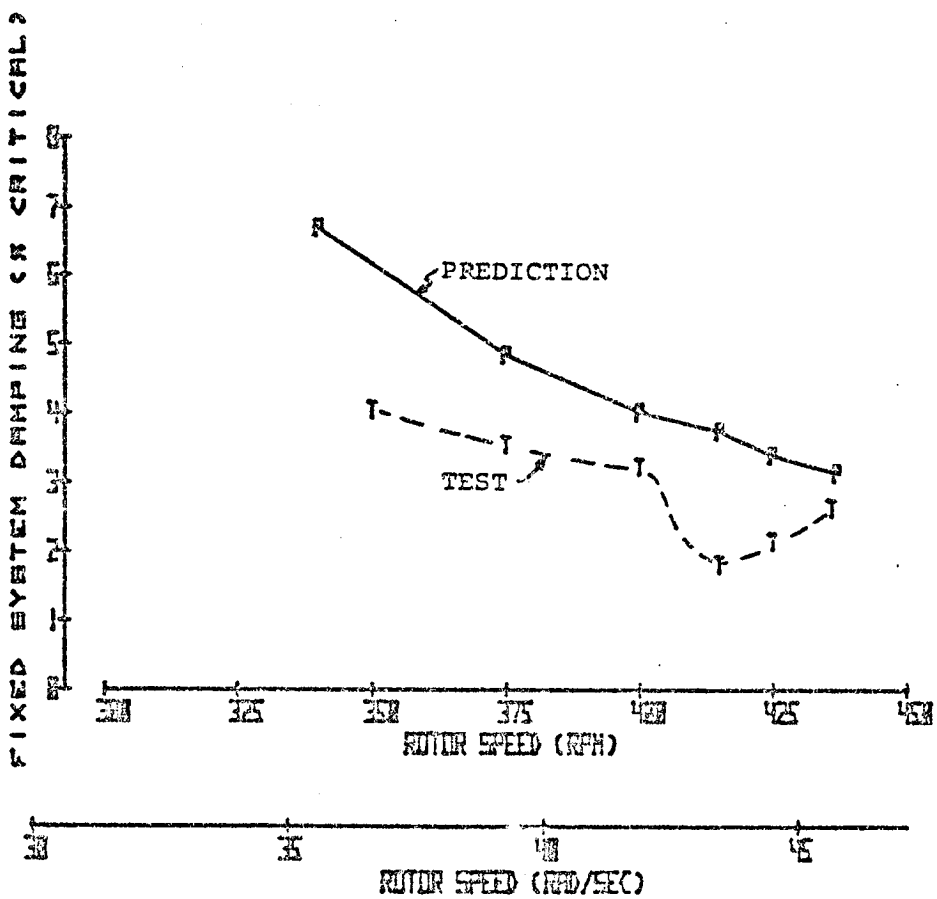

FIGURE 6.15 PREDICTED AND TEST DAMPING FOR THE FIRST BMR/RTA WIND TUNNEL RUN WITH BLADES INSTALLED - ZERO AIRSPEED

The second method determines damping levels from curve fits of an input/output transfer function which may be obtained from sinusoidal sweep testing or wide band frequency random testing over the frequency range of interest. The moving block method was used almost exclusively to obtain stability data for the BMR/RTA, and test results for BMR/RTA damping data contained in this report are based on the moving block method of analysis for damping data. For damping determination by the moving block method, the system was excited in the fixed system through the non-rotating swashplate using the Dynamic Control System (DCS). DCS inputs were at the lead-lag regressing frequency. The excitation amplitude was gradually increased until acceptable response was observed, but the excitation amplitude was limited to a safe value so that rotor vibratory load limits were not exceeded. A response measurement was selected for analysis on the Dynamic Analysis System (DAS); the excitation was stopped, a record of the decay of the selected signal was recorded on the DAS, and the decaying signal was then analyzed to determine the damping level.

The test procedure for the moving block analysis was to:

a. Excite the system at ground resonance (lead-lag regressing) frequency nutation control on DCS. This could be replaced by using longitudinal cyclic input on DCS.

b. Very slowly increase the amplitude until a "predetermined limit" was reached on any component.

c. Shut off the excitation and record the transient decay of one or more of the following:

Flexbeam chord bending 11.0A
Flexbeam chord bending 14.25 (multi-blade coordinates)
Flexbeam chord bending 43.0A
Blade chord bending 55.36
Longitudinal RTA accelerometers
Lateral RTA accelerometers

d. Perform moving block analysis by:

Selecting start and stop time for analysis.
Selecting parameter for analysis.
Obtaining spectral analysis and selecting frequency for analysis.
Selecting block size.
Computer does moving block analysis.
Selecting time period for fit of log amplitude decay.
Display of damping and frequency results.

The multi-blade coordinate analysis could be combined with the moving block analysis method after performing a multi-blade coordinate analysis of corresponding instrumentation on all four rotating arms simultaneously. Flexbeam chord bending gages available for multi-blade coordinate analysis were located at radial station 14.25. In addition to using the DAS for stability analysis, one channel of the Oscillograph Recorder (OGR) was used to display a filtered flexbeam chord bending gage (4547) at station 11.0 on beam A. This gage was band pass filtered from 3 to 5 Hz to reject 1/rev and steady (zero frequency) beam bending moments. This signal could be monitored to determine adequacy of the excitation level and could give an immediate qualitative indication of the level of stability. A sample signal is indicated in Figure 6.16.

6.3.4 Types of Excitation

Discrete frequency sinusoidal excitation was generally used for excitation of aeroelastic stability modes before analysis of decays by the moving block method. However, during the initial hover run, steps of either collective pitch, lateral cyclic, or longitudinal cyclic were introduced to produce a low level of response for initial evaluation of stability levels in hover. As mentioned above, swept sine excitation and banded frequency random excitation in the frequency range of interest were also considered for obtaining transfer functions for determining

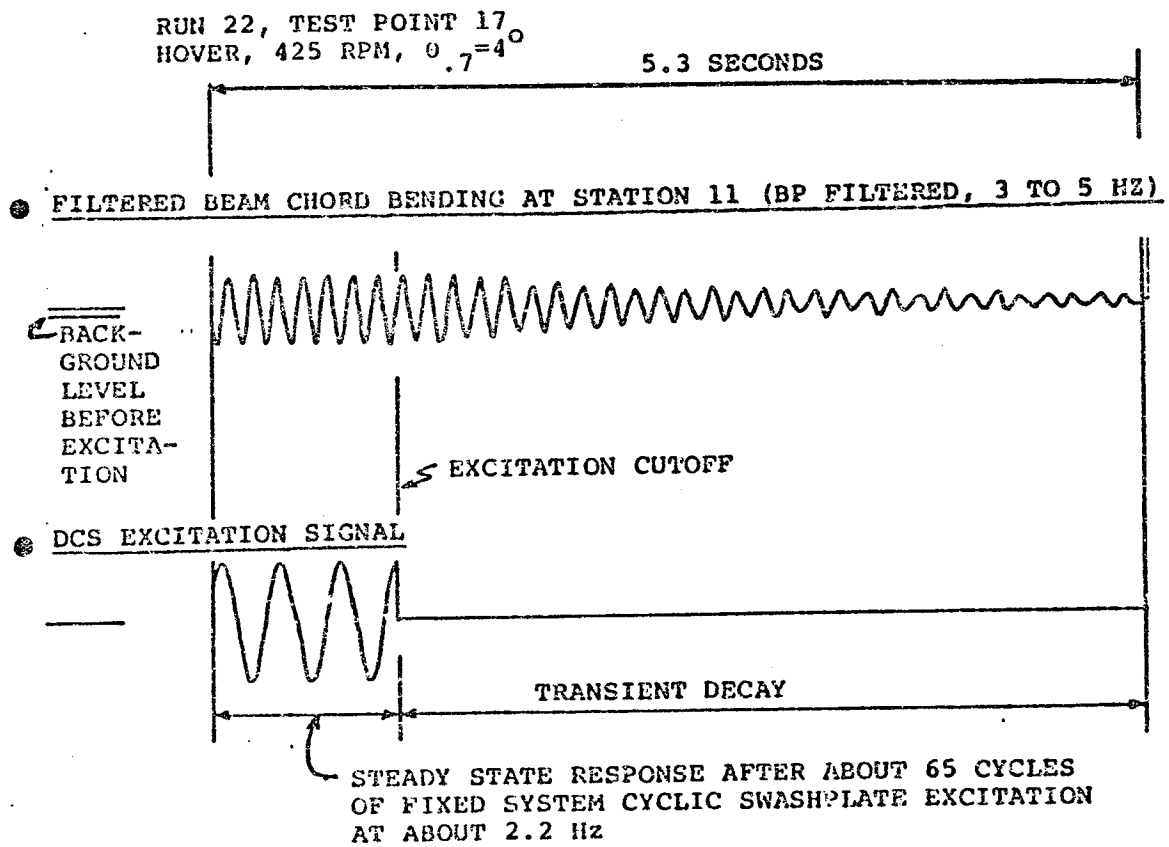

FIGURE 6.16 SAMPLE TRACE OF DECAY OF FILTERED BEAM CHORD BENDING AT STATION 11.

damping by the instrumental variables method. However, only a few attempts were made to use the instrumental variables method, and all stability data presented in this report are from the moving block method of analysis of transient decaying signals.

All types of excitation were introduced by exciting the swashplate in the fixed system using the DCS. For discrete frequency sinusoidal excitation, two kinds excitation were generally introduced at the lead-lag regressing frequency:

1) lateral cyclic only

2) nutation excitation which combined lateral and longitudinal cyclic excitation in a phase relationship which would best excite the lead-lag regressing mode.

Thus to use the DCS there were three variables to select for discrete frequency sinusoidal excitation:

1) lateral or nutation excitation

2) excitation frequency (lead-lag regressing frequency)

3) excitation amplitude

Excitation amplitude on the DCS amplitude control was indicated in counts. The maximum input amplitude used was 500 counts, which corresponded to approximately .75 degrees of cyclic excitation.

6.3.5 Data Analysis Methods

As mentioned above, several methods of data analysis were considered for determining damping from test data:

1) instrumental variables: determing damping from curve fits of transfer function

2) moving block analysis of a decaying signal

3) manual analysis of a filtered flexbeam chord bending decaying signal (as a backup).

The moving block method was used as the primary method after limited attempts at using the instrumental variable method in combination with multi-blade coordinate analysis. The moving block method was used with both the multi-blade coordinate analysis cyclic signals and with a single flexbeam chord bending signal (generally Data Code 4547, radial station 11, beam A). The latter signal was in the rotating system. For determining aeroelastic stability, either measurements in the

rotating system or the fixed system could be analyzed. In Figure 6.17, Y_{BR} and Y_{HUB} are rotating and fixed system motions, respectively. A physical relationship between blade rotating system motions and fixed system hub motions is implied on sheet 1 of Figure 6.17. The chordwise blade motion Y_{BR} in the rotating system has a component Y_{BF} in the lateral direction in the fixed system. As an example let the blade motion in the rotating system be sinusoidal at the blade first chord mode frequency:

$$Y_{BR} = \bar{Y}_{BR} \text{ SIN } \omega_\zeta t$$

Where

ω_ζ = blade first chord mode frequency, rad/sec

t = time, sec

$\bar{Y}_{BR}$ = amplitude of blade motion, cm

The fixed system component of this motion in the lateral direction is:

$$Y_{BF} = Y_{BR} \text{ COS } \Omega t$$

$$= \bar{Y}_{BR} \text{ (SIN } \omega_\zeta t \text{ COS } \Omega t)$$

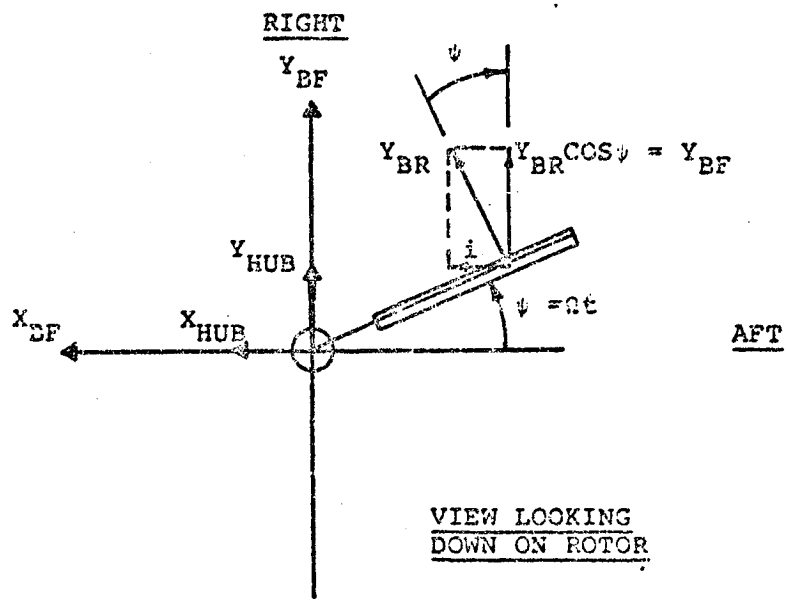

Ω = ROTOR SPEED, RAD/SEC

Y_{BR} = ROTATING SYSTEM BLADE MOTION AT POINT i IN BLADE FIRST CHORD MODE

Y_{BF} = LATERAL FIXED SYSTEM BLADE MOTION AT POINT i IN THE BLADE FIRST CHORD MODE

LET

$$Y_{BR} = \bar{Y}_{BR} \ \text{SIN}\omega_\zeta t$$

WHERE

ω_ζ = THE FIRST CHORD MODE FREUQENCY, RAD/SEC

t = TIME, SEC

THEN

$$Y_{BF} = \bar{Y}_{BR} \ \text{SIN}\ \omega_\zeta t \ \text{COS}\ \Omega\ t$$

$$= 1/2\ \bar{Y}_{BR} \left[\text{SIN}\ (\Omega-\omega_\zeta)t + \text{SIN}\ (\Omega+\omega_\zeta)t \right]$$

REGRESSING MODE FREQUENCY

PROGRESSING MODE FREQUENCY

FIGURE 6.17 EXAMPLE OF DECAYING SIGNALS IN FIXED AND ROTATING SYSTEM FOR AEROELASTIC STABILITY MODE (SHEET 1 OF 2)

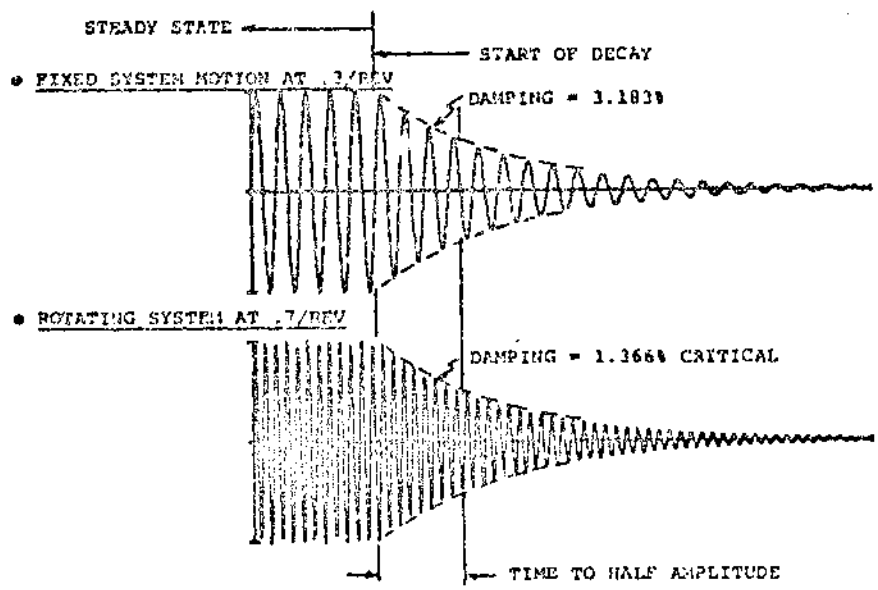

Ω = ROTOR 1/REV FREQUENCY

$\omega_{FIXED\ SYSTEM} = \Omega - \omega_{ROTATING}$

$\zeta_{FIXED} = \text{FIXED SYSTEM DAMPING} = \zeta_{ROTATING}\left(\frac{\omega_{ROTATING}}{\Omega-\omega_{ROTATING}}\right)$

FOR THE EXAMPLE SHOWN ABOVE:

$\omega_{ROTATING} = .7/REV$

$\omega_{FIXED} = (1-.7) = .3/REV$

$\zeta_{ROTATING}$ = ROTATING SYSTEM DAMPING = 1.366% CRITICAL

$\zeta_{FIXED} = 1.366 \times .7/.3 = 3.183\%$ CRITICAL

$T_{1/2} = 12.03/(f\zeta)$, SECONDS, FOR BOTH ROTATING AND FIXED SYSTEM MEASUREMENTS

f = FREQUENCY OF DECAYING SIGNAL, Hz
ζ = RATIO OF CRITICAL DAMPING, PERCENT

FIGURE 6.17 EXAMPLE OF DECAYING SIGNALS IN FIXED AND ROTATING SYSTEM FOR AEROELASTIC STABILITY MODE. (SHEET 2 OF 2)

$$= \frac{1}{2} Y_{BR} \left[\text{SIN}\ (\Omega - \omega_\zeta)t + \text{SIN}(\Omega + \omega_\zeta t)\right]$$

Thus the lateral component of blade motion in the fixed system has two frequency components. One is the lead-lag regressing mode frequency, $\Omega-\omega_\zeta$, and the other is the lead-lag progressing mode frequency, $\Omega+\omega_\zeta$. For the soft-in-plane BMR rotor ($\omega_\zeta < \Omega$ at normal rotor speed), the frequency of interest is the regressing mode frequency.

As indicated in Figure 6.17, sheet 1, lateral hub motion Y_{HUB} may also occur so that coupling between fixed system blade and hub motions may occur. This coupling is most likely to occur when a body mode natural frequency equals or nearly equals the rotor lead-lag regressing mode frequency. From sheet 1 of Figure 6.17, it can be seen that similar relationships can be developed for the longitudinal components of blade motions which could couple with longitudinal hub motions. Mathematical relationships for coupling between the rotor lead-lag regressing mode and the hub have been developed in the literature; see for example Reference 15.

When the coupled system consisting of the rotor and the body (RTA) is excited in the fixed system at the lead-lag regressing mode frequency, the rotor will respond in the rotating system at the first chord mode frequency, ω_ζ. Body motions will occur in the fixed system at the lead-lag regressing mode frequency, $\Omega-\omega_\zeta$.

After excitation is stopped, the rate of decay of motions in the fixed and rotating systems will be the same, e.g., the times to half amplitude will be the same. Assume that the rotating system motion is decaying due to damping after a fixed system sinusoidal excitation (at the lead-lag regressing frequency) has stopped. Assume that the rotating system blade motion is:

$$Y_{BR} = \bar{Y}_{BR} e^{-at} \text{ SIN } \omega_\zeta t$$

The corresponding lateral fixed system component blade motion is:

$$Y_{BF} = 1/2 \bar{Y}_{BR} e^{-at} \text{ SIN } (\Omega - \omega_\zeta t).$$

Critical damping is defined as the minimum viscous damping which will allow a displaced system to return to its undisplaced position without further oscillation. The fraction of critical damping which a system has in a particular mode of oscillation is related to the exponential decay rate of free vibration:

$\zeta = \frac{a}{\omega}$ = ratio of critical damping

ω = frequency of free vibration

For the rotating system oscillation Y_{ER}, the ratio of critical damping is:

$$\zeta_{BR} = \frac{a}{\omega_\zeta} . = \text{rotating system ratio of critical damping.}$$

For a fixed component of motion Y_{BF}, the ratio of critical damping is:

$$\zeta_{BF} = \frac{a}{\Omega-\omega_\zeta} = \text{fixed system ratio of critical damping}$$

Then the relationship between damping ratios determined in the fixed and rotating systems for aeroelastic stability modes involving the rotor lead-lag regressing mode is:

$$\frac{\zeta_{BF}}{\zeta_{BR}} = \frac{\omega_\zeta}{\Omega-\omega_\zeta} = \frac{\text{fixed system ratio of critical damping}}{\text{rotating system ratio of critical damping}}$$

Therefore, a rotating system signal will have a lower ratio of critical damping than the corresponding fixed system signal. Attempts at analyzing fixed system RTA accelerometers and multi-blade cyclic chord bending signals gave poor results compared to analyzing a single rotating system chord bending gage and computing the corresponding damping which would have been observed in the fixed system. All critical damping data shown in figures in this report are equivalent fixed system

damping. Figure 6.17 shows the relationship used to compute damping in the fixed system from damping in the rotating system. This conversion from rotating to fixed system has a potential for introducing significant errors, particularly at low rotor speeds where the first chord frequency is very near the rotor rotational frequency. As seen in Figure 6.17, the difference between these two frequencies is used in the computing of the relationship between fixed system and rotating system damping. As discussed below, the chord mode frequency obtained from the moving block analysis is known only to an accuracy of 0.125 Hz for analysis of a typical time sample of 8.0 seconds.

An expression for the BMR first chord mode frequency based on decay traces from Boeing Vertol whirl tower tests is believed to be slightly more accurate than the DAS first chord mode frequency spectral analysis results. These whirl tower results may be used for configurations which did not have damper strips added to the flexbeams. This expression for chord mode frequency is:

$$\omega_\zeta = 2\pi \left(4.75 + 1.24 \left(\frac{\Omega}{375} - 1\right) - .02\,\theta_{.7}\right)$$

where,

ω_ζ = first chord mode frequency, rad/sec

Ω = rotor speed, RPM

$\theta_{.7}$ = collective pitch at 70% blade radius, degrees

This expression was used to compute chord mode frequencies for use in the expression to convert rotating system damping to fixed system damping for configurations without damper strips. This expression for first chord mode frequency is not consistent with DAS software. For configurations with damper strips added, the DAS spectral analysis value for rotating first chord mode frequency was used to compute the factor for converting rotating system damping to fixed system damping.

Another way of presenting stability data is to indicate time to decay to half amplitude. As indicated in Figure 6.17, time to half amplitude is the same for both rotating and fixed system signals for a coupled rotor/body mode. Therefore, the time to half amplitude can be computed directly from the rotating system measurement, and a small error in the chord mode frequency from the moving block analysis would produce only a small error in the computed time to half amplitude (see the expression for time to half amplitude in Figure 6.17). The expression for first chord frequency based on Boeing Vertol whirl tower tests was used to compute time to half amplitude for configurations where no damper strips were added. When damper strips were added, DAS spectral analysis re ults for first chord frequency were used to compute times to half amplitude. Generally, in this report, stability data from the BMR/RTA test are presented in both formats, i.e., fixed system ratio of critical damping and time to half amplitude.

The moving block analysis is conducted on the DAS through an interactive graphics terminal. Figure 6.18 shows typical displays from the graphics terminal. One display shows the sample rate (typically 64 samples per second), the time length of the data sample to be analyzed (typically 8.0 seconds), and the flight conditions: tunnel speed, rotor speed, collective pitch, and angle of attack. These data are all input by the engineer operating the graphics terminal. The operating procedure is to record a sample of decaying data after excitation is terminated by the engineer operating the DCS. The engineer operating the DAS initiates collecting a data sample when given a signal from the DCS controller indicating that excitation has been terminated. After data collection, a spectral analysis of the sample is completed and displayed (Figure 6.18). The graphics terminal operator specifies a narrow frequency band including the frequency of interest for the moving block analysis. In Figure 6.18, a flexbeam chord bending gage is being analyzed, and the frequency of interest is the first chord bending mode just below 5 Hz. The block size is also specified for the moving block analysis: 1/2 was generally used meaning that a 4 second moving block size was used for an 8 second time sample; this smooths variations in the signal with time. The moving block technique analyzes the decaying transient signal at the peak frequency amplitude found within the frequency range specified by the DAS operator. The log decay is then displayed for the selected peak frequency; the terminal operator selects a time period to compute a linear fit to this

```
@  TEST CONDITIONS

     RUN NO.=23      POINT= 6

     *** SINGLE CHANNEL ***
          CH14


     --- INPUT DATA FOR MOVING BLOCK ANALYSIS ---

     SIGNAL LEVEL CODE=88      SAMPLE RATE=   64.0(HZ)

     TIME FOR DATA RECORDING= 8.00(SEC.)

     $$$ ZEROS INCLUDED $$$
     WIND TUNNEL SPEED = 90.00
     ROTATION SPEED =  410.0
     COLLECTIVE PITCH =  4.00
     BODY ANGLE OF ATTACK = -8.00

     ACQUIRE ANALOG DATA OR RETURN(R)
?
```

FIGURE 6.18 TYPICAL GRAPHICS TERMINAL OUTPUT FOR MOVING BLOCK ANALYSIS (SHEET 1 OF 3)

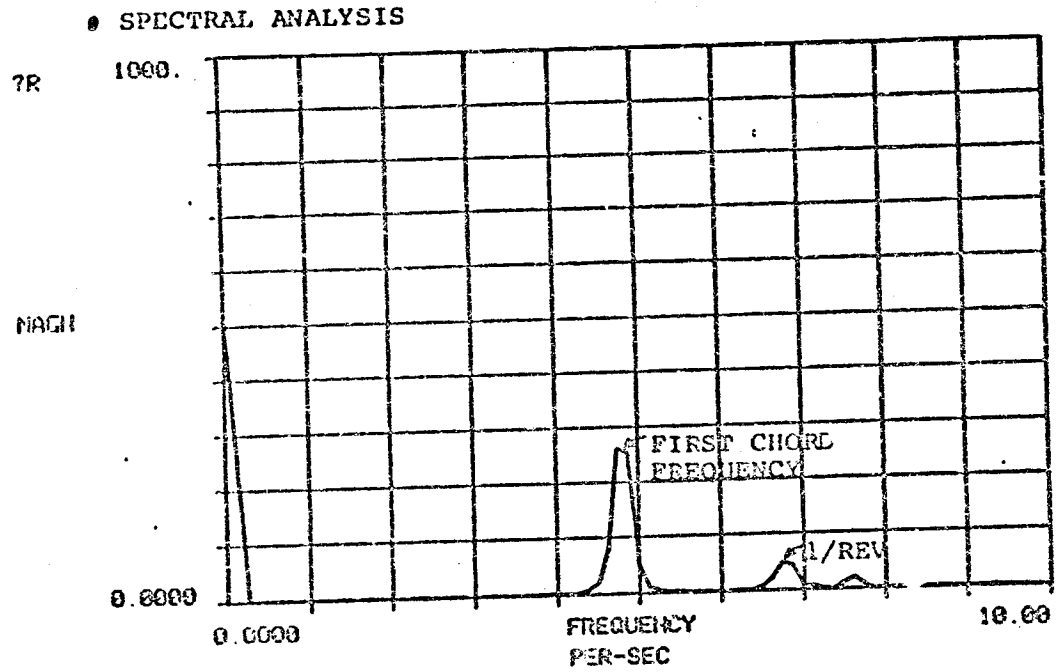

FIGURE 6.18 TYPICAL GRAPHICS TERMINAL OUTPUT FOR MOVING BLOCK ANALYSIS (SHEET 2 OF 3)

- MOVING BLOCK ANALYSIS

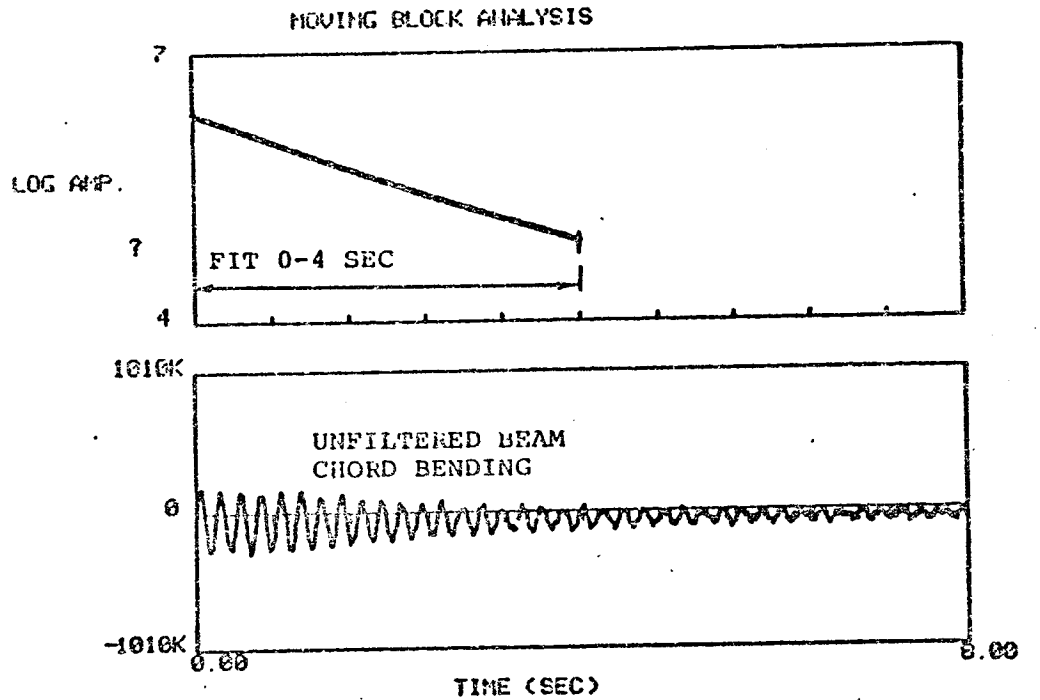

$\Omega = \frac{410 \text{ RPM}}{60} = 6.83$ Hz

ANALYSIS FREQUENCY

ROTATING SYSTEM DAMPING = 1.21%

$$\text{FIXED SYSTEM DAMPING} = \left(\frac{4.75}{6.83-4.75}\right) \times 1.21\% = 2.76\%$$

FIGURE 6.18 TYPICAL GRAPHICS TERMINAL OUTPUT FOR MOVING BLOCK ANALYSIS (SHEET 3 OF 3)

decay, and the corresponding damping level is computed. In the example in Figure 6.18, the fit time was from 0 to 4 seconds, and the rotating system damping was 1.21 percent; the fixed system damping was 2.76 percent (the conversion from rotating to fixed system damping was eventually added as a part of the moving block analysis on the DAS). The unfiltered signal was also displayed on the graphics terminal; in the example in Figure 6.18, the signal contains mostly data at the chord bending frequency. At low rotor speeds, the unfiltered chord bending data would also contain a very large one/rev signal.

6.4 FLYING QUALITIES TESTING

The flying qualities testing was very similar to the 1G flight testing. The rpm was set at 425 and the tunnel speed brought to the desired setting. Collective pitch was adjusted to maintain a lift coefficient of .072. The shaft angle was varied until the rate of descent was zero, and longitudinal and lateral cyclic pitch were adjusted to attain the predicted aircraft pitch and roll moments of the BO-105/BMR. Then approximately .4 degree input changes of positive and negative longitudinal and lateral cyclic pitch were put in successively through the Dynamic Control System. For each input, time history data was taken of the multi-blade flap and chord bending flexbeam gages so that fixed system hub loads response data could be computed.

7.0 PRETEST ANALYSIS METHODOLOGY

7.1 STABILITY ANALYSIS METHODOLOGY

7.1.1 Description of C-90 Program

Boeing Vertol's C-90 analysis computer program has been described in some detail in Reference 16. This program was used to predict expected damping levels on the BMR/RTA. Figure 7.1 shows general features of the C-90 computer program. The program can compute aeroelastic stability mode damping for ground resonance, hover, and forward flight. It uses modal representations of the rotor blades and the airframe, and has the capability to incorporate rotor isolation elements between the rotor transmission and the airframe. A computational flow diagram for C-90 is shown in Figure 7.2. Input required for C-90 are described in Reference 17. A steady state rotor loads analysis is required to compute the blade steady deflected positions, and a rotor blade modal analysis must be performed to generate blade modal data at the steady deflected position for input to the C-90 program.

7.1.2 Correlation of Predicted C-90 Stability Results with Flight Test Data for the BMR

To validate the capability of comp ter program C-90 to predict aeroelastic stability levels, C-90 analyses were conducted to determine damping data for comparison with data obtained during BMR/BO-105 flight tests conducted by Boeing Vertol (Reference 18). Results of this analysis/test comparison are shown in Figures 7.3 through 7.6 from Reference 16. These figures show

comparisons of predicted and test values of damping versus airspeed for level flight; versus rate of climb at 60 knots; and versus collective pitch position at 50 and 100 knots. Test and C-90 analysis damping data are in very good agreement in these figures. Figures 7.7 and 7.8 show C-90 analysis versus test comparisons for damping data for the BMR rotor on the Vertol whirl tower. Again, C-90 analysis results and the test results are in very good agreement. All results in Figures 7.3 through 7.8 are equivalent fixed system damping at approximately the lead-lag regressing mode frequency.

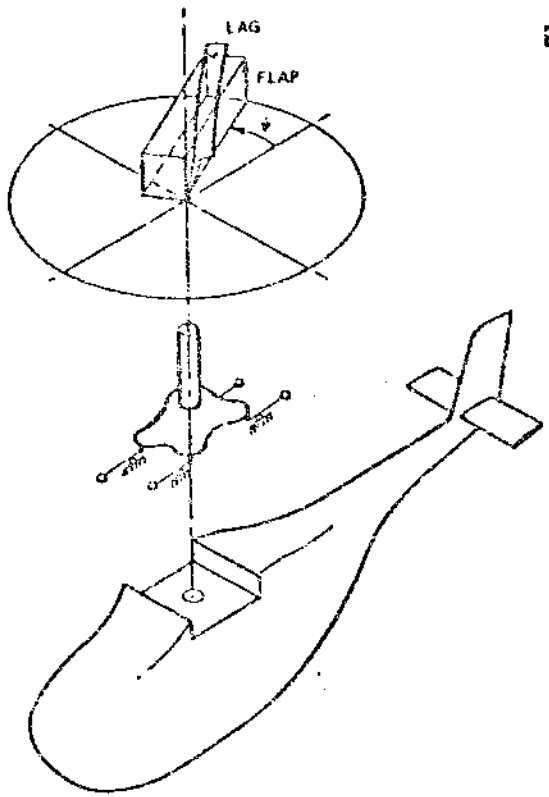

MATHEMATICAL MODEL FOR C-90 PROGRAM

ROTOR

- 4 BLADES
- 6 FULLY COUPLED FLAP-LAG TORSION MODES PER BLADE
- ACCOUNT FOR BLADE STEADY-STATE DEFLECTION
- CAN HANDLE BLADE TWIST
- TABLE LOOK UP AERO
- HOVER AND FORWARD FLIGHT
- REVERSE FLOW

IRIS

- 4 IRIS EACH IN LONGITUDINAL, LATERAL AND VERTICAL DIRECTION
- EACH HAD SPRING, MASS & DAMPER

FUSELAGE

15 ARBITRARY FUSELAGE MODES

SOLUTION

- EIGENVALUE/EIGENVECTOR SOLUTION OF LINEARIZED PERTURBATION EQUATIONS USING FLOQUET THEORY

FIGURE 7.1 MATHEMATICAL MODEL FOR C-90 PROGRAM

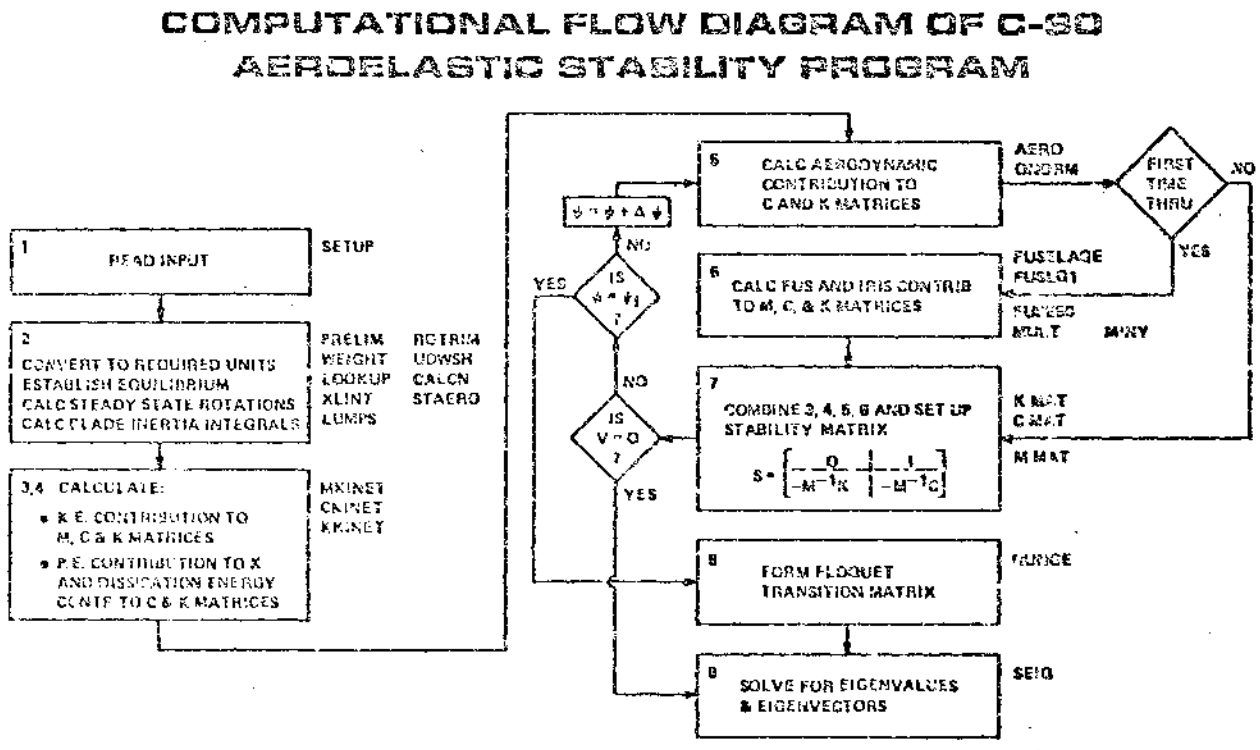

FIGURE 7.2 COMPUTATIONAL FLOW DIAGRAM FOR C-90 AEROELASTIC STABILITY PROGRAM

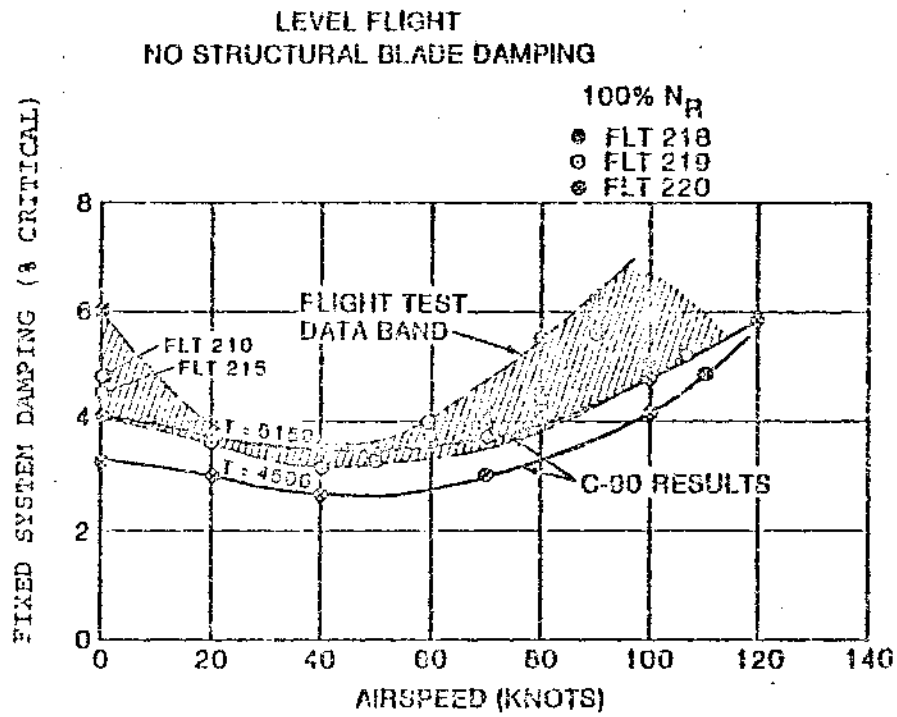

FIGURE 7.3 C-90 COMPARISON WITH FLIGHT DATA - BMR/BO-105 STABILITY IN FORWARD FLIGHT

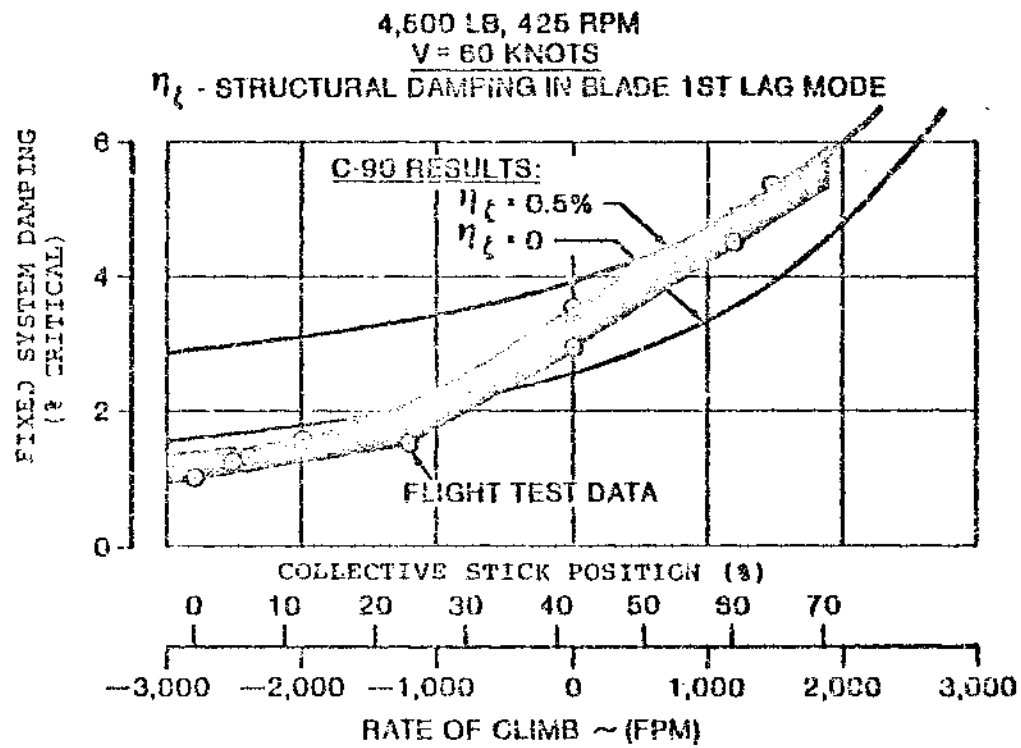

FIGURE 7.4 C-90 VS FLIGHT DATA AT 60 KNOTS: BMR/BO-105 IN CLIMBS AND DESCENTS

FIGURE 7.5 C-90 VS FLIGHT DATA AT 50 KNOTS: BHR/BO-105
STABILITY IN CLIMBS AND DESCENTS

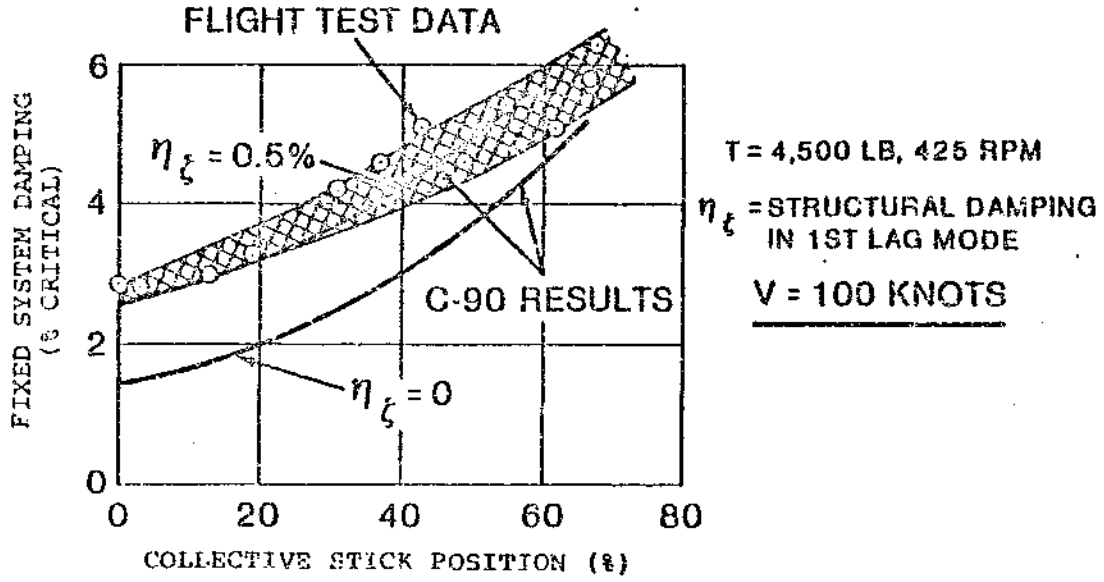

FIGURE 7.6 C-90 VS FLIGHT DATA AT 100 KNOTS: BMR/BO-105 STABILITY IN CLIMBS AND DESCENTS

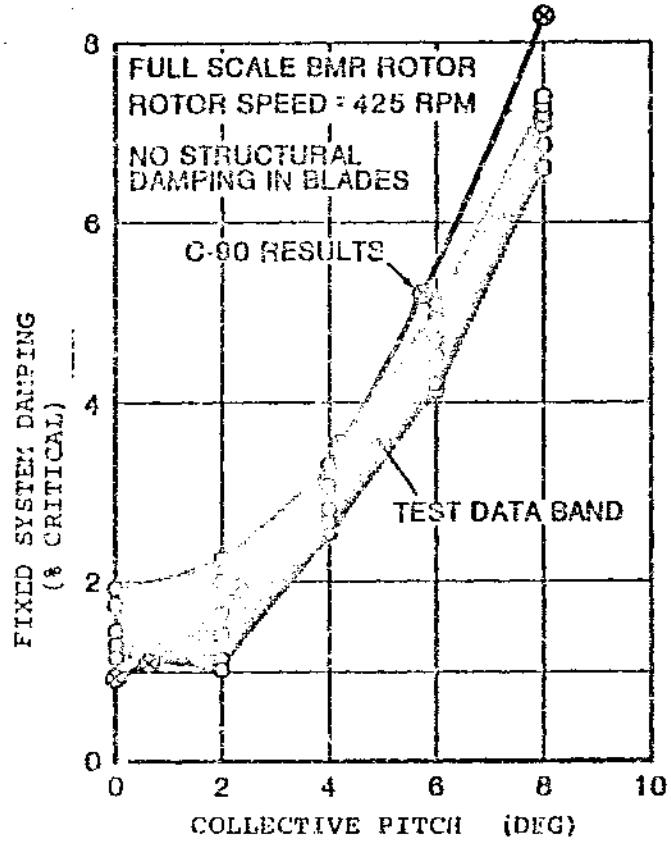

FIGURE 7.7 C-90 COMPARISON WITH WHIRL TOWER TESTS - EFFECT OF COLLECTIVE PITCH

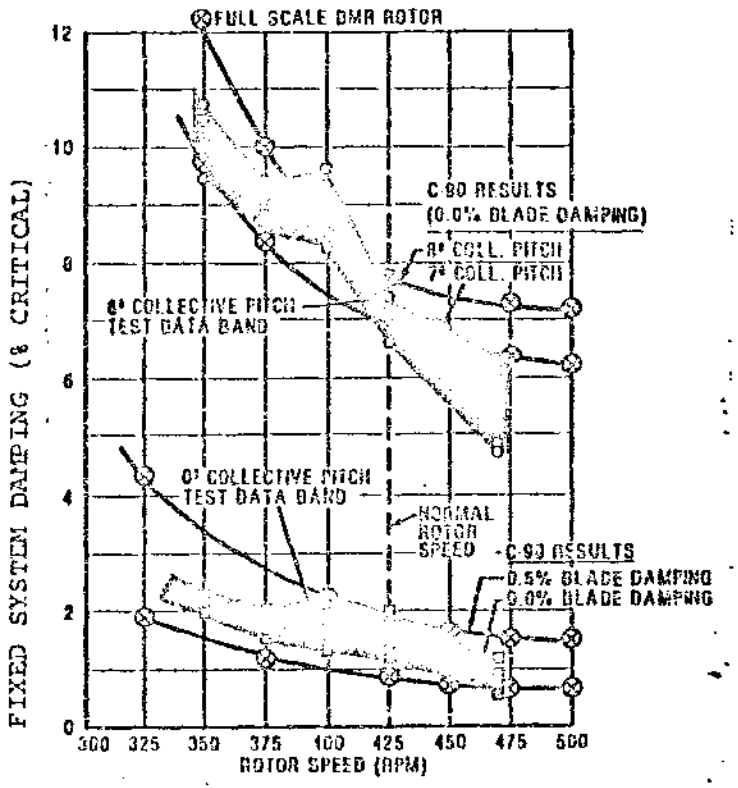

FIGURE 7.8 C-90 COMPARISON WITH BMR WHIRL TOWER TESTS - EFFECT OF ROTOR SPEED AND BLADE STRUCTURAL DAMPING

7.2 LOADS ANALYSIS METHODOLOGY

7.2.1 Description of C-60 Program

Boeing Vertol has developed an aeroelastic rotor loads analysis, the C-60 Program, which calculates:

- blade loads and motions for steady-state flight conditions
- control-system forces
- steady and vibratory hub loads
- rotor performance
- rotor trim

for articulated, teetering, and hingeless rotors with two to nine blades. The blades may be of arbitrary planform, twist, and airfoil section variation with radius. This analysis is limited to steady flight conditions.

The analysis considers coupled flap and torsion deflections and uncoupled chordwise deflections of the rotor blades. The blade is represented by 25 lumped masses connected by elastic elements. The model can include planform sweep at two locations and spanwise variations of shear center, vertical neutral axis, chordwise center of gravity, and pitch axis. The associated-matrix method is used to relate the tip-boundary conditions to the root-boundary conditions. The solution is expressed as a Fourier series and the coefficients are obtained by inverting the matrix equation that relates the tip-and root-boundary conditions.

Airload calculations include airfoil-section geometry, compressibility, stall, three-dimensional flow, unsteady aerodynamics with center of pressure shift, and nonuniform downwash. Static airfoil tables are used to account for compressibility, static stall, and airfoil shape. The unsteady aerodynamic loads are calculated by modifying the static loading resulting from the airfoil tables to include Theodorsen's shed-wake function, dynamic stall effects based on oscillating-airfoil data, and yawed flow across the blade.

The wake is modeled as a tip and root vortex trailed from each blade for nonuniform inflow calculations. Through an iterative procedure, each trailed vortex is made compatible with the calculated blade-lift distribution; the lift distribution is compatible with the nonuniform downwash field. The vortex wake is assumed to be rigid and to drift relative to the hub with a constant velocity composed of the thrust-induced uniform downwash added to the speed of the aircraft. The nonuniform downwash field can be recalculated at any stage of the analysis to account for the redistribution of airloads resulting from elastic blade deflections.

The nonlinear aerodynamic loads and the coupled flap and pitch responses are calculated iteratively. Up to 20 iterations are used to obtain the final solution. This iterated solution accounts for the nonlinear coupling between the blade deflections and airloads that result from stall and compressibility.

A summary of the analytical features is provided in Figure 7.9.

The uncoupled lag response calculation includes an option to analyze a multiple load path retention system such as the dual beam BMR configuration. This option adds an additional program loop in which the chord moments and shears and the axial force are used to initialize a special subroutine which computes the chord motion of the dual retention system. The deflections and slopes are harmonically analyzed and imposed as new boundary conditions on the chord portion of C-60 at the outboard end of the beams. A new pass through the chord portion of C-60 is made and new moments, shears, and axial force are computed. These are compared to the previous iteration until convergence is achieved.

7.2.2 Verification of C-60 Program

Figures 7.10 through 7.13 show a comparison of loads predicted by C-60 with BMR/RTA test results for a selected test point at 90 knots. The 90 knot condition was selected because it does not contain transition effects or very high advancing tip Mach Number effects. The flap bending steady and vibratory moment correlation is very good, as is the vibratory chord moment correlation. The steady chord moment correlation is fair to poor. Figures 7.12 and 7.13 present only the total chord bending moment. Since a major portion of the chord bending moment at the blade to flexbeam attachment is transmitted as differential axial force in the beams, local beam chord bending moments

● BLADE DYNAMICS
- LUMPED PARAMETER BLADE IDEALIZATION (20 MASSES)
- COUPLED FLAP-PITCH
- UNCOUPLED CHORD

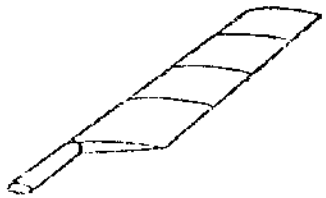

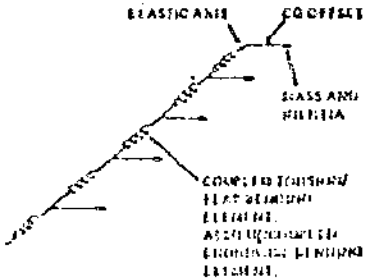

● AERODYNAMICS
- NON-LINEAR, COMPRESSIBLE, UNSTEADY AERODYNAMICS (FOR LIFT, DRAG, AND PITCHING MOMENT)

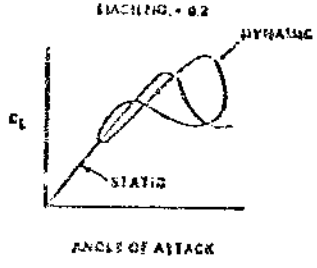

- YAWED FLOW

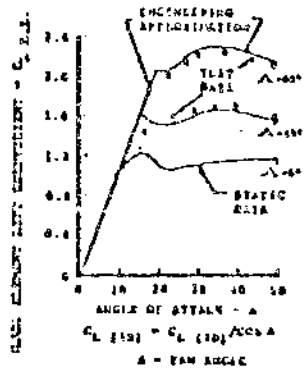

● SOLUTION
- AUTOMATIC TRIM MATCH (MATCHES TRIM PROGRAM FORCES)

- HARMONIC SOLUTION
- ITERATIVE NON-LINEAR AERO-ELASTIC COUPLING

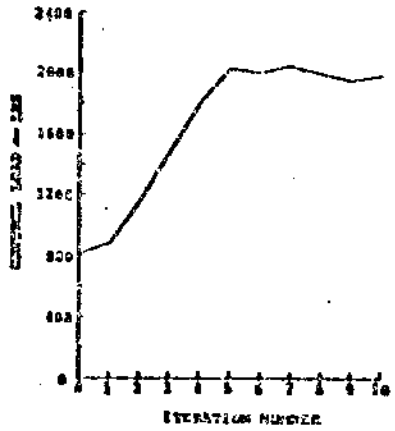

FIGURE 7.9 ANALYTICAL FEATURES OF PROGRAM C-60

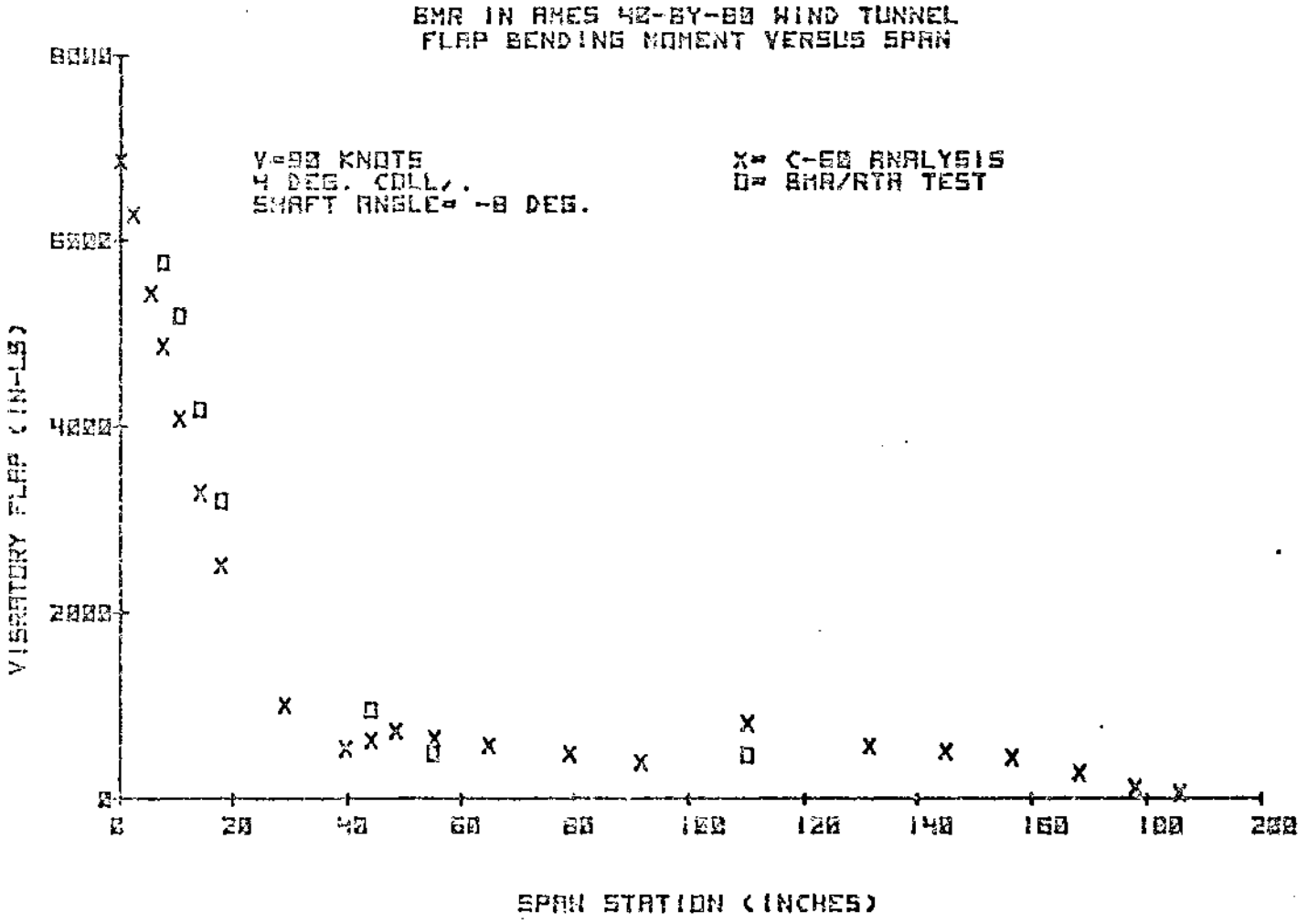

FIGURE 7.10 CORRELATION WITH ANALYSIS - VIBRATORY FLAP MOMENT VERSUS SPAN AT 90 KNOTS

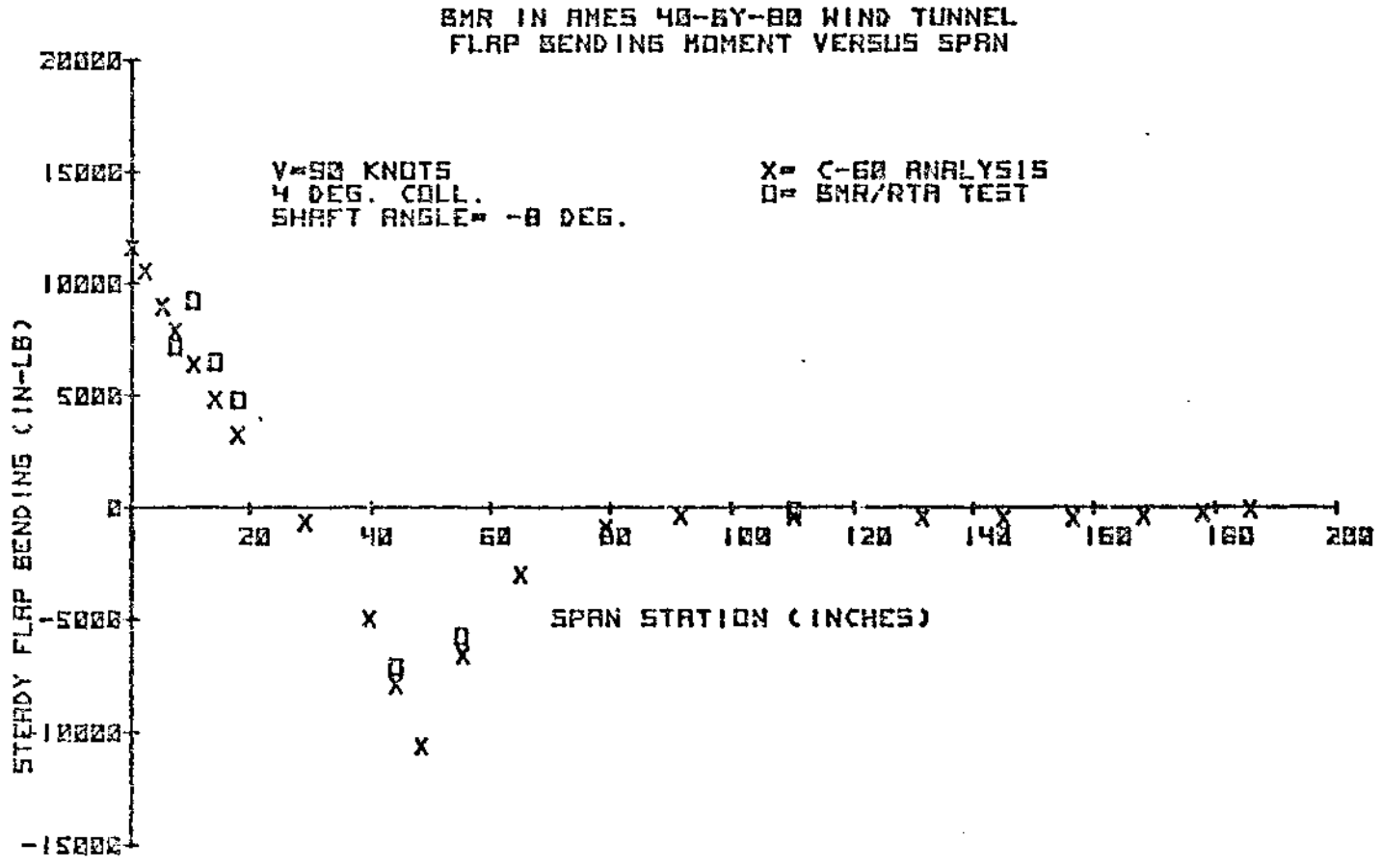

FIGURE 7.11 CORRELATION WITH ANALYSIS - STEADY FLAP MOMENT VERSUS SPAN AT 90 KNOTS

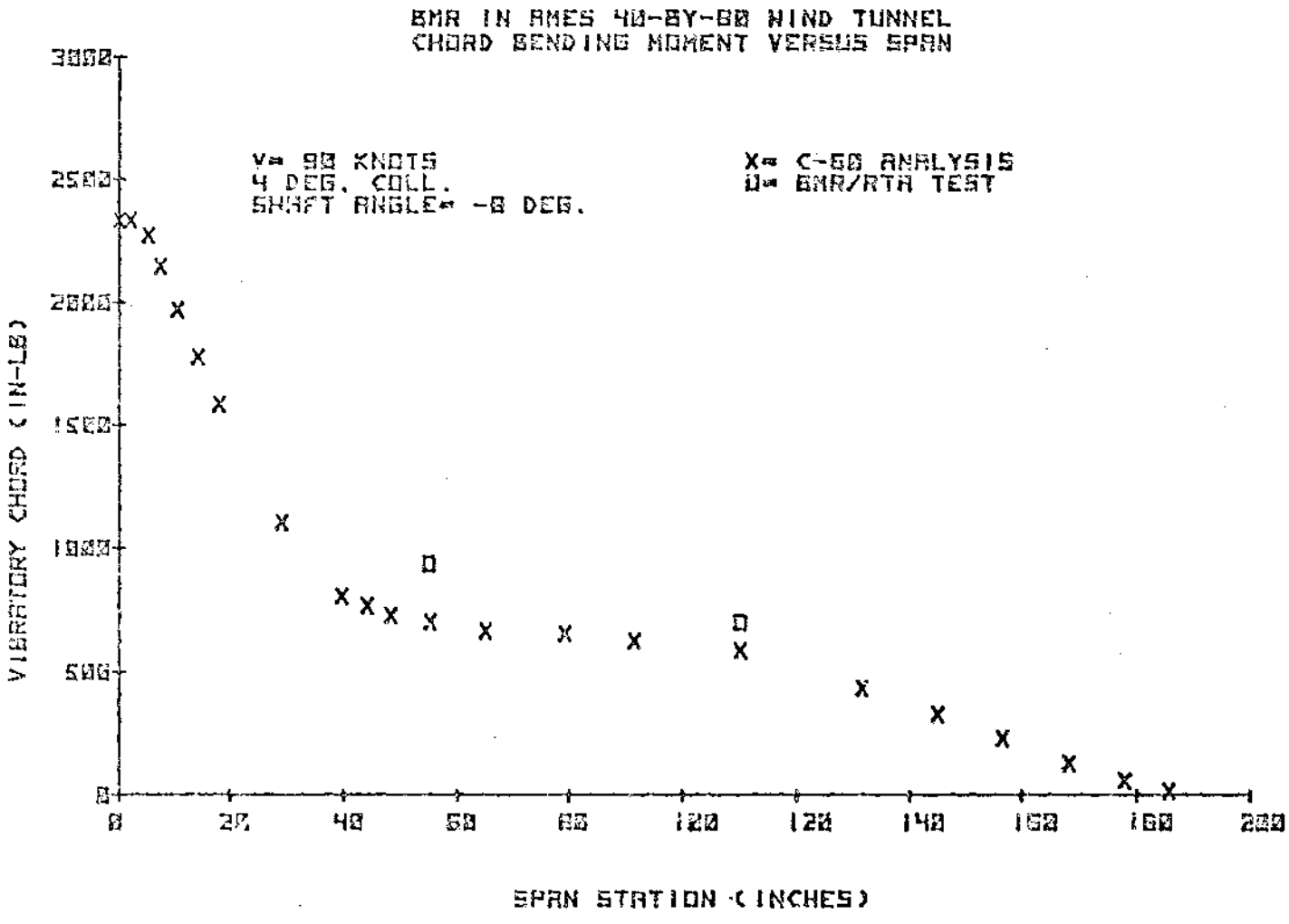

FIGURE 7.12 CORRELATION WITH ANALYSIS - VIBRATORY CHORD MOMENT VERSUS SPAN AT 90 KNOTS

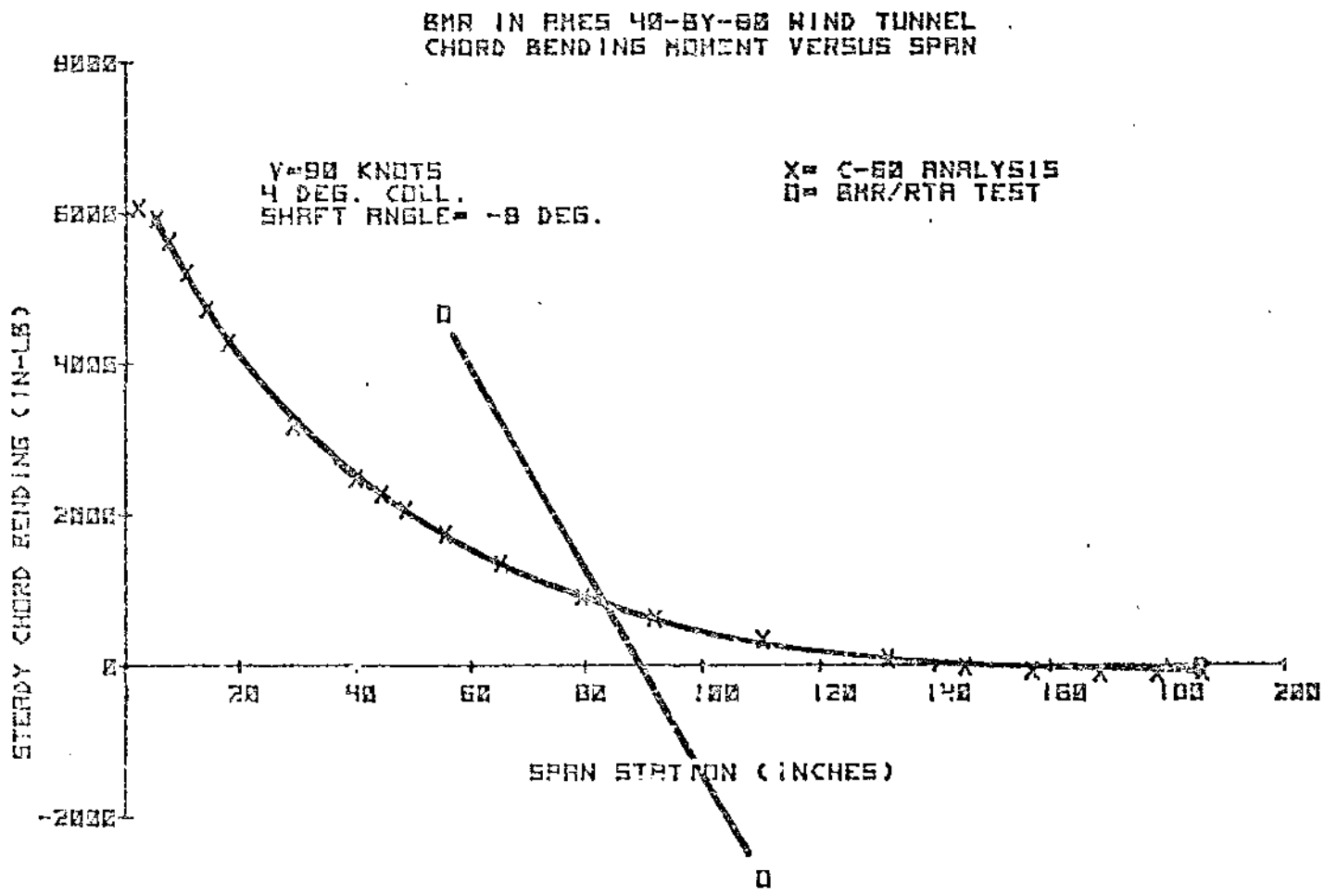

FIGURE 7.13 CORRELATION WITH ANALYSIS - STEADY CHORD MOMENT VERSUS SPAN AT 90 KNOTS

are small relative to blade root moments at station 55.36 inches. The theory as shown treats the flexbeams as an equivalent single beam, then computes the local chord moments. The total chord moment measured at station 14.25 inches is not presented in the correlation plots. This bridge was installed to measure relative changes in chord bending response only for multiblade stability analysis during control excitations. The calibration conditions for this bending bridge consisted of equal local shear and moment distributions for the leading and trailing beam. Under rotating conditions, when the local distributions are not the same and centrifugal force is present, the laboratory calibrations are not applicable.

Figures 7.14 through 7.17 show correlation for BMR/RTA test results in which the control inputs were adjusted to match the 1/rev flapping of the BMR/BO-105 flight test results at 29.5 knots. Again, the flap bending correlation is excellent, while both the steady and vibratory chord moment correlation is poor. Figure 7.18 presents an explanation for this result. This figure shows the computed lag deflection versus radius for the C-60 equivalent beam method and the local chord bending subroutine. It can be seen that the two results are not compatible. Without a converged solution, the individual beam chord bending moments predicted for stations 11 and 43 will be based on a chord bending mode shape in the flexbeams which is not consistent with the blade chord bending mode shape. A discontinuity in the mode shape will exist at the blade attachment joint.

Further effort is required to refine the iteration process so that a converged solution can be obtained.

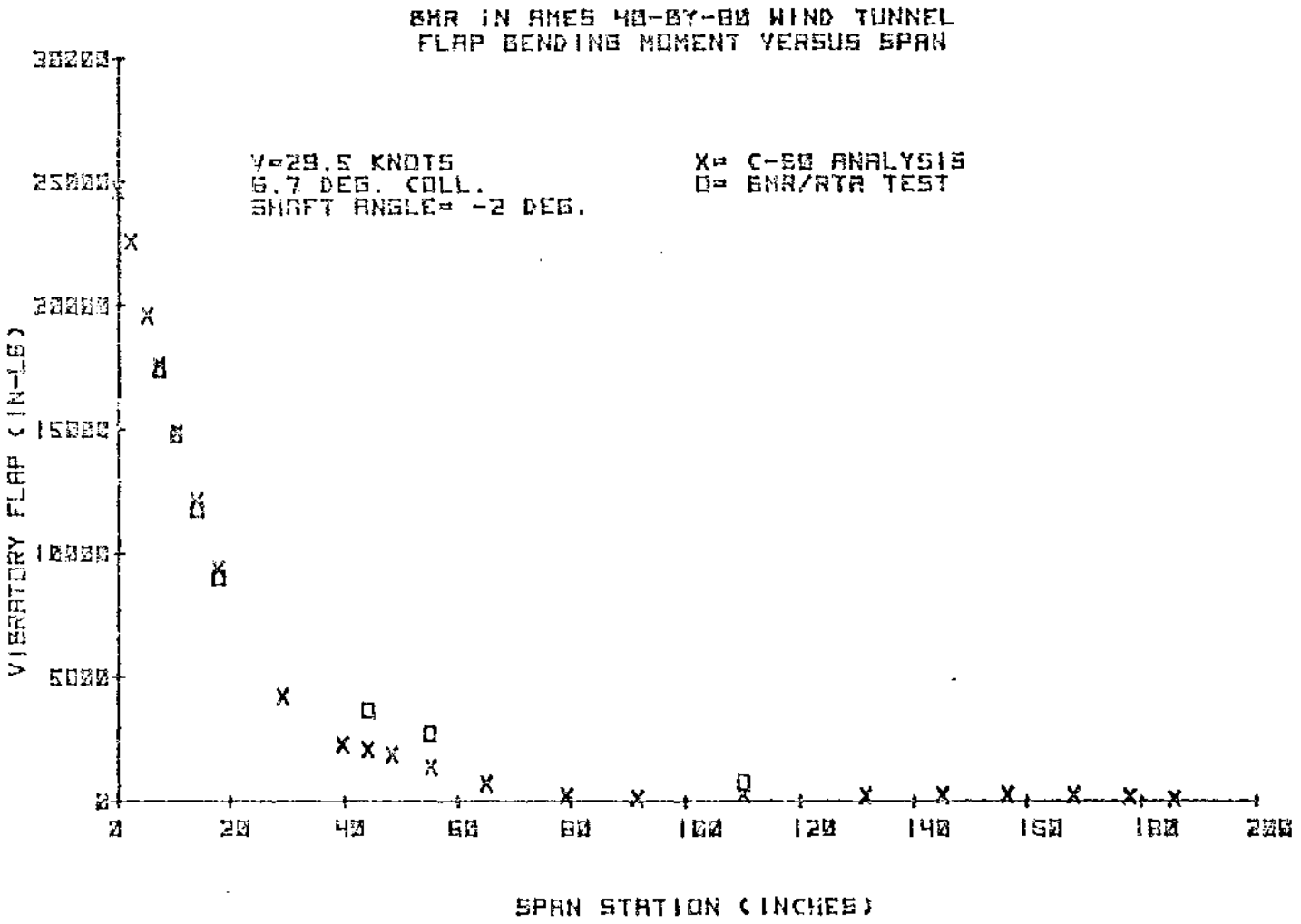

FIGURE 7.14 CORRELATION WITH ANALYSIS - VIBRATORY FLAP MOMENT VERSUS SPAN AT 29.5 KNOTS

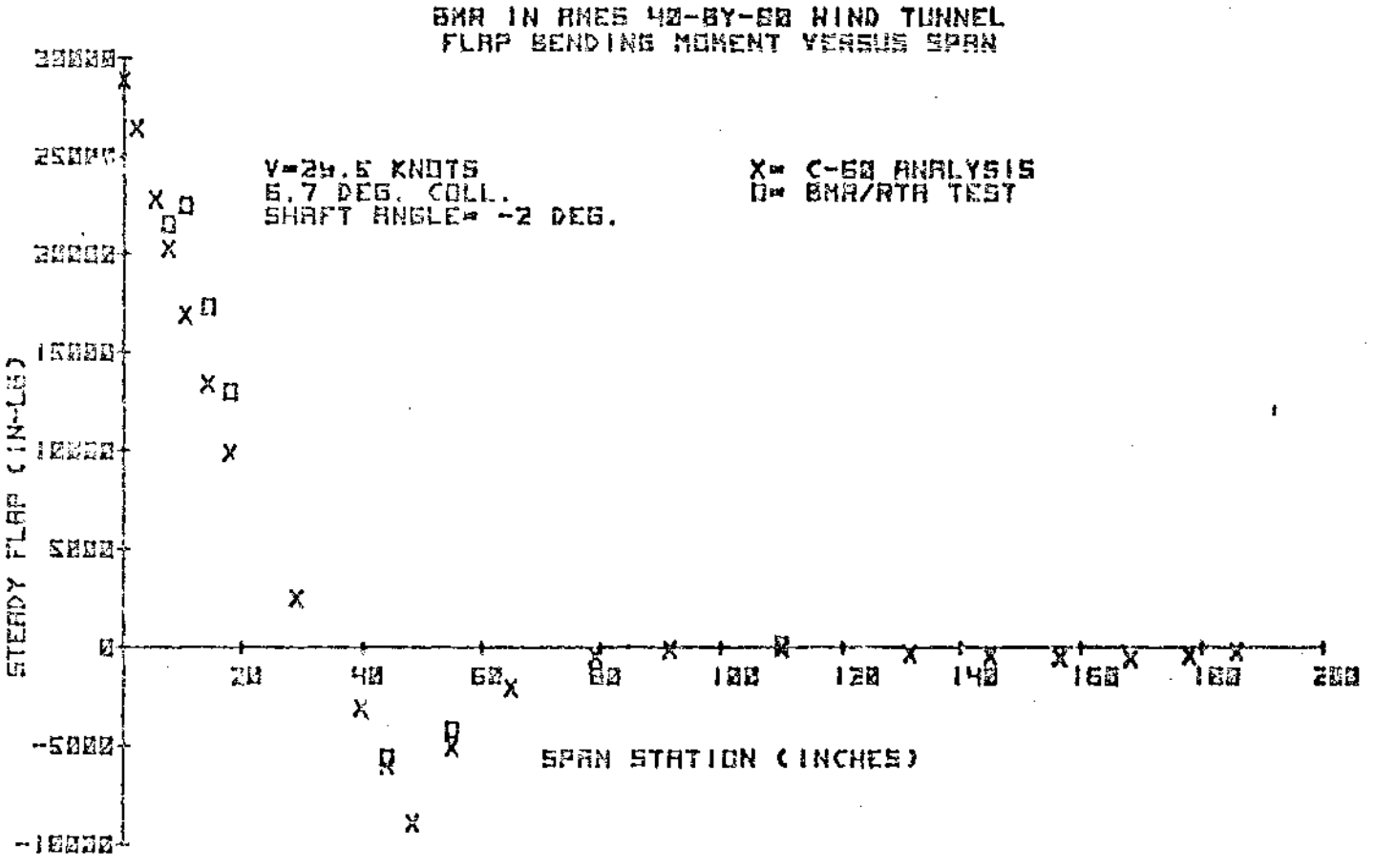

FIGURE 7.15 CORRELATION WITH ANALYSIS - STEADY FLAP MOMENT VERSUS SPAN AT 29.5 KNOTS

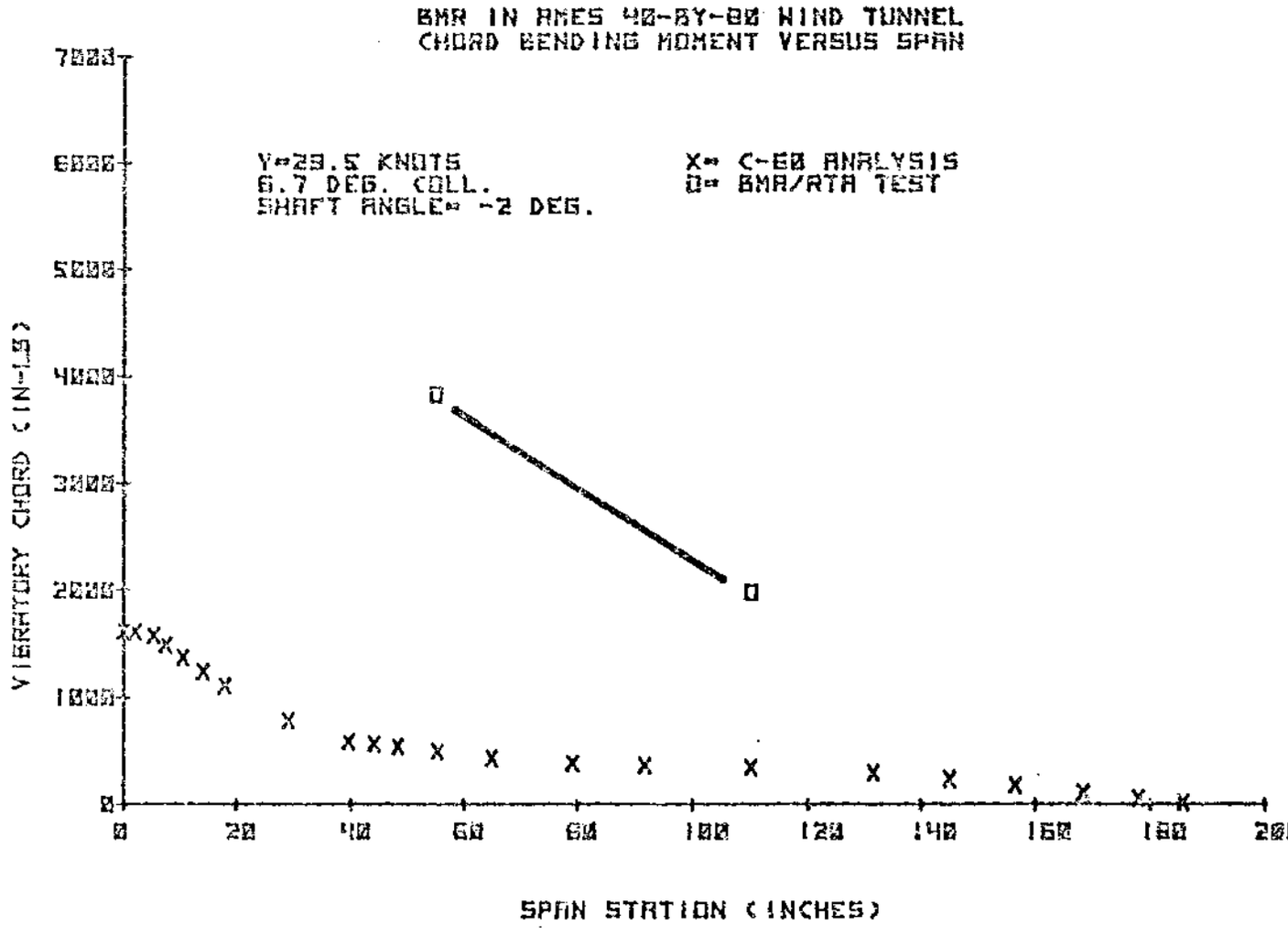

FIGURE 7.16 CORRELATION WITH ANALYSIS - VIBRATORY CHORD MOMENT VERSUS SPAN AT 29.5 KNOTS

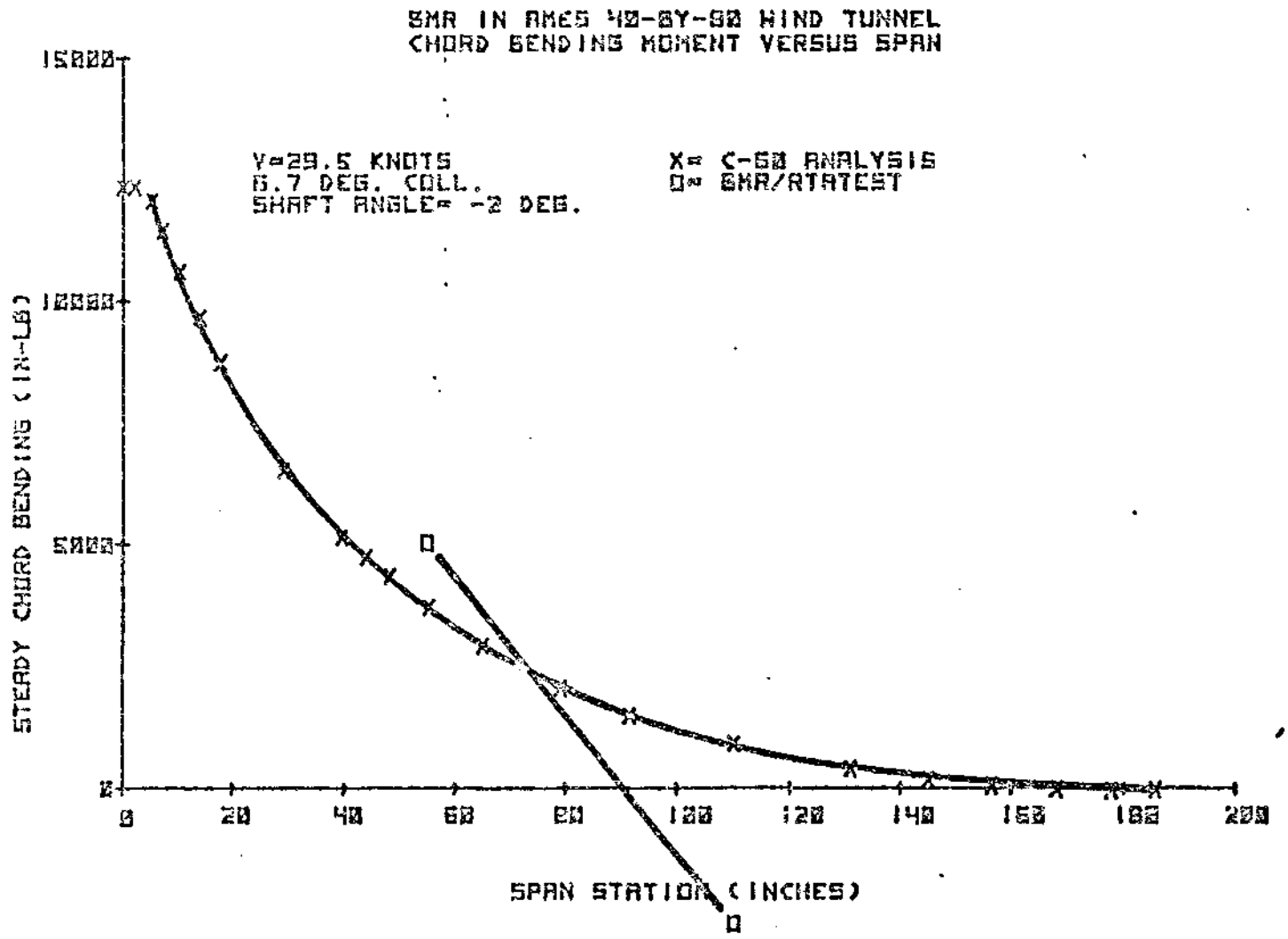

FIGURE 7.17 CORRELATION WITH ANALYSIS - STEADY CHORD MOMENT VERSUS SPAN AT 29.5 KNOTS

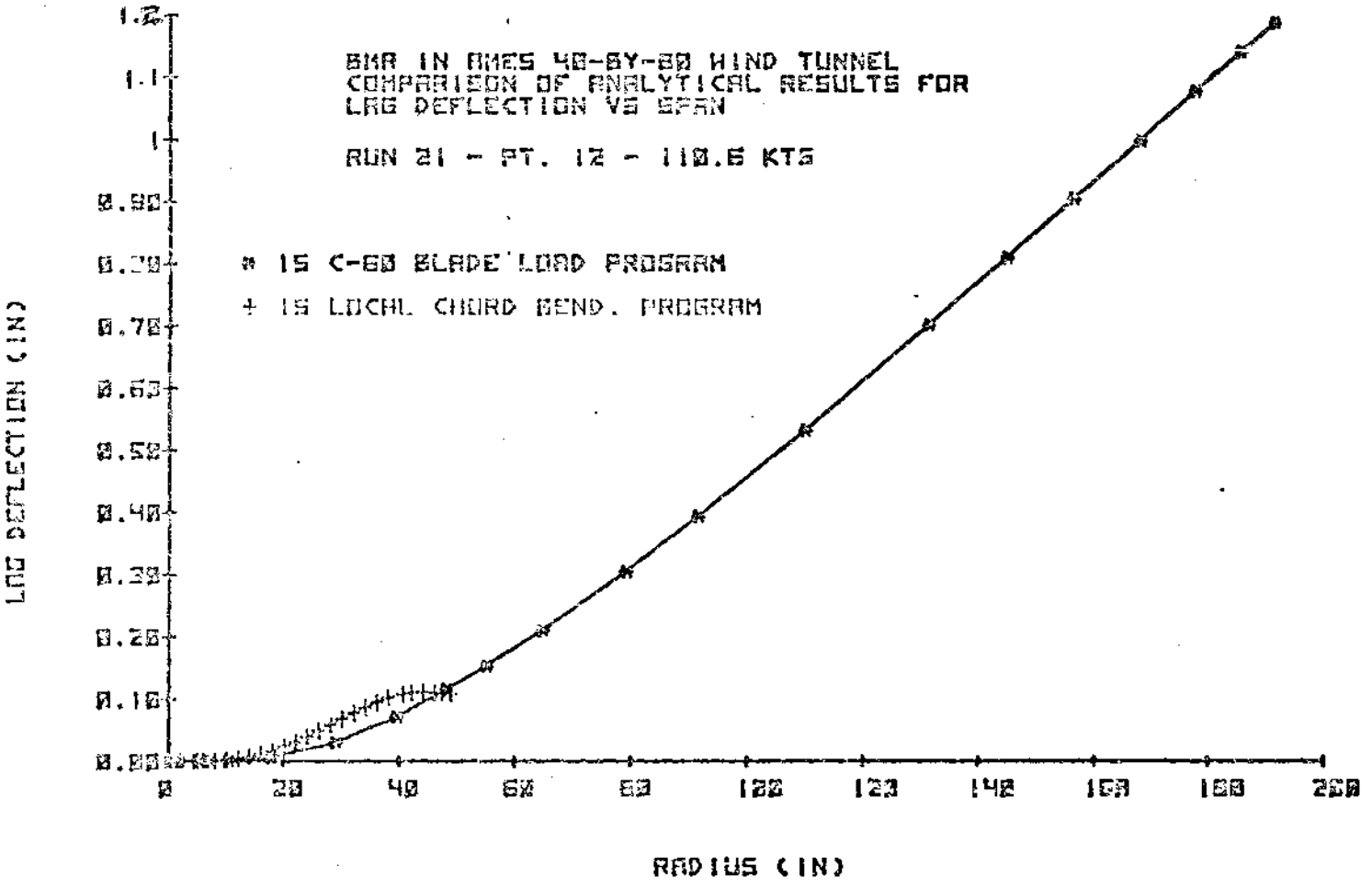

FIGURE 7.18 COMPARISON OF C-60 AND DUAL BEAM CHORD DEFLECTION SHAPES

7.3 PERFORMANCE ANALYSIS METHODOLOGY

7.3.1 Description of B-67 Program

The performance of rotors in forward flight is calculated using program B-67 DD. This is a rotor performance and airloads analysis in which the blades are treated as lifting lines. The trailed vortex wake is represented by a number of concentrated vortices. The program iterates to obtain a mutually consistent induced flow and aerodynamic loading. Two flap bending modes and one torsion mode may be included. The analysis is applicable to blades of arbitrary twist and planform, and the effects of radial flow and unsteady aerodynamics on the airfoil characteristics are included. The features of B-67 are presented in Figure 7.19.

7.3.2 Verification of B-67 Program

Figure 7.20 shows good correlation of B-67 theory with wind tunnel test data for a three-bladed rotor. In Figure 7.21 the measured azimuthal load variation near the tip of a CH-47 rotor blade compares well with B-67 predictions.

ROTOR AIRLOADS AND PERFORMANCE ANALYSI WITH NON-UNIFORM INDUCED INFLOW

MODEL

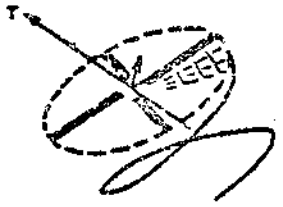

BLOCK DIAGRAM

INPUT
FLIGHT CONDITIONS
BLADE CHARACTERISTICS
REQUIRED THRUST AND SIDE FORCE

↓

COMPUTE UNIFORM DOWN-WASH ROTOR SOLUTION

↓

APPROXIMATE TRAILED VORTEX SHEET BY A SERIES OF VORTEX FILAMENTS FOR 45° BEHIND BLADE AND A CONCENTRATED TIP VORTEX AFTER 45° (UNIFORM DRIFT RATE). CALCULATE NON-UNIFORM DOWNWASH AND LOCAL AERODYNAMICS AT 13 RADIAL POSITIONS AND 15° AZIMUTHAL INCREMENTS. COMPUTE NON-UNIFORM DOWNWASH ROTOR SOLUTION.

↓

OUTPUT
OVERALL ROTOR PERFORMANCE PARAMETERS.
RADIAL AND AZIMUTHAL VARIATION OF MACH NUMBER, ANGLE OF ATTACK C_y, C_d, INDUCED VELOCITY, AND OTHER LOCAL PARAMETERS.

BASIC FEATURES

1. NON-UNIFORM DOWNWASH.
2. ARTICULATED, TEETERING & RIGID ROTORS.
3. RIGID BLADE.
4. UTILIZES EXTENDED LIFT TABLES.

OPTIONAL FEATURES

A. YAWED FLOW –
IMPROVES ESTIMATE OF ROTOR LIFTING CAPABILITY AT $\psi = 0°$, 180° DUE TO SWEEP EFFECTS.

B. ELASTICITY AND UNSTEADY AERODYNAMICS –
1. UNSTEADY AERO: YIELDS FAVORABLE STALL DELAYS ON C_y AND C_m.
2. BLADE ELASTICITY: IMPROVES ESTIMATE OF LOCAL ANGLE OF ATTACK, & EVALUATION, AND LOCAL BLADE AIRLOADS.
3. ITEMS 1) AND 2) ENABLE THE USE OF 2 D AIRFOIL DECKS INCLUDING STALL CHARACTERISTICS AS MEASURED DURING STATIC SECTION TESTS.

FIGURE 7.19 FEATURES OF B-67

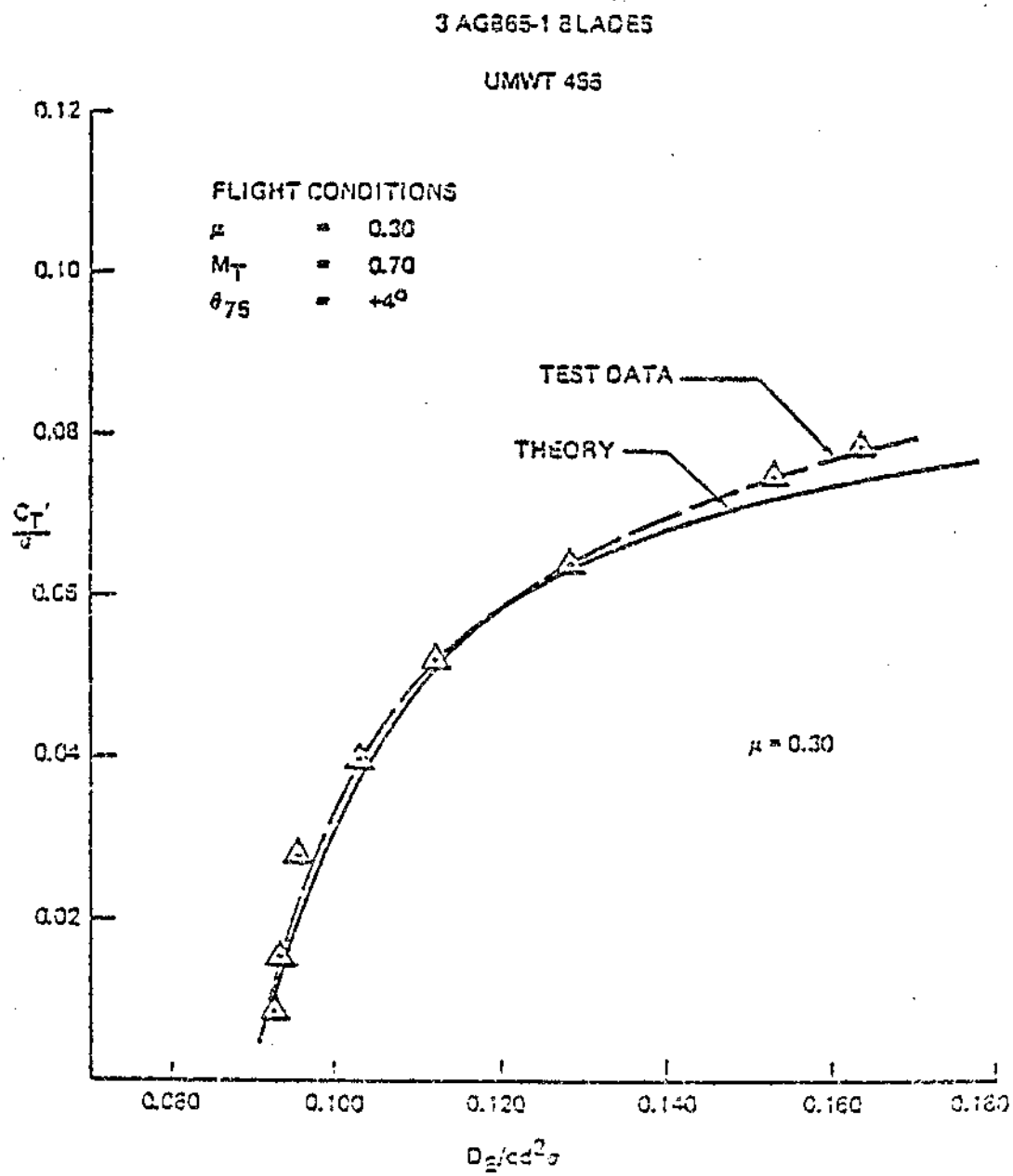

FIGURE 7.20 CORRELATION OF FORWARD FLIGHT ANALYSIS (B-67) WITH TEST DATA

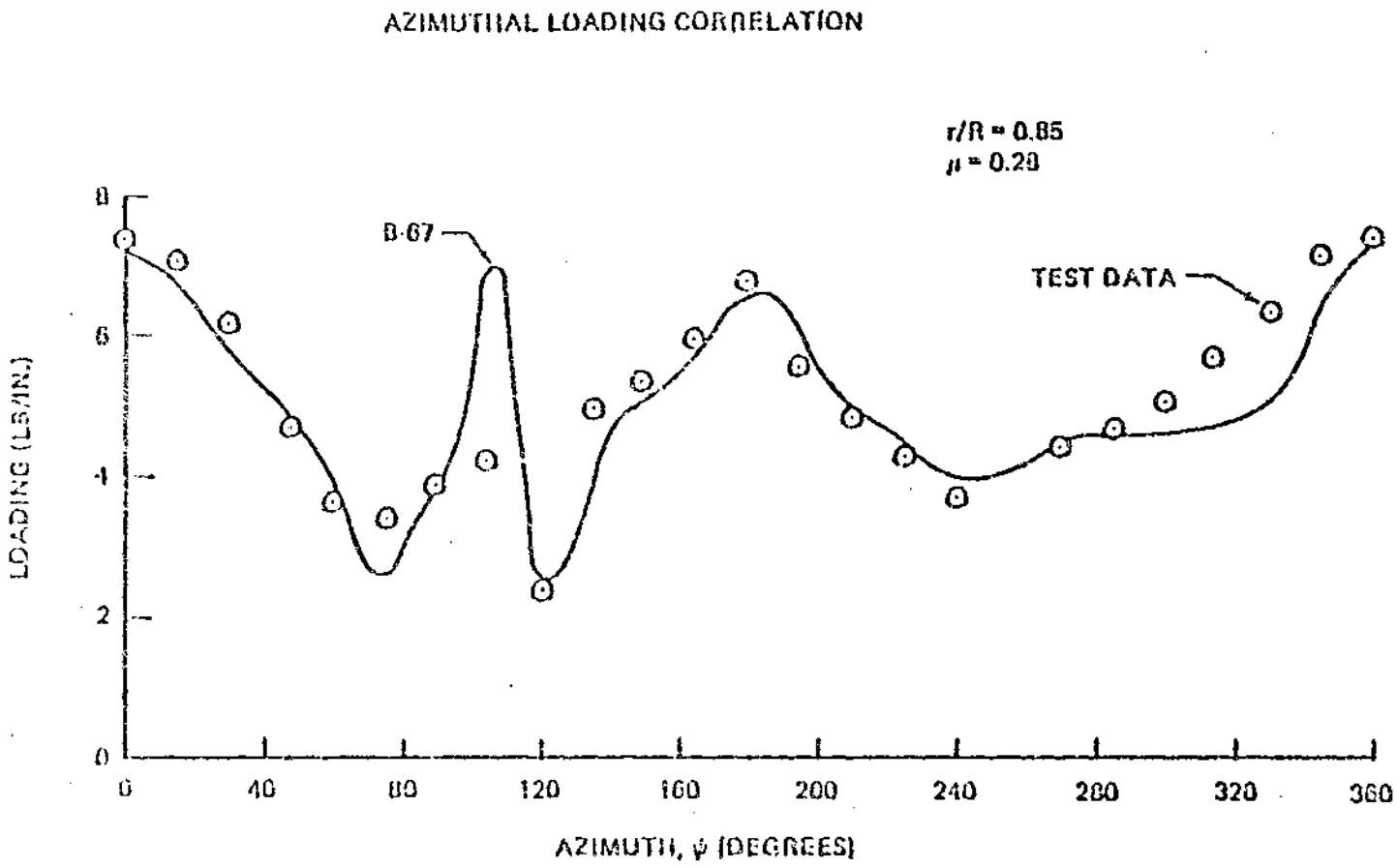

FIGURE 7.21 B-67 FORWARD FLIGHT ANALYSIS PREDICTS BLADE LOADING

8.0 TEST RESULTS

8.1 STABILITY

Aeroelastic stability test results are presented in this section in terms of percent critical damping and time to half amplitude obtained from decay tests. Attempts were made to estimate the degree of data scatter by selected repetition at certain test conditions. Repeatability of damping results was found to be dependent on the stability level. Good repeatability was generally found in the two to four percent fixed system critical damping ratio level. Poor repeatability was generally obtained above ten percent fixed system critical damping ratio. Data scatter was also found to be smaller at rotor speeds of 400 rpm and higher where the first chord mode frequency was well below the rotor 1/rev frequency.

8.1.1 Baseline Configuration Results

8.1.1.1 Damping Versus Airspeed

8.1.1.1.1 Damping Versus Airspeed with Collective Pitch and Shaft Angle Variations

Figures 8.1 and 8.2 show fixed system damping ratio and time to half amplitude versus airspeed at normal rotor speed. Results are for a shaft angle of -6 degrees and for collective pitch angles at 70 percent radius of 3 to 10 degrees. Data is presented for airspeeds from hover to 120 knots. Note that the shaft angle for hover was -10 degrees. Figure 8.1 shows that at a constant collective pitch, fixed system damping generally remains the same or increases slightly as airspeed increases

from hover to 60 knots. Between 60 and 90 knots, fixed system damping remains constant for 3 to 6 degrees collective pitch, and decreases as airspeed increases from 60 to 90 knots at 8 degrees collective pitch. At collective pitch angles of 4 to 8 degrees, damping decreases as airspeed increases from 90 to 120 knots.

Damping is stable at all airspeeds and collective pitches indicated in Figure 8.1. Damping increases with collective pitch at all airspeeds; a minimum damping of slightly less than 2 percent critical occurred at 3 degrees collective pitch; a maximum damping of about 11 percent was obtained at 10 degrees collective pitch in hover.

Figure 8.2 shows time to half amplitude data versus airspeed corresponding to fixed system damping ratio data shown in Figure 8.1. Time to half amplitude data have an inverse relationship to fixed system damping data: a low value of damping corresponds to a high value of time to half amplitude. The maximum value of time to half amplitude is about 2.5 seconds at 3 degrees collective pitch at 60 knots; the minimum value obtained is less than one half second at 10 degrees collective pitch for hover.

Figures 8.3 and 8.4 show damping ratio and time to half amplitude data versus airspeed for speeds from hover to 143 knots for collective pitch angles from 0 to 10 degrees and shaft

angles from -8 to -12 degrees. Results are generally in agreement with those of Figures 8.1 and 8.2; the trend of decreasing damping with increasing airspeed for speeds above 90 knots at constant collective pitch and shaft angle is confirmed. Damping data do not appear to be very sensitive to shaft angle based on results shown in Figures 8.3 and 8.4.

8.1.1.1.2 Damping Versus Airspeed for 1.0 G Level Flight Level flight testing was conducted to obtain performance data but no aeroelastic stability data were obtained for these conditions. Trim values of collective pitch and shaft angles versus airspeed for the 1.0 G level flight condition are shown in Figure 8.5. Figure 8.6 shows trim values of collective pitch and shaft angle versus airspeed for the zero flapping condition where the lift equals 5000 pounds (take-off gross weight) and the flat plate drag area equals 9.0 square feet. That is the flat plate area of the rotor with the hub and RTA tares removed, and matches the flat plate area of the BO-105 rotor. Based on interpolating the damping data obtained in the test at zero flapping conditions which bracketed the range of trim conditions shown in Figure 8.6, the damping values for a 5000 pound lift, F_e = 9.0 square feet condition are plotted in Figure 8.7 versus airspeed. This approximates 1.0g flight damping data. Figure 8.7 shows estimated damping for 1.0 G level flight to be about 7 percent in hover, decreasing to about 3.5 percent at 60 knots, and increasing to about 6.5 percent at 120 knots.

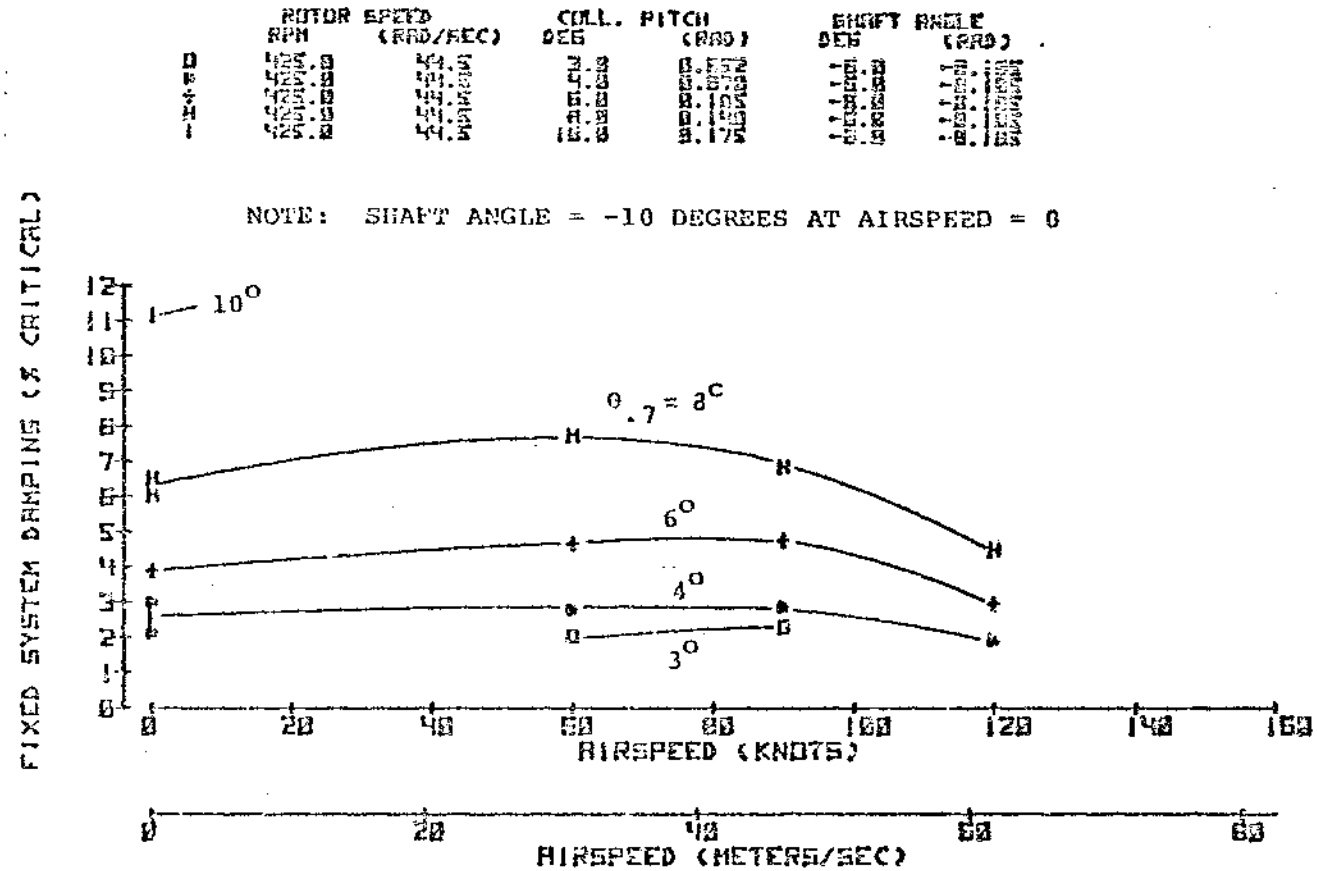

FIGURE 8.1 FORWARD FLIGHT - FIXED SYSTEM DAMPING VS AIRSPEED AND COLLECTIVE PITCH - AT NORMAL ROTOR SPEED AND -6 DEGREE SHAFT ANGLE - BASELINE CONFIGURATION

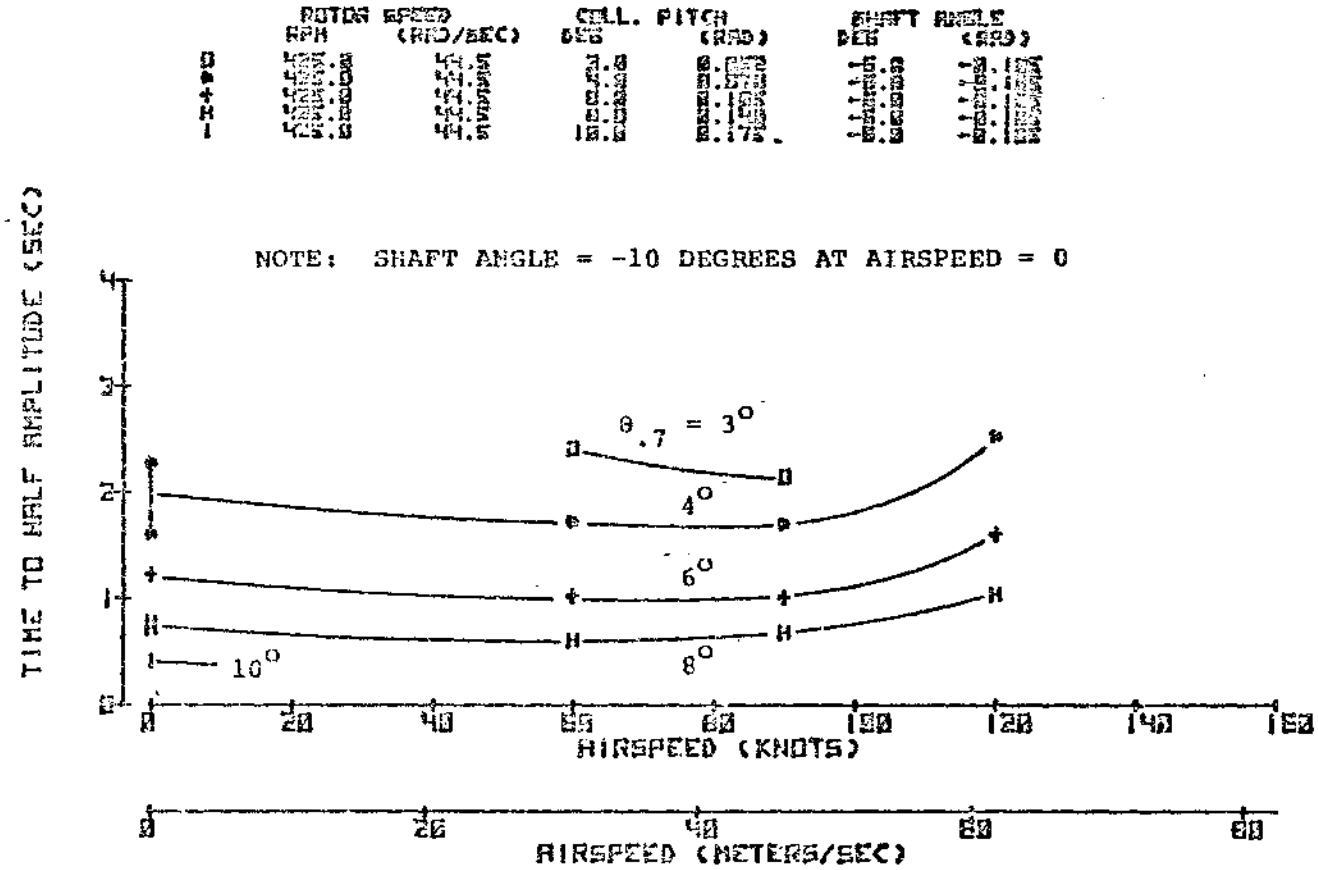

FIGURE 8.2 FORWARD FLIGHT - TIME TO HALF AMPLITUDE VS AIRSPEED AND COLLECTIVE PITCH - AT NORMAL ROTOR SPEED AND -6 DEGREE SHAFT ANGLE - BASELINE CONFIGURATION

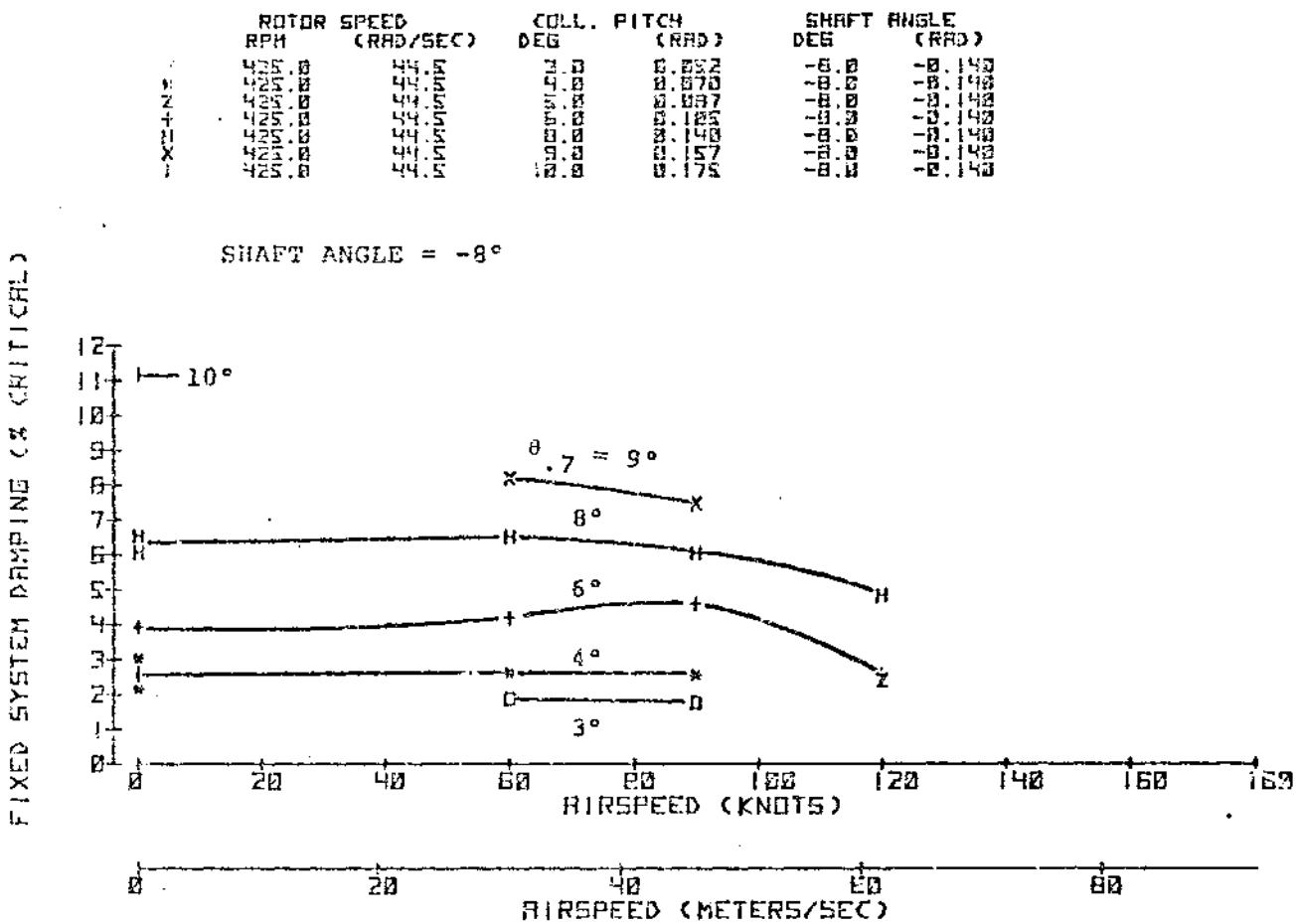

FIGURE 8.3 FORWARD FLIGHT - FIXED SYSTEM DAMPING VS AIRSPEED AND COLLECTIVE PITCH - AT NORMAL ROTOR SPEED AND -8 TO -12 DEGREE SHAFT ANGLE - BASELINE CONFIGURATION (SHEET 1 OF 3)

	ROTOR SPEED RPM	(RAD/SEC)	COLL. PITCH DEG	(RAD)	SHAFT ANGLE DEG	(RAD)
A	425.0	44.5	7.0	0.122	-10.0	-0.175
B	425.0	44.5	8.0	0.140	-10.0	-0.175
C	425.0	44.5	9.0	0.157	-10.0	-0.175
D	425.0	44.5	10.0	0.175	-10.0	-0.175

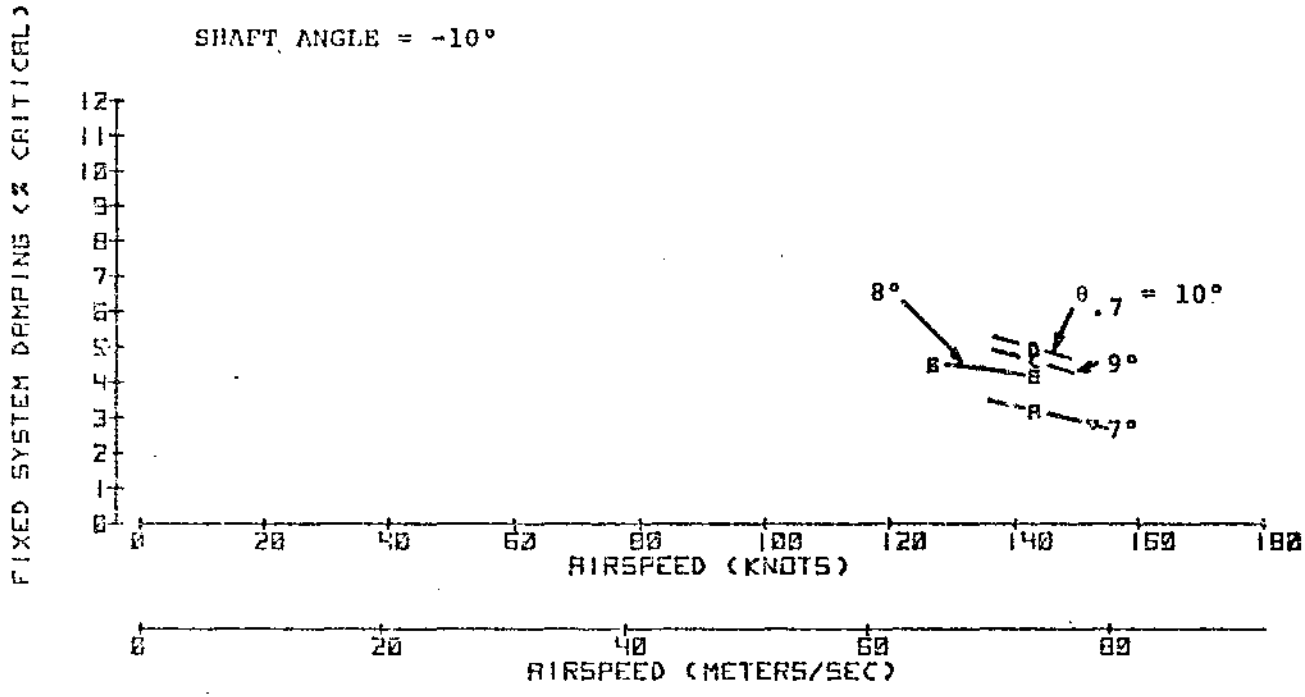

FIGURE 8.3 FORWARD FLIGHT - FIXED SYSTEM DAMPING VS AIRSPEED AND COLLECTIVE PITCH - AT NORMAL ROTOR SPEED AND -8 TO -12 DEGREE SHAFT ANGLE - BASELINE CONFIGURATION (SHEET 2 OF 3)

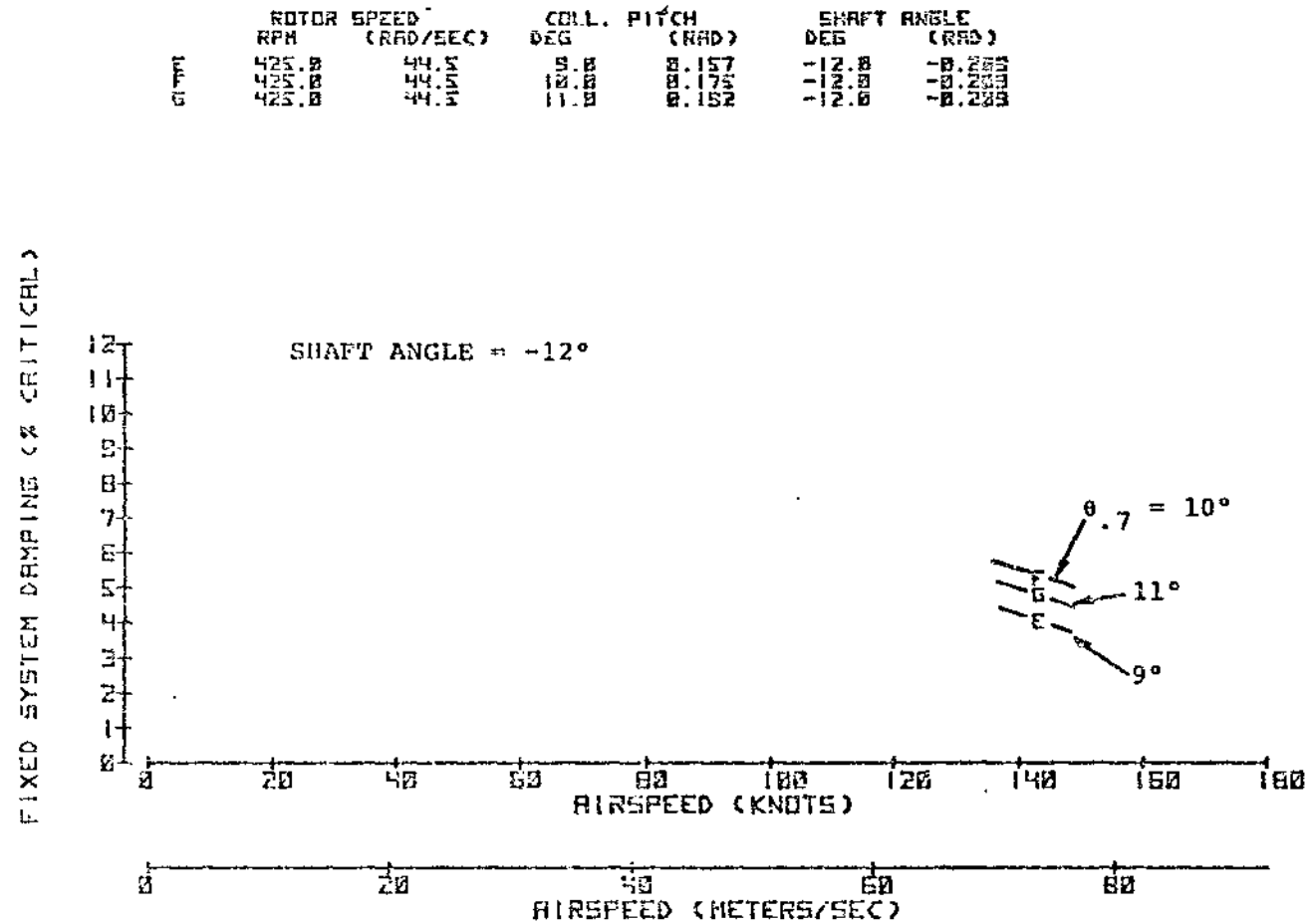

FIGURE 8.3 FORWARD FLIGHT - FIXED SYSTEM DAMPING VS AIRSPEED AND COLLECTIVE PITCH - AT NORMAL ROTOR SPEED AND -8 TO -12 DEGREE SHAFT ANGLE BASELINE CONFIGURATION (SHEET 3 OF 3)

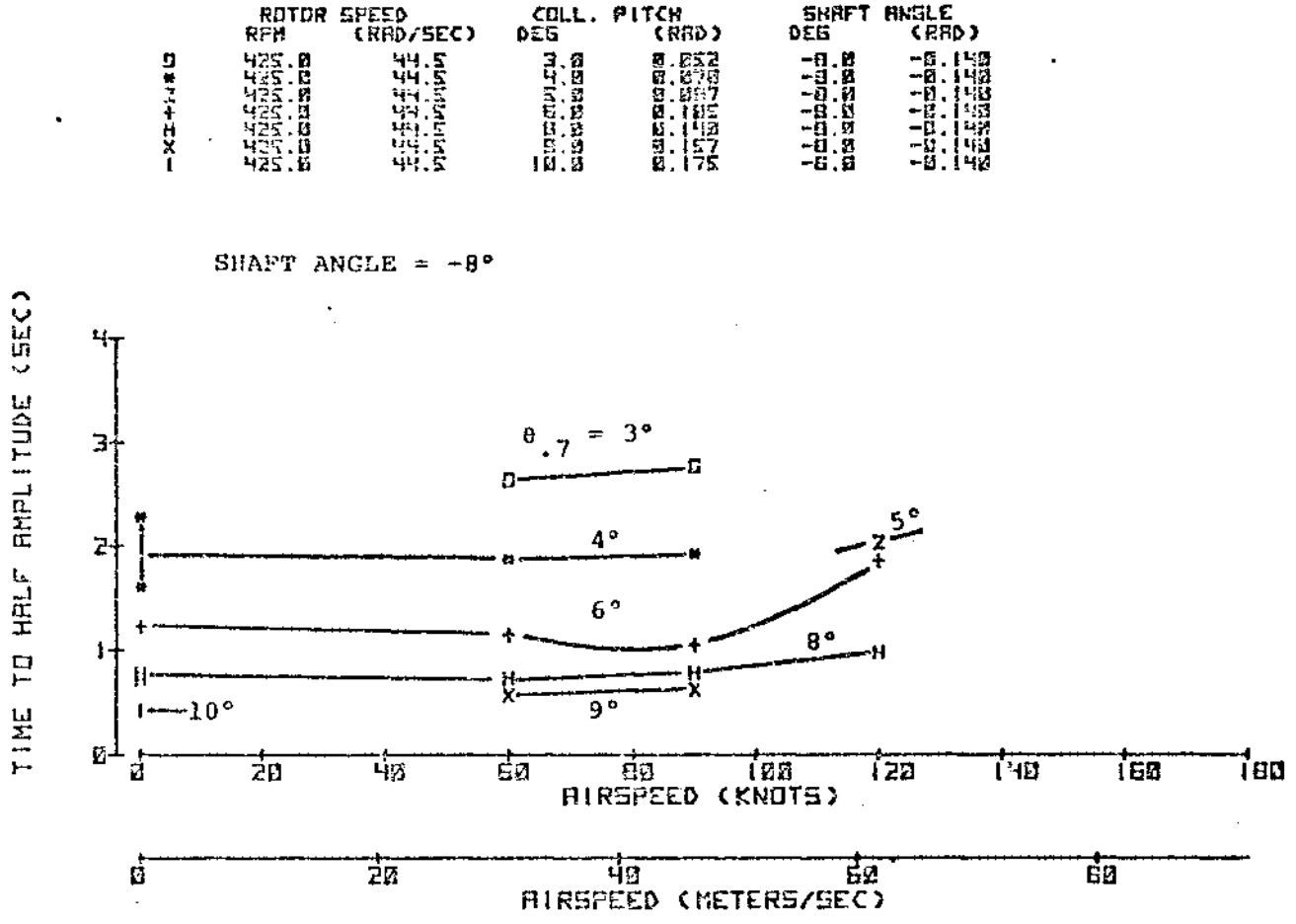

FIGURE 8.4 FORWARD FLIGHT - TIME TO HALF AMPLITUDE VS AIRSPEED AND COLLECTIVE PITCH - AT NORMAL ROTOR SPEED AND -8 TO -12 DEGREE SHAFT ANGLE - BASELINE CONFIGURATION (SHEET 1 OF 3)

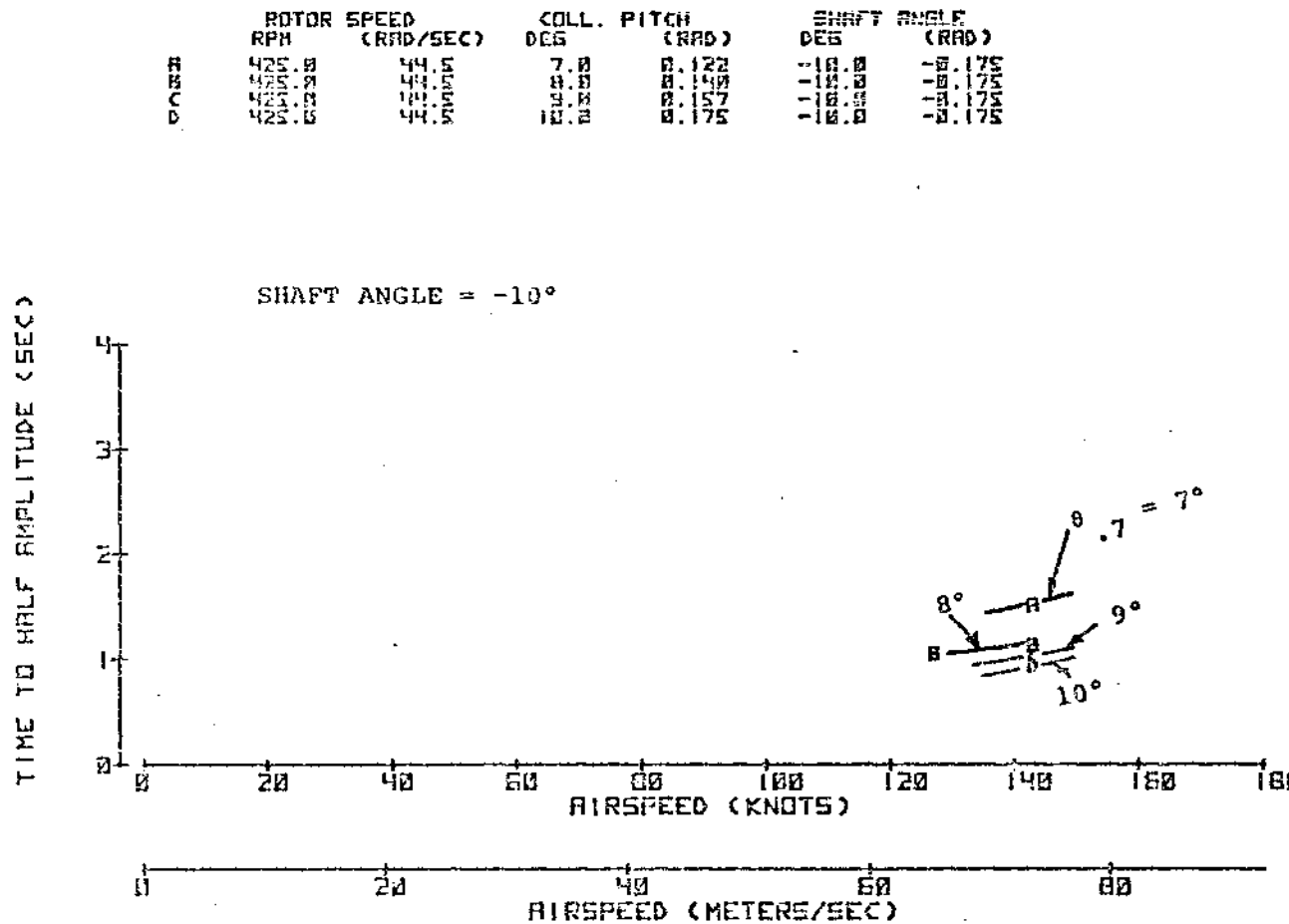

FIGURE 8.4 FORWARD FLIGHT - TIME TO HALF AMPLITUDE VS AIRSPEED AND COLLECTIVE PITCH - AT NORMAL ROTOR SPEED AND -8 TO -12 DEGREE SHAFT ANGLE - BASELINE CONFIGURATION (SHEET 2 OF 3)

	ROTOR SPEED RPM	(RAD/SEC)	COLL. PITCH DEG	(RAD)	SHAFT ANGLE DEG	(RAD)
E	425.0	44.5	9.0	0.157	-12.0	-0.209
F	425.0	44.5	10.0	0.175	-12.0	-0.209
G	425.0	44.5	11.0	0.192	-12.0	-0.209

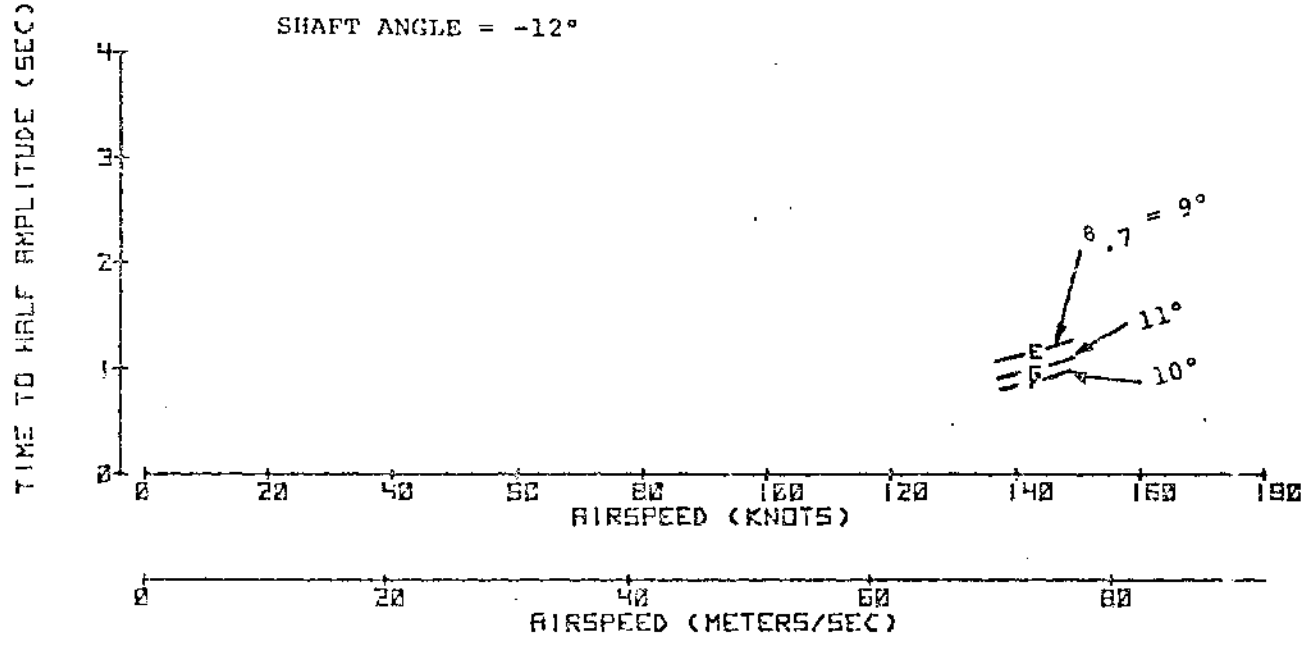

FIGURE 8.4 FORWARD FLIGHT - TIME TO HALF AMPLITUDE VS AIRSPEED AND COLLECTIVE PITCH - AT NORMAL ROTOR SPEED AND -8 TO -12 DEGREE SHAFT ANGLE - BASELINE CONFIGURATION (SHEET 3 OF 3)

FIGURE 8.5 TRIM VALUES FOR SHAFT ANGLE AND COLLECTIVE PITCH FOR 1.0G LEVEL FLIGHT AT 425 RPM

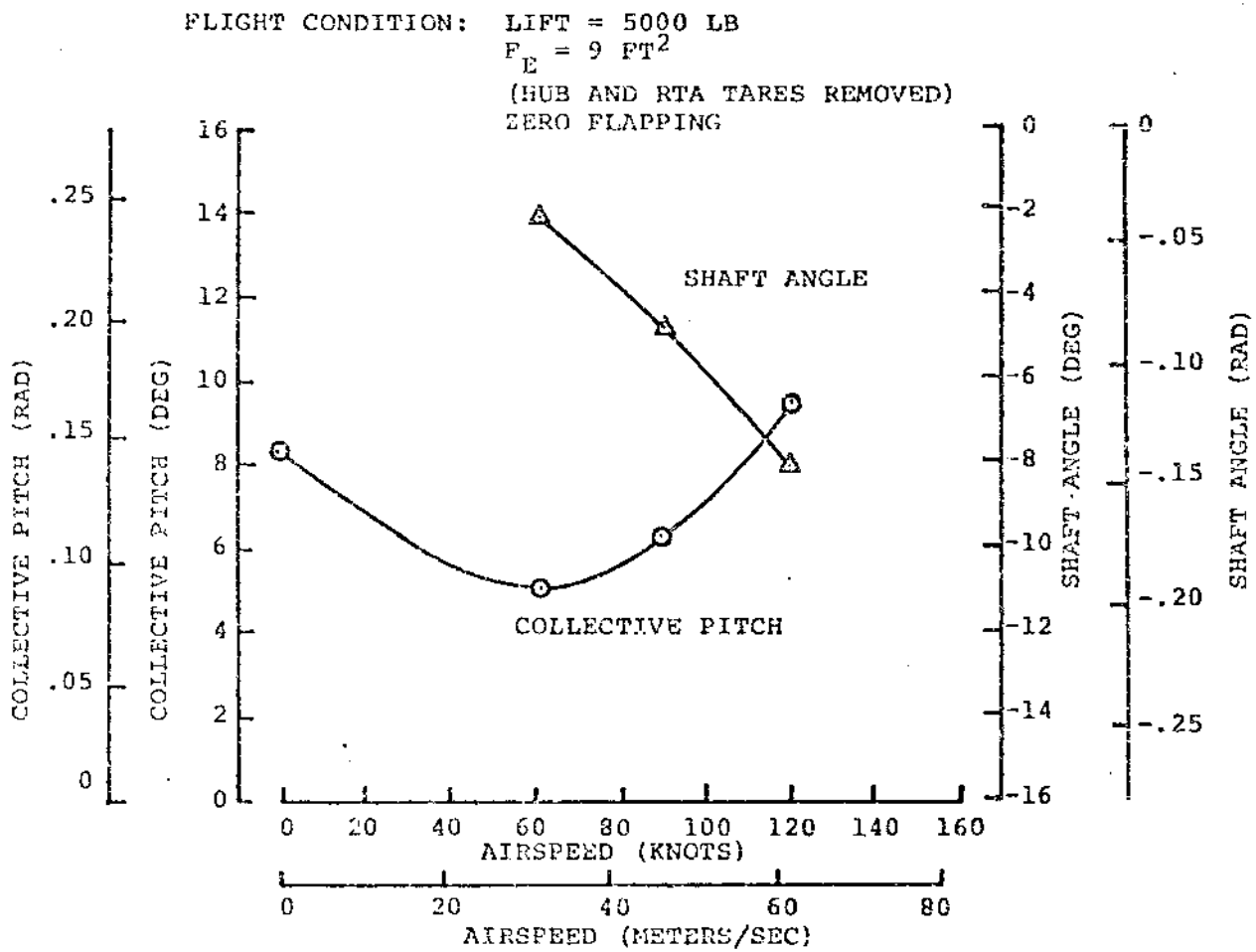

FIGURE 3.6 INTERPOLATED TRIM VALUES FOR SHAFT ANGLE AND COLLECTIVE PITCH FOR 5000 LB LIFT AND BODY F_E = 9.0 SQ FT WITH CYCLIC FOR ZERO FLAPPING

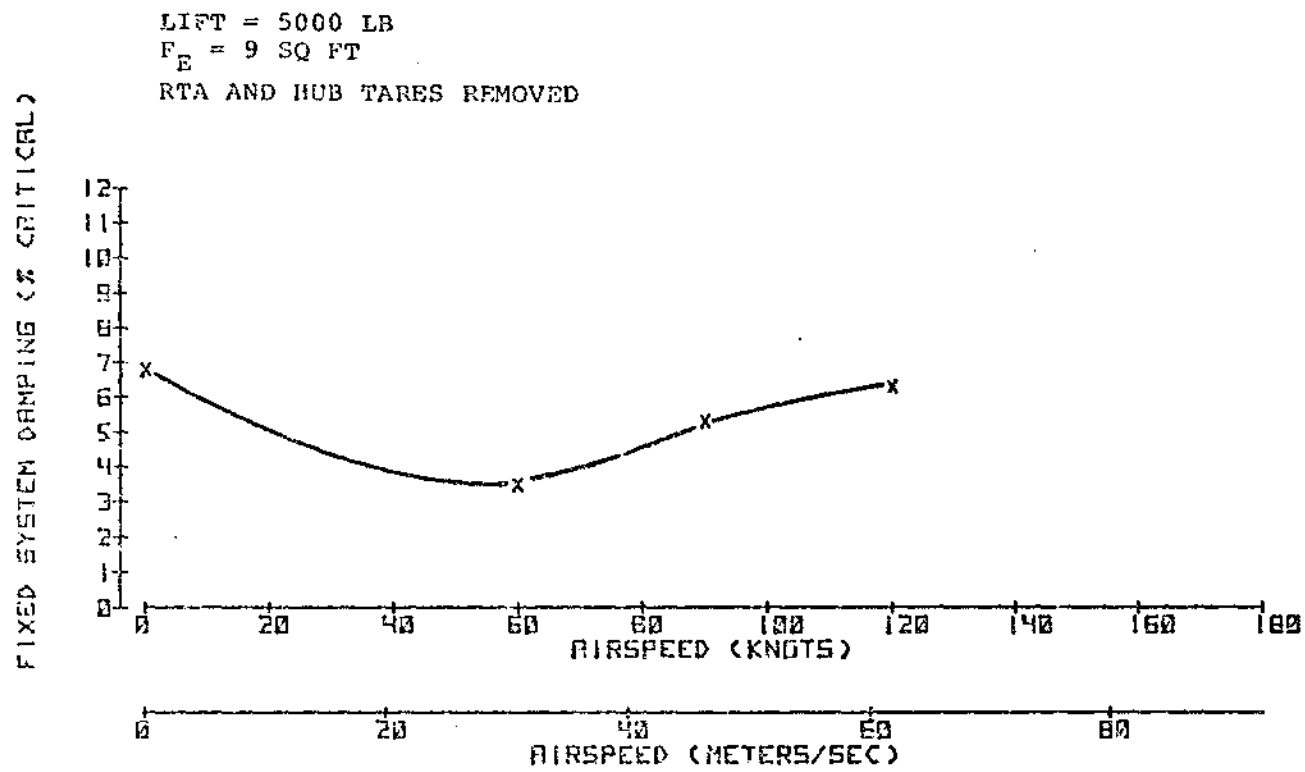

FIGURE 8.7 INTERPOLATED DAMPING VS AIRSPEED FOR 5000 LB LIFT AND F_E = 9 SQ FT - NORMAL ROTOR SPEED - BASELINE CONFIGURATION

8.1.1.2 Damping Versus Collective Pitch and Rotor Speed

8.1.1.2.1 Initial Hover Stability Results

Initial testing consisted of hover testing for a collective pitch of 4 degrees for a rotor speed variation from 350 to 436 rpm. Collective pitch sweeps were then made at 350, 375, 400, 415, and 425 rpm. Fixed system damping data and time to half amplitude for these initial test conditions are shown in Figures 8.8 and 8.9, respectively. Figure 8.8 shows that fixed system damping generally decreases with increasing rotor speed at constant collective pitch and increases with collective pitch for a constant rotor speed. At collective pitch values of 4, 6, and 8 degrees, a slight reduction in damping is seen at the 415 rpm rotor speed. This is the rotor speed where a coalescence of the rotor regressing chord mode frequency with the body pitch mode frequency is expected to occur.

A significant amount of data scatter is indicated in Figures 8.8 and 8.9. An improved trim procedure was developed, and additional hover test data were obtained using this improved procedure.

8.1.1.2.2 Hover Stability Results with Nonzero Cyclic Inputs

Figures 8.10 and 8.11 show fixed system damping levels and time to half amplitude for hover with nonzero longitudinal and lateral cyclic pitch inputs in an effort to trim out nominal one per rev flapping. Results are shown for rotor speeds from 375 to 437 rpm and for collective pitch values from 4 to 10 de-

grees. Results are similar to those obtained from initial hover testing. The rotor speed range between 400 and 425 rpm was studied in more detail, but no specific indication of reduced damping near 415 rpm was indicated with the nonzero cyclic inputs.

8.1.1.2.3 Summary of Hover Stability Results

Figures 8.12 and 8.13 show summaries of hover damping data and time to half amplitude data for rotor speeds of 350, 375, 400, 425 and 437 rpm and for collective pitch values of from 0 to 11 degrees. Hover data for both initial hover testing and hover testing with nonzero cyclic inputs were averaged to obtain hover summary data presented in Figures 8.12 and 8.13.

8.1.1.2.4 Stability at 90 Knots

Figures 8.14 through 8.17 show damping and time to half amplitude data for rotor speeds of 335, 400 and 425 rpm for collective pitch values from 2 to 10 degrees and for shaft angles of -6 and -8 degrees. Damping and time to half amplitude data are similar at shaft angles of -6 and -8 degrees. Data at 90 knots are similar to hover data (Figures 8.12 and 8.13) at the same rotor speed and collective pitch values.

8.1.1.3 Effects of Shaft Angle

Figures 8.18 through 8.21 present damping and time to half amplitude data versus collective pitch and shaft angle at 60, 90, and 120 knots. Data are shown at 90 knots for rotor speeds of

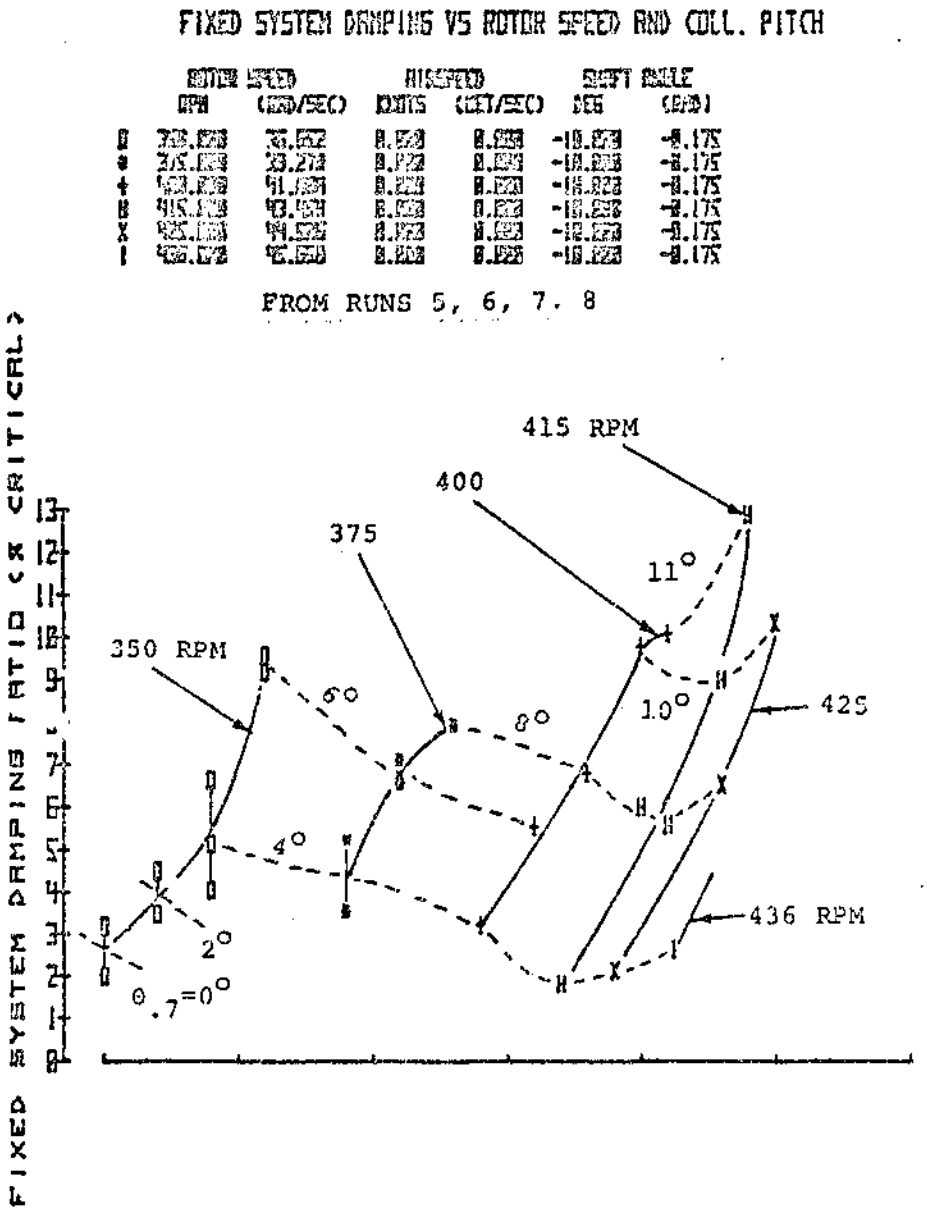

FIGURE 8.8 HOVER - FIXED SYSTEM DAMPING VS ROTOR SPEED AND COLLECTIVE PITCH - INITIAL DATA - BASELINE CONFIGURATION

TIME TO HALF AMPLITUDE VS ROTOR SPEED AND COLL. PITCH

	ROTOR SPEED RPM	ROTOR SPEED (RAD/SEC)	[illegible]	[illegible]	SHAFT ANGLE [illegible]	SHAFT ANGLE (RAD)
□	[illegible]	[illegible]	[illegible]	[illegible]	[illegible]	[illegible]
■	[illegible]	[illegible]	[illegible]	[illegible]	[illegible]	[illegible]
+	[illegible]	[illegible]	[illegible]	[illegible]	[illegible]	[illegible]
⊞	[illegible]	[illegible]	[illegible]	[illegible]	[illegible]	[illegible]
×	[illegible]	[illegible]	[illegible]	[illegible]	[illegible]	[illegible]
⊥	[illegible]	[illegible]	[illegible]	[illegible]	[illegible]	[illegible]

FROM RUNS 5, 6, 7, 8

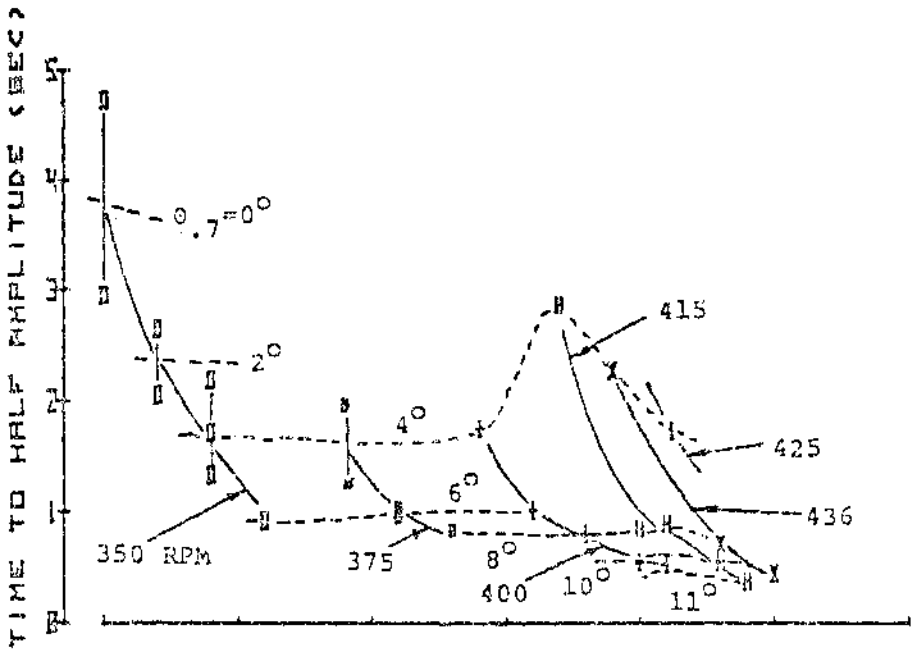

FIGURE 8.9 HOVER - TIME TO HALF AMPLITUDE VS ROTOR SPEED AND COLLECTIVE PITCH - INITIAL DATA - BASELINE CONFIGURATION

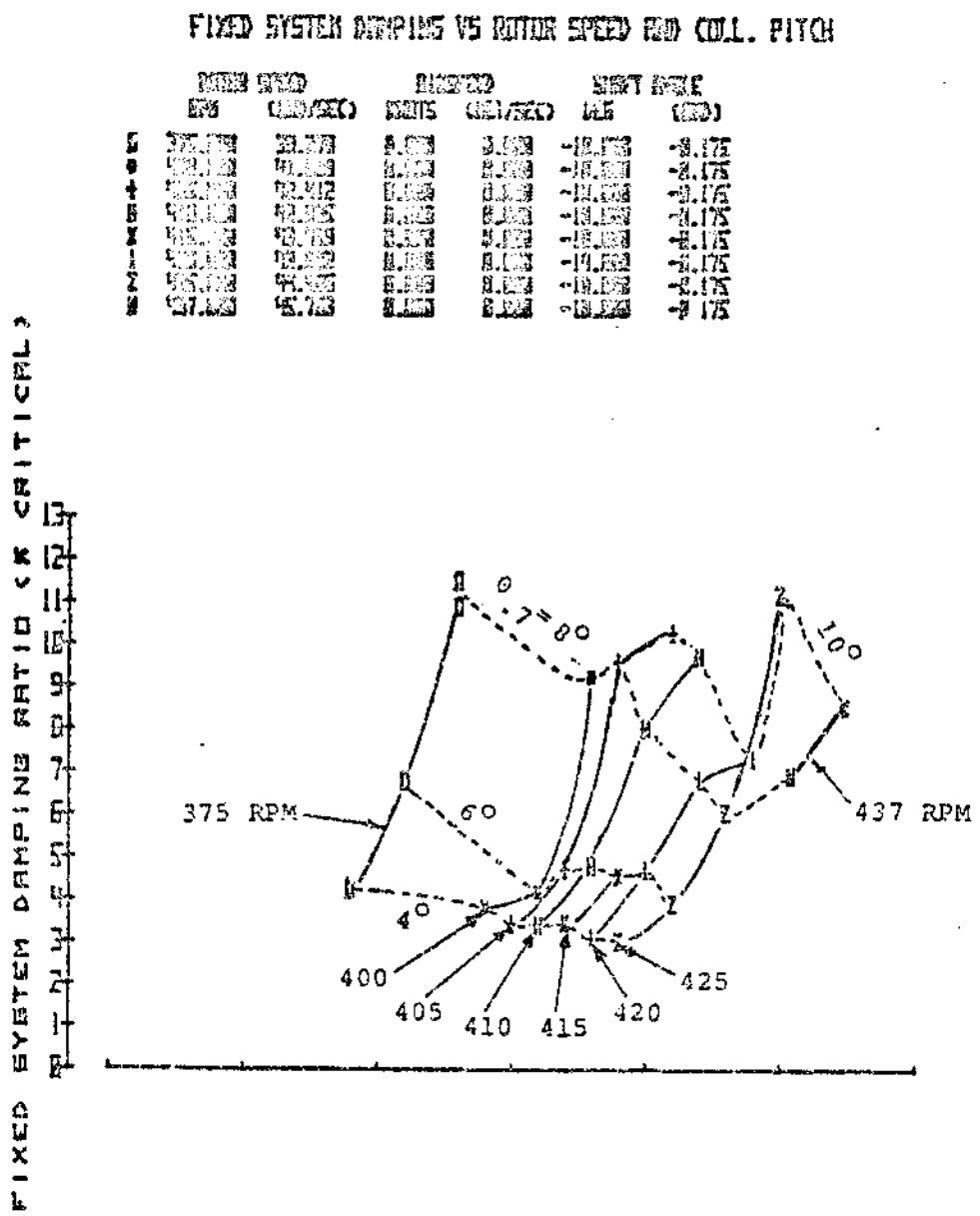

FIGURE 8.10 HOVER - FIXED SYSTEM DAMPING VS ROTOR SPEED AND COLLECTIVE PITCH - NONZERO CYCLIC - BASELINE CONFIGURATION

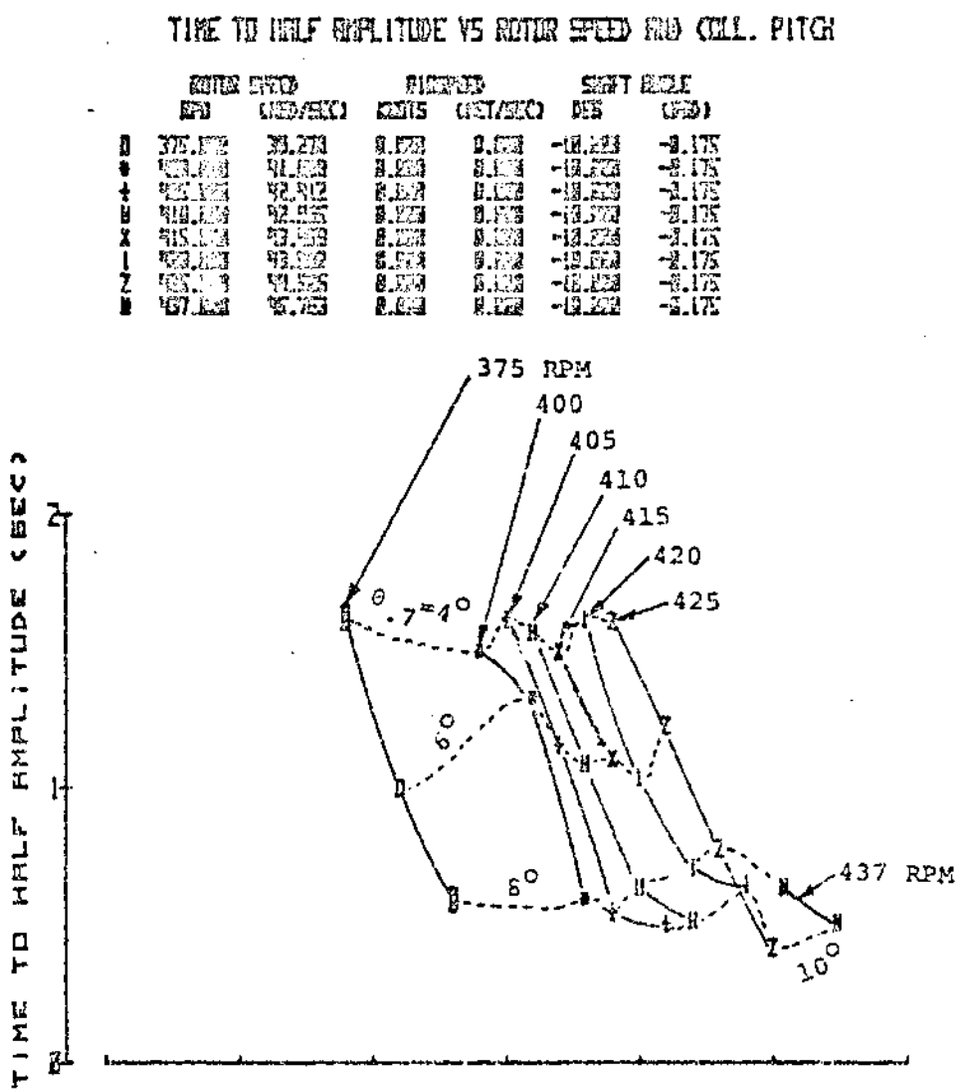

FIGURE 8.11 HOVER - TIME TO HALF AMPLITUDE VS ROTOR SPEED AND COLLECTIVE PITCH - NONZERO CYCLIC - BASELINE CONFIGURATION

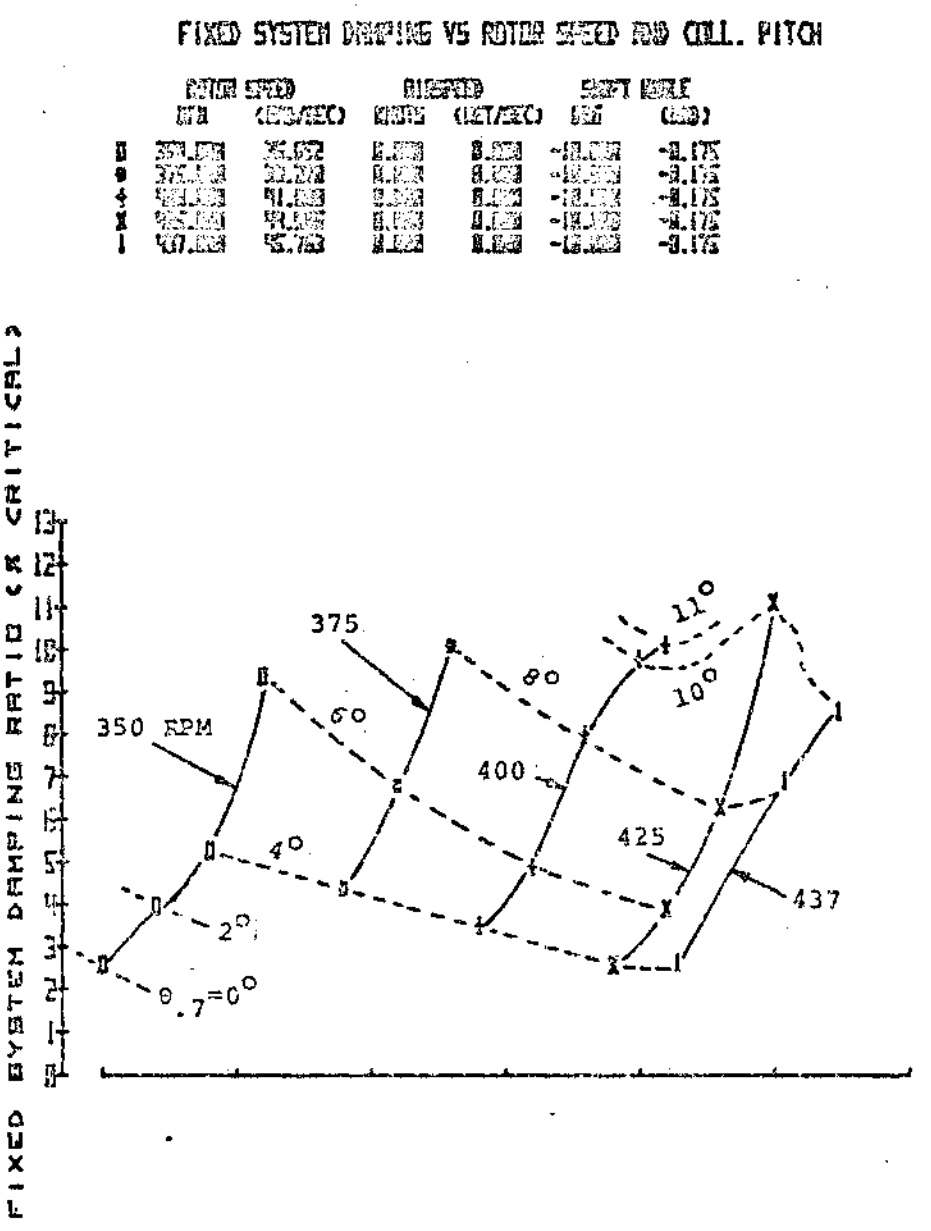

FIGURE 8.12 HOVER - SUMMARY OF FIXED SYSTEM DAMPING DATA VS ROTOR SPEED AND COLLECTIVE PITCH - BASELINE CONFIGURATION

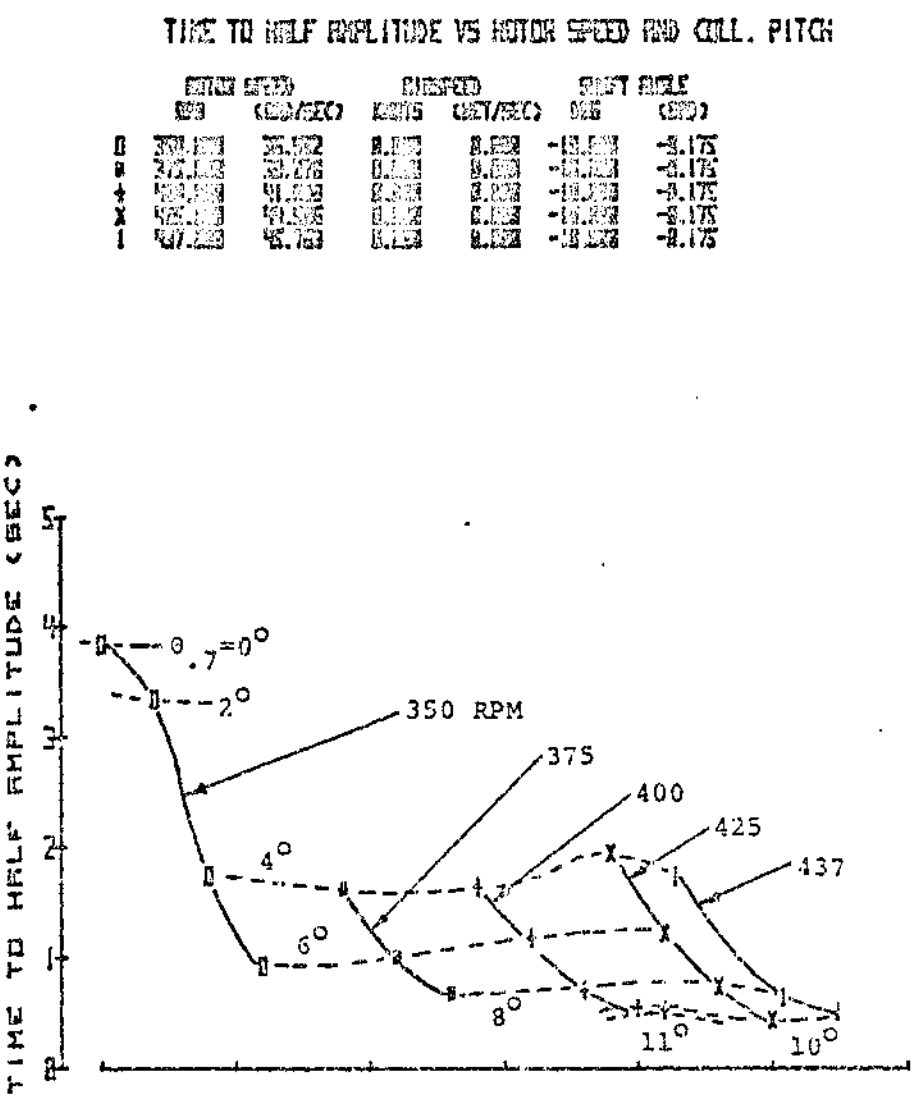

FIGURE 8.13 HOVER - SUMMARY OF TIME TO HALF AMPLITUDE DATA VS ROTOR SPEED AND COLLECTIVE PITCH - BASELINE CONFIGURATION

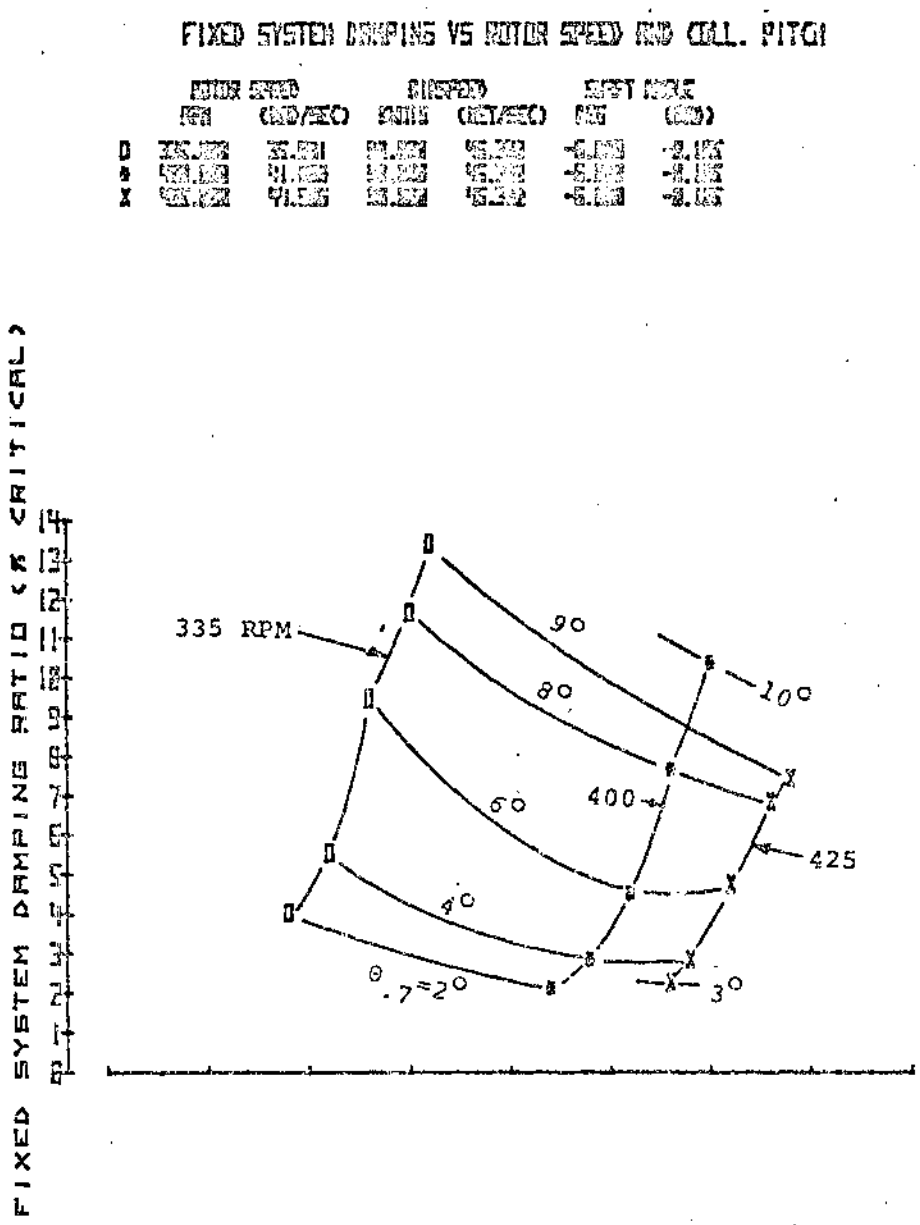

FIGURE 8.14 FIXED SYSTEM DAMPING AT 90 KNOTS VS ROTOR SPEED AND COLLECTIVE PITCH - FOR A -6 DEGREE SHAFT ANGLE - BASELINE CONFIGURATION

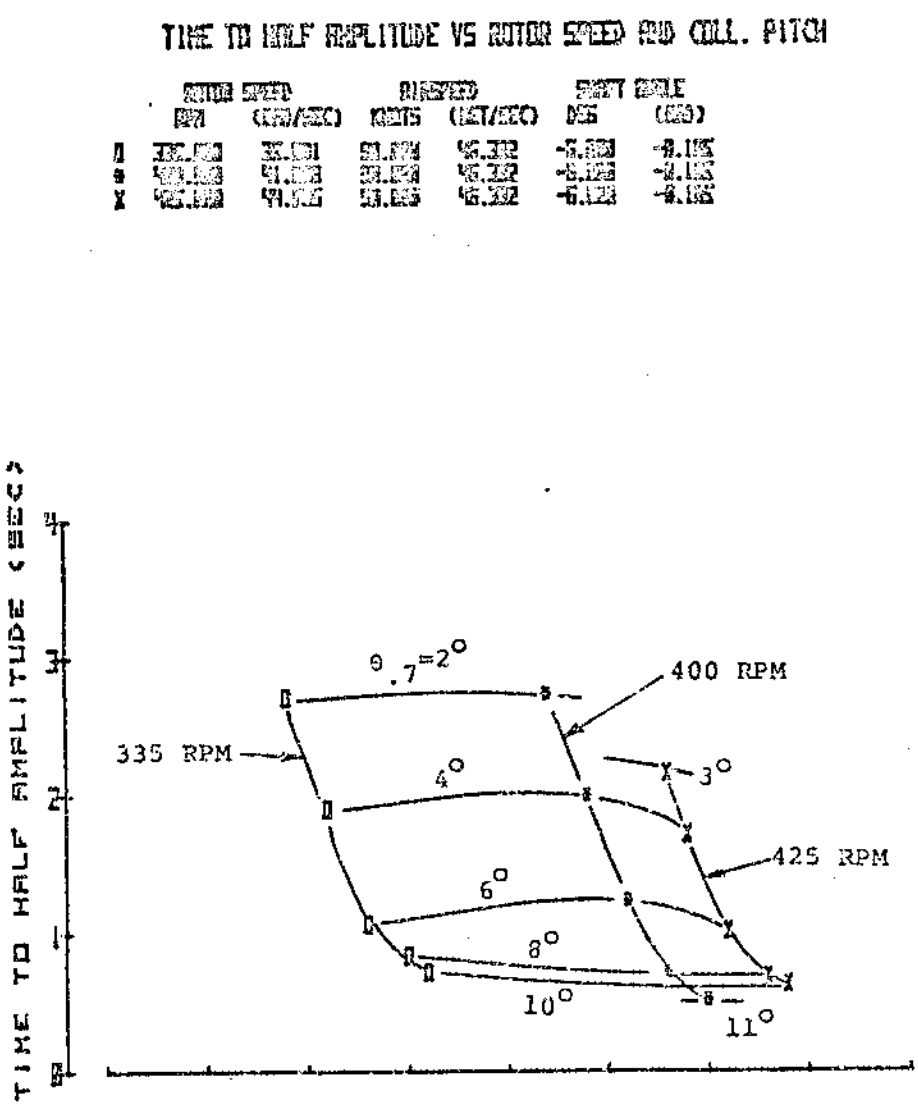

FIGURE 8.15 TIME TO HALF AMPLITUDE AT 90 KNOTS VS ROTOR SPEED AND COLLECTIVE PITCH - FOR A -6 DEGREE SHAFT ANGLE - BASELINE CONFIGURATION

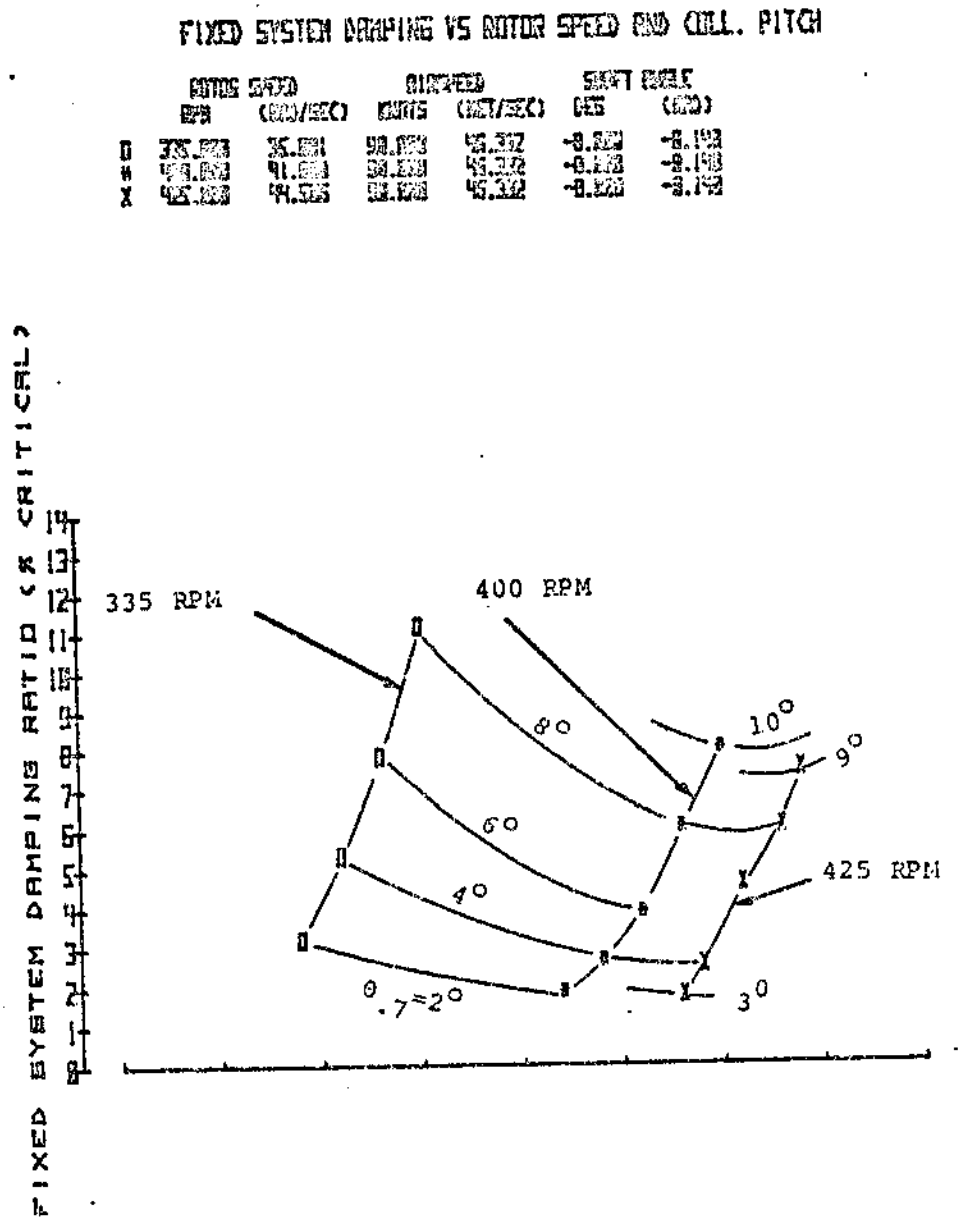

FIGURE 8.16 FIXED SYSTEM DAMPING AT 90 KNOTS VS ROTOR SPEED AND COLLECTIVE PITCH FOR A -8 DEGREE SHAFT ANGLE-BASELINE CONFIGURATION

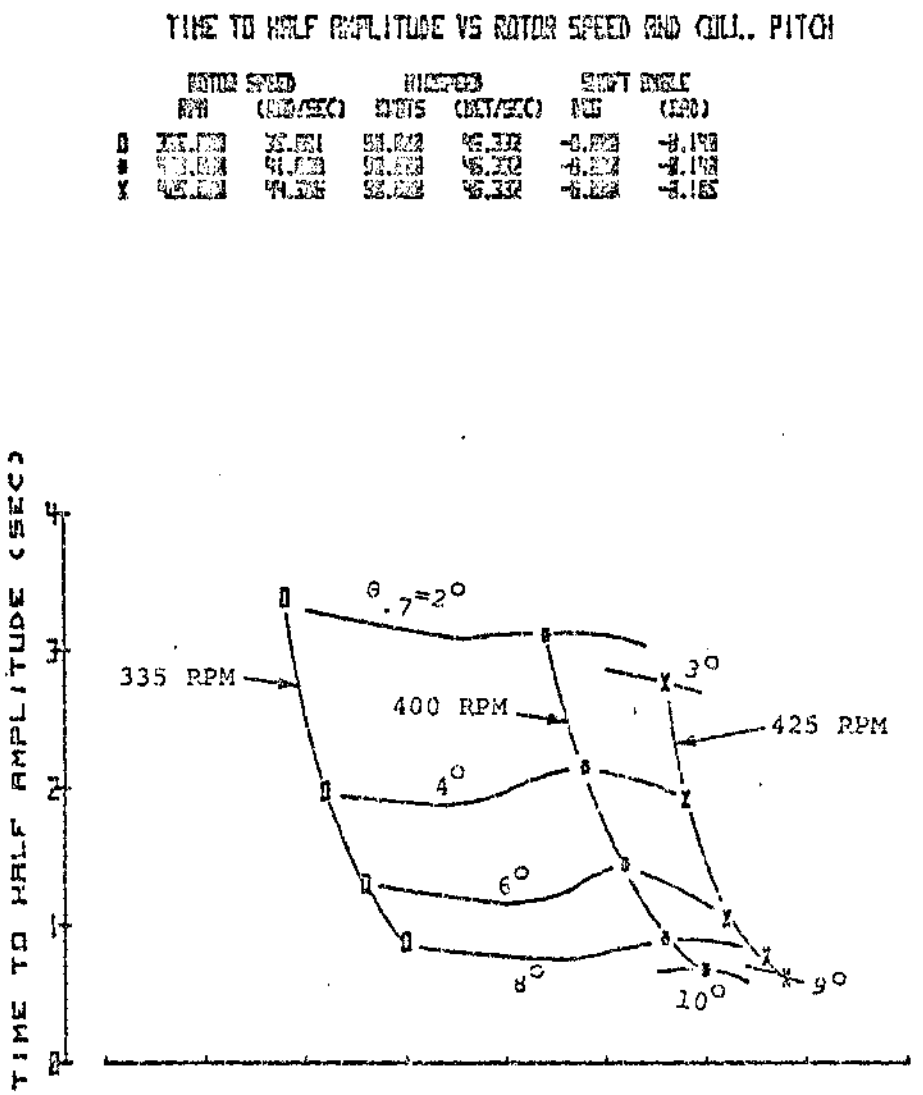

FIGURE 8.17 TIME TO HALF AMPLITUDE AT 90 KNOTS VS ROTOR SPEED AND COLLECTIVE PITCH FOR A -8 DEGREE SHAFT ANGLE-BASELINE CONFIGURATION

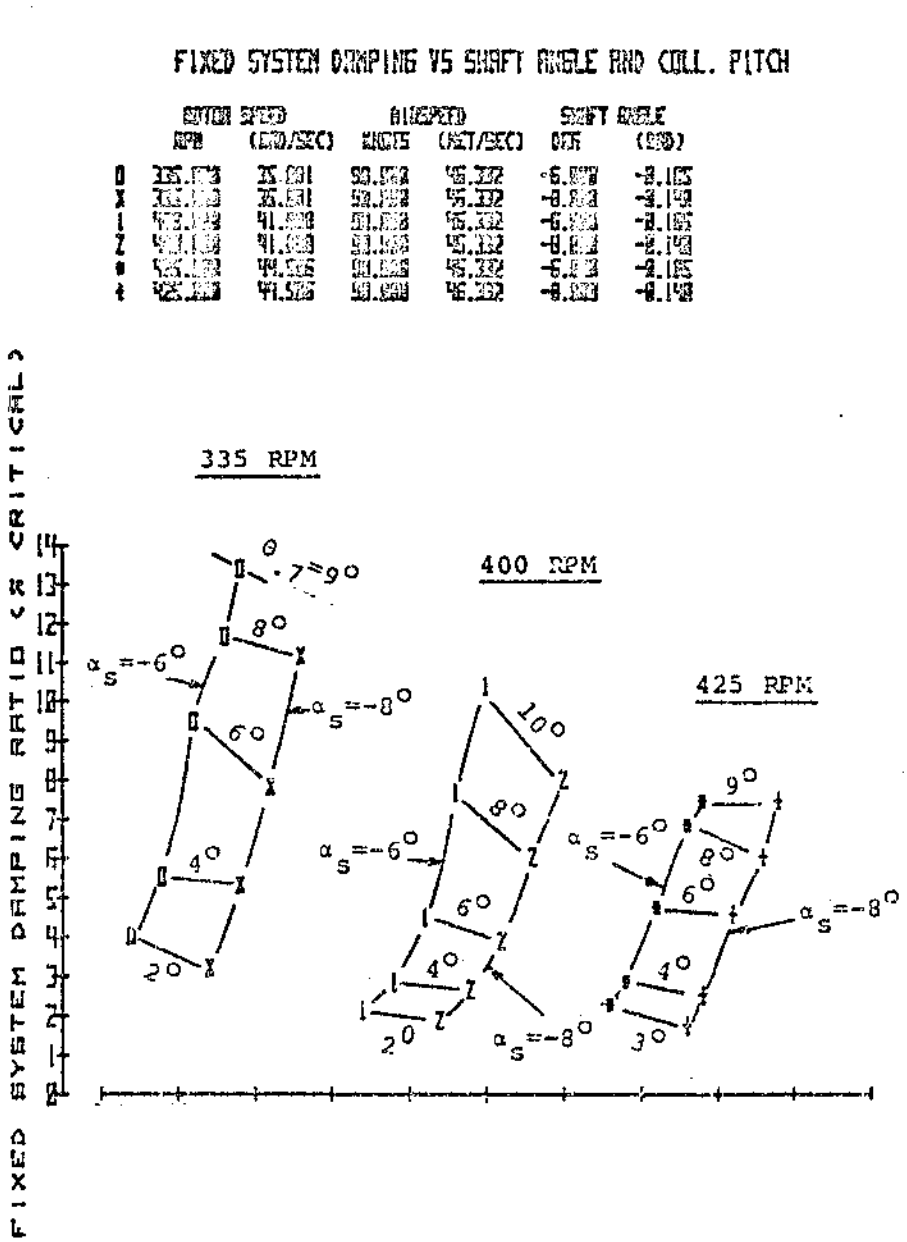

FIGURE 8.18 FIXED SYSTEM DAMPING AT 90 KNOTS VS COLLECTIVE PITCH AND SHAFT ANGLE - BASELINE CONFIGURATION

TIME TO HALF AMPLITUDE VS SHAFT ANGLE AND COLL. PITCH

	ROTOR SPEED		AIRSPEED		SHAFT ANGLE	
	RPM	(RAD/SEC)	KNOTS	(FEET/SEC)	DEG	(RAD)
□	[illegible]	[illegible]	[illegible]	[illegible]	[illegible]	[illegible]
X	[illegible]	[illegible]	[illegible]	[illegible]	[illegible]	[illegible]
⊥	[illegible]	[illegible]	[illegible]	[illegible]	[illegible]	[illegible]
Z	[illegible]	[illegible]	[illegible]	[illegible]	[illegible]	[illegible]
⊕	[illegible]	[illegible]	[illegible]	[illegible]	[illegible]	[illegible]
+	[illegible]	[illegible]	[illegible]	[illegible]	[illegible]	[illegible]

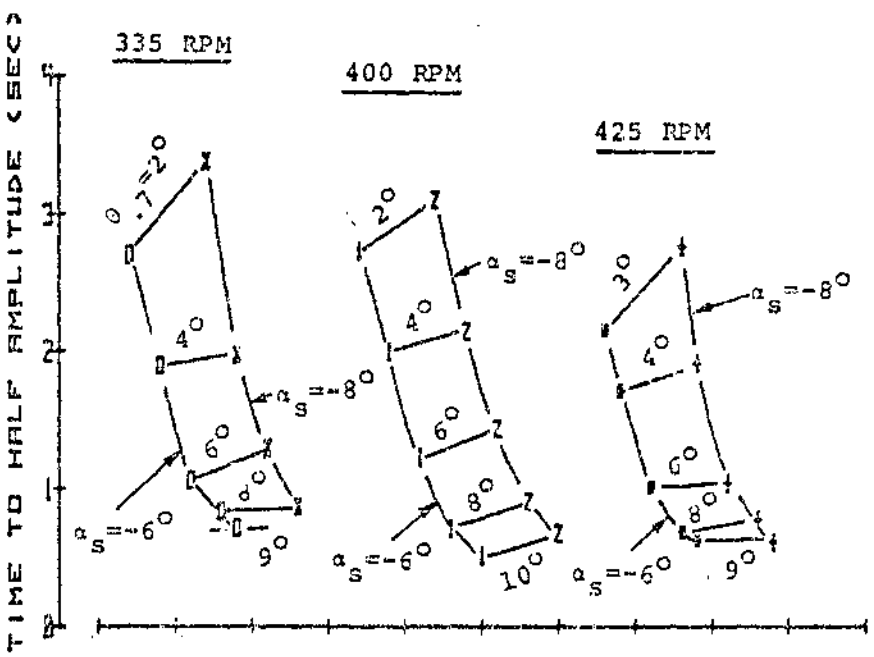

FIGURE 8.19 TIME TO HALF AMPLITUDE AT 90 KNOTS VS COLLECTIVE PITCH AND SHAFT ANGLE - BASELINE CONFIGURATION

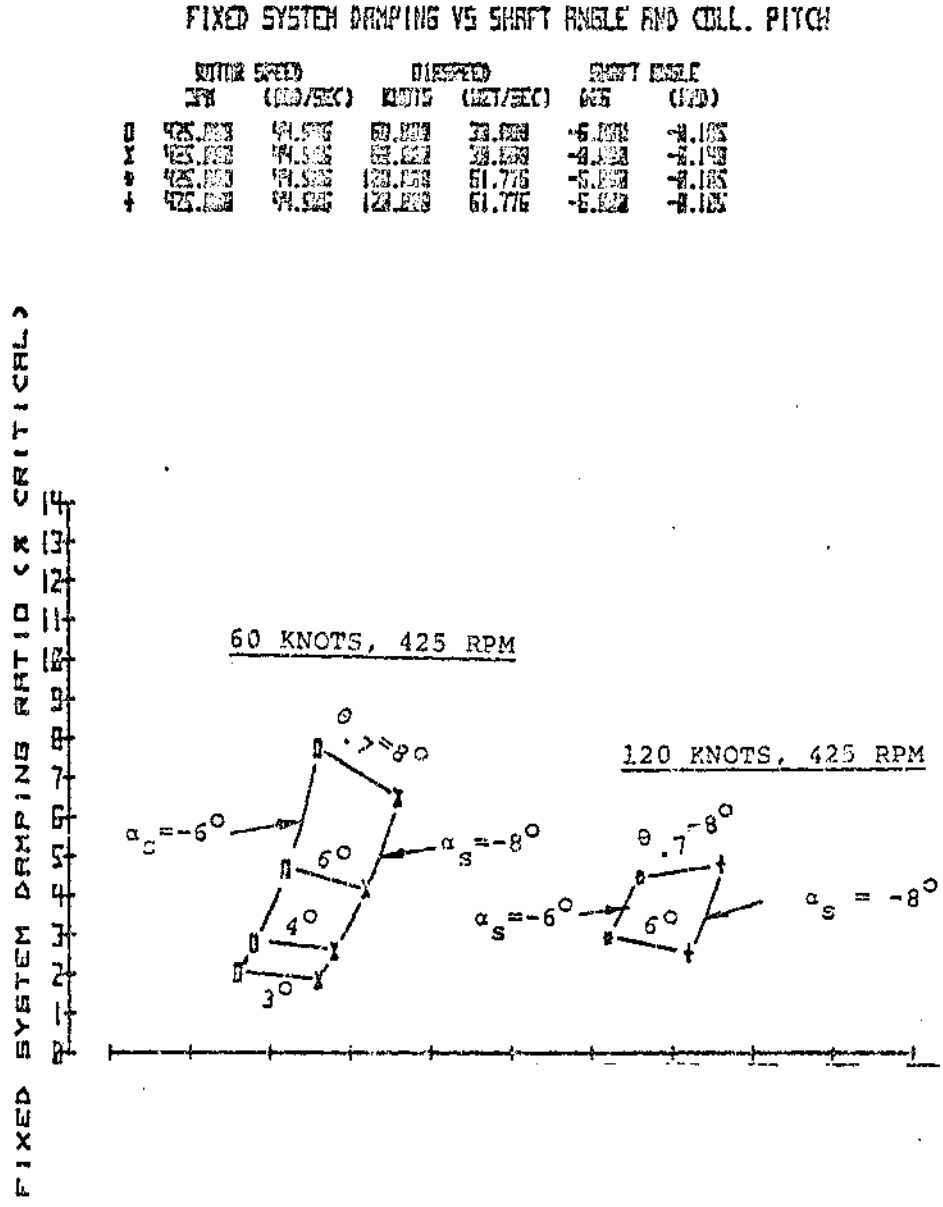

FIGURE 8.20 FIXED SYSTEM DAMPING AT 60 AND 120 KNOTS VS COLLECTIVE PITCH AND SHAFT ANGLE - BASELINE CONFIGURATION

TIME TO HALF AMPLITUDE VS SHAFT ANGLE AND COLL. PITCH

	ROTOR SPEED RPM	ROTOR SPEED (RAD/SEC)	AIRSPEED KNOTS	AIRSPEED (FEET/SEC)	SHAFT ANGLE DEG	SHAFT ANGLE (RAD)
□	[illegible]	[illegible]	[illegible]	[illegible]	[illegible]	[illegible]
X	[illegible]	[illegible]	[illegible]	[illegible]	[illegible]	[illegible]
◇	[illegible]	[illegible]	[illegible]	[illegible]	[illegible]	[illegible]
+	[illegible]	[illegible]	[illegible]	[illegible]	[illegible]	[illegible]

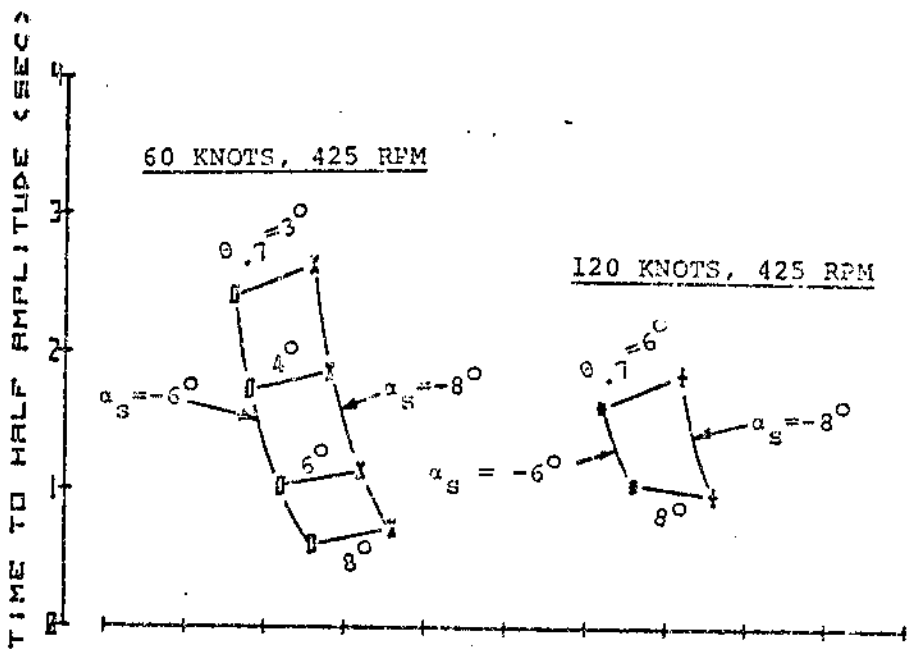

FIGURE 8.21 TIME TO HALF AMPLITUDE AT 60 AND 120 KNOTS VS COLLECTIVE PITCH AND SHAFT ANGLE - BASELINE CONFIGURATION

335, 400 and 425 rpm while data at 60 and 120 knots are for 425 rpm. Data are shown for shaft angles of -6 and -8 degrees for collective pitch values ranging from 2 to 9 degrees. Although damping does not appear to be very sensitive to shaft angle, the most dominant trend with shaft angle variation from -6 to -8 degrees is a slight decrease in damping levels (slight increase in time to half amplitude). These changes are generally near the data scatter level (estimated to be about plus or minus one half percent critical damping).

8.1.1.4 Effects of Configuration Changes

8.1.1.4.1 Effects of Varying Control Stiffness

Analytical and experimental studies have indicated that a decrease in control system stiffness would increase aeroelastic stability mode damping (References 3 and 12). The test plan called for installing a pitch link with softer axial stiffness to reduce the total control system stiffness so that the effect of control system stiffness on the BMR aeroelastic stability mode damping could be determined. As discussed in Section 3.1.5 of this report, experimental evaluation of the baseline and "soft" pitch link stiffnesses indicated that an 11 percent reduction of total control system stiffness (i.e., blade root end support total torsional stiffness) had been achieved; the total control system stiffness had been reduced from 56,680 to 50,700 in-lb/rad.

Figures 8.22 to 8.27 show comparisons of damping and time to half amplitude data obtained with the baseline and soft pitch links; these data were obtained with the Ames 40-by-80 foot wind tunnel balance dampers removed (see discussion of effects of removing balance dampers in section 8.1.1.7). Figures 8.22 and 8.23 show stability data for hover; data are shown for rotor speeds of 375, 400, and 425 rpm and collective pitch values of 4, 6, and 8 degrees. At 375, and 400 rpm, the soft pitch link configuration appears to be significantly less stable, while at 425 rpm, essentially no difference in stability is indicated.

Figures 8.24 and 8.25 show stability data at 90 knots versus rotor speed at 4 degrees collective pitch and a shaft angle of -8 degrees. Generally very little difference is indicated by stability levels in Figures 8.24 and 8.25; with perhaps a slightly lower damping level indicated for the soft pitch link configuration (i.e., the opposite of the trend indicated in hover). Figures 8.26 and 8.27 show stability data at 90 knots versus collective pitch at 425 rpm for a shaft angle of -4 degrees. As in Figures 8.24 and 8.25, the stability level appears to be lower for the soft pitch link configuration.

Damping in hover at 375 and 400 rpm appeared to be significantly increased by reducing control system stiffness. Although increased damping due to reduced control system stiffness was not confirmed by stability data at 90 knots, hover results are

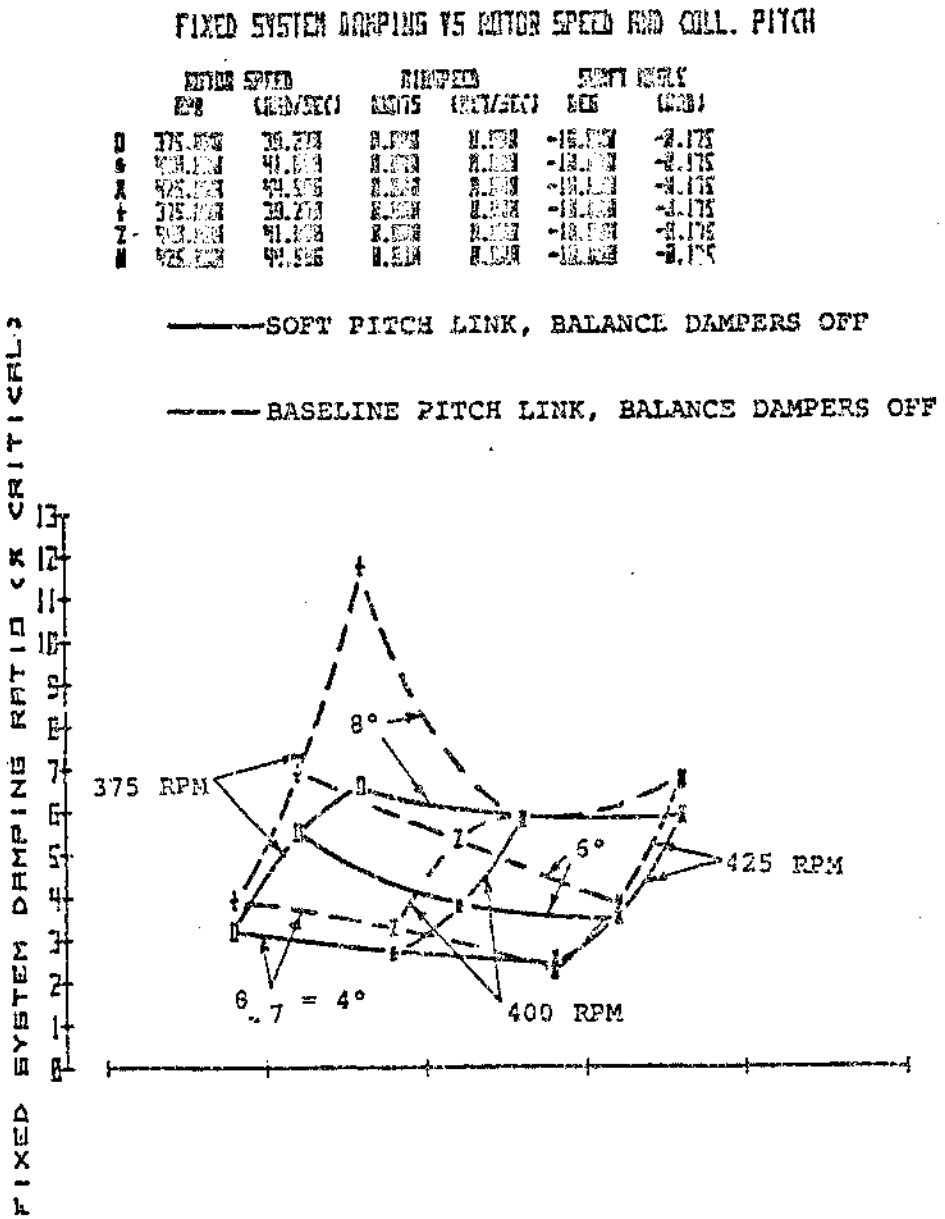

FIGURE 8.22 EFFECT OF PITCH LINK STIFFNESS - DAMPING VS ROTOR SPEED AND COLLECTIVE PITCH - HOVER

TIME TO HALF AMPLITUDE VS ROTOR SPEED AND COLL. PITCH

	[illegible] RPM	[illegible] (KNOTS)	[illegible] (KNOTS)	[illegible] (KNOTS)	[illegible] DEG	[illegible] (DEG)
D	[illegible]	[illegible]	[illegible]	[illegible]	[illegible]	[illegible]
B	[illegible]	[illegible]	[illegible]	[illegible]	[illegible]	[illegible]
A	[illegible]	[illegible]	[illegible]	[illegible]	[illegible]	[illegible]
C	[illegible]	[illegible]	[illegible]	[illegible]	[illegible]	[illegible]
Z	[illegible]	[illegible]	[illegible]	[illegible]	[illegible]	[illegible]
M	[illegible]	[illegible]	[illegible]	[illegible]	[illegible]	[illegible]

———SOFT PITCH LINK, BALANCE DAMPERS OFF

– – – –BASELINE PITCH LINK, BALANCE DAMPERS OFF

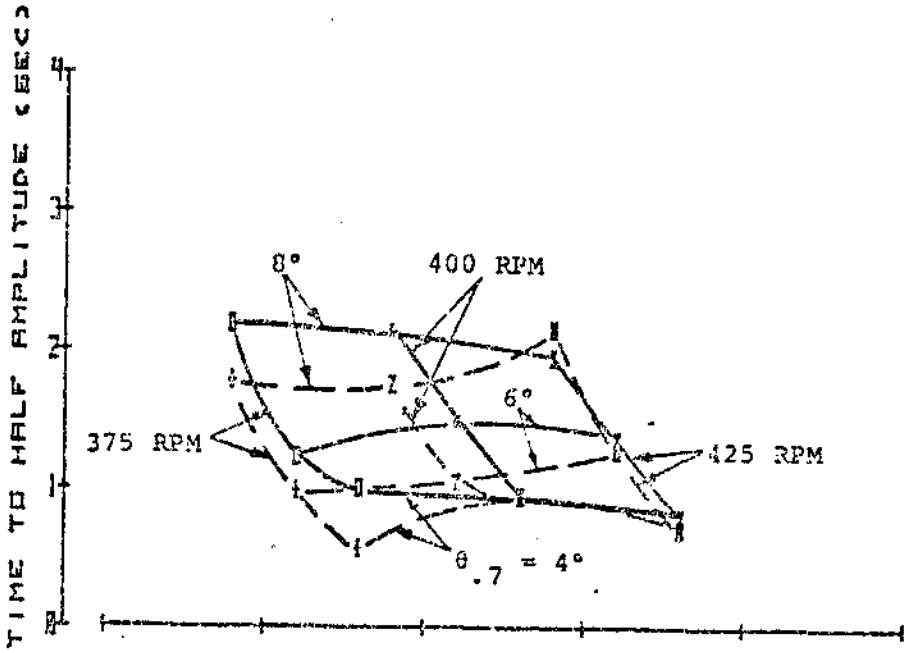

FIGURE 8.23 EFFECT OF PITCH LINK STIFFNESS - TIME TO HALF AMPLITUDE VS ROTOR SPEED - HOVER

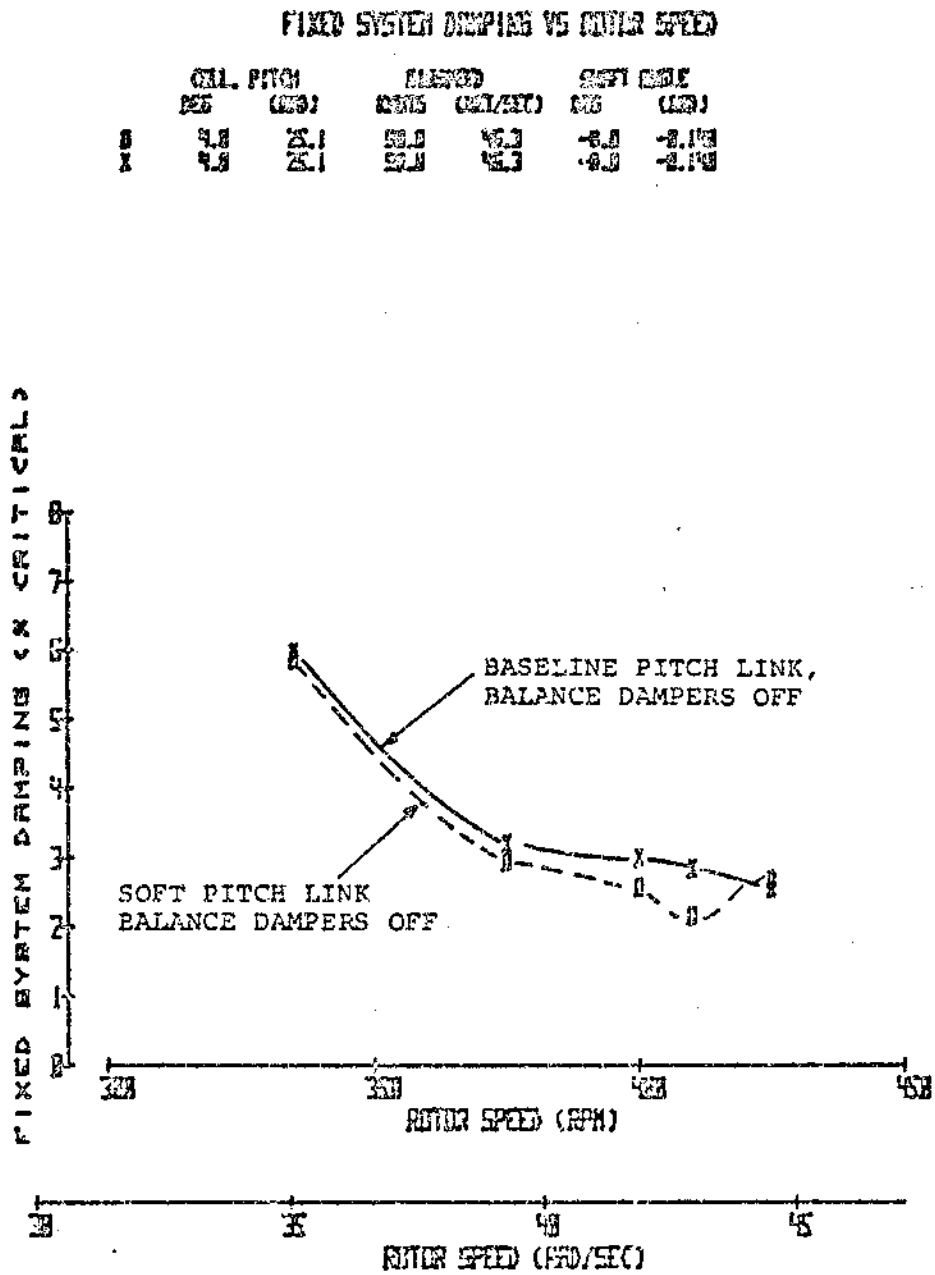

FIGURE 8.24 EFFECT OF PITCH LINK STIFFNESS - DAMPING VS ROTOR SPEED AT 90 KNOTS

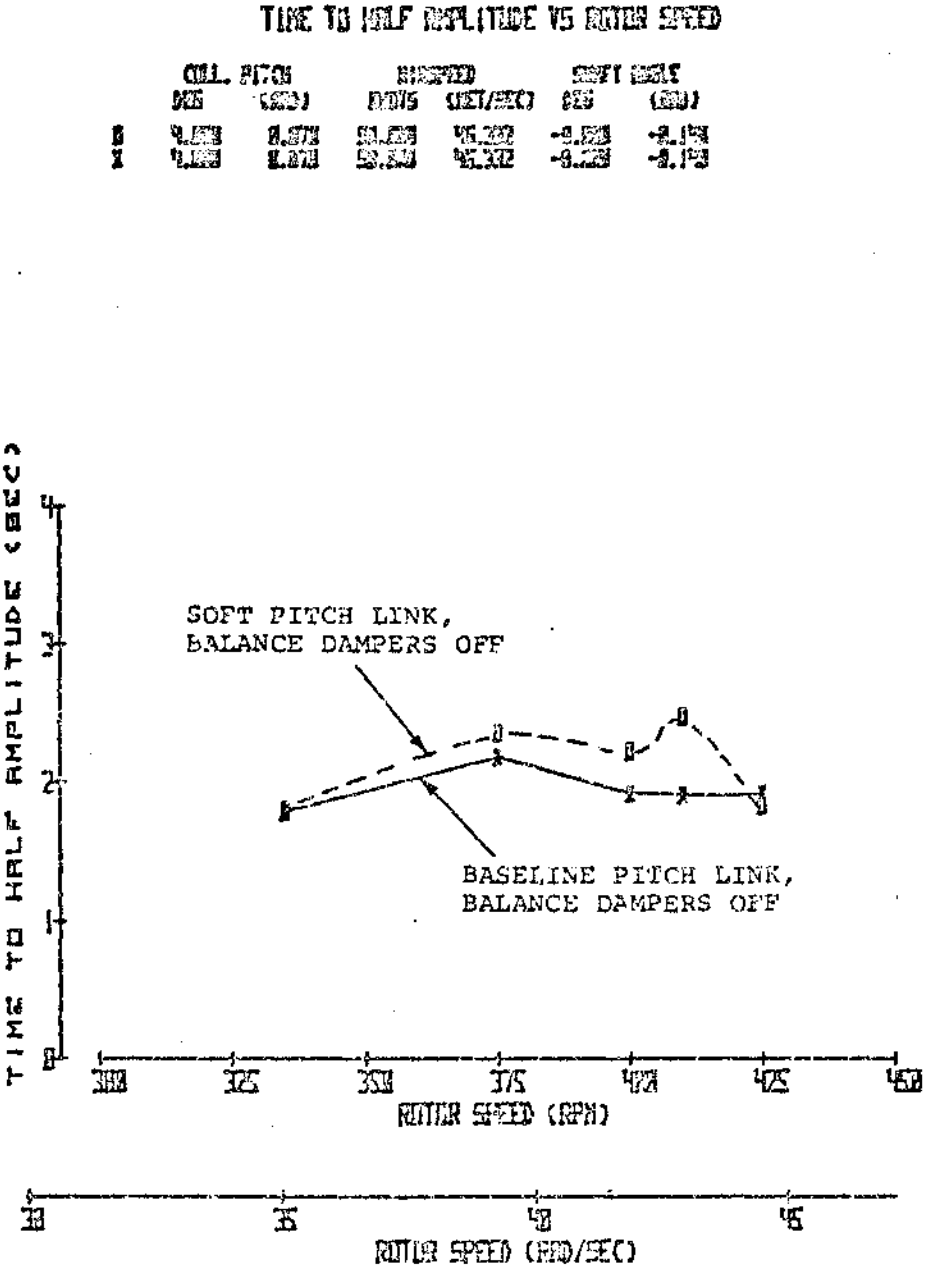

FIGURE 8.25 EFFECT OF PITCH LINK STIFFNESS - TIME TO HALF AMPLITUDE VS ROTOR SPEED AT 90 KNOTS

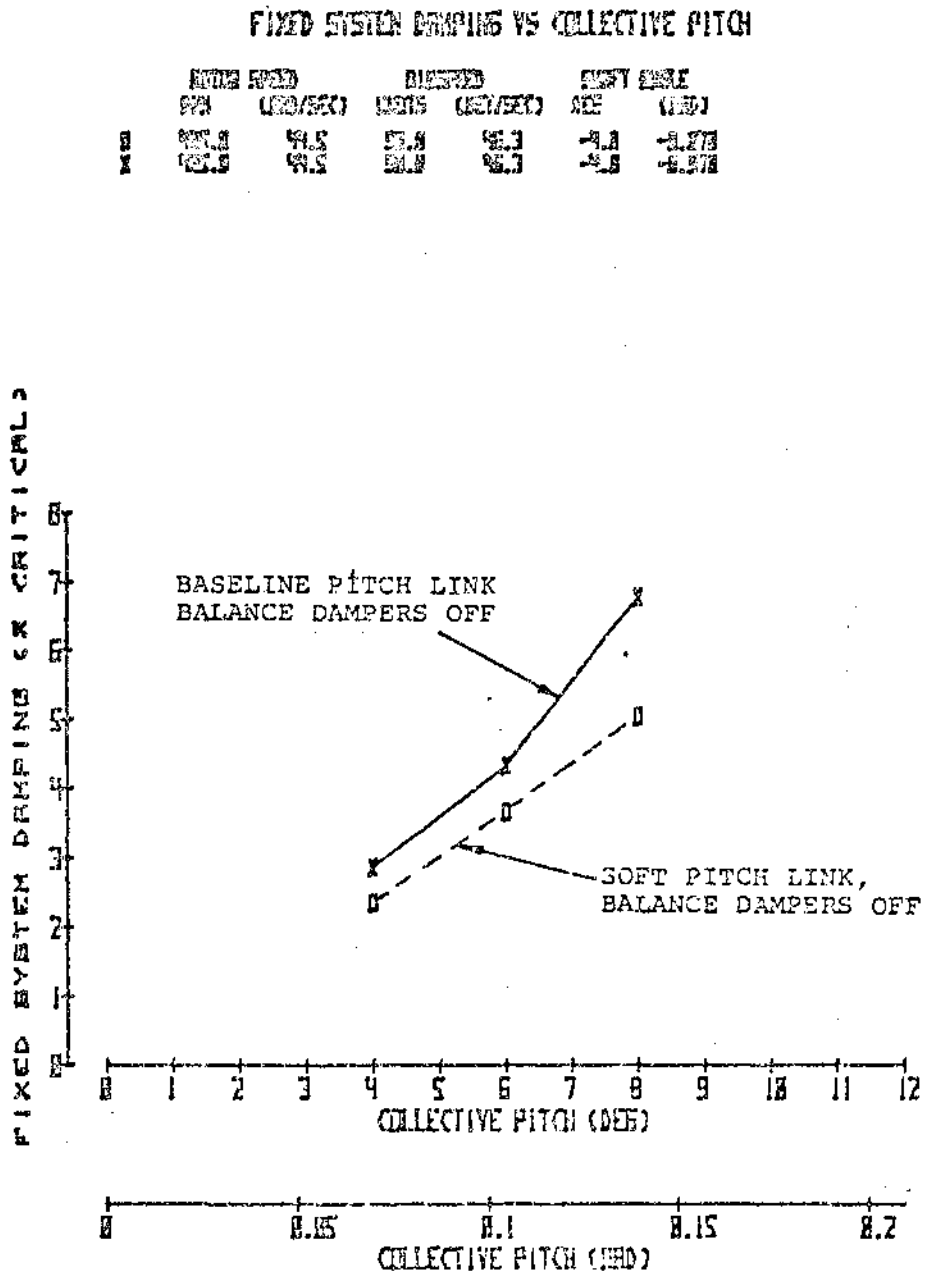

FIGURE 8.26 EFFECT OF PITCH LINK STIFFNESS - DAMPING VS COLLECTIVE PITCH AT 90 KNOTS

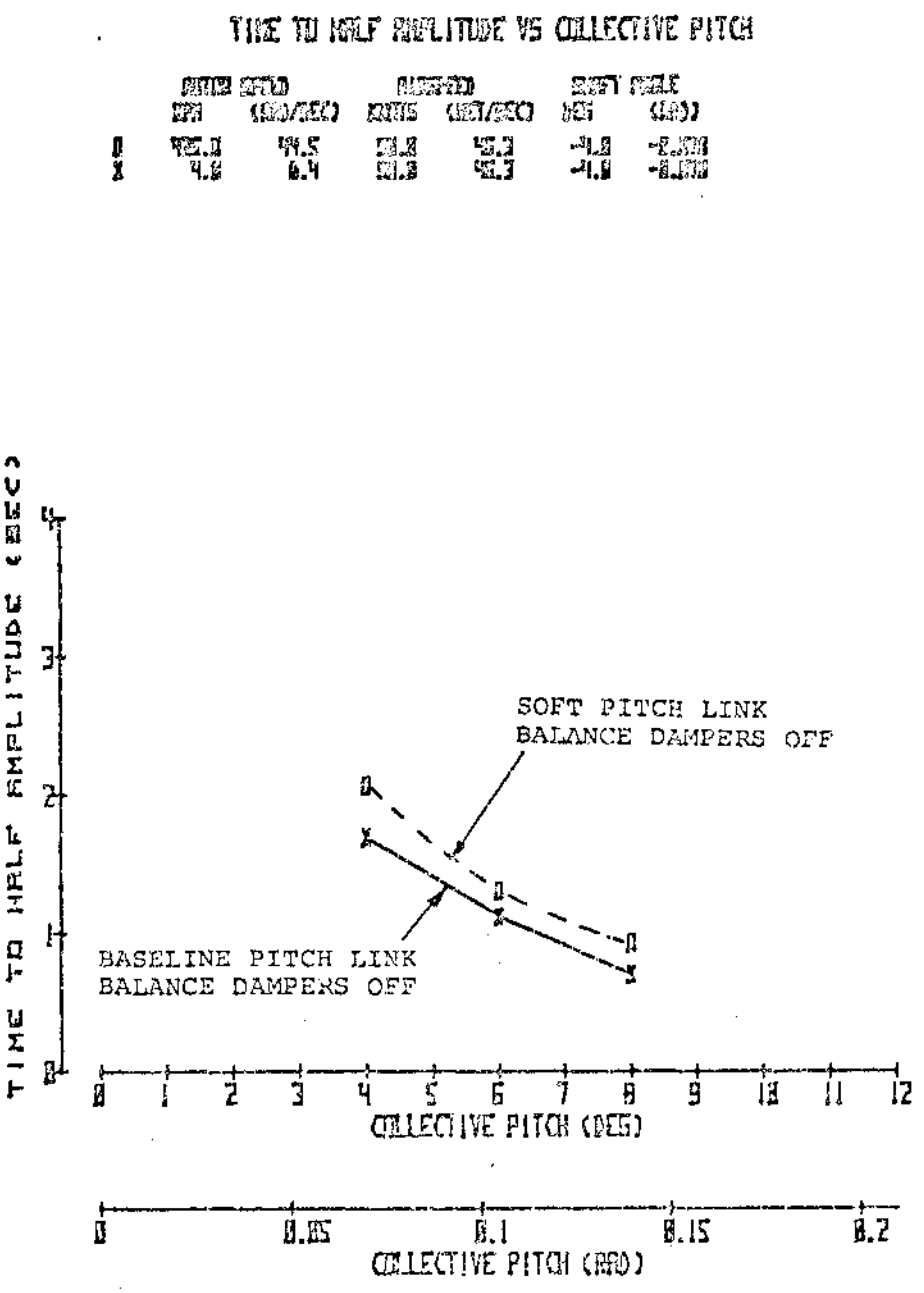

FIGURE 8.27 EFFECT OF PITCH LINK STIFFNESS - TIME TO HALF AMPLITUDE VS COLLECTIVE PITCH AT 90 KNOTS

encouraging. Additional tests are recommended where the torsional stiffness at the root end of the rotor blade is reduced to approximately 70 percent of the baseline.

8.1.1.4.2 Effect of Blade Structural Damping

The effects of adding elastomeric damping strips to the BMR open section "c" beams are shown in Figures 8.28 through 8.35. Figures 8.28 and 8.29 show stability data versus rotor speed for hover at 4 degrees collective pitch. Fixed system damping ratios are increased by about 1.5 percent critical between 375 and 425 rpm; time to half amplitude is decreased by about 0.7 seconds at 425 rpm. Figures 8.30 and 8.31 show damping data versus collective pitch at 425 rpm. Damping increases by nearly 2 and 4 percent at 4 and 8 degrees collective pitch, respectively, with the damping strips added. Figure 8.31 shows that time to half amplitude is decreased by 0.7 seconds at 4 degrees collective pitch and by lesser amounts at higher collective pitch values at 425 rpm in hover. Figures 8.32 through 8.35 show effects of added blade structural damping versus rotor speed at 90 knots for shaft angles of -6 and -8 degrees. At 425 rpm, the damping level is increased by about 1.0 and 1.5 percent critical at -6 and -8 degree shaft angles, respectively; damping is increased by larger amounts at lower rotor speeds. Time to half amplitude is decreased by about 0.7 seconds.

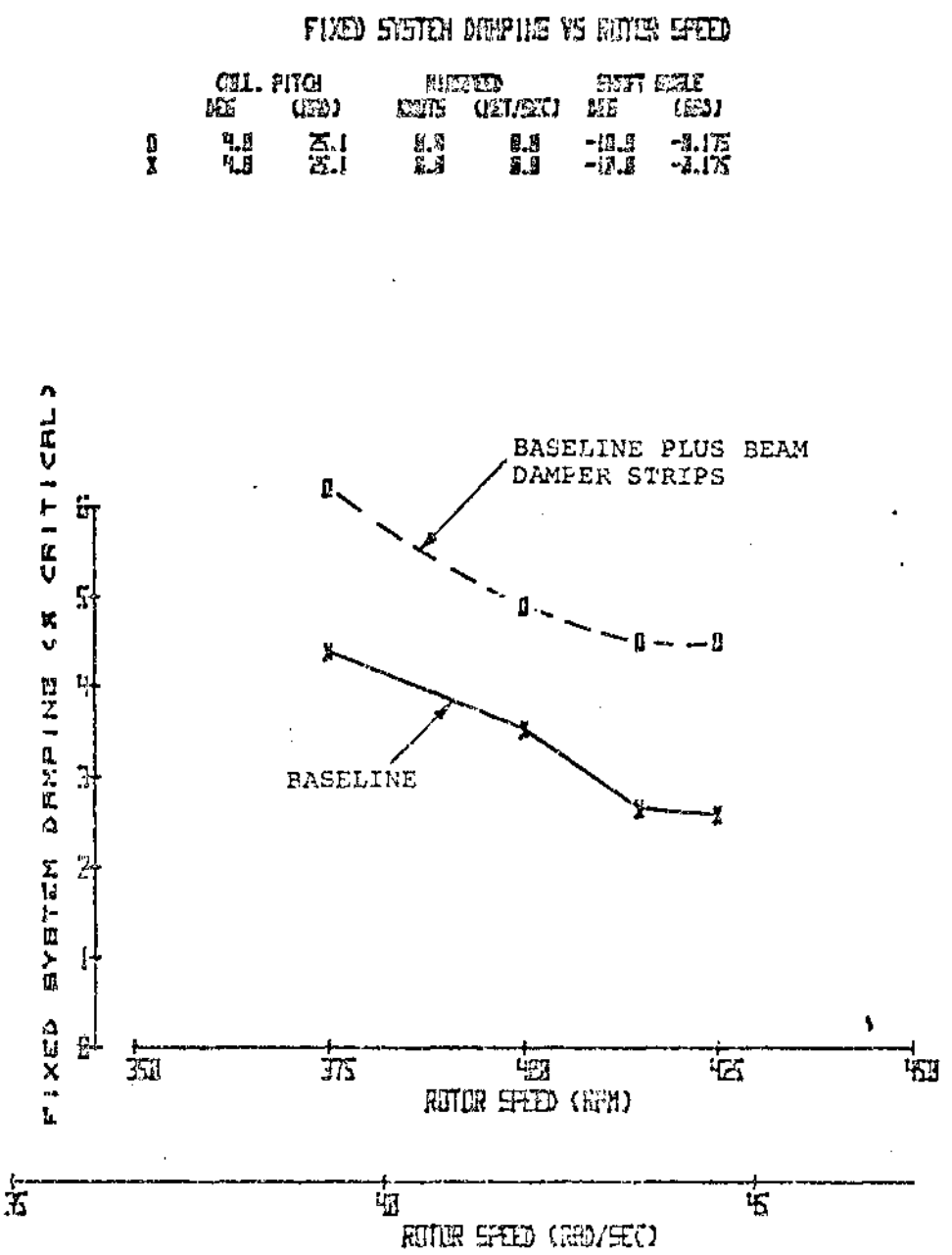

FIGURE 8.28 EFFECT OF BLADE STRUCTURAL DAMPING - DAMPING VS ROTOR SPEED - HOVER

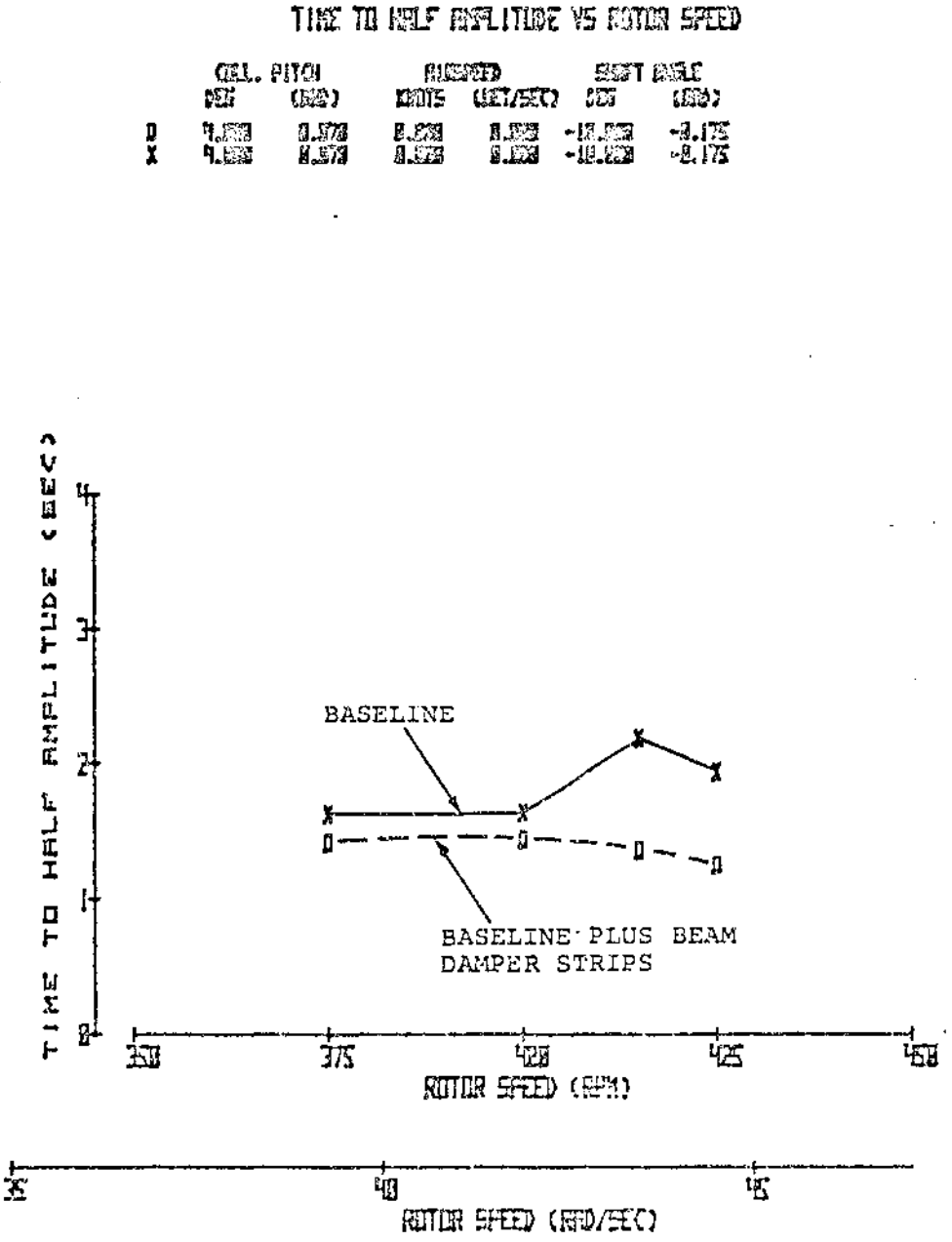

FIGURE 8.29 EFFECT OF BLADE STRUCTURAL DAMPING - TIME TO HALF AMPLITUDE VS ROTOR SPEED - HOVER

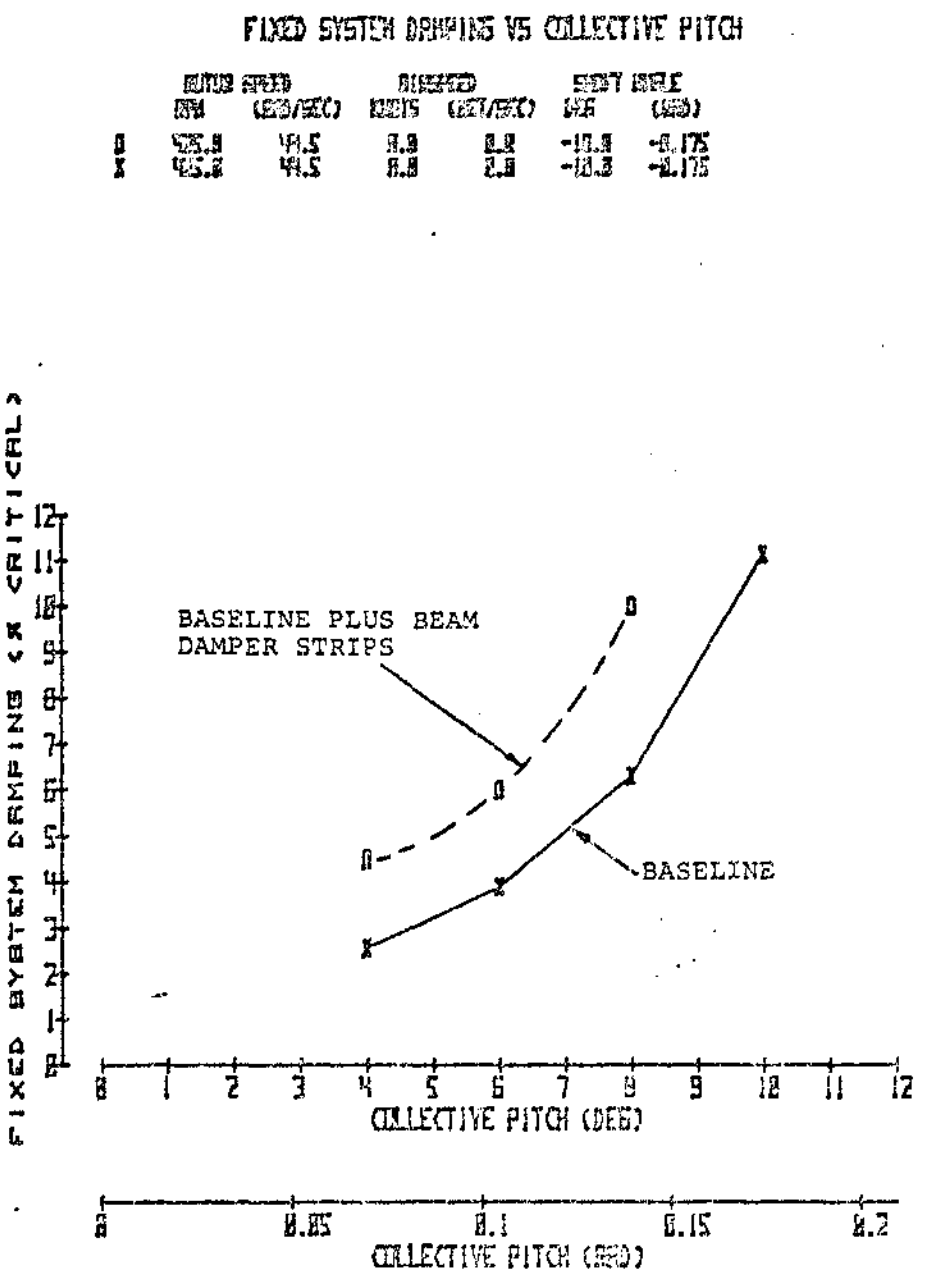

FIGURE 8.30 EFFECT OF BLADE STRUCTURAL DAMPING - DAMPING VS COLLECTIVE PITCH - HOVER

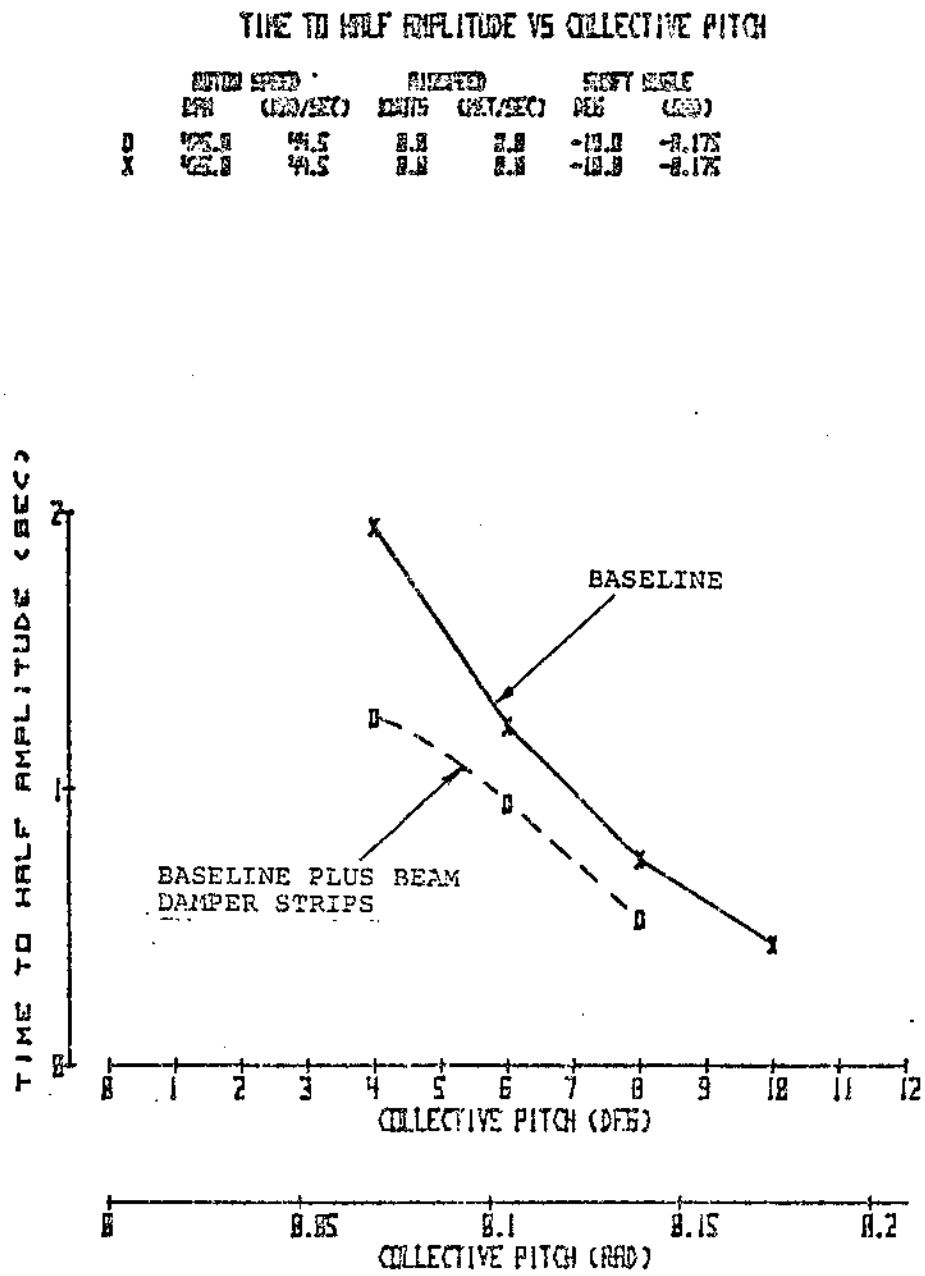

FIGURE 8.31 EFFECT OF BLADE STRUCTURAL DAMPING - TIME TO HALF AMPLITUDE VS COLLECTIVE PITCH - HOVER

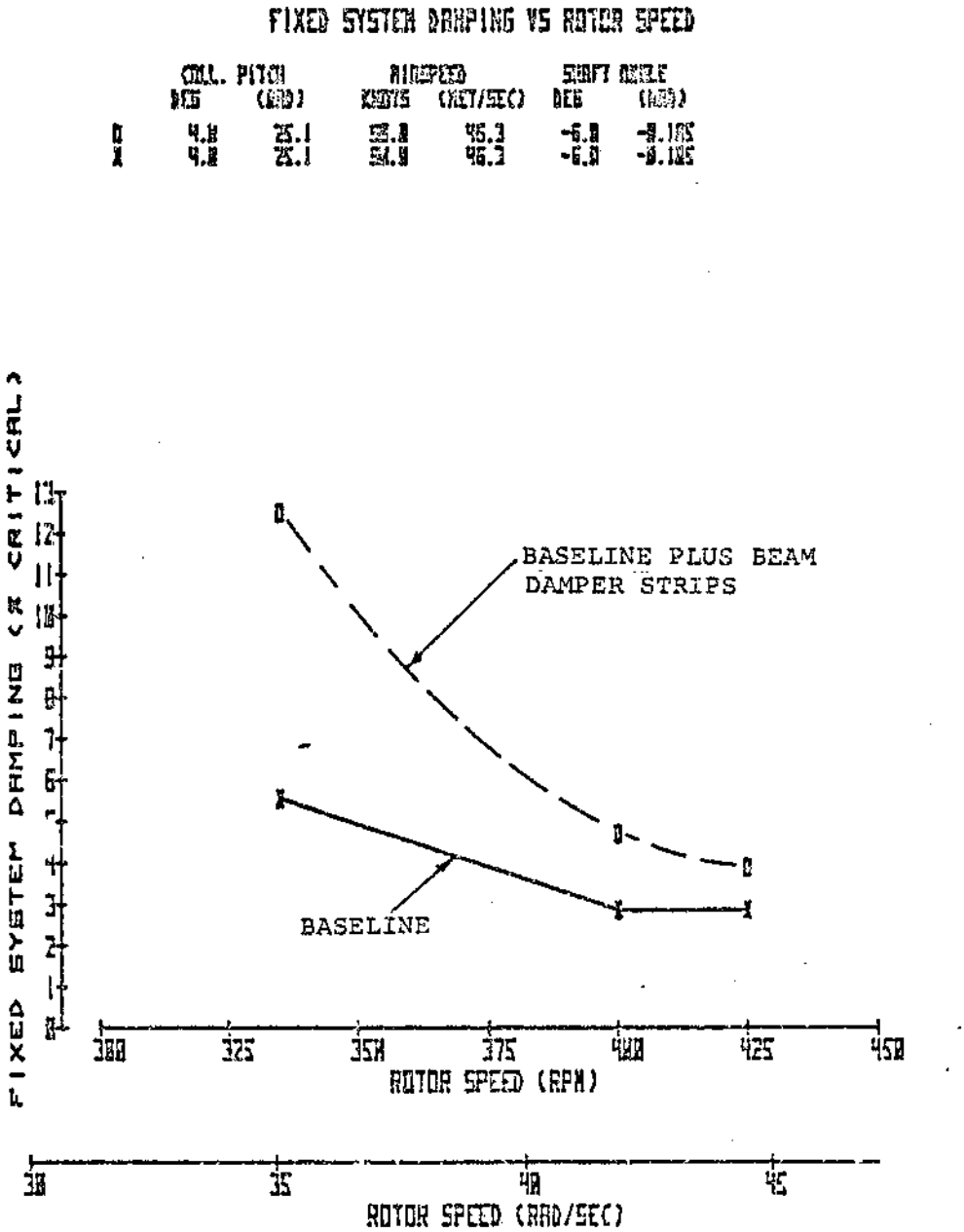

FIGURE 8.32 EFFECT OF BLADE STRUCTURAL DAMPING - DAMPING VS ROTOR SPEED AT 90 KNOTS AND -6 DEGREE SHAFT ANGLE

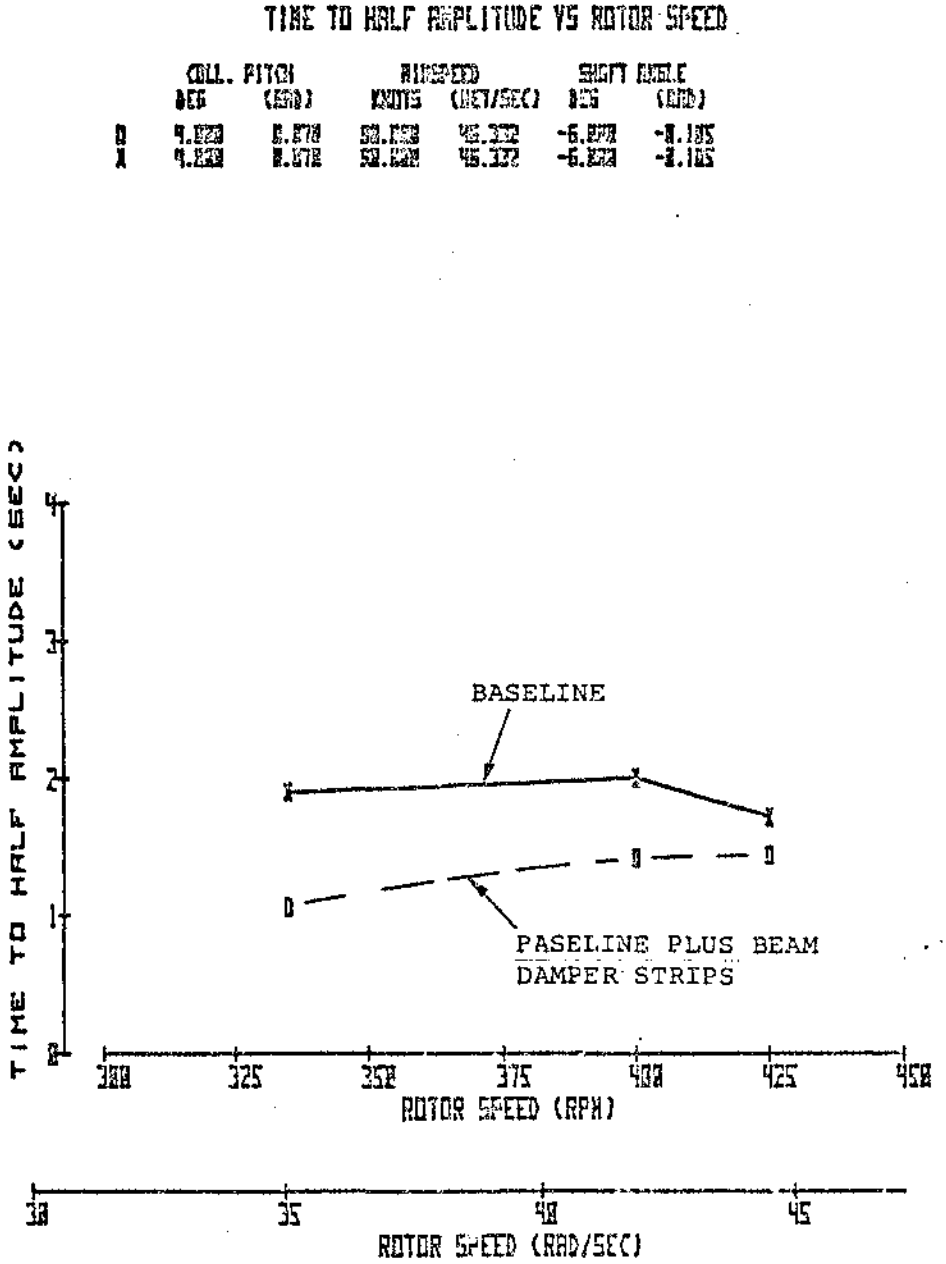

FIGURE 8.33 EFFECT OF BLADE STRUCTURAL DAMPING - TIME TO HALF AMPLITUDE VS ROTOR SPEED AT 90 KNOTS AND -6 DEGREE SHAFT ANGLE

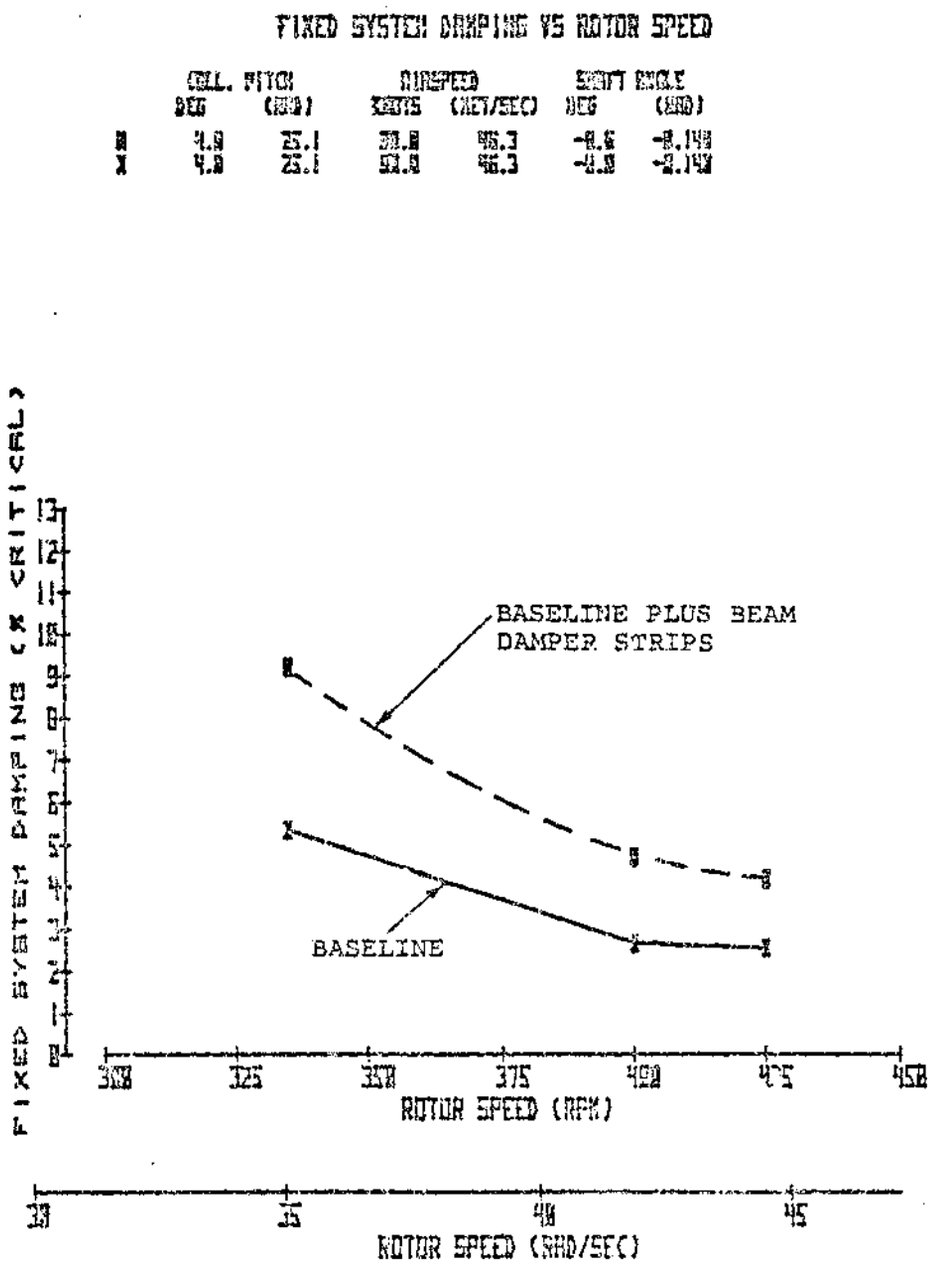

FIGURE 8.34 EFFECT OF BLADE STRUCTURAL DAMPING - DAMPING AT 90 KNOTS and -8 DEGREE SHAFT ANGLE

C-3

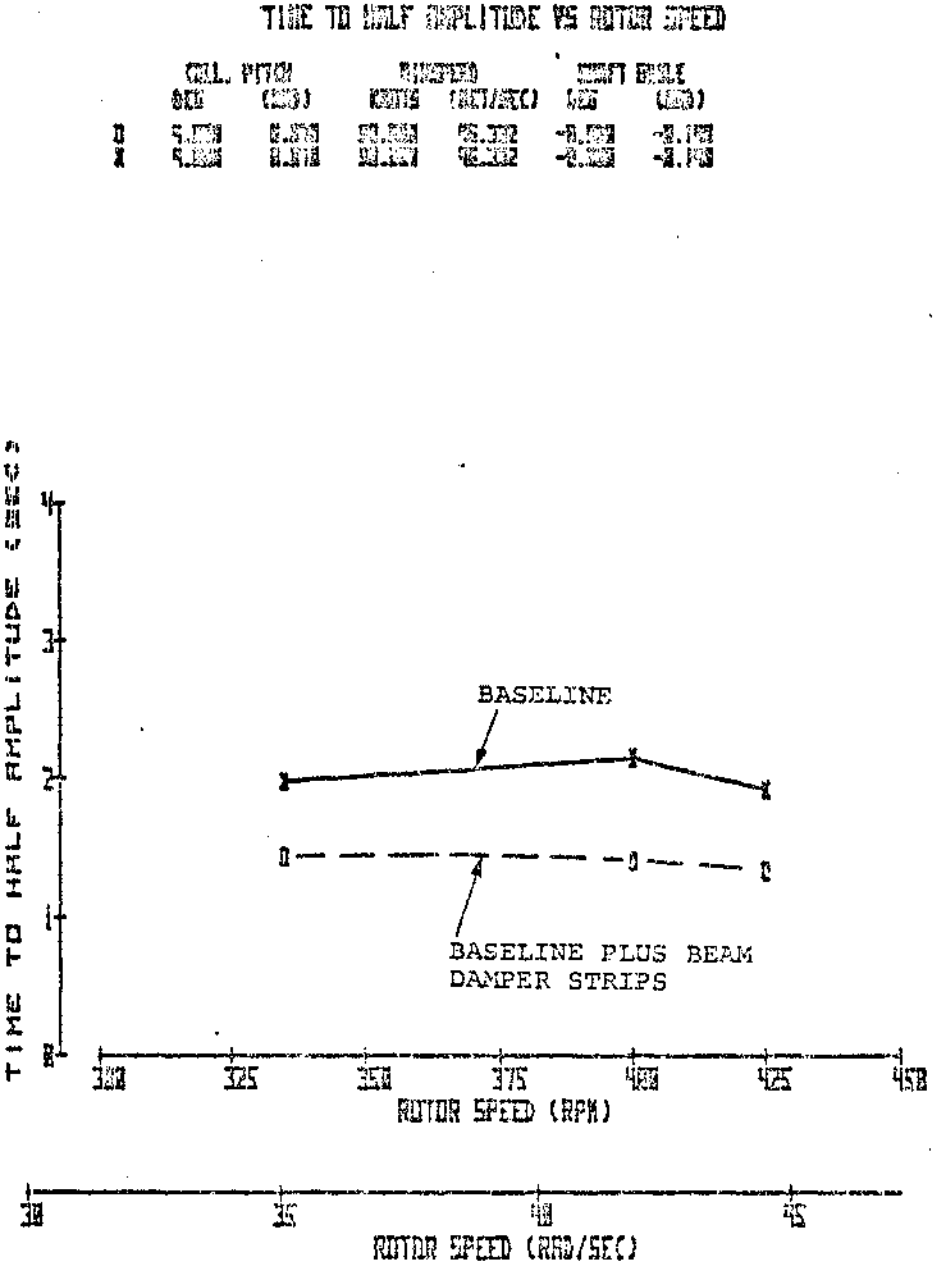

FIGURE 8.35 EFFECT OF BLADE STRUCTURAL DAMPING - TIME TO HALF AMPLITUDE AT 90 KNOTS AND -8 DEGREE SHAFT ANGLE

Adding the beam damper strips increased the first chord mode frequency slightly in addition to adding chord mode damping. Approximate frequency changes were obtained from the moving block spectral analysis frequencies. In addition, non-rotating chord mode natural frequency and damping tests were performed at Boeing Vertol after the BMR Ames wind tunnel test. Non-rotating decay test results with beam damper strips are compared with earlier Boeing Vertol BMR chord mode non-rotating damping results in Figure 8.36. For a 1.5 inch tip amplitude the chord mode damping ratio is 2.4 percent with beam damping strips added compared to 1.2 percent critical for the baseline. Figure 8.37 shows first chord mode frequency from moving block spectral analysis of beam chord bending data during the BMR Ames wind tunnel test and from Boeing Vertol non-rotating first chord mode decay tests. Frequency data for the baseline for rotating conditions are based on time histories of decays of chord bending data from Boeing Vertol whirl tower tests. The first chord mode frequency is seen to increase by about 0.3 Hz (about .04/Rev) at 425 rpm with the damper strips added.

8.1.1.5 Effect of Removing Balance Dampers

The wind tunnel balance dampers were removed to determine the effect on aeroelastic stability of the BMR/RTA. Figures 8.38 through 8.43 show effects of removing balance dampers in hover and at 90 knots. Figures 8.38 and 8.39 show hover stability data versus rotor speed at 4, 6, and 8 degrees collective pitch with and without balance dampers. The difference in stability

- BASELINE BMR

- BMR WITH DAMPER STRIPS ADDED

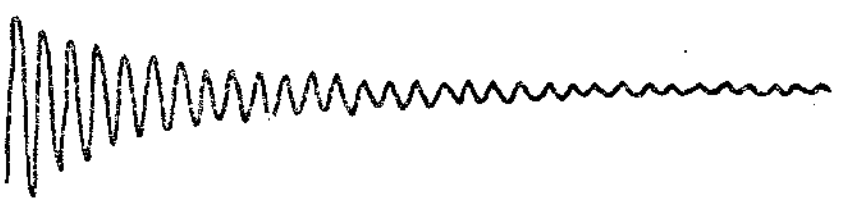

FIGURE 8.36 TYPICAL BMR NONROTATING FIRST CHORD MODE DECAY WITH AND WITHOUT FLEX BEAM DAMPER STRIPS

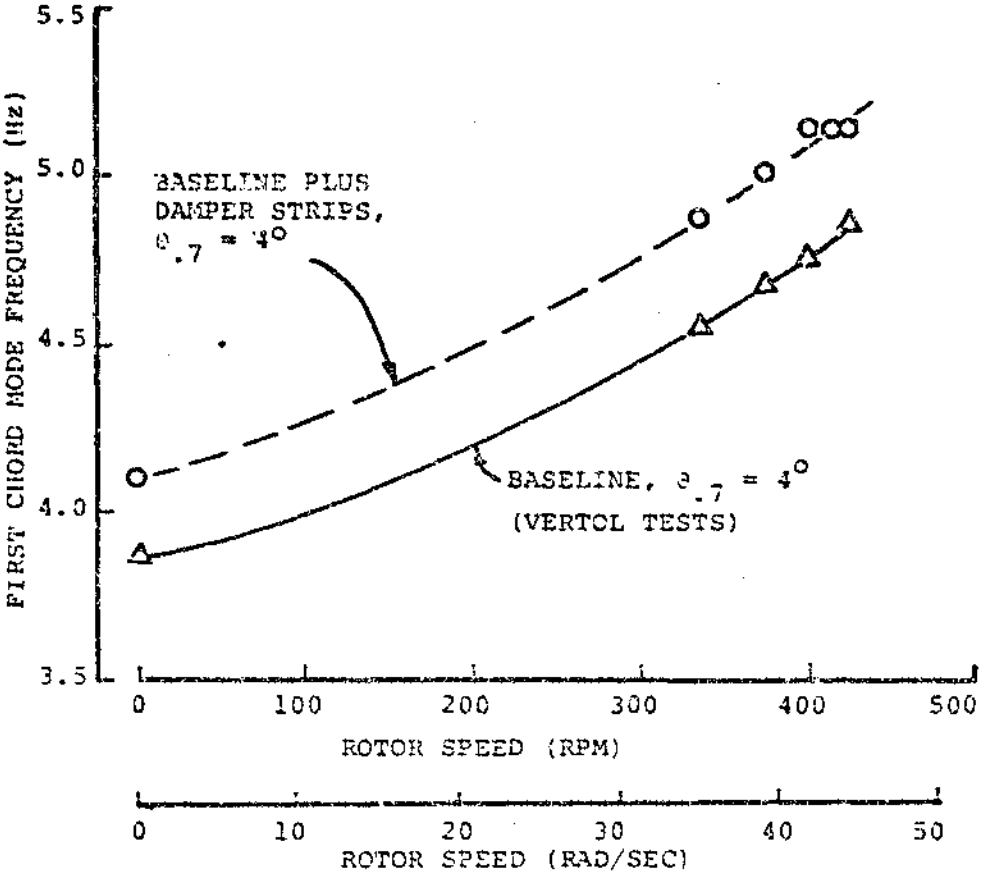

FIGURE 8.37 FIRST CHORD MODE FREQUENCY WITH AND WITHOUT DAMPER STRIPS VS ROTOR SPEED

levels appear to be due to data scatter. Figures 8.40 and 8.41 show the effects of removing balance dampers on stability versus rotor speed at 90 knots at 4 degrees collective pitch. Figures 8.42 and 8.43 show the effect of removing balance dampers on damping versus collective pitch at 425 rpm at 90 knots. Stability results in Figures 8.40 through 8.43 indicate even more strongly than hover data that no significant change in BMR/RTA aeroelastic stability occurred due to removal of the wind tunnel balance dampers.

8.1.1.6 Effects of Excitation Amplitude

The effect of excitation amplitude on the magnitude of aeroelastic stability levels determined from the test was checked, and results are presented in Figure 8.44. Cyclic excitation levels were input in terms of counts where 500 counts corresponds to approximately .75 degrees of cyclic excitation. Results for damping levels are shown in Figure 8.44 for the baseline configuration in hover at 6 degrees collective pitch and 375 rpm and for the "soft" pitch link, balance dampers off configuration at 4 degrees collective pitch and 425 rpm. These results indicate that the damping levels obtained from the test are not very sensitive to excitation magnitude for excitation levels above 100 counts. Typical excitation levels were 125 counts during stability testing.

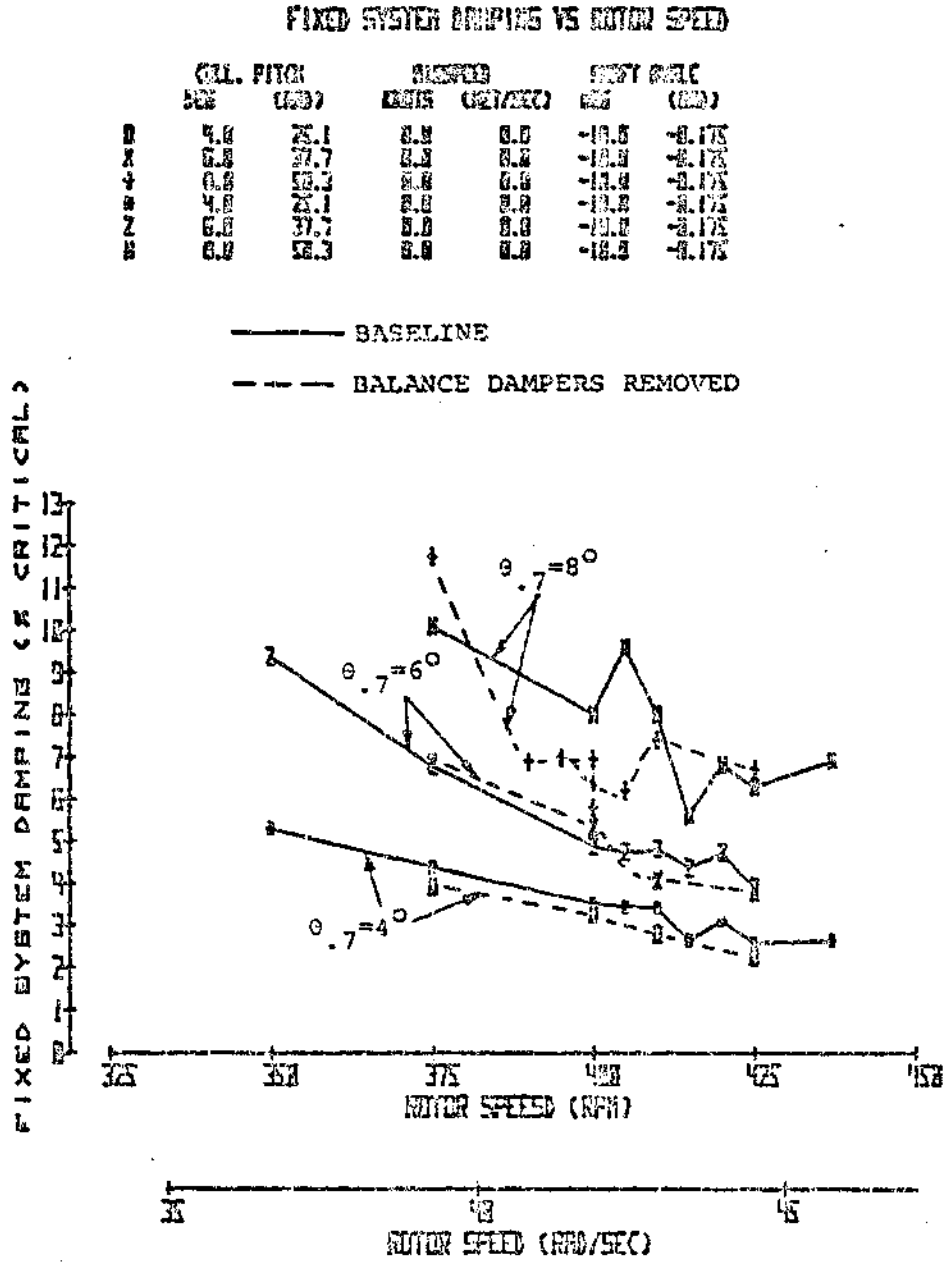

FIGURE 8.38 EFFECT OF REMOVING BALANCE DAMPERS - DAMPING VS ROTOR SPEED - HOVER

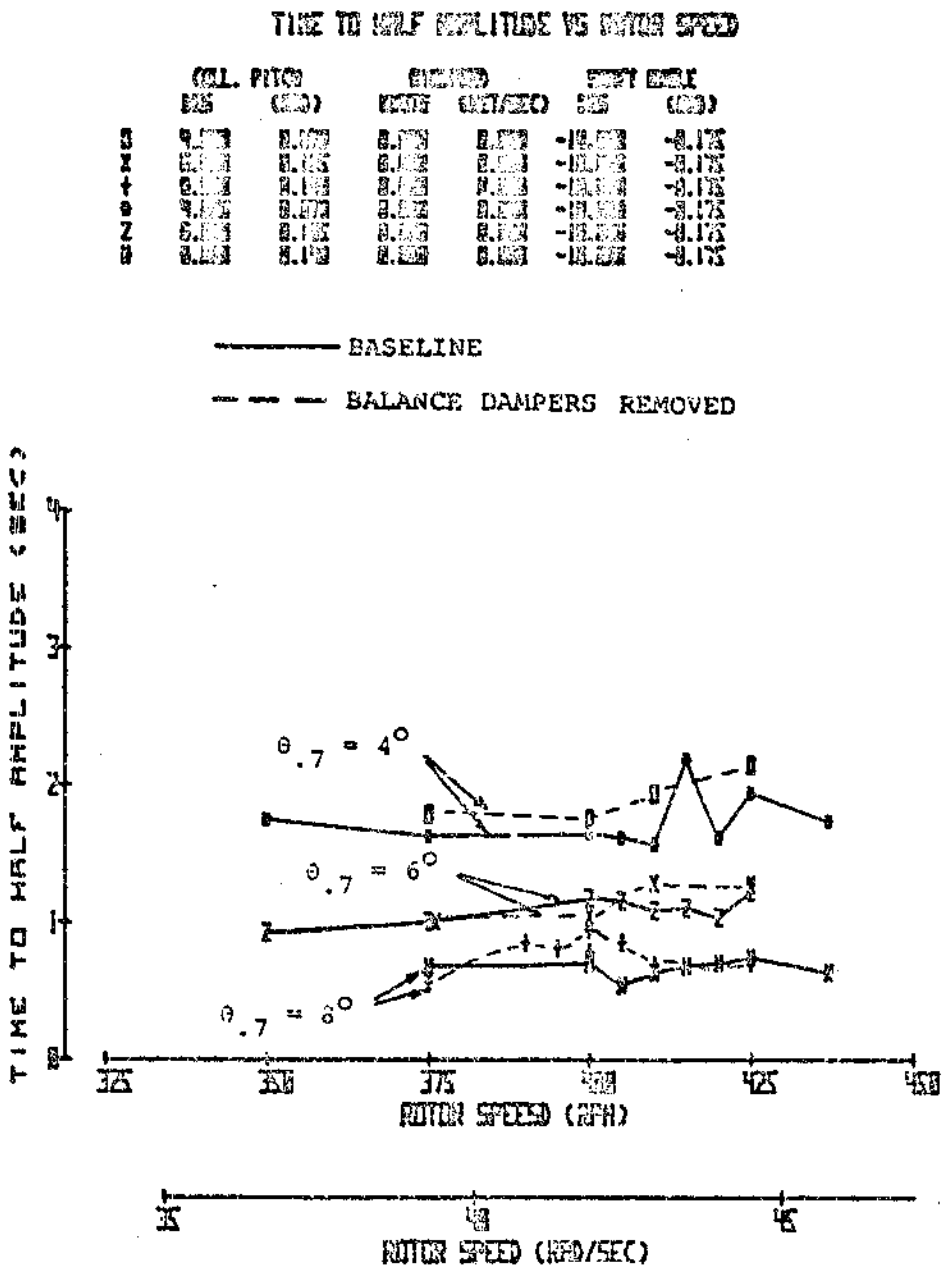

FIGURE 8.39 EFFECT OF REMOVING BALANCE DAMPERS - TIME TO HALF AMPLITUDE VS ROTOR SPEED - HOVER

FIXED SYSTEM DAMPING VS ROTOR SPEED

	COLL. PITCH DEG	(DEG)				

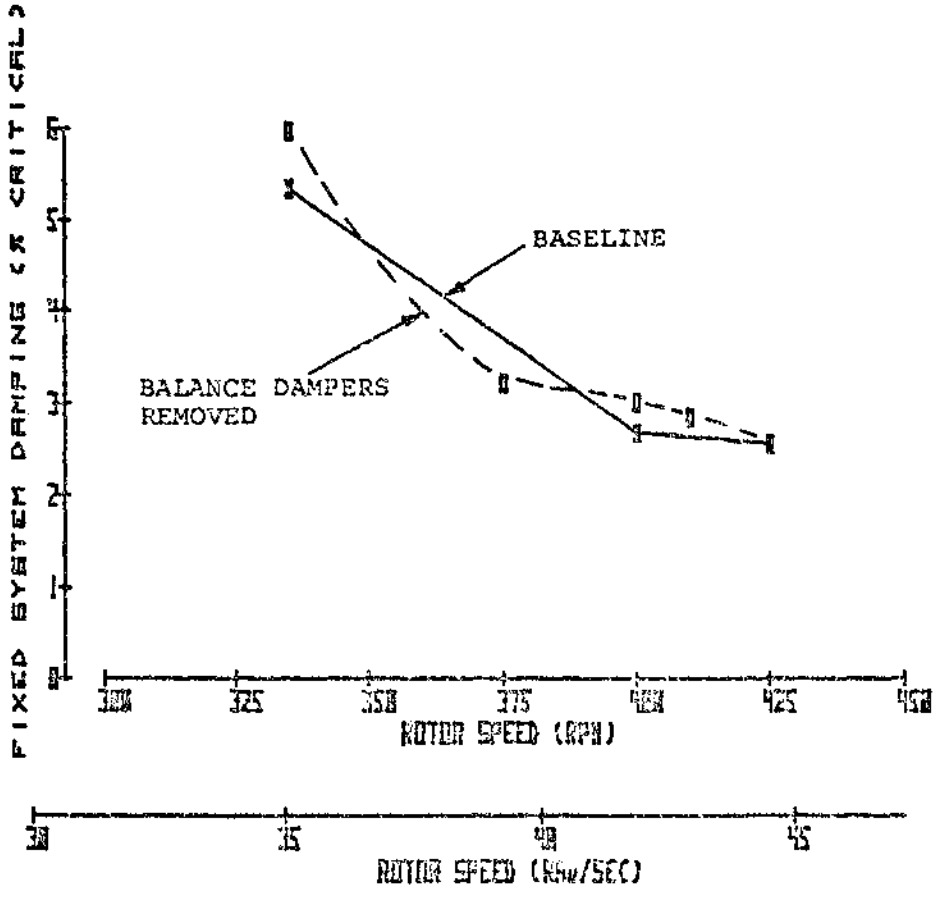

FIGURE 8.40 EFFECT OF REMOVING BALANCE DAMPERS - DAMPING VS ROTOR SPEED AT 90 KNOTS

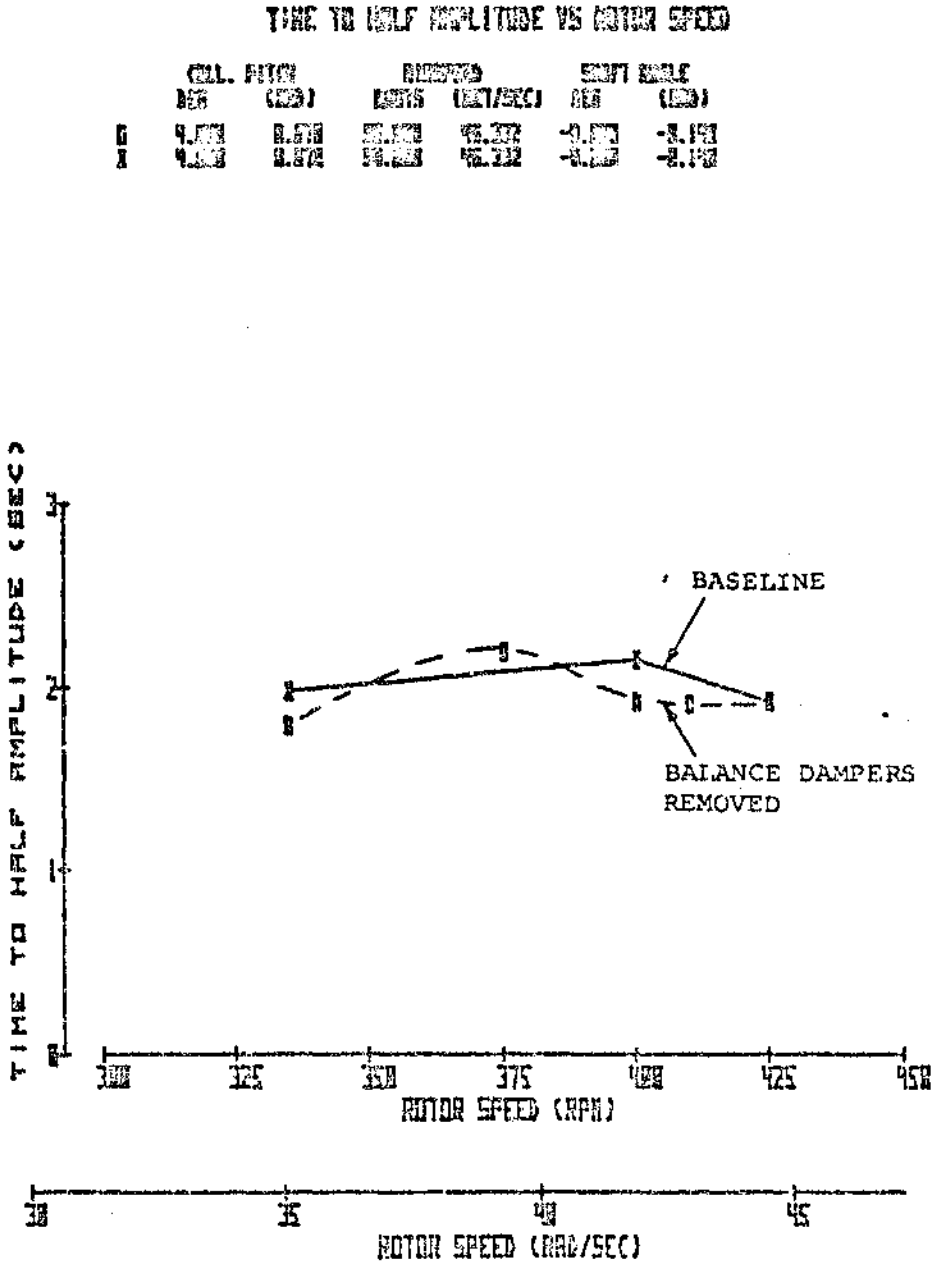

FIGURE 8.41 EFFECT OF REMOVING BALANCE DAMPERS - TIME TO HALF AMPLITUDE VS ROTOR SPEED AT 90 KNOTS

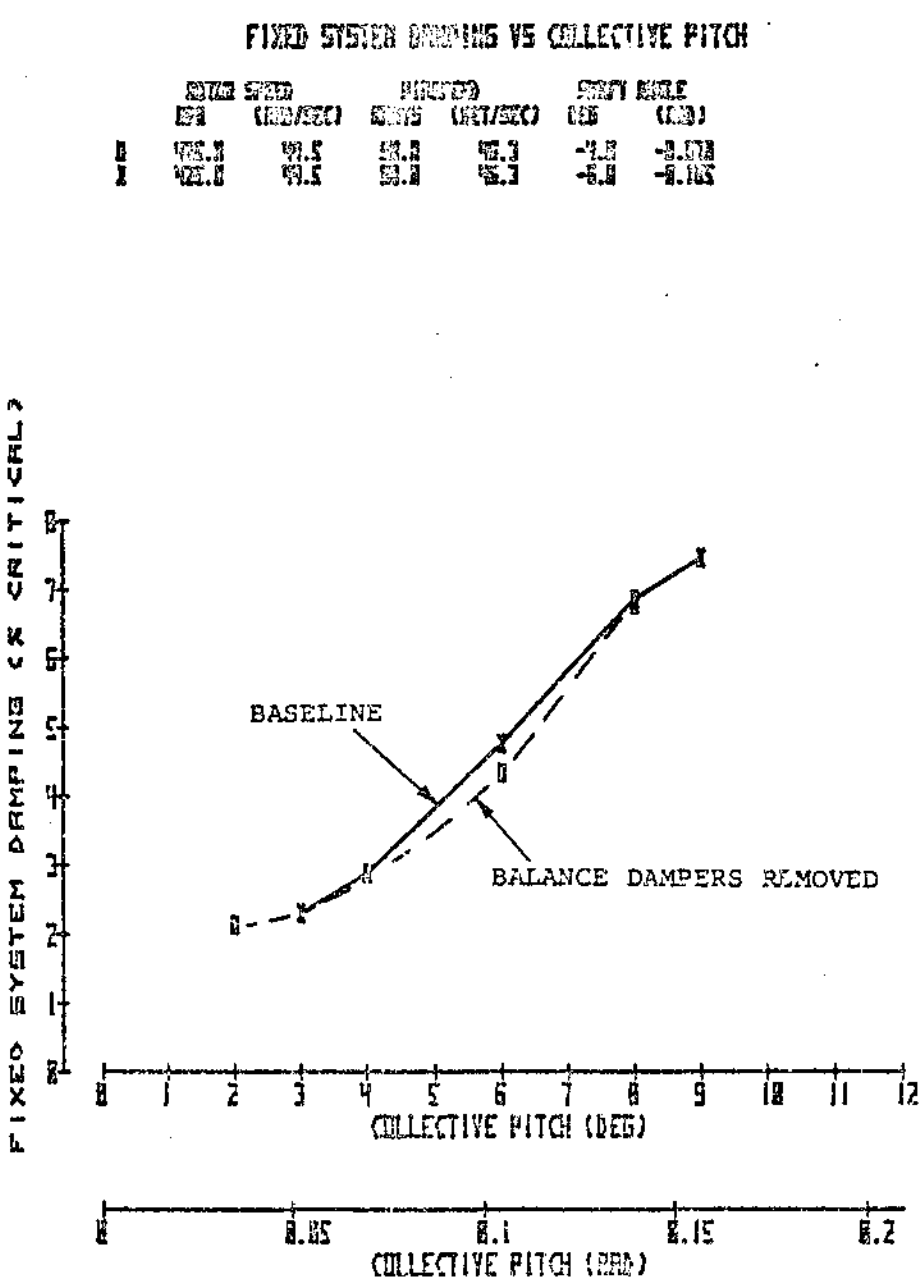

FIGURE 8.42 EFFECT OF REMOVING BALANCE DAMPERS - DAMPING VS COLLECTIVE PITCH AT 90 KNOTS

TIME TO HALF AMPLITUDE VS COLLECTIVE PITCH

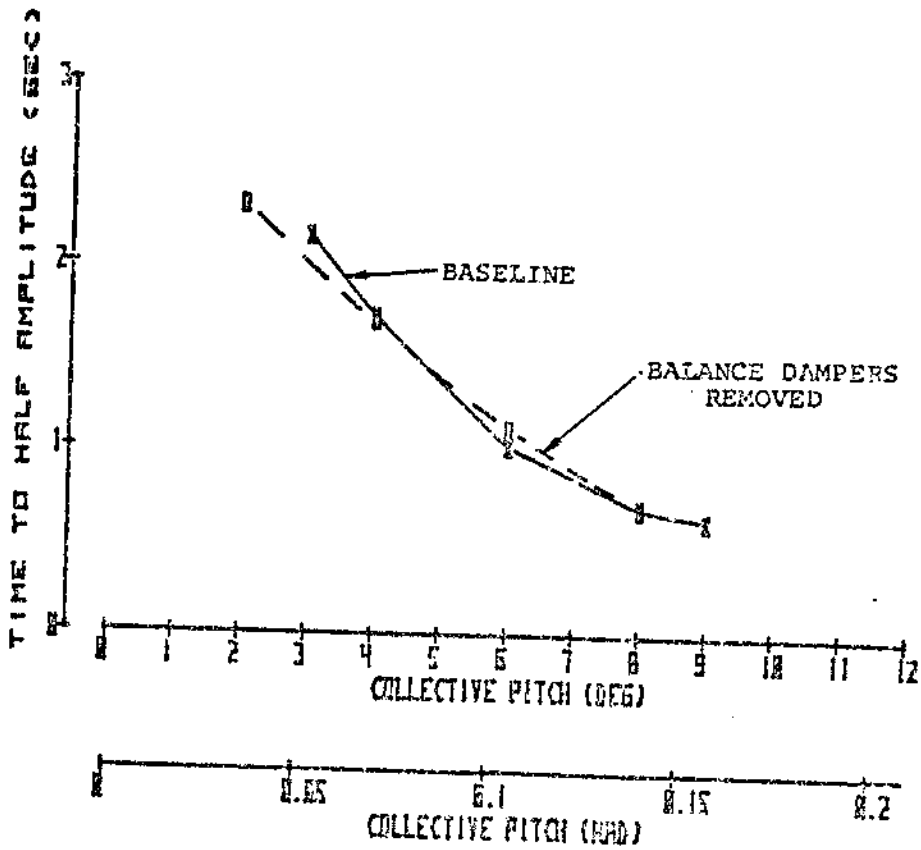

FIGURE 8.43 EFFECT OF REMOVING BALANCE DAMPERS - TIME TO HALF AMPLITUDE VS COLLECTIVE PITCH AT 90 KNOTS

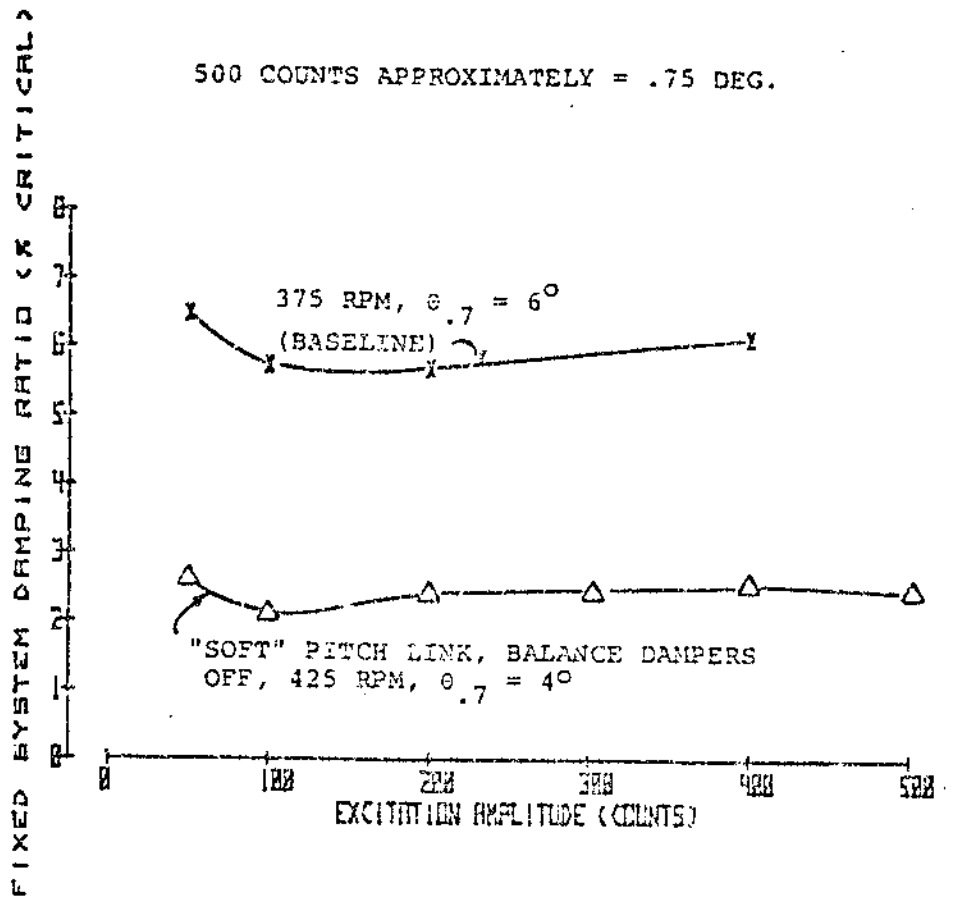

FIGURE 8.44 DAMPING VS EXCITATION AMPLITUDE FOR HOVER

8.1.1.7 Effects of Trim Values of Cyclic Pitch

The effect on stability of varying the longitudinal and lateral cyclic trim values by magnitudes of the order of ±1.0 degree was determined and results are presented in Figures 8.45 and 8.46 for hover. Figure 8.45 shows no general trend for damping as trim values of lateral and longitudinal cyclic pitch are varied. Figure 8.46 shows damping versus resultant trim value of lateral and longitudinal cyclic pitch; again, no general trend of damping with cyclic pitch amplitude is indicated.

8.1.2 Correlation with Analysis

As discussed previously, analyses were conducted using Vertol's C-90 computer program to predict damping levels to be expected while testing the BMR/RTA in the Ames 40-by-80 foot wind tunnel. Comparisons of predicted stability levels and measured stability levels obtained during the BMR/RTA tests are presented below.

8.1.2.1 Hover - Predicted and Test Values of Damping Versus Rotor Speed and Collective Pitch

Figure 8.47 shows a comparison of predicted and test values of damping in hover for rotor speeds from 350 to 437 rpm and for collective pitch values from 0 to 11 degrees. The qualitative comparisons of these predicted and test results is generally good: both show increasing damping levels with increasing collective pitch and decreasing damping levels with increasing rotor speed. The quantitative comparisons are also generally

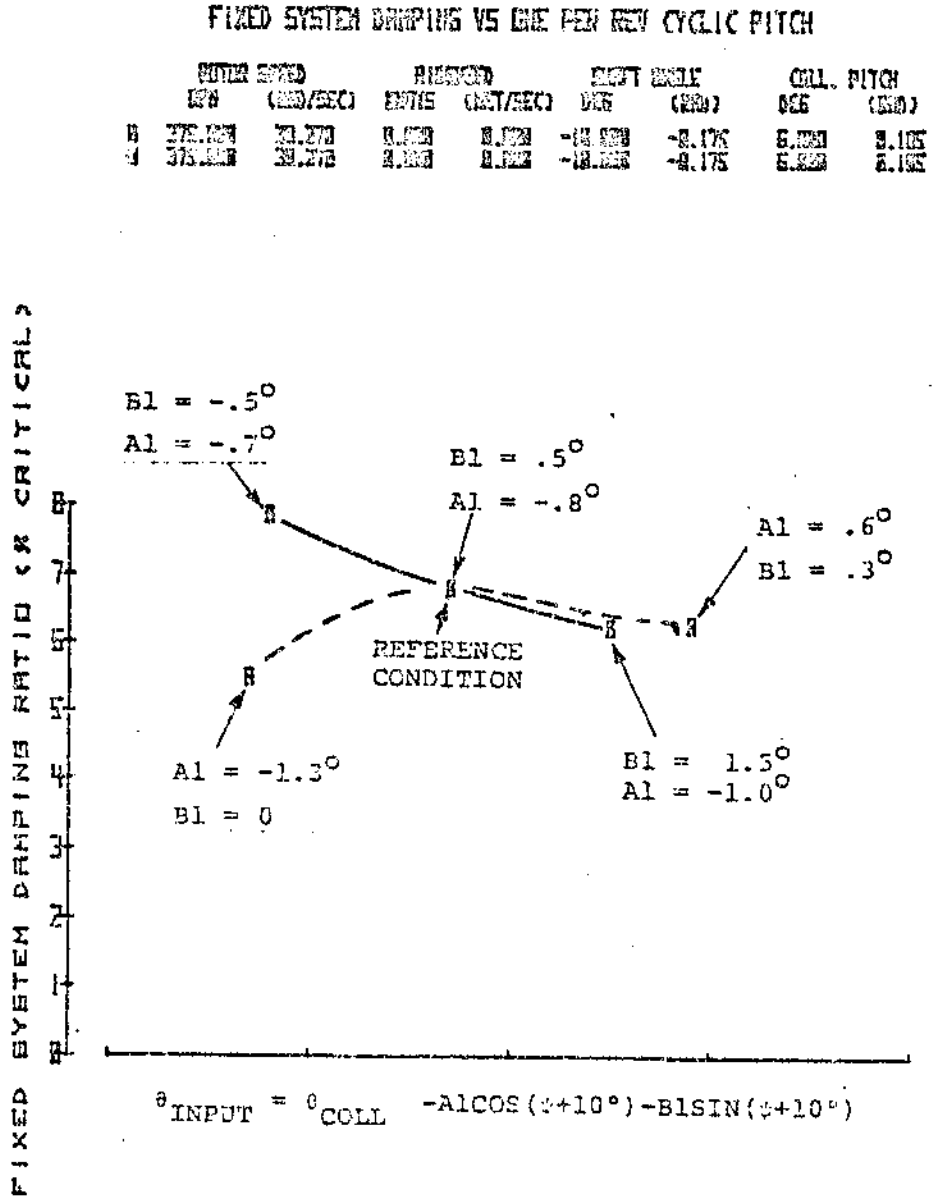

FIGURE 8.45 HOVER - FIXED SYSTEM DAMPING VS LATERAL AND LONGITUDINAL CYCLIC PITCH - BASELINE CONFIGURATION

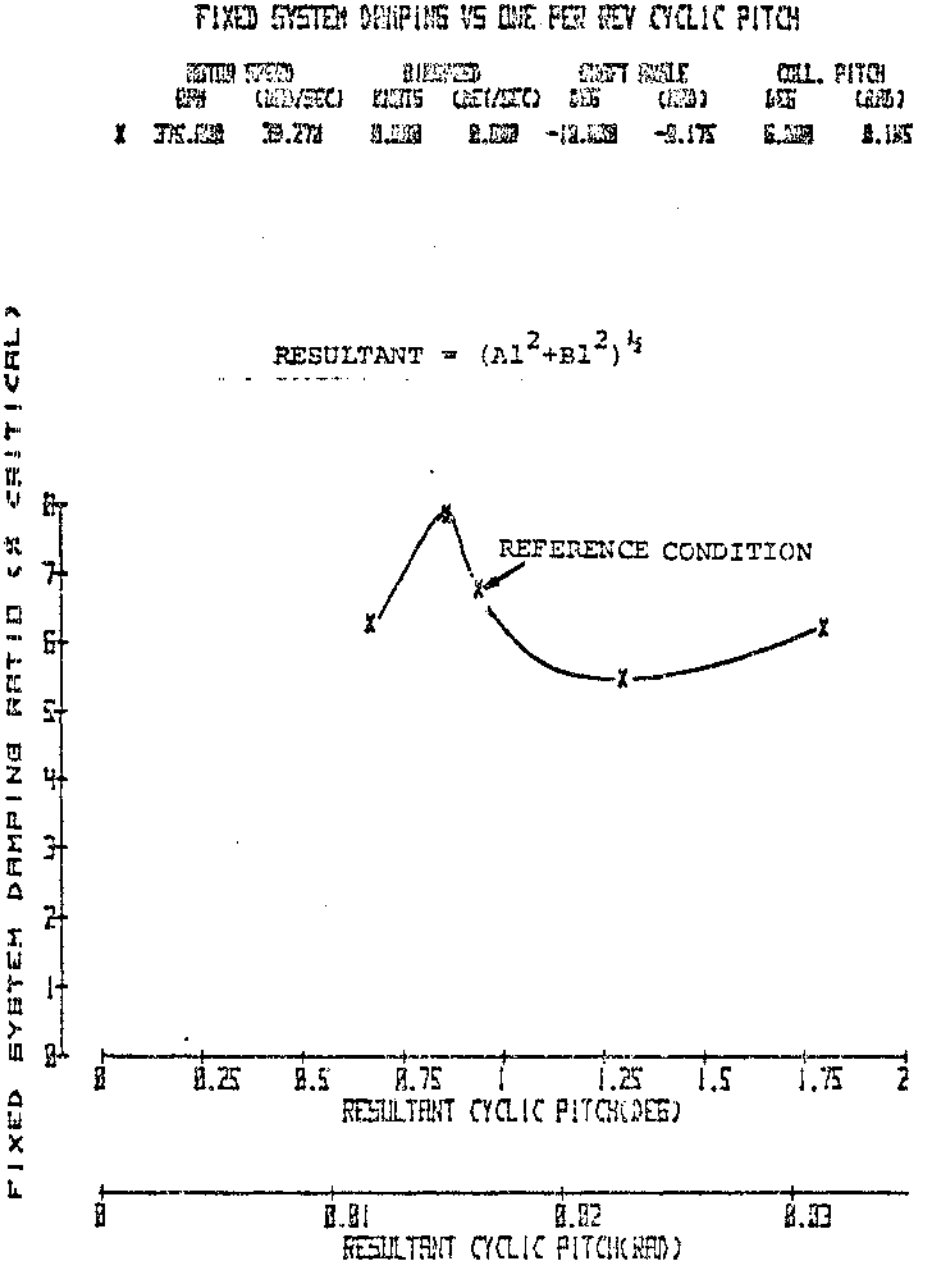

FIGURE 8.46 HOVER - FIXED SYSTEM DAMPING VS RESULTANT ONE/REV CYCLIC PITCH - BASELINE CONFIGURATION

very good, particularly at 425 rpm and at the lowest values of collective pitch tested (where the lowest values of damping were obtained).

8.1.2.2 Forward Flight Test and Prediction Comparison

8.1.2.2.1 Test and Prediction Comparison for Stability at 90 Knots

Figure 8.48 shows test and prediction results for damping versus rotor speed and collective pitch at 90 knots for a shaft angle of -6 degrees. Data are shown for collective pitch values from 0 to 10 degrees for predicted results and for 2 to 9 degrees for test results. Qualitative trends for both test and predicted results are generally similar to those seen in hover with damping increasing with increasing collective pitch and decreasing with increasing rotor speed. Predicted damping levels are generally in good agreement with test results at 2 degrees collective pitch; however, predicted damping levels of 90 knots increase more rapidly with collective pitch than test results. At 8 degrees collective pitch and 335 rpm, predicted damping is about 5 percent of critical damping above test results. At 8 degrees collective and 425 rpm, predicted damping is about 3 percent of critical above the test level.

8.1.2.2.2 Predicted and Test Damping Versus Airspeed and Collective Pitch at -6 Degree Shaft Angle

Figure 8.49 shows predicted and test levels of damping versus airspeed and collective pitch at a -6 degree shaft angle and

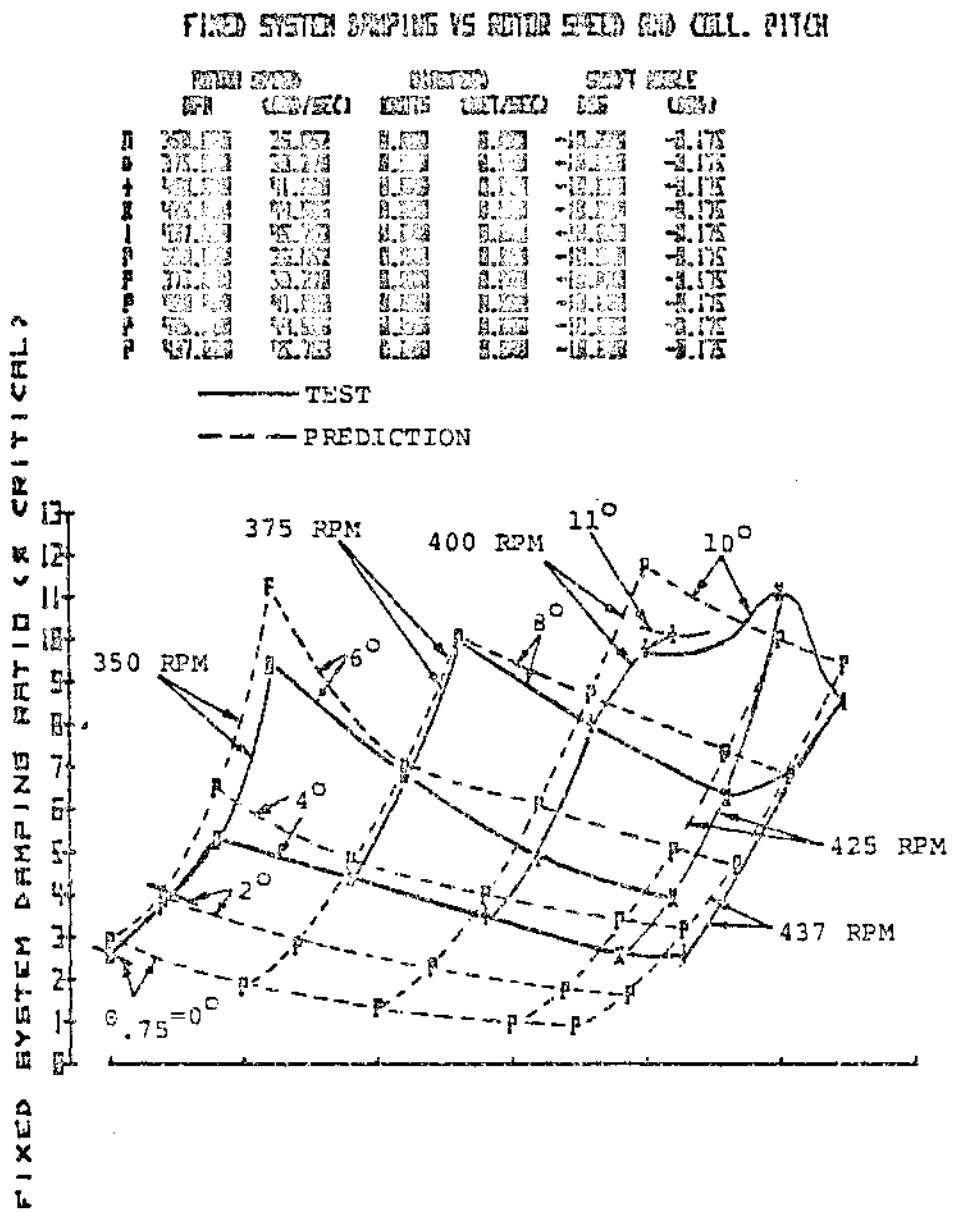

FIGURE 8.47 HOVER - COMPARISON OF PREDICTION AND TEST RESULTS - FIXED SYSTEM DAMPING DATA VS ROTOR SPEED AND COLLECTIVE PITCH - BASELINE CONFIGURATION

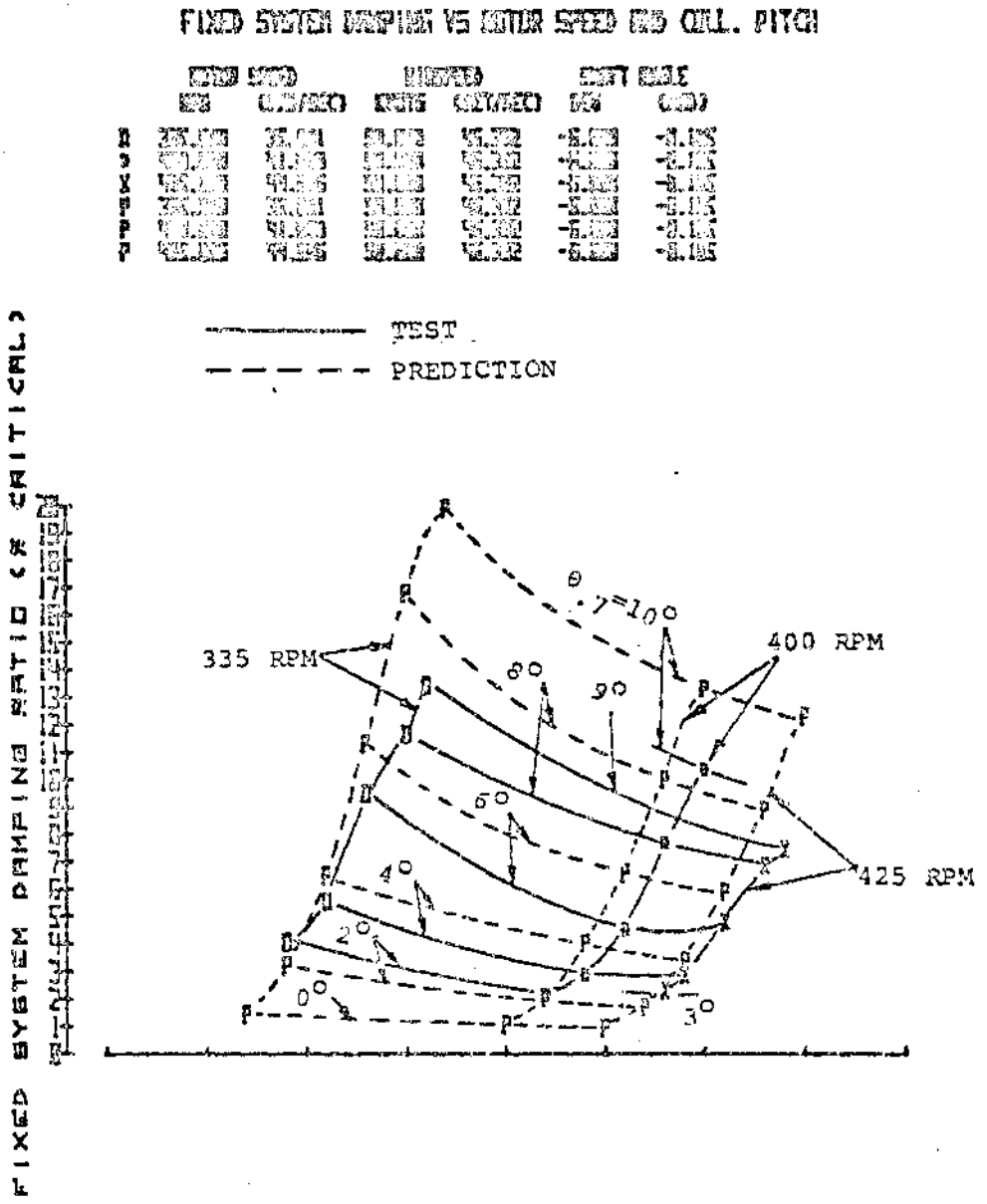

FIGURE 8.48 COMPARISON OF PREDICTION AND TEST RESULTS AT 90 KNOTS - FIXED SYSTEM DAMPING VS ROTOR SPEED AND COLLECTIVE PITCH - BASELINE CONFIGURATION

425 rpm rotor speed (hover test points are for a -10 degree shaft angle). Test data are shown for collective pitch values from 3 to 10 degrees and for airspeeds from 0 to 120 knots. Predicted results are shown for collective pitch values of 4 and 8 degrees for airspeeds from 0 to 180 knots. This prediction/test comparison indicates:

1) Prediction and test values for damping are in reasonable agreement between 0 and 90 knots at 4 degrees collective pitch.

2) Between 0 and 90 knots the trend of damping with airspeed is similar for predicted and test results, but predicted damping levels increase more rapidly with collective pitch.

3) Test results show a decrease in damping level with increasing airspeed at constant collective pitch above 90 knots, while predicted damping levels show damping increasing with airspeed above 90 knots for constant collective pitch values.

8.1.2.2.3 Predicted and Test Damping Versus Airspeed for 1.0 G Level Flight

Figure 8.50 shows a comparison of predicted and test values of damping versus airspeed at 1.0 G level flight. Test values are for a 4500 pound lift and 9 square feet flat plate drag area

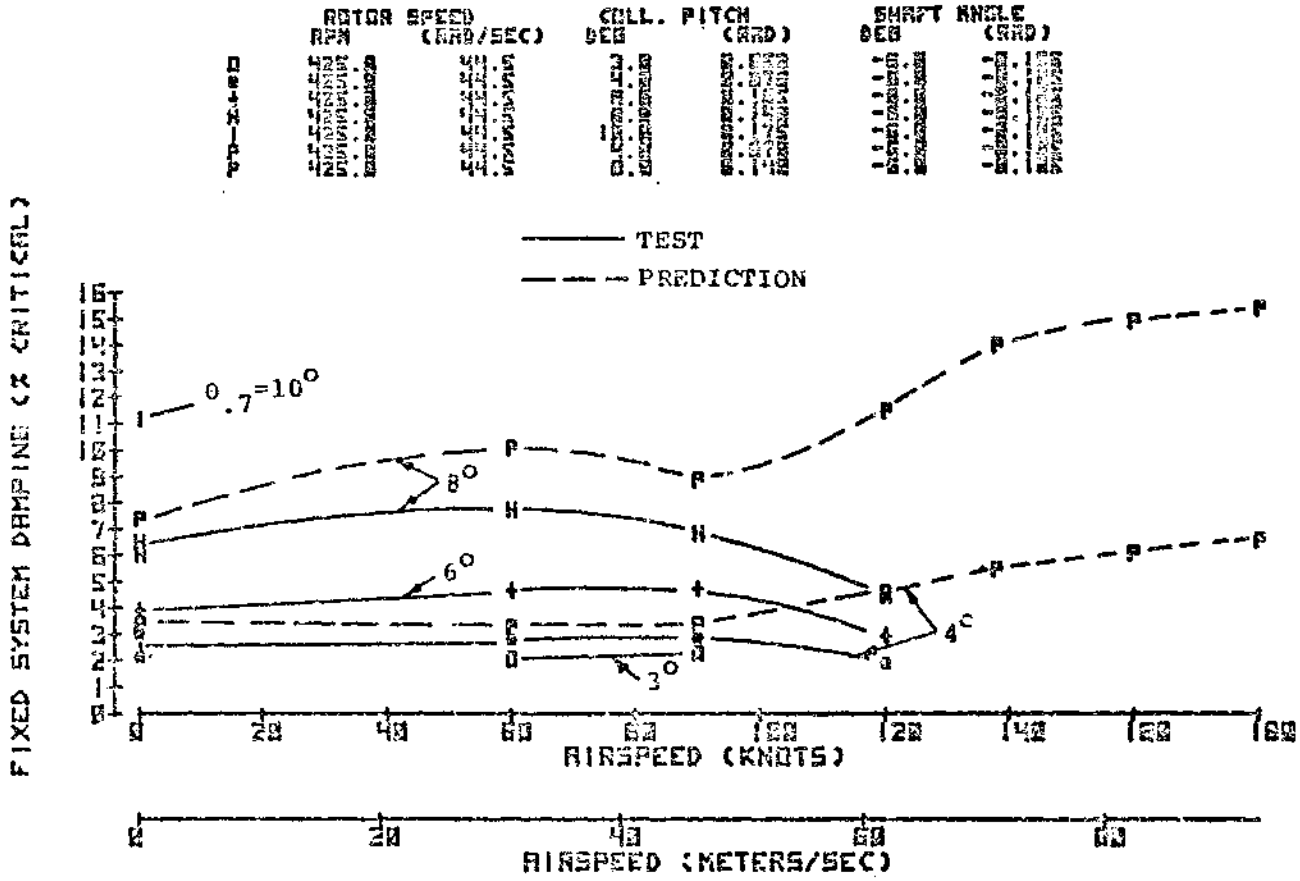

FIGURE 8.49 TEST VS PREDICTED DAMPING VS AIRSPEED AND COLLECTIVE PITCH AT NORMAL ROTOR SPEED AND -6 DEGREE SHAFT ANGLE - BASELINE CONFIGURATION

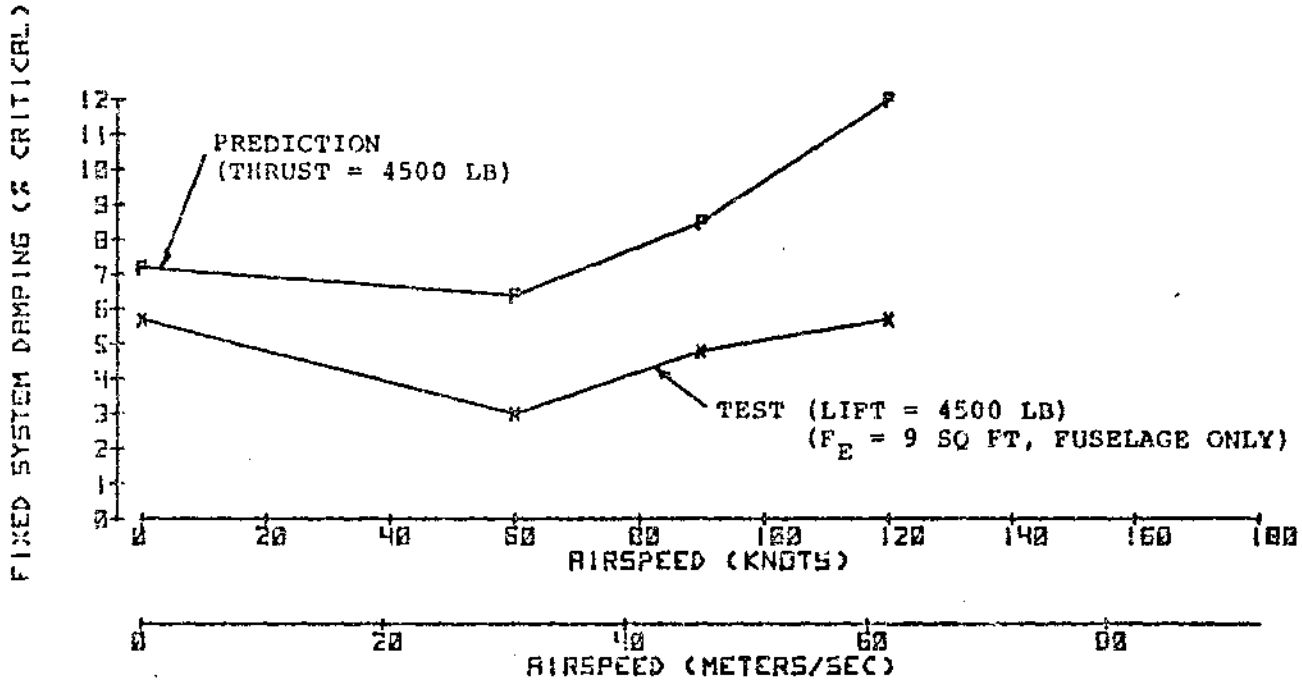

FIGURE 8.50 TEST AND PREDICTED DAMPING VS AIRSPEED AT 4500 LB LIFT AND 425 RPM - BASELINE CONFIGURATION

obtained in a manner identical to that used to get the results shown in Figure 8.7. Similar trim values were used to obtain predicted values for damping from Figure 6.12 which shows damping versus airspeed and shaft angle for 4500 pounds thrust at 425 rpm. The comparison in Figure 8.50 indicates that predicted and test levels of damping are in fair agreement for hover. As airspeed increases, both test and predicted values of damping decrease, but the test value decreases more rapidly. Between 60 and 120 knots, both test and predicted damping levels increase, but the predicted damping level increases more rapidly with airspeed than the test level of damping. At 120 knots, the test level of damping is approximately 6 percent of critical while the predicted level is approximately 12 percent of critical damping.

8.1.2.3 Effect of First Chord Mode Structural Damping on Test and Predicted Stability

Figures 8.51 and 8.52 shows the incremental increase in fixed system damping for a one percent increase in first chord mode structural damping in hover at 425 rpm rotor speed versus collective pitch. Figure 8.51 shows test and theoretical damping versus first chord mode structural damping at fixed collective pitch and rotor speed. The slopes of these curves are plotted in Figure 8.52. Test and predicted levels are in good agreement, and both show a sensitivity to collective pitch. Generally, about a 2 percent increase in fixed system damping is

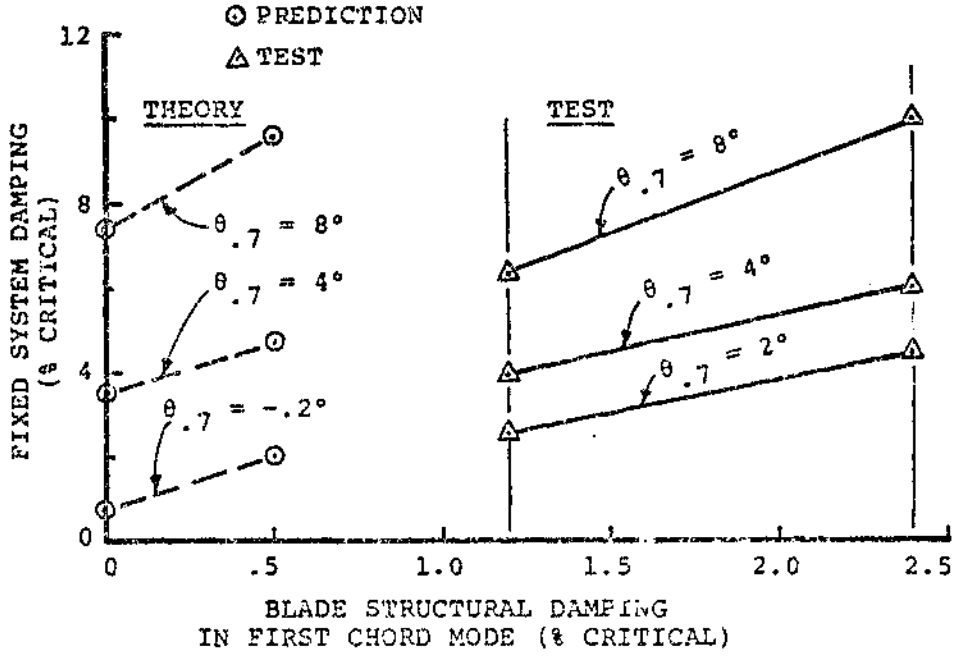

FIGURE 8.51 TEST VS THEORY - SENSITIVITY OF FIXED SYSTEM DAMPING TO CHORD MODE STRUCTURAL DAMPING - AS A FUNCTION OF COLLECTIVE PITCH AT 425 RPM IN HOVER.

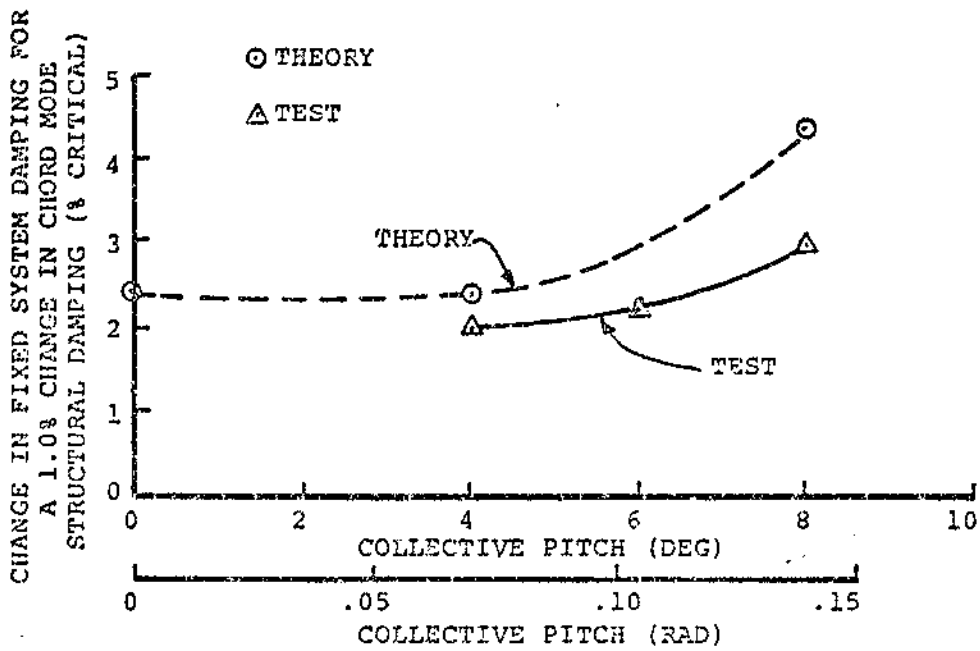

FIGURE 8.52 TEST VS PREDICTED EFFECT OF CHORD MODE STRUCTURAL DAMPING ON FIXED SYSTEM DAMPING VS. COLLECTIVE PITCH AT 425 RPM FOR HOVER.

indicated for a 1 percent increase in first chord mode damping in hover at 425 rpm for collective pitch values from 0 to 6 degrees.

8.1.3 Correlation of BMR/RTA Stability Test Data with Other BMR Stability Test Data

8.1.3.1 Comparison of BMR/RTA Stability Data with Stability Data from Boeing Vertol BMR Whirl Tower Tests

Figures 8.53 and 8.54 compare BMR/RTA hover stability data with BMR whirl tower stability data obtained from Boeing Vertol tests. Figure 8.53 shows damping levels versus collective pitch from zero to 8 degrees at 425 rpm; Ames test data are near the bottom of scatter of whirl tower test data. Figure 8.54 shows data versus rotor speed from 350 to 420 rpm for whirl tower data and for 350 to 425 rpm for BMR/RTA wind tunnel data. Whirl tower data are shown at 0 and 8 degrees collective pitch. Wind tunnel data are shown: at 0 and 2 degrees collective pitch at 350 rpm; at 350, 375, 400, and 425 rpm at 4 and 6 degrees collective pitch; and at 375, 400, and 425 rpm at 8 degrees collective pitch. BMR whirl tower and BMR/RTA test damping data are generally in agreement at 8 degrees collective pitch. At 350 rpm, whirl tower test data at 8 degrees appears to be low compared to what would have been expected from the wind tunnel test. Whirl tower damping data at 0 degrees collective pitch appears to be in agreement with BMR/RTA damping data obtained at low collective pitch values.

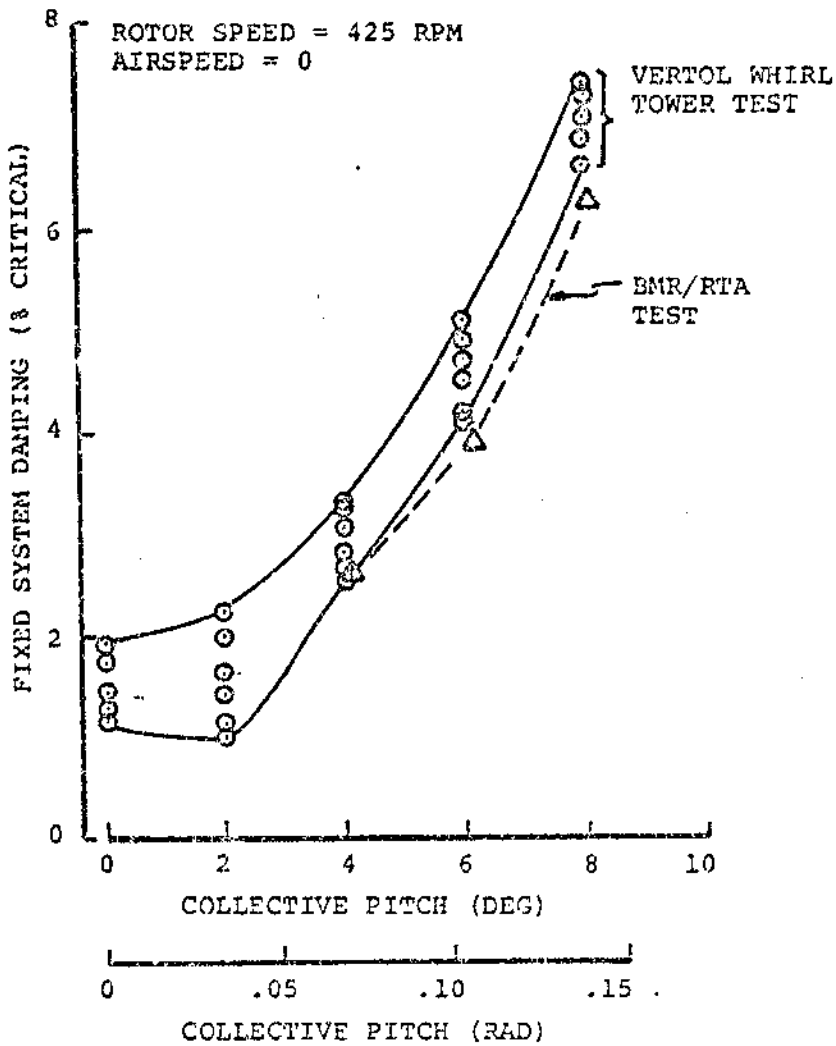

FIGURE 8.53 COMPARISON OF BMR/RTA AND BMR WHIRL TOWER TEST DAMPING DATA VS COLLECTIVE PITCH AT 425 RPM

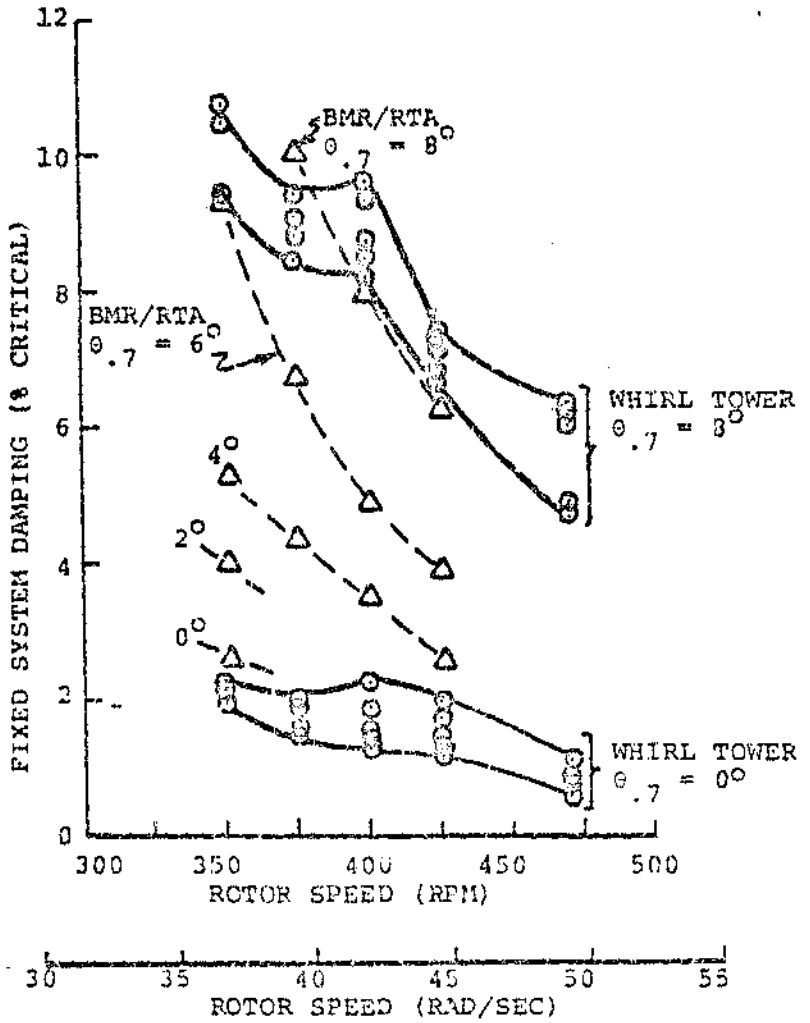

FIGURE 8.54 COMPARISON OF BMR/RTA AND BMR WHIRL TOWER TEST DAMPING VS ROTOR SPEED

8.1.3.2 Comparison of BMR/RTA Hover Damping Data with Damping Data Obtained from BMR/BO-105 Ground Resonance Test Data

Figures 8.55 and 8.56 show a limited comparison of BMR/RTA hover stability data with ground resonance damping data obtained when the BMR was tested on a BO-105 aircraft. Figure 8.55 compares damping versus collective pitch for ground resonance tests at 425 rpm. BMR/BO-105 data are shown for the BMR on the BO-105 with its standard landing gear and for the BMR on the BO-105 with a slightly stiffened landing gear. These results are for ground resonance tests on a concrete surface. Comparison of BMR/RTA hover damping and BMR/BO-105 ground resonance damping indicates that the BMR/RTA generally shows the level of damping and the trend with collective pitch indicated for the BMR/BO-105 at normal rotor speed on concrete. There are some variations from the general trend of damping versus collective pitch seen in the BMR/BO-105 damping data but not seen in the BMR/RTA data. For example, note the dip in damping versus collective pitch seen just below 4 degrees collective pitch for the unstiffened gear and at just above 4 degrees collective pitch for the stiffened gear. These "dips" in damping at certain collective pitch values might be due to coalescing of the lead-lag regressing frequency with a body mode frequency for the BMR/BO-105. Figure 8.56 shows a comparison of BMR/RTA hover damping data and BMR/BO-105 ground resonance damping data at a BMR/RTA rotor speed of 400 rpm and a BMR/BO-105 rotor speed of 404 rpm; again the BMR/RTA test results agree with the general results for the BMR/BO-105 except at a

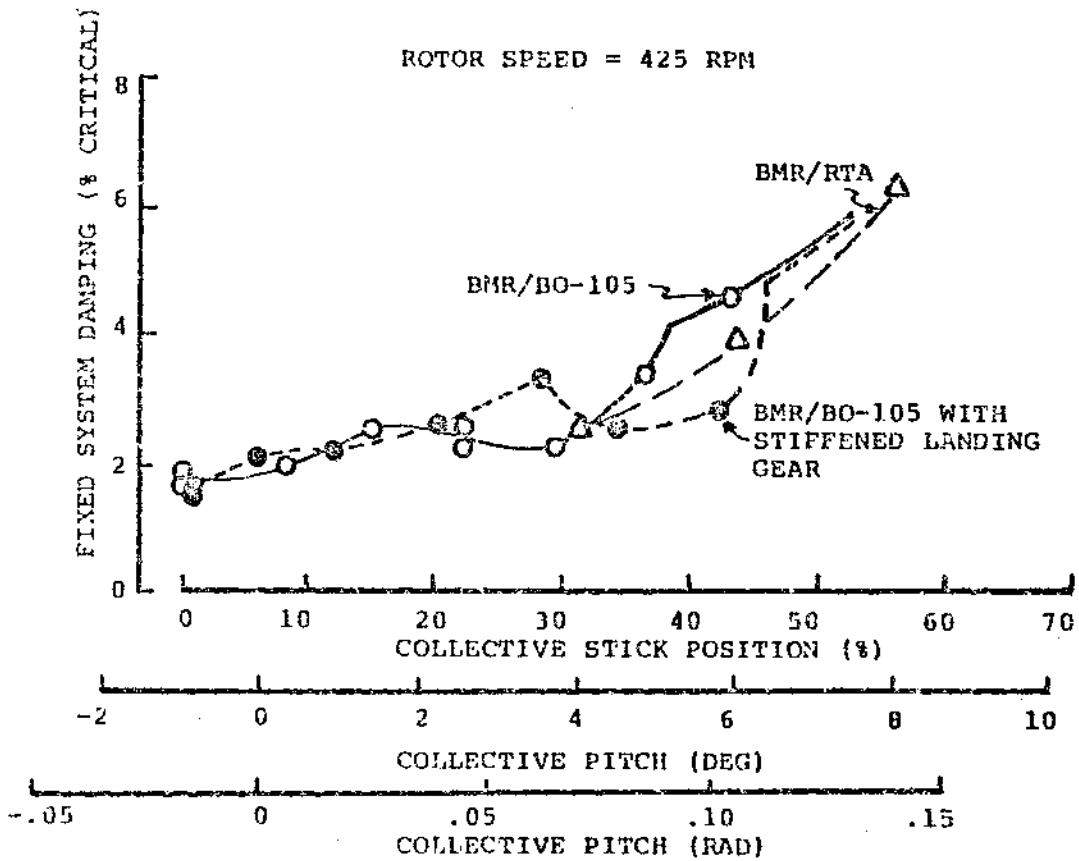

FIGURE 8.55 COMPARISON OF BMR/RTA AND BMR/BO-105 GROUND RESONANCE MODE DAMPING VS COLLECTIVE PITCH AT 425 RPM

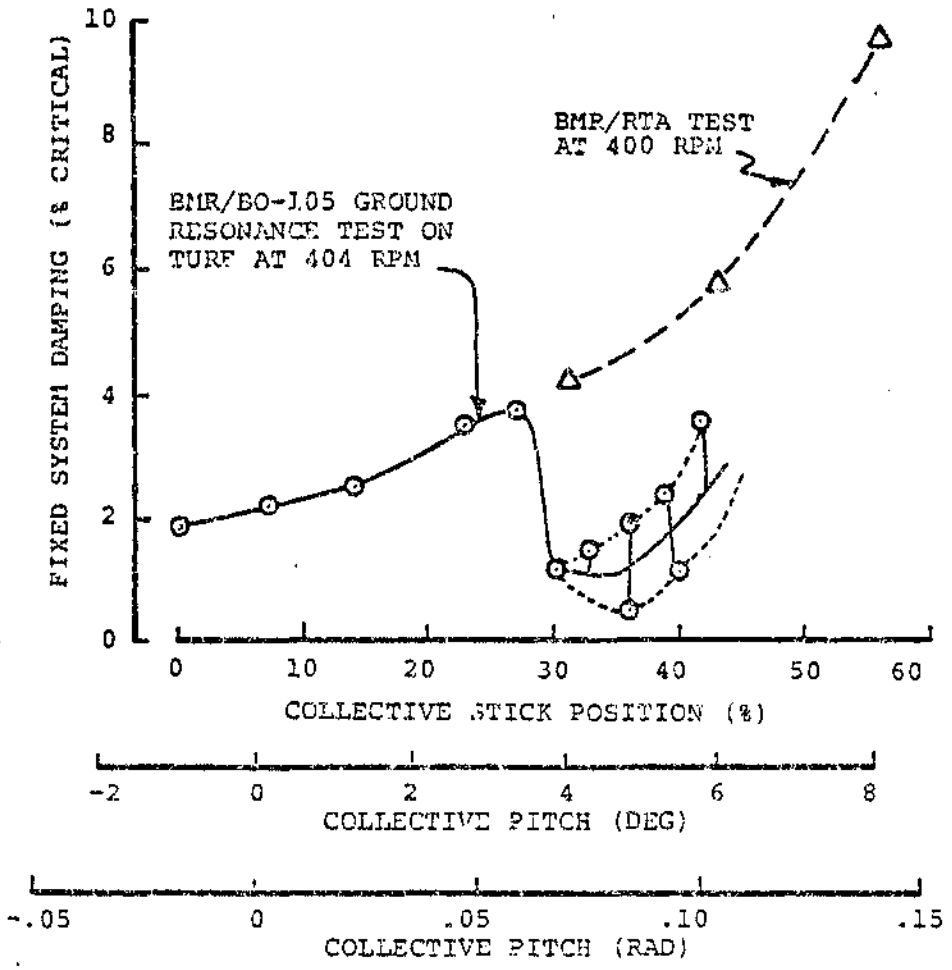

FIGURE 8.56 COMPARISON OF BMR/RTA AND BMR/BO-105 GROUND RESONANCE TEST DAMPING VS COLLECTIVE PITCH NEAR 400 RPM

collective pitch near 4 degrees. Again a reduction in damping for the BMR/BO-105 is indicated over a narrow range of collective pitch values near 4 degrees. The BMR/BO-105 results are for the BO-105 on turf with the stiffened landing gear. The range of data for the BMR/BO-105 test data between 4 and 6 degrees collective pitch is attributed to variations in the BMR/BO-105 trim condition and the degree of contact between the BO-105 landing gear and the ground.

These results indicate the BMR/RTA data are useful for indicating the inherent level of damping available from the rotor when no potential for coupled rotor/body mode instability exists. Stability testing on the RTA in the Ames 40-by-80 wind tunnel would be useful for determining inherent rotor damping levels and for evaluating rotor configuration variations for improving stability.

8.1.3.3 Comparison of BMR/RTA and BMR/BO-105 Damping Data Versus Airspeed for 1.0 G Level Flight

Figure 8.57 shows a comparison of estimated BMR/RTA test damping versus airspeed for level flight trim conditions at 425 rpm with corresponding data obtained in the BMR/BO-105 flight testing. BMR/RTA damping data are slightly higher at 0 and 60 knots; BMR/RTA data are within the BMR/BO-105 scatter band at 93 and 111 knots. These results support the conclusion of the previous section that the BMR/RTA tests indicate the inherent level of rotor damping available when no tendency toward insta-

bility exists. No tendency toward an instability (i.e., a reduction in damping due to coalescence of a body mode frequency with the lead-lag regressing frequency) was indicated during BMR/BO-105 hover and forward flight testing over a wide range of rotor speeds and rates of climb and descent (a wide range of collective pitch values) including autorotations.

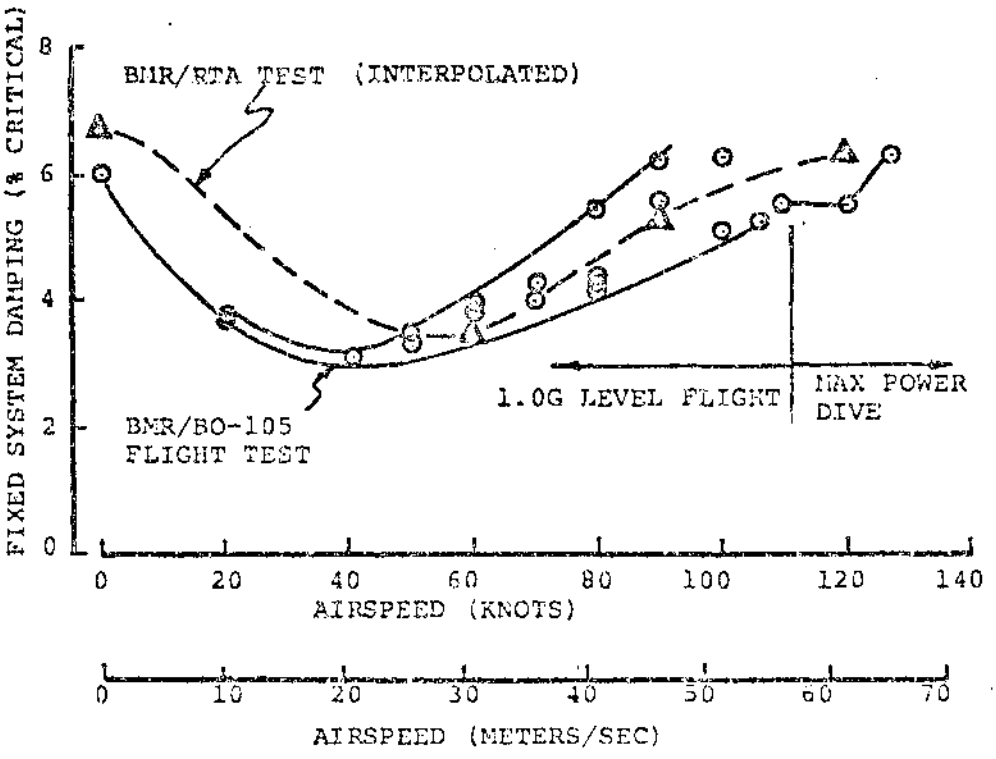

FIGURE 8.57 COMPARISON OF BMR/RTA AND BMR/BO-105 TEST DAMPING FOR 1.0G LEVEL FLIGHT AT 425 RPM

8.2 LOADS

8.2.1 Definition of Critical Load Parameters

Loads have been evaluated on the basis of measured data from blade and individual beam instrumentation, torque tube chord and torsion bridges, and pitch link axial loading. Torque tube flapping values were relatively low throughout the test and are not presented since torque tube chord bending was significantly more critical. Pitch control component measurements (actuators, stationary control rods and swashplate gages) were also relatively low throughout the test and therefore only pitch link loads are presented in this report.

As determined by the measured loads from the test compared to the endurance limit, the critical parameters were flexbeam flap bending and torque tube chord bending in the vibratory mode. During envelope expansion, peak loading was critical for flap and chord bending at the outboard end of the beam and blade root flap bending. Stability testing was limited by peak torque tube chord bending was critical for low collective settings. During dynamic excitations, fatigue endurance limits were momentarily exceeded in the chord bending mode. Inboard flexbeam sections were more critical than outboard sections and the blade root section was even less critical. Blade root torsion steady plus alternating approached the limit load cut-off during the two runs intended to achieve the maximum possible airspeed (runs 18 and 23). The cut-off for blade torsion was established on the basis of maximum loads applied during bench testing. Loading

to a higher level would have established a higher cut-off. In this respect, the flexbeam limits are more critical.

Data presented in the load trends section (3.2.2) are based on test results obtained with the baseline configuration with balance dampers in place. Configuration variations and the effect of removing the balance dampers are discussed in later sections. Aircraft attitudes, control settings, and fixed system measurements have been obtained from the static file. All vibratory load levels shown use the smoothed data as opposed to the raw test data. This insures that only periodic forces and/or motions are considered in assessing load trends, configuration changes (parameter variations), and correlation with flight testing.

8.2.2 Load Trends

8.2.2.1 Vibratory Loads in Hover

For hover testing in the wind tunnel, the rotor shaft was tilted nose down to a -10 degree shaft angle to minimize the effect of recirculation within the tunnel section. Since it is not possible to completely eliminate recirculation effects, there are variations in tunnel flow which would require a continuous fine adjustment in cyclic to maintain minimum 1/rev flapping. While an automated flight control system can cope with such a requirement, the manual console adjustment is a relatively coarse adjustment when compared with an automated system. Coupling the control adjustment capability with the inherent sensitivity of the hingeless rotor to variations in airloading does not contribute to good repeatability for hover results. The variations of flap and chord bending moments displayed below illustrate the high degree of sensitivity to control adjustments for the hover test condition.

FLAP BENDING MOMENT VS CYCLIC INPUT IN DEGREES

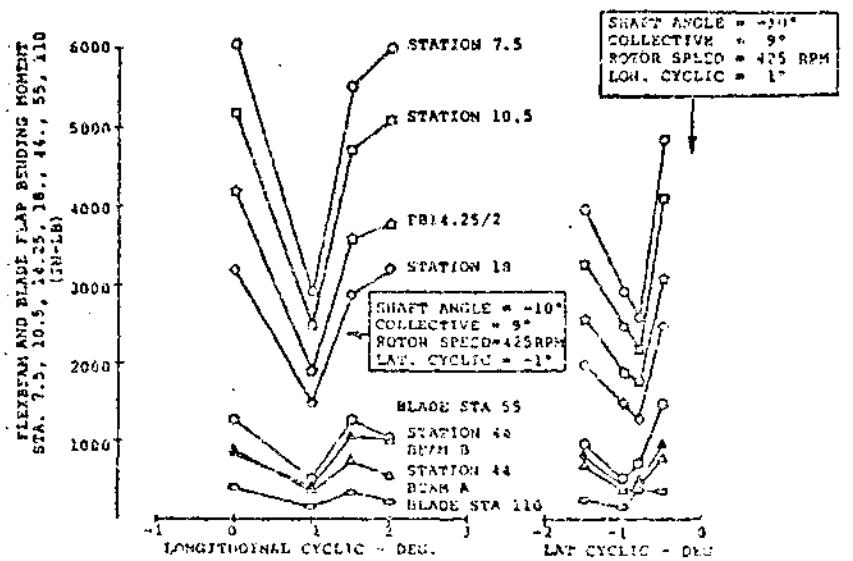

CHORD BENDING MOMENT VS CYCLIC INPUT IN DEGREES

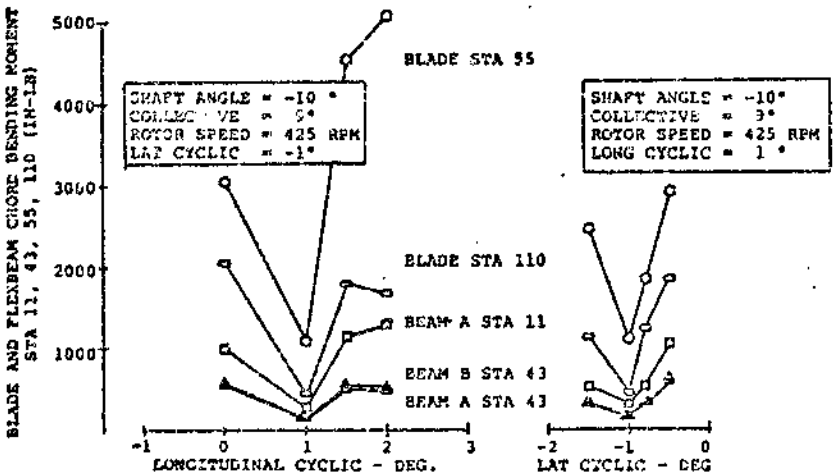

Due to the previously discussed sensitivity, the differences in shaft attitude between the wind tunnel and the aircraft, and main to tail rotor interactions, no attempt has been made to correlate wind tunnel data with flight test results in the hover mode.

With respect to trends in the hover mode, the potential for cyclic trim effects being as significant as differences between two points due to a change in a test control variable (such as

collective, shaft angle, or rotor speed) precluded any attempt to define load trends in the hover condition.

8.2.2.2 Blade Load Trends

Figures 8.58 through 8.61 present blade flap moments as a function of airspeed for a constant shaft angle and collective setting. Both midspan and root sections show the expected build-up in vibratory moments at higher airspeeds. Root section moments indicate a build-up in magnitude in the transitional speed range (20 to 60 knots). Steady midspan flap moments trend from flap up to flap down with increasing airspeed while steady flap moments at the blade root section are flap down throughout the speed range from 0 to 143 knots with a flap down moment trend at the higher airspeeds.

Blade flap bending moments as a function of collective are presented for the test range of airspeeds in Figures 8.62 through 8.65. Vibratory flap moments are most sensitive to collective variation at 60 knots. The trend of decreasing vibratory flap moments with increasing collective at constant rpm and shaft angle for the blade root evidenced by the 120 knot data is not in agreement with the expected trend or the other measured flap bending moments. Steady flap moments show a trend of linear increasing upward flapping with collective at constant rpm and shaft angle as expected. Blade flap bending at station 55 evidenced significant variation in the magnitude of the 4/rev

content as collective changed while the 1st, 2nd and 3rd harmonics showed little change with collective at 143 knots. This lack of a definite trend at this airspeed (Figure 8.64) is the result of significant variations in the magnitude of the 4/rev component.

As a function of shaft angle at constant rpm and collective, vibratory flap moments show a slightly greater than linear trend to increasing values as the shaft angle becomes more positive (nose-up for the RTA). Blade root section flapping does not follow this general trend at higher airspeeds (120 and 143 knots). At these airspeeds, the effect of shaft angle was not seen because the rotor was generally tested to lift levels below 3500 pounds, considerably less than the lifts of 5300 pounds at 60 and 90 knots. Figure 8.66 through 8.69 present blade flap moments as a function of shaft angle.

Within the operating range of rotor speed no significant effects of rotor speed were observed. In hover, considerable variation in vibratory load measurement was realized as a result of tunnel recirculation effects. When plotted as a function of rotor speed, considerable variations in blade root flapping are evident which were not observed with tunnel "q".

Figures 8.70 through 8.73 present chord bending as a function of airspeed at constant rpm, collectives and shaft angle.

Vibratory chord bending at both midspan and the root section show a signficantly higher level in the intermediate speed range (40 to 80 knots) with relatively low values at hover and 143 knots. The higher levels are not limiting since values are well within the chord bending endurance limits of ±6300 and ±9400 inch-pounds for the midspan and root sections, respectively. Steady chord bending moments are relatively constant with leading edge compression at midspan and leading edge tension at the root.

Blade chord bending moments as a function of collective at constant rpm and collective are presented in Figures 8.74 through 8.77. Above rotor thrust levels of 2000 pounds, vibratory chord bending moments exhibit a relatively rapid build-up with increasing collective. Below 2000 pounds rotor thrust, chord moments show a trend to higher vibratory levels with lower collective. This low collective trend is rather shallow for the test data. Steady chord bending moments for the midspan section show little variation indicating a low sensitivity to airspeed or shaft angle effects. At the blade root section, the effects of shaft angle and airspeed are shown by the spread between the various combinations plotted.

Figures 8.78 through 8.81 present blade chord bending as a function of shaft angle at constant rpm and collective. Vibratory chord moments increase with more positive shaft angle. Midspan section steady chord bending is relatively insensitive

to shaft angle. At the blade root section, there appears to be a combined effect of collective and shaft angle which gives an increasingly more positive chord moment at 143 knots.

No significant effects of rotor speed were observed within the operating range. During start-up and shutdown of the rotor, a crossing of the first chordwise mode at approximately 260 rotor rpm resulted in a momentary build-up of chord bending moments.

Figures 8.82 and 8.83 show the variation in blade root torque as a function of collective. Load changes are gradual and it can be seen that for the vibratory loads there is a much more pronounced effect with airspeed than with collective. Trends with shaft angle are very gradual also as shown in Figures 8.84 and 8.85.

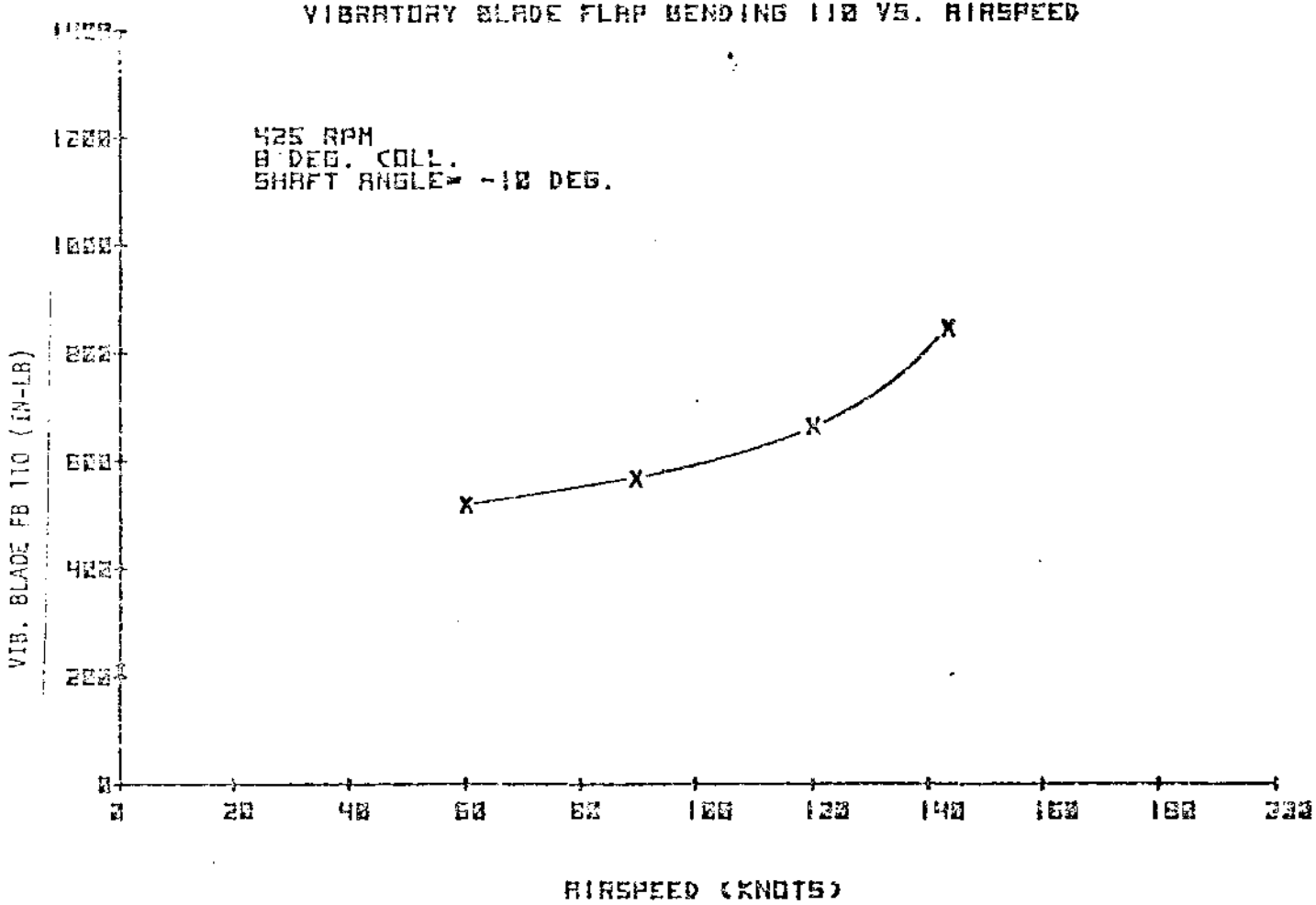

FIGURE 8.58 VIBRATORY FLAP BENDING 110 VERSUS AIRSPEED

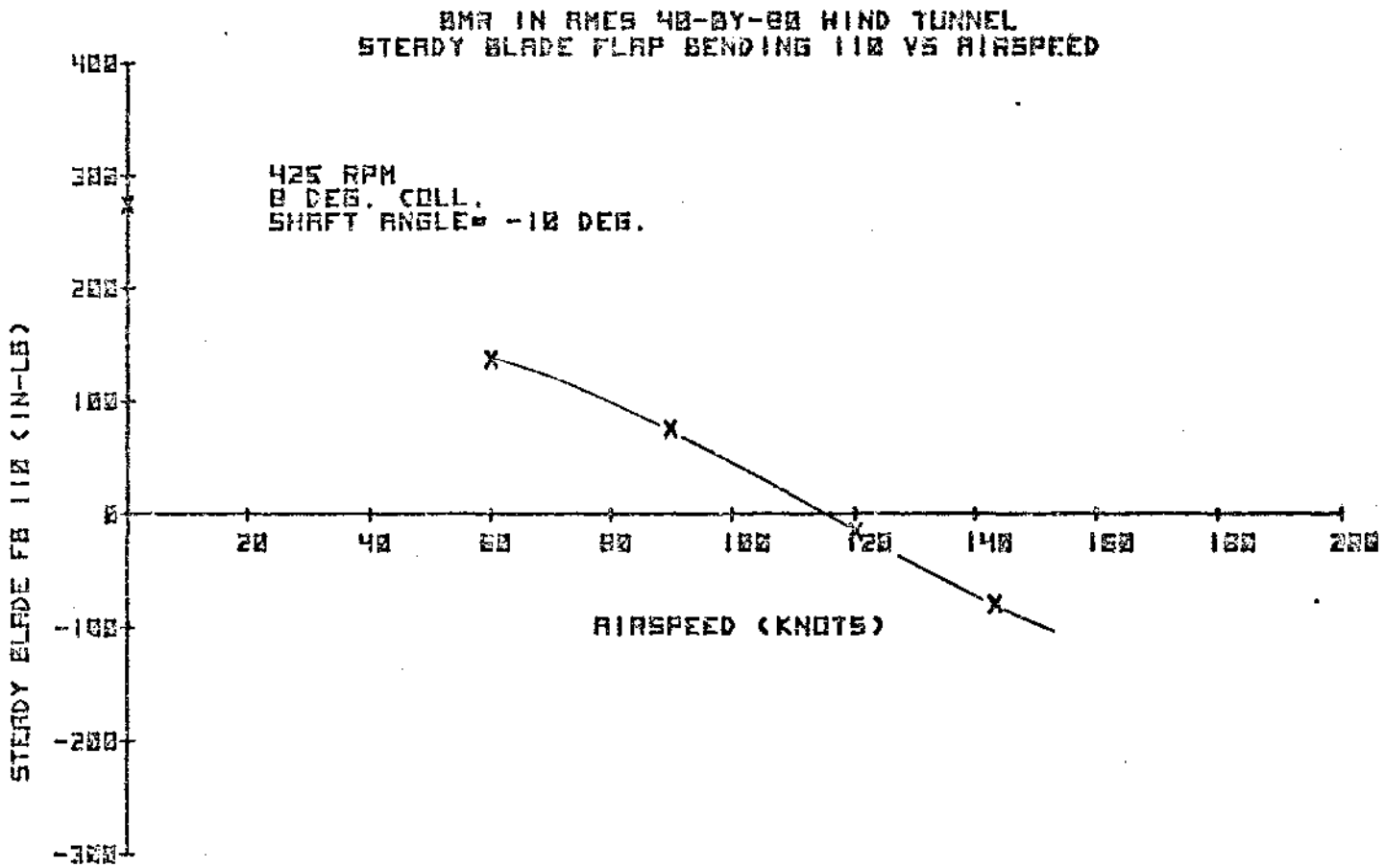

FIGURE 8.59 STEADY FLAP BENDING 110 VERSUS AIRSPEED

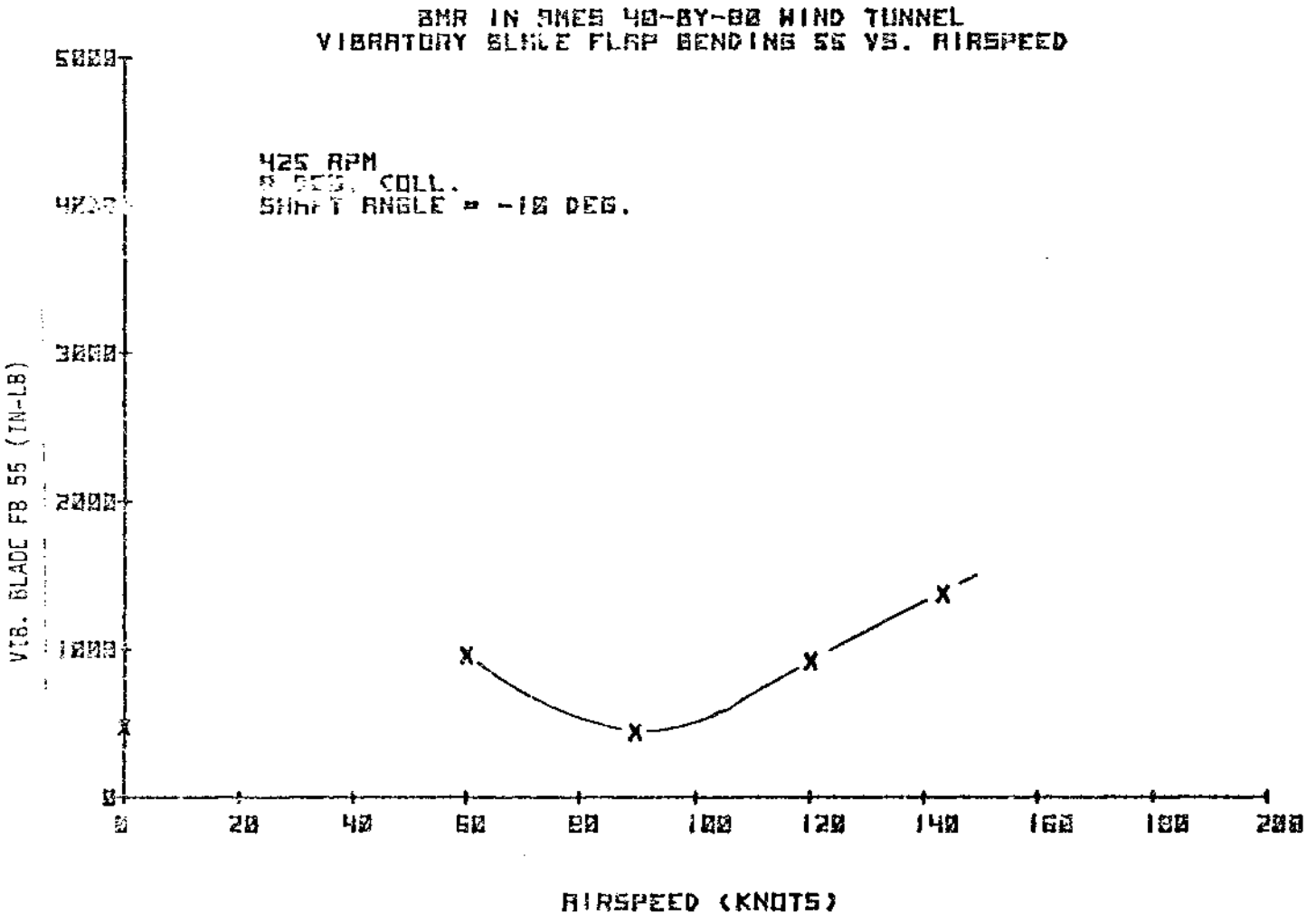

FIGURE 8.60 VIBRATORY FLAP BENDING 55 VERSUS AIRSPEED

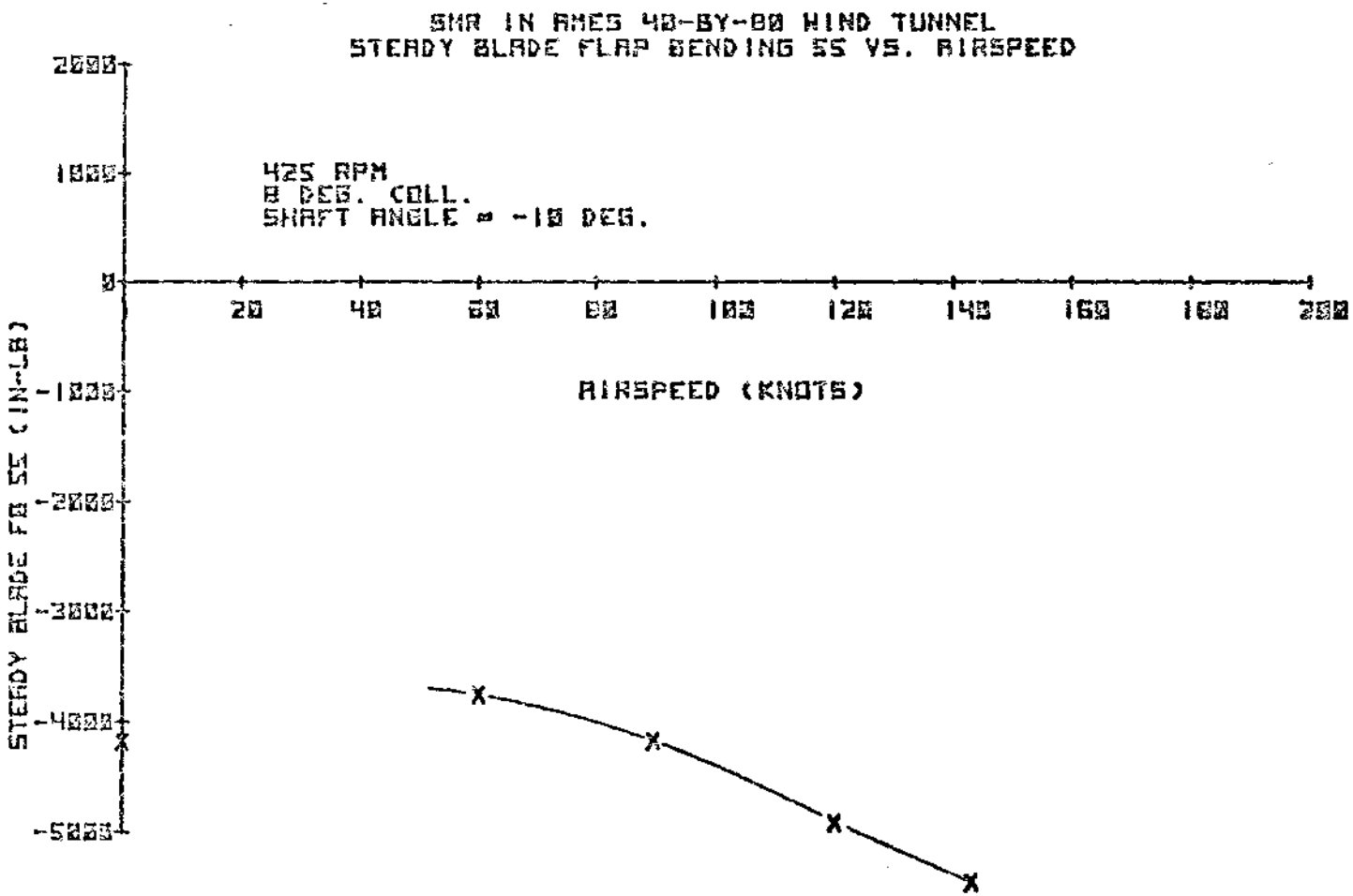

FIGURE 8.61 STEADY FLAP BENDING 55 VERSUS AIRSPEED

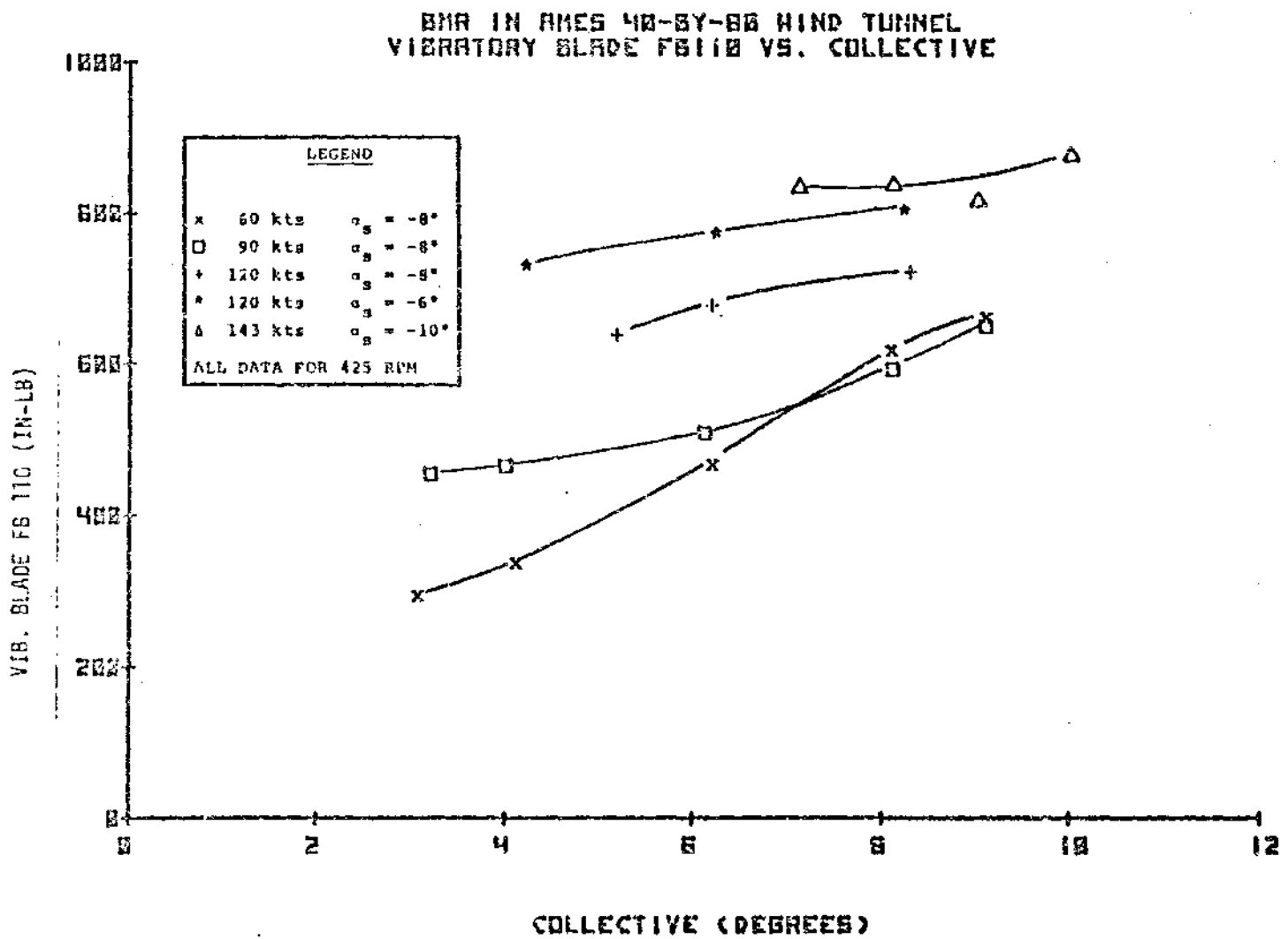

FIGURE 8.62 VIBRATORY FLAP BENDING 110 VERSUS COLLECTIVE

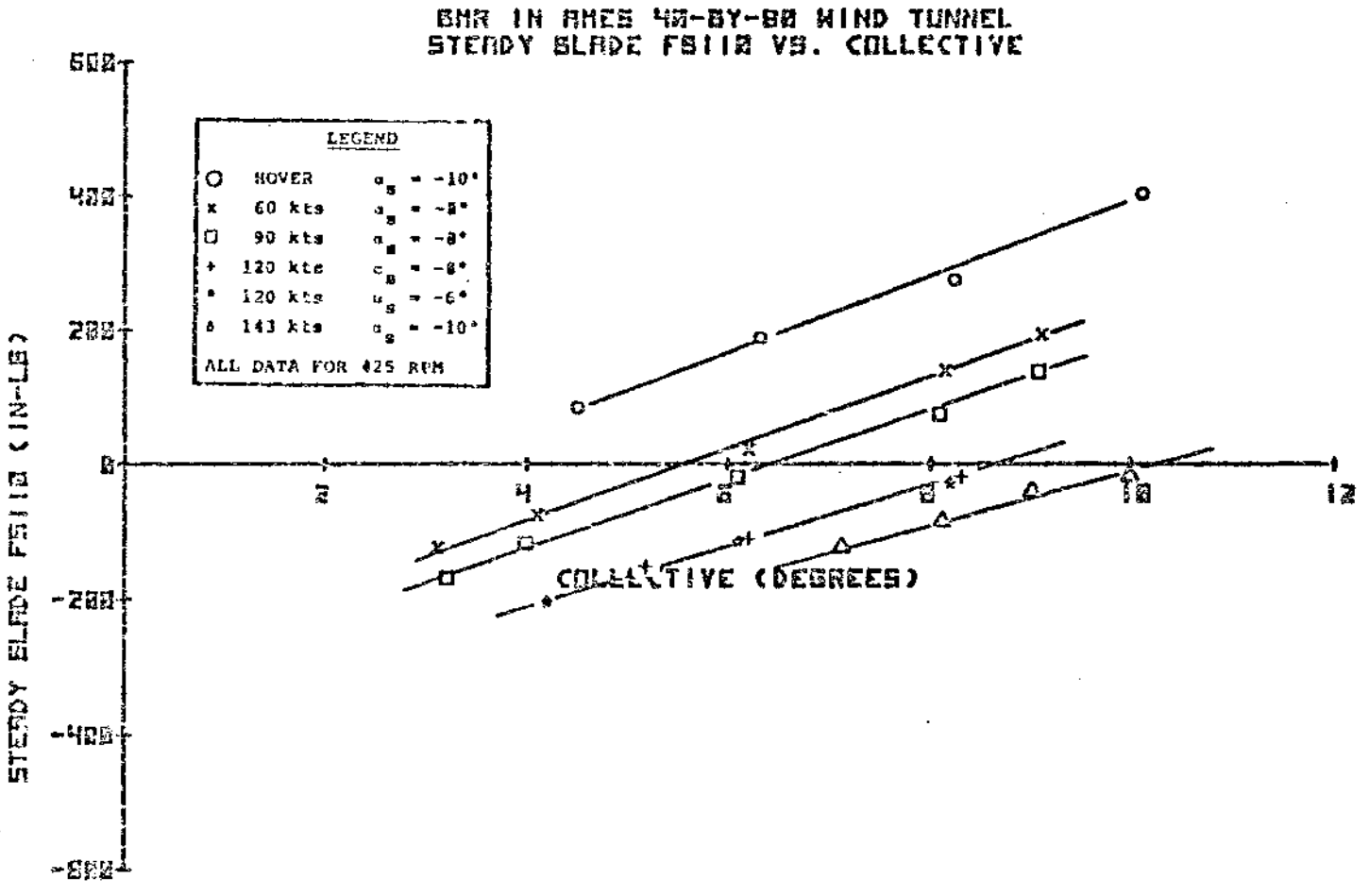

FIGURE 8.63 STEADY FLAP BENDING 110 VERSUS COLLECTIVE

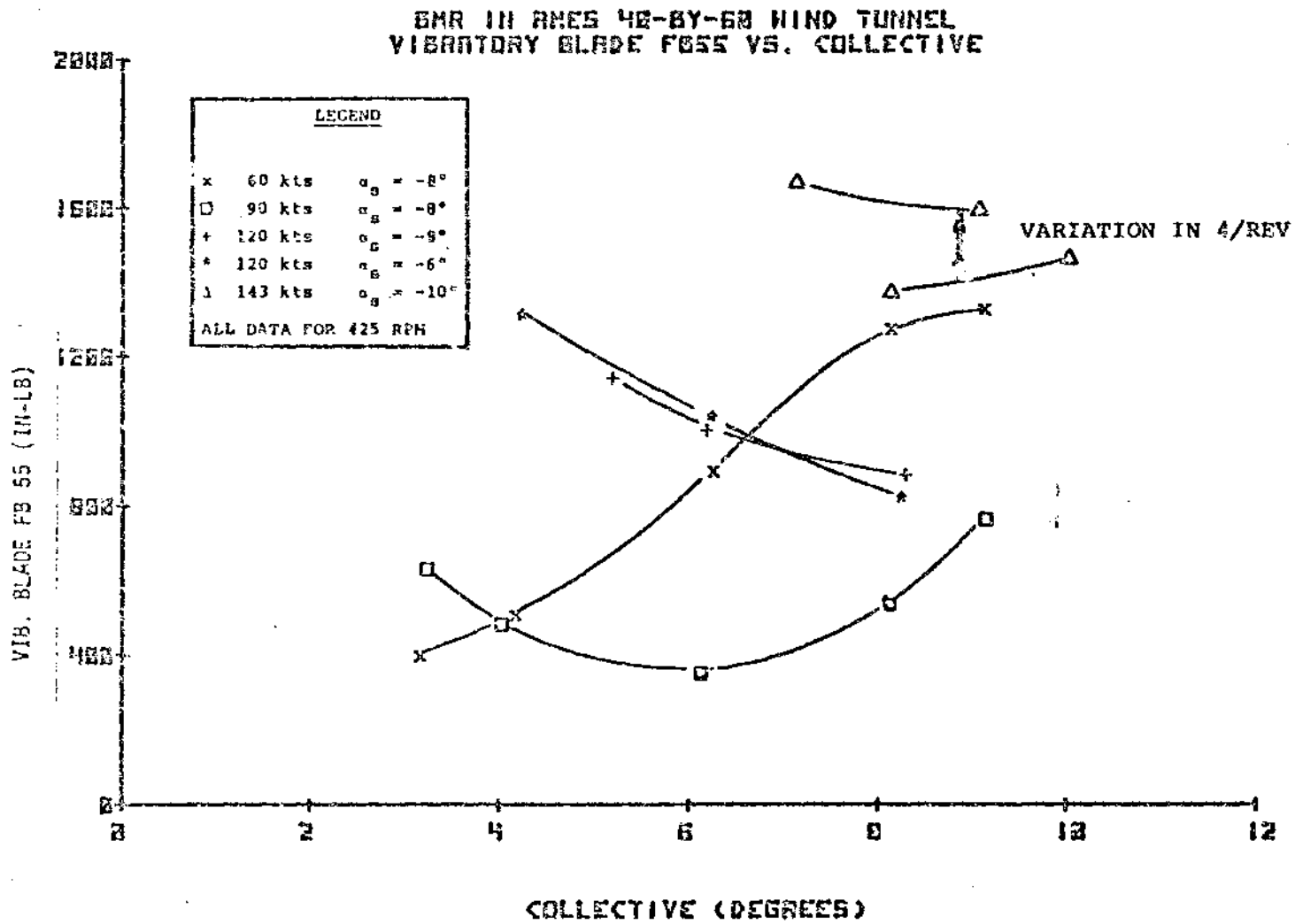

FIGURE 8.64 VIBRATORY FLAP BENDING 55 VERSUS COLLECTIVE

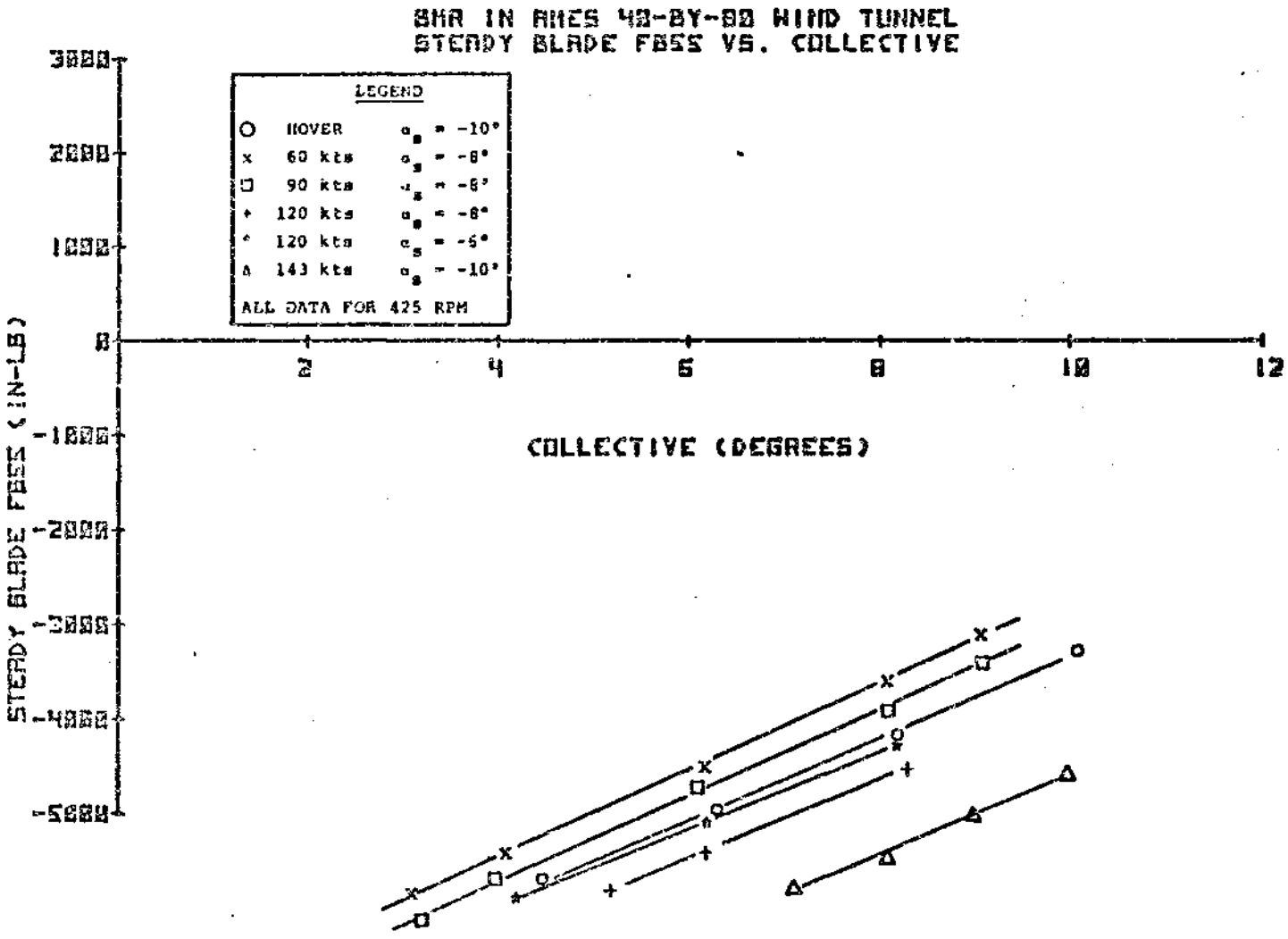

FIGURE 8.65 STEADY FLAP BENDING 55 VERSUS COLLECTIVE

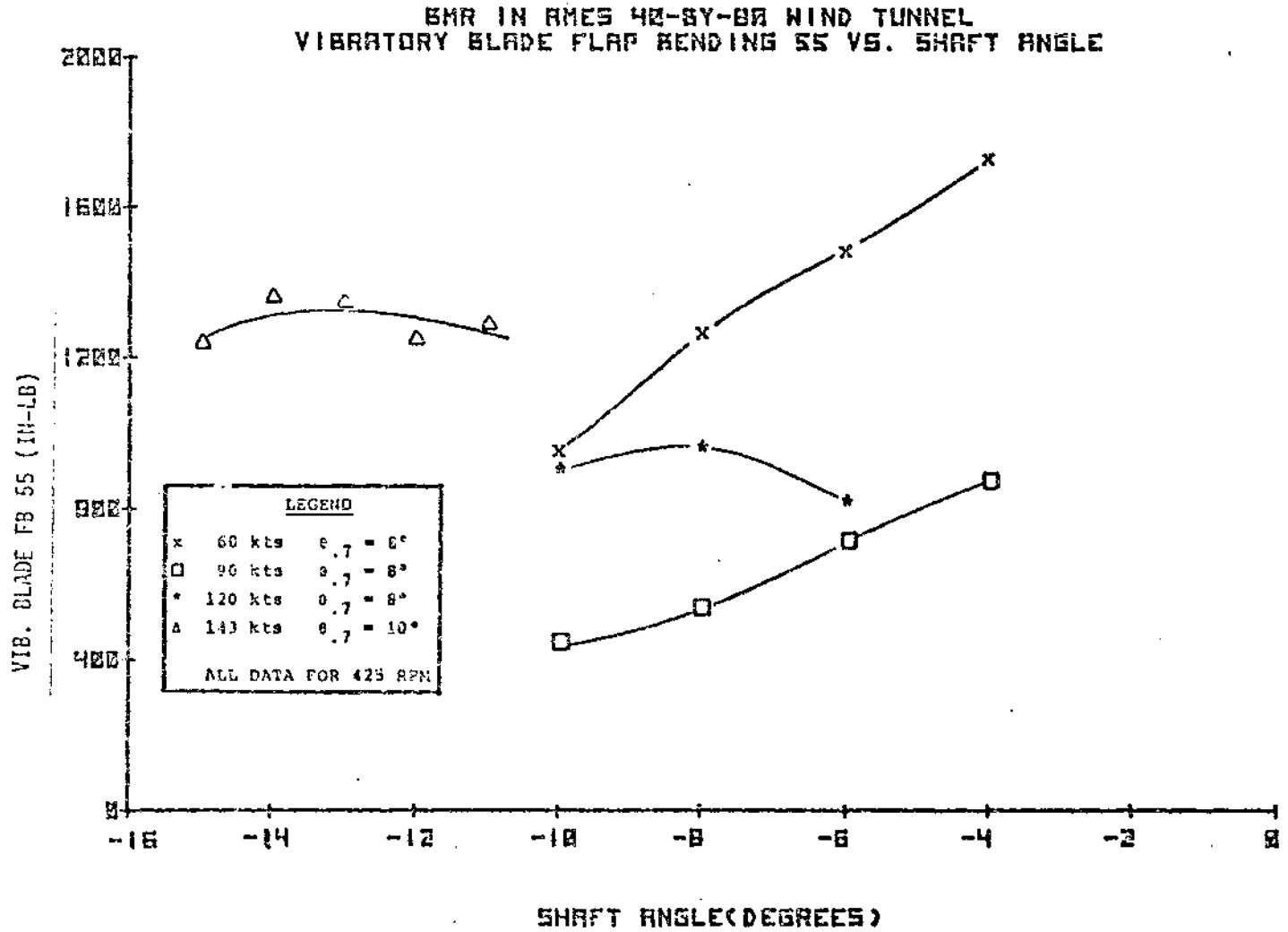

FIGURE 8.66 VIBRATORY FLAP BENDING 55 VERSUS SHAFT ANGLE

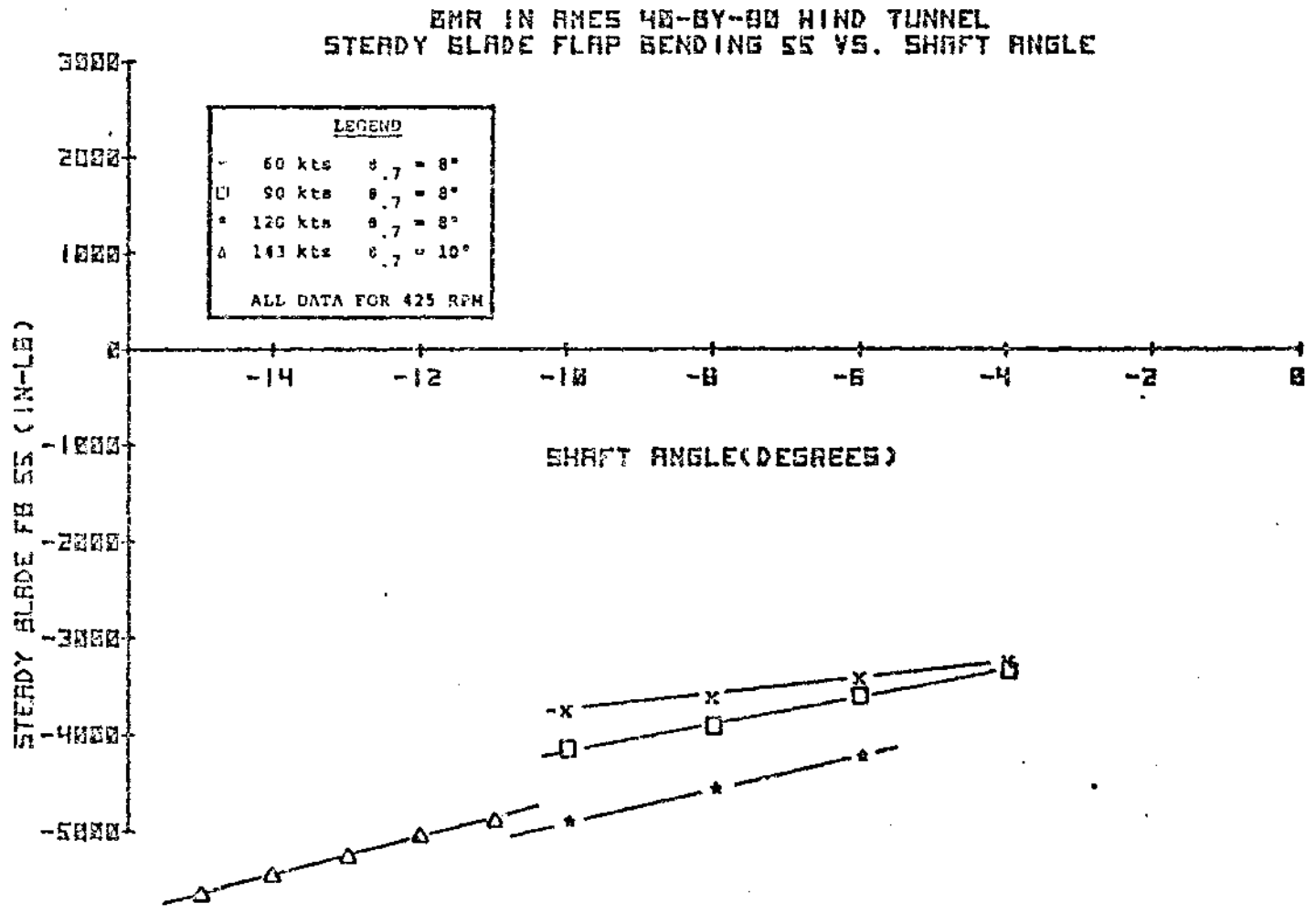

FIGURE 8.67 STEADY FLAP BENDING 55 VERSUS SHAFT ANGLE

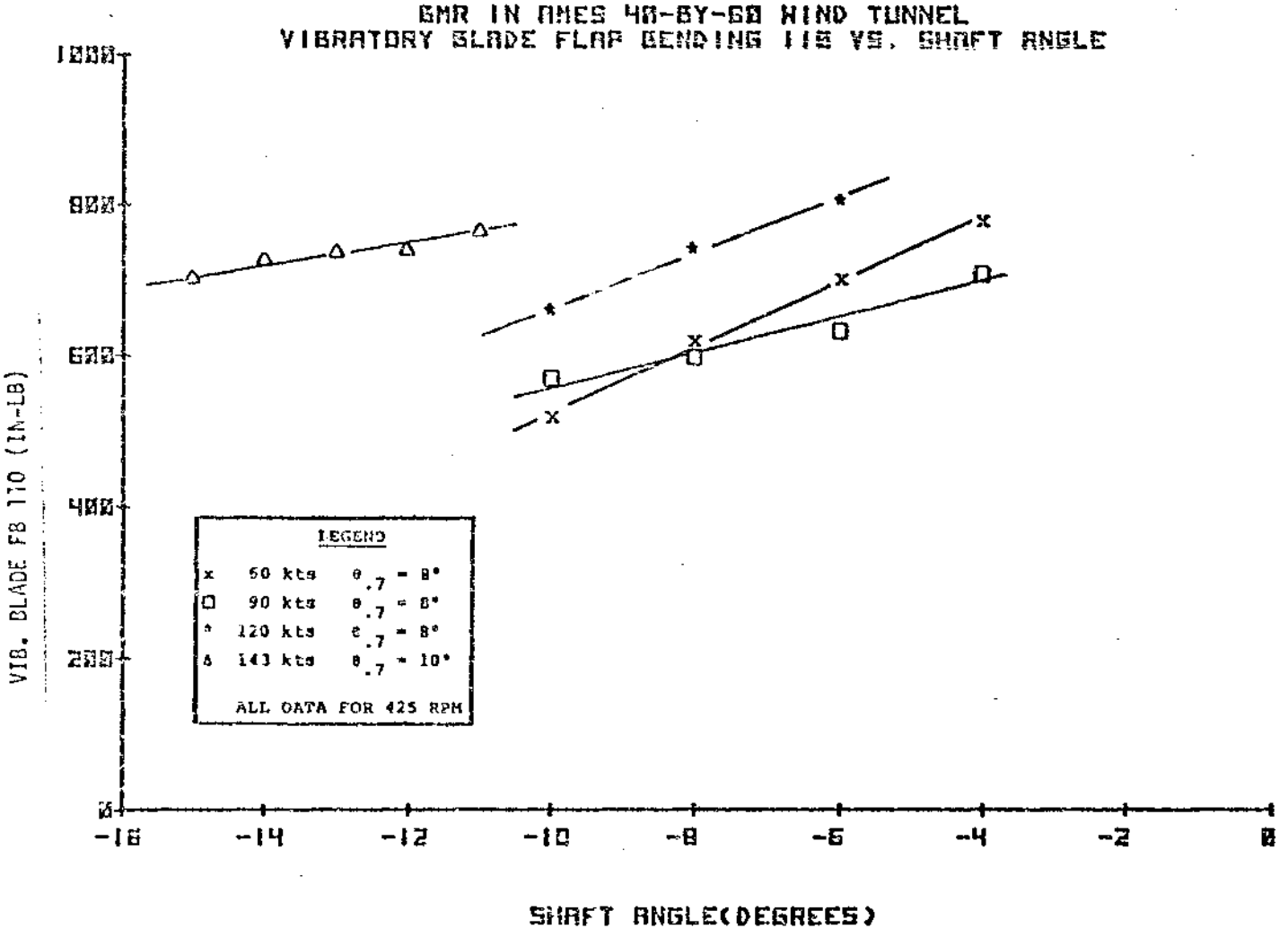

FIGURE 8.68 VIBRATORY FLAP BENDING 110 VERSUS SHAFT ANGLE

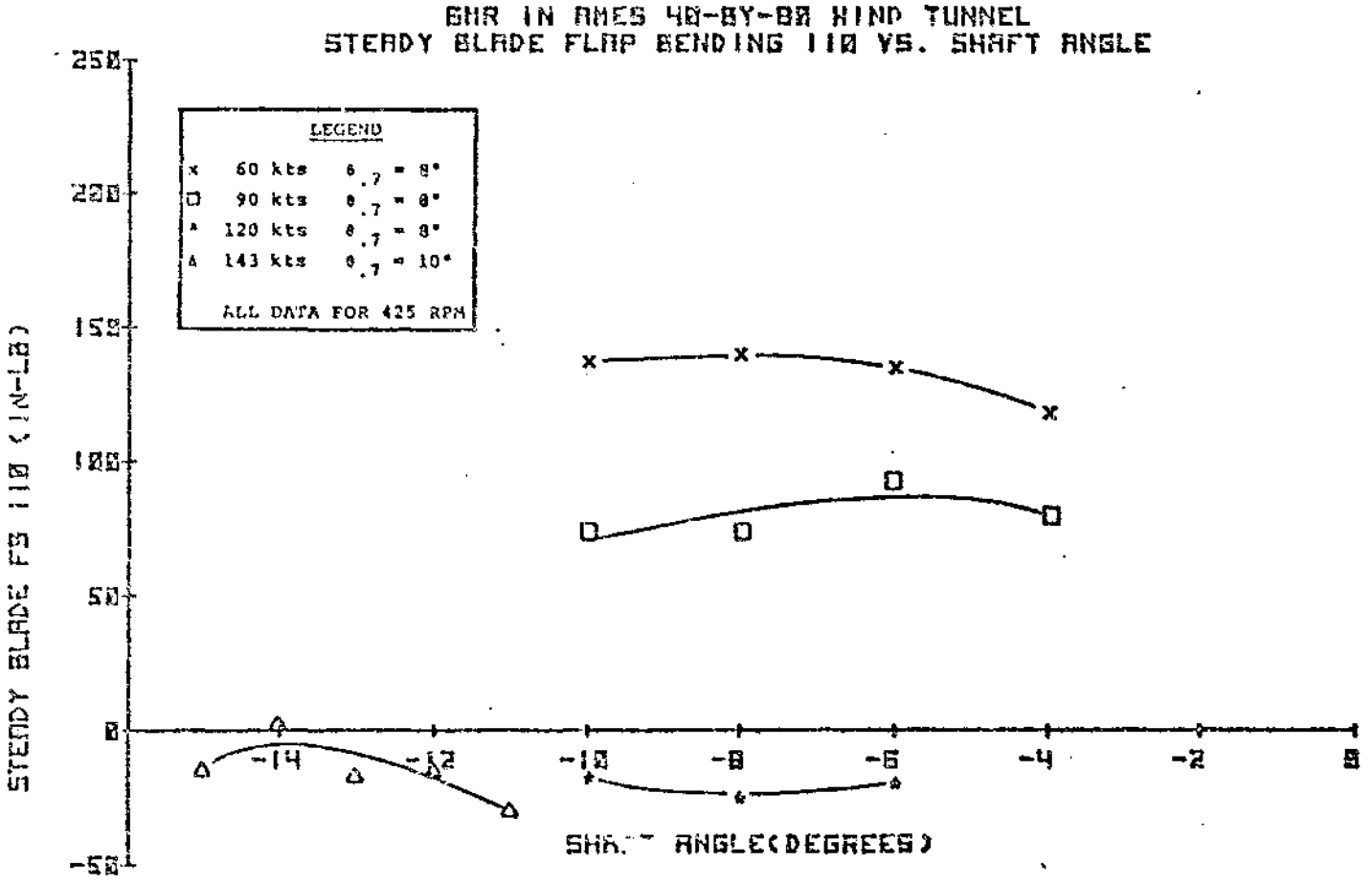

FIGURE 3.69 STEADY FLAP BENDING 110 VERSUS SHAFT ANGLE

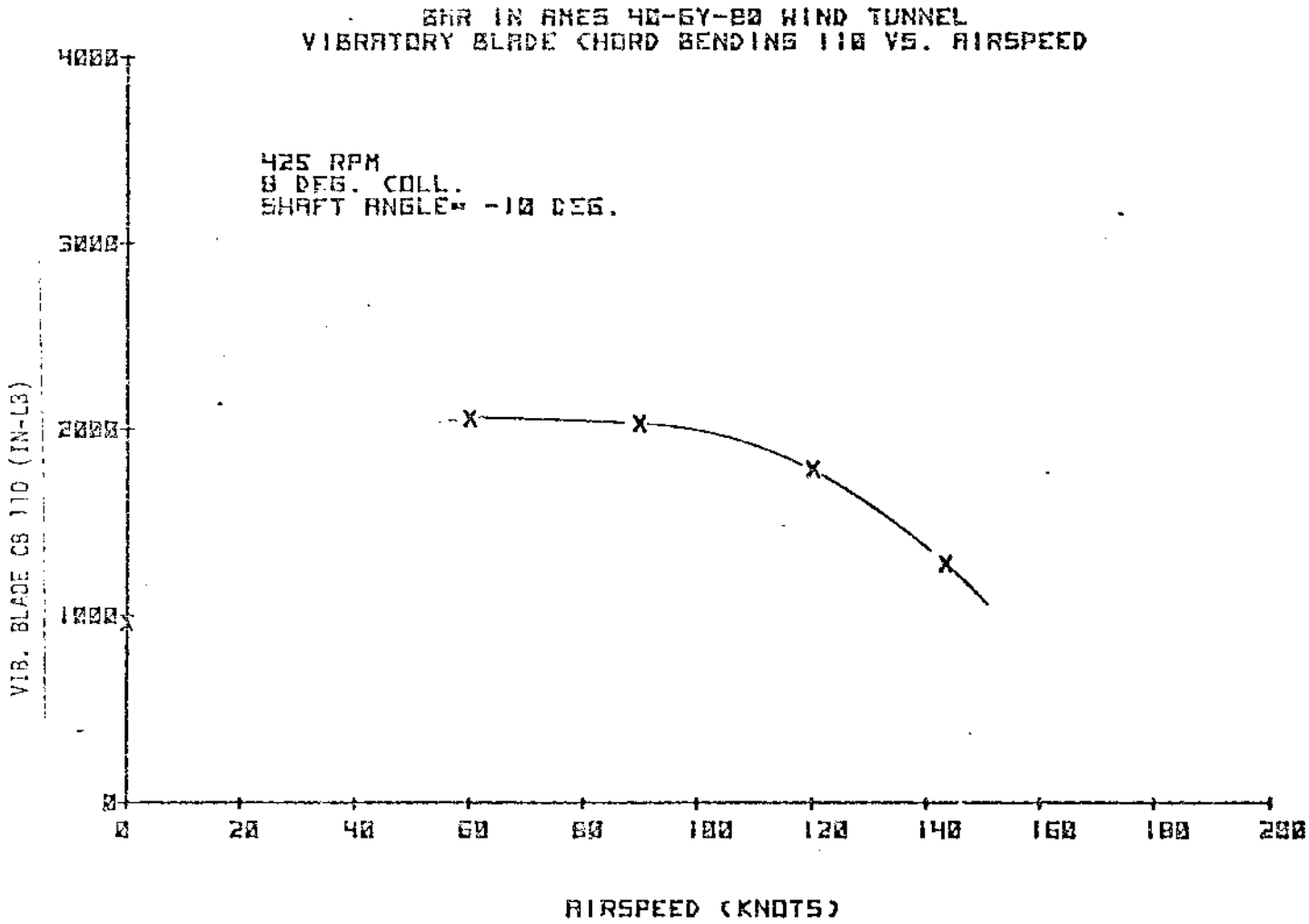

FIGURE 8.70 VIBRATORY CHORD BENDING 110 VERSUS AIRSPEED

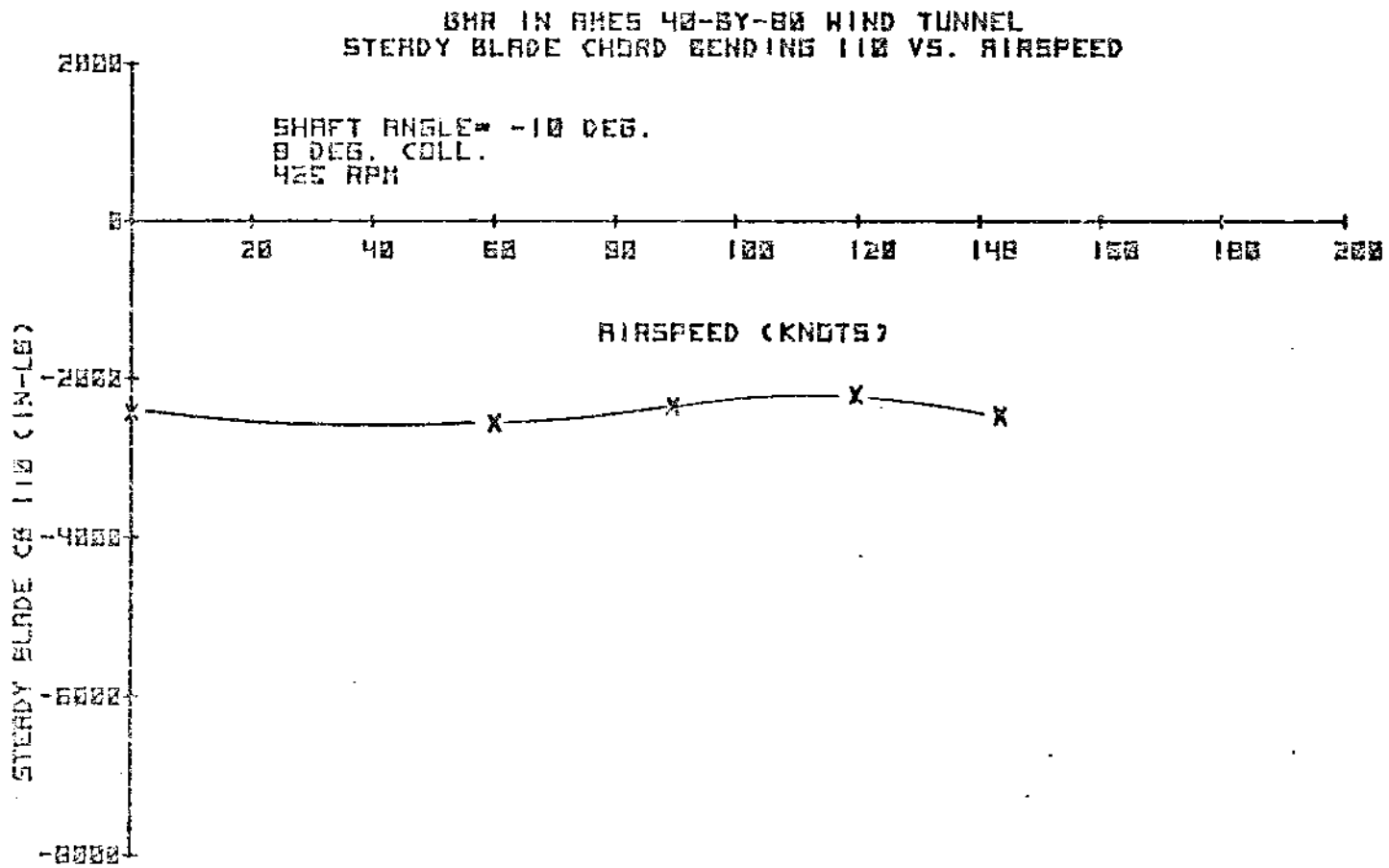

FIGURE 8.71 STEADY CHORD BENDING 110 VERSUS AIRSPEED

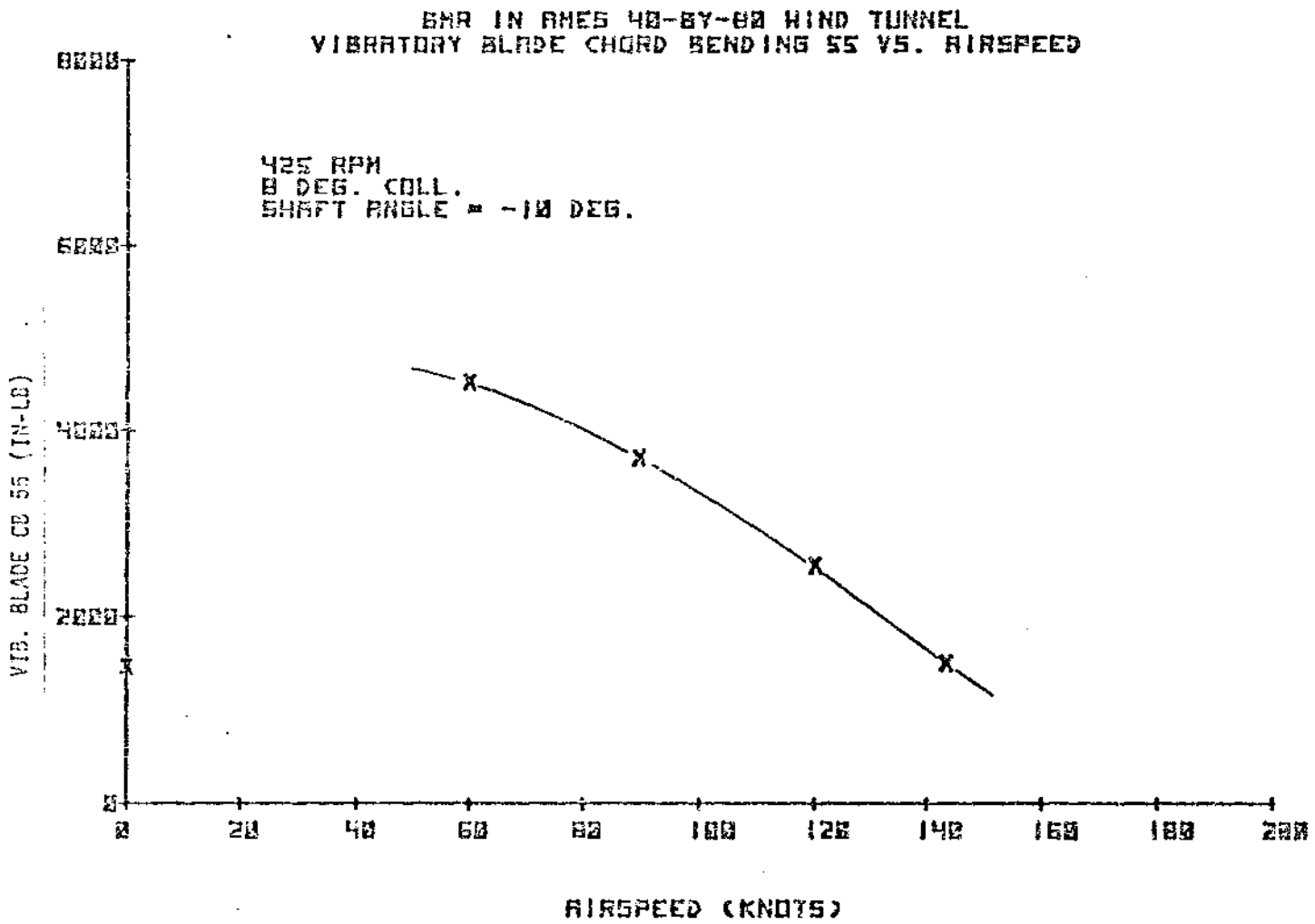

FIGURE 8.72 VIBRATORY CHORD BENDING 55 VERSUS AIRSPEED

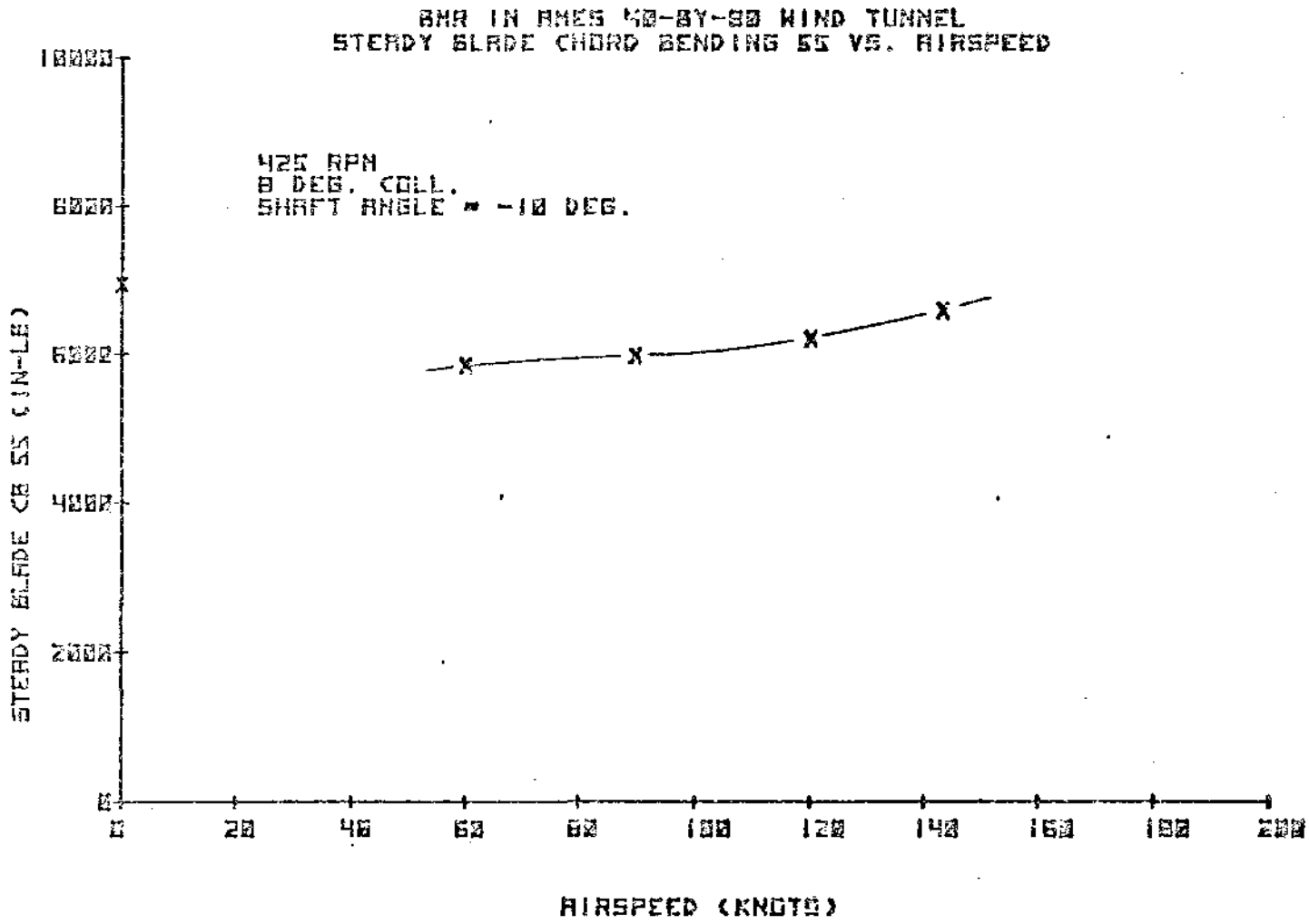

FIGURE 8.73 STEADY CHORD BENDING 55 VERSUS AIRSPEED

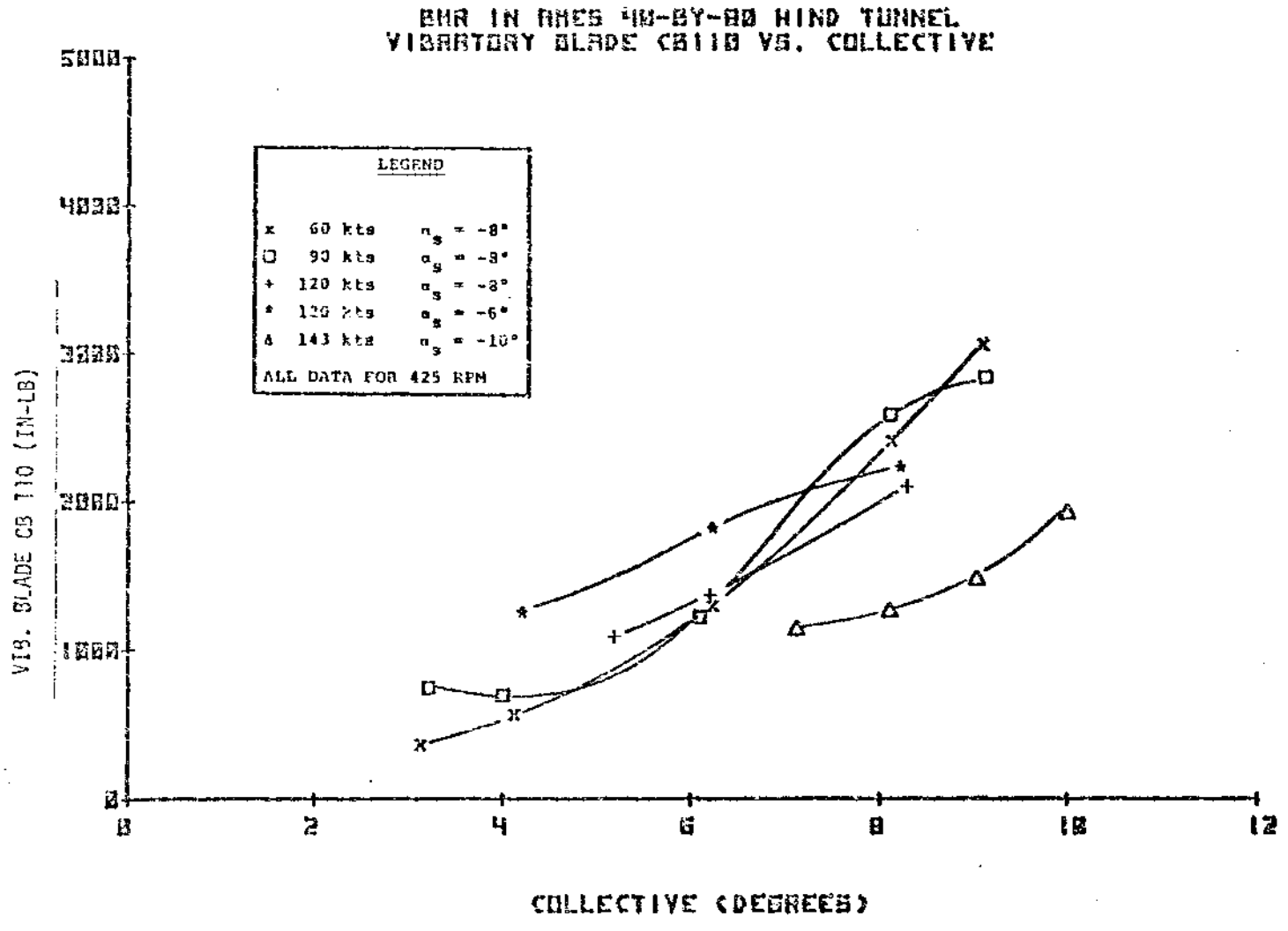

FIGURE 8.74 VIBRATORY CHORD BENDING 110 VERSUS COLLECTIVE

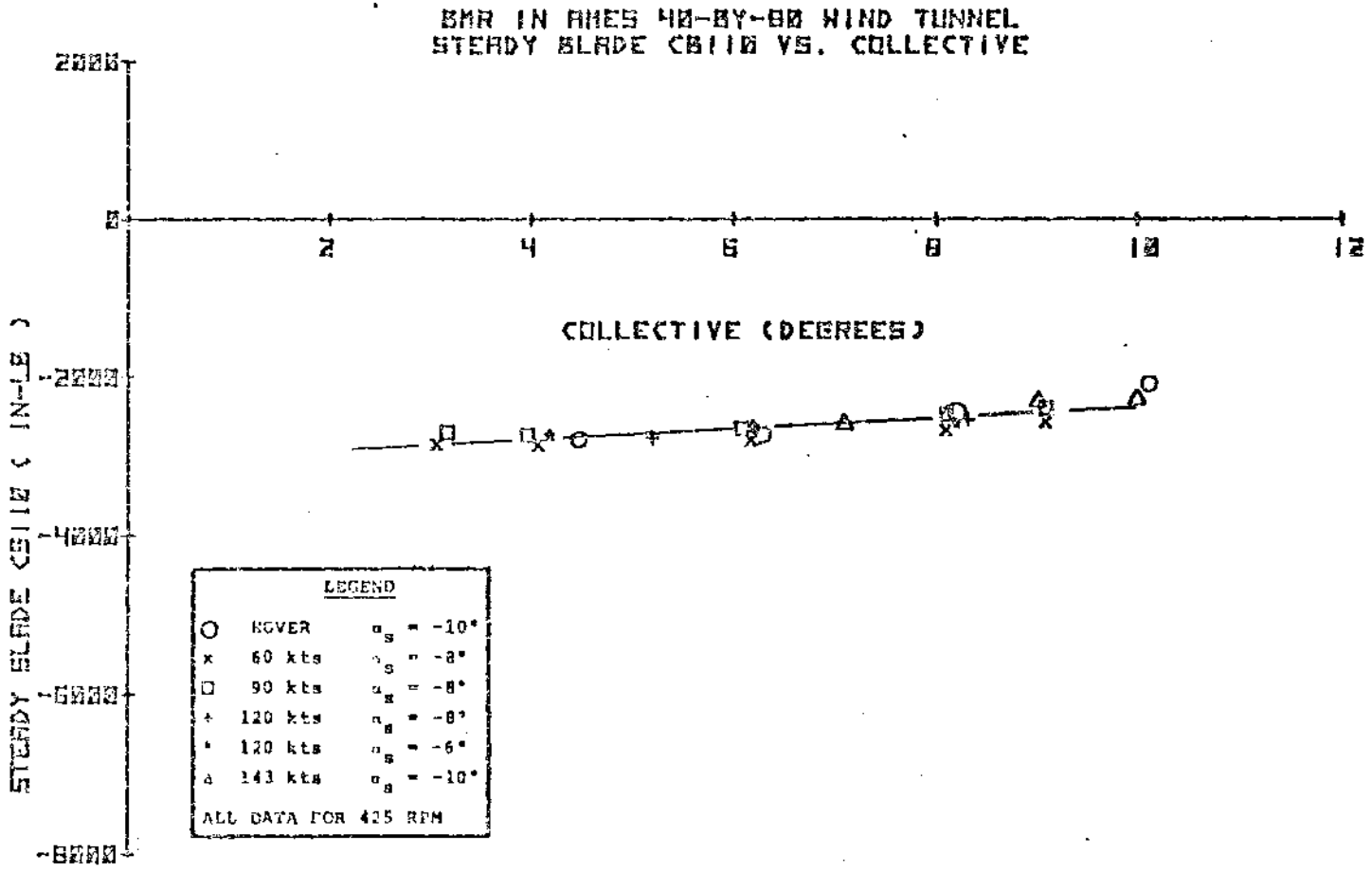

FIGURE 8.75 STEADY CHORD BENDING 110 VERSUS COLLECTIVE

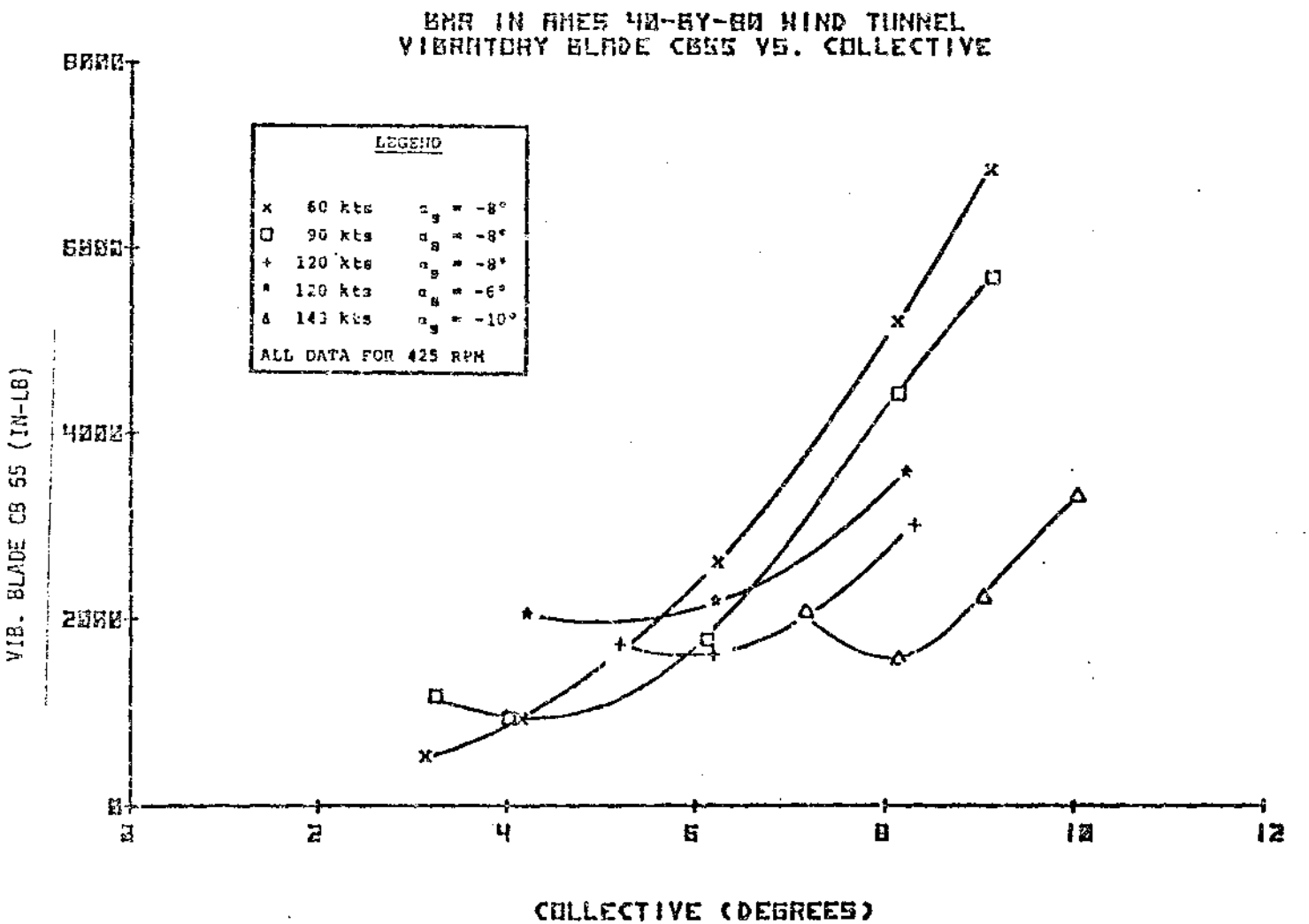

FIGURE 8.76 VIBRATORY CHORD BENDING 55 VERSUS COLLECTIVE

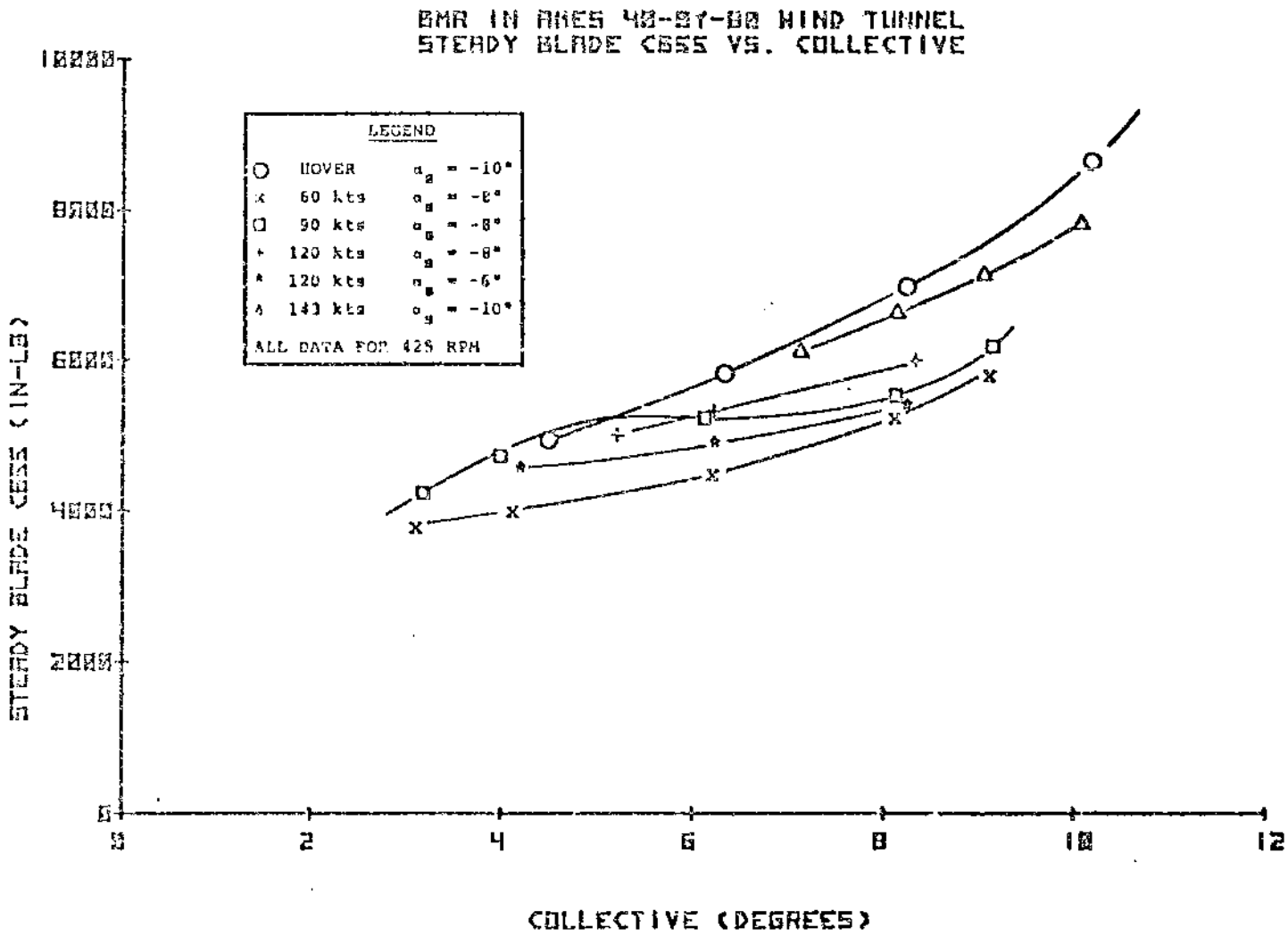

FIGURE 8.77 STEADY CHORD BENDING 55 VERSUS COLLECTIVE

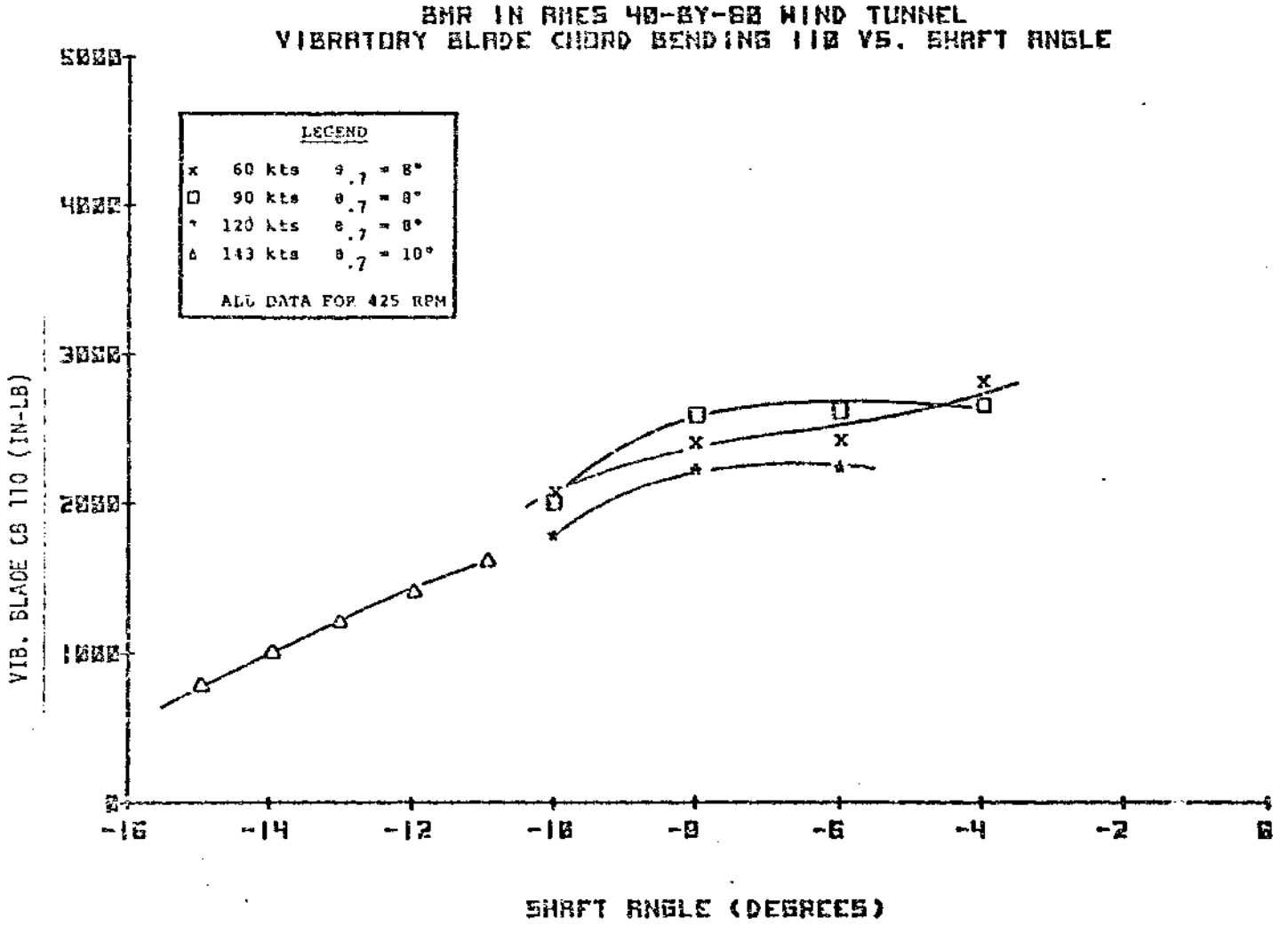

FIGURE 6.78 VIBRATORY CHORD BENDING 110 VERSUS SHAFT ANGLE

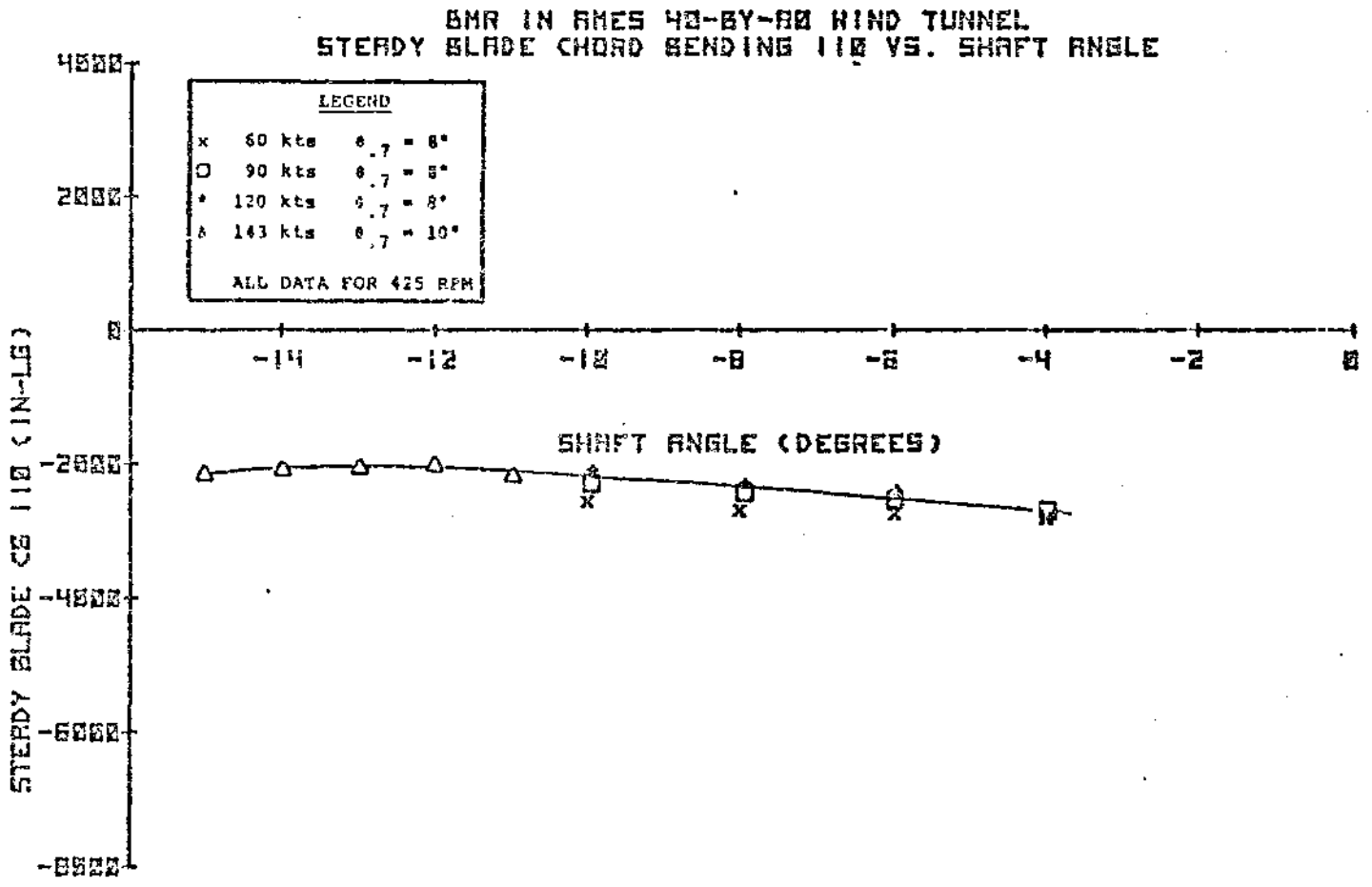

FIGURE 8.79 STEADY CHORD BENDING 110 VERSUS SHAFT ANGLE

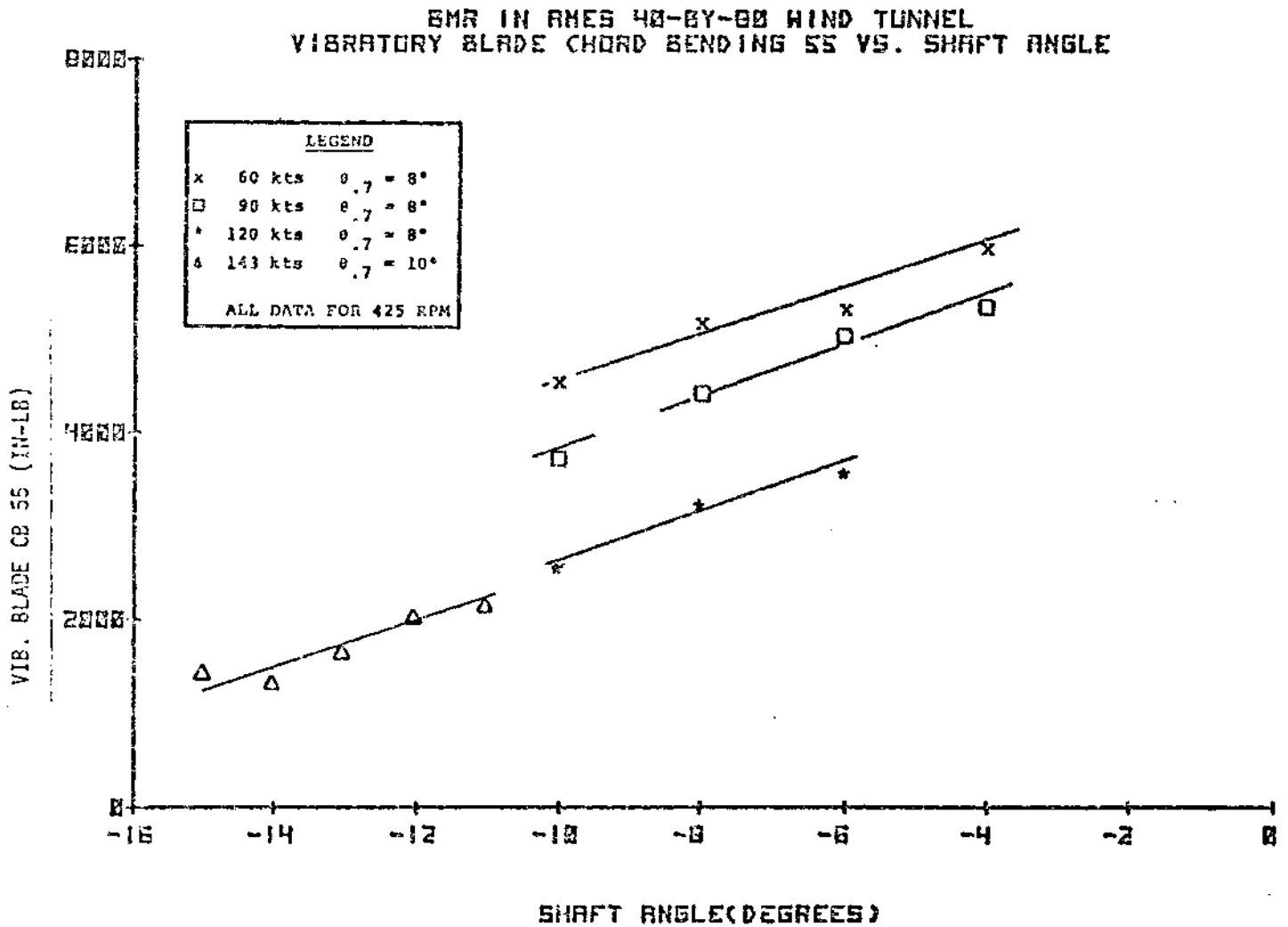

FIGURE 8.80 VIBRATORY CHORD BENDING 55 VERSUS SHAFT ANGLE

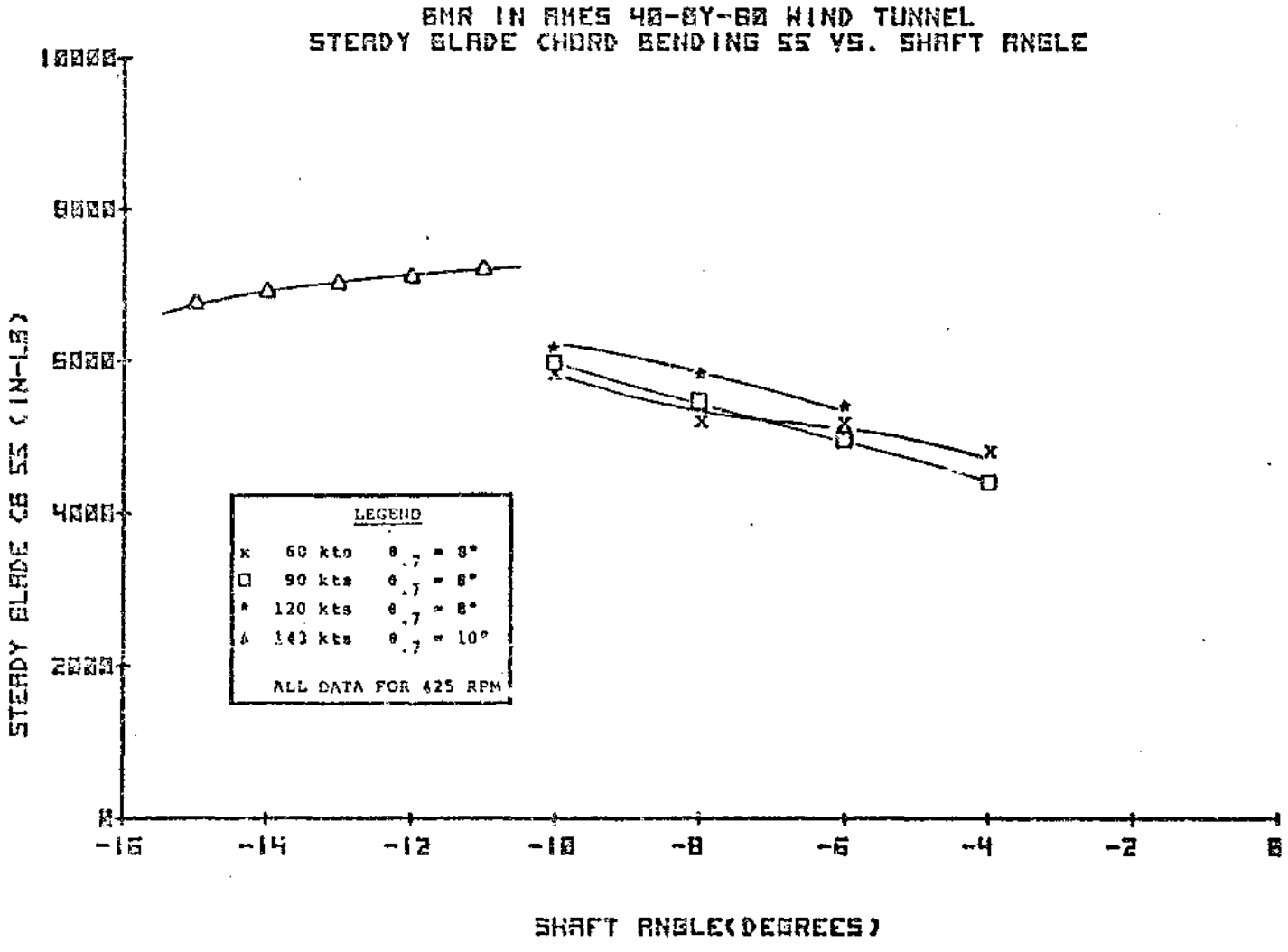

FIGURE 8.81 STEADY CHORD BENDING 55 VERSUS SHAFT ANGLE

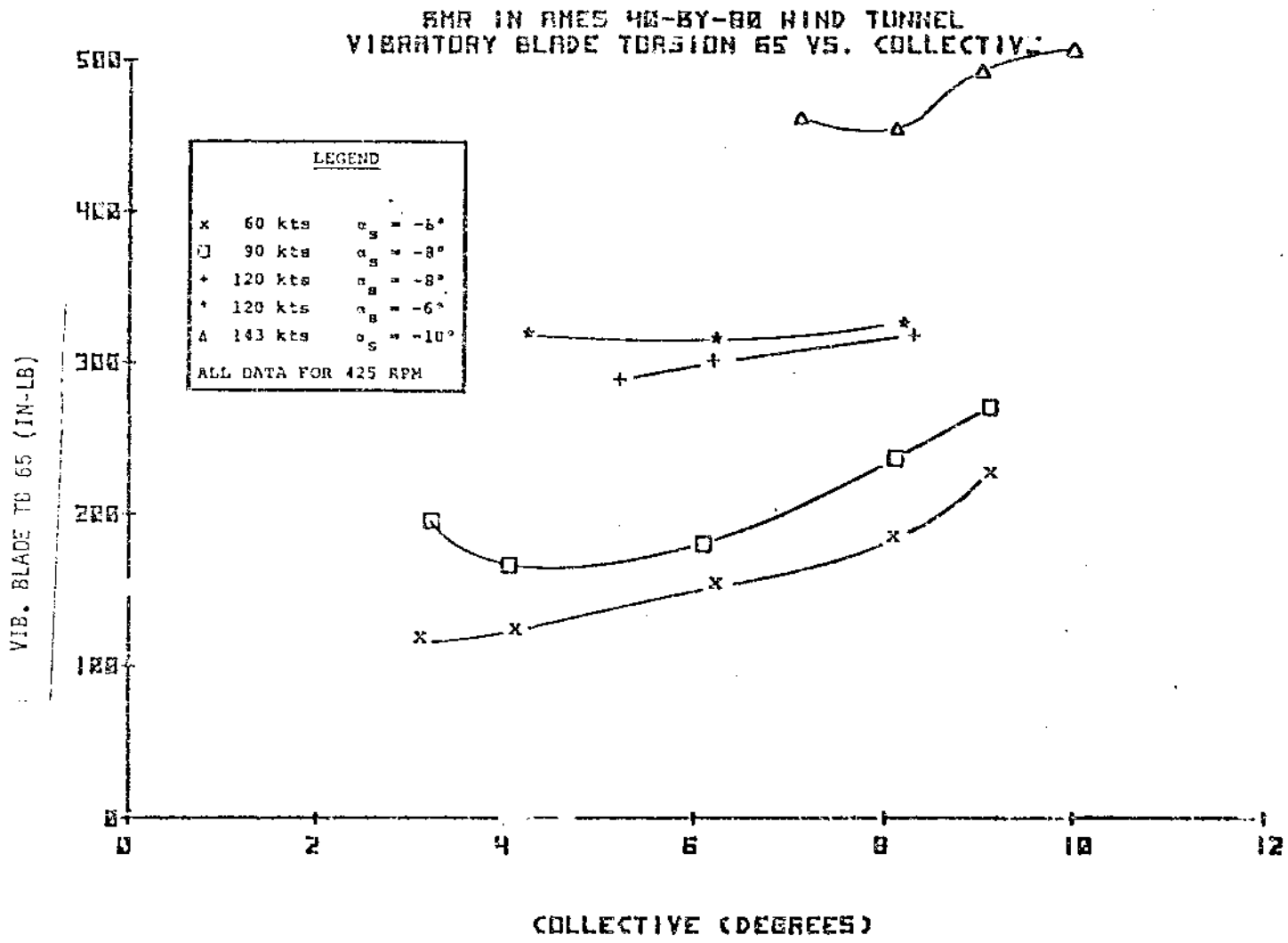

FIGURE 8.82 VIBRATORY BLADE TORSION 65 VERSUS COLLECTIVE

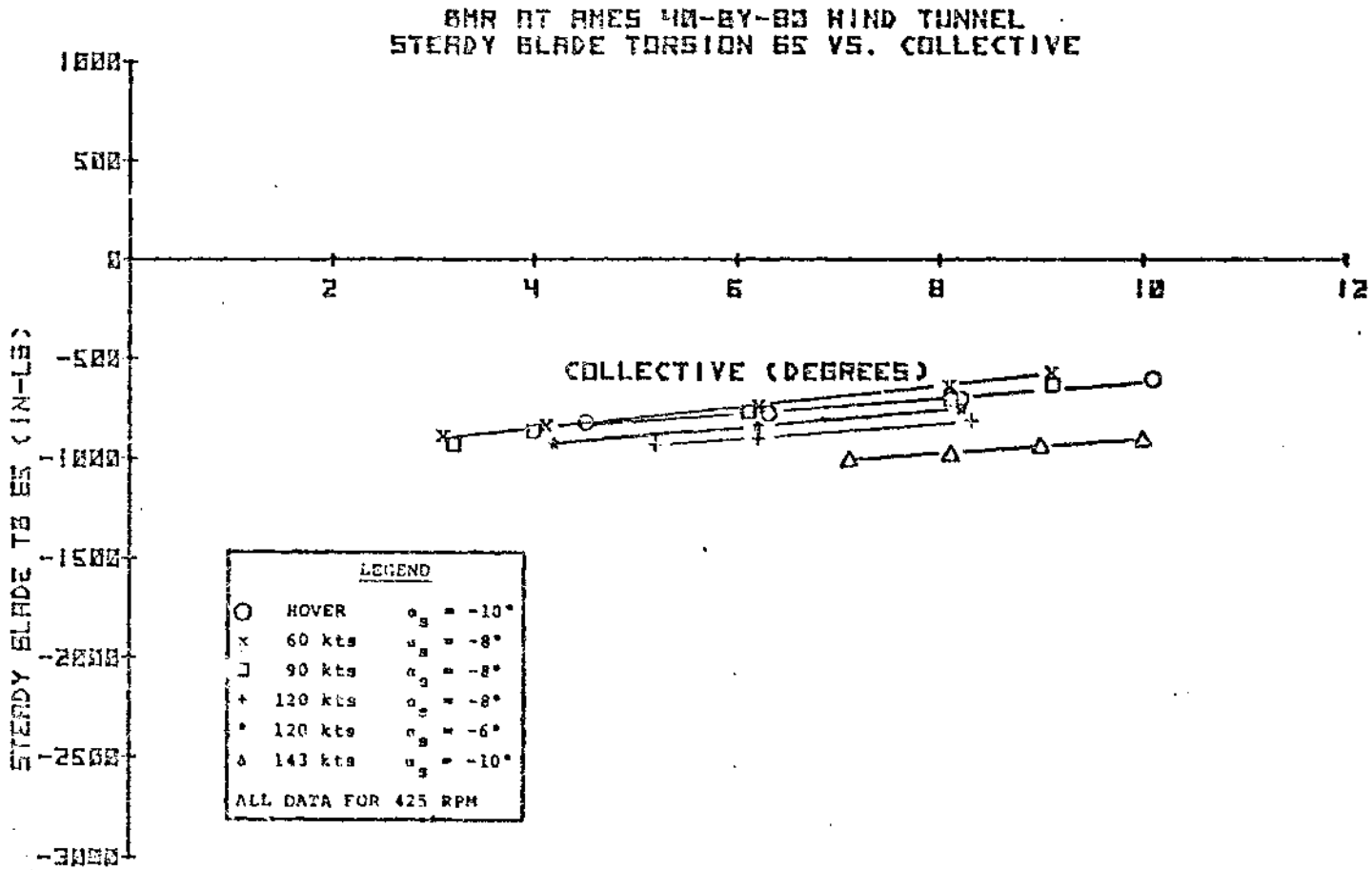

FIGURE 8.83 STEADY TORSION 65 VERSUS COLLECTIVE

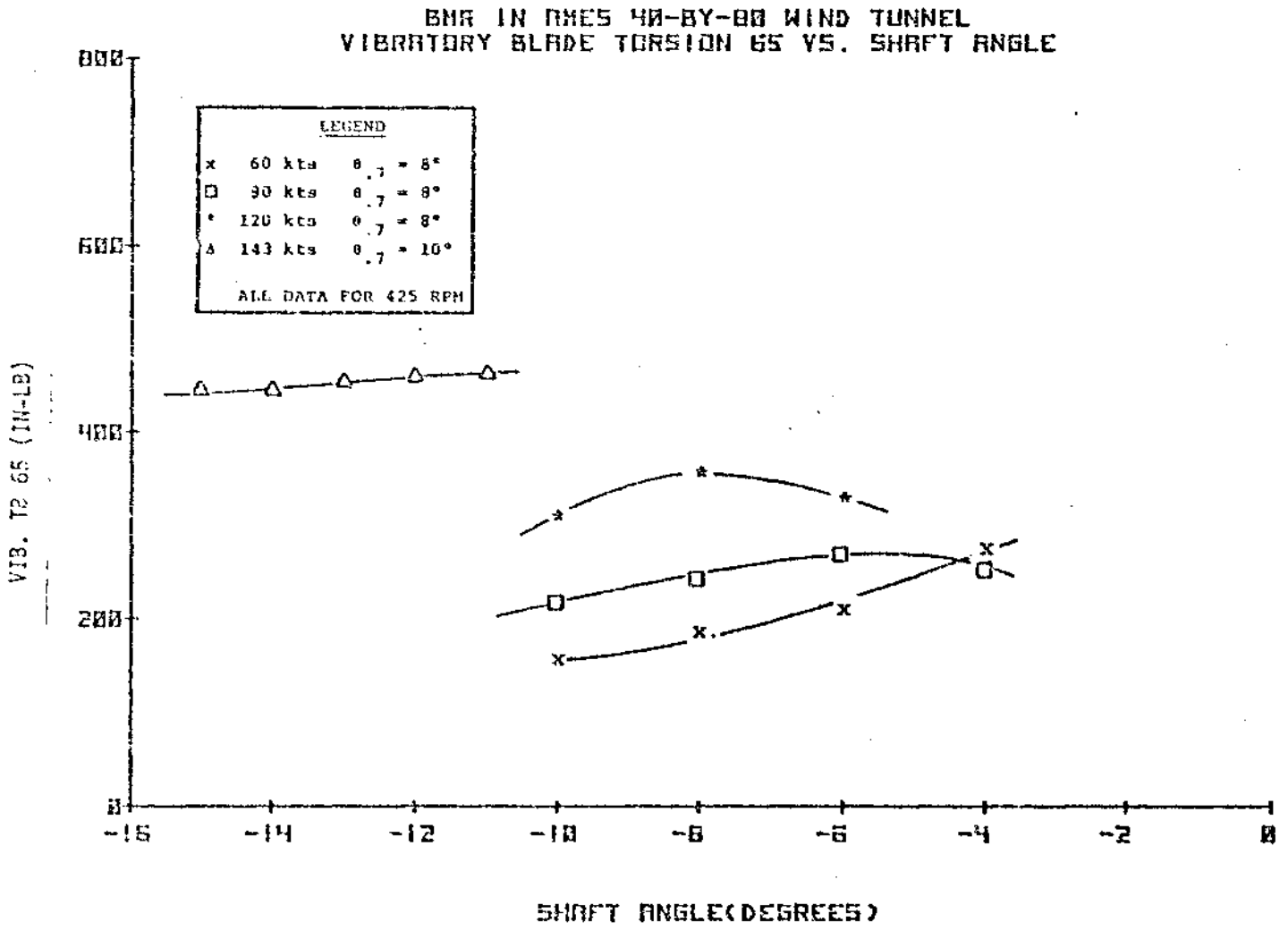

FIGURE 8.64 VIBRATORY BLADE TORSION 65 VERSUS SHAFT ANGLE

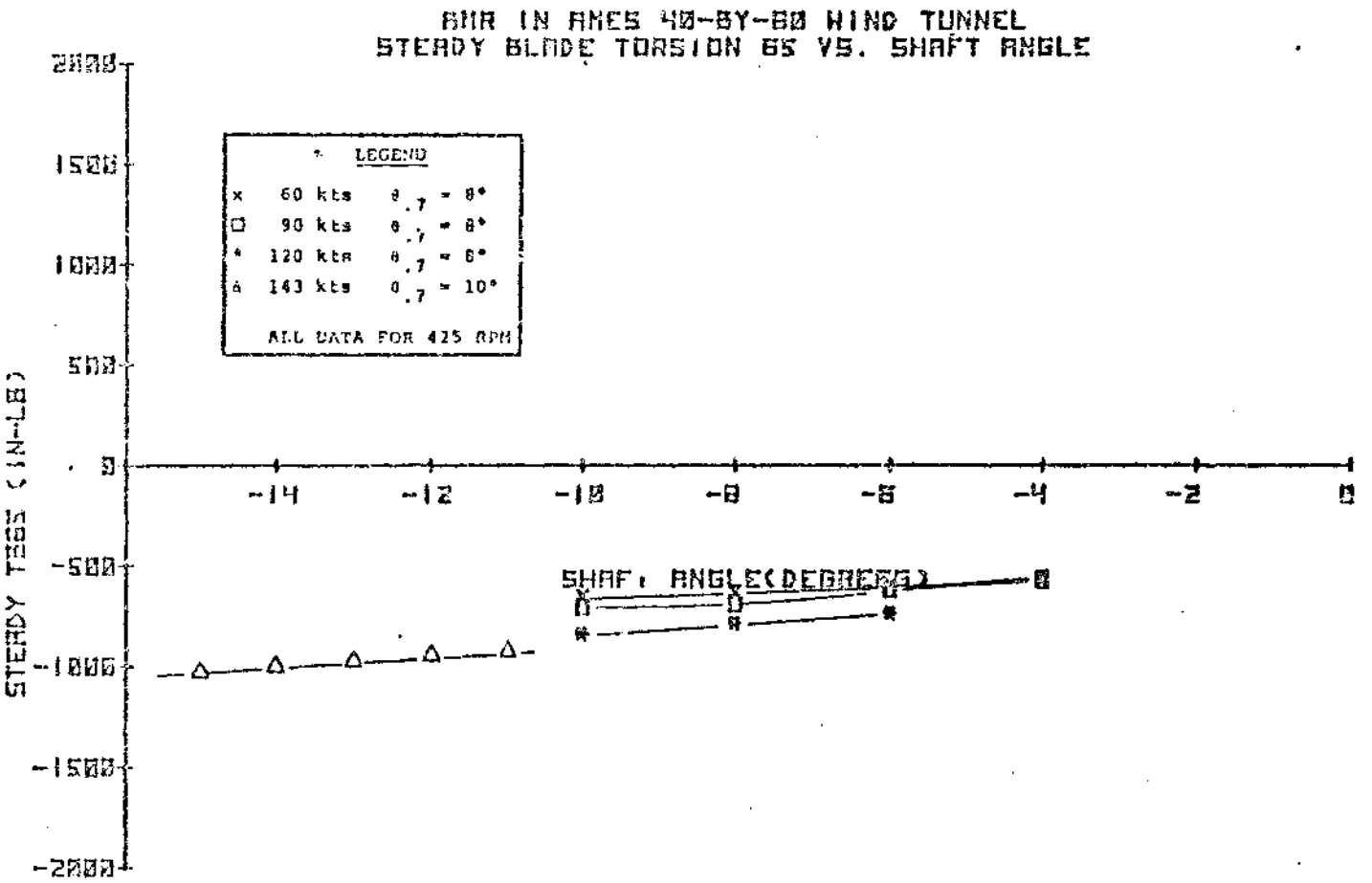

FIGURE 8.85 STEADY TORSION 65 VERSUS SHAFT ANGLE

8.2.2.3 Flexbeam Load Trends

Flexbeam flap moments as a function of airspeed are presented in Figures 8.86 through 8.97. Vibratory flap moments exhibit the expected trend with relatively constant vibratory levels out to about 90 knots, with a knee and subsequent build-up at higher airspeeds. The spanwise distribution indicates that the outboard and inboard ends are most critical. The most critical location is span station 44 inches on the trailing beam (Figure 8.88). The peak load limit (steady plus vibratory) for this same station is one of the constraints on additional envelope expansion. Peak load limits for the flexbeam were set at 80% of the load level achieved in static proof tests. Those load levels were the predicted limit loads for a 3.5g load factor within the BO-105 flight envelope. Flap down bending is the critical peak flapping mode. As can be seen in the steady flap plots, considerable peak value margin exists in transition with critical flap down steadies occurring at high airspeeds.

Vibratory flapping moments show increases with higher collective settings at constant rpm and shaft angle consistent with the build-up in airloads. At low collective settings, there is some small load build-up reflecting increased sensitivity to trim. Figures 8.98 through 8.109 present flap moments versus collective pitch for stations 44, 18, and 10.5 for both the leading and trailing beam. Slope differences in the steady moments between leading and trailing beams reflect the effect of twist along the span of the flexbeams.

Total vibratory flexbeam flapping at station 44 increases with increasing positive shaft angles at constant rpm and collective, which is consistent with results shown for the blade root section. This effect is less pronounced at the more inboard flexbeam stations. Data are presented in Figures 8.110 through 8.117. The differences in load distribution between the leading and trailing beams may be due to the blade clevis rotation causing a different flap mode shape in each beam and the chord bending motion causing differential centrifugal stiffening. These same effects are visible in the steady flap moments which exhibit a linear increase in flap bending as the shaft angle becomes more positive.

Flexbeam chord bending moments as a function of airspeed at constant rpm, collective and shaft angle are shown in Figures 8.118 through 8.121. Vibratory chord bending moments show a significantly higher level in the intermediate speed range (40 to 80 knots) with relatively low values at hover and 143 knots. This trend is identical to the blade chord bending trend. Inboard and outboard moments on beam A (leading beam) indicate an "S" shaped bending mode. Differences between beam A and beam B steady chord moments at station 43 indicate opposing rotations at the outboard end of the flexbeams. A potential source for this action is an assymmetric line of action of the centrifugal force which would tend to produce a different mode shape for the leading and trailing beam. The chord bending gage on beam B failed prior to this phase of the testing.

Figures 8.122 through 8.125 present the variation of flexbeam chord bending moment with collective at constant rpm and shaft angle. Vibratory moments increase rapidly with higher collective settings. The distribution between leading and trailing beams tends to be equal in the vibratory mode. By contrast, steady moments are leading edge tension in the leading beam and trailing edge tension in the trailing beam consistent with a bowing effect across the tie between the beams at the blade attachment point.

Figures 8.126 through 8.129 present flexbeam chord bending moments as a function of shaft angle at constant rpm and collective. Vibratory moments tend to be shared equally by the leading and trailing beams. Outboard chord bending shows a limited variation with shaft angle. There is a general correspondence between the midspan versus the root section of the blade (Figures 8.78 through 8.81) and the outboard versus the inboard end of the flexbeam. The cumulative effects of shear force and twist result in greater changes in moments at the inboard sections of the blade and flexbeam as the shaft angle is varied at constant rpm and collective. Moment levels at the outboard sections show little or no change with shaft angle. The dual beam concept results in differential centrifugal forces and chord shears between the leading and trailing beams with relatively small local chord moments. Small changes in the chord shears at the outboard end show up as larger changes in the

local chord moment at the flexbeam root end due to the large moment arm from station 49 in the inboard end.

During start-up and shut-down of the rotor, the one per rev crossing of the first chordwise mode resulted in momentary chord bending responses in excess of the endurance limit. The outboard chord bending was more critical than the inboard chord bending for this excitation. During excitation of the rotor for stability data, the inboard chord bending section was critical. No significant rotor speed effects were observed in the operating speed range.

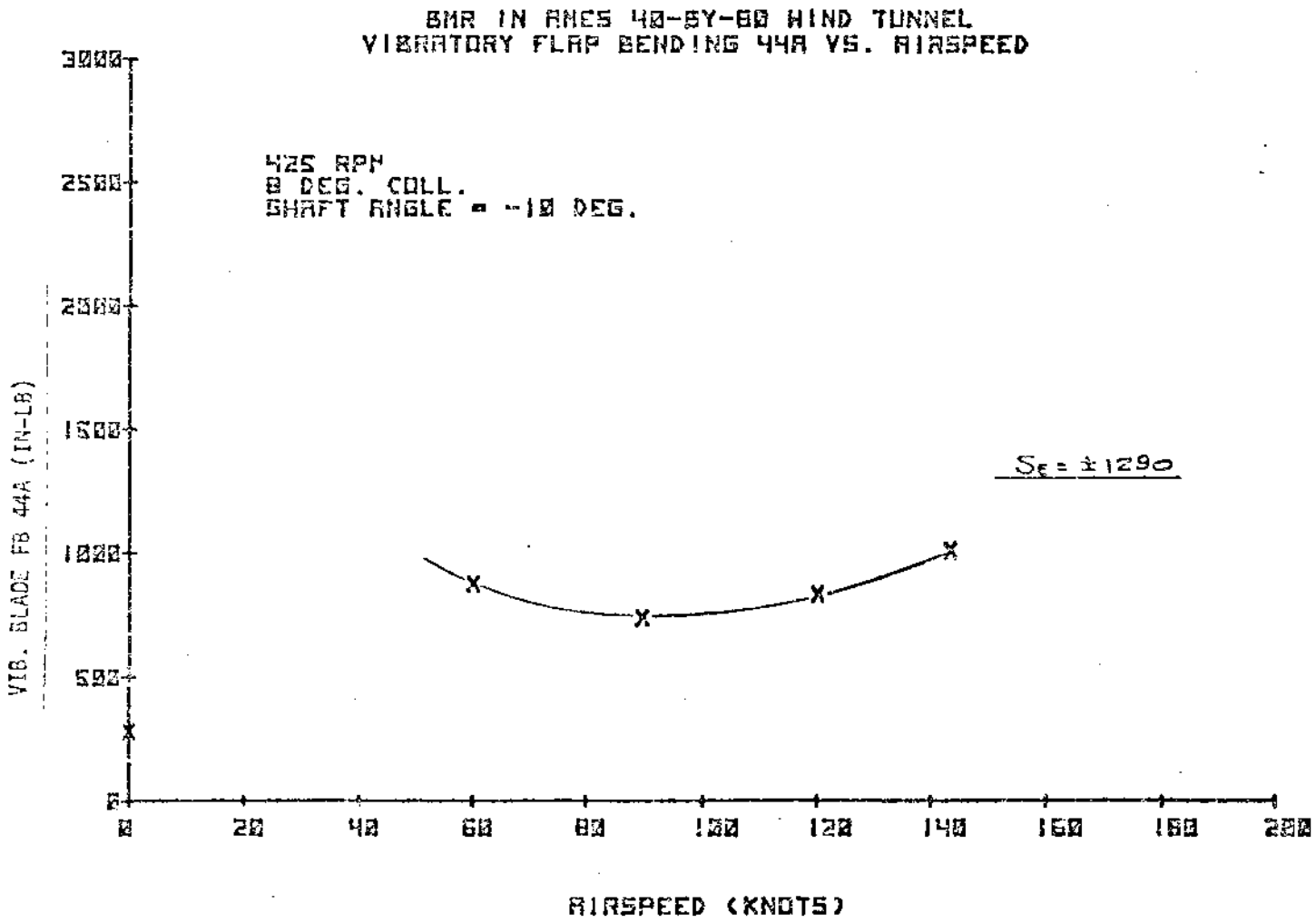

FIGURE 8.86 VIBRATORY FLAP BENDING 44A VERSUS AIRSPEED

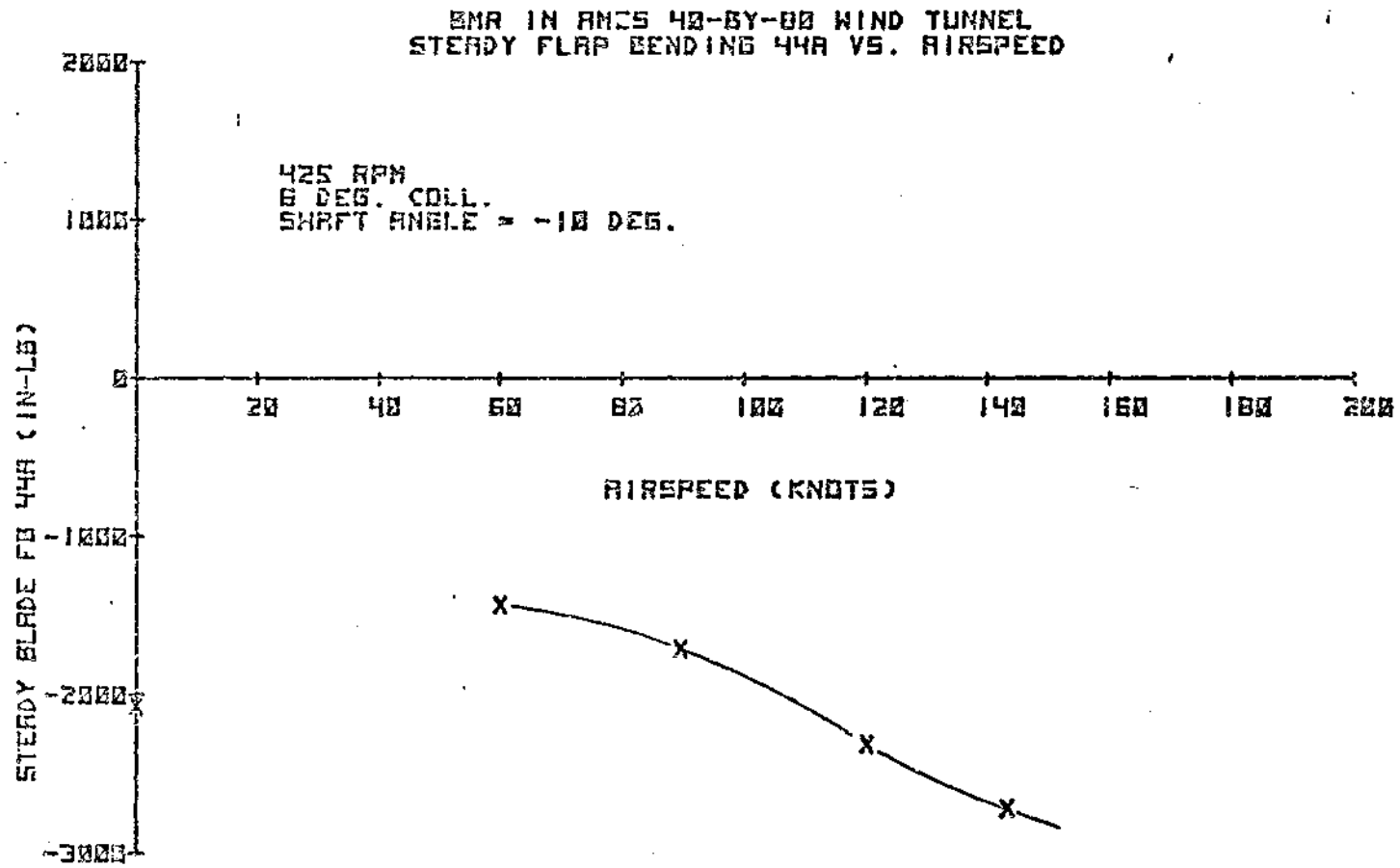

FIGURE 8.87 STEADY FLAP BENDING 44A VERSUS AIRSPEED

$S_L = -7200$

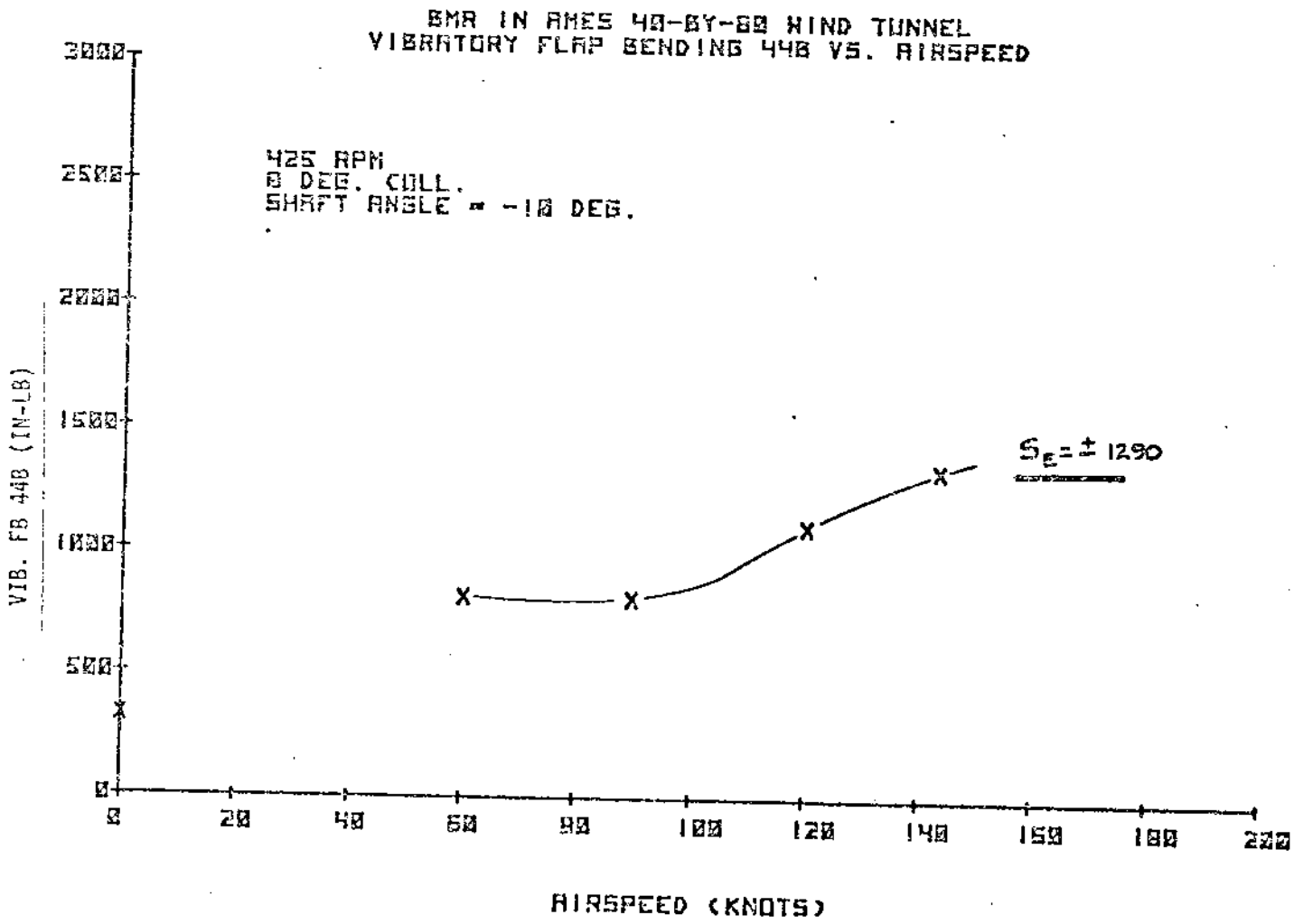

FIGURE 8.88 VIBRATORY FLAP BENDING 44B VERSUS AIRSPEED

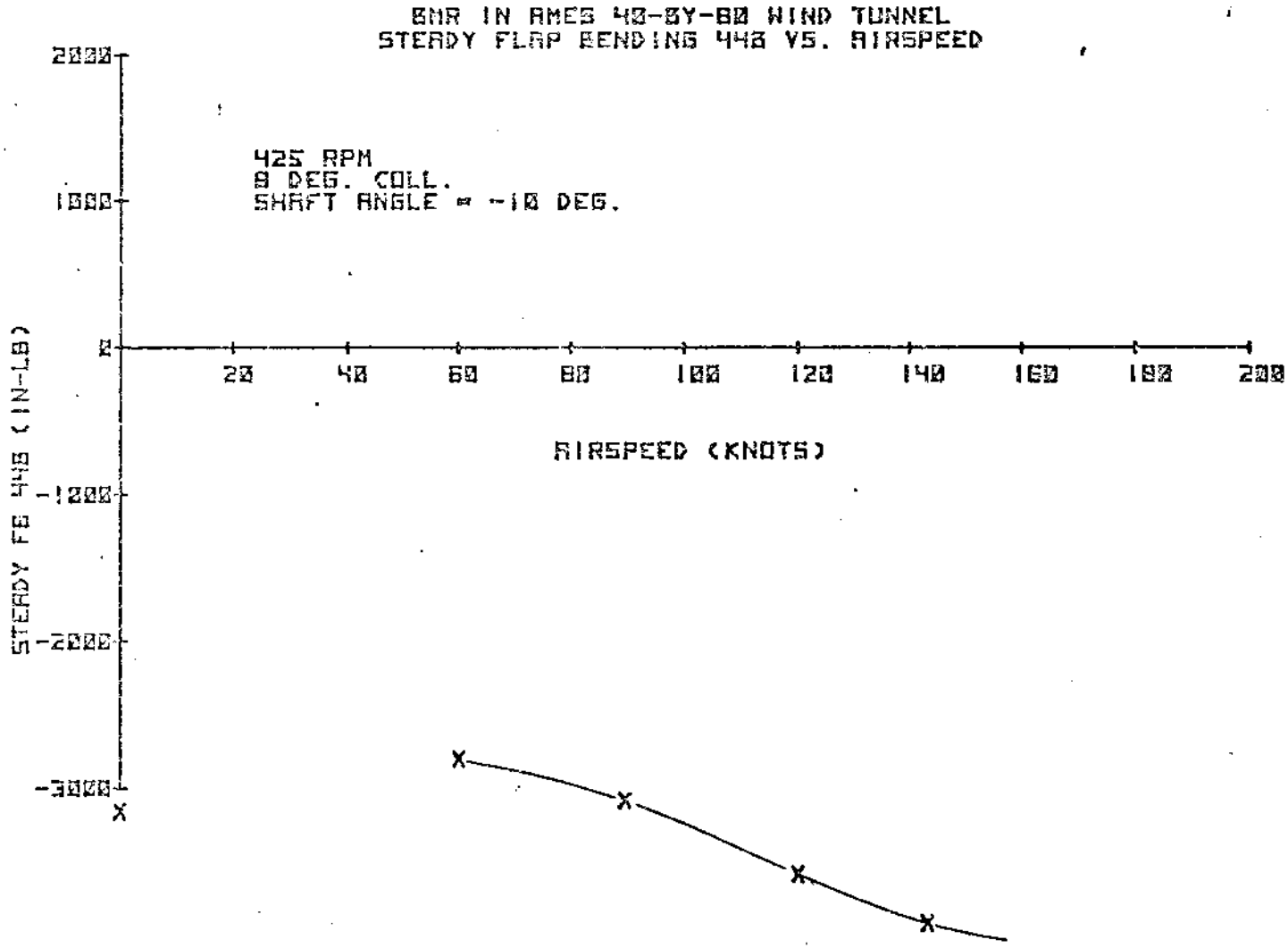

FIGURE 8.89 STEADY FLAP BENDING 44B VERSUS AIRSPEED

$S_L = -7200$

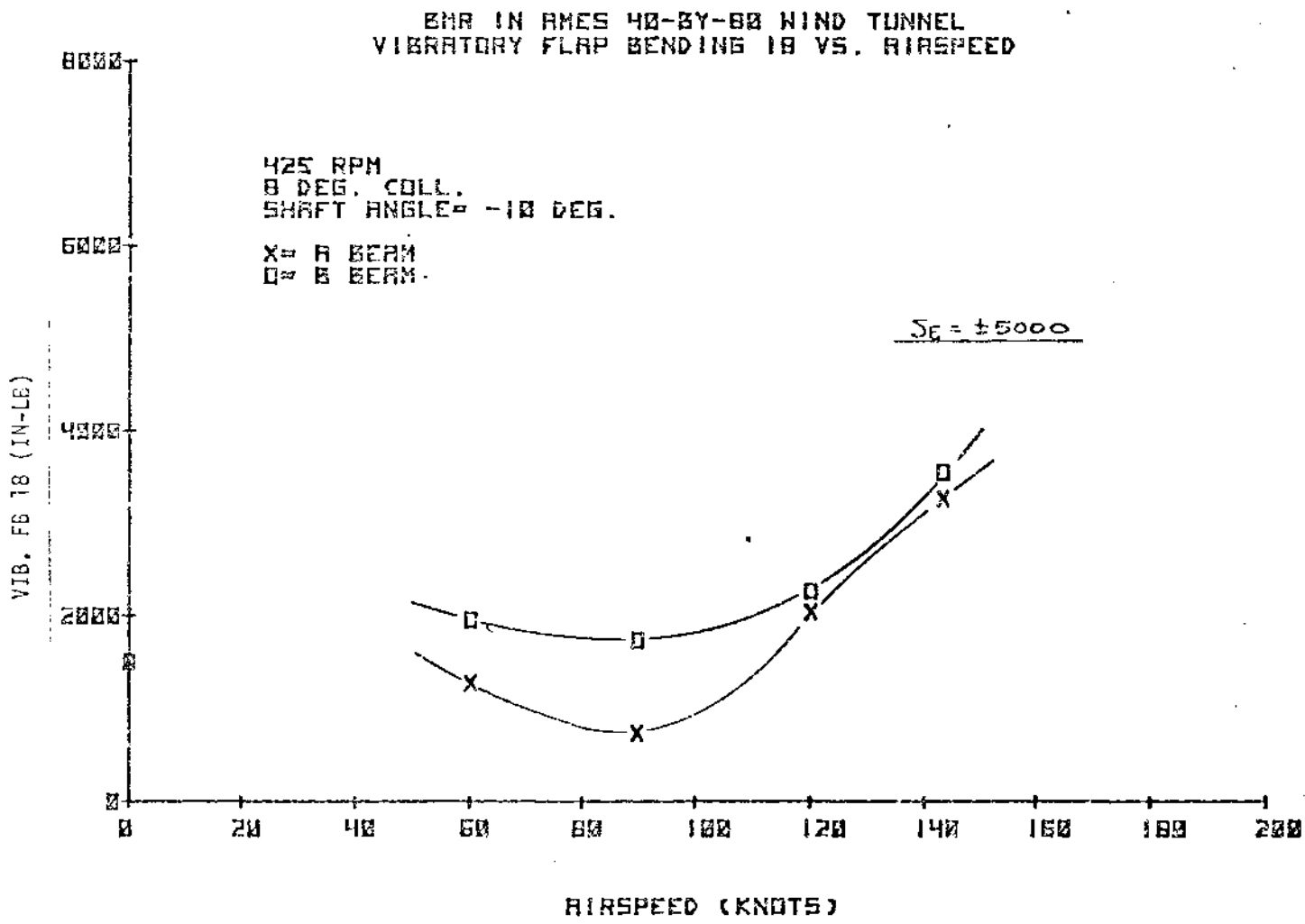

FIGURE 8.90 VIBRATORY FLAP BENDING 18 VERSUS AIRSPEED

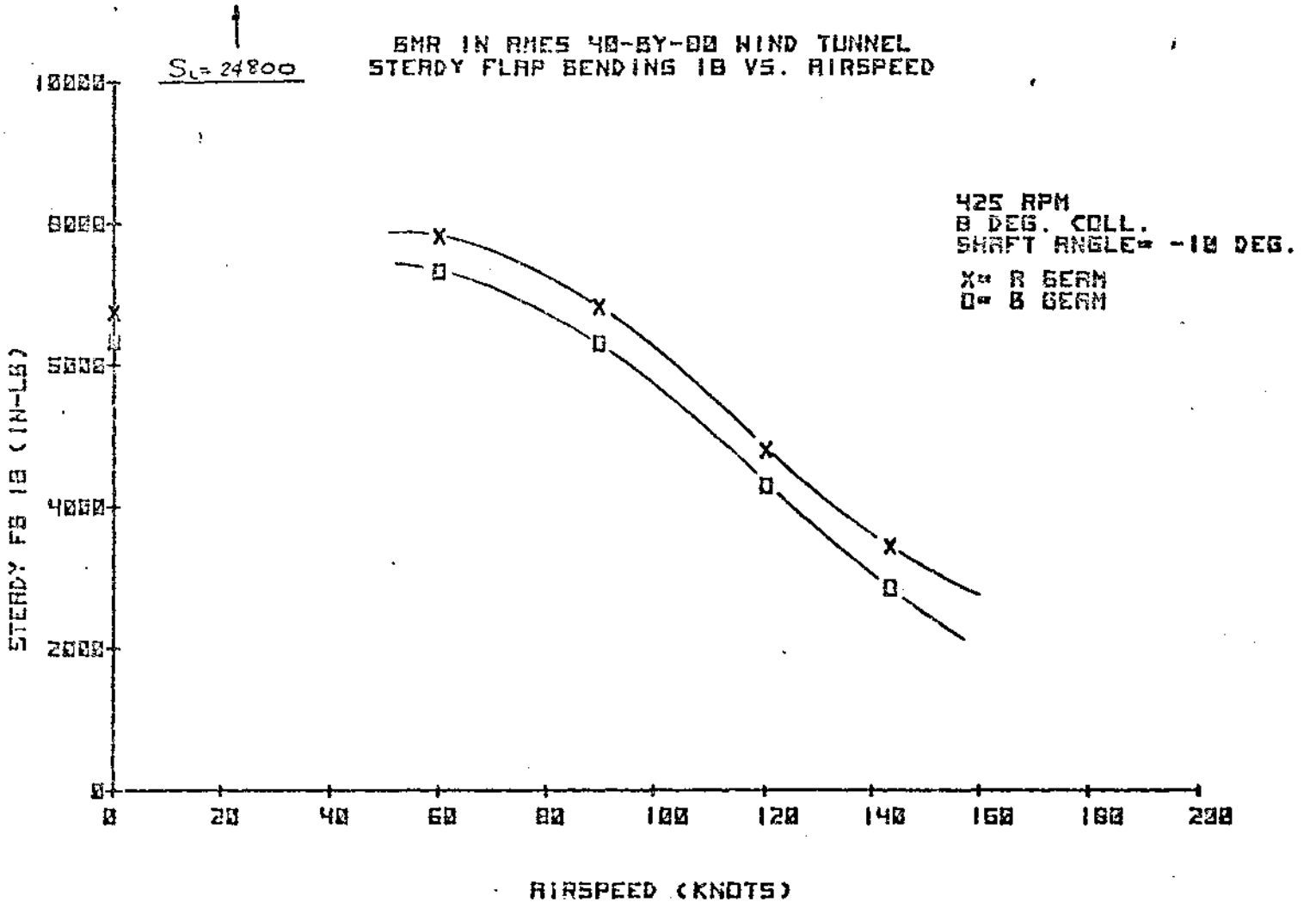

FIGURE 8.91 STEADY FLAP BENDING 1B VERSUS AIRSPEED

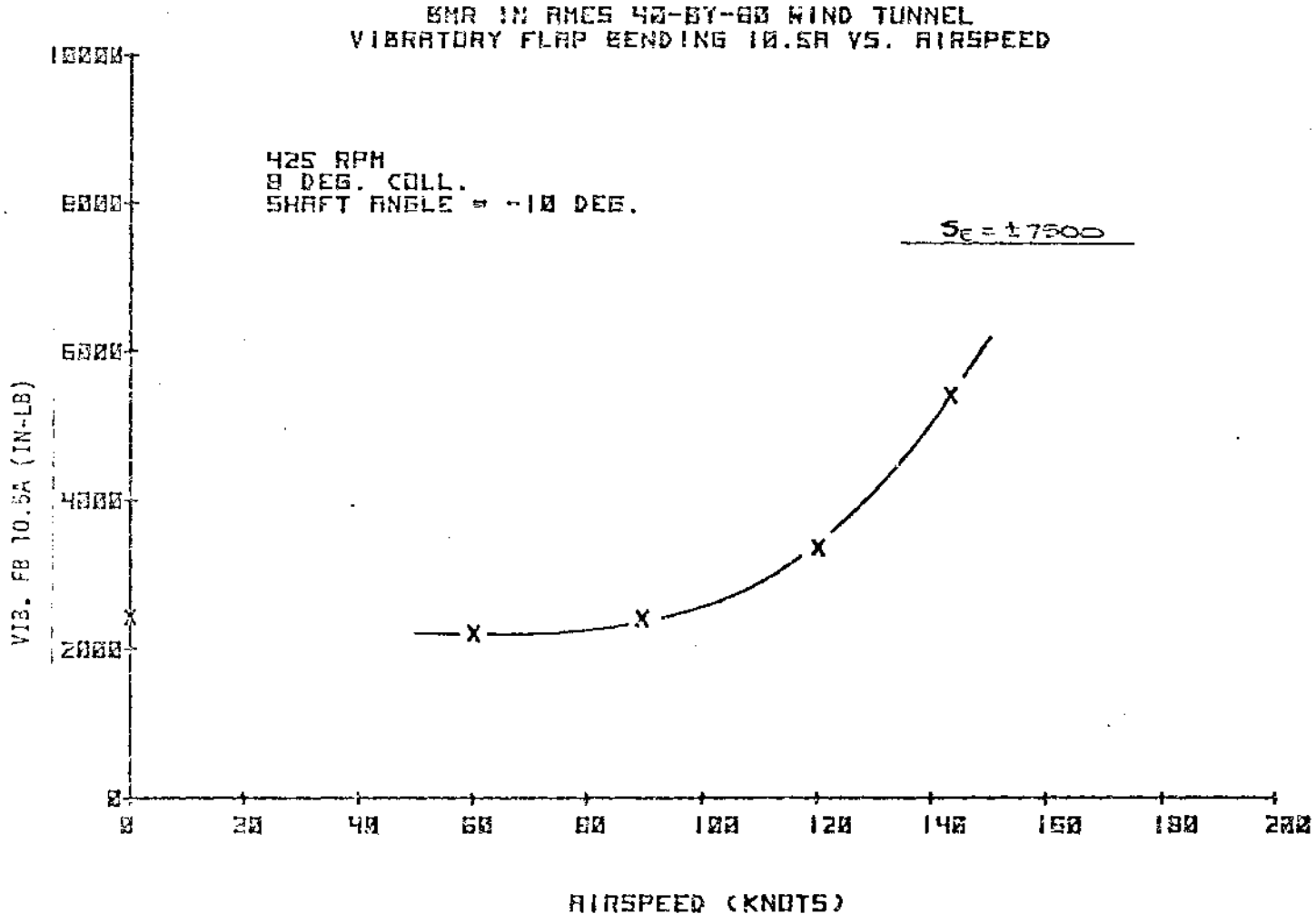

FIGURE 8.92 VIBRATORY FLAP BENDING 10.5A VERSUS AIRSPEED

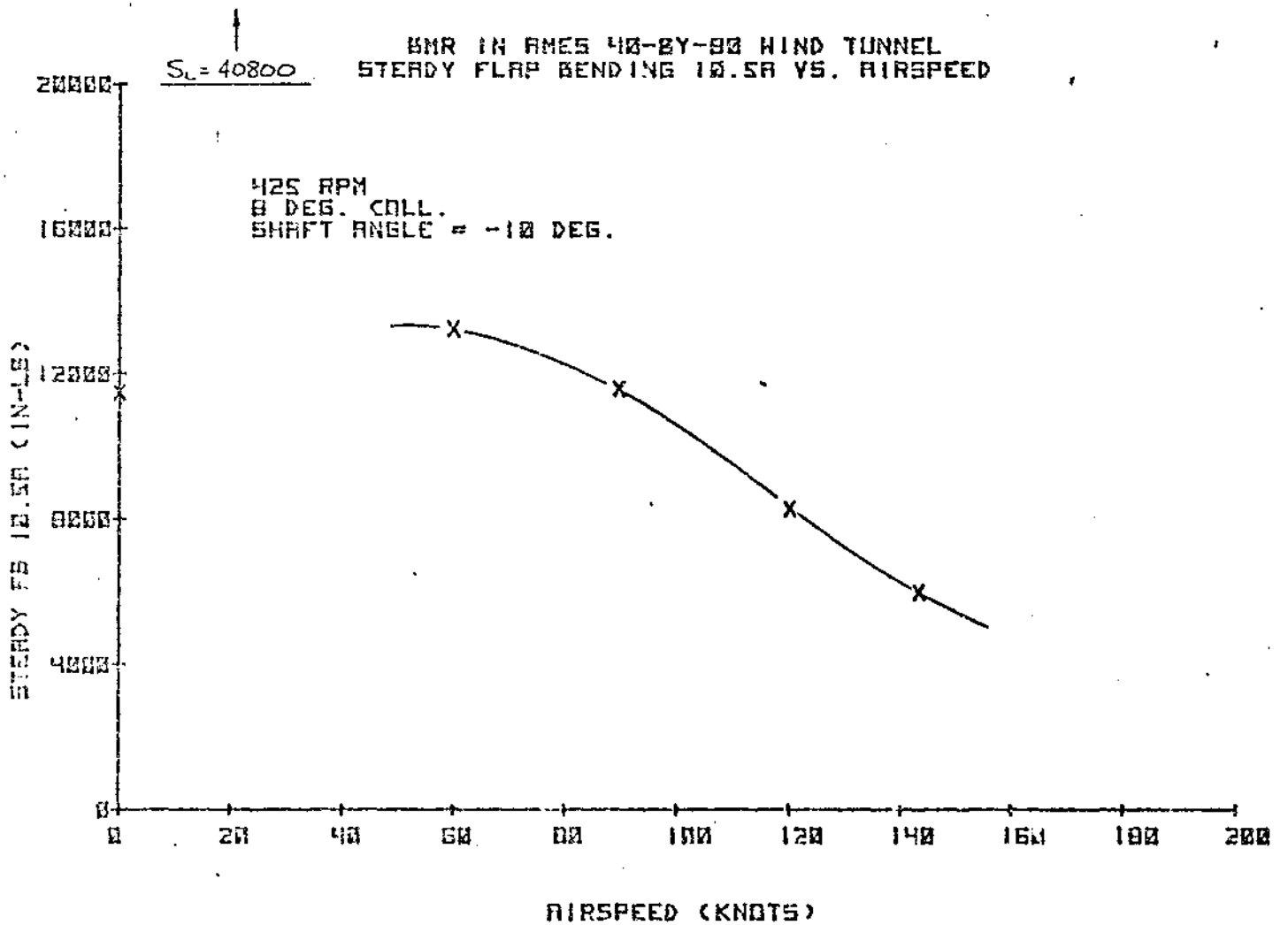

FIGURE 8.93 STEADY FLAP BENDING 10.5A VERSUS AIRSPEED

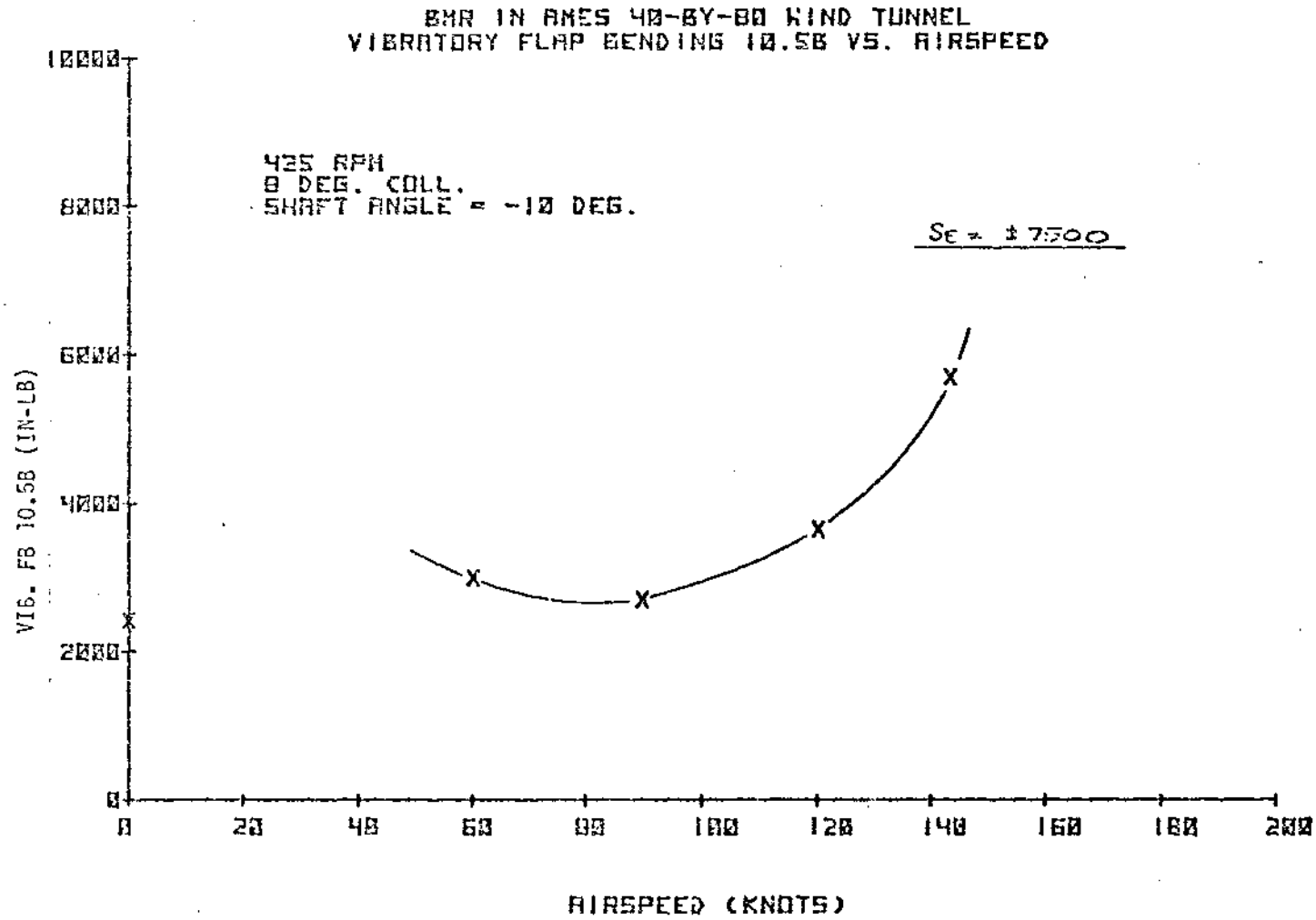

FIGURE 8.94 VIBRATORY FLAP BENDING 10.5B VERSUS AIRSPEED

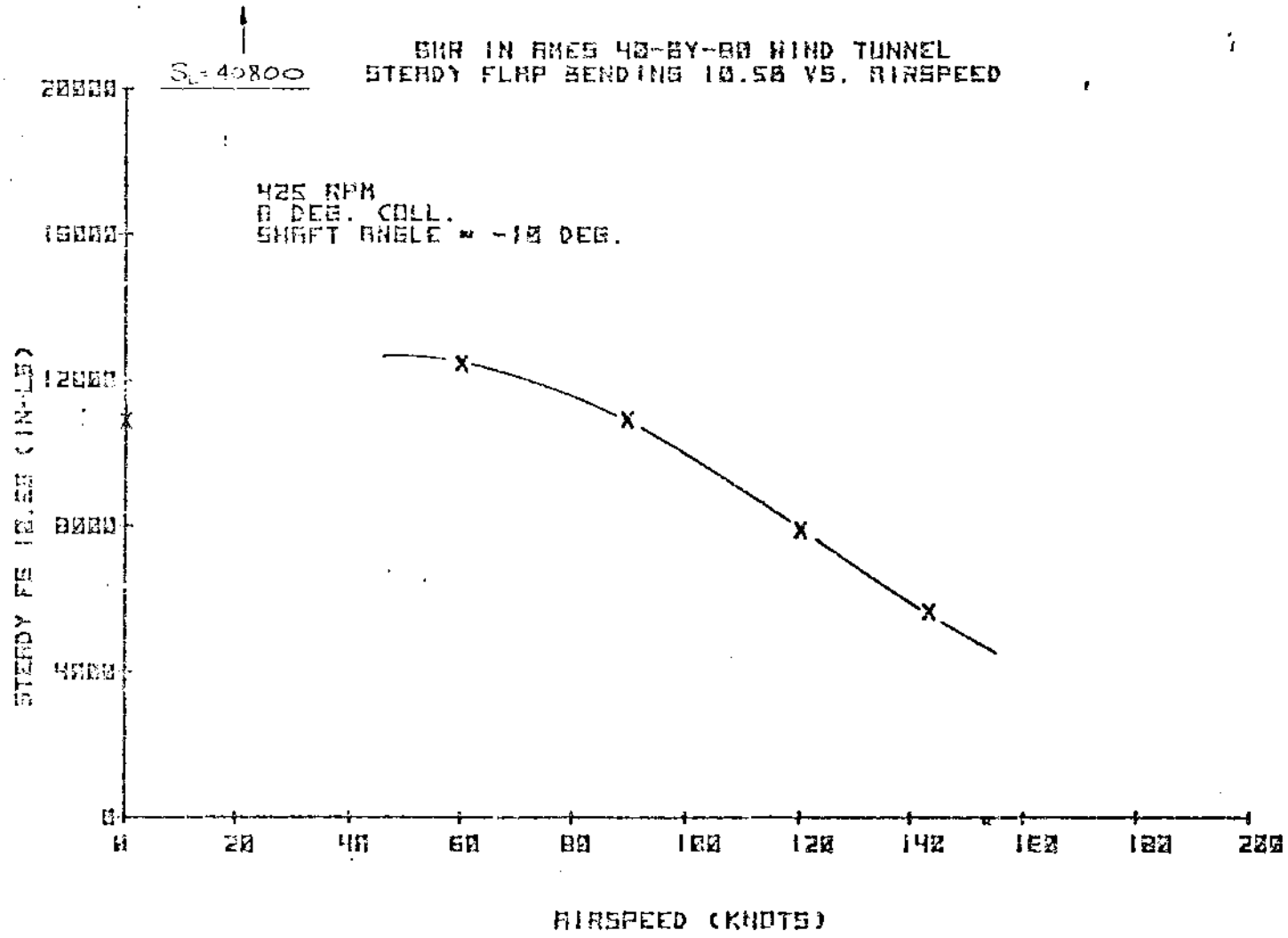

FIGURE 8.95 STEADY FLAP BENDING 10.5B VERSUS AIRSPEED

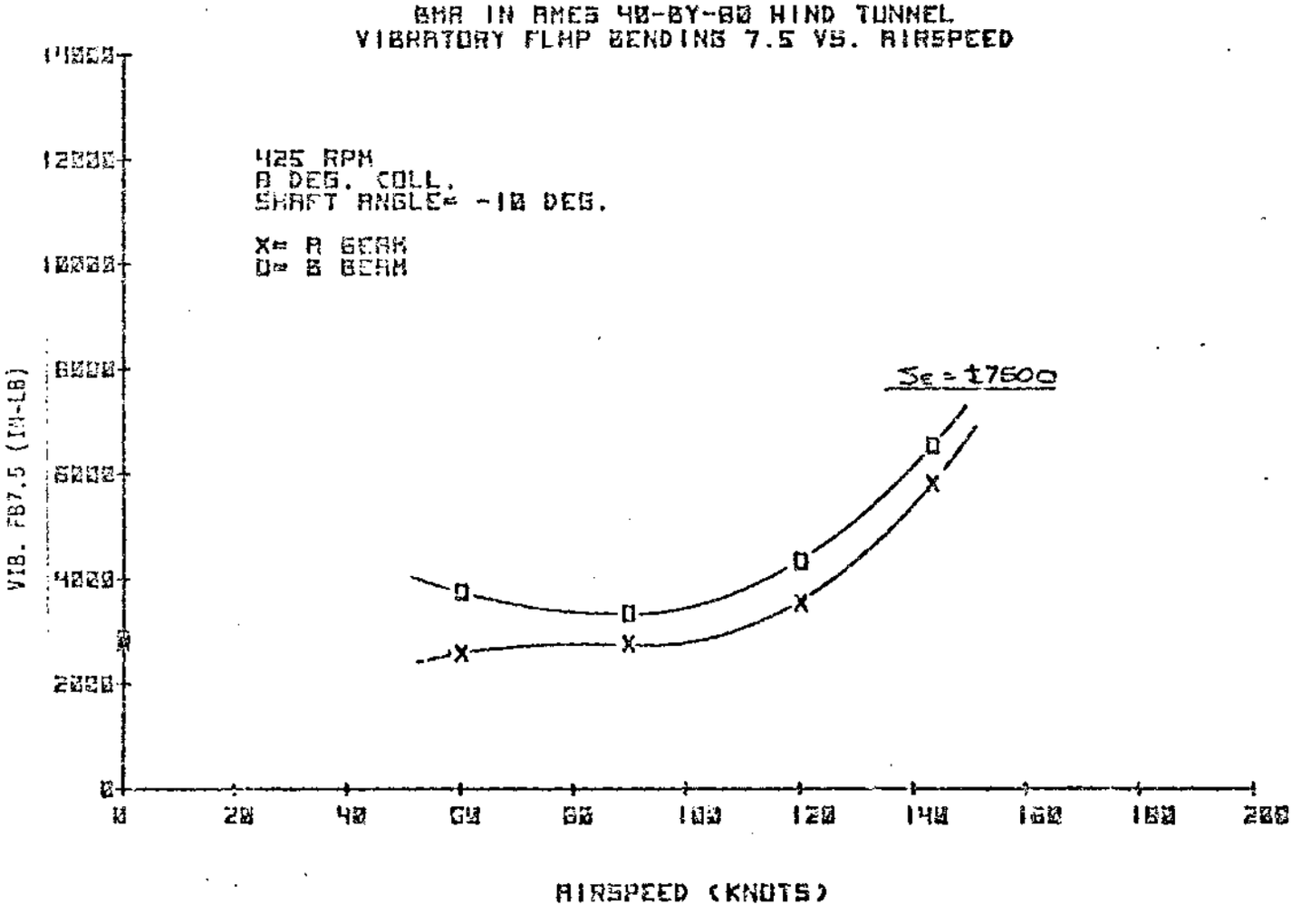

FIGURE 8.96 VIBRATORY FLAP BENDING 7.5 VERSUS AIRSPEED

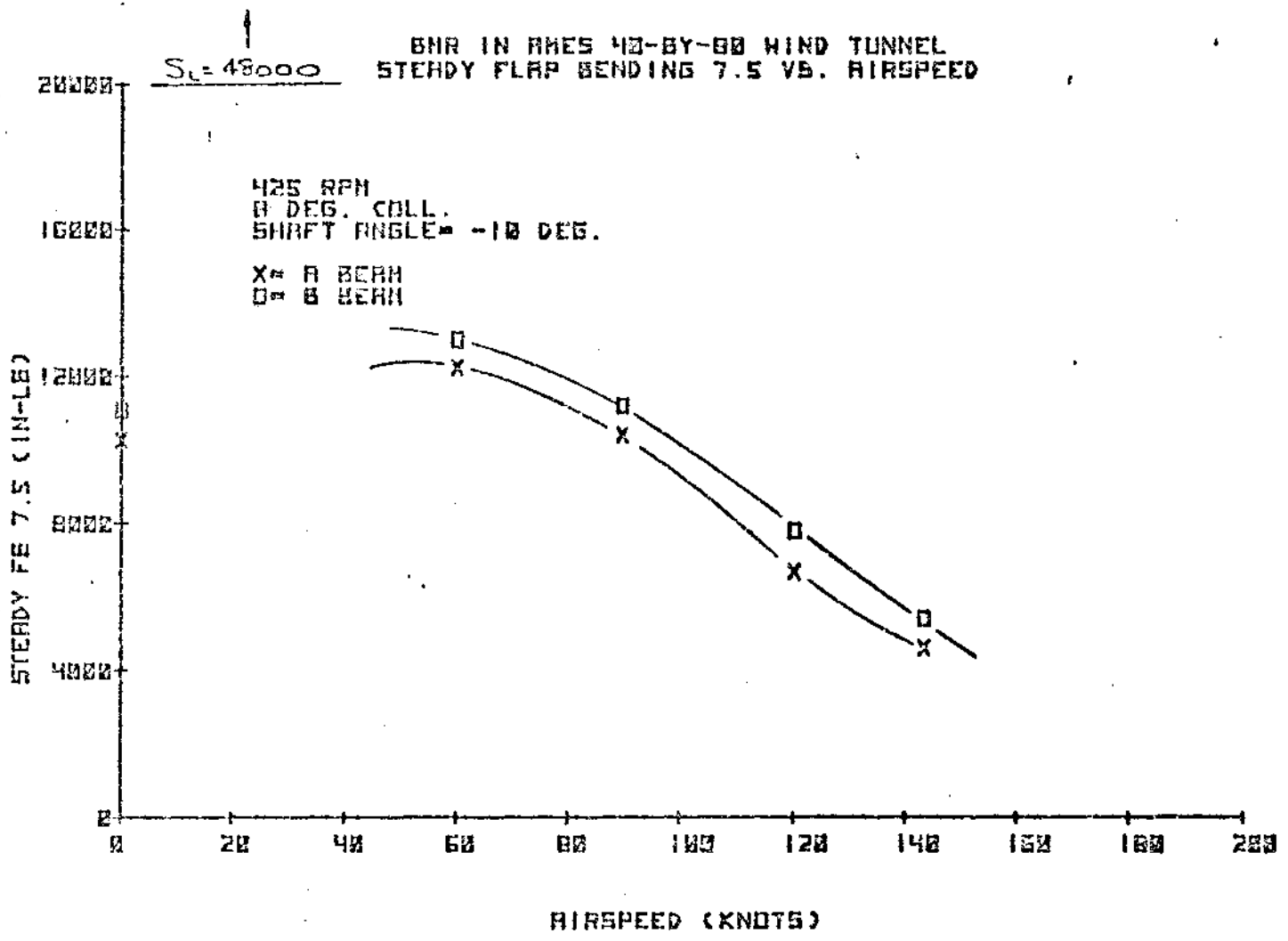

FIGURE 8.97 STEADY FLAP BENDING 7.5 VERSUS AIRSPEED

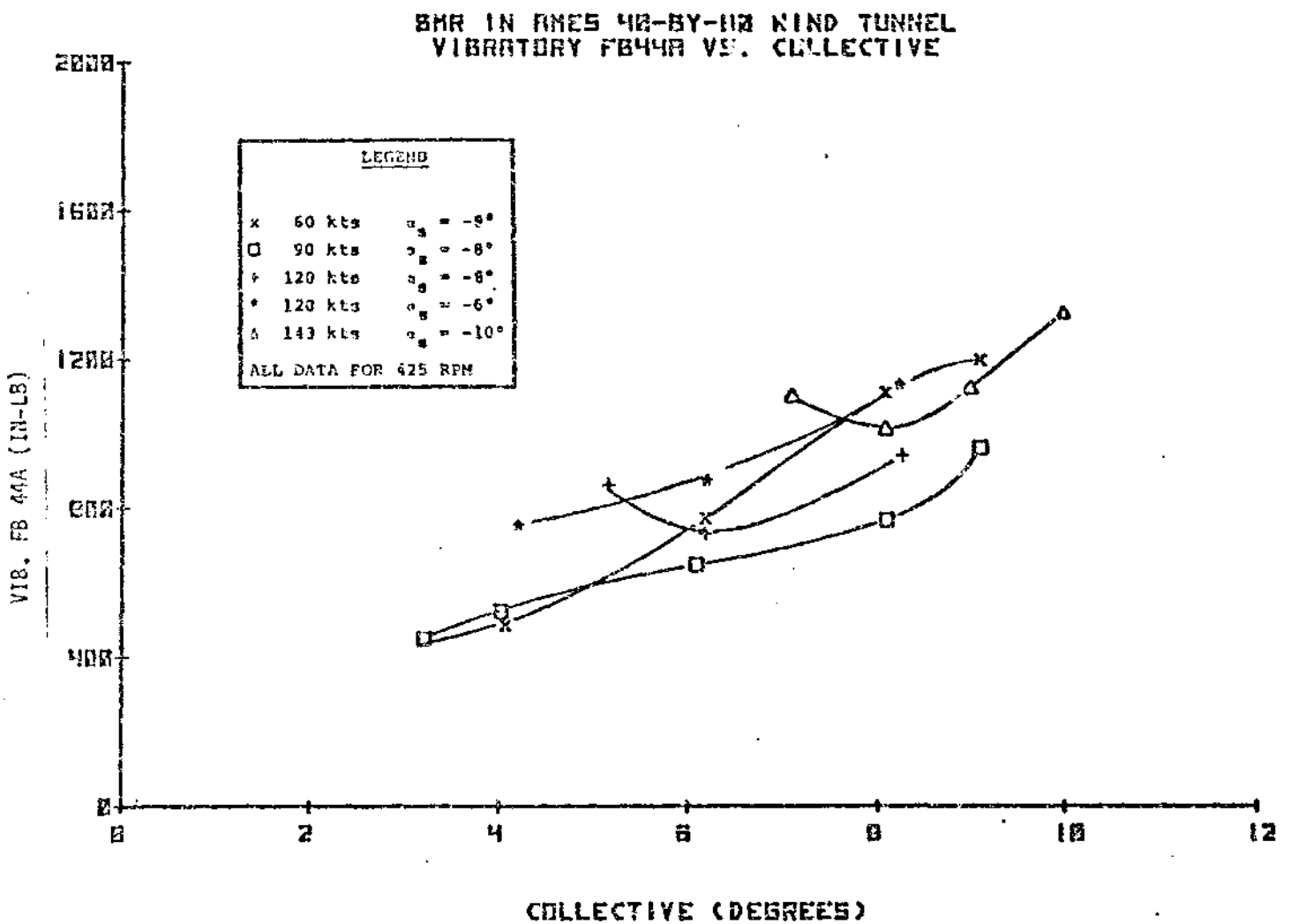

FIGURE 8.98 VIBRATORY FLAP BENDING 44A VERSUS COLLECTIVE

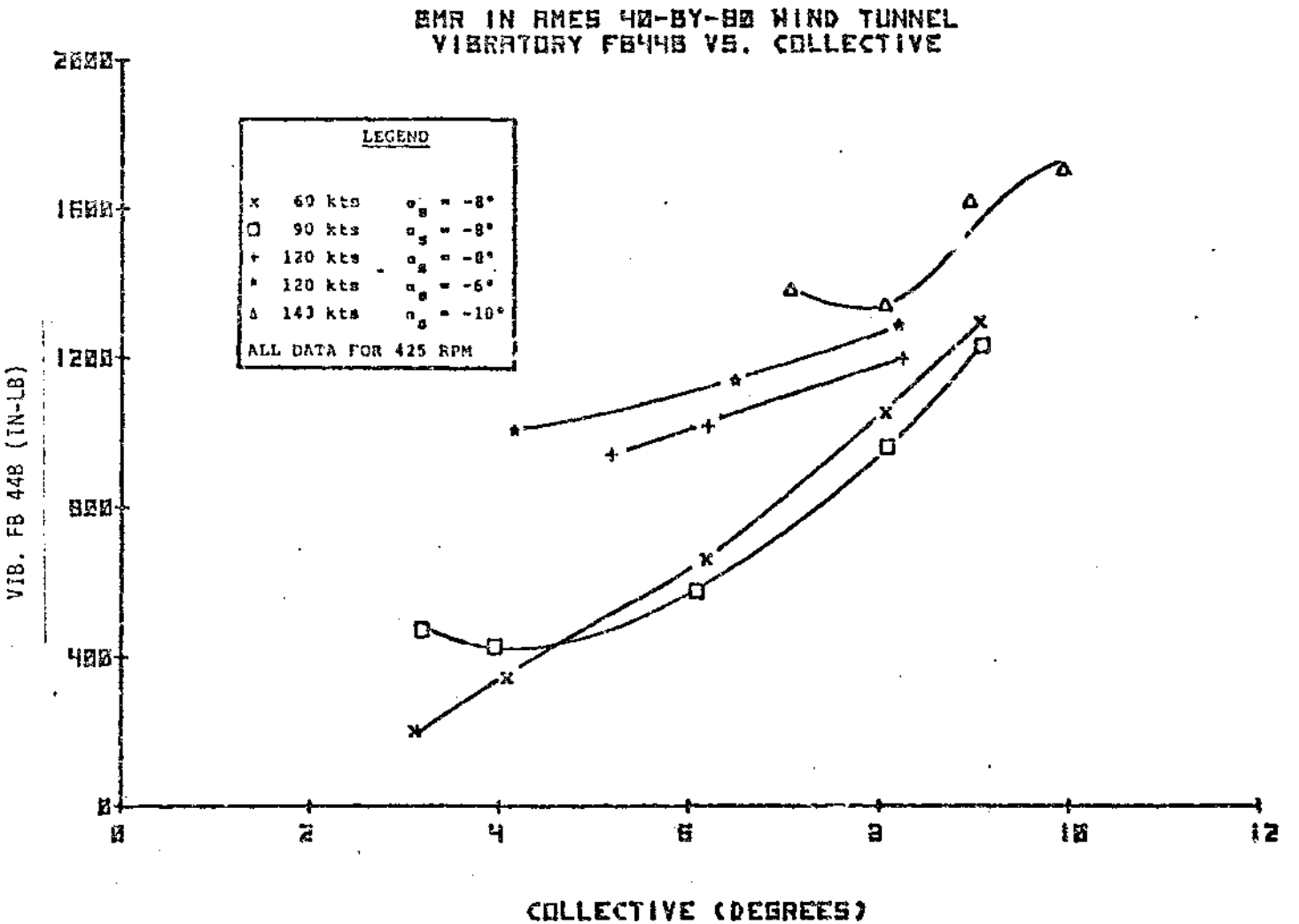

FIGURE 8.99 VIBRATORY FLAP BENDING 44B VERSUS COLLECTIVE

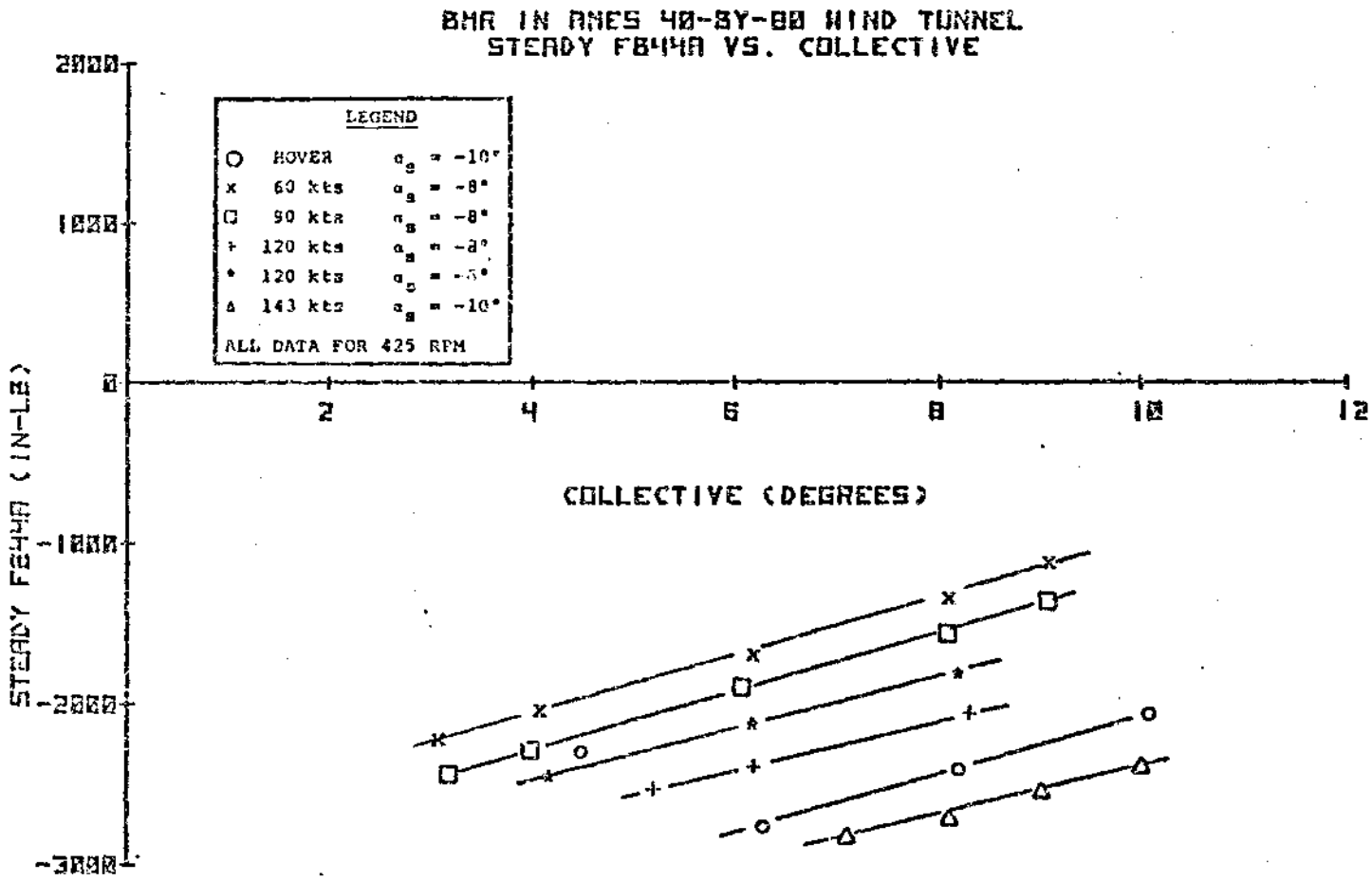

FIGURE 8.100 STEADY FLAP BENDING 44A VERSUS COLLECTIVE

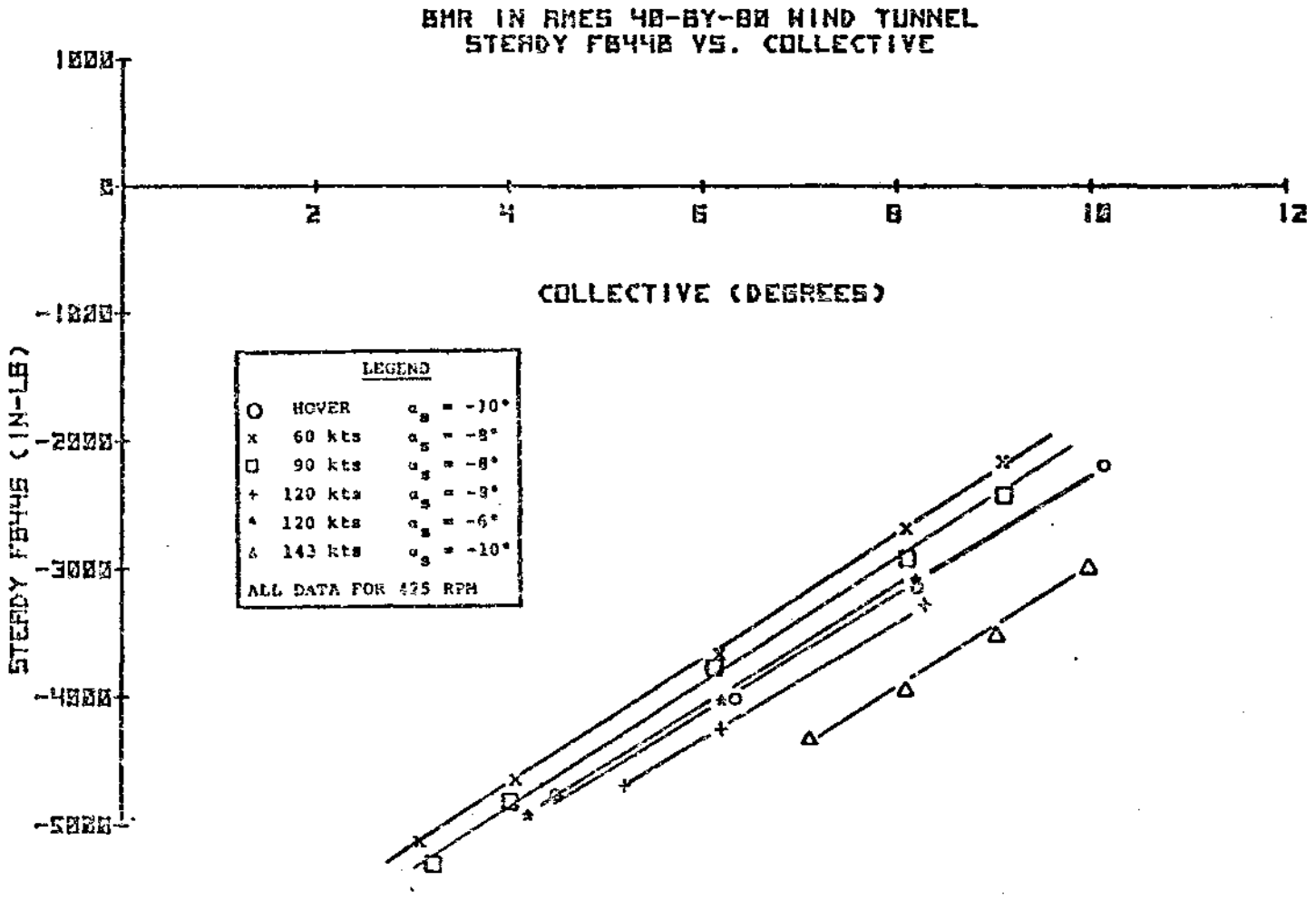

FIGURE 8.101 STEADY FLAP BENDING 44B VERSUS COLLECTIVE

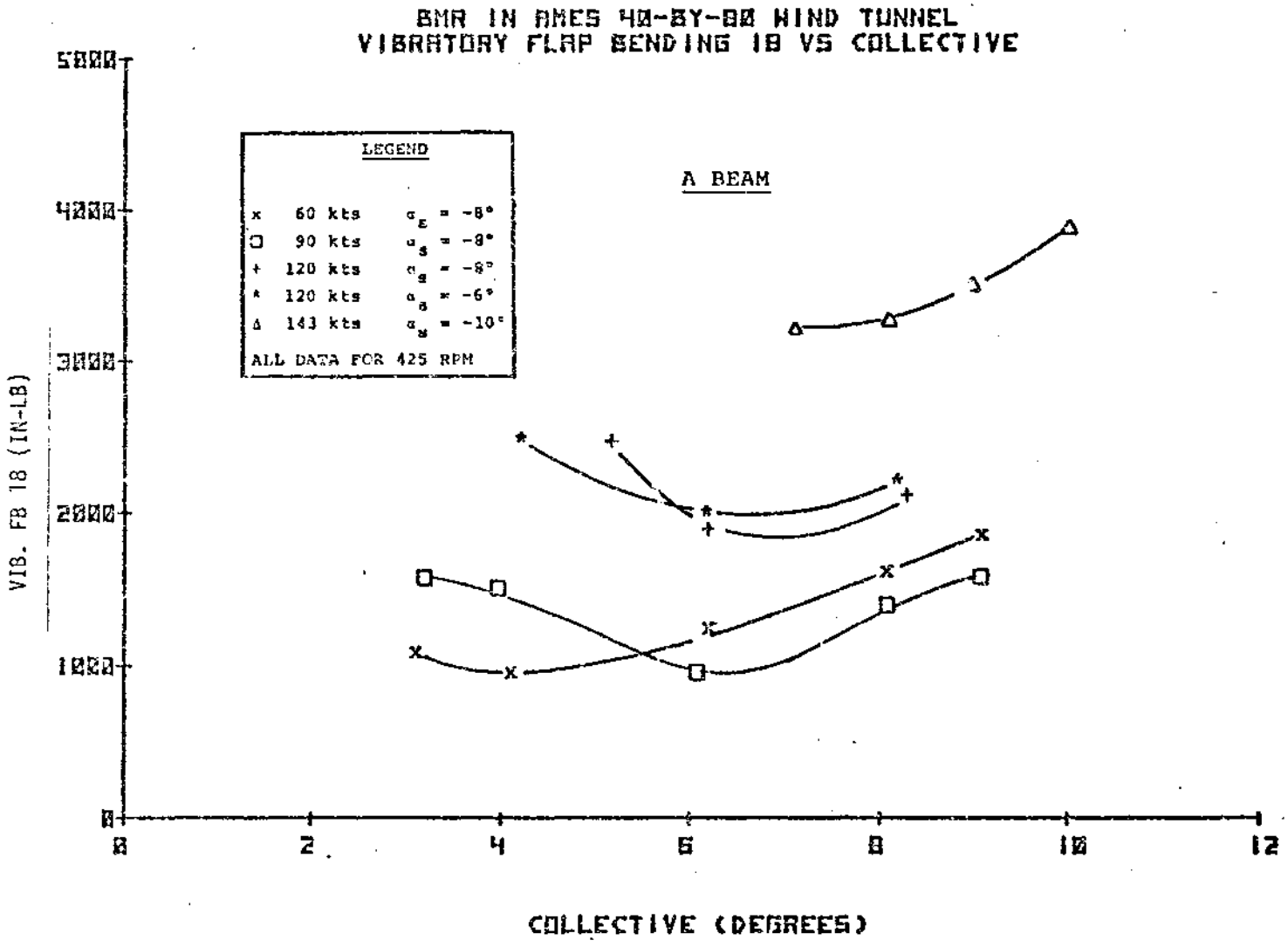

FIGURE 8.102 VIBRATORY FLAP BENDING 1BA VERSUS COLLECTIVE

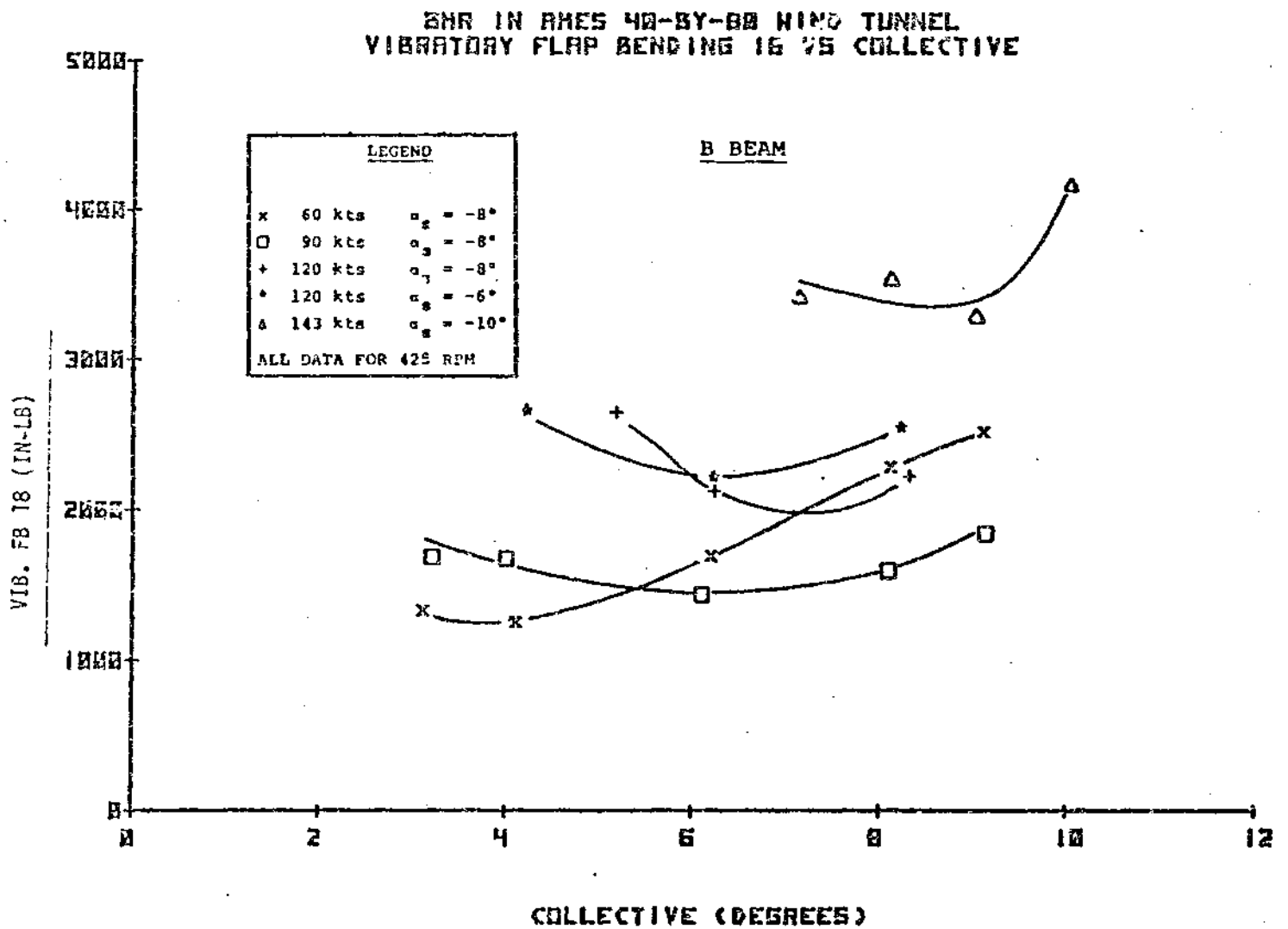

FIGURE 8.103 VIBRATORY FLAP BENDING 1BB VERSUS COLLECTIVE

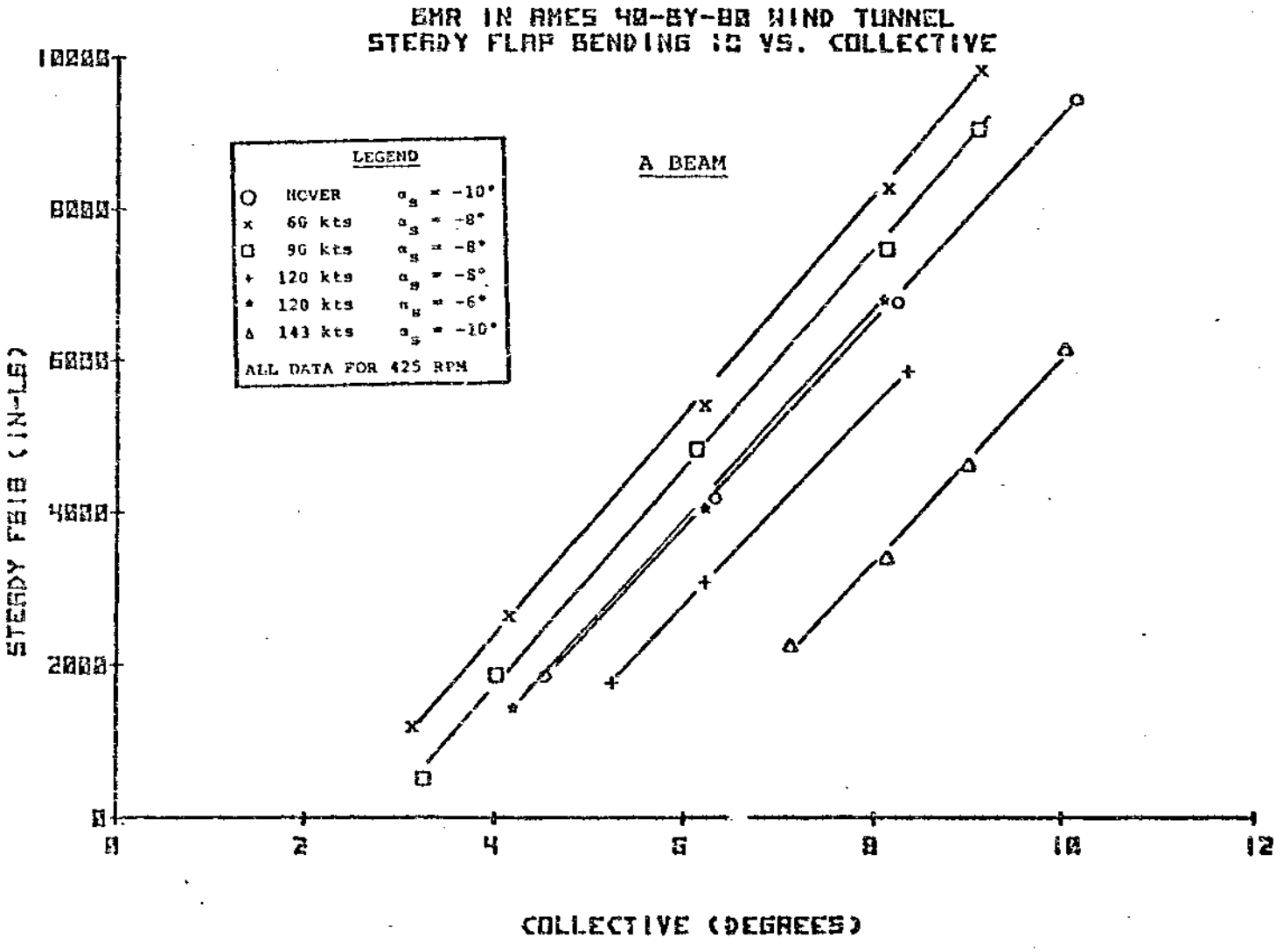

FIGURE 8.104 STEADY FLAP BENDING 18A VERSUS COLLECTIVE

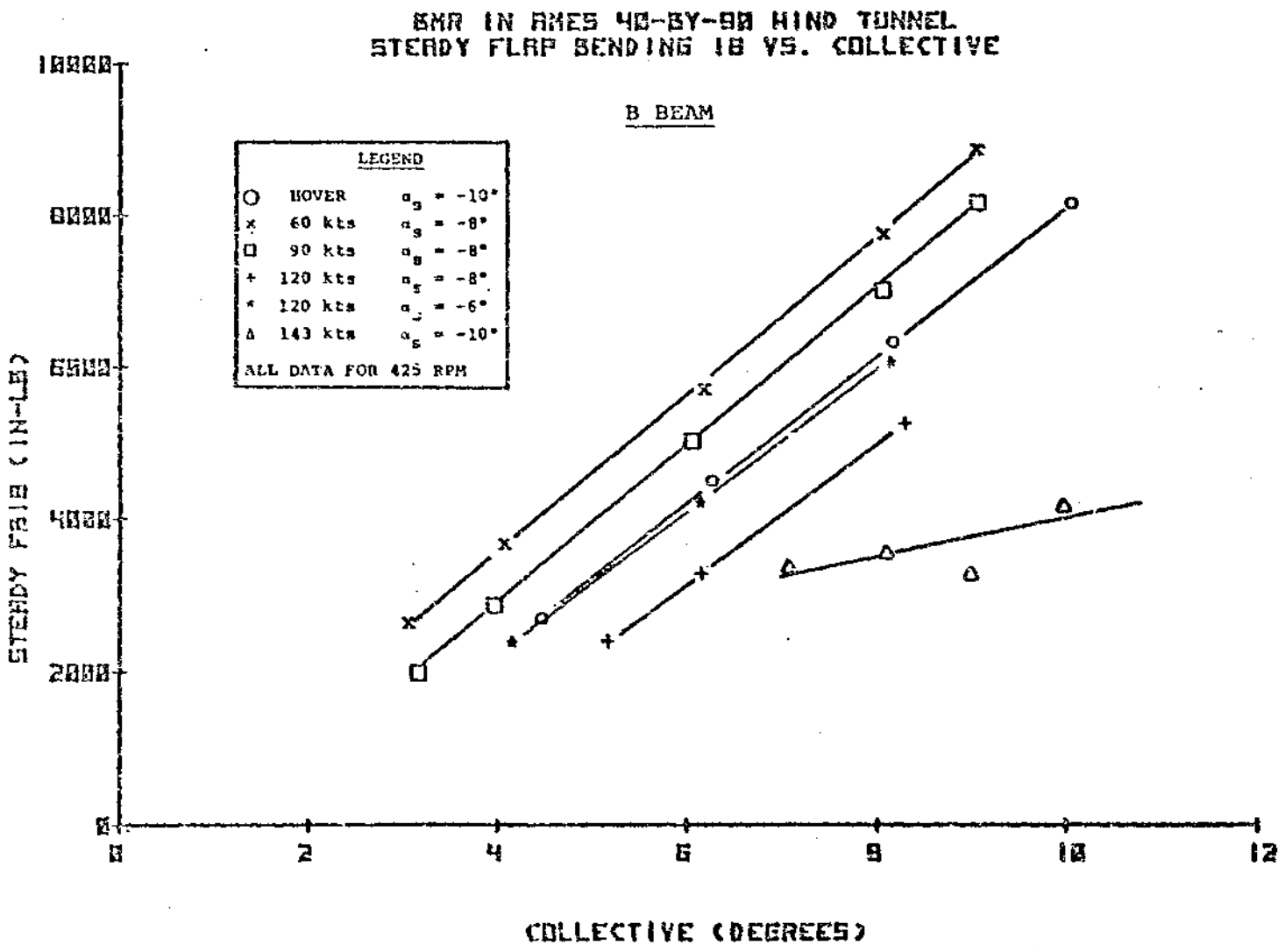

FIGURE 8.105 STEADY FLAP BENDING 1BB VERSUS COLLECTIVE

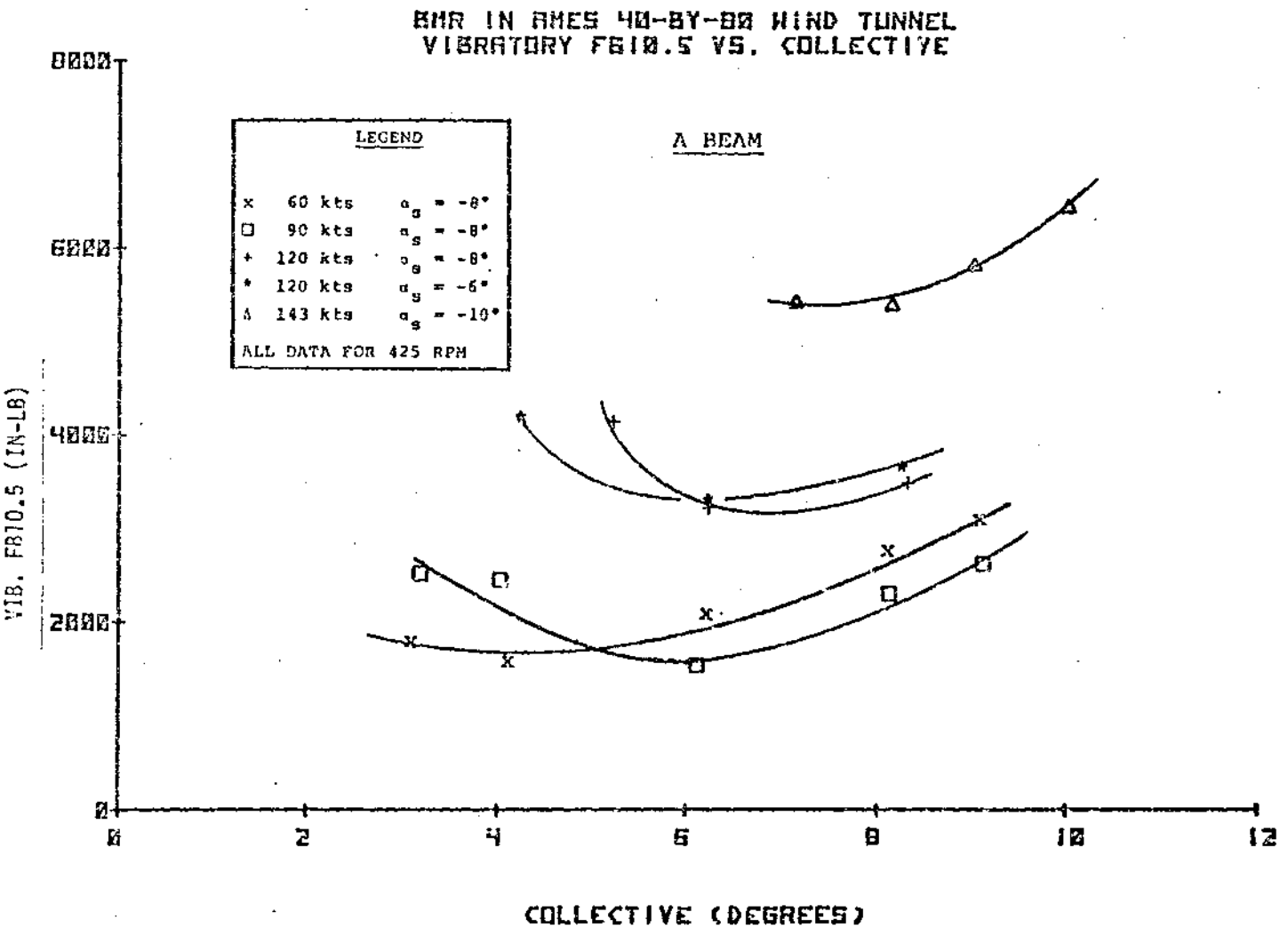

FIGURE 8.106 VIBRATORY FLAP BENDING 10.5A VERSUS COLLECTIVE

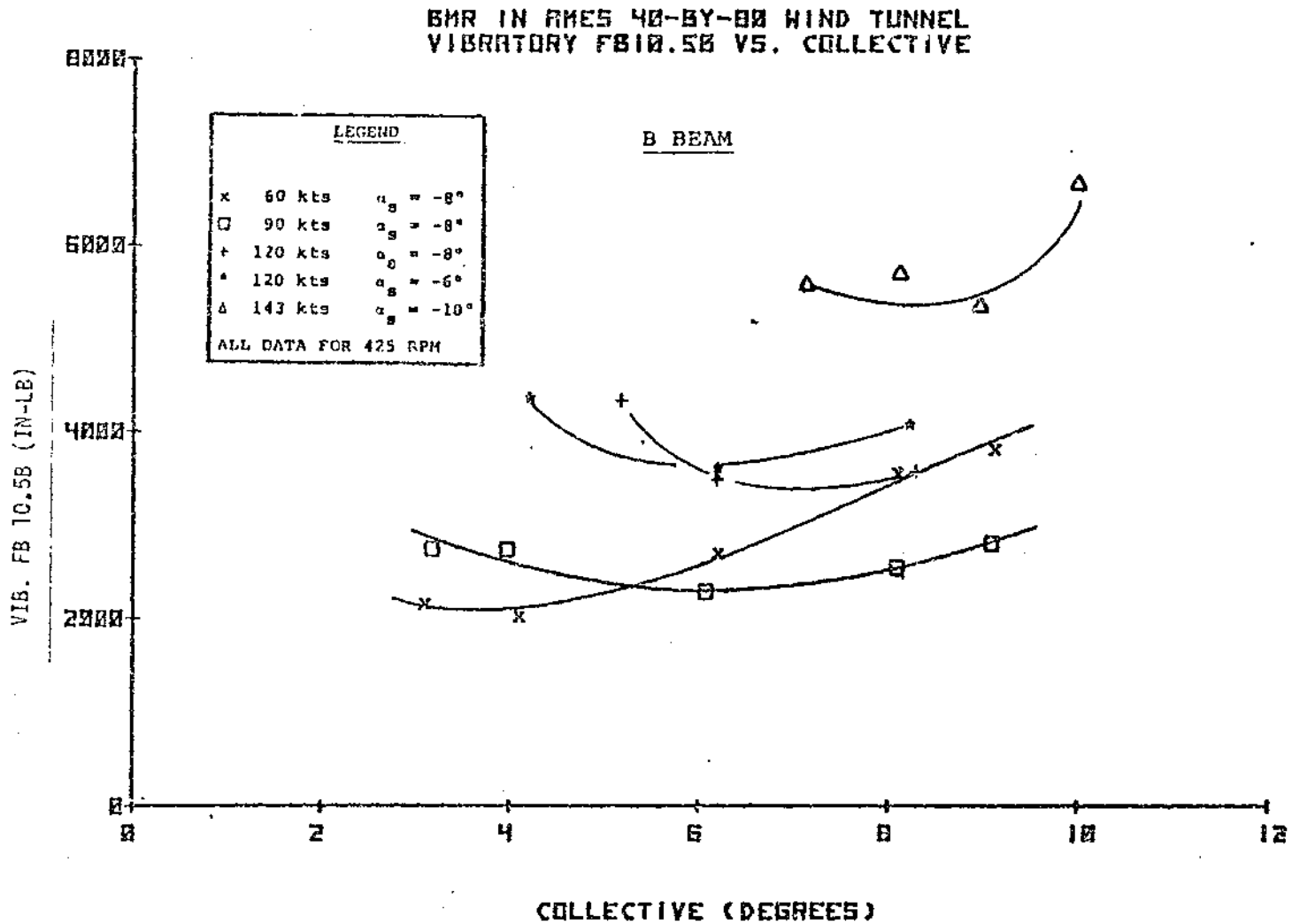

FIGURE 8.107 VIBRATORY FLAP BENDING 10.5B VERSUS COLLECTIVE

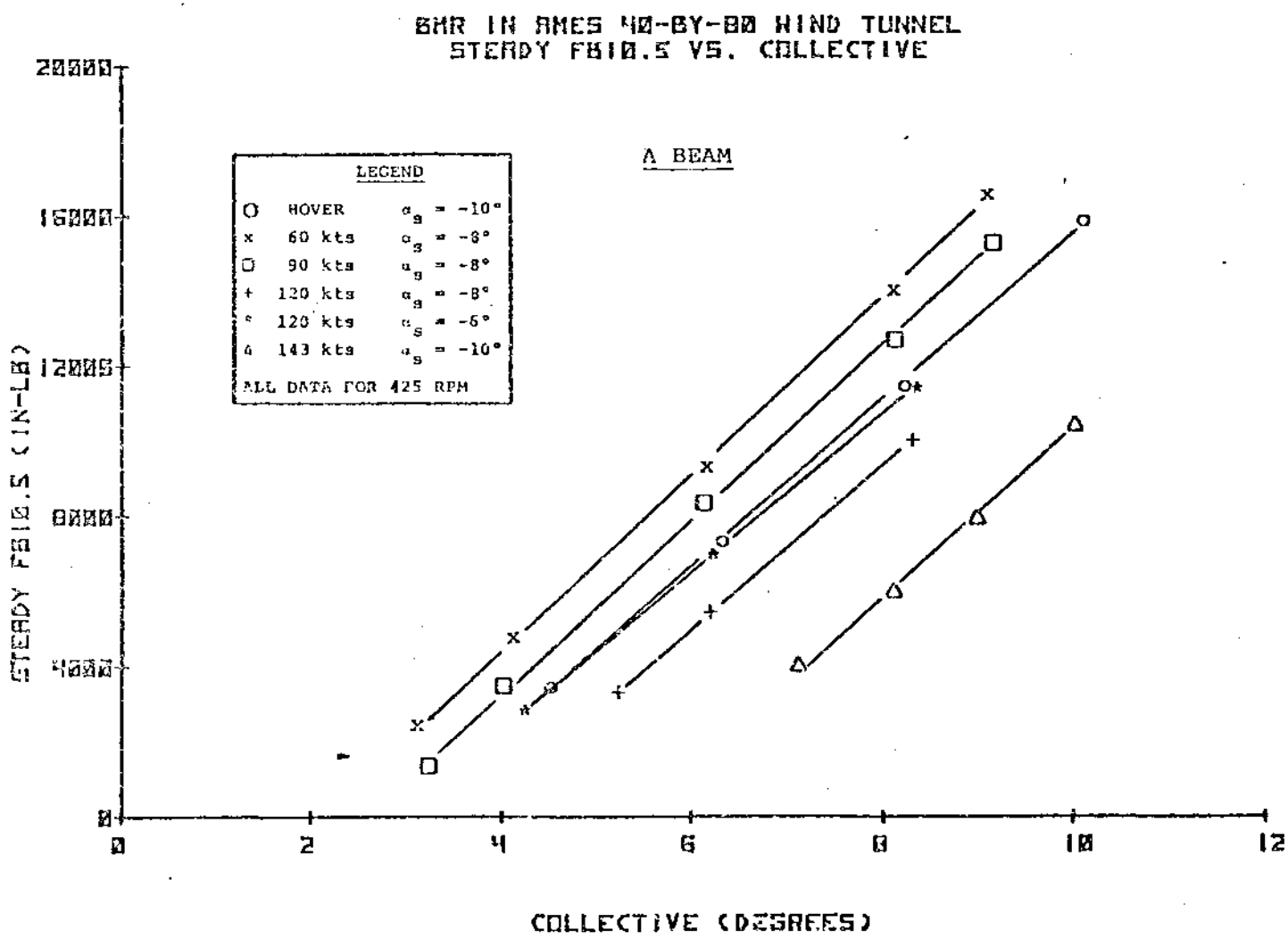

FIGURE 8.108 STEADY FLAP BENDING 10.5A VERSUS COLLECTIVE

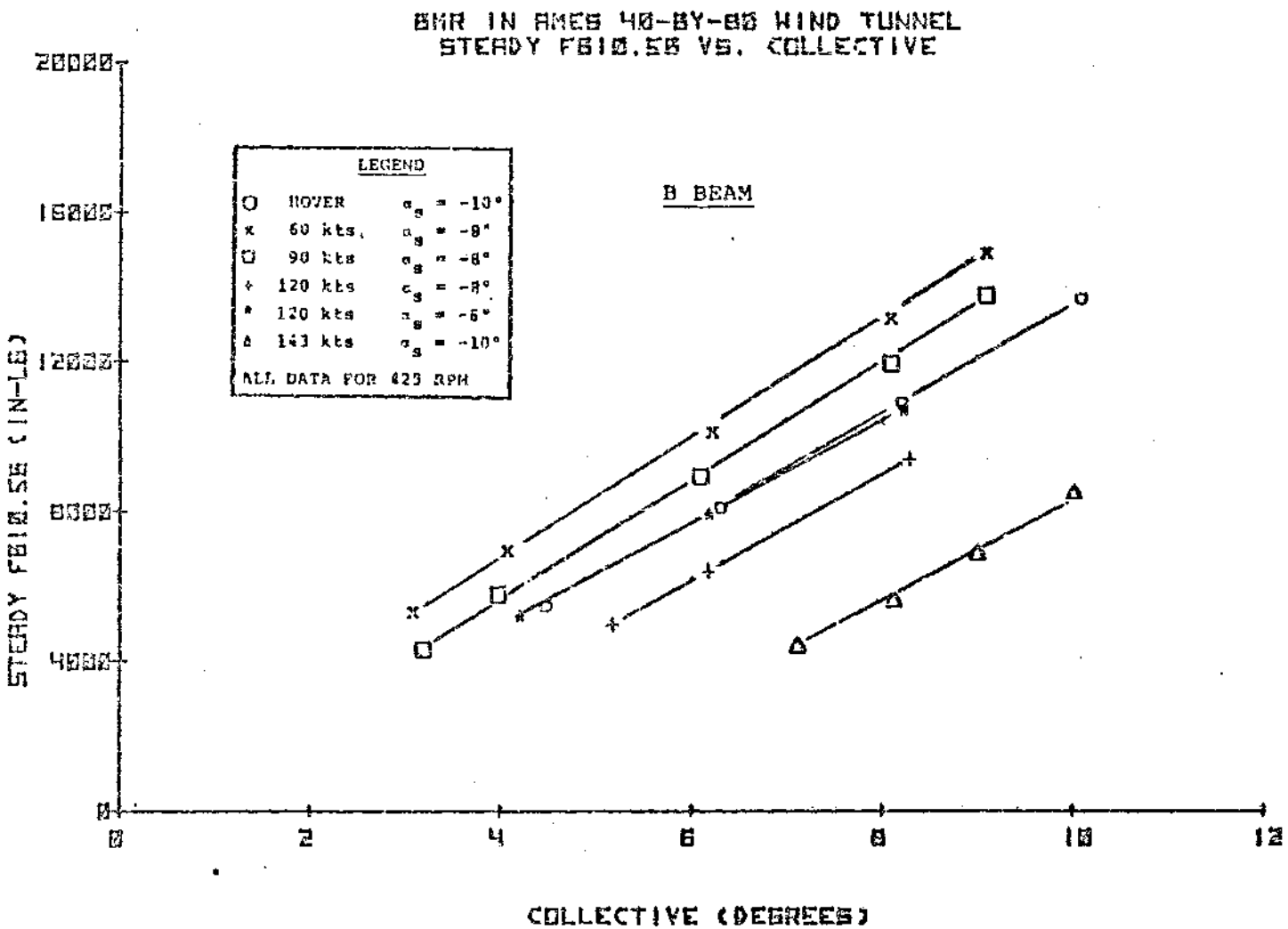

FIGURE 8.109 STEADY FLAP BENDING 10.5B VERSUS COLLECTIVE

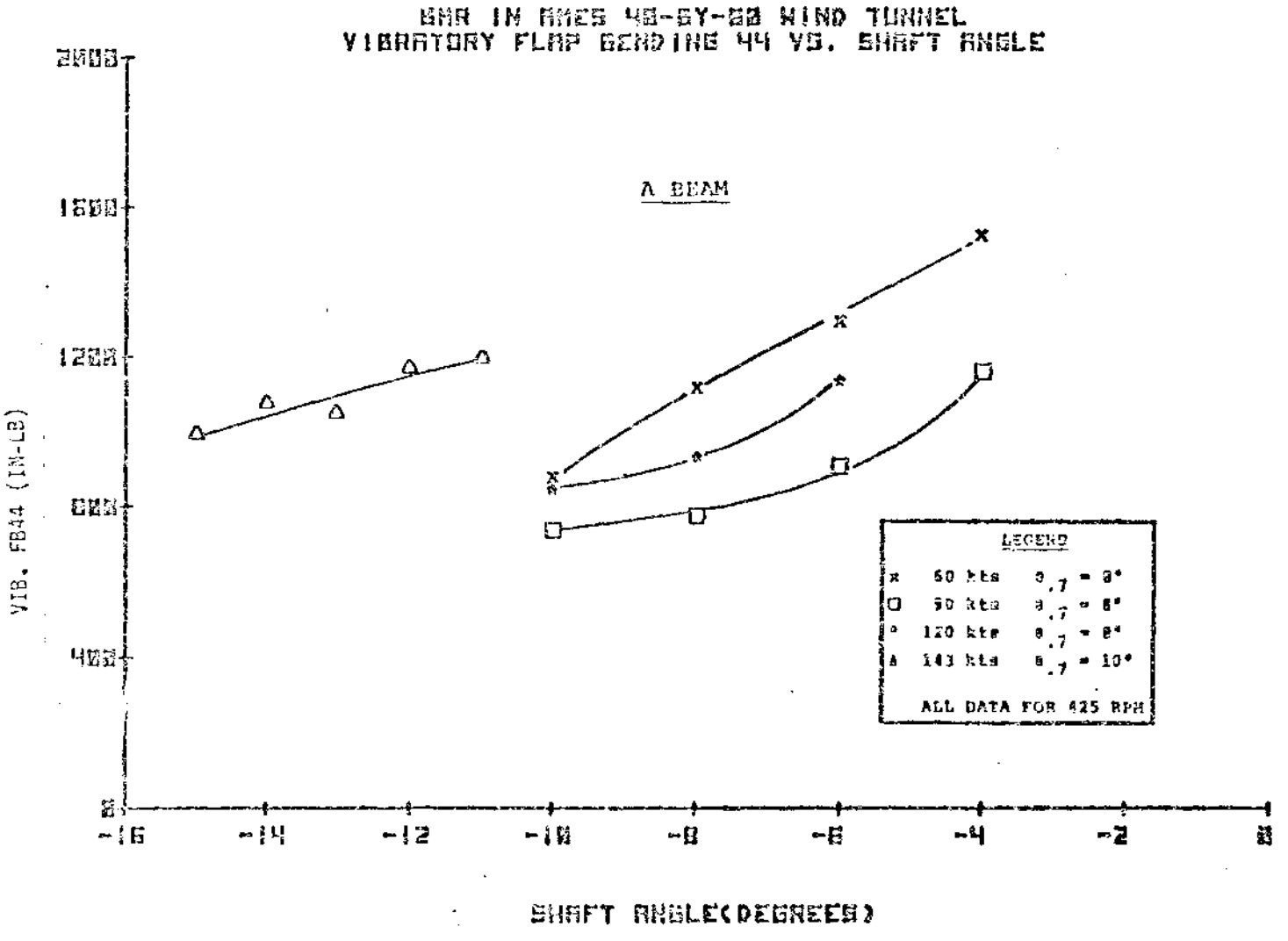

FIGURE 8.110 VIBRATORY FLAP BENDING 44 VERSUS SHAFT ANGLE
(SHEET 1 OF 2)

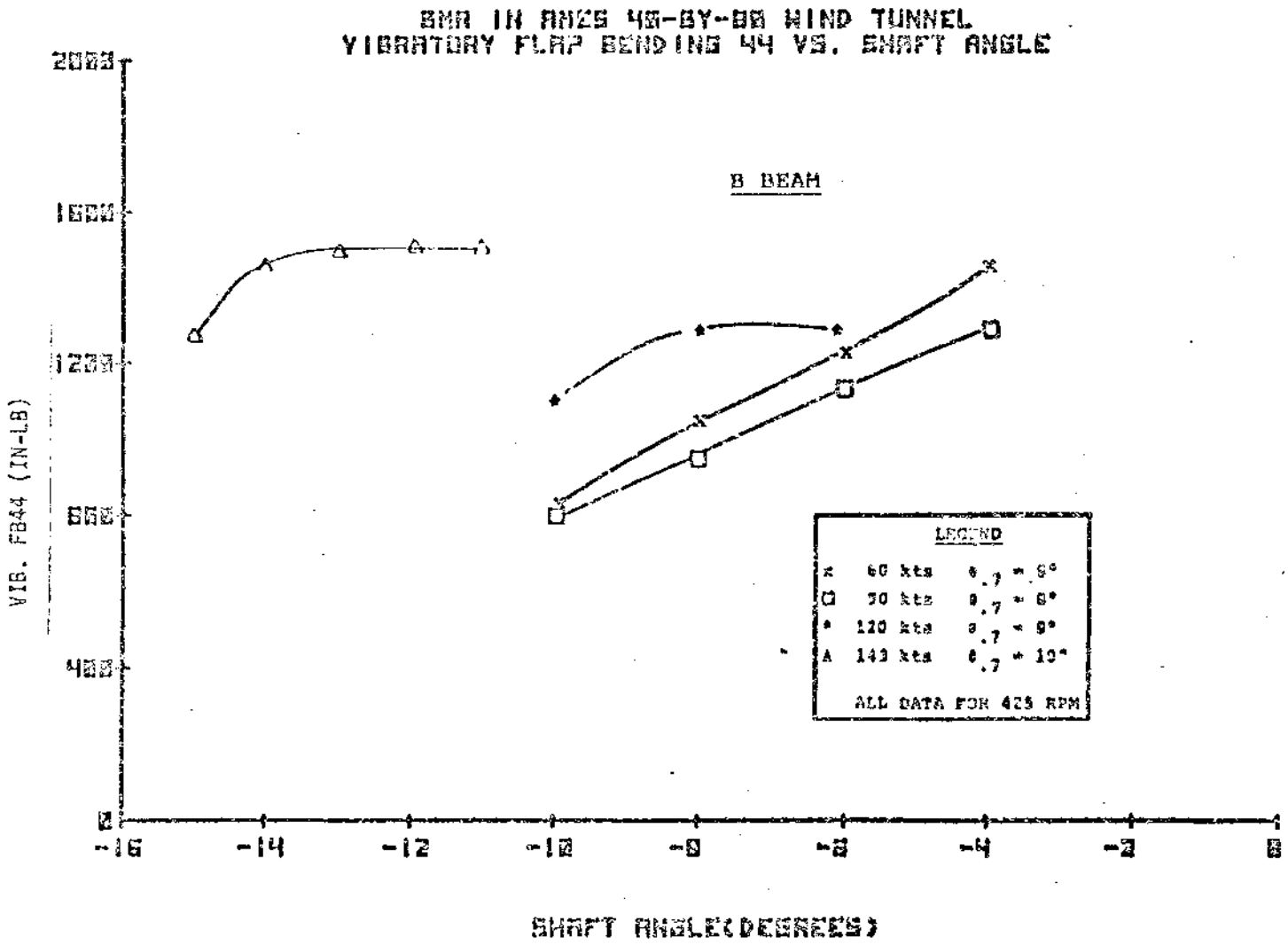

FIGURE 8.110 VIBRATORY FLAP BENDING 44 VERSUS SHAFT ANGLE
(SHEET 2 OF 2)

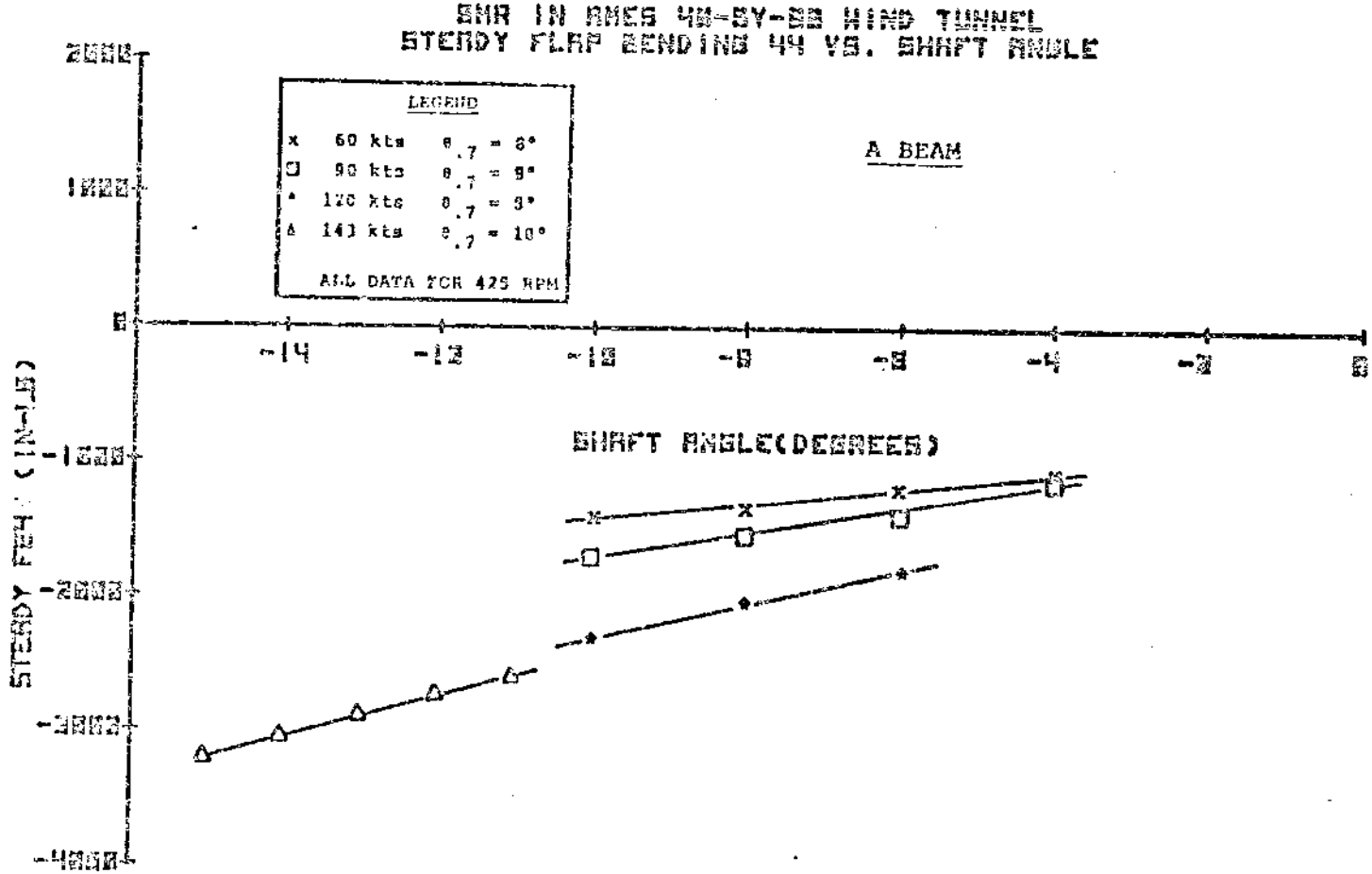

FIGURE 8.111 STEADY FLAP BENDING 44 VERSUS SHAFT ANGLE (SHEET 1 OF 2)

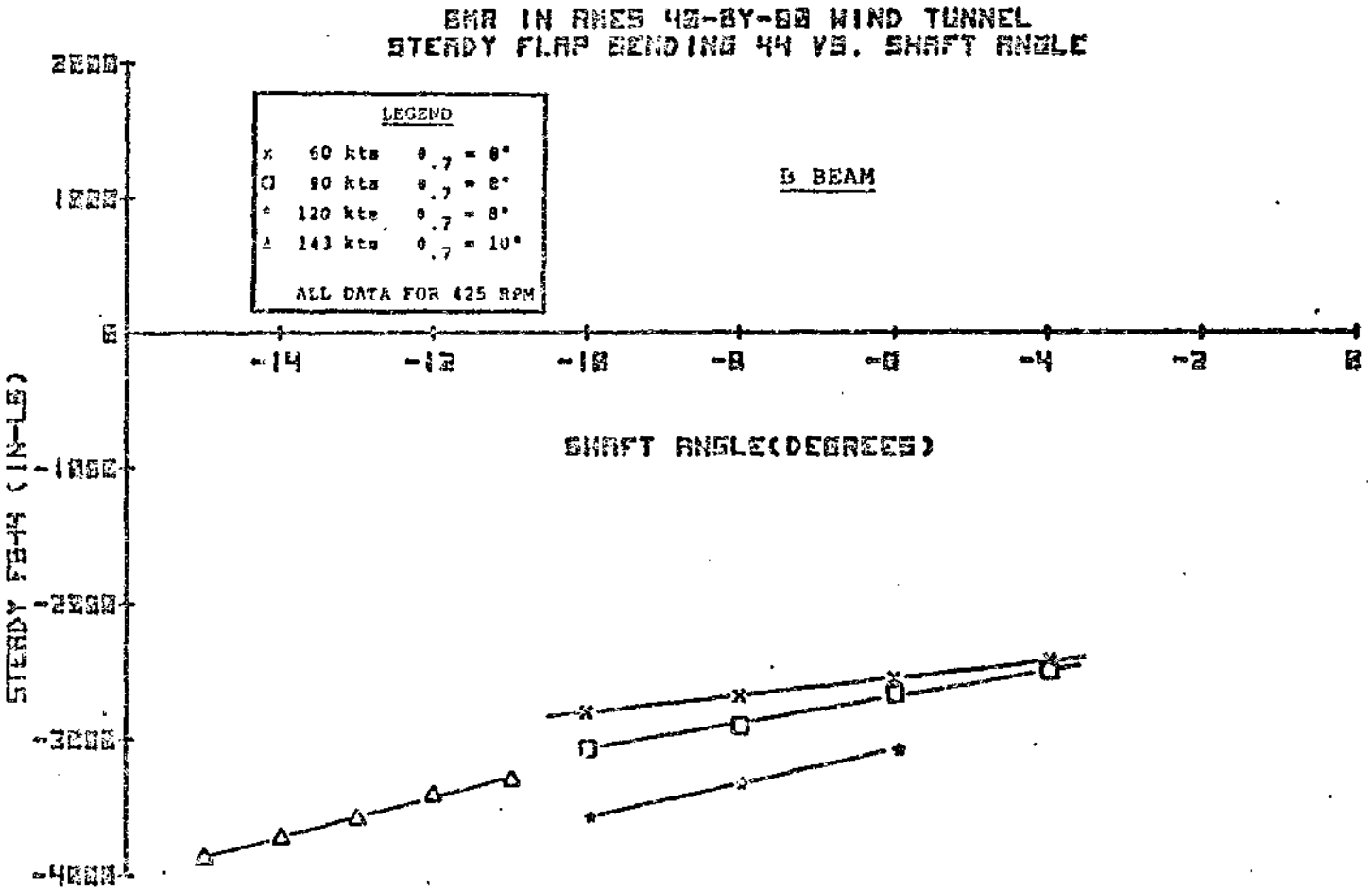

FIGURE 8.111 STEADY FLAP BENDING 44 VERSUS SHAFT ANGLE
(SHEET 2 OF 2)

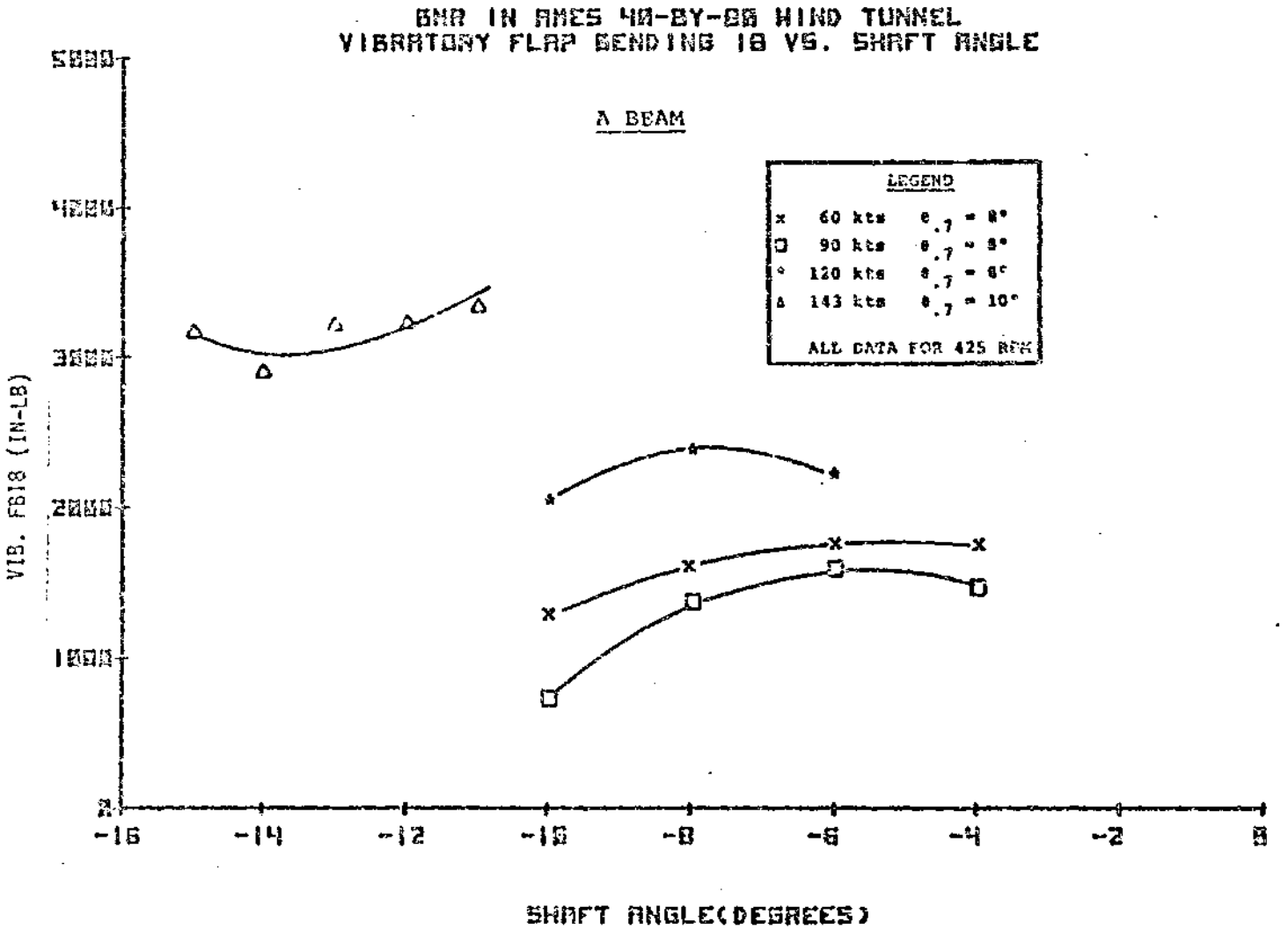

FIGURE 8.112 VIBRATORY FLAP BENDING 1B VERSUS SHAFT ANGLE
(SHEET 1 OF 2)

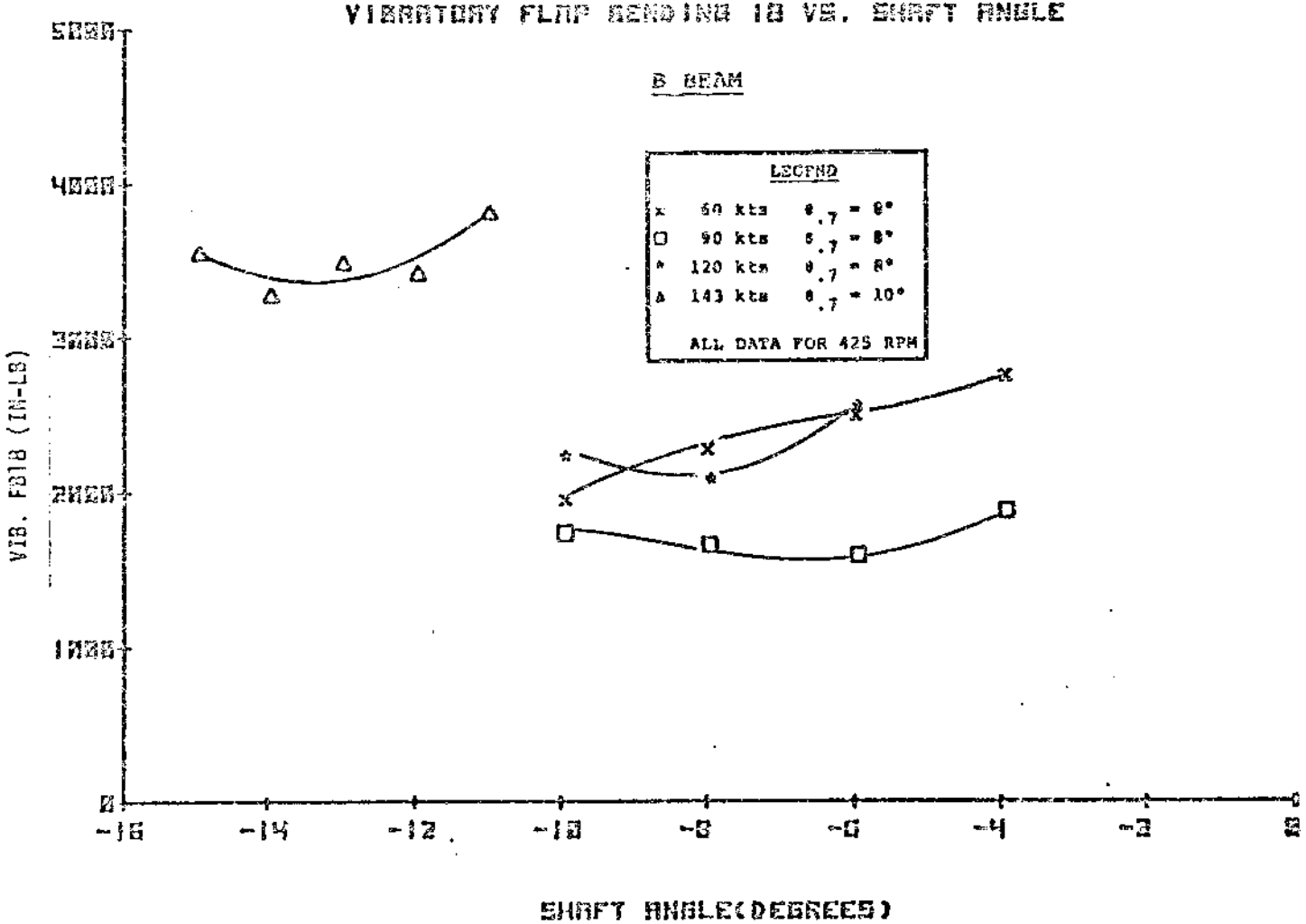

FIGURE 8.112 VIBRATORY FLAP BENDING 18 VERSUS SHAFT ANGLE
(SHEET 2 OF 2)

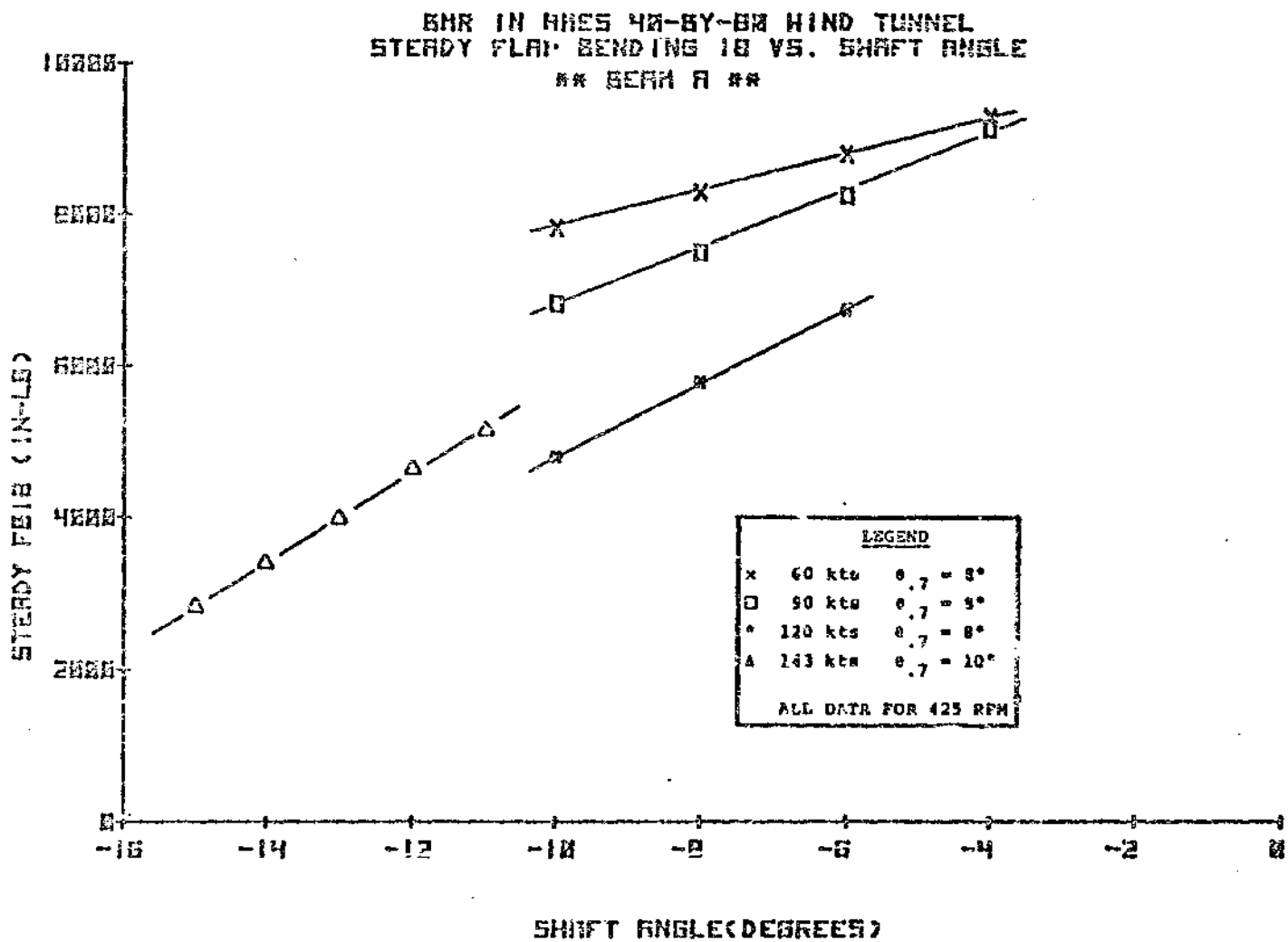

FIGURE 8.113 STEADY FLAP BENDING 1B VERSUS SHAFT ANGLE
(SHEET 1 OF 2)

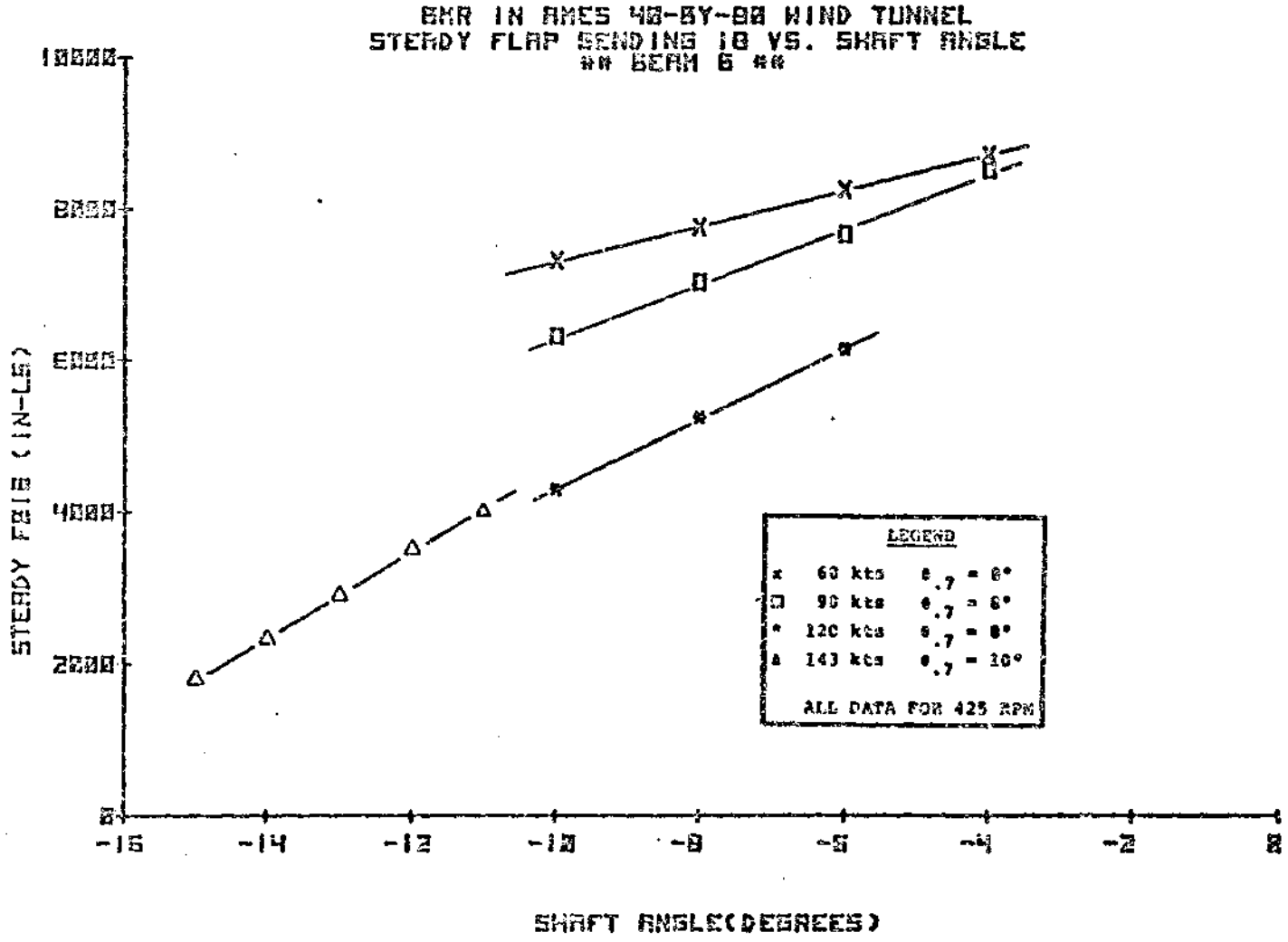

FIGURE 8.113 STEADY FLAP BENDING 18 VERSUS SHAFT ANGLE
(SHEET 2 OF 2)

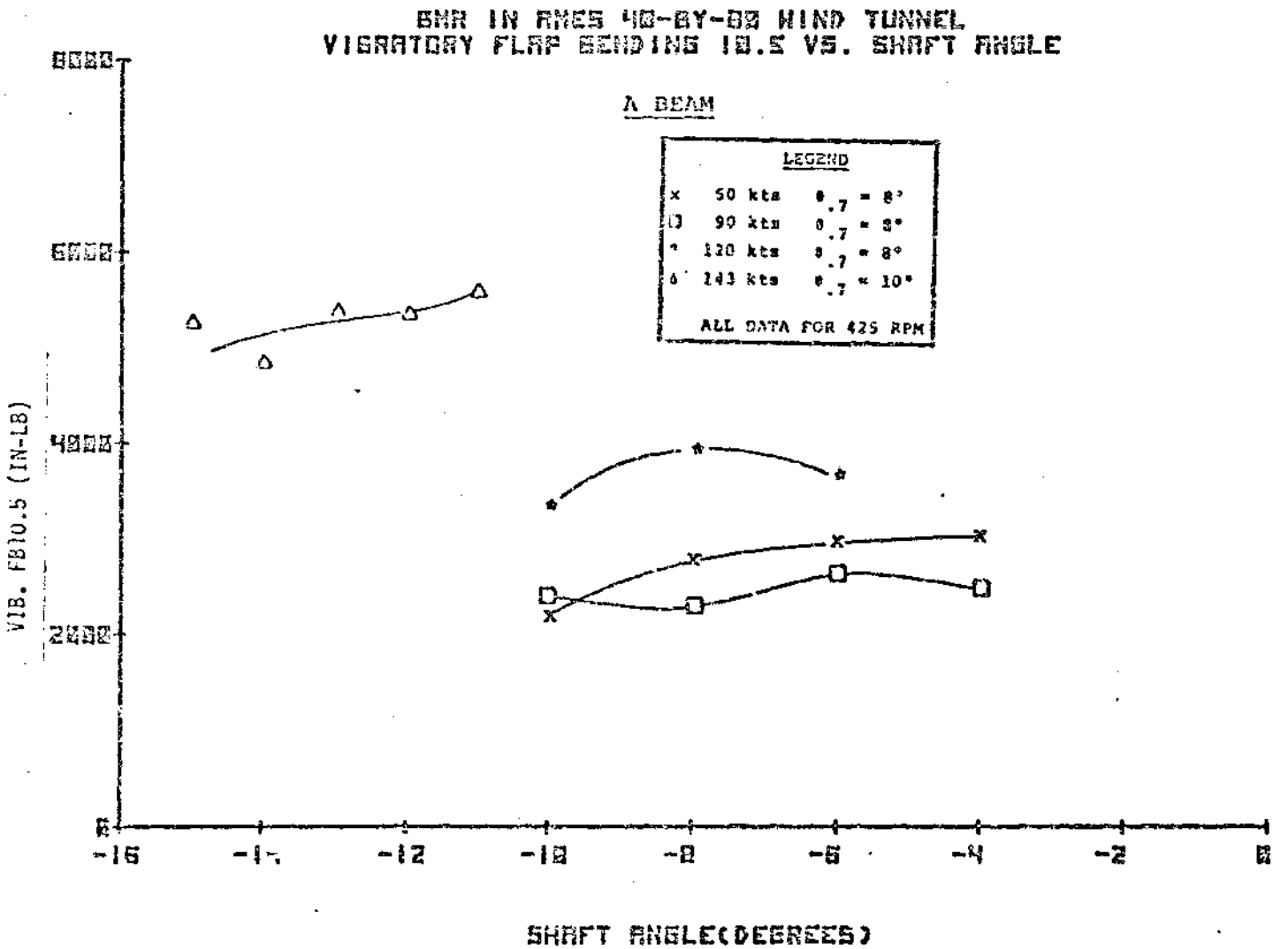

FIGURE 8.114 VIBRATORY FLAP BENDING 10.5 VERSUS SHAFT ANGLE
(SHEET 1 OF 2)

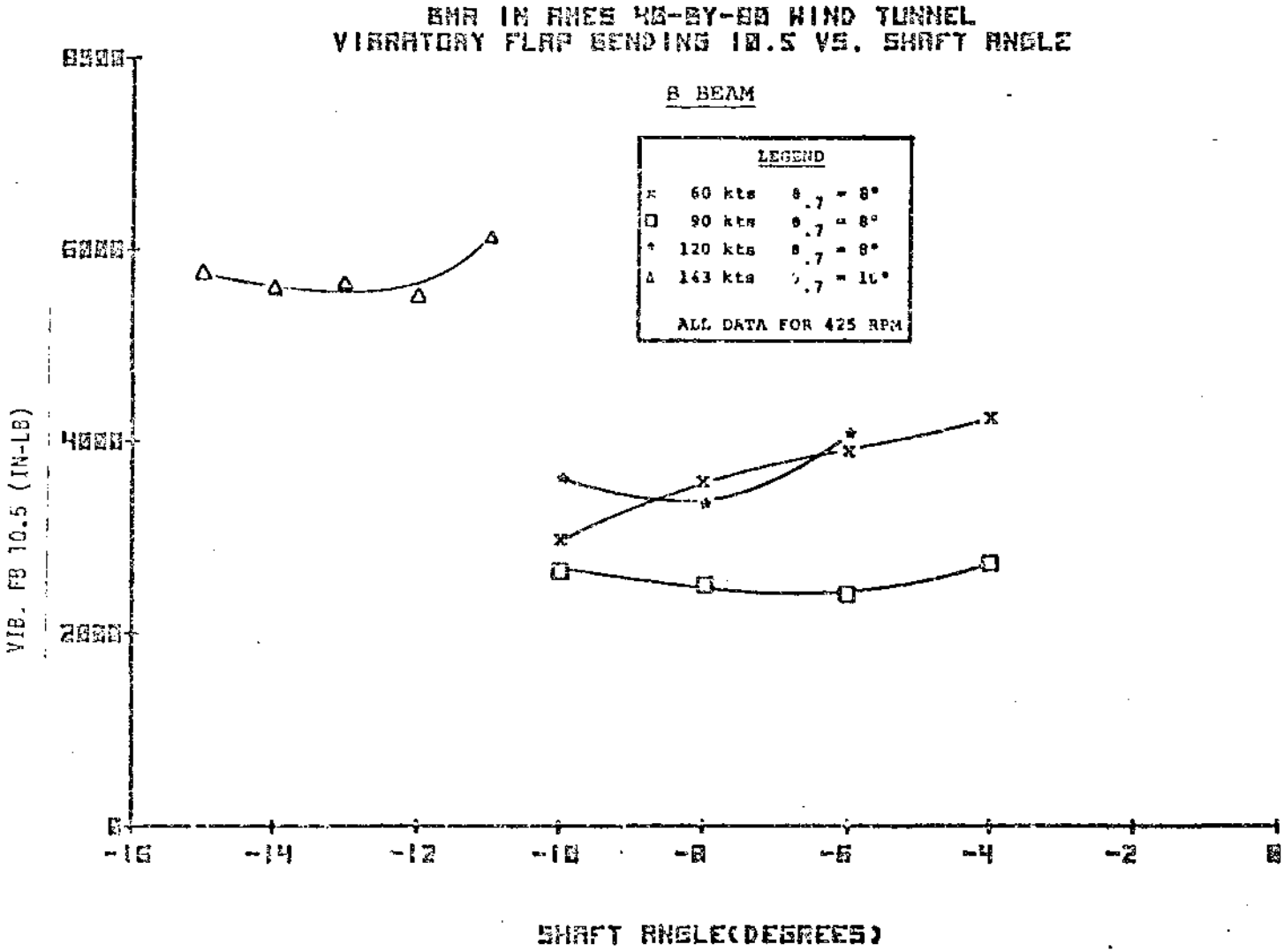

FIGURE 8.114 VIBRATORY FLAP BENDING 10.5 VERSUS SHAFT ANGLE
(SHEET 2 OF 2)

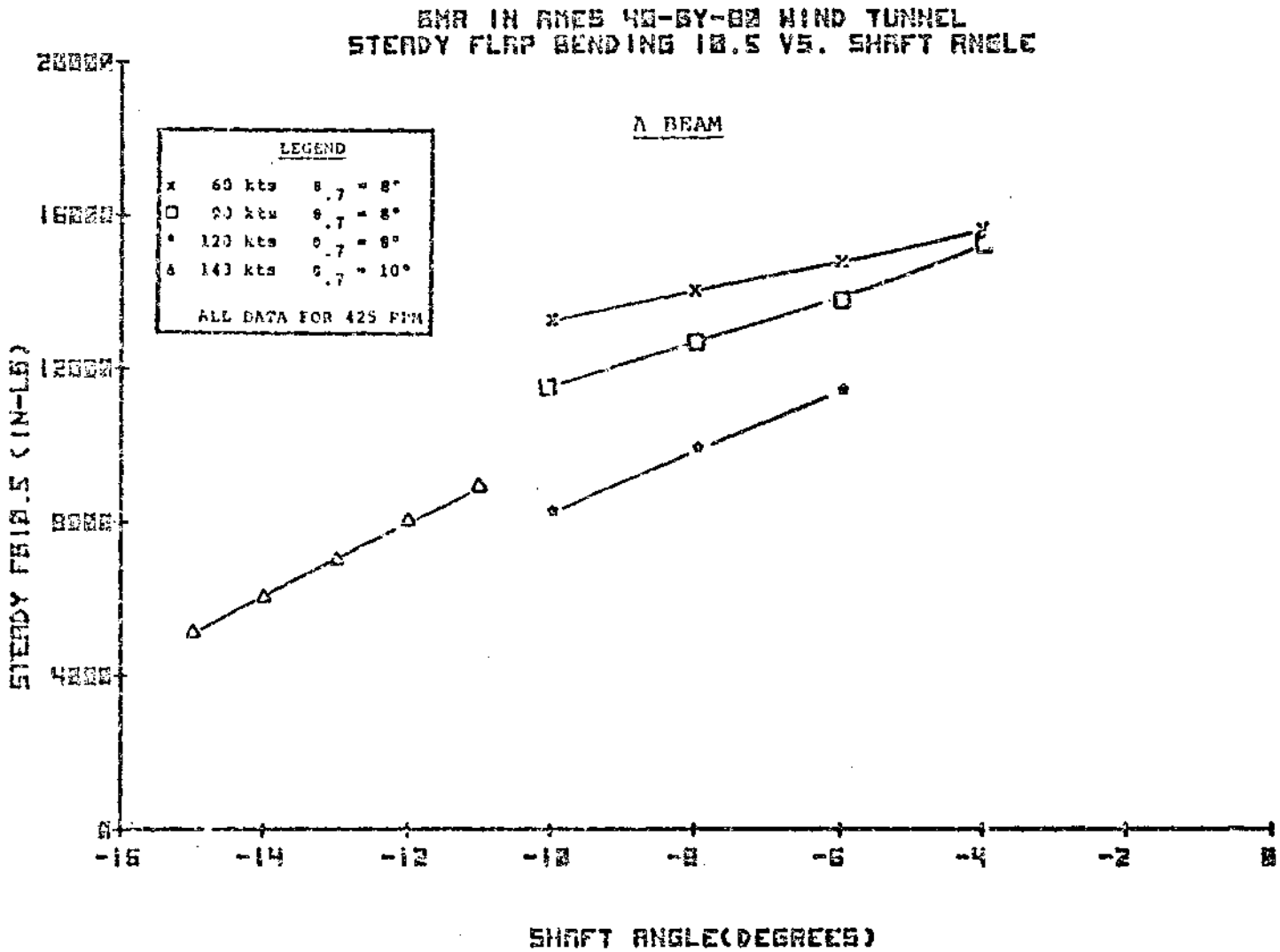

FIGURE 8.115 STEADY FLAP BENDING 10.5 VERSUS SHAFT ANGLE
(SHEET 1 OF 2)

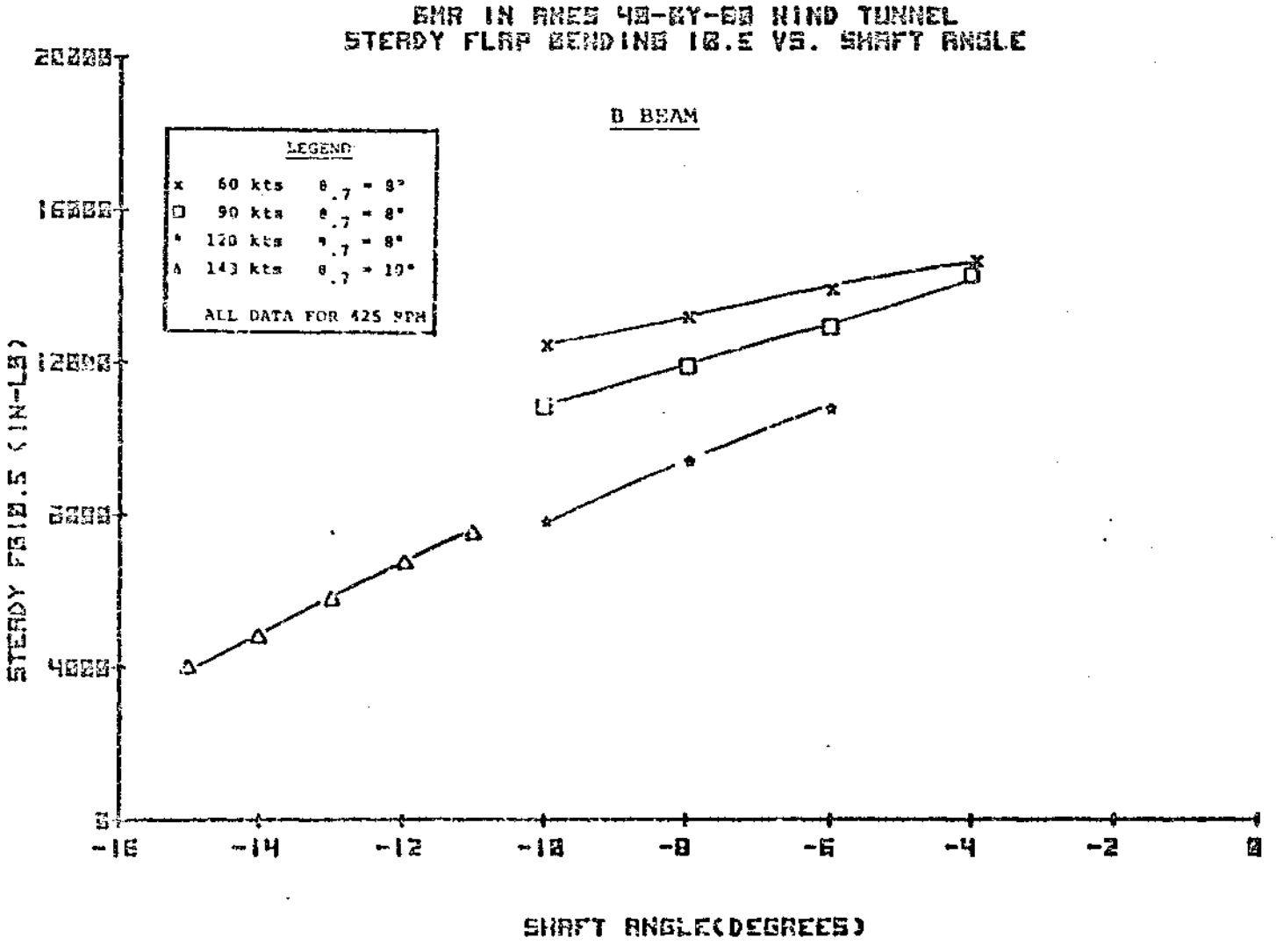

FIGURE 8.115 STEADY FLAP BENDING 10.5 VERSUS SHAFT ANGLE
(SHEET 2 OF 2)

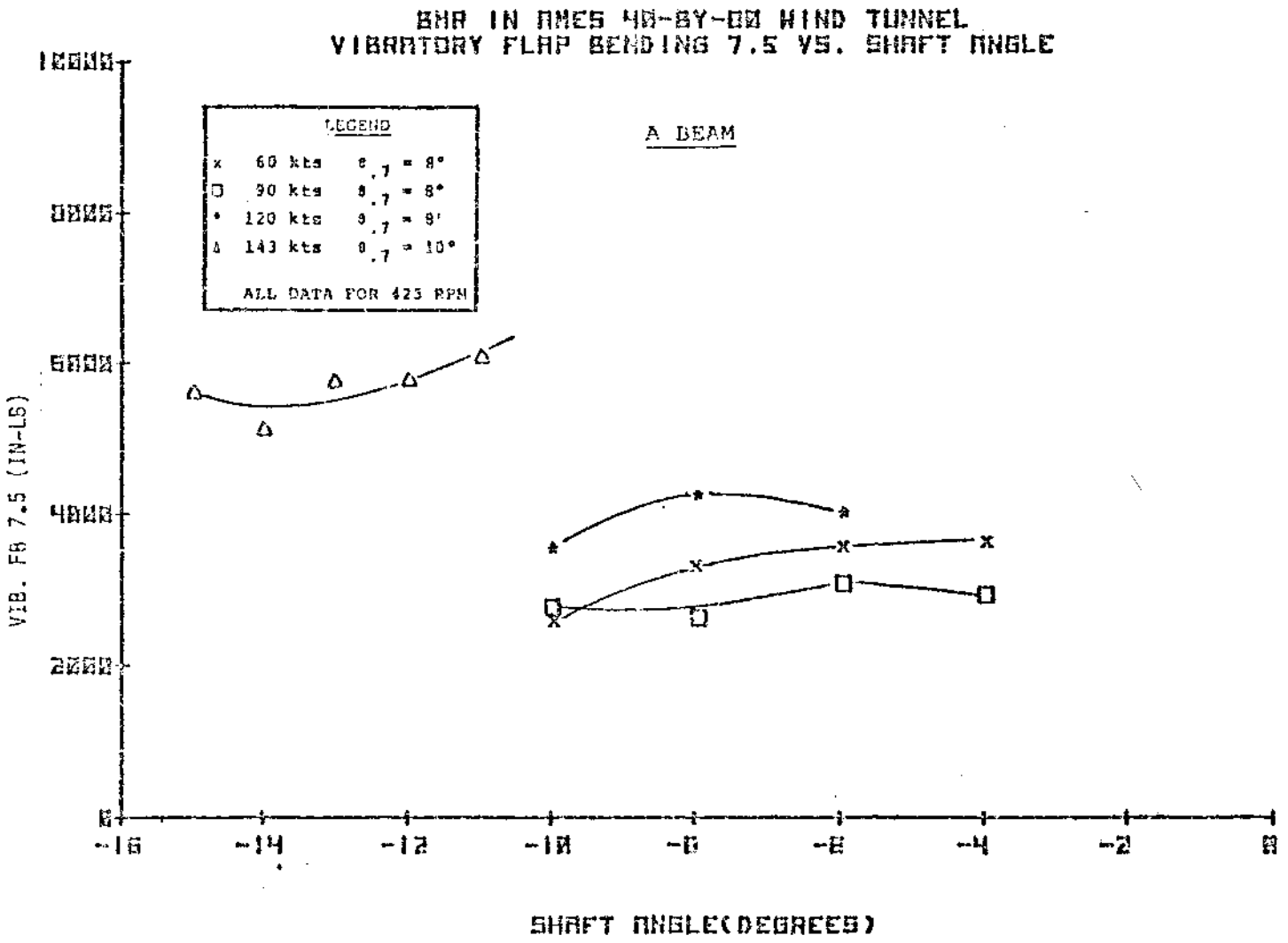

FIGURE 8.116 VIBRATORY FLAP BENDING 7.5 VERSUS SHAFT ANGLE
(SHEET 1 OF 2)

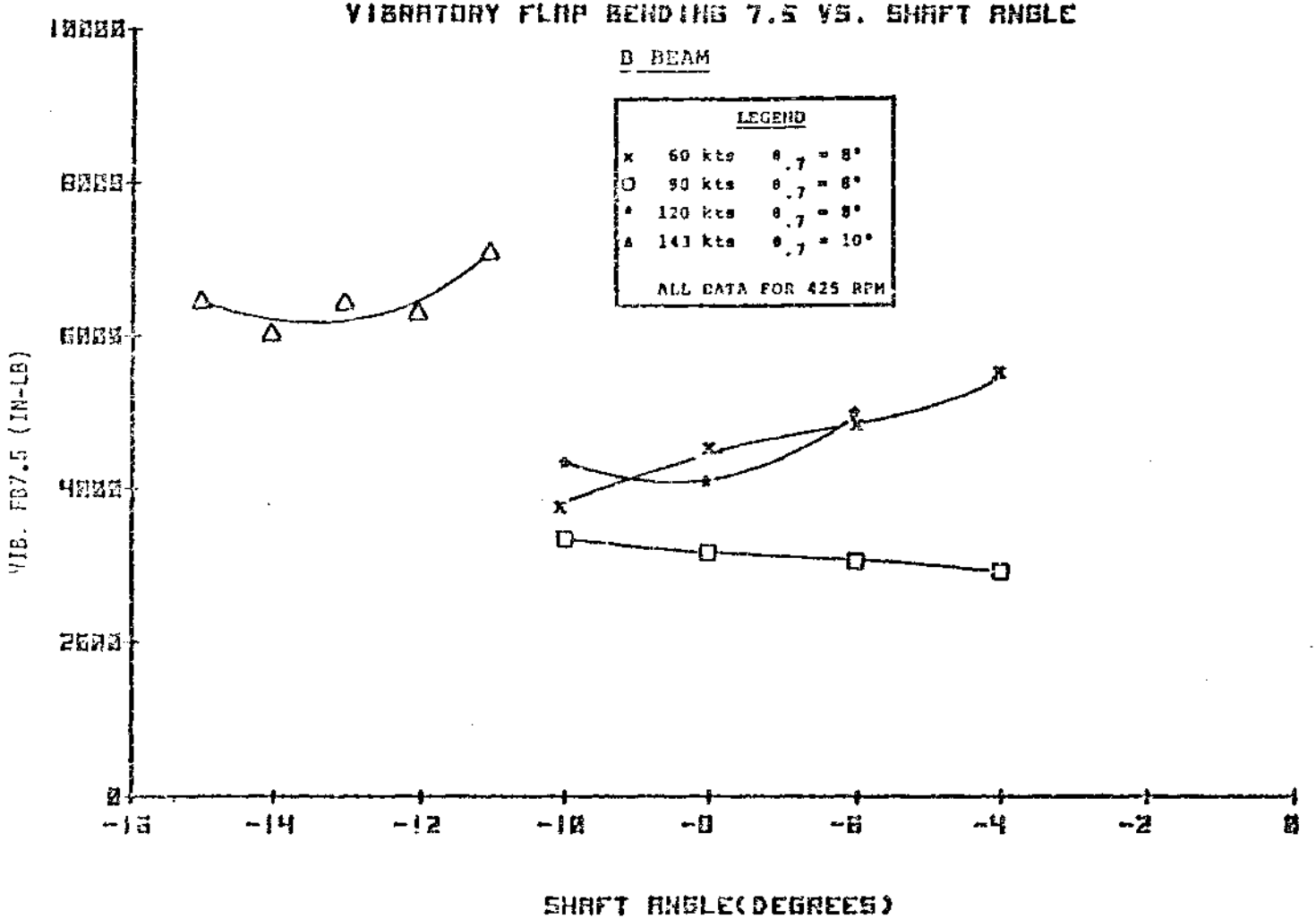

FIGURE 8.116 VIBRATORY FLAP BENDING 7.5 VERSUS SHAFT ANGLE
(SHEET 2 OF 2)

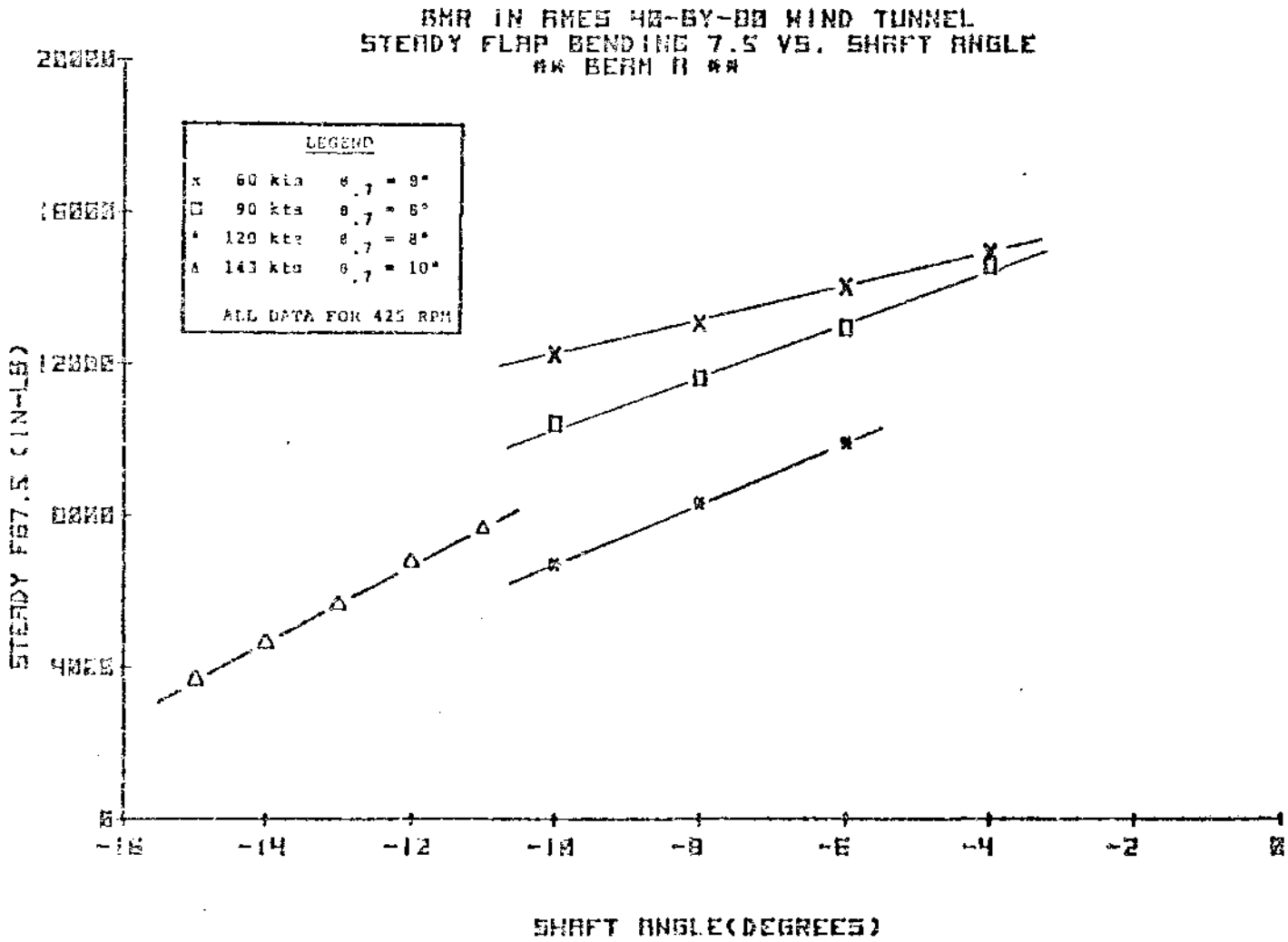

FIGURE 8.117 STEADY FLAP BENDING 7.5 VERSUS SHAFT ANGLE
(SHEET 1 OF 2)

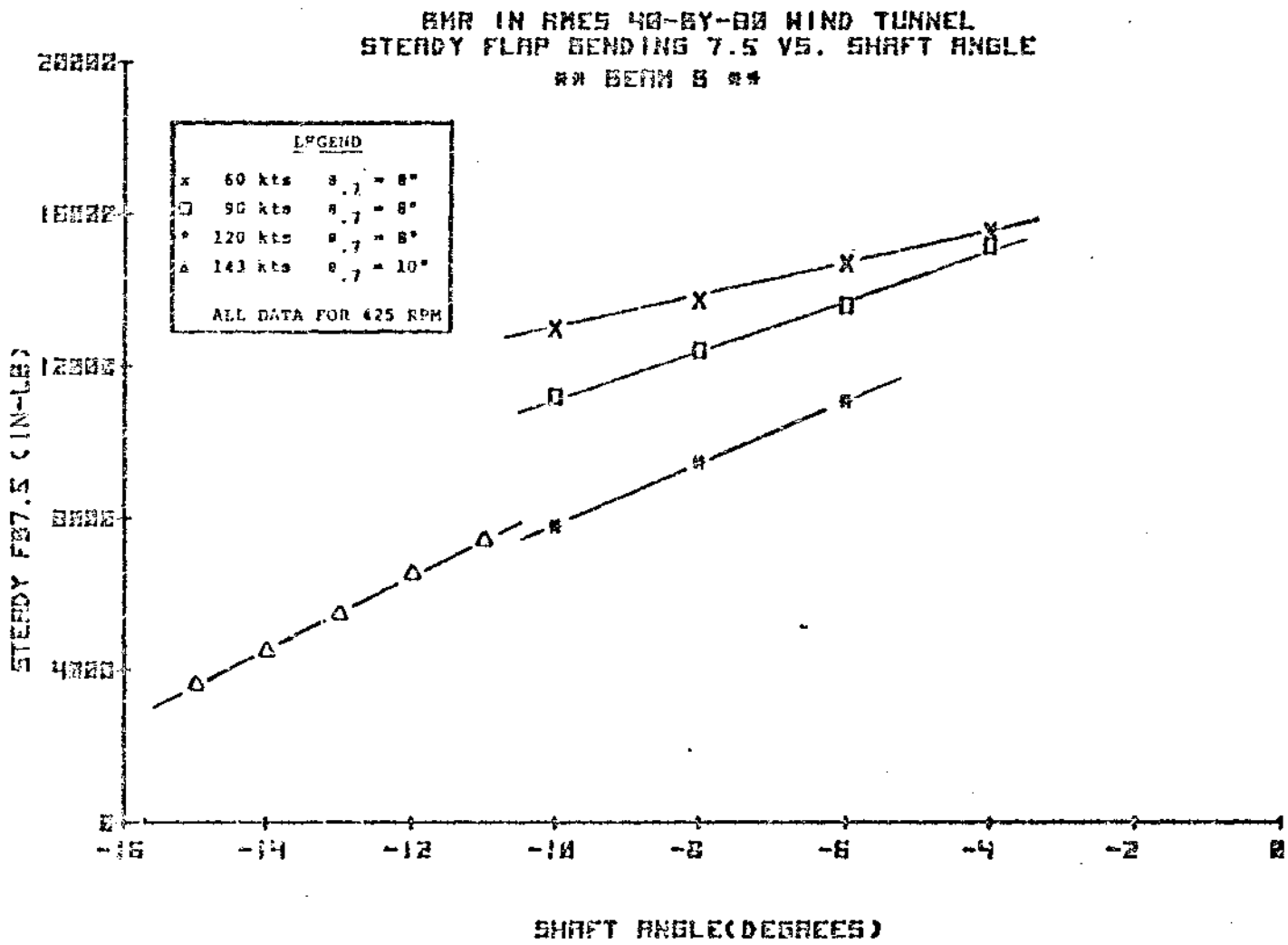

FIGURE 8.117 STEADY FLAP BENDING 7.5 VERSUS SHAFT ANGLE
(SHEET 2 OF 2)

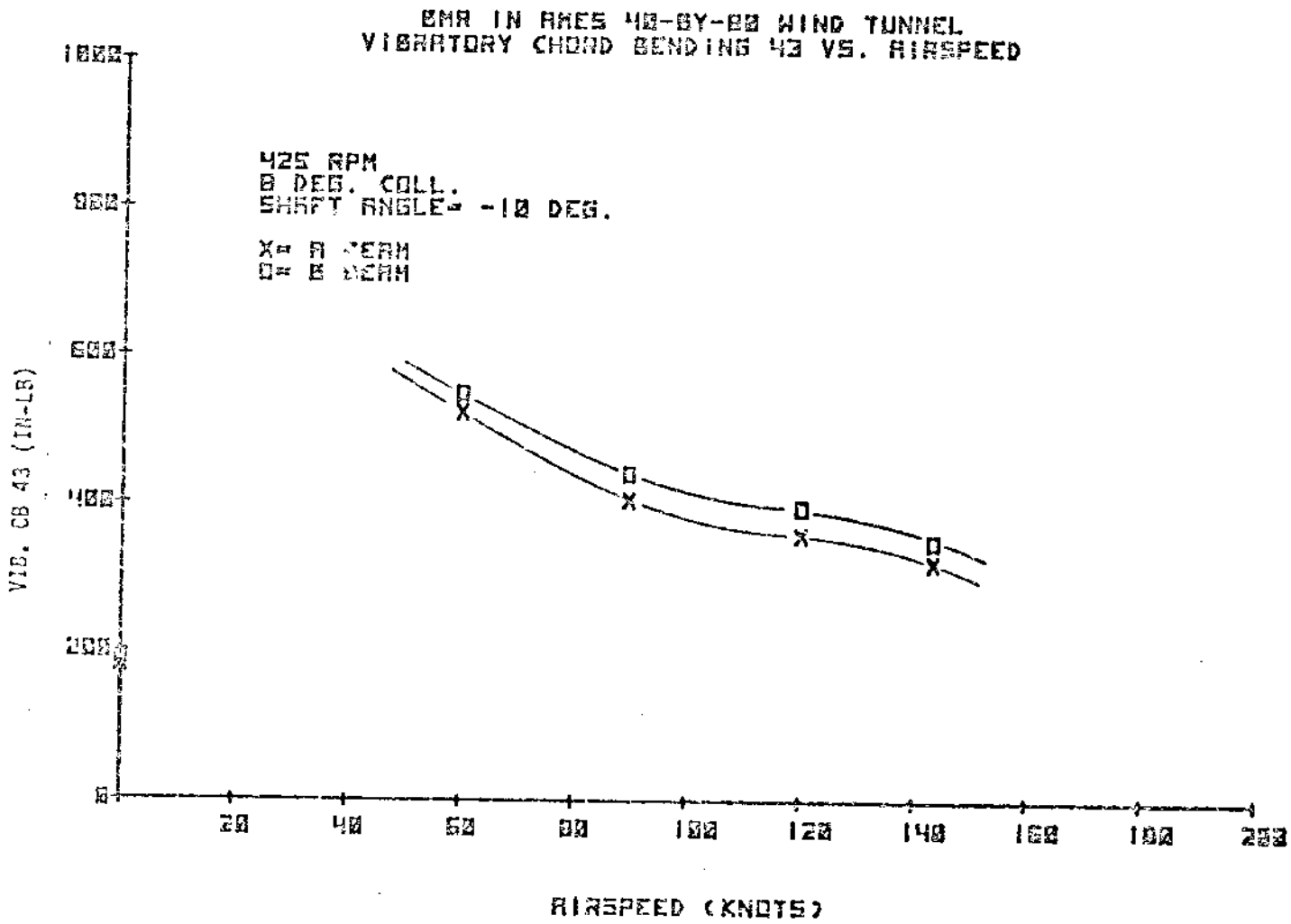

FIGURE 8.118 VIBRATORY CHORD BENDING 43 VERSUS AIRSPEED

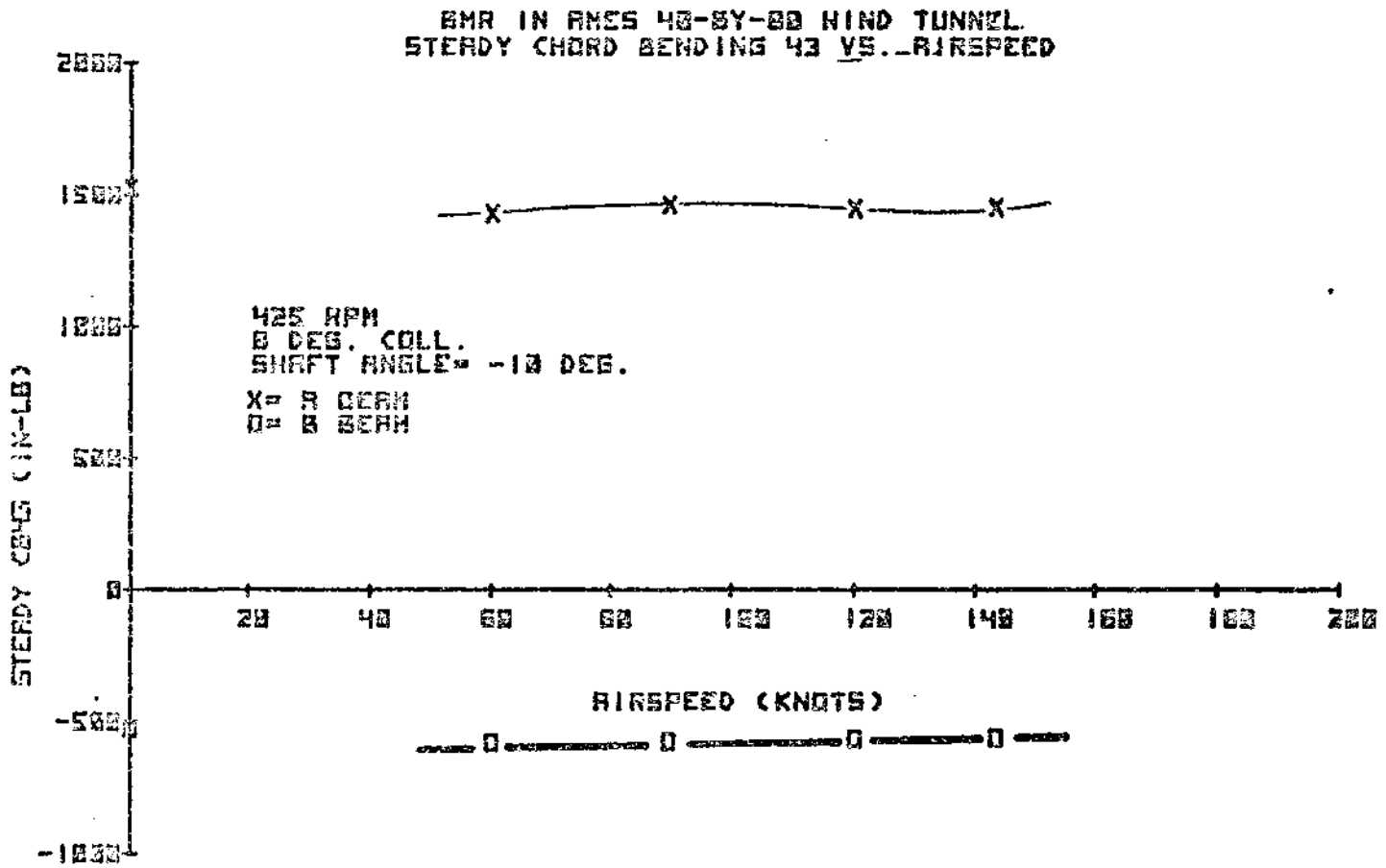

FIGURE 8.119 STEADY CHORD BENDING 43 VERSUS AIRSPEED

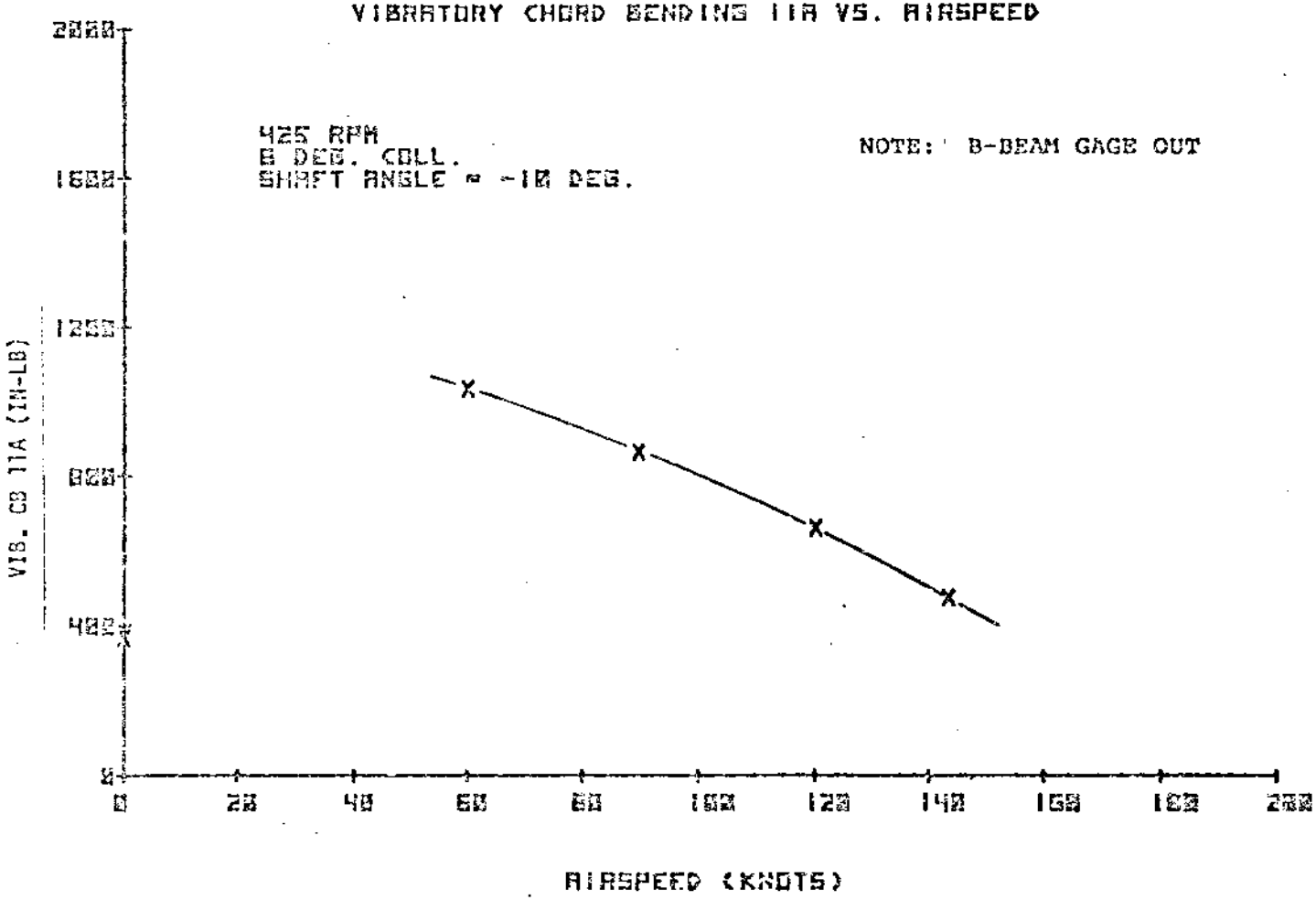

FIGURE 8.120 VIBRATORY CHORD BENDING 11A VERSUS AIRSPEED

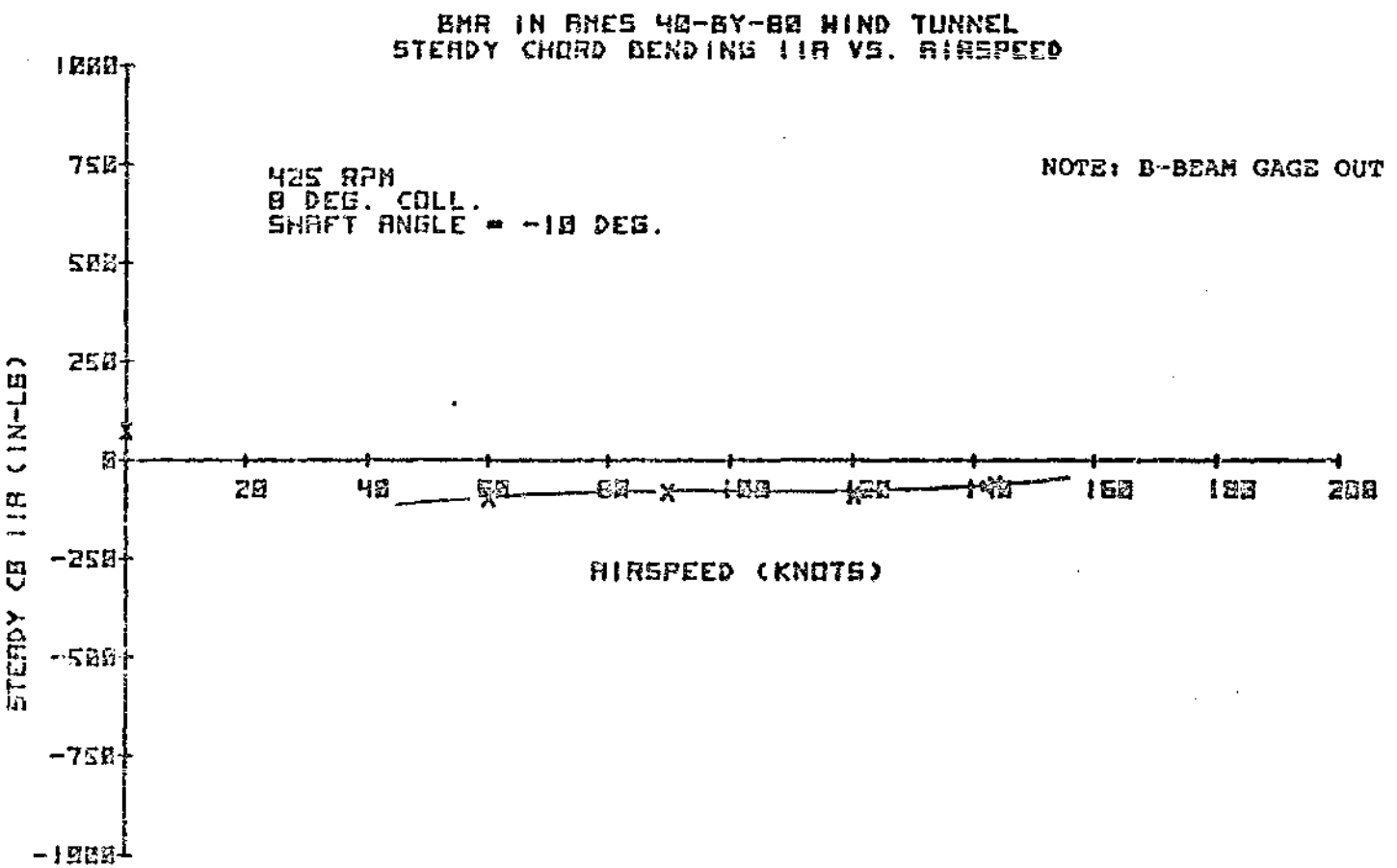

FIGURE 8.121 STEADY CHORD BENDING 11A VERSUS AIRSPEED

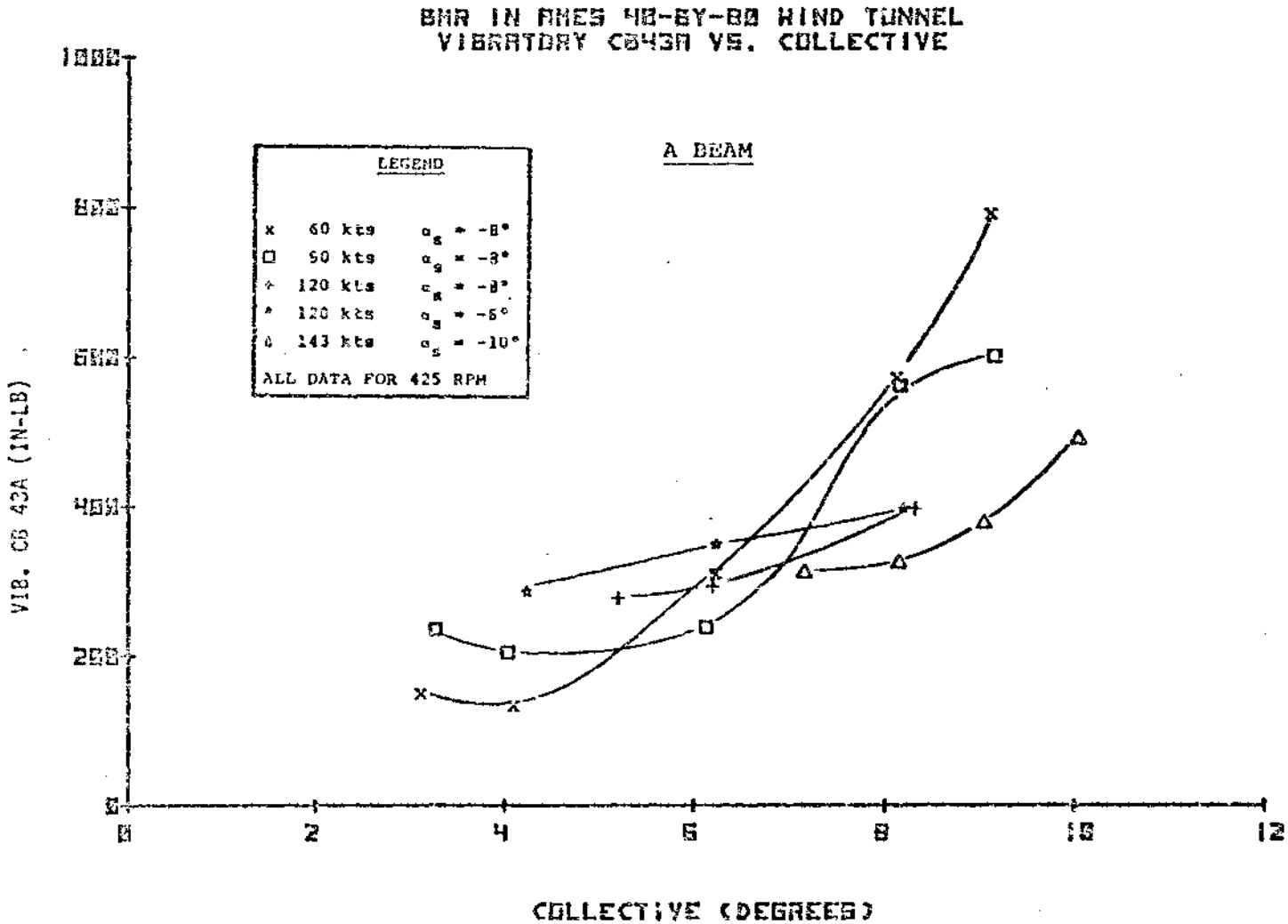

FIGURE 8.122 VIBRATORY CHORD BENDING 43 VERSUS COLLECTIVE (SHEET 1 OF 2)

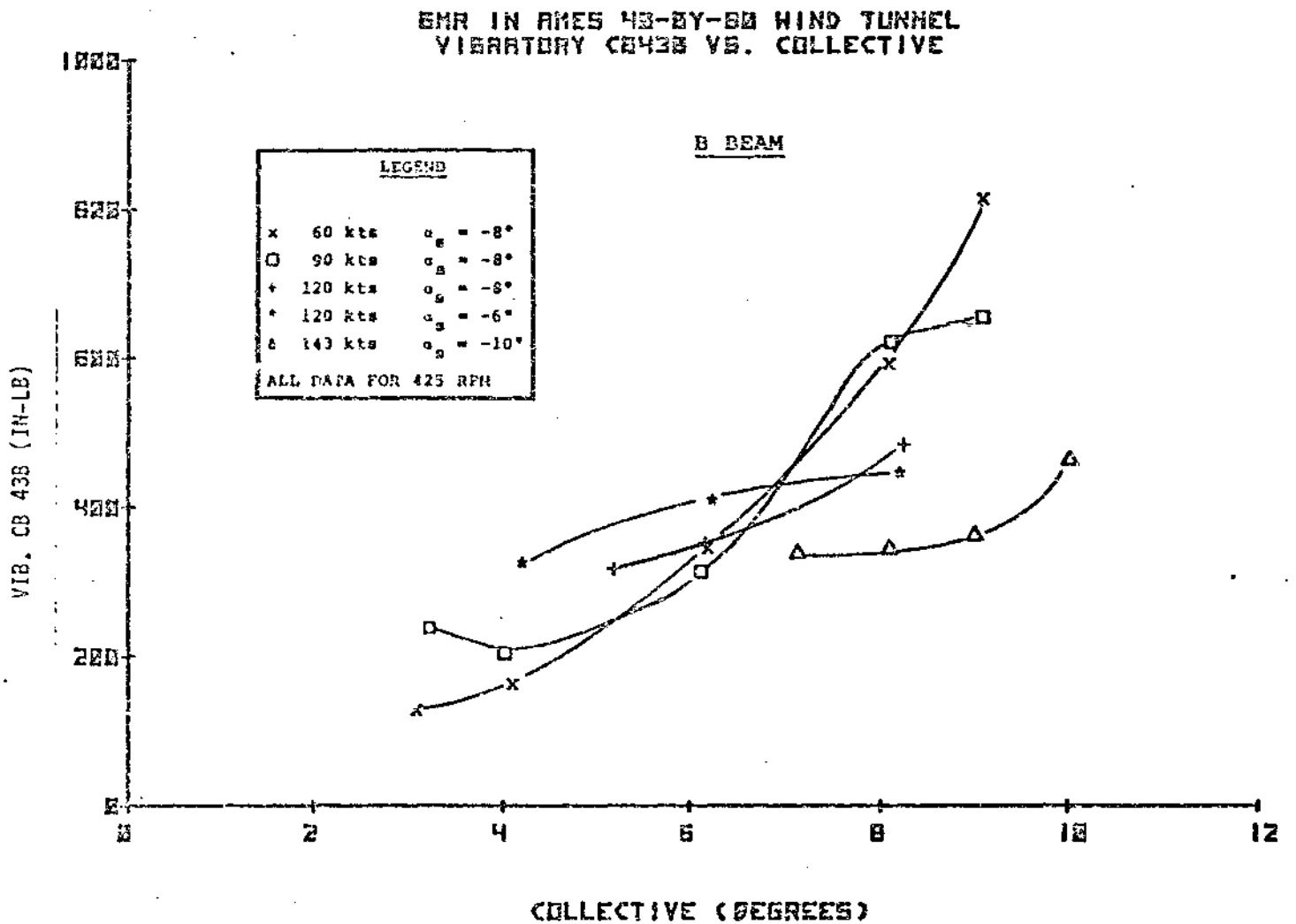

FIGURE 8.122 VIBRATORY CHORD BENDING 43 VERSUS COLLECTIVE (SHEET 2 OF 2)

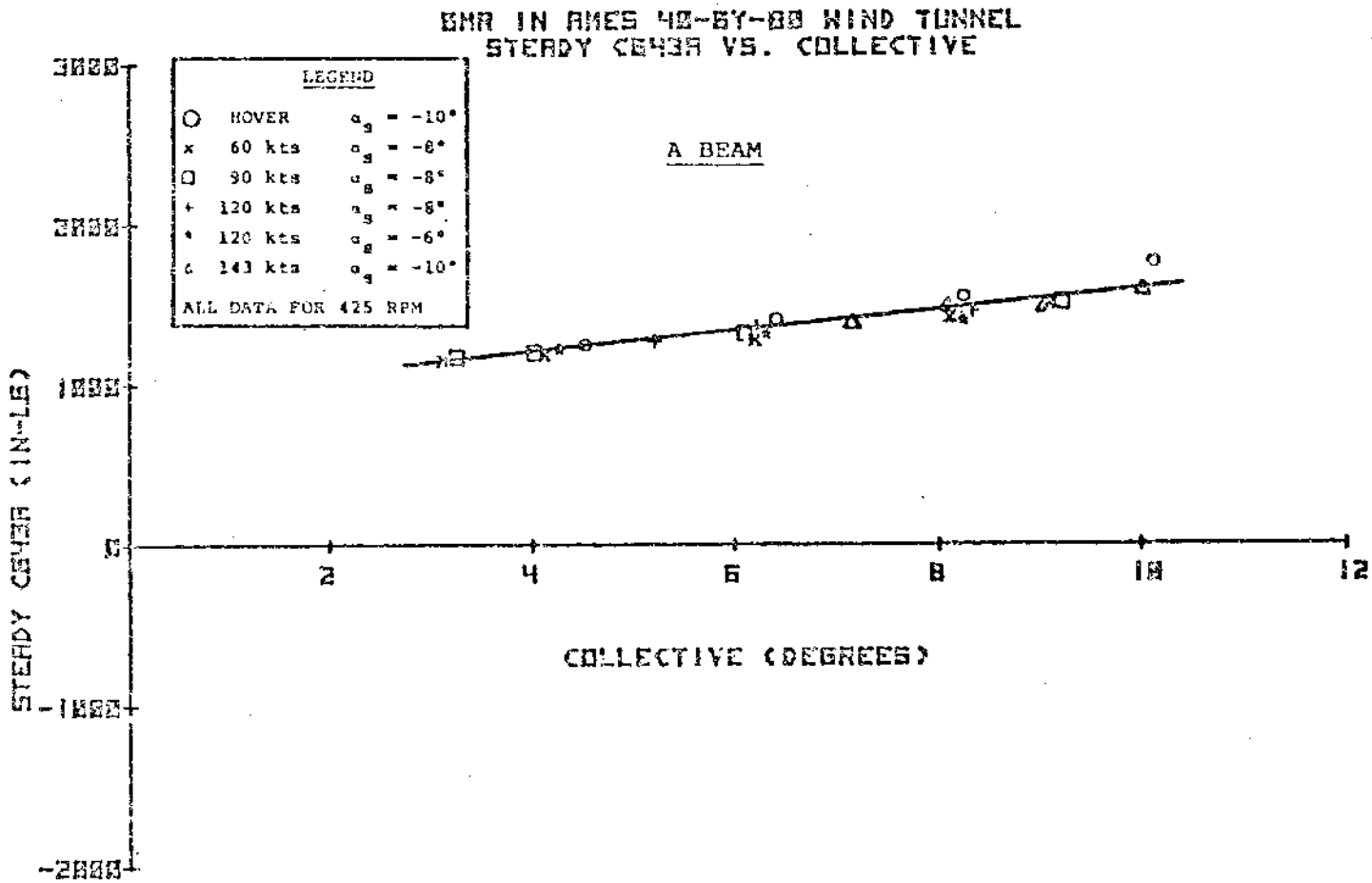

FIGURE 3.123 STEADY CHORD BENDING 43 VERSUS COLLECTIVE
(SHEET 1 OF 2)

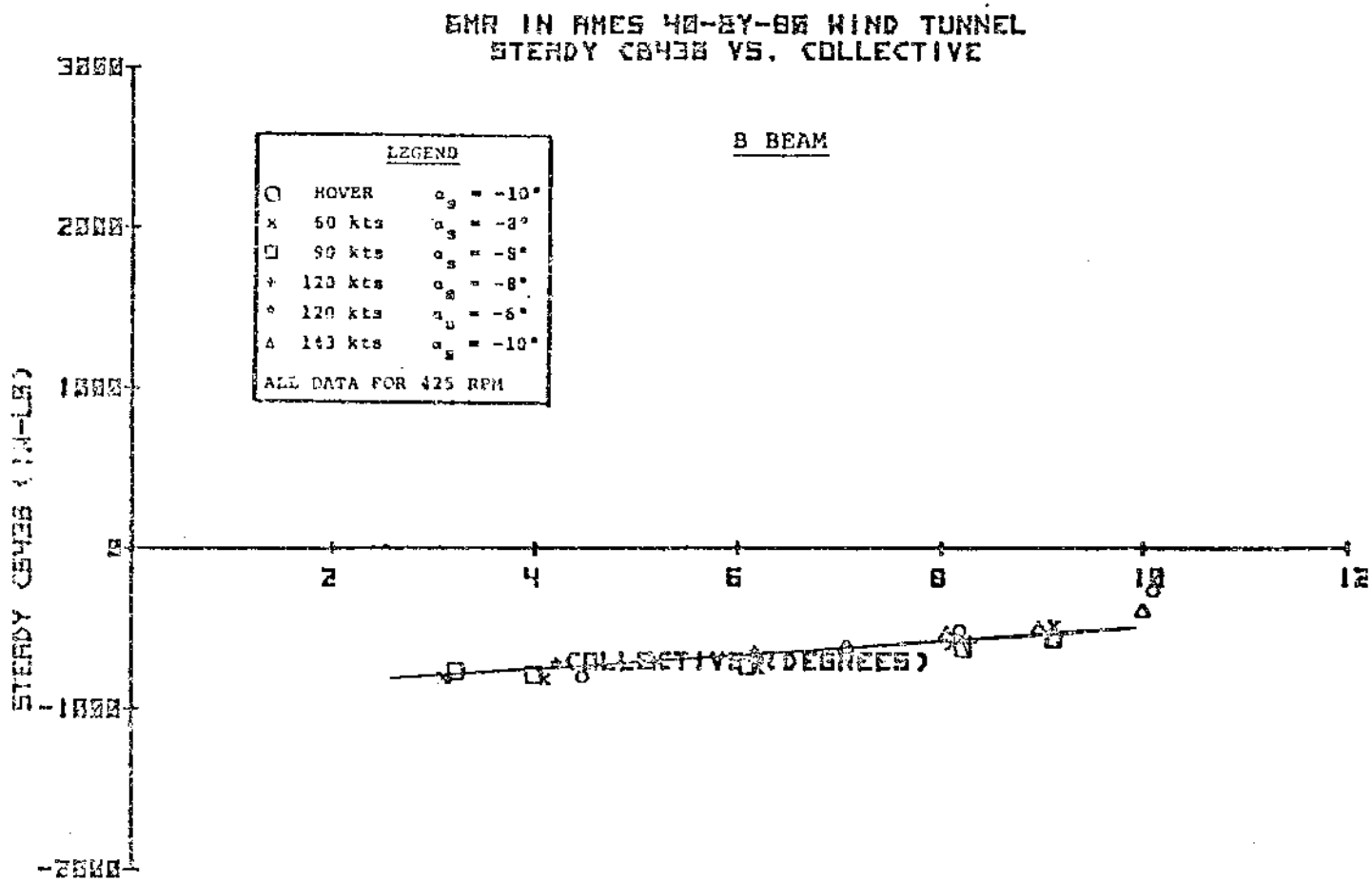

FIGURE 8.123 STEADY CHORD BENDING 43 VERSUS COLLECTIVE
(SHEET 2 OF 2)

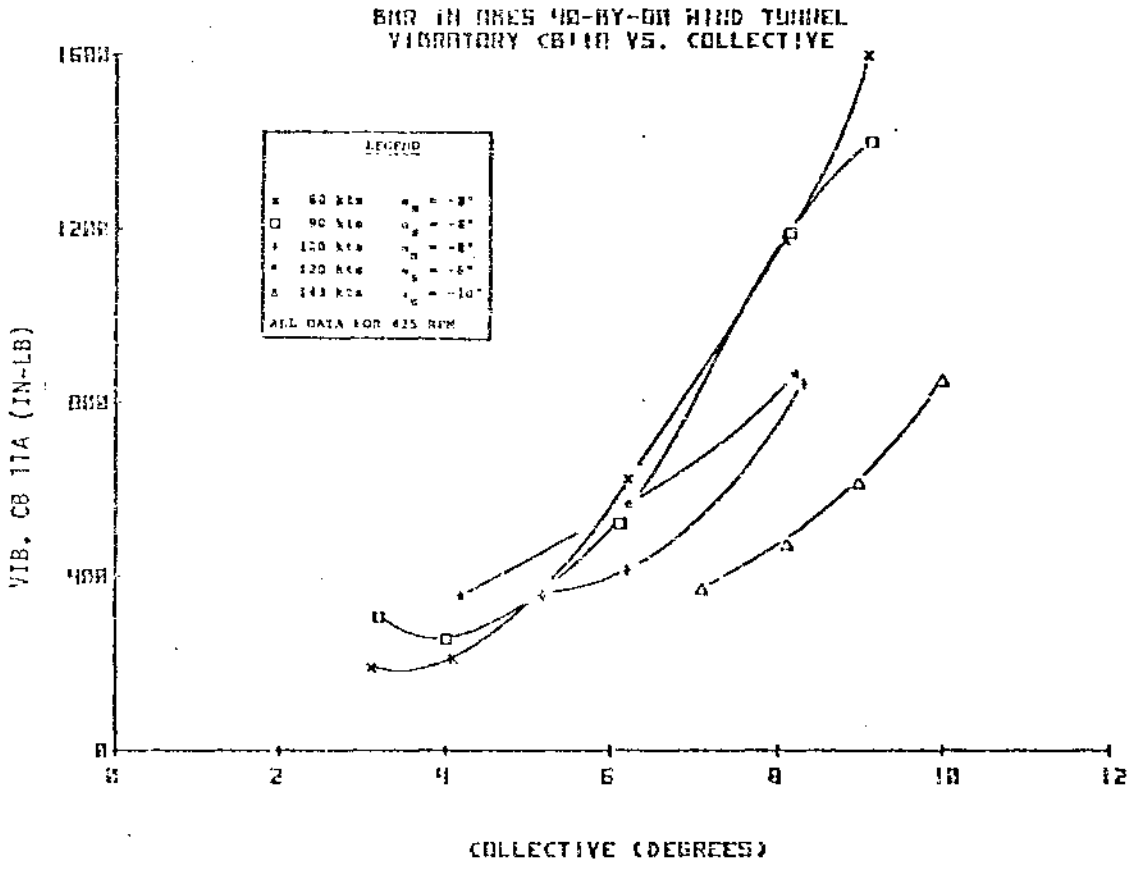

FIGURE 8.124 VIBRATORY CHORD BENDING 11A VERSUS COLLECTIVE

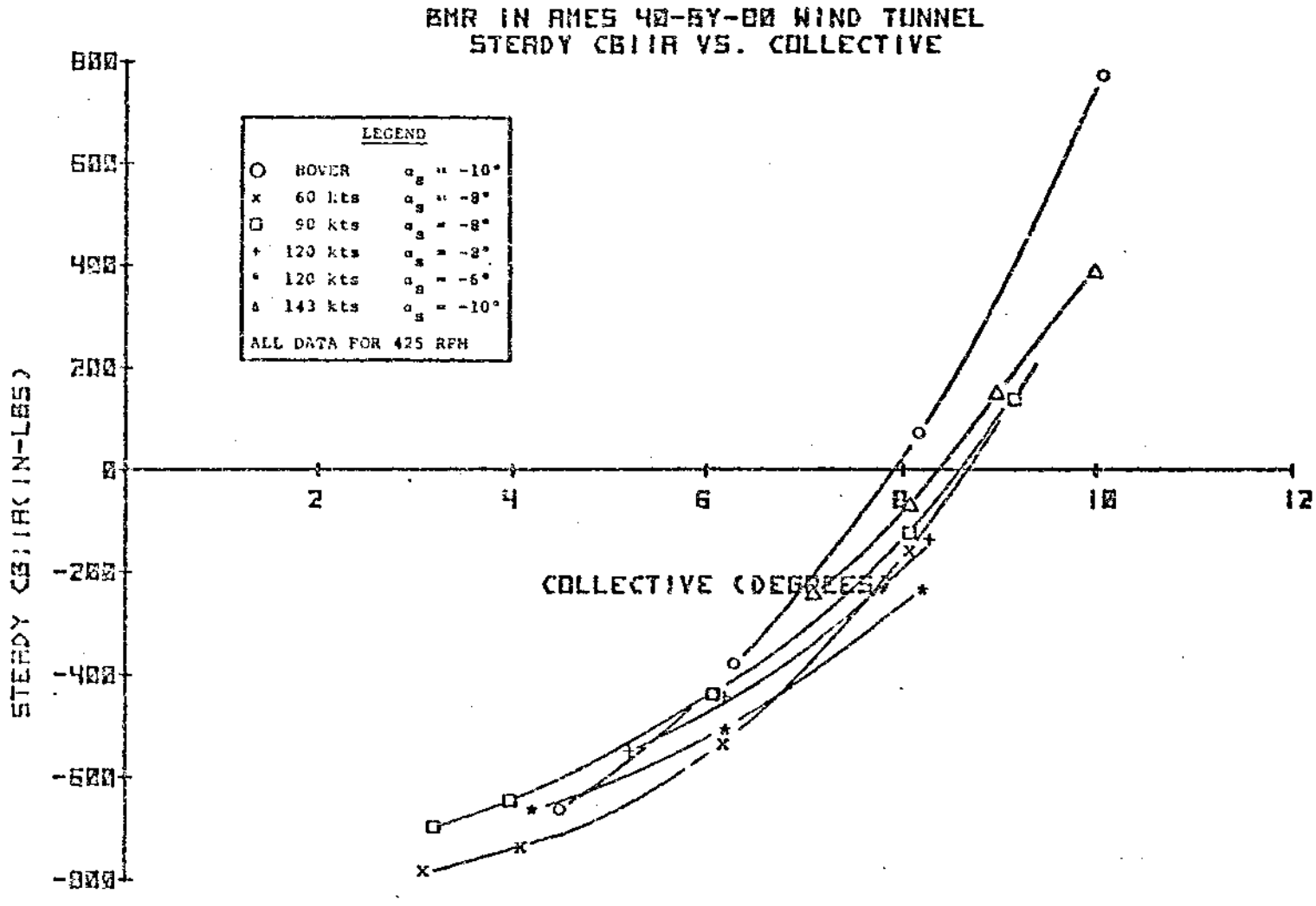

FIGURE 8.125 STEADY CHORD BENDING 11A VERSUS COLLECTIVE

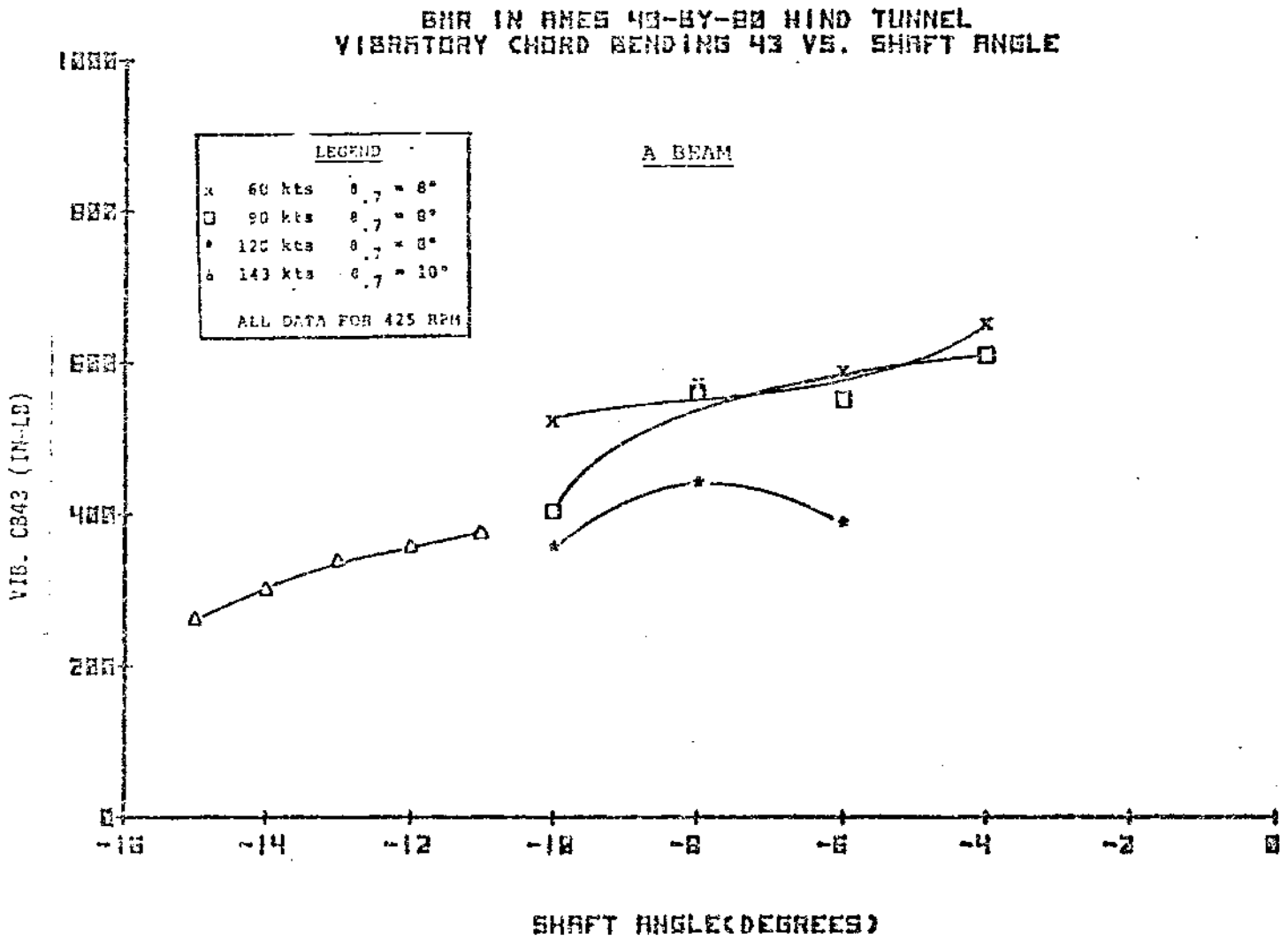

FIGURE 8.126 VIBRATORY CHORD BENDING 43 VERSUS SHAFT ANGLE
(SHEET 1 OF 2)

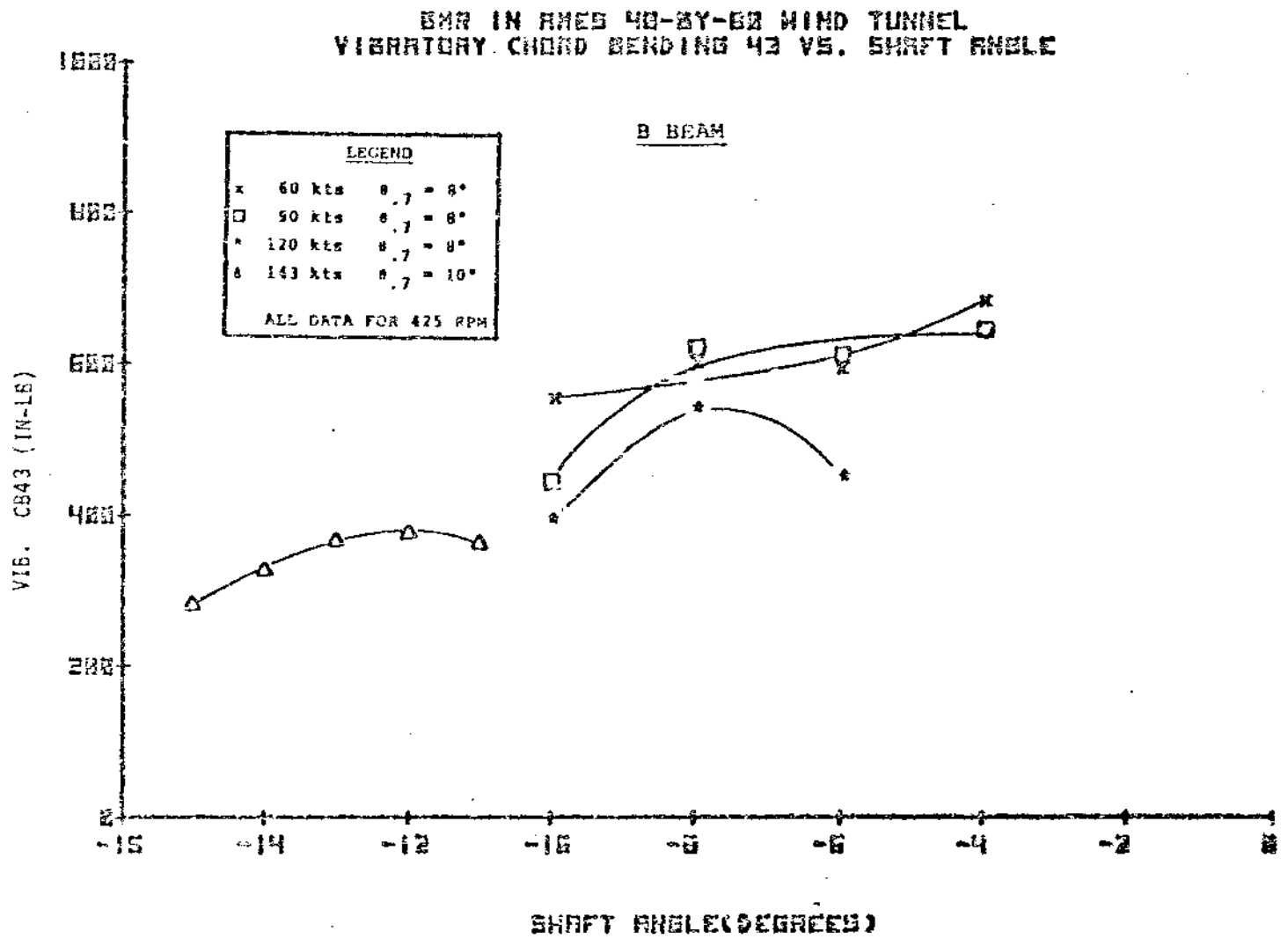

FIGURE 8.126 VIBRATORY CHORD BENDING 43 VERSUS SHAFT ANGLE
(SHEET 2 OF 2)

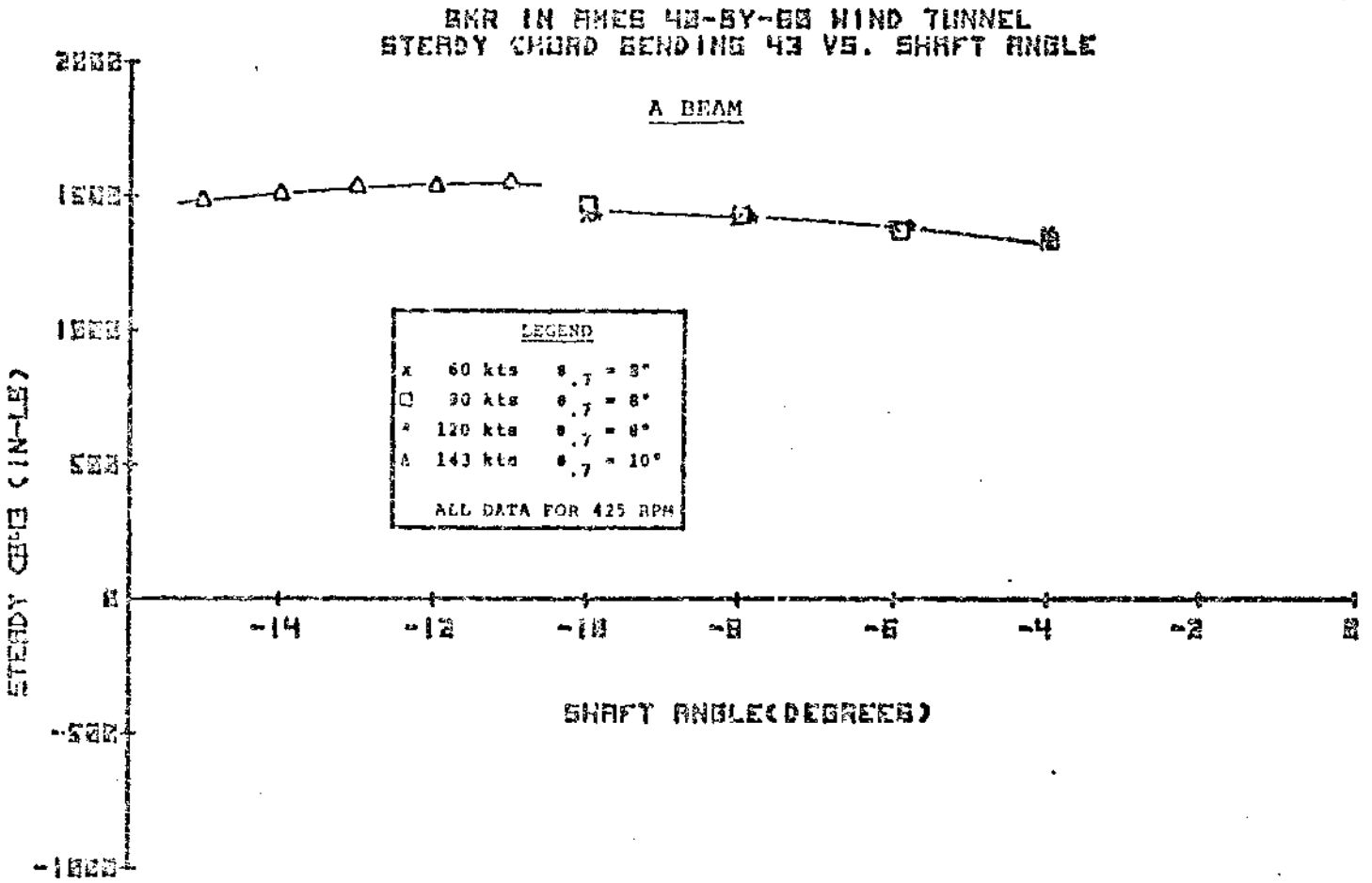

FIGURE 8.127 STEADY CHORD BENDING 43 VERSUS SHAFT ANGLE
(SHEET 1 OF 2)

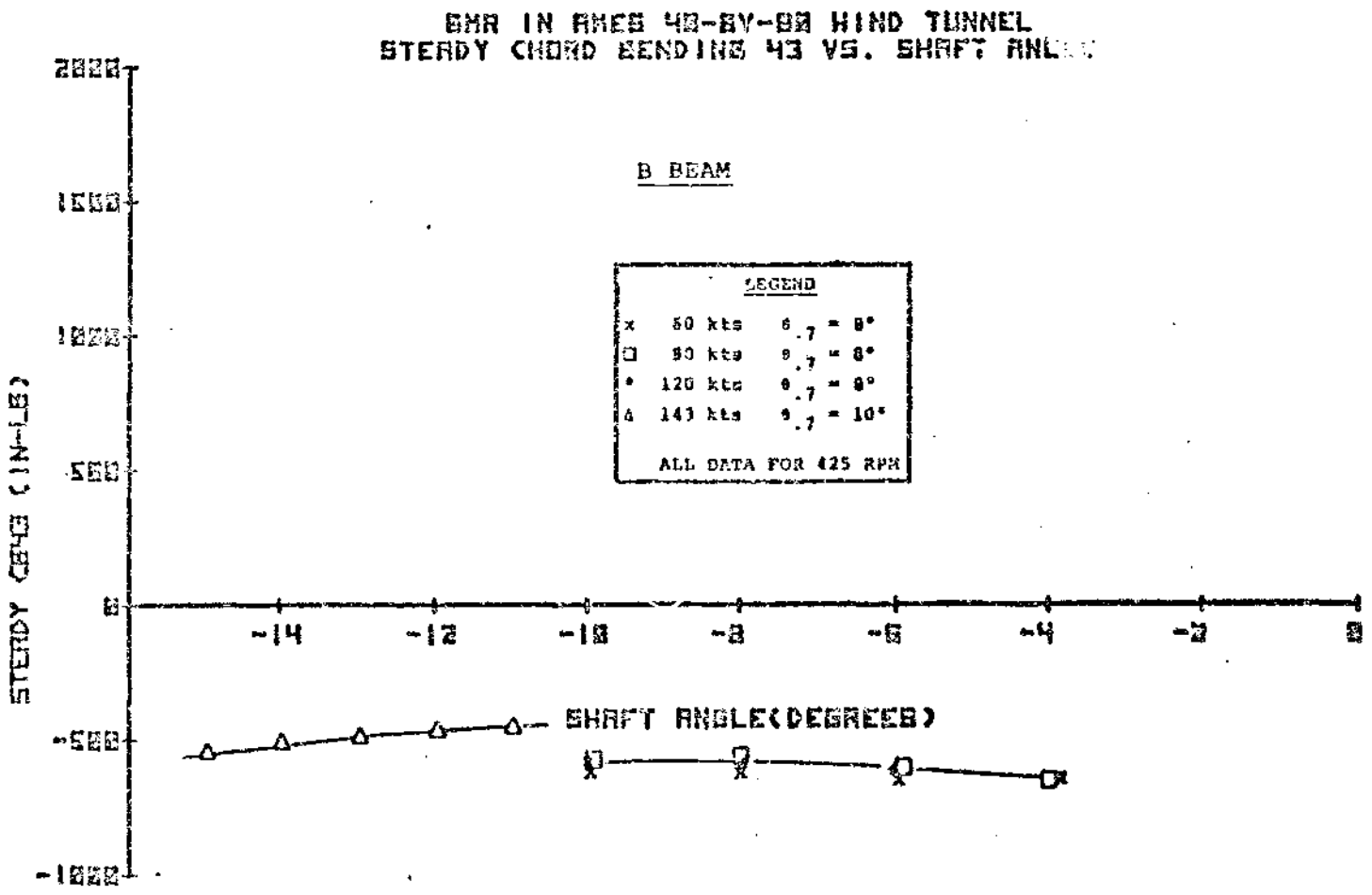

FIGURE 9.127 STEADY CHORD BENDING 43 VERSUS SHAFT ANGLE
(SHEET 2 OF 2)

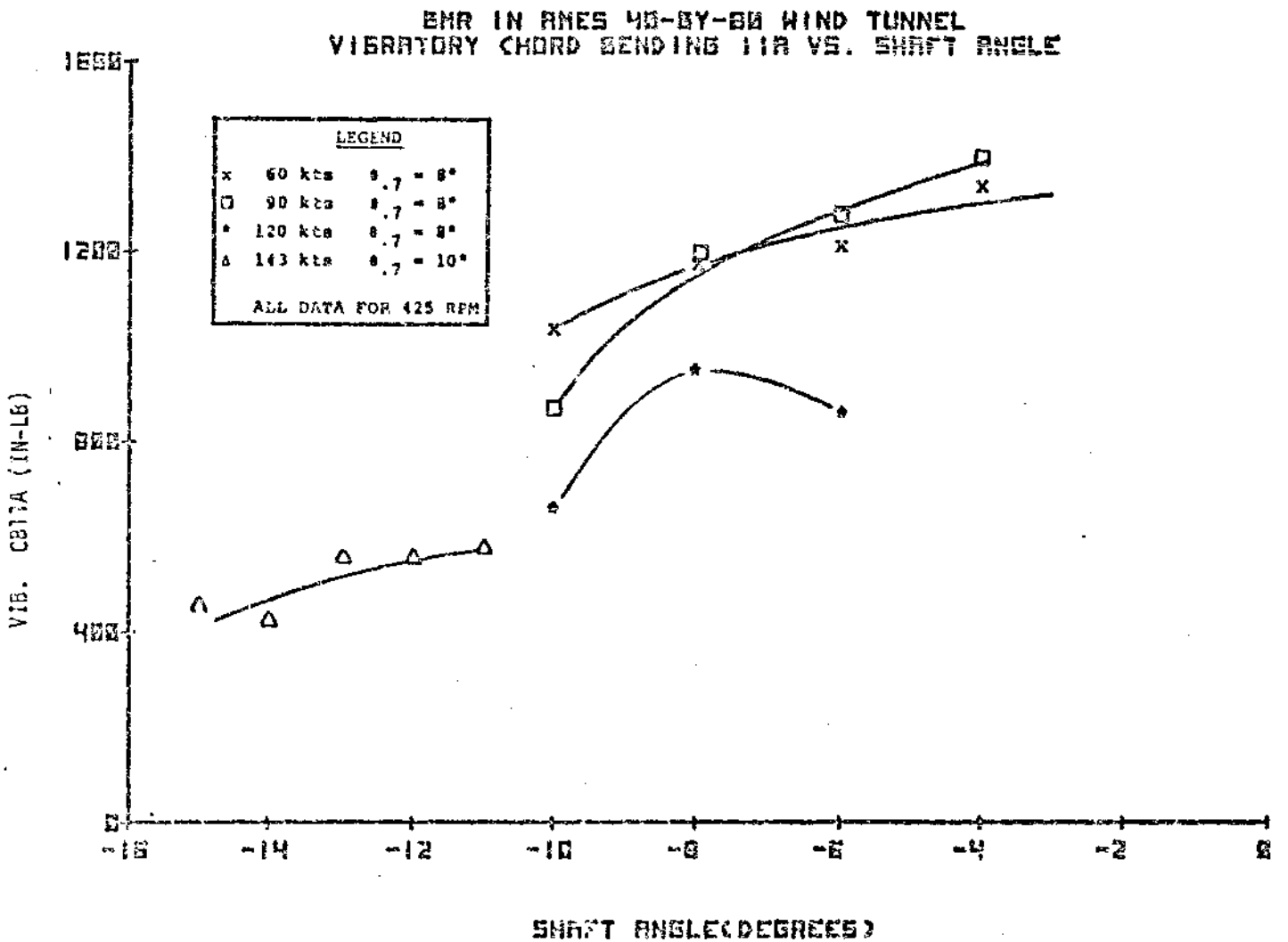

FIGURE 8.128 VIBRATORY CHORD BENDING 11A VERSUS SHAFT ANGLE

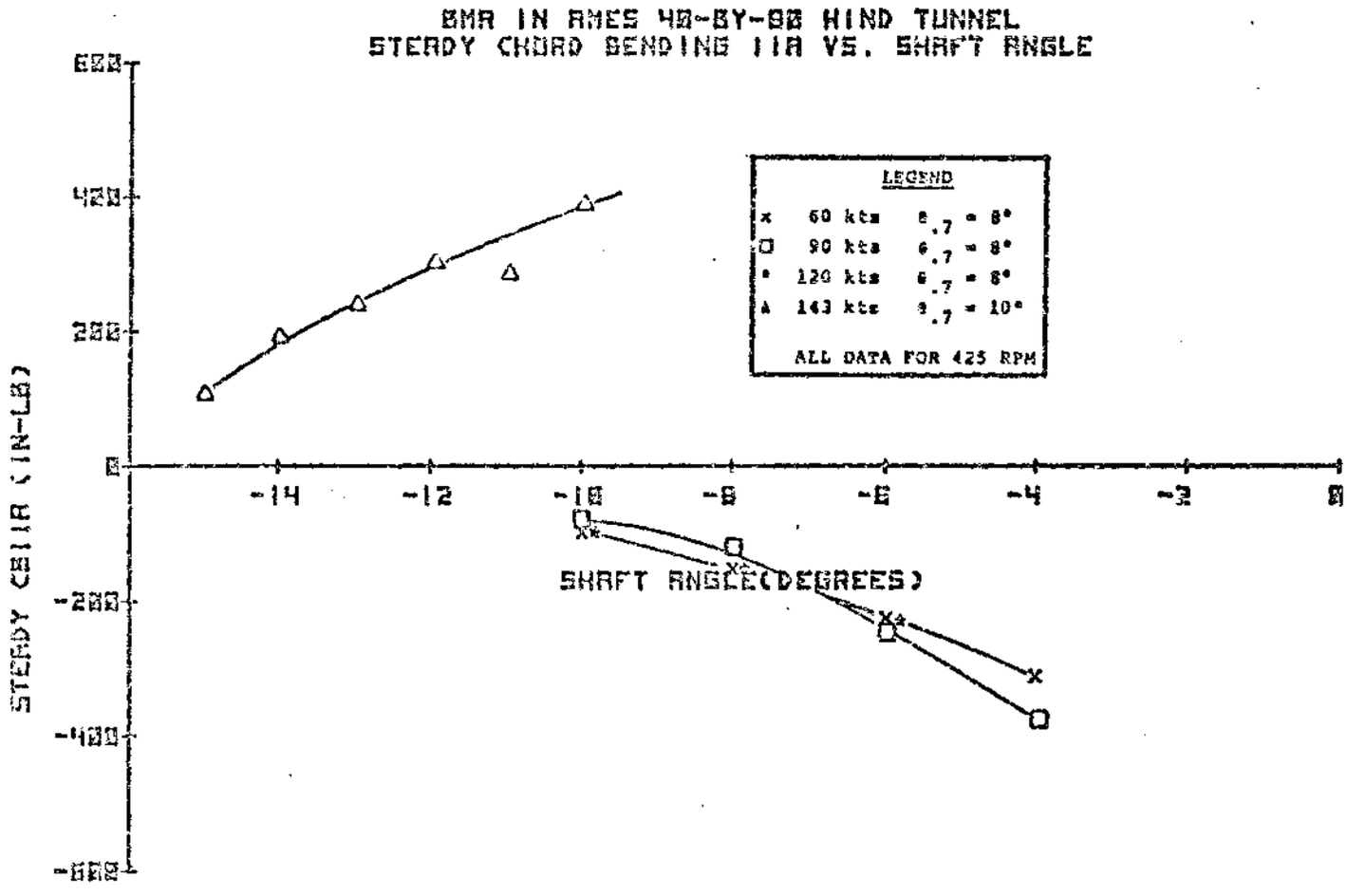

FIGURE 8.129 STEADY CHORD BENDING 11A VERSUS SHAFT ANGLE

8.2.2.4 Torque Tube and Pitch Link Load Trends

Torque tube chord bending as a function of airspeed is presented in Figures 8.130 and 8.131. Steady chord bending exhibits only a slight dependence on airspeed and follows the same trend as steady torsion in the torque tube. It appears that there is a chordwise displacement which is related to the torsional rotation of the clevis and the inherent flap-pitch-chord coupling. The variation with airspeed may be more related to torsional deflection along the blade span at the higher airspeeds.

Figures 8.132 through 8.135 present torque tube torsion and pitch link load as a function of airspeed. These figures show a distinct correlation between pitch link load and torque tube torsion. This reflects the forces required to produce the desired pitch changes around the azimuth by rotation of the attachment clevis.

Figures 8.136 and 8.137 present torque tube chord bending trends as a function of collective at constant rpm and shaft angle. There is a nearly linear increase in vibratory chord bending that reaches the endurance limit within the test range of collective. Peak chord bending moments (steady plus vibratory) are limiting on the low side of the desired collective range and prevented stability evaluation at zero collective.

Vibratory pitch link load and torque tube torsion show a strong dependence on collective at constant rpm and shaft angle for all forward airspeeds. A very pronounced dependence on collective is shown in the steady pitch link load and torque tube torsion, which varies directly with collective setting. Figures 8.138 through 8.141 display measured loads versus collective for torque tube torsion and axial pitch link load.

Figures 8.142 and 8.143 present torque tube chord bending versus shaft angle at constant rpm and collective. Shaft angle variations produce relatively little change in either vibratory or steady chord bending. The most pronounced effect is due to airspeed or collective changes. This reinforces the concept of a lag displacement related to clevis rotation and the corresponding wind-up between the flexbeam attachment points.

Torque tube torsion and pitch link load trends with shaft angle are presented in Figures 8.144 through 8.147. Vibratory loads show a linearly increasing trend with more positive shaft angles. Steady loads show a slight influence of shaft angle at 143 knots airspeed only.

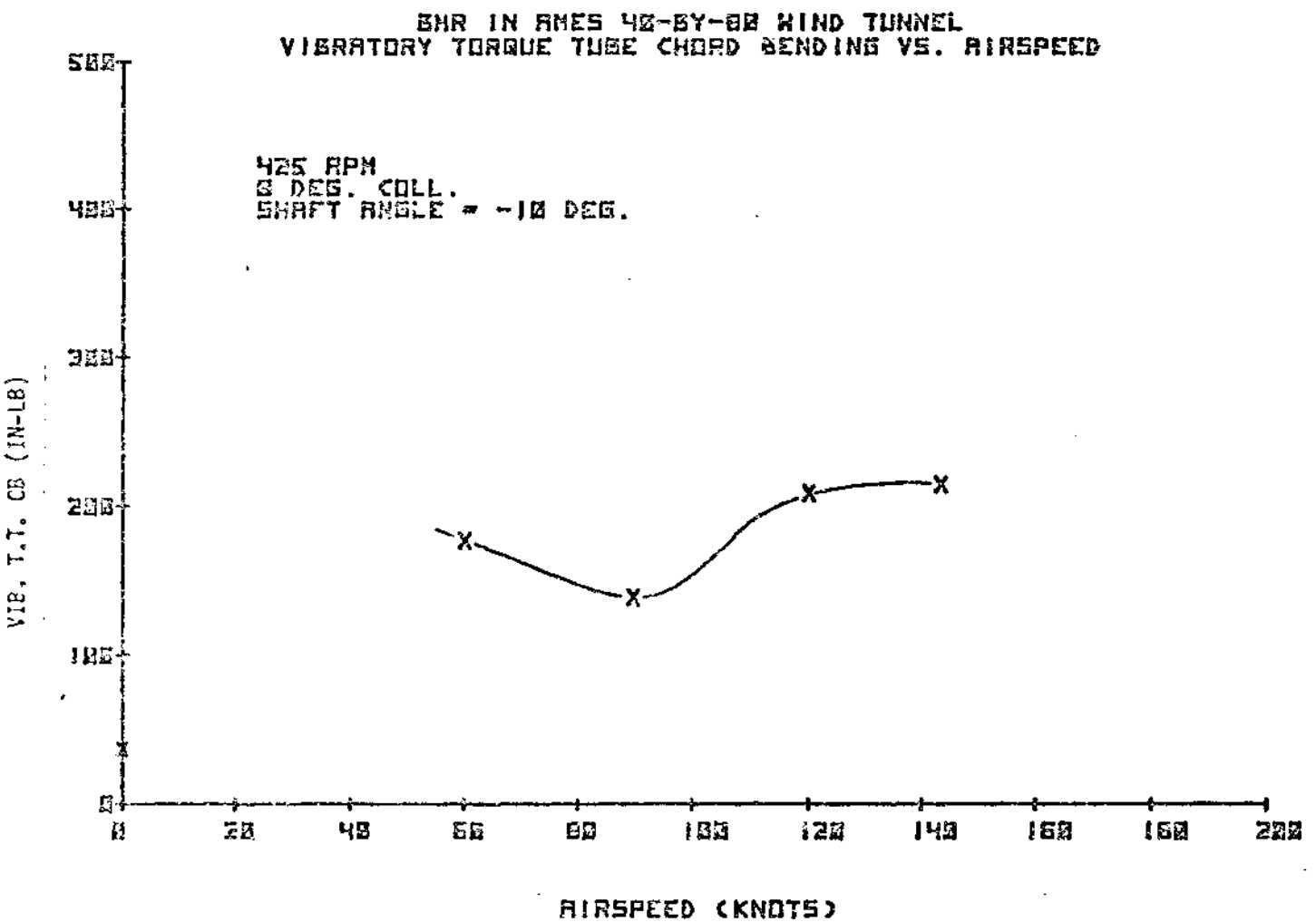

FIGURE 8.130 VIBRATORY TORQUE TUBE CHORD BENDING VERSUS AIRSPEED

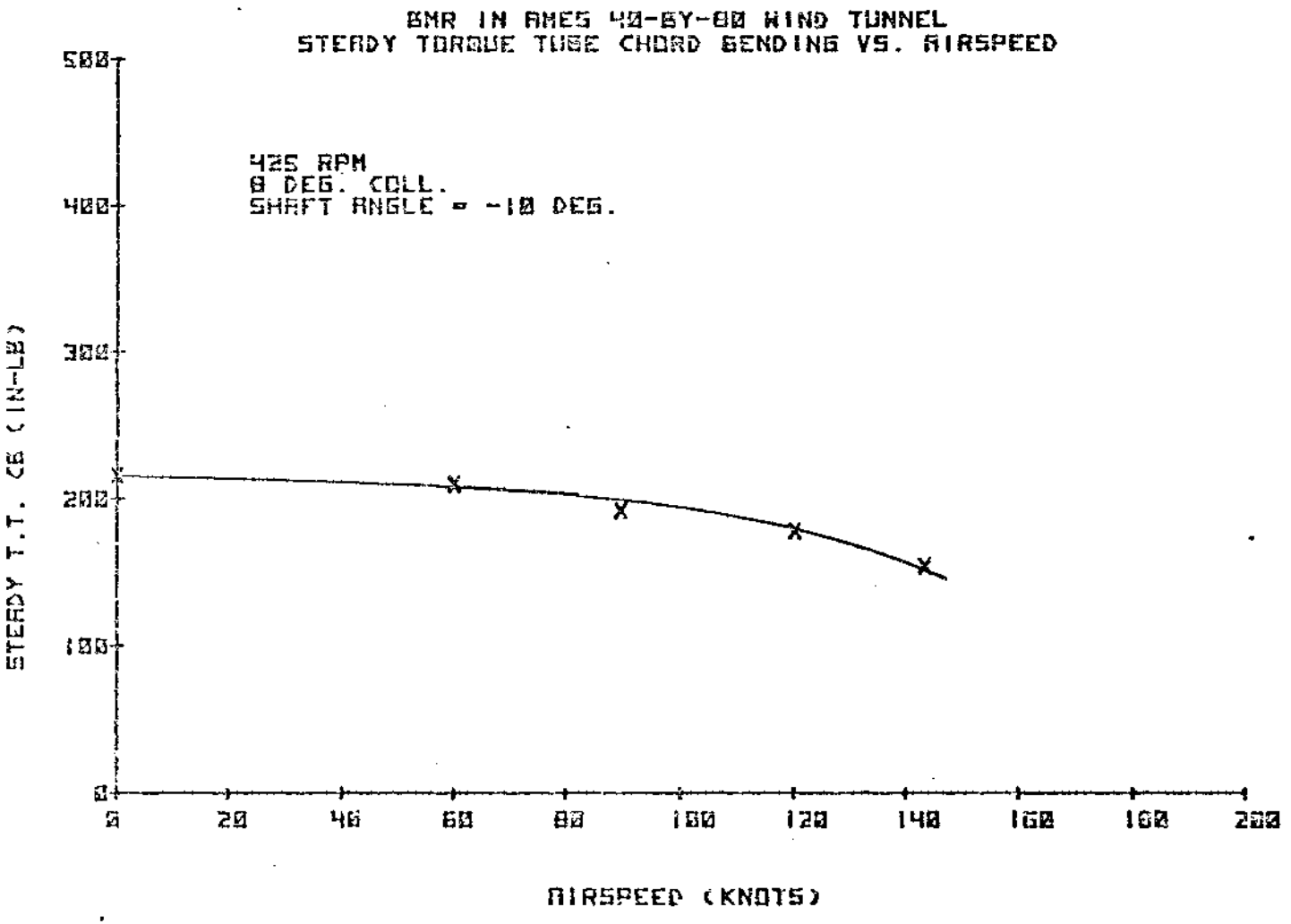

FIGURE 8.131 STEADY TORQUE TUBE CHORD BENDING VERSUS AIRSPEED

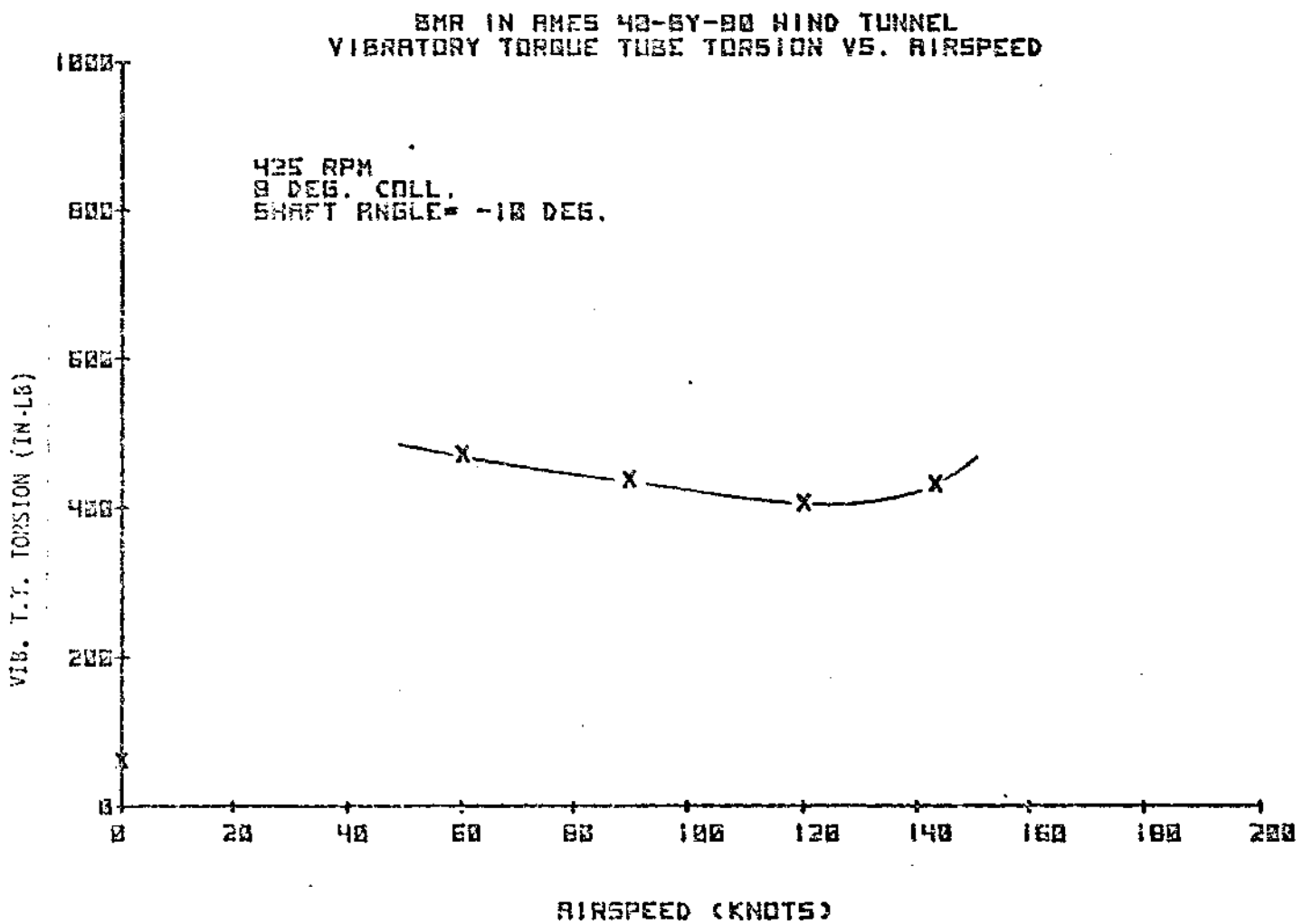

FIGURE 8.132 VIBRATORY TORQUE TUBE TORSION VERSUS AIRSPEED

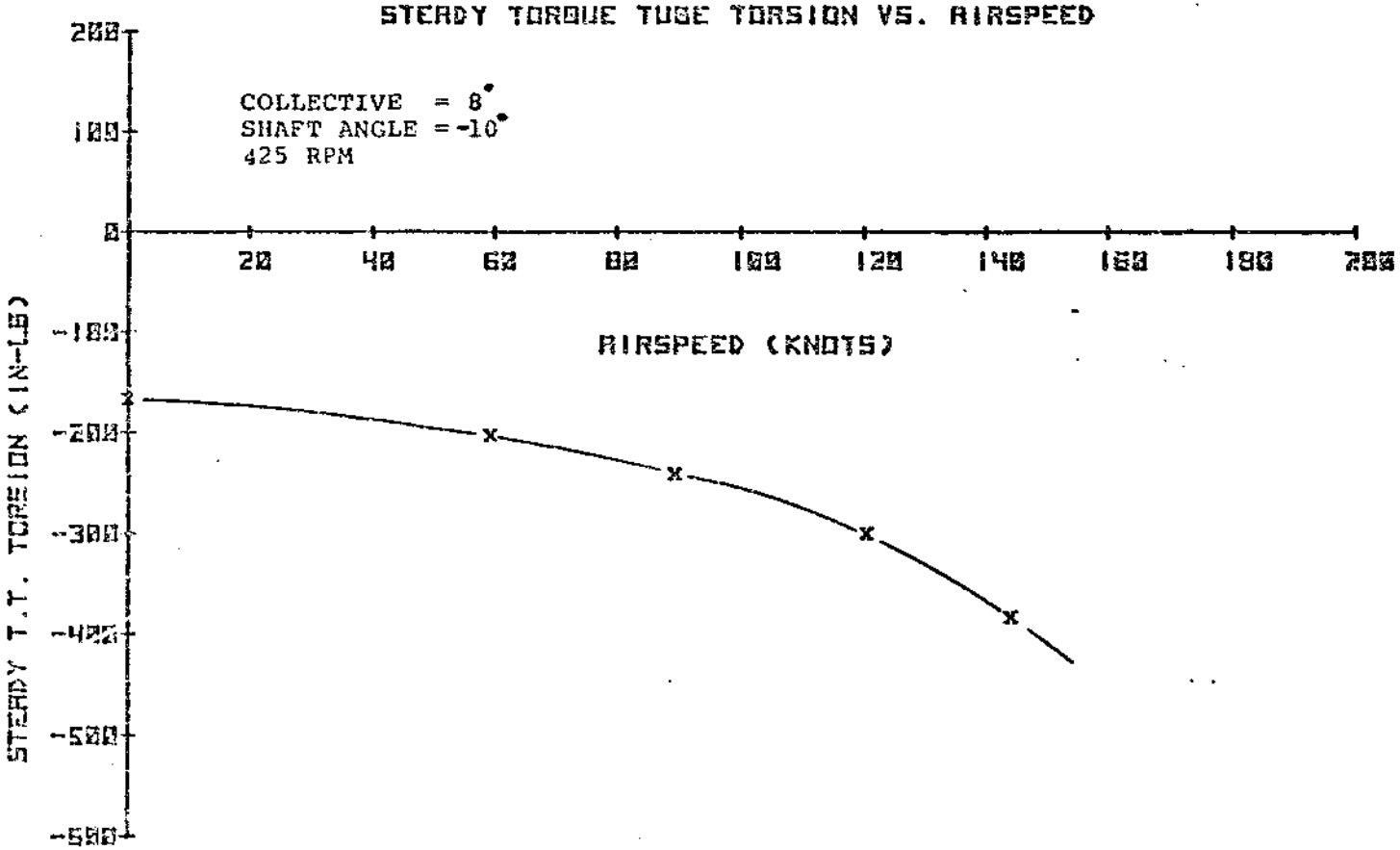

FIGURE 8.133 STEADY TORQUE TUBE TORSION VERSUS AIRSPEED

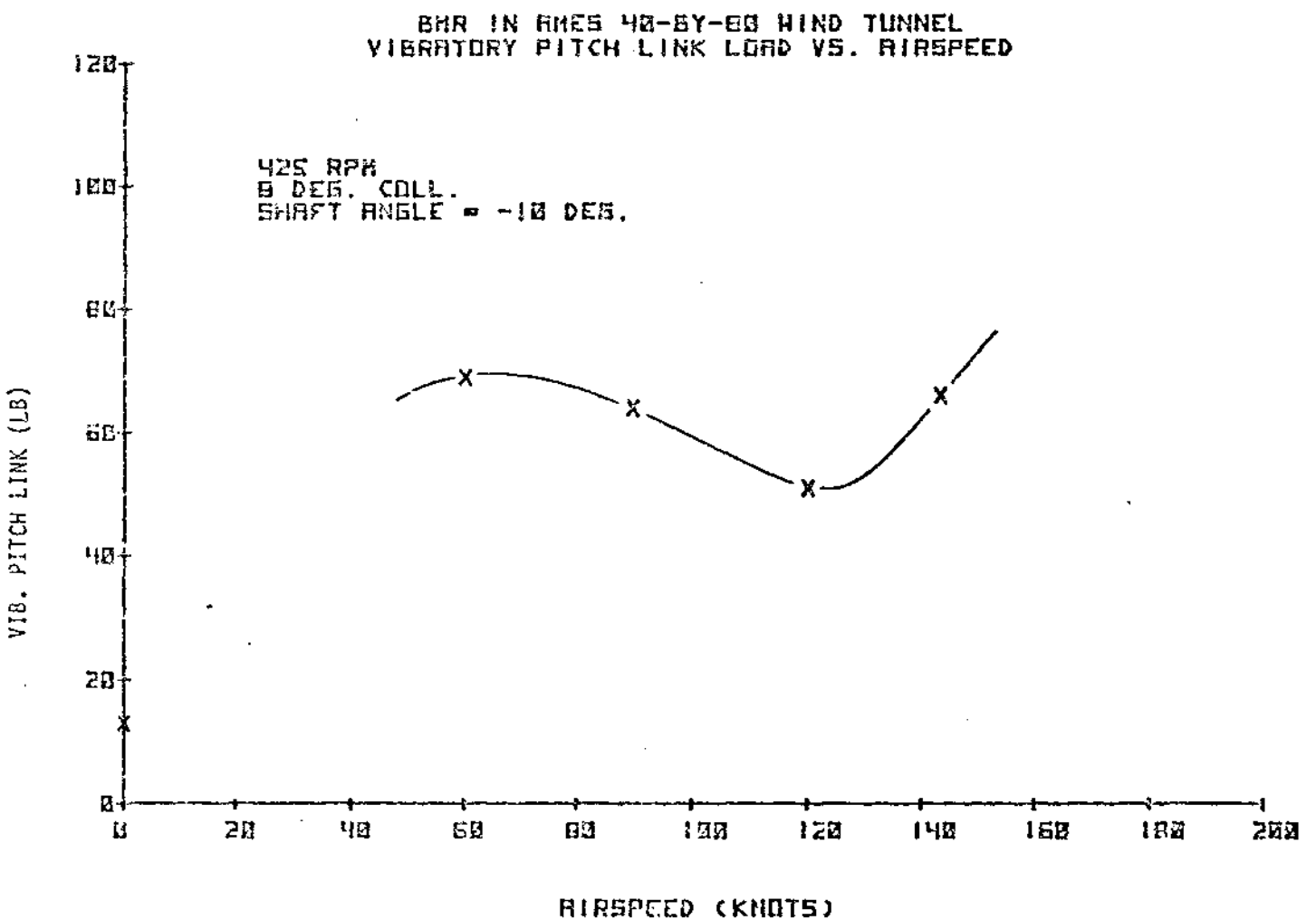

FIGURE 8.134 VIBRATORY PITCH LINK LOAD VERSUS AIRSPEED

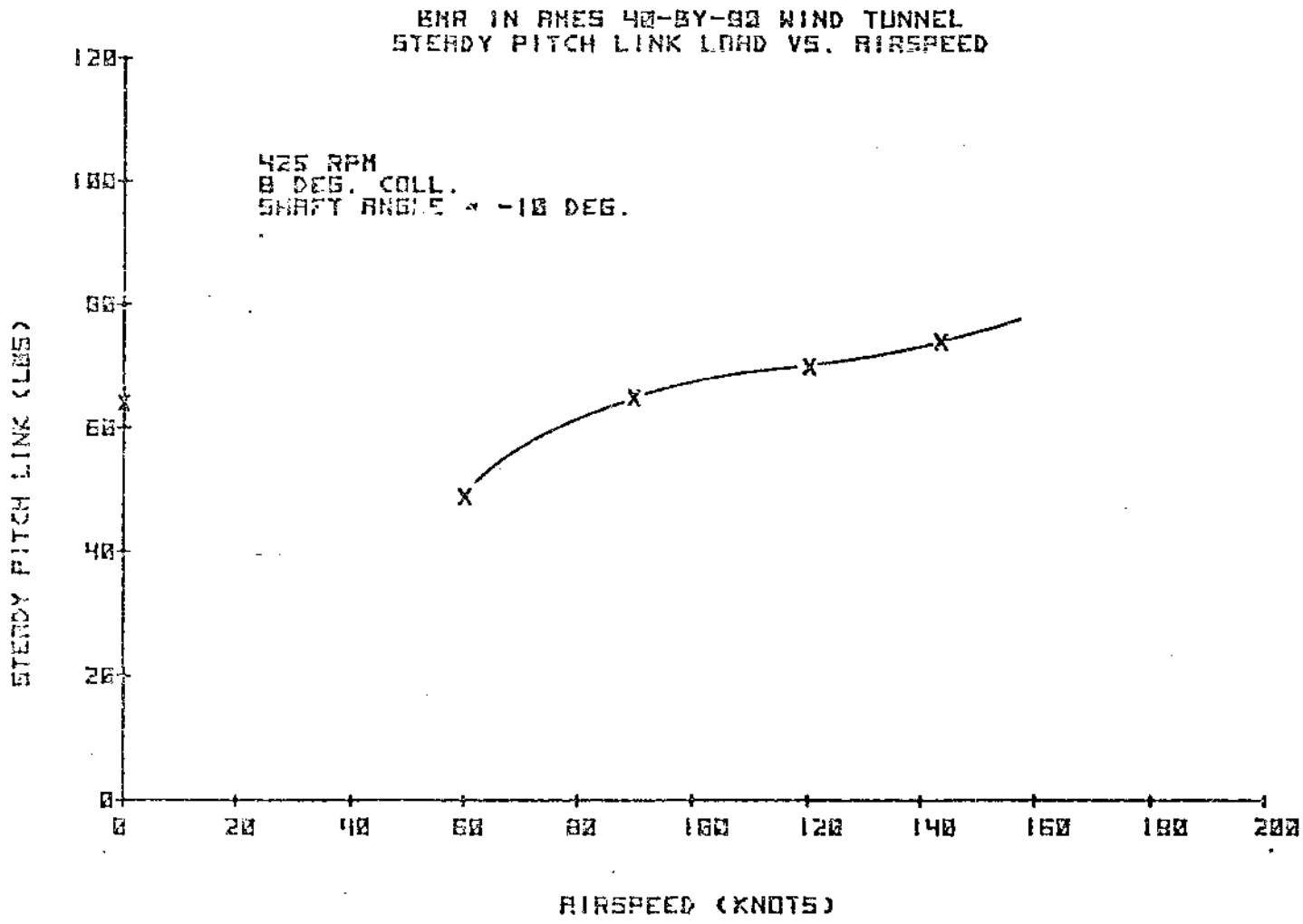

FIGURE 8.135 STEADY PITCH LINK LOAD VERSUS AIRSPEED

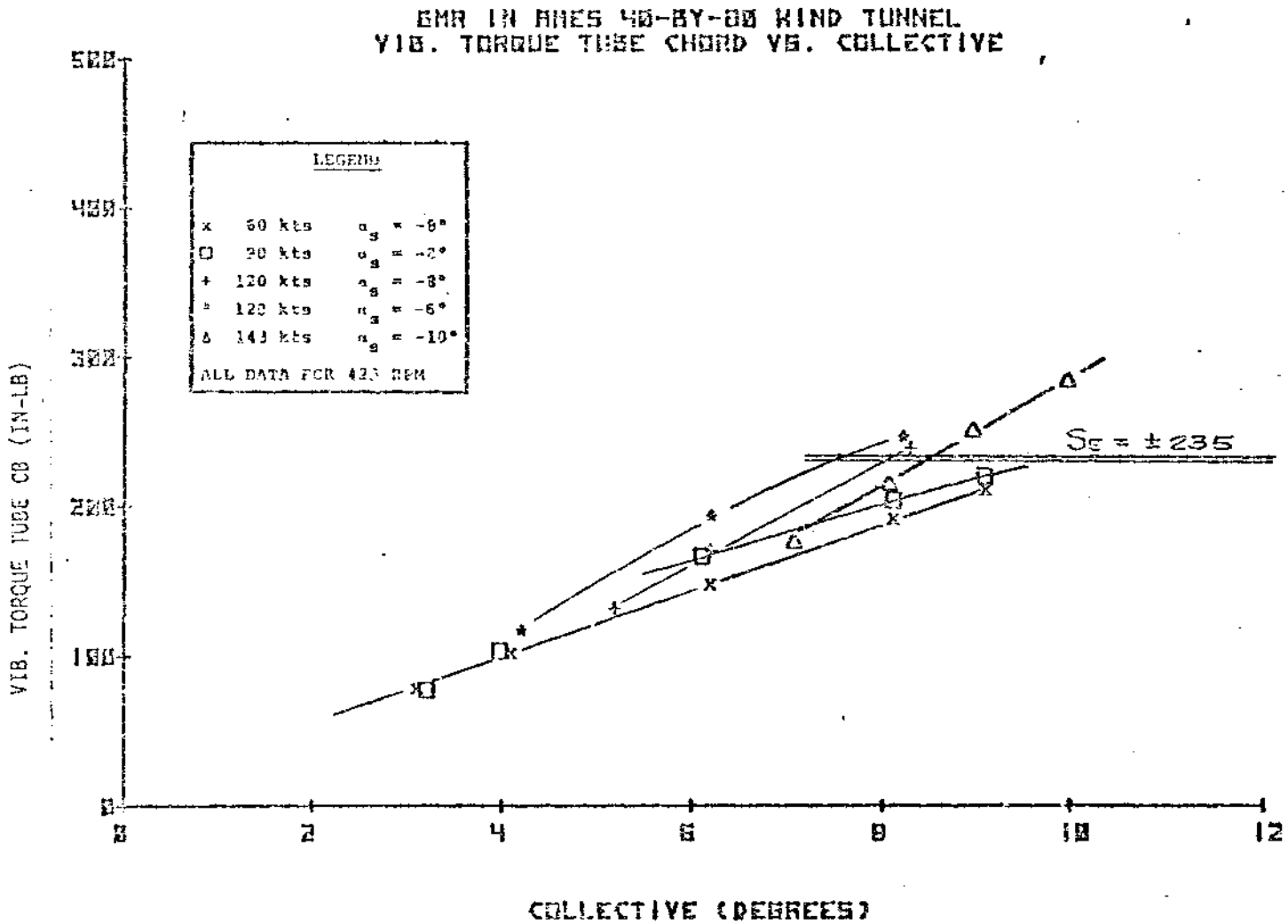

FIGURE 8.136 VIBRATORY TORQUE TUBE CHORD BENDING VERSUS COLLECTIVE

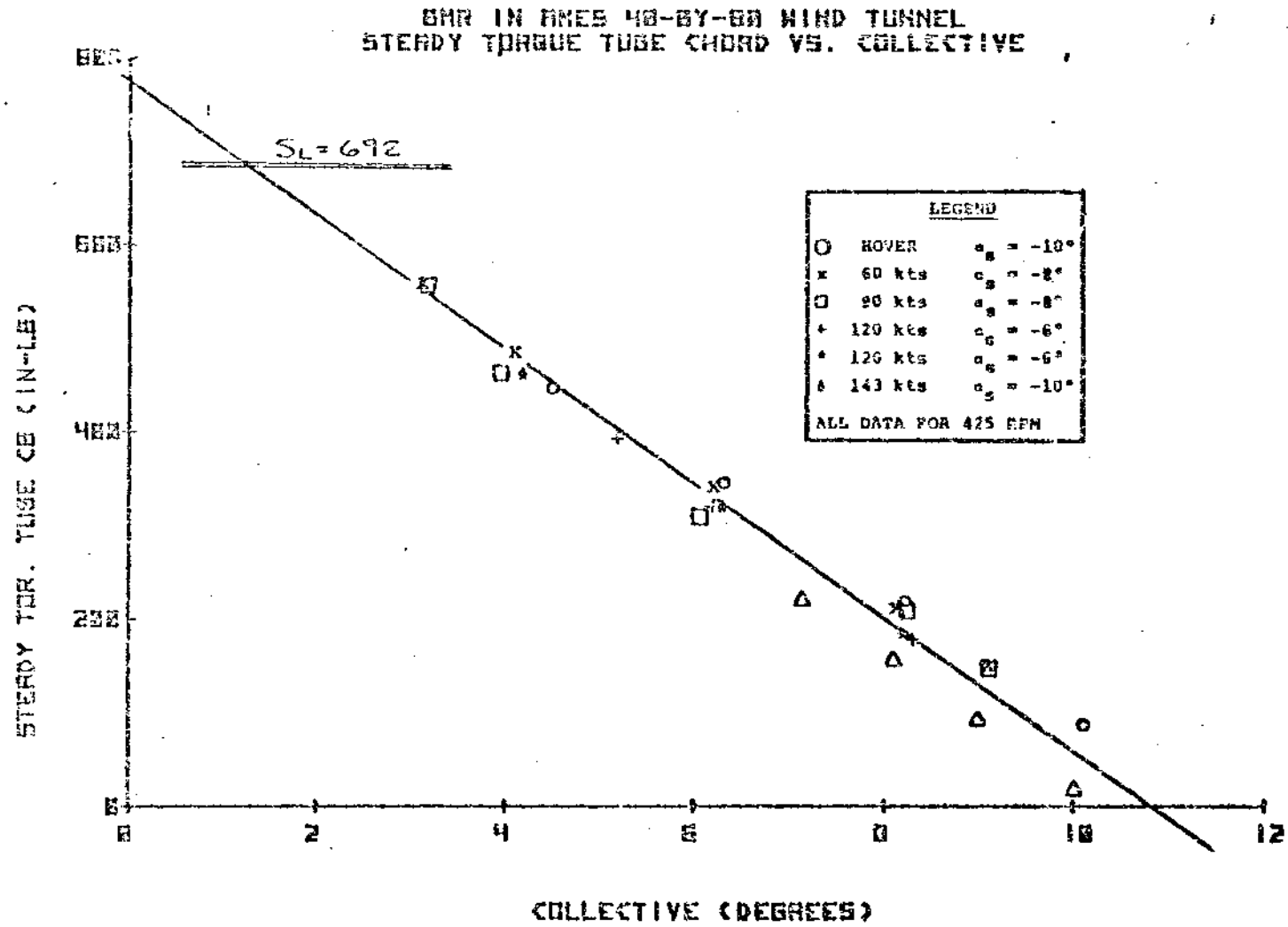

FIGURE 8.137 STEADY TORQUE TUBE CHORD BENDING VERSUS COLLECTIVE

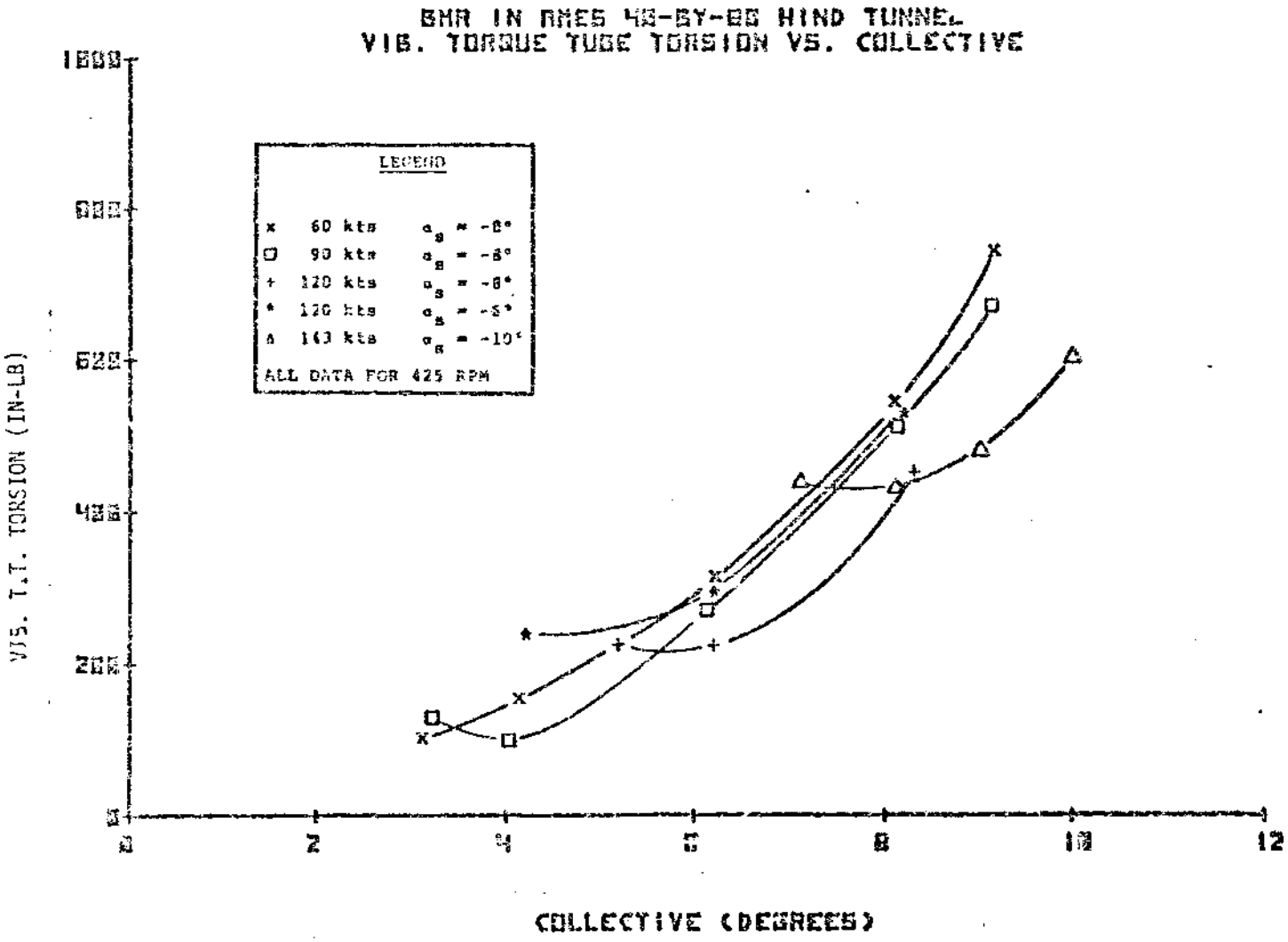

FIGURE 8.138 VIBRATORY TORQUE TUBE TORSION VERSUS COLLECTIVE

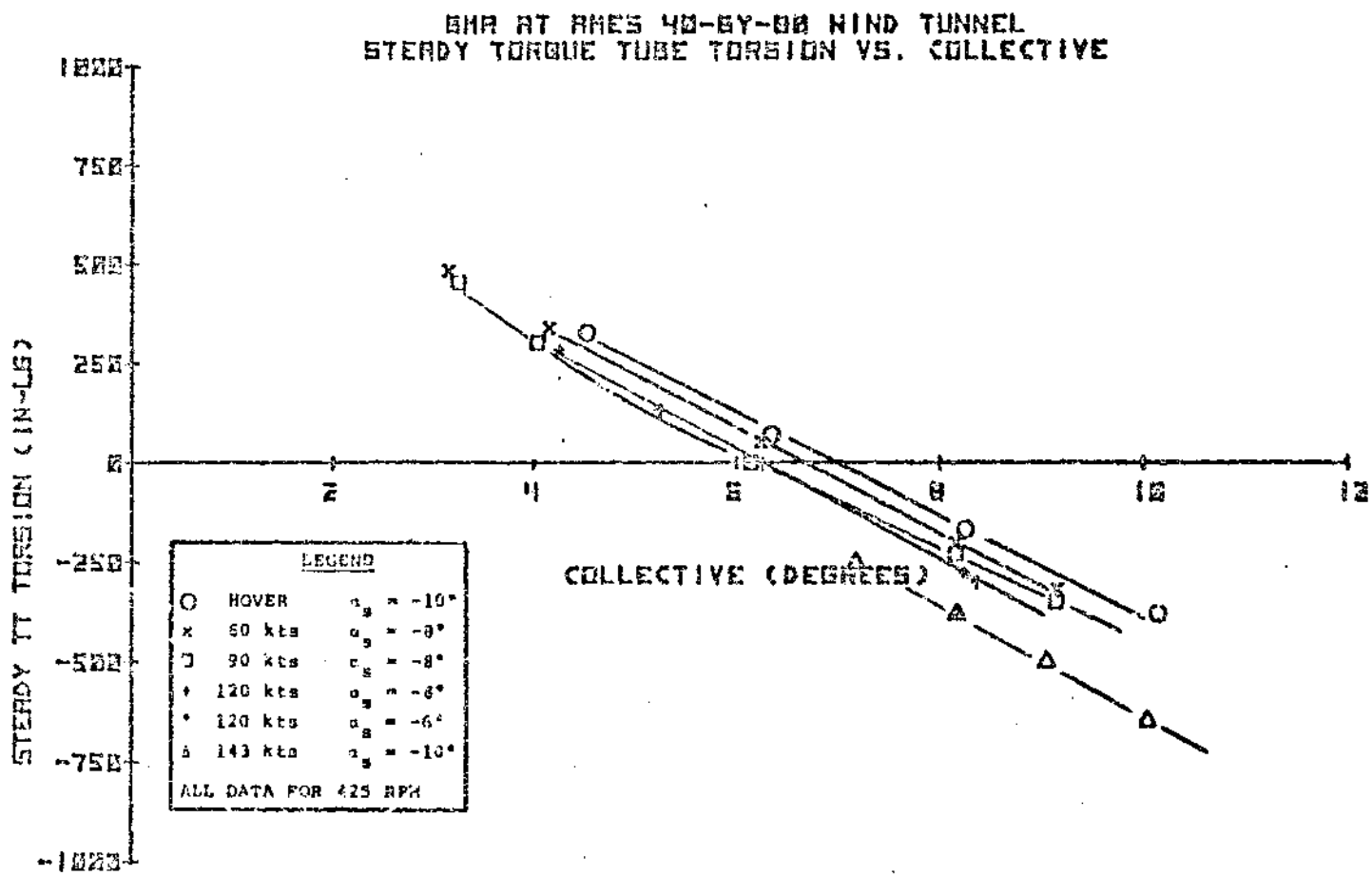

FIGURE 8.139 STEADY TORQUE TUBE TORSION VERSUS COLLECTIVE

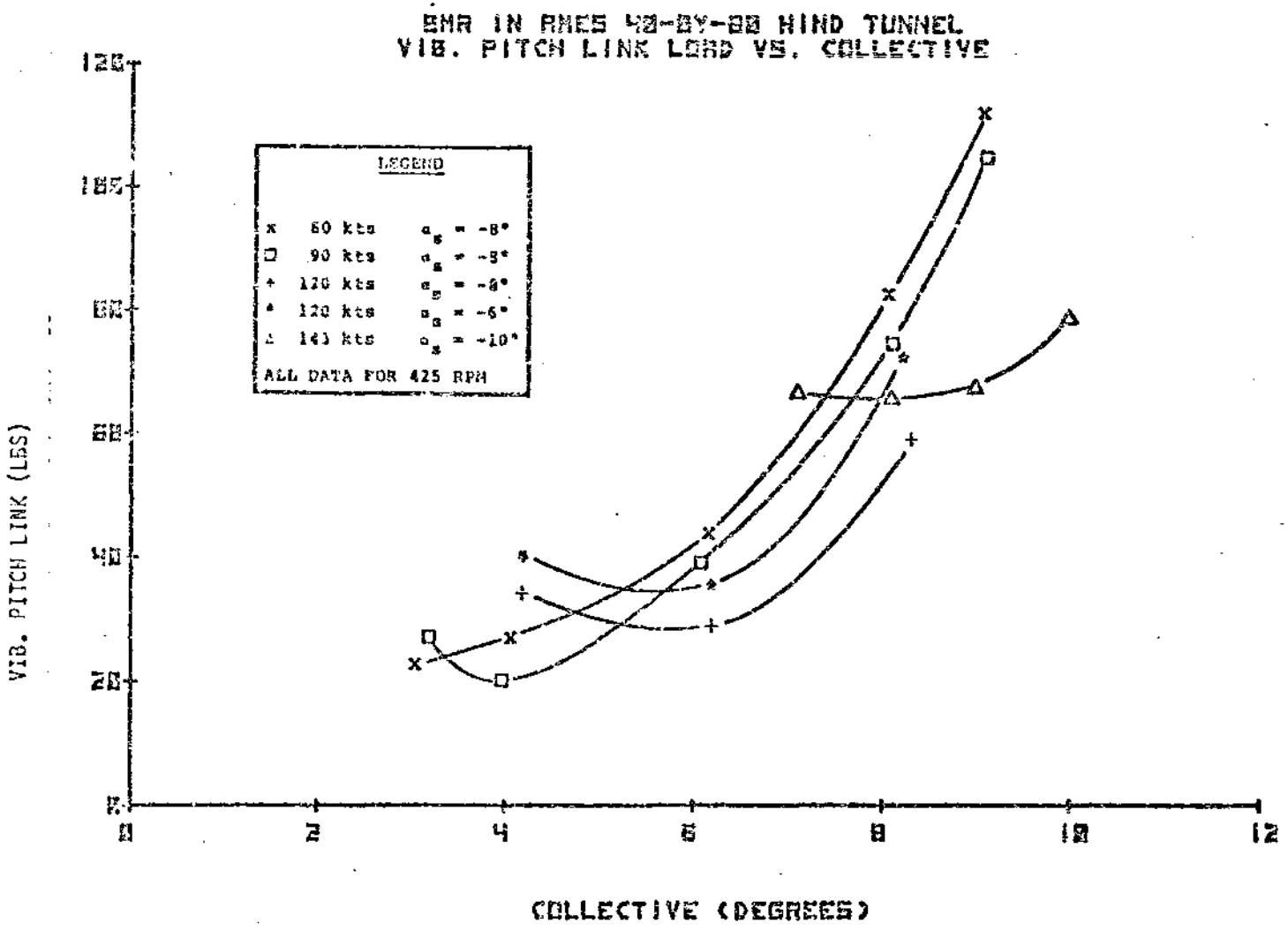

FIGURE 3.140 VIBRATORY PITCH LINK LOAD VERSUS COLLECTIVE

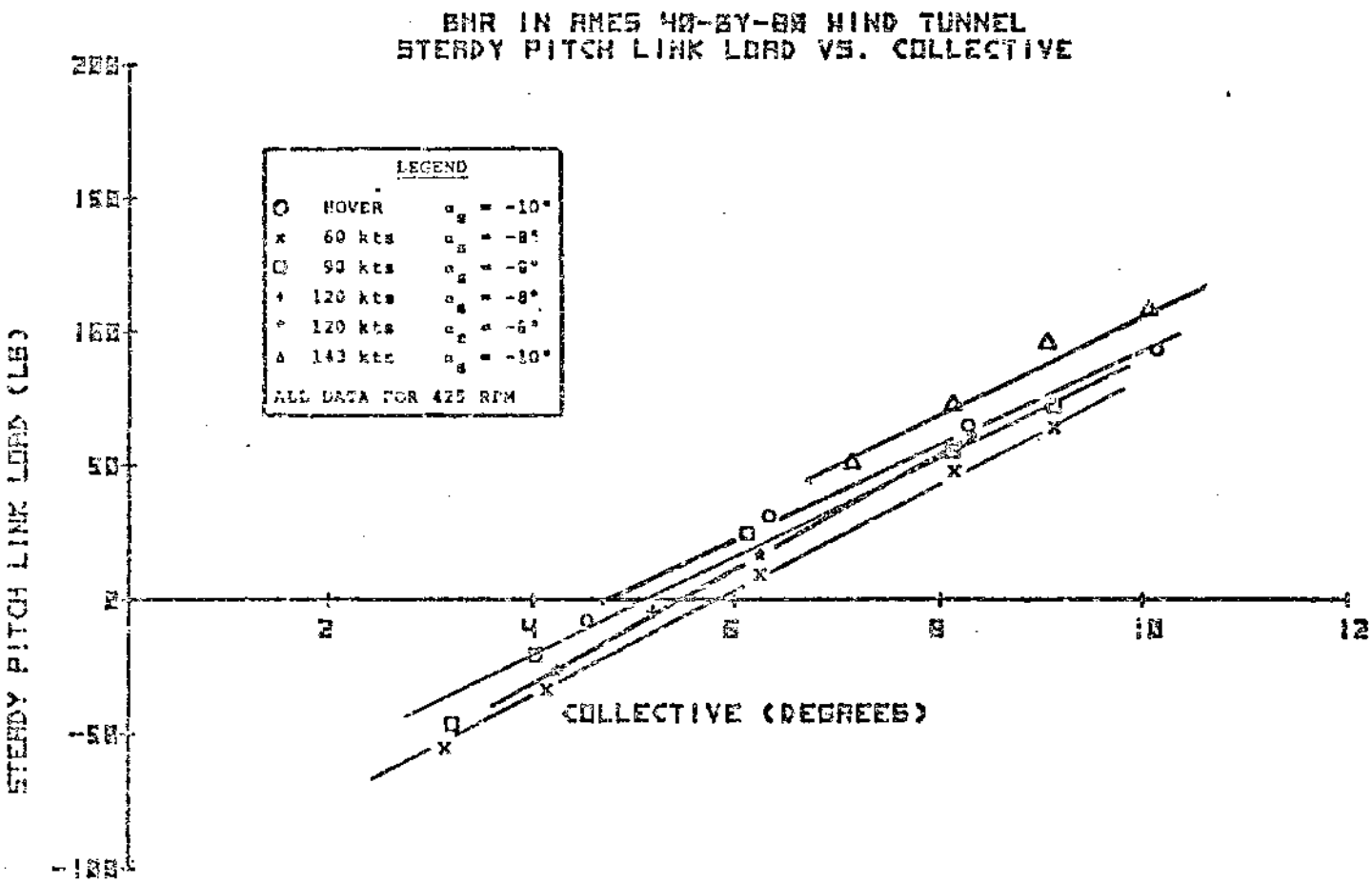

FIGURE 8.141 STEADY PITCH LINK LOAD VERSUS COLLECTIVE

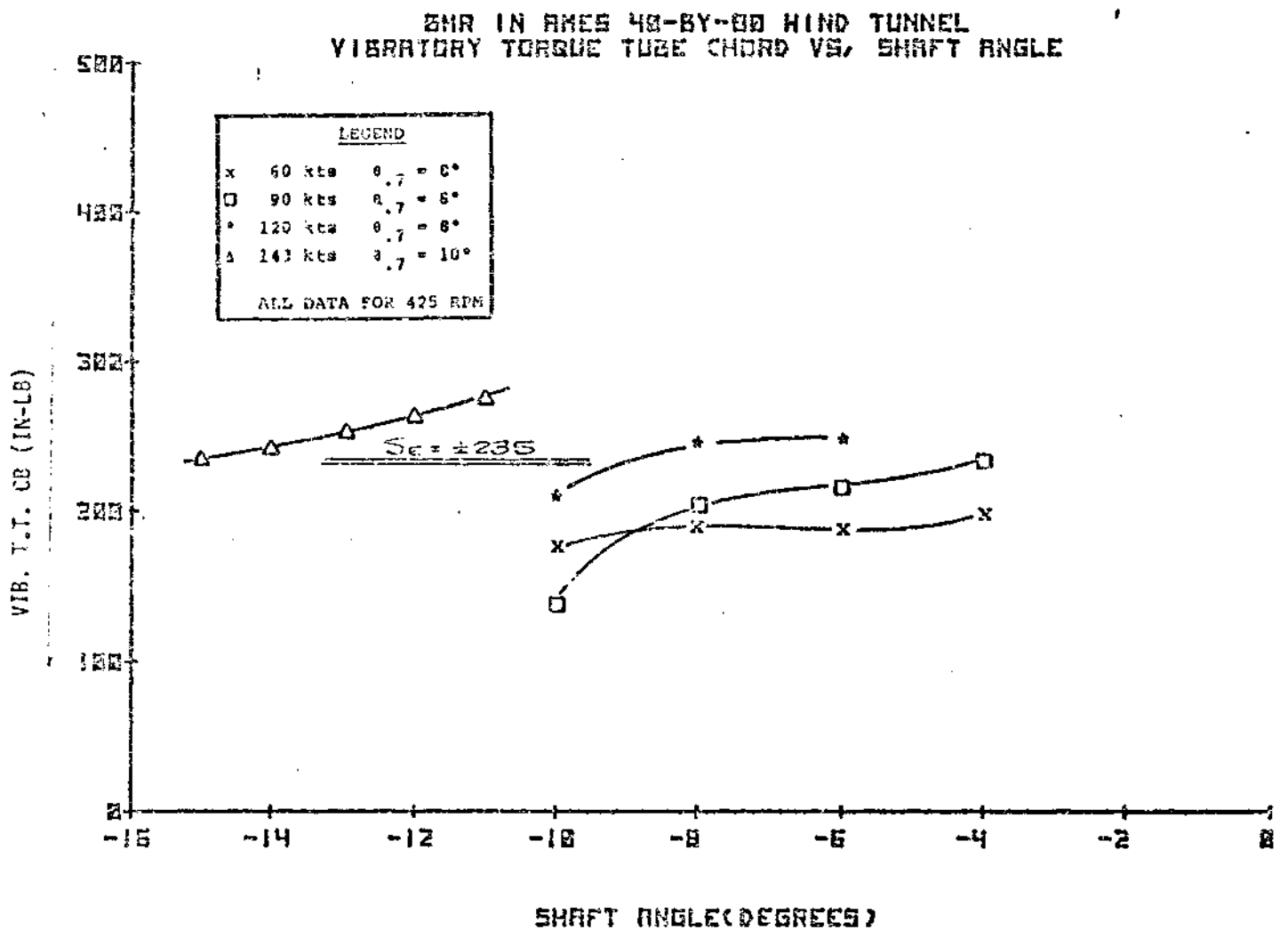

FIGURE 8.142 VIBRATORY TORQUE TUBE CHORD BENDING VERSUS SHAFT ANGLE

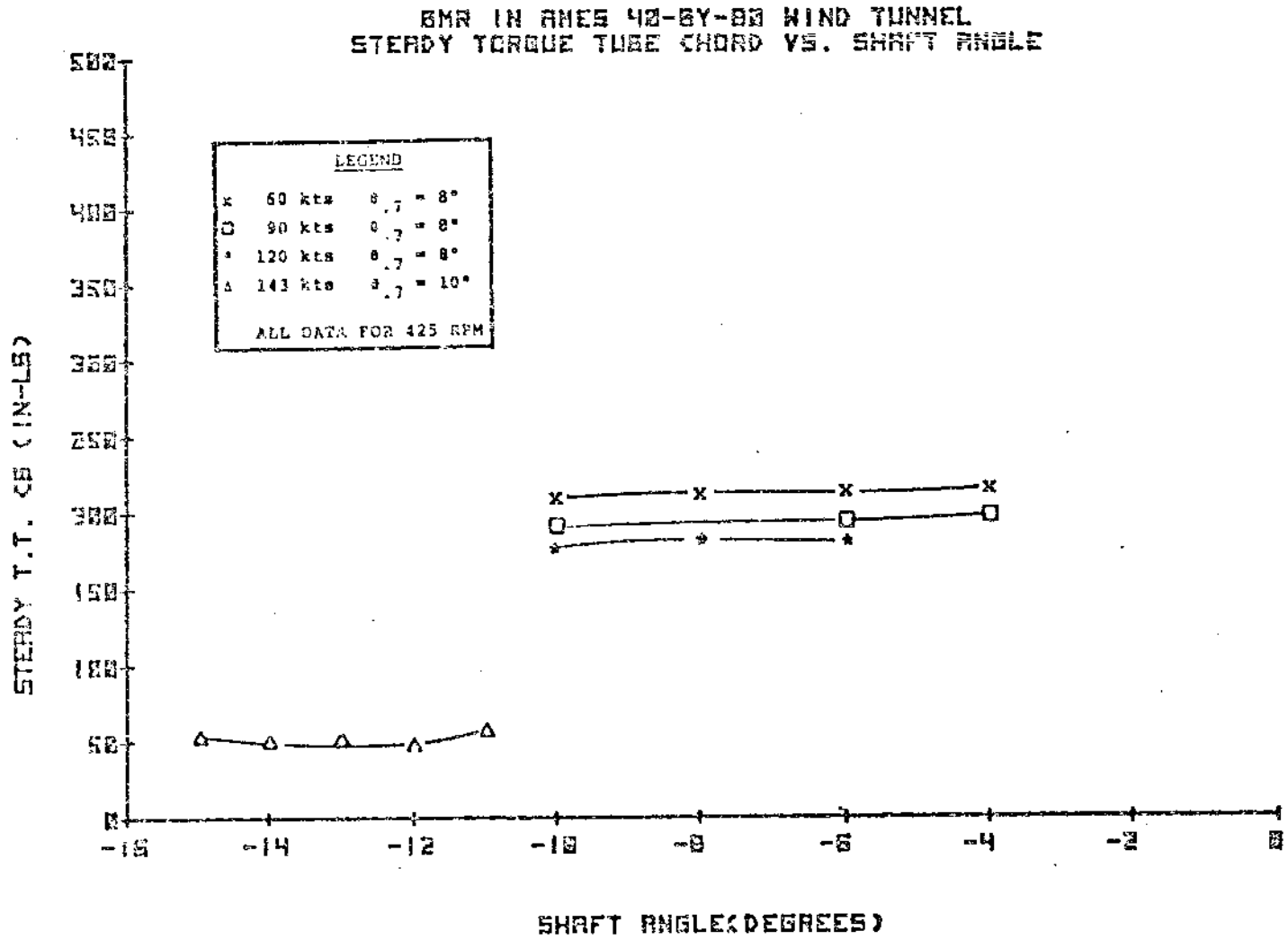

FIGURE 8.143 STEADY TORQUE TUBE CHORD BENDING VERSUS SHAFT ANGLE

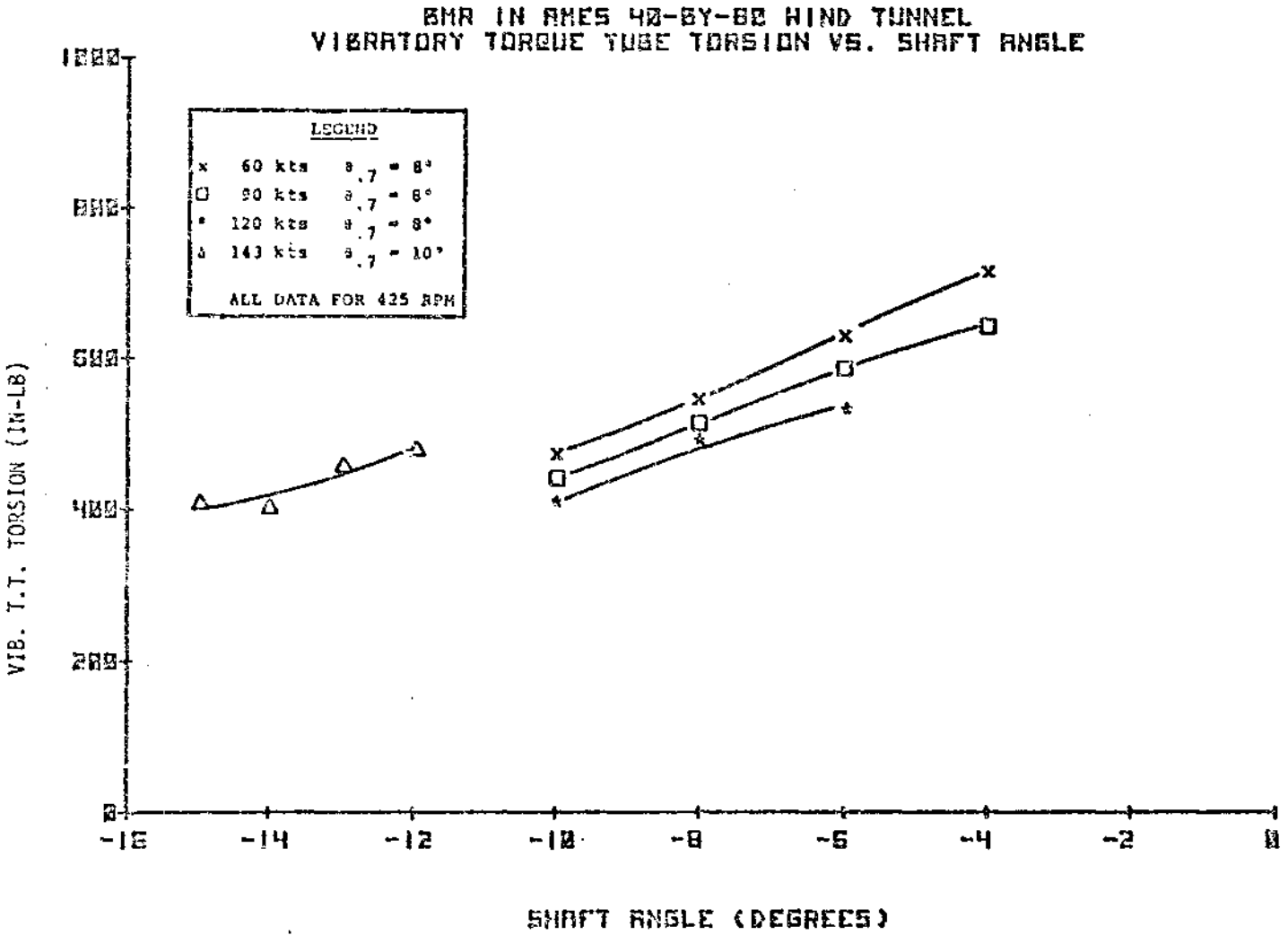

FIGURE 8.144 VIBRATORY TORQUE TUBE TORSION VERSUS SHAFT ANGLE

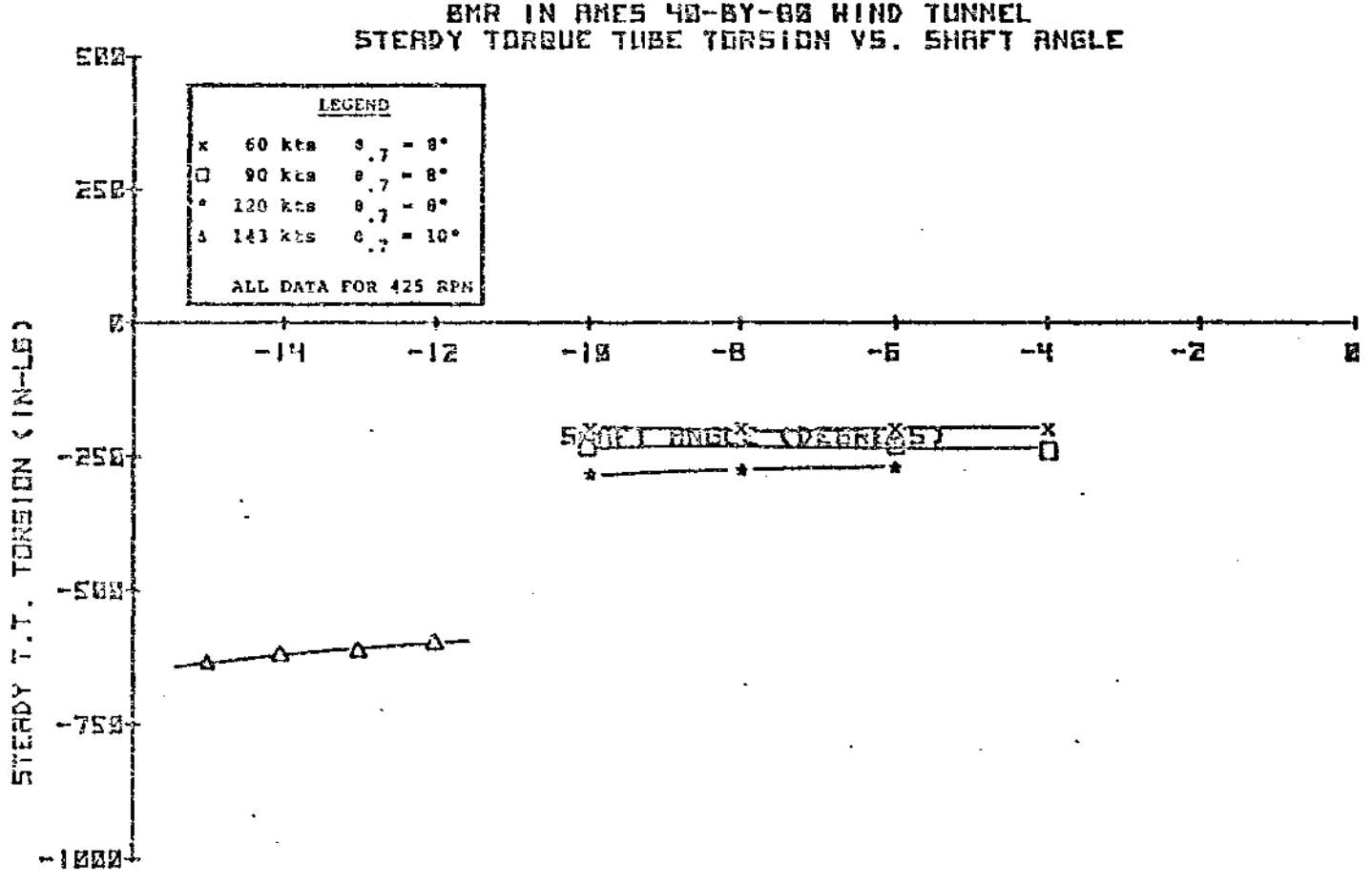

FIGURE 9.145 STEADY TORQUE TUBE TORSION VERSUS SHAFT ANGLE

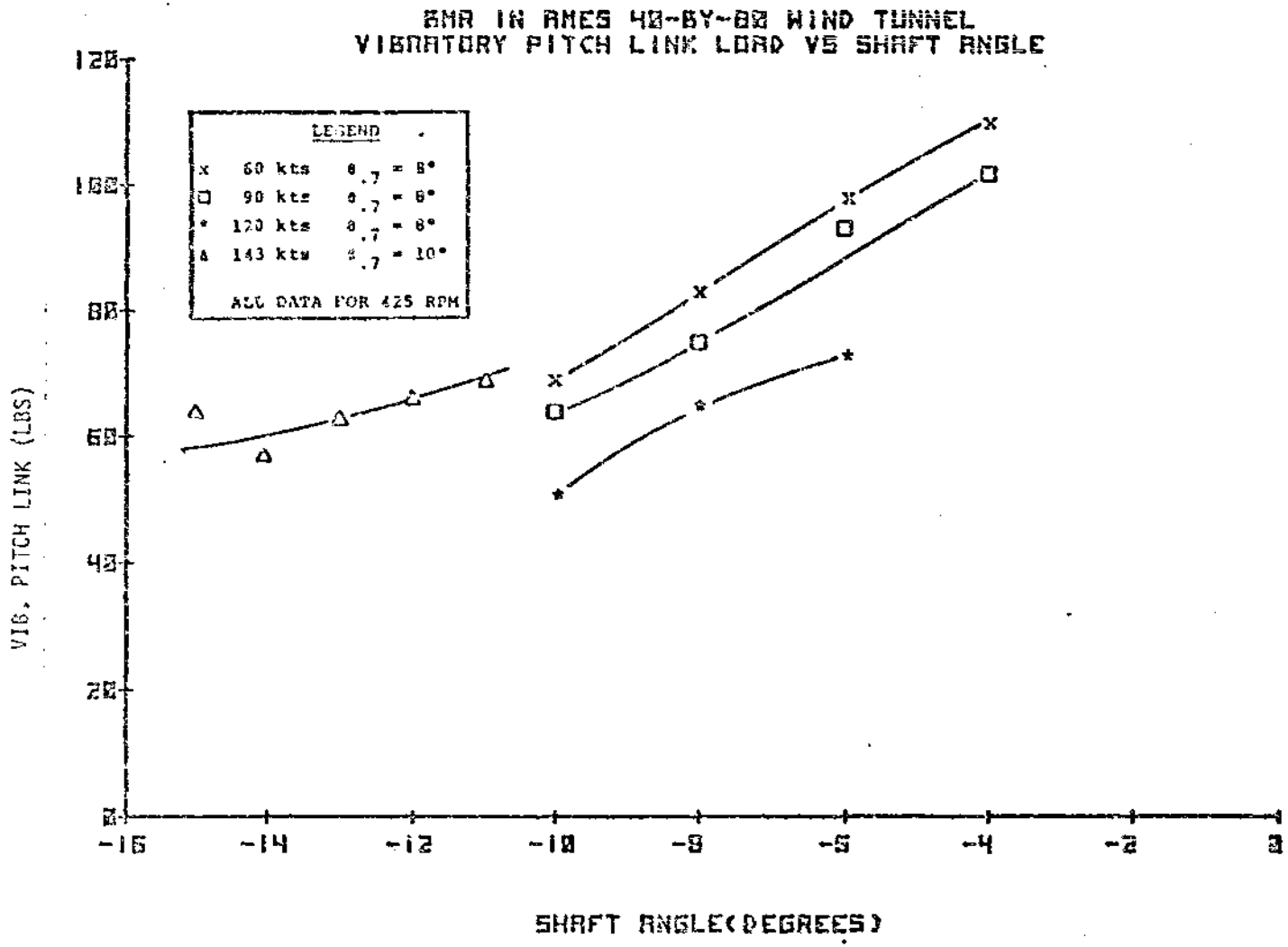

FIGURE 8.146 VIBRATORY PITCH LINK LOAD VERSUS SHAFT ANGLE

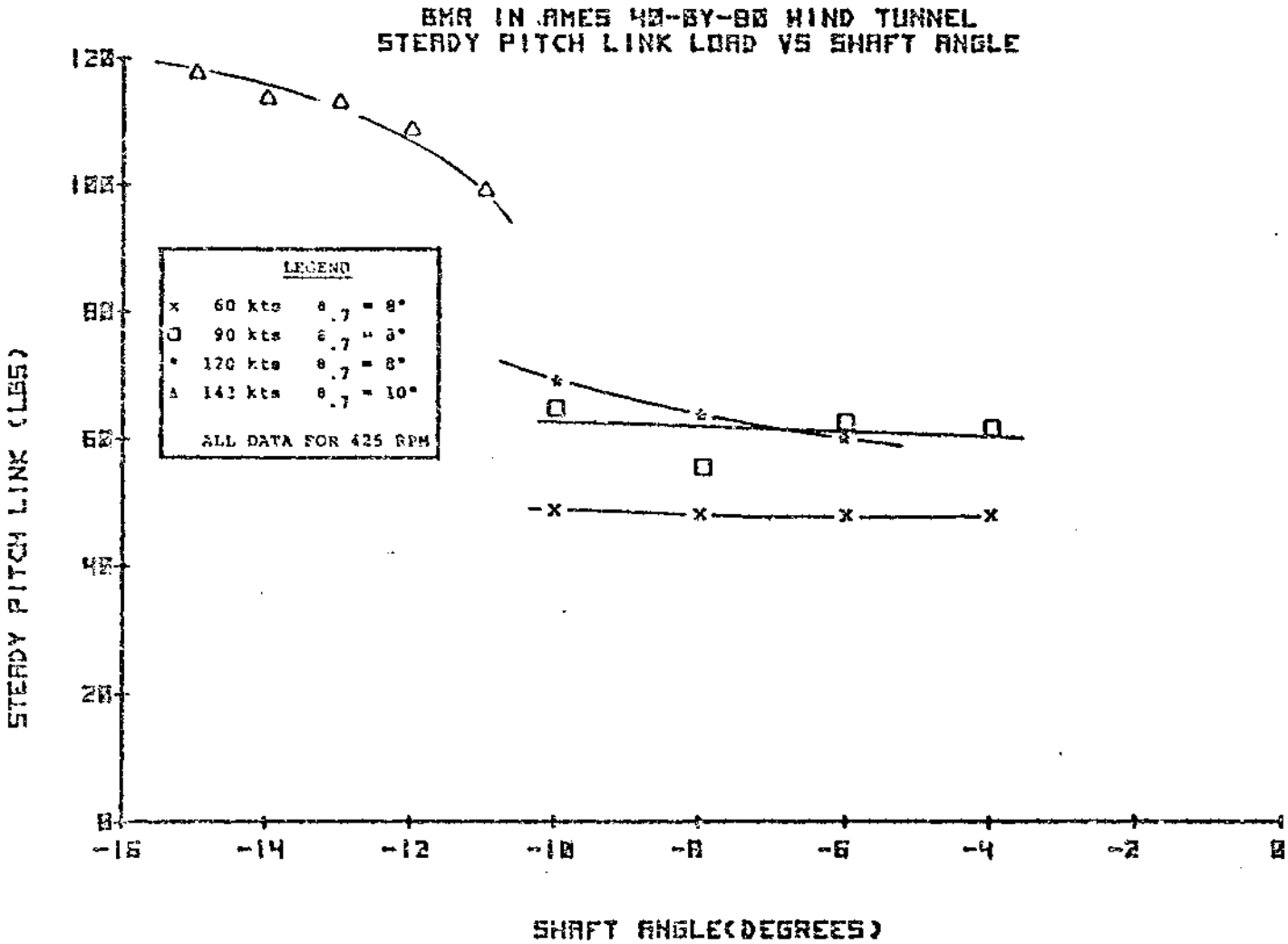

FIGURE 8.147 STEADY PITCH LINK LOAD VERSUS SHAFT ANGLE

8.2.2.5 Configuration Changes

The configuration changes were evaluated in hover and forward speed. These configuration changes were made to investigate their effect on aeroelastic stability. The first configuration tested incorporated a set of "soft" pitch links with a reduced axial spring rate (5755 lb/in vs 26,666 lb/in for the baseline configuration). The overall effect of the change was an 11% reduction in control system stiffness. The addition of elastomeric damper strips to the upper and lower flanges of both the leading and trailing beams was the second configuration change to be tested. In addition to the configuration changes, the effect of removing the AMES tunnel balance dampers was investigated.

Similar results were obtained for the "soft pitch links" and "damper strips installed" configurations. Both the blade pitch at the beam-to-blade attachment and the division of the vibratory blade torque between the control system and flexbeams are dependent upon the relative stiffness between the torque tube/ control load path and the flexbeam flapwise bending which restrains torsional rotation of the clevis relative to the rotor hub. This effect can be seen in the data presented for these two configurations and compared to the baseline in Figures 8.148 through 8.171. Total vibratory flap bending at station 44 was obtained by adding the 10 harmonics (including effect of phase angle) for beams A and B and reconstituting the resultant harmonics for total flap bending.

In considering the effect of the relation between the control loads path and flexbeam stiffness on pitch angle at the blade attachment clevis, it is instructive to consider two extremes. If the flexbeams were completely rigid, then the control actuator motion would produce wind-up in the torque tube with no rotation of the clevis. On the other hand, very flexible flexbeams would result in almost no wind-up in the torque tube as the control actuator motion would go directly into clevis rotation. It can be concluded from these two extremes that any modification which increases the stiffness of the flexbeams (in the vertical bending mode which restrains clevis rotation) relative to the torque tube/pitch link will have the effect of reducing the blade clevis rotation for the same control input.

A comparison of rotor lift, as reported in the static file is presented in the following tabulation for a nominal collective setting of 4 degrees:

ROTOR LIFT (Lbs)

Rotor Speed (RPM)	Baseline Configuration	Soft Pitch Links	Damper Strips Installed	Baseline 3.2° Coll.
335	1162	802	887	
400	1727	1387	1377	
425	2392	1652	1587	1773

In Figures 8.148 through 8.171, shifts in steady load levels are consistent with a lower blade pitch angle for the configuration variations. This is most evident at 425 rpm. The one exception to this trend is chord bending at station 11 with damper strips installed. For this case, the increased chord bending stiffness results in a shift in the steady moments in the opposite direction of reduced collectives.

A baseline data point (run 15, test point 4, 90 knots, -8° shaft angle) with 3.2 degrees collective was superimposed on Figures 8.148 - 8.171. This point was chosen because the resultant lift is similar to the lift values for the configuration changes at 425 rpm. This point shows the effect of a collective change only on the baseline configuration. It can be seen that the shifts in steady moments due to the configuration changes are

compatible with the shift due to a reduction in blade pitch. In view of the reduction in lift for the configuration changes compared to the baseline and the shift in steady moments, it can be concluded that the blade pitch angles were lower for the configuration changes for the same control input.

Shifts in vibratory load levels are consistent with changes in blade pitch except for flap bending at station 10.5. At this station there is a significant reduction in 1/rev flap bending while Figures 8.106 and 8.107 do not show this sensitivity to collective.

The waveforms for station 10.5 at 425, 400 and 335 rpm are plotted in Figures 8.186 - 8.188.

Steady torque tube torsion is increased consistent with a smaller rotation at the outboard attachment for the same displacement at the pitch arm. (An increase in the wind-up along the torque tube for both soft pitch links and damper strips installed). A compressive pitch link load increment is required to achieve a more nose-up torque tube torsion (increased wind-up). Figure 8.169 shows this shift.

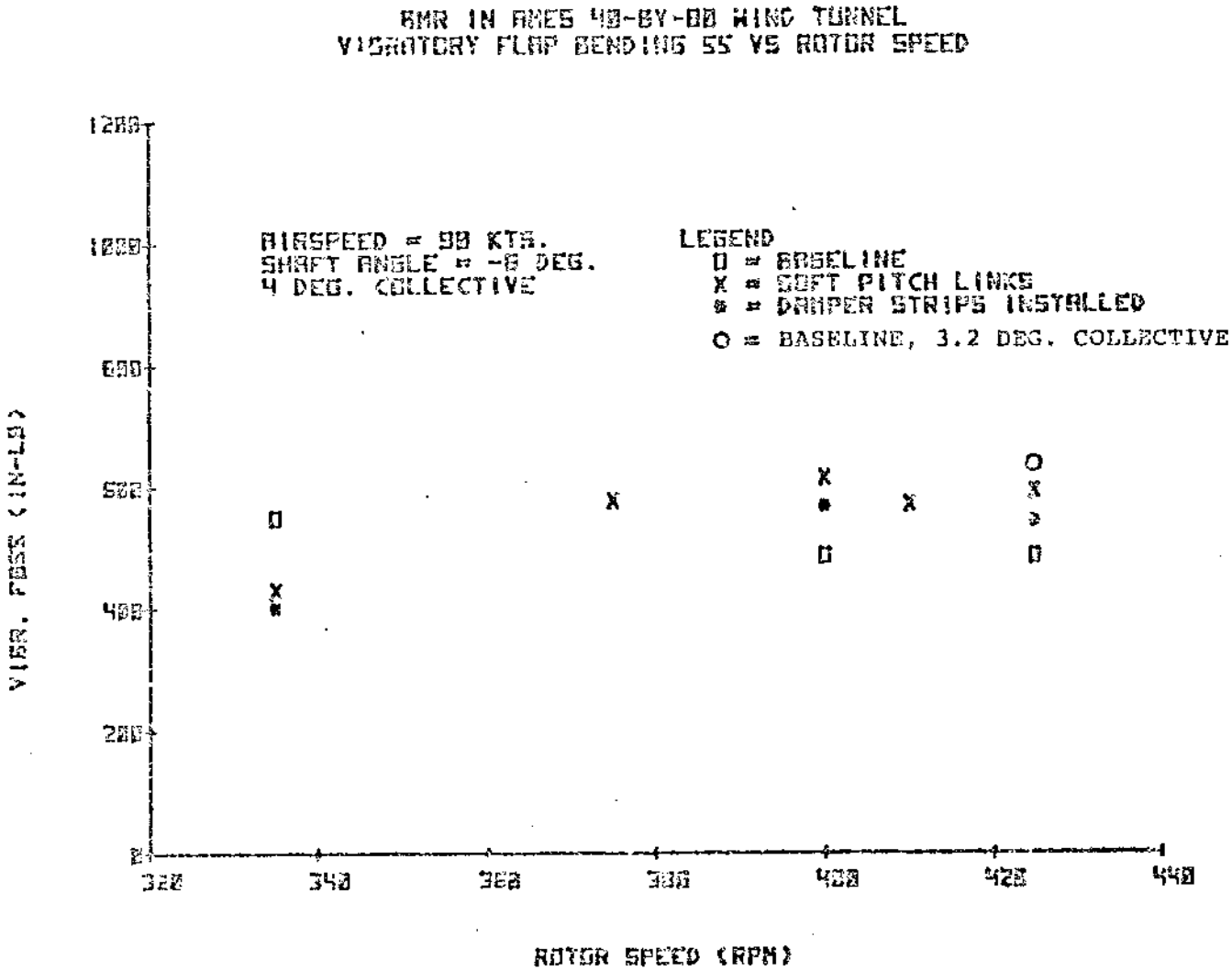

FIGURE 6.148 EFFECT OF SOFT PITCH LINKS AND DAMPER STRIPS VIBRATORY FLAP BENDING 5S VS ROTOR SPEED

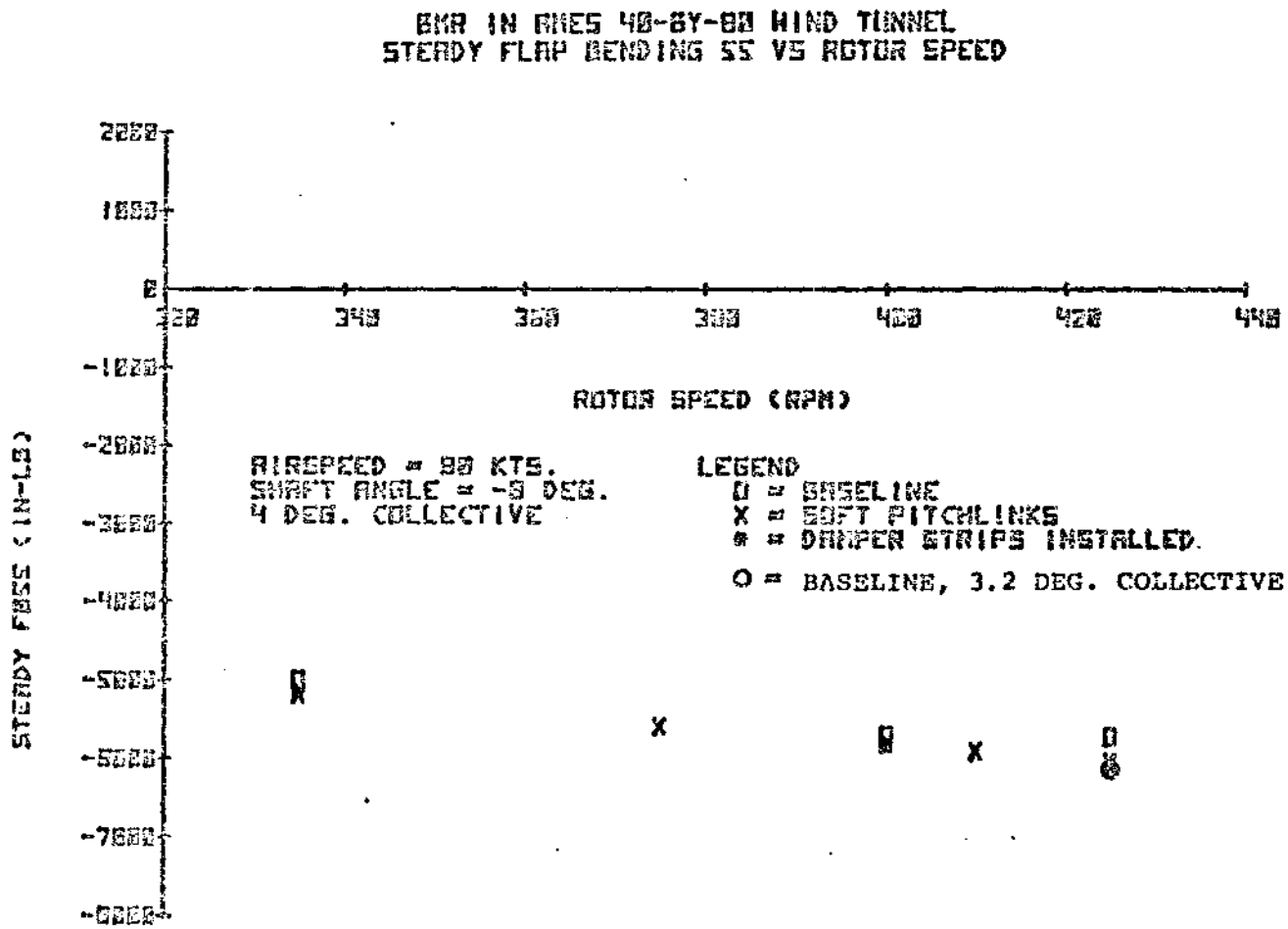

FIGURE 8.149 EFFECT OF SOFT PITCH LINKS AND DAMPER STRIPS STEADY FLAP BENDING 55 VS ROTOR SPEED

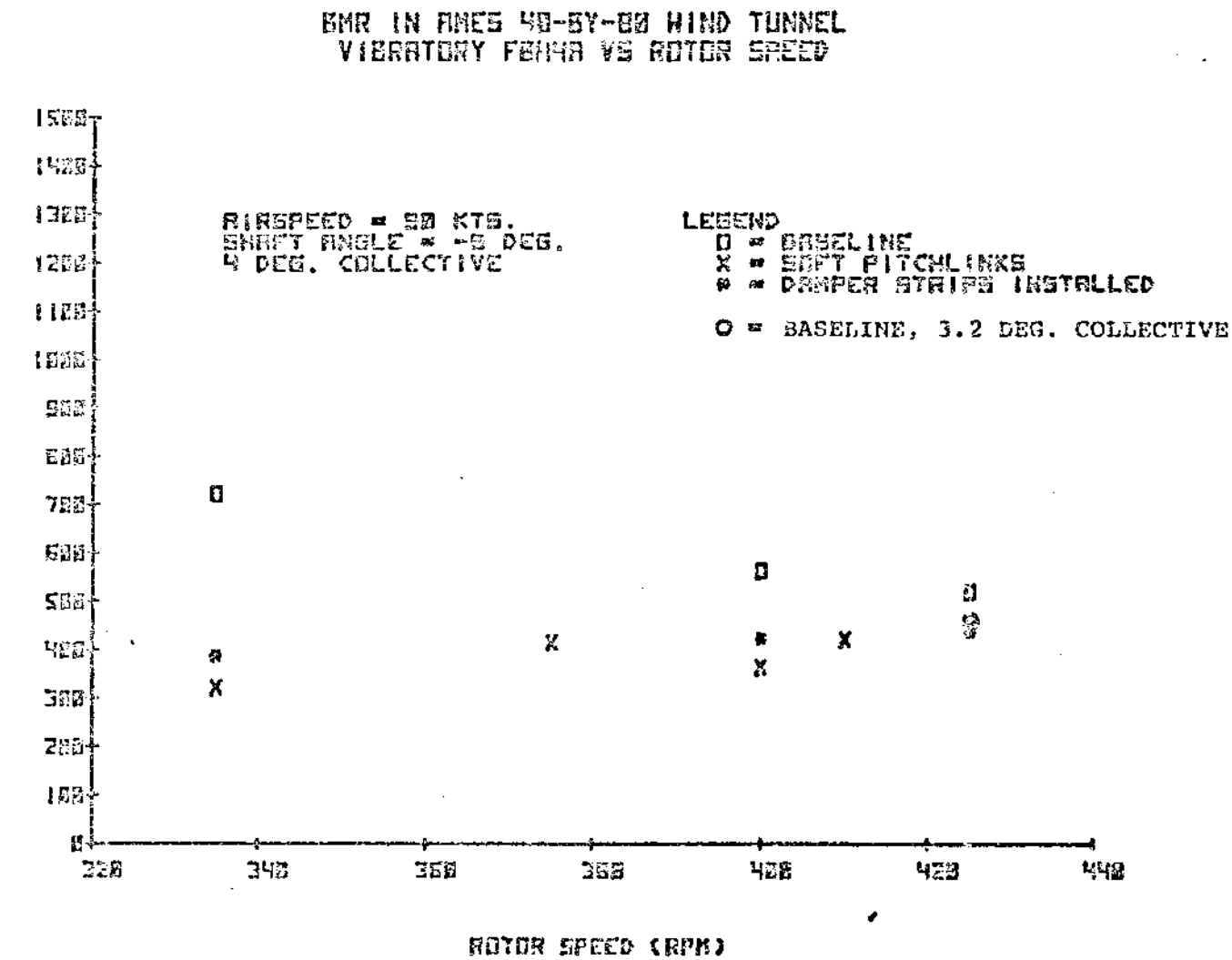

FIGURE 8.150 EFFECT OF SOFT PITCH LINKS AND DAMPER STRIPS VIBRATORY FLAP BENDING 44 BEAM A VS ROTOR SPEED

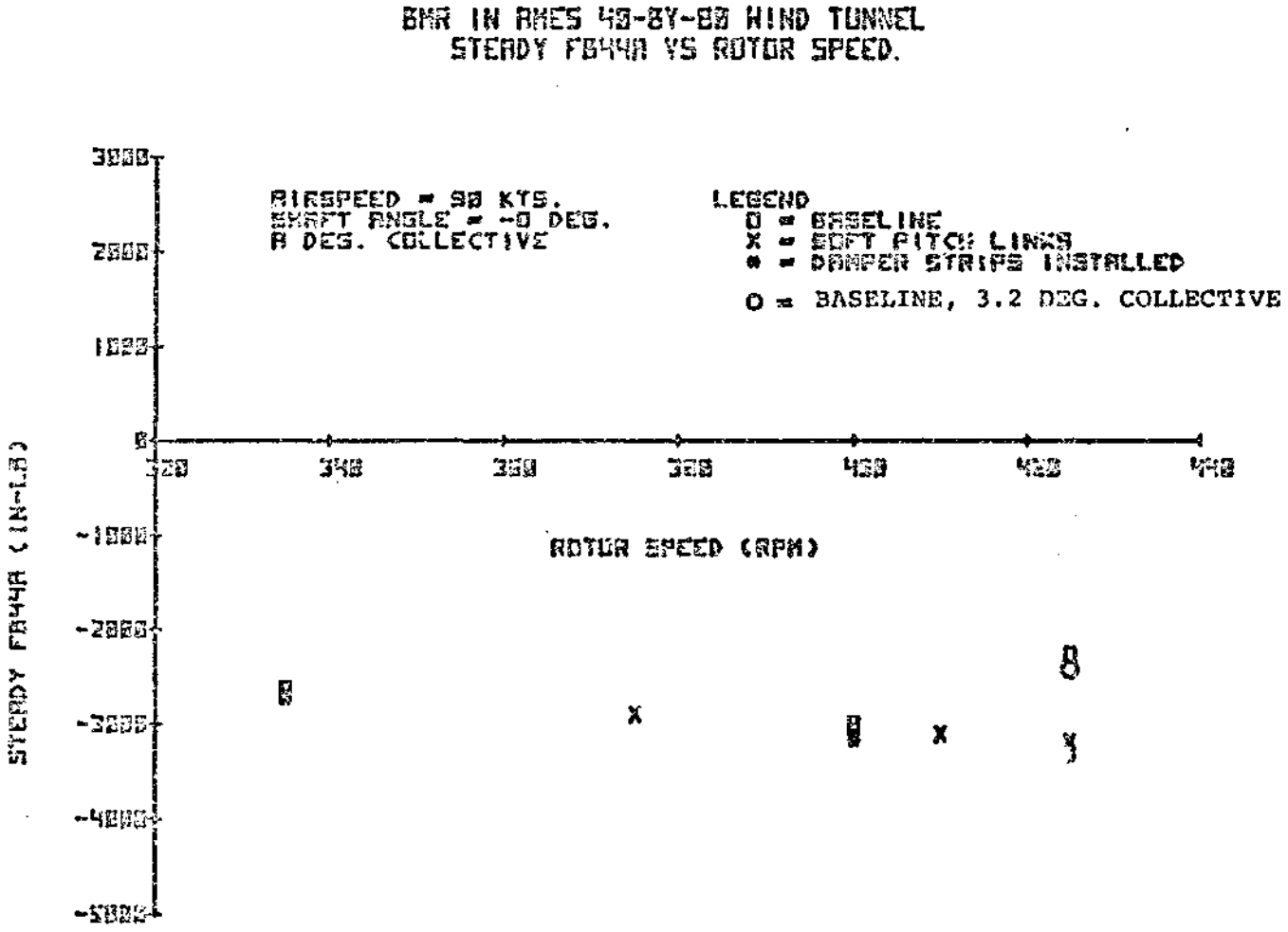

FIGURE 8.151 EFFECT OF SOFT PITCH LINKS AND DAMPER STRIPS
STEADY FLAP BENDING 44 BEAM A VS ROTOR SPEED

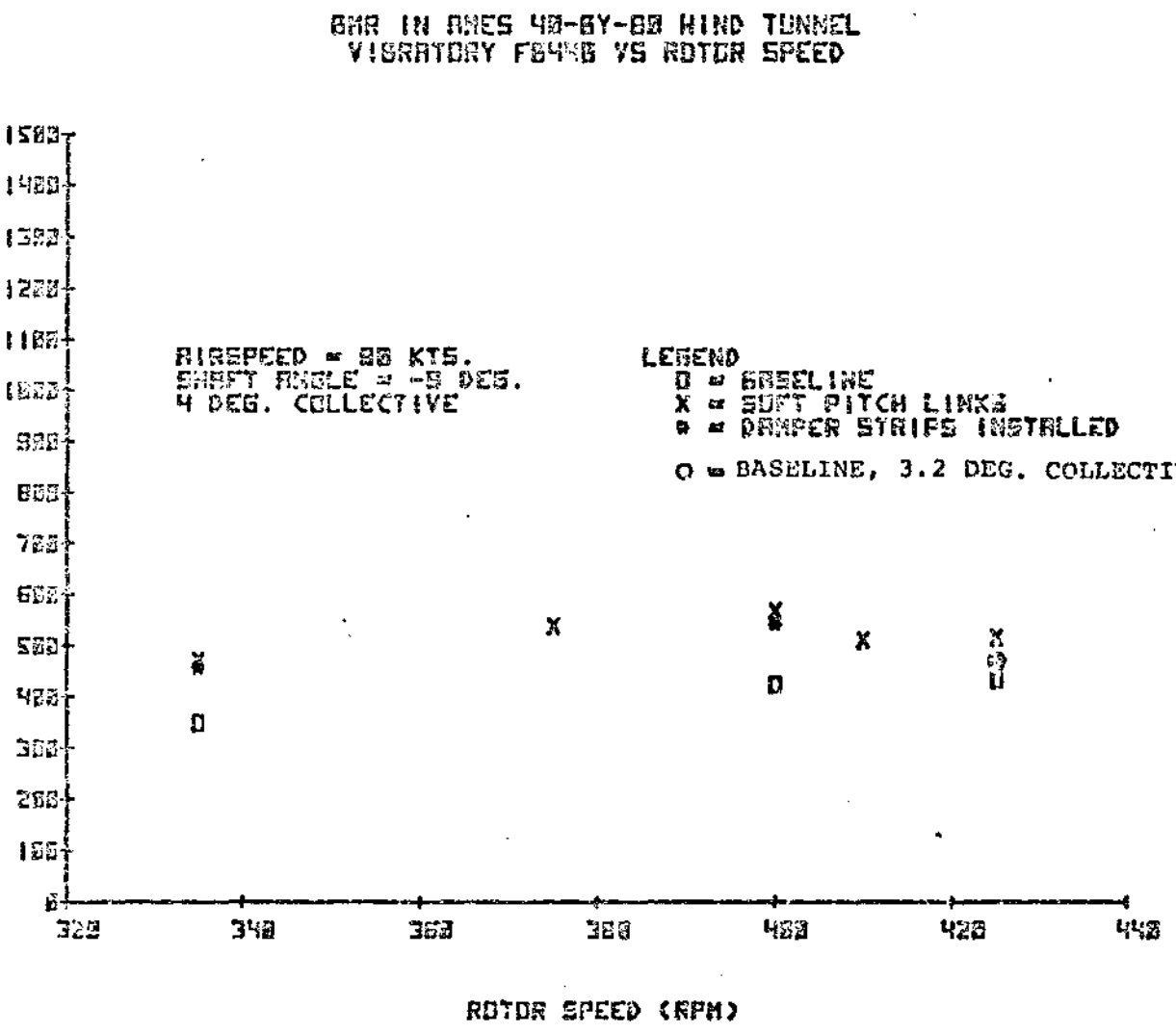

FIGURE 8.152 EFFECT OF SOFT PITCH LINKS AND DAMPER STRIPS
VIBRATORY FLAP BENDING BEAM B VS ROTOR SPEED

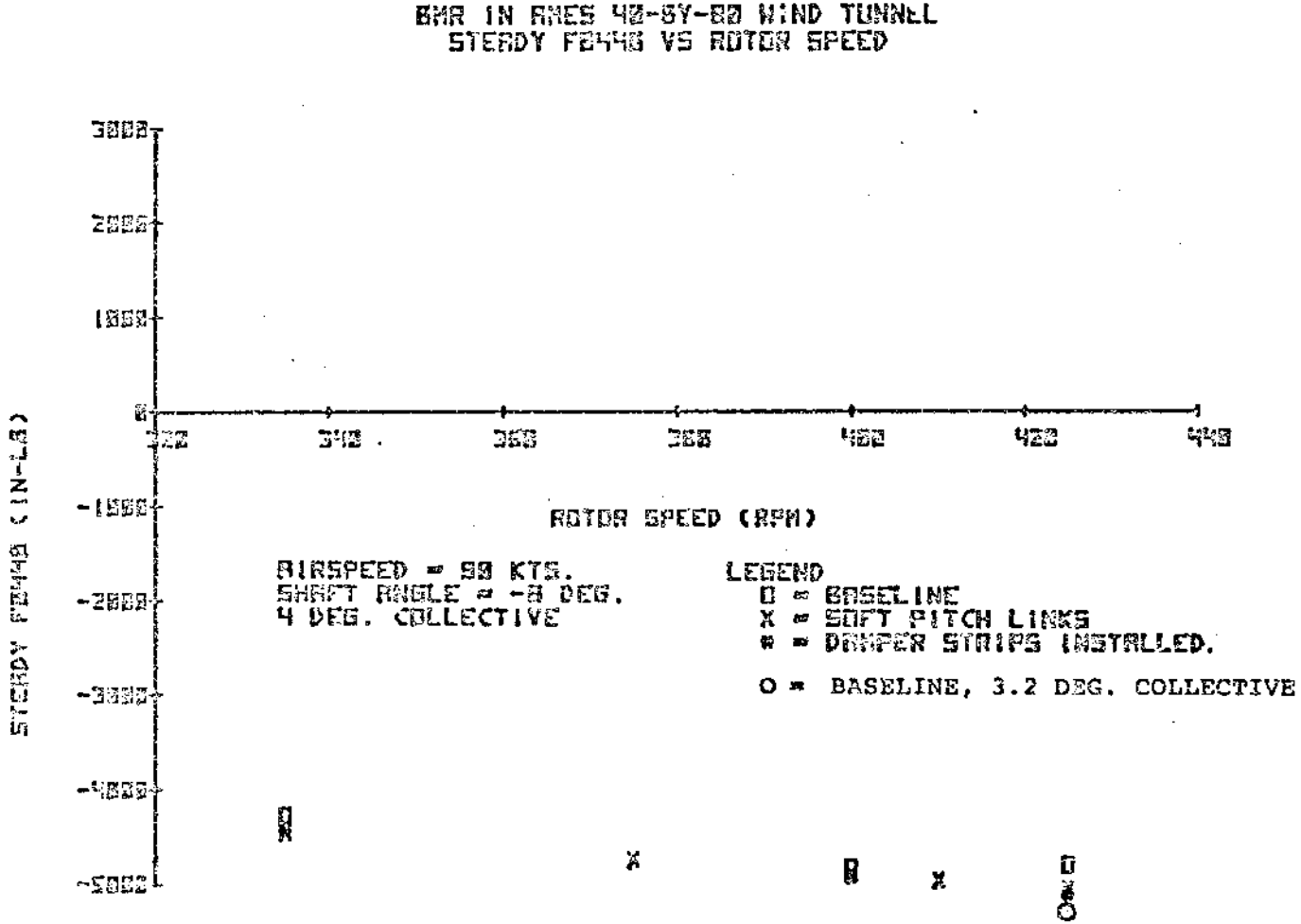

FIGURE 8.153 EFFECT OF SOFT PITCH LINKS AND DAMPER STRIPS
STEADY FLAP BENDING BEAM B VS ROTOR SPEED

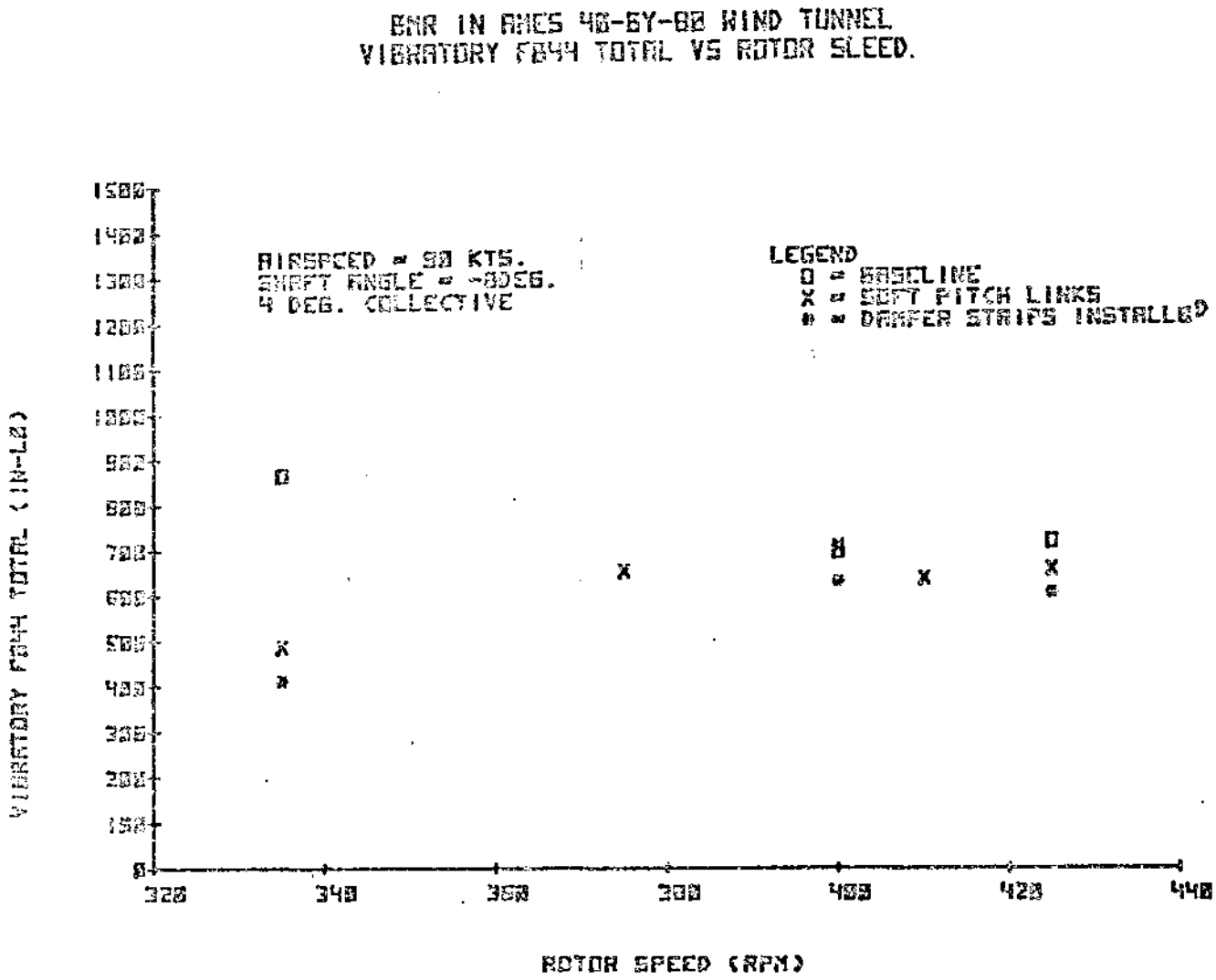

FIGURE 8.154 EFFECT OF SOFT PITCH LINKS AND DAMPER STRIPS VIBRATORY FLAP BENDING 44 (TOTAL) VS ROTOR SPEED

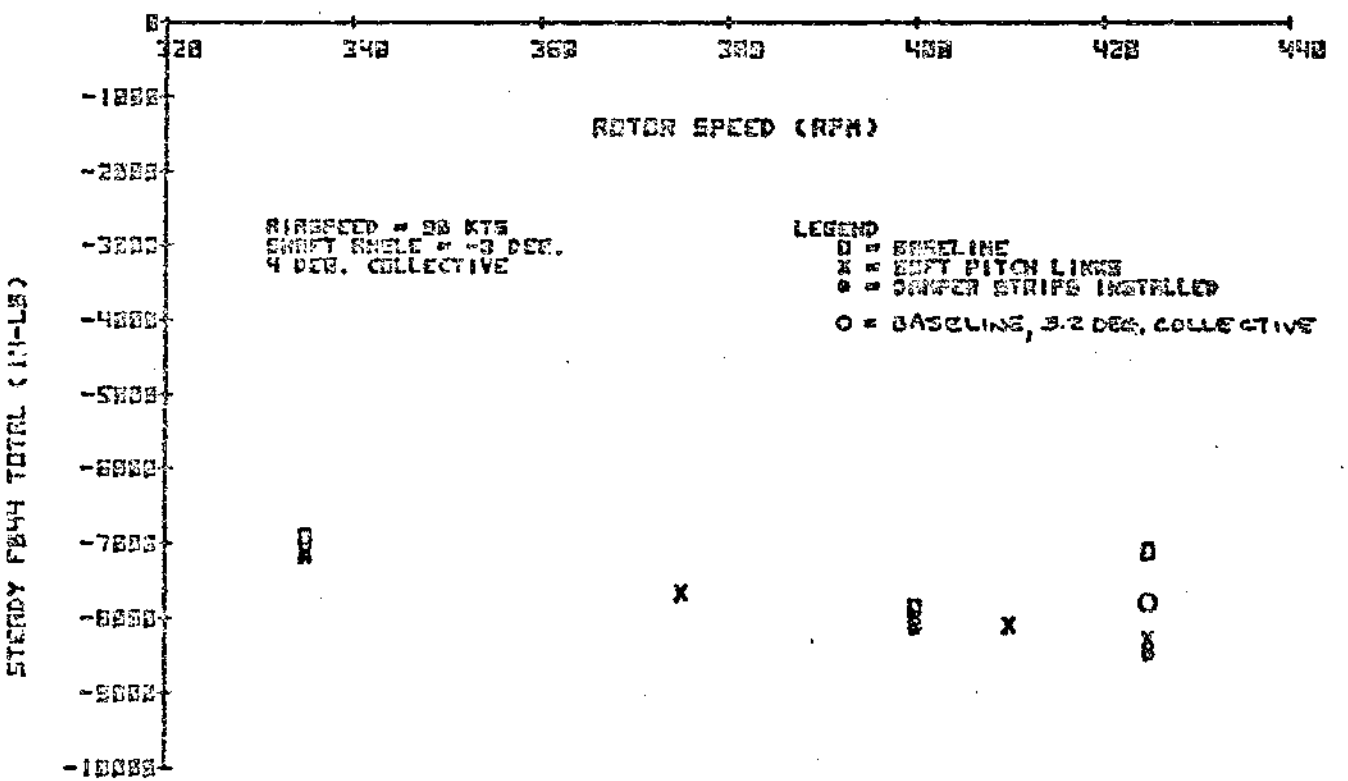

FIGURE 8.155 EFFECT OF SOFT PITCH LINKS AND DAMPER STRIPS STEADY FLAP BENDING 44 (TOTAL) VS ROTOR SPEED

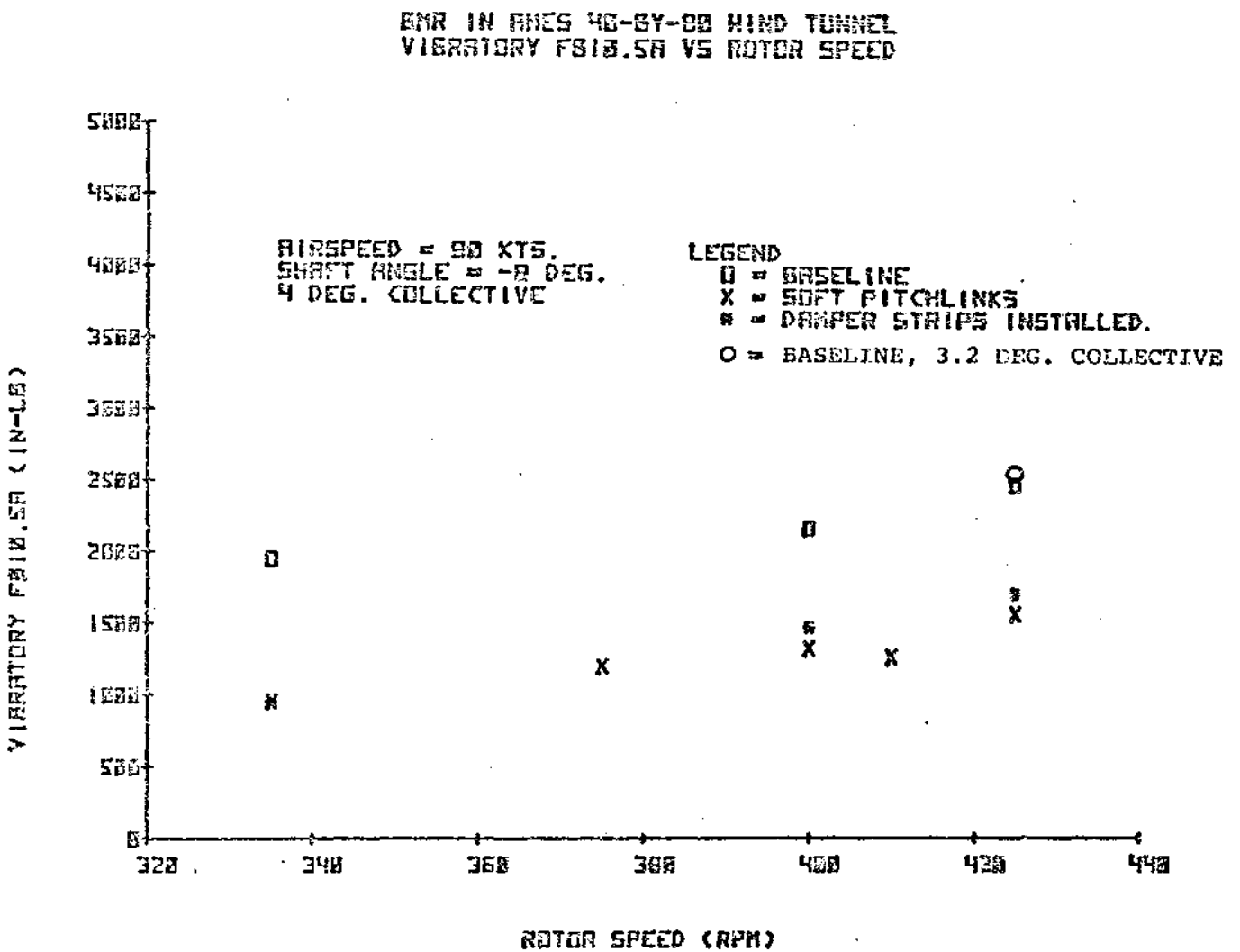

FIGURE 8.156 EFFECT OF SOFT PITCH LINKS AND DAMPER STRIPS
VIBRATORY FLAP BENDING 10.5 BEAM A VS ROTOR SPEED

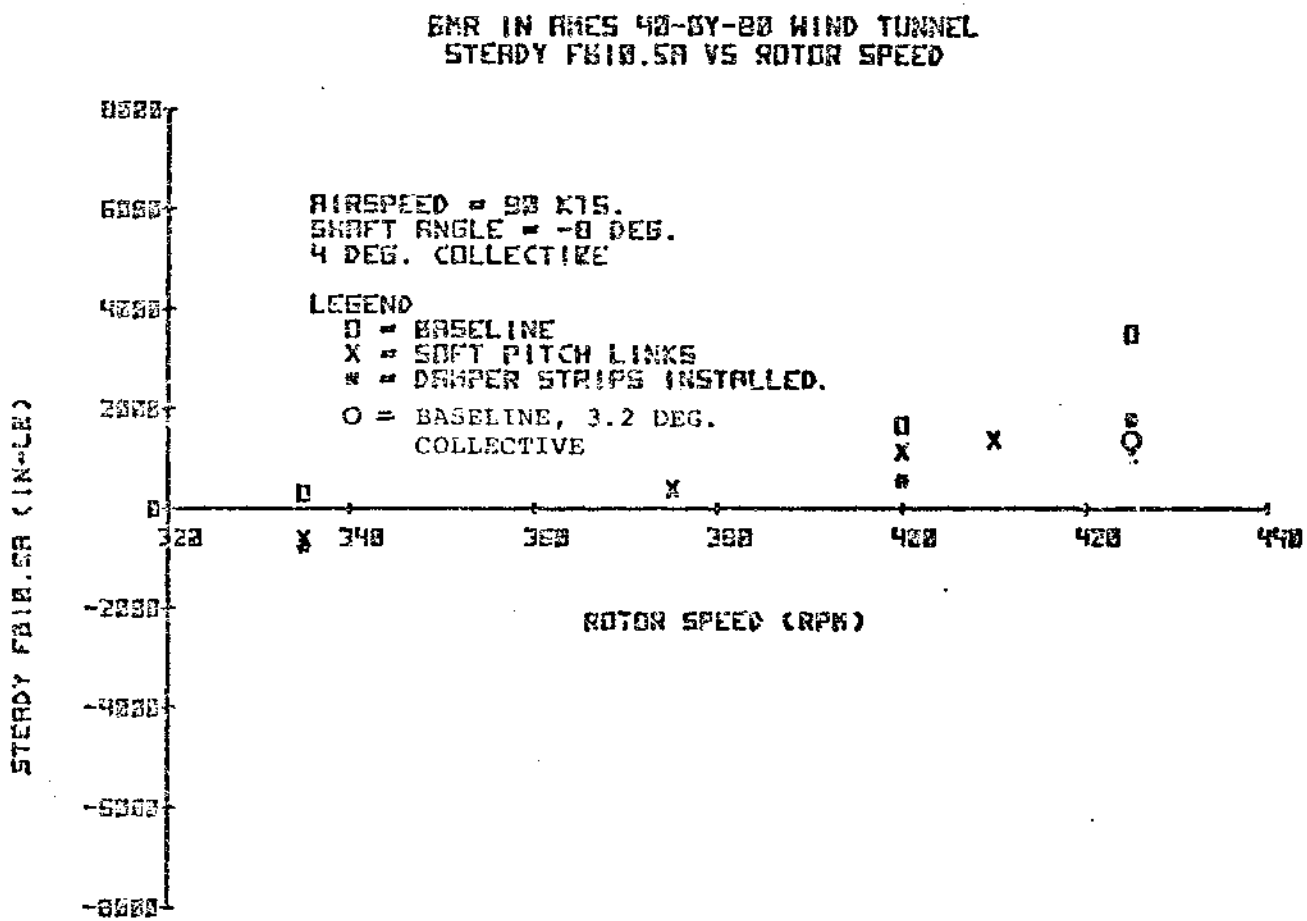

FIGURE 8.157 EFFECT OF SOFT PITCH LINKS AND DAMPER STRIPS STEADY FLAP BENDING 10.5 BEAM A VS ROTOR SPEED

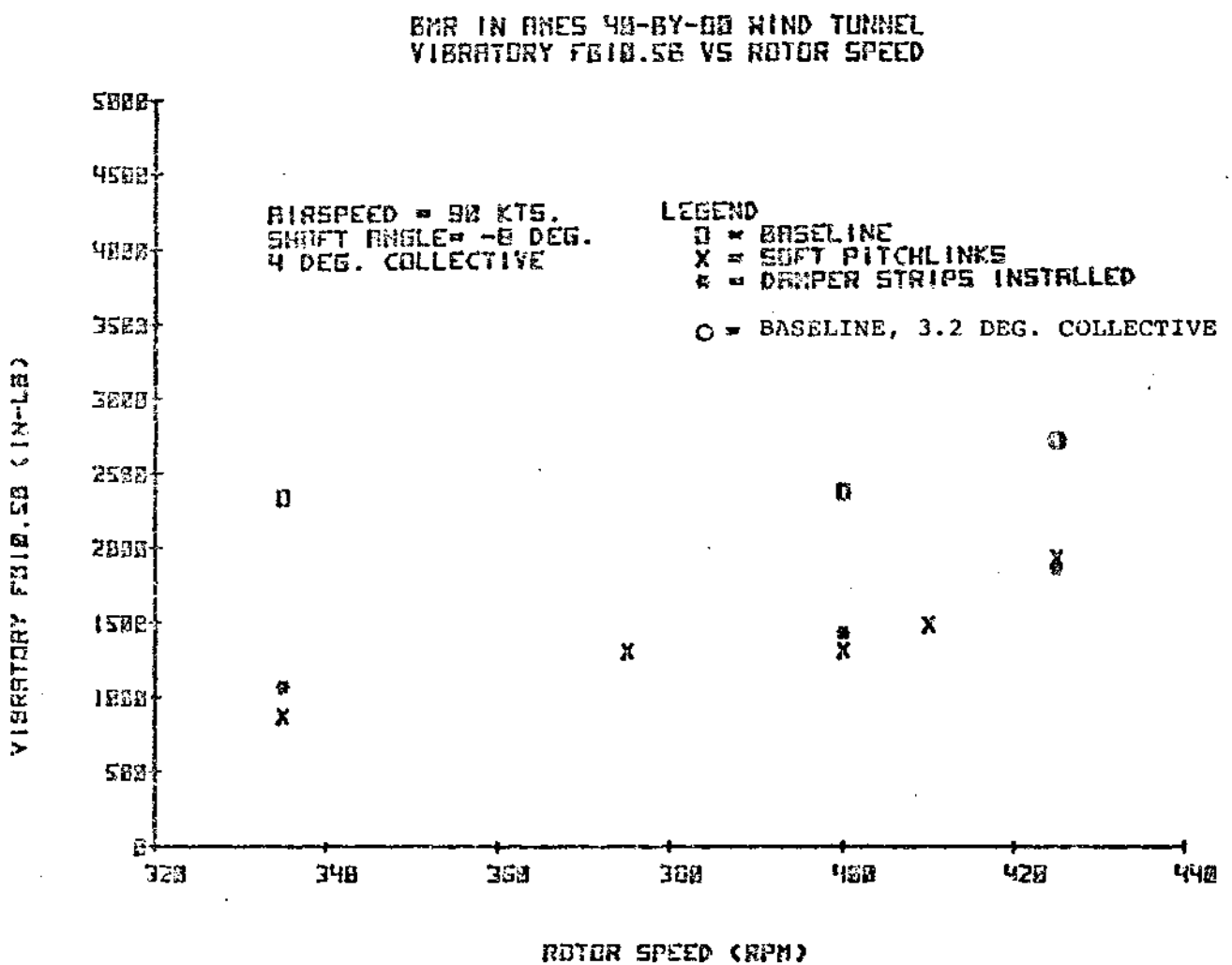

FIGURE 8.158 EFFECT OF SOFT PITCH LINKS AND DAMPER STRIPS VIBRATORY FLAP BENDING 10.5 BEAM B VS ROTOR SPEED

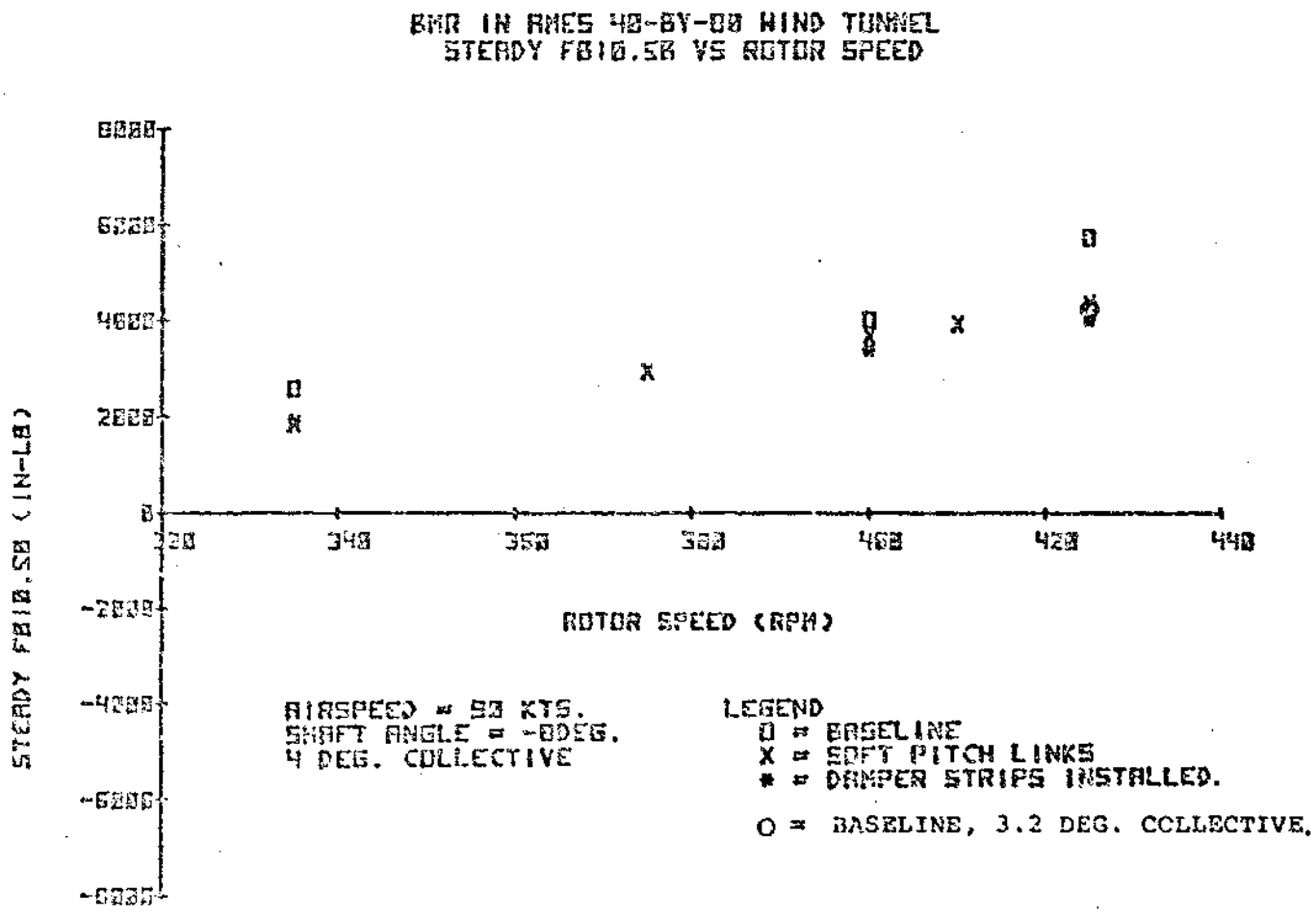

FIGURE 8.159 EFFECT OF SOFT PITCH LINKS AND DAMPER STRIPS
STEADY FLAP BENDING 10.5 BEAM B VS ROTOR SPEED

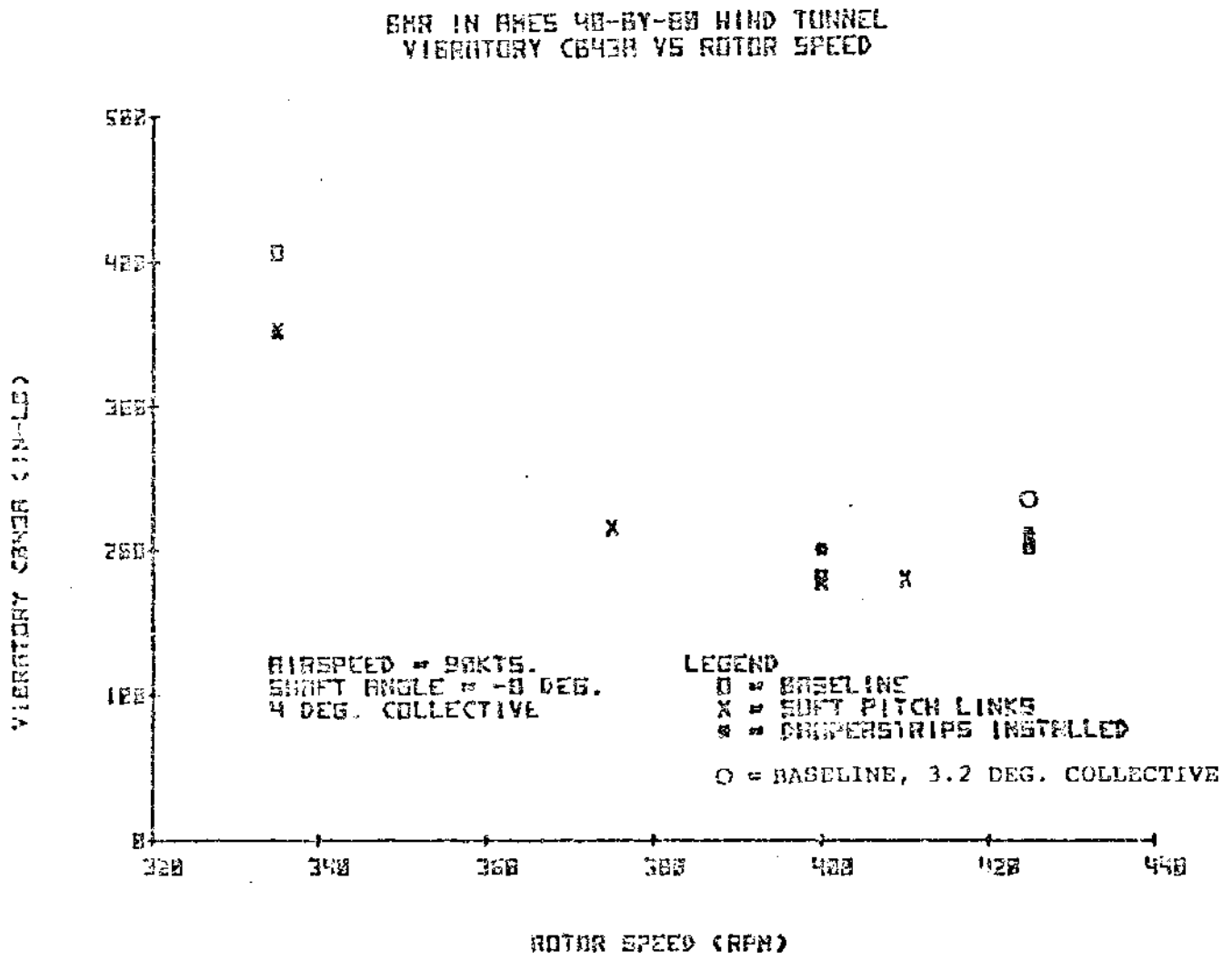

FIGURE 8.160 EFFECT OF SOFT PITCH LINKS AND DAMPER STRIPS
VIBRATORY CHORD BENDING 43 BEAM A VS ROTOR SPEED

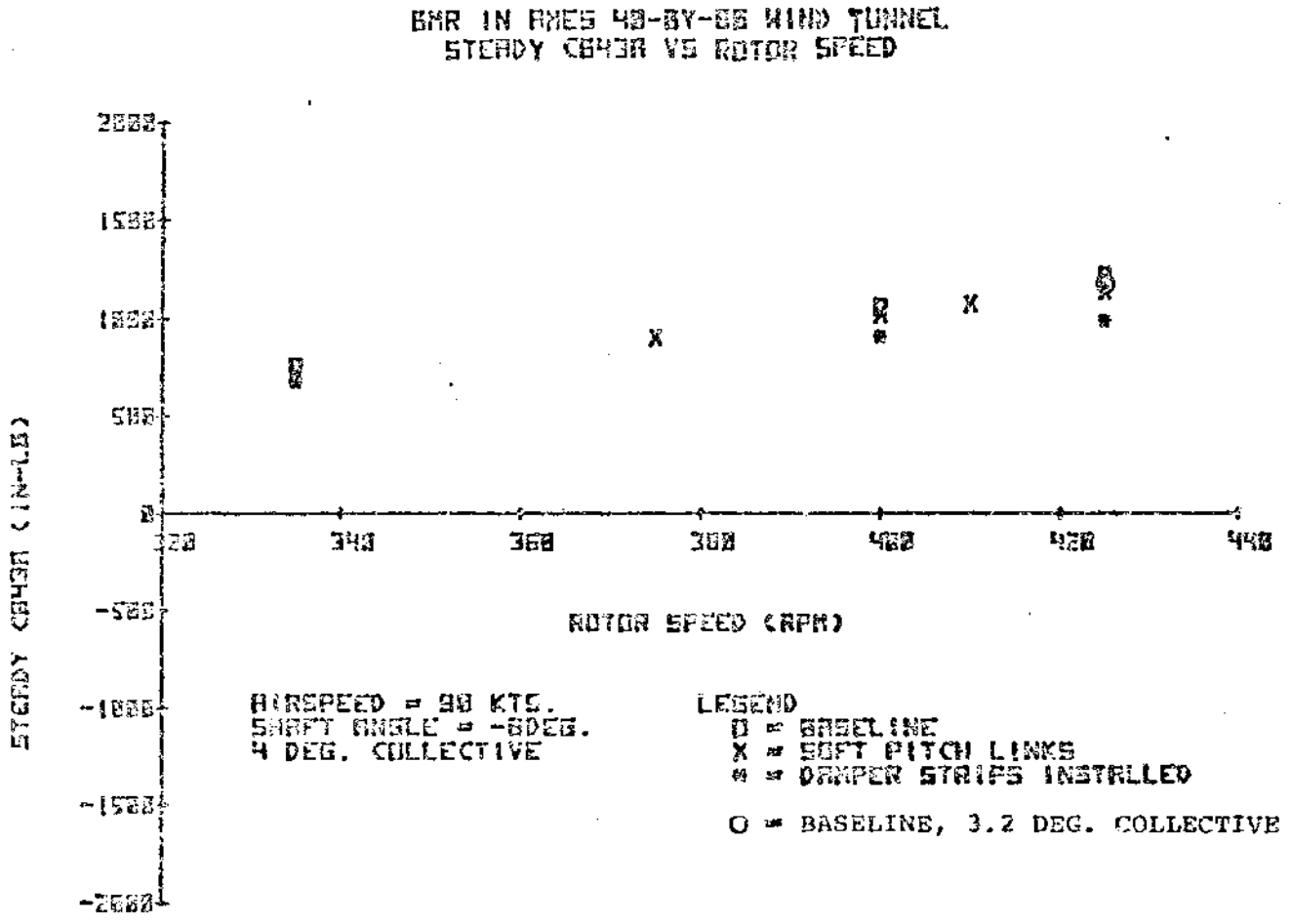

FIGURE 8.161 EFFECT OF SOFT PITCH LINKS AND DAMPER STRIPS
STEADY CHORD BENDING 43 BEAM A VS ROTOR SPEED

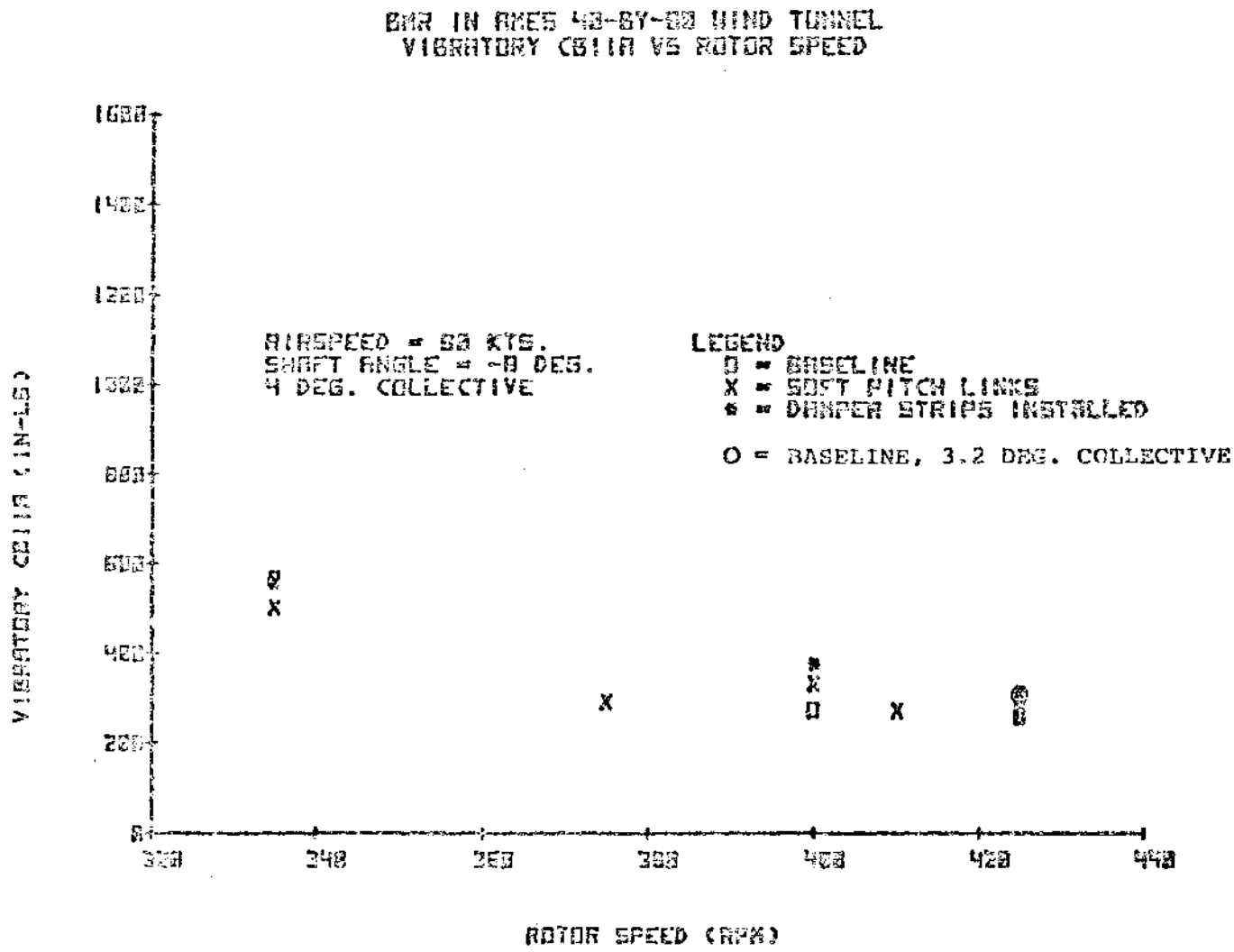

FIGURE 8.162 EFFECT OF SOFT PITCH LINKS AND DAMPER STRIPS VIBRATORY CHORD BENDING 11 BEAM A VS ROTOR SPEED

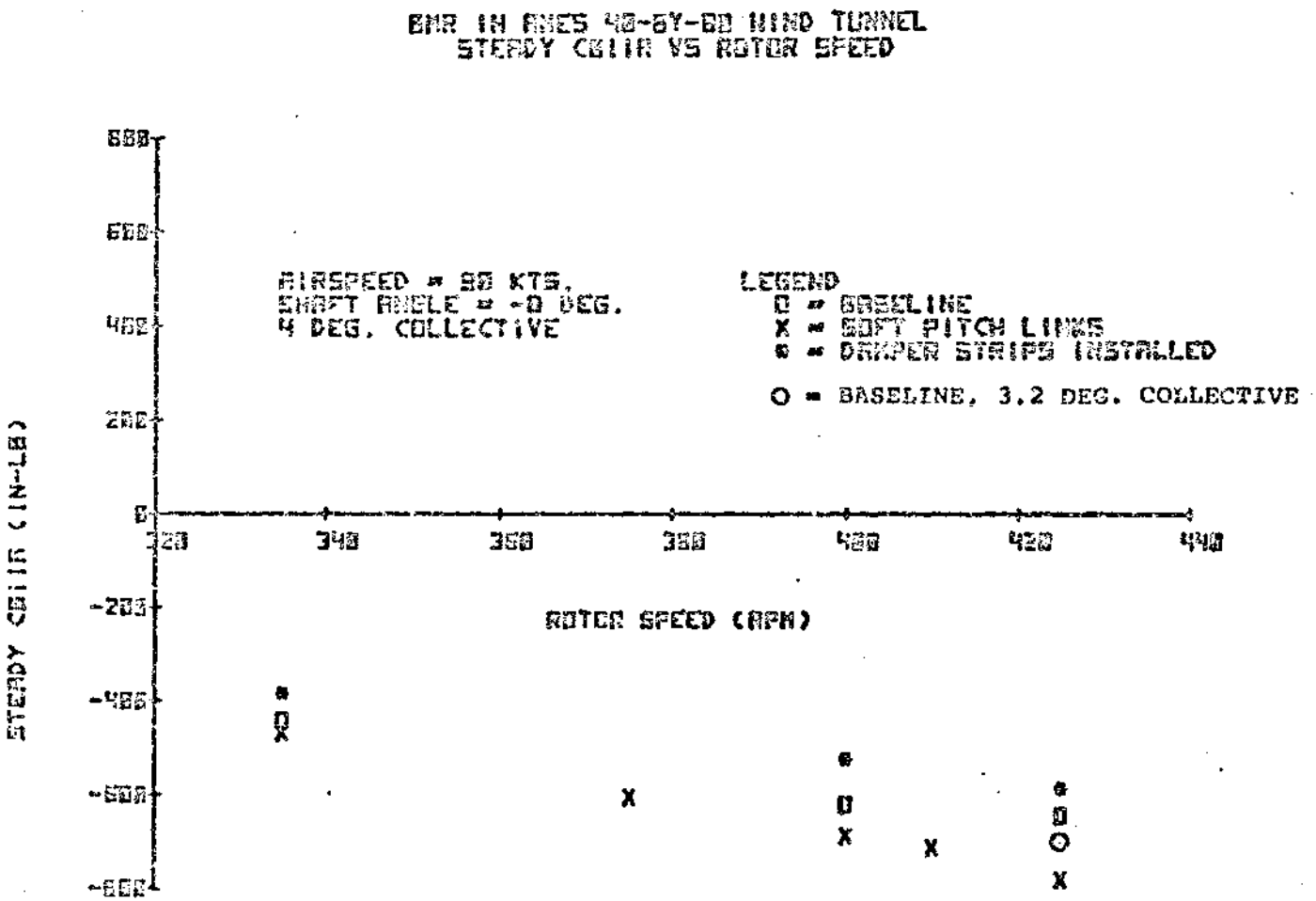

FIGURE 8.163 EFFECT OF SOFT PITCH LINKS AND DAMPER STRIPS
STEADY CHORD BENDING 11 BEAM A VS ROTOR SPEED

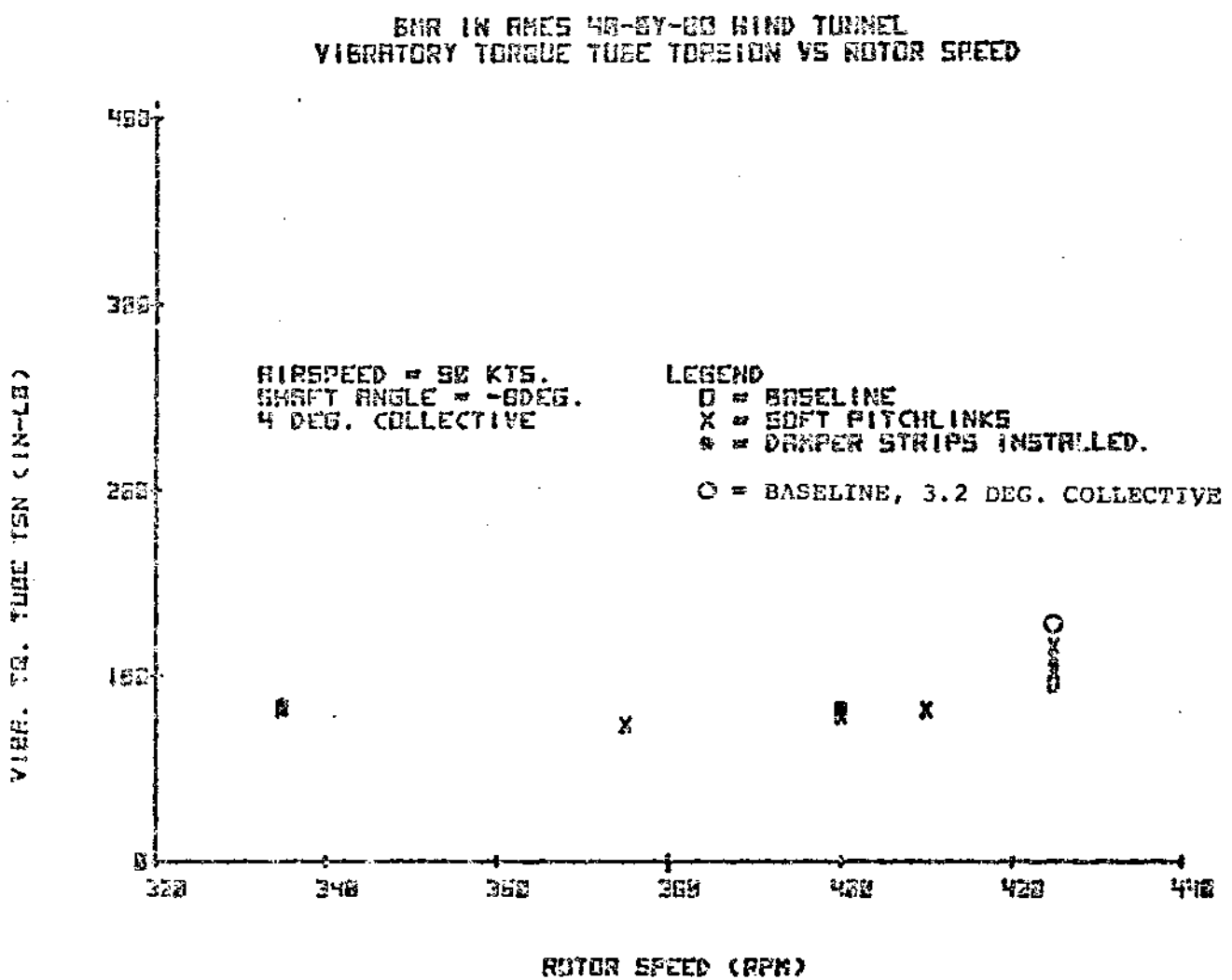

FIGURE 8.164 EFFECT OF SOFT PITCH LINKS AND DAMPER STRIPS VIBRATORY TORQUE TUBE TORSION VS ROTOR SPEED

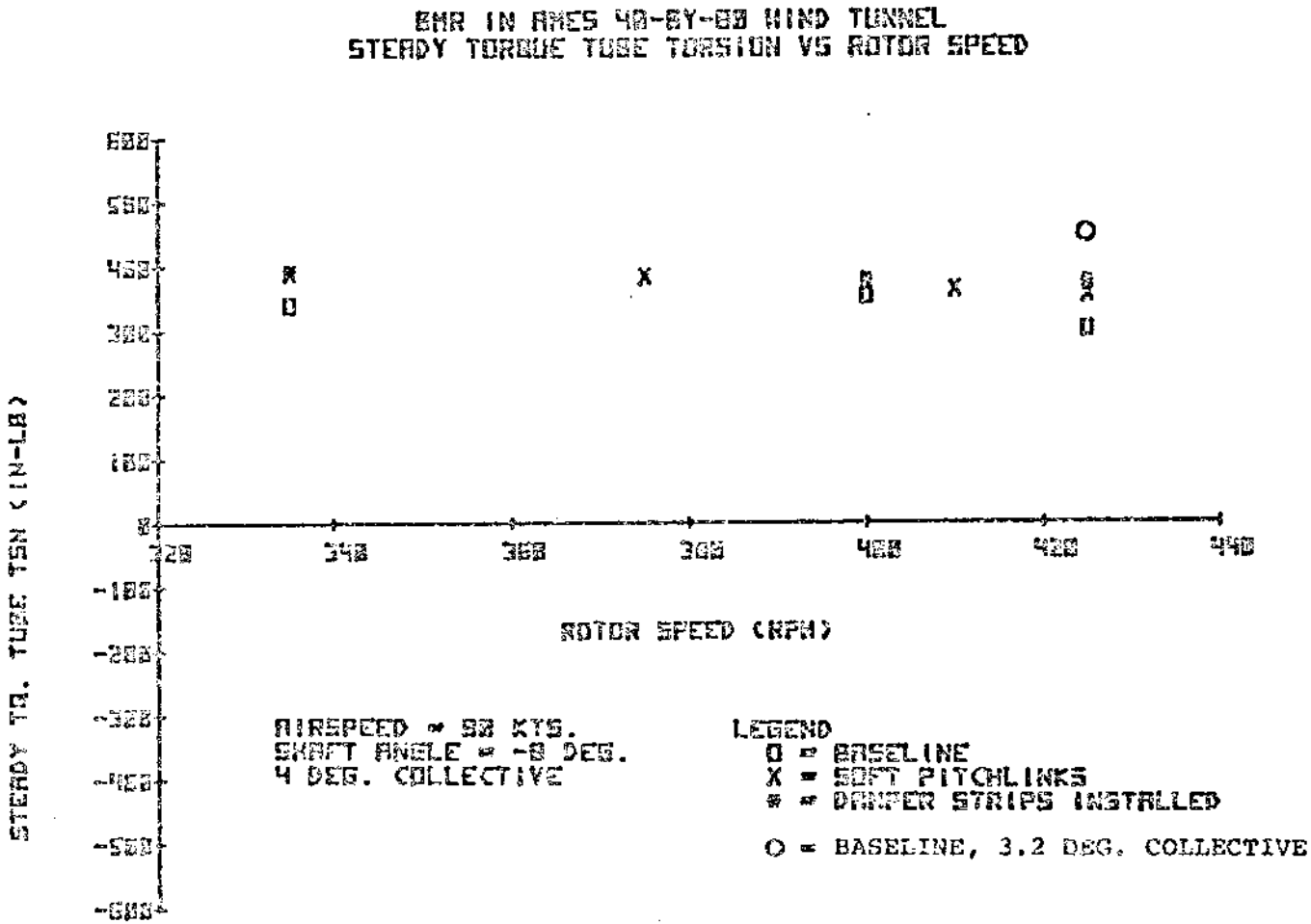

FIGURE 8.165 EFFECT OF SOFT PITCH LINKS AND DAMPER STRIPS
STEADY TORQUE TUBE TORSION VS ROTOR SPEED

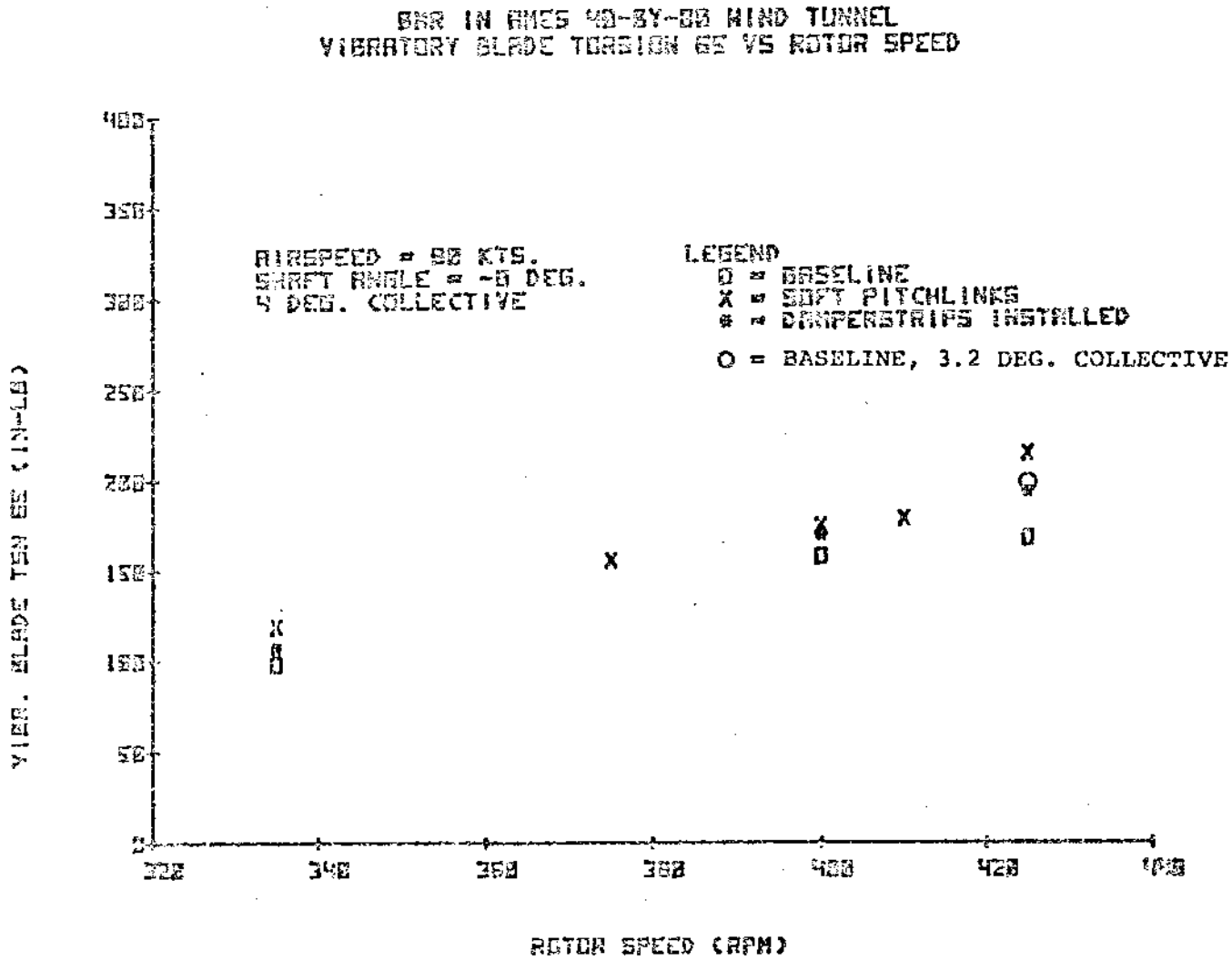

FIGURE 8.166 EFFECT OF SOFT PITCH LINKS AND DAMPER STRIPS VIBRATORY BLADE TORSION 6S VS ROTOR SPEED

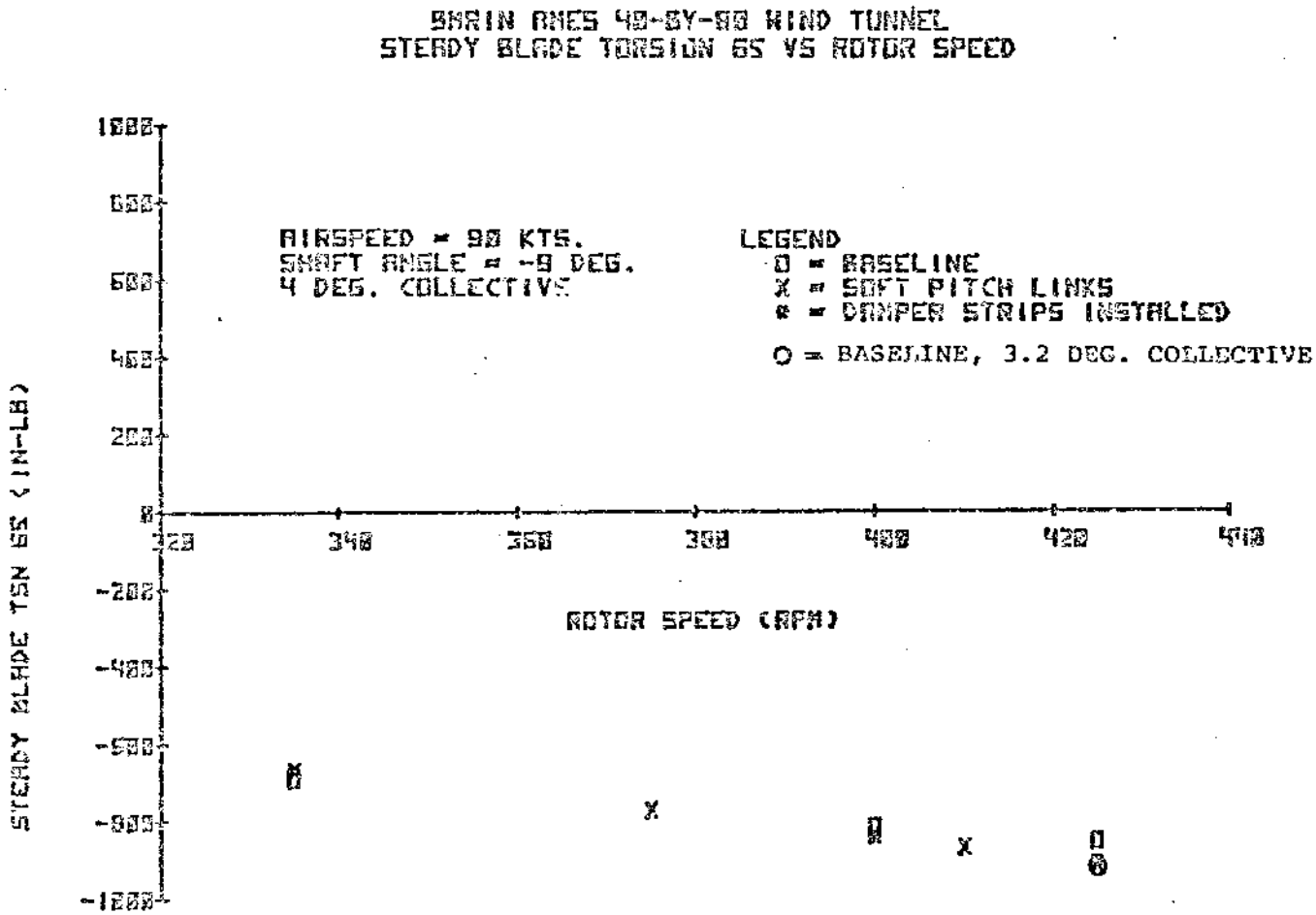

FIGURE 8.167 EFFECT OF SOFT PITCH LINKS AND DAMPER STRIPS
STEADY BLADE TORSION GS VS ROTOR SPEED

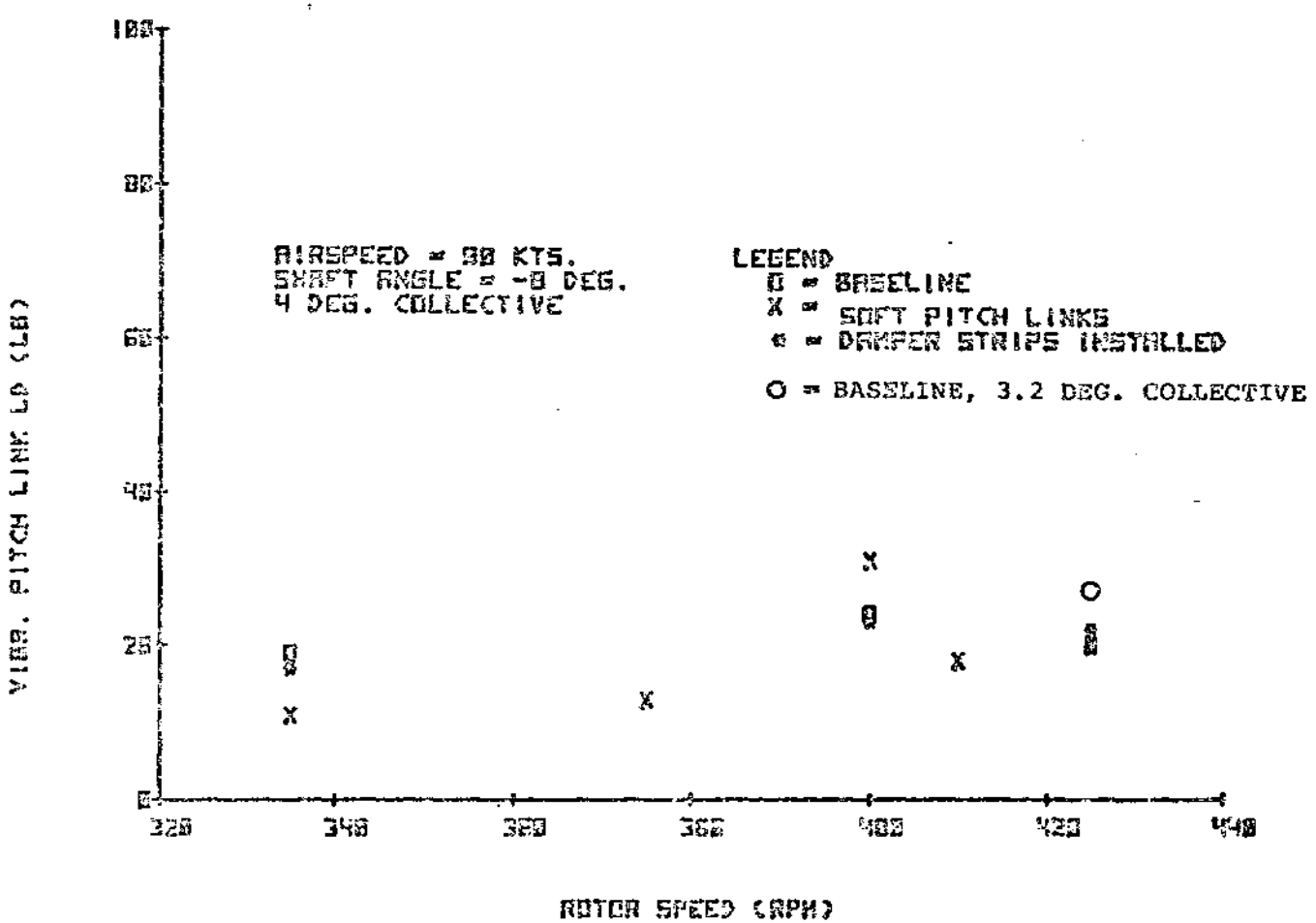

FIGURE 8.168 EFFECT OF SOFT PITCH LINKS AND DAMPER STRIPS
VIBRATORY PITCH LINK LOAD VS ROTOR SPEED

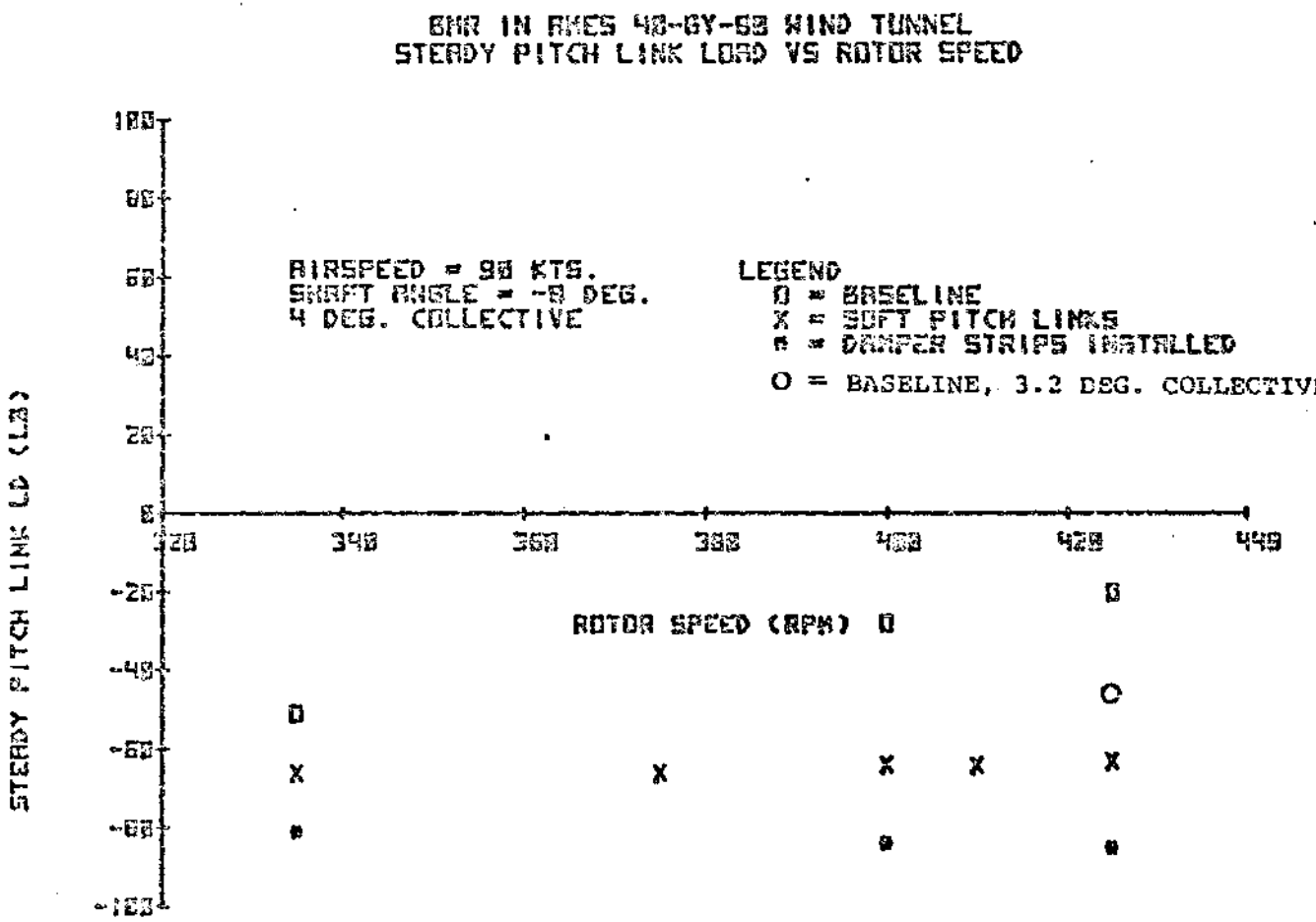

FIGURE 8.169 EFFECT OF SOFT PITCH LINKS AND DAMPER STRIPS
STEADY PITCH LINK LOAD VS ROTOR SPEED

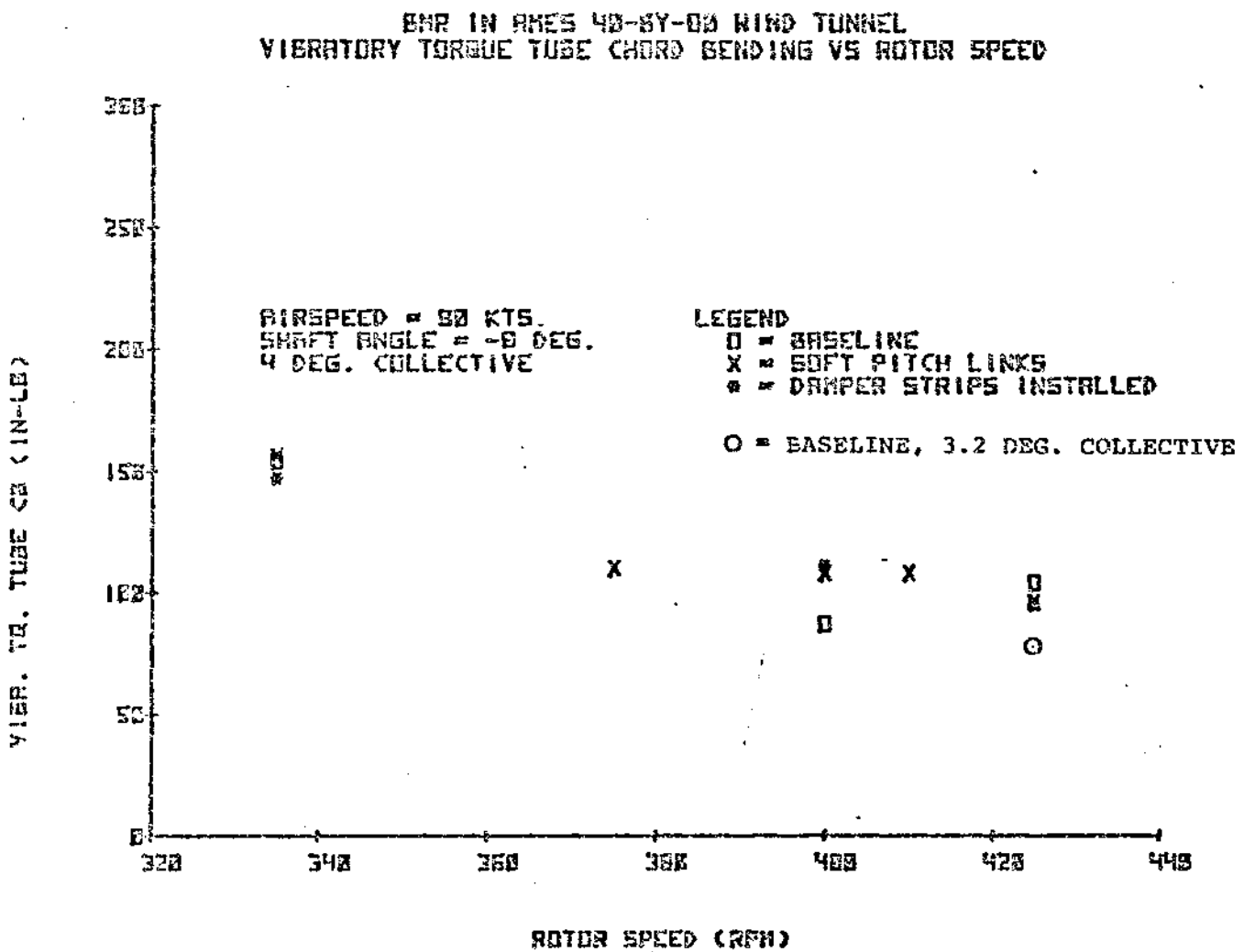

FIGURE 8.170 EFFECT OF SOFT PITCH LINKS AND DAMPER STRIPS VIBRATORY TORQUE TUBE CHORD BENDING VS ROTOR SPEED

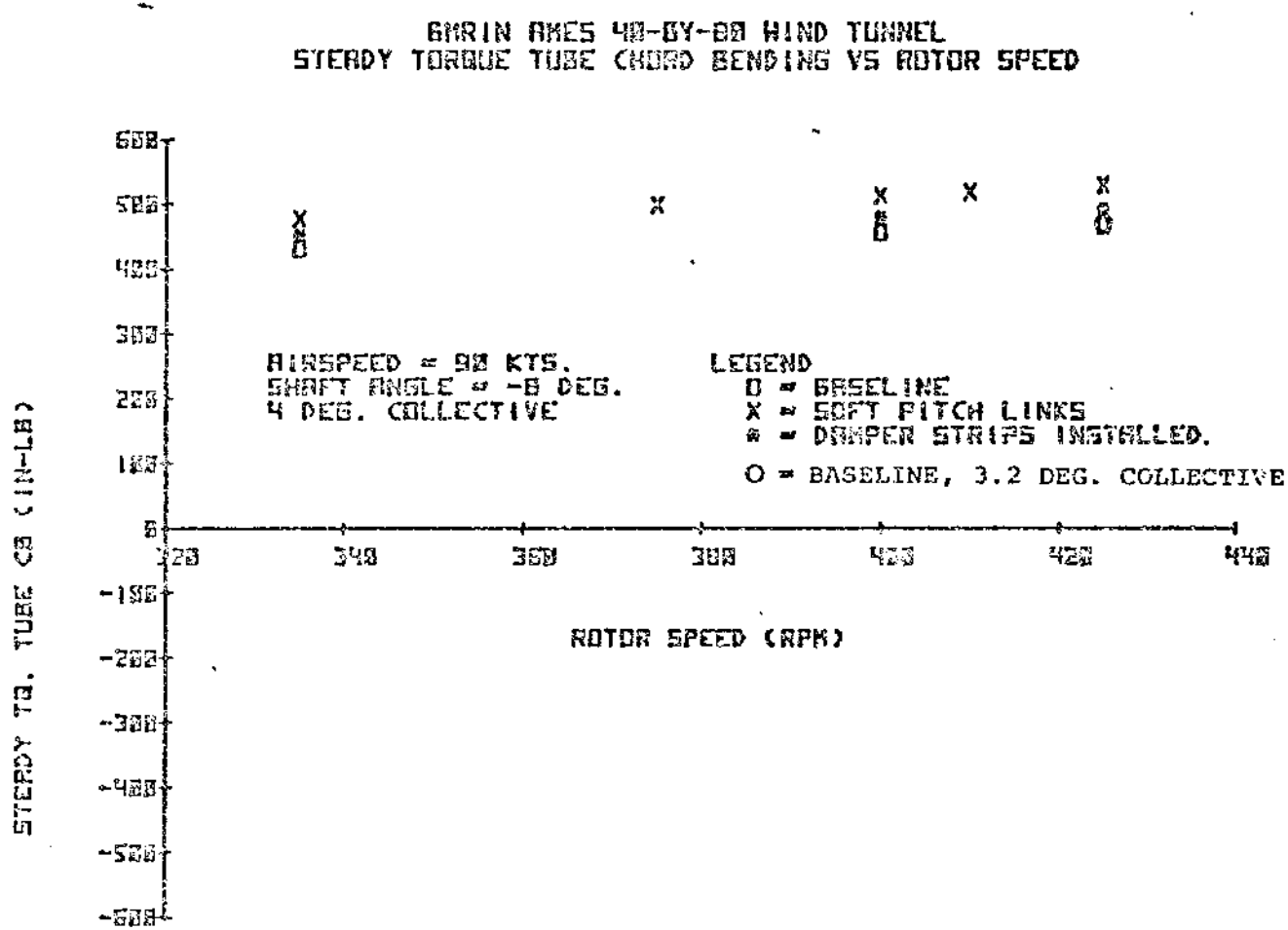

FIGURE 8.171 EFFECT OF SOFT PITCH LINKS AND DAMPER STRIPS STEADY TORQUE TUBE CHORD BENDING VS ROTOR SPEED

8.2.2.5.1 Soft Pitch Links

In addition to the plots in the previous section, the soft pitch link effect is also exhibited by the harmonic content as shown in Figures 8.172 through 8.178. While the total vibratory loads show a significant reduction in flap bending at station 10.5 only, the harmonic content shows significant reduction in 1/rev loading for both flexbeam flap bending stations (10.5 and 44). There is also significantly more 2/rev content at station 10.5. In addition, axial pitch link load shows significant changes, with an increase in 6/rev and 10/rev at 400 rpm and a decrease in 1/rev at all rotor speeds tested. A comparison of the pitch link axial load and the torque tube torsion shows that there is not a direct correspondence in the vibratory response.

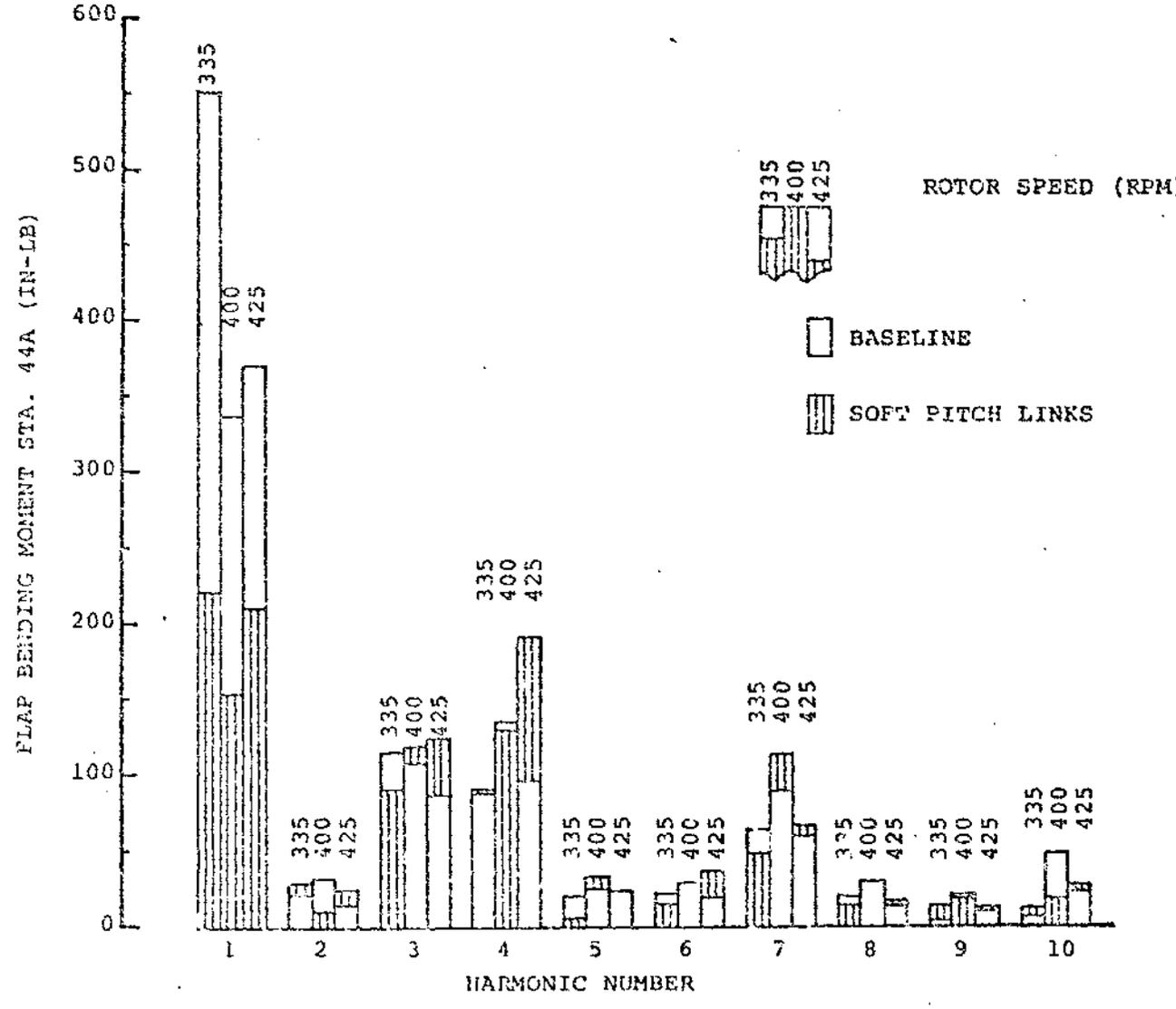

FIGURE 8.172 FLAP BENDING STATION 44 BEAM A - HARMONIC CONTENT FOR BASELINE & SOFT PITCH LINKS

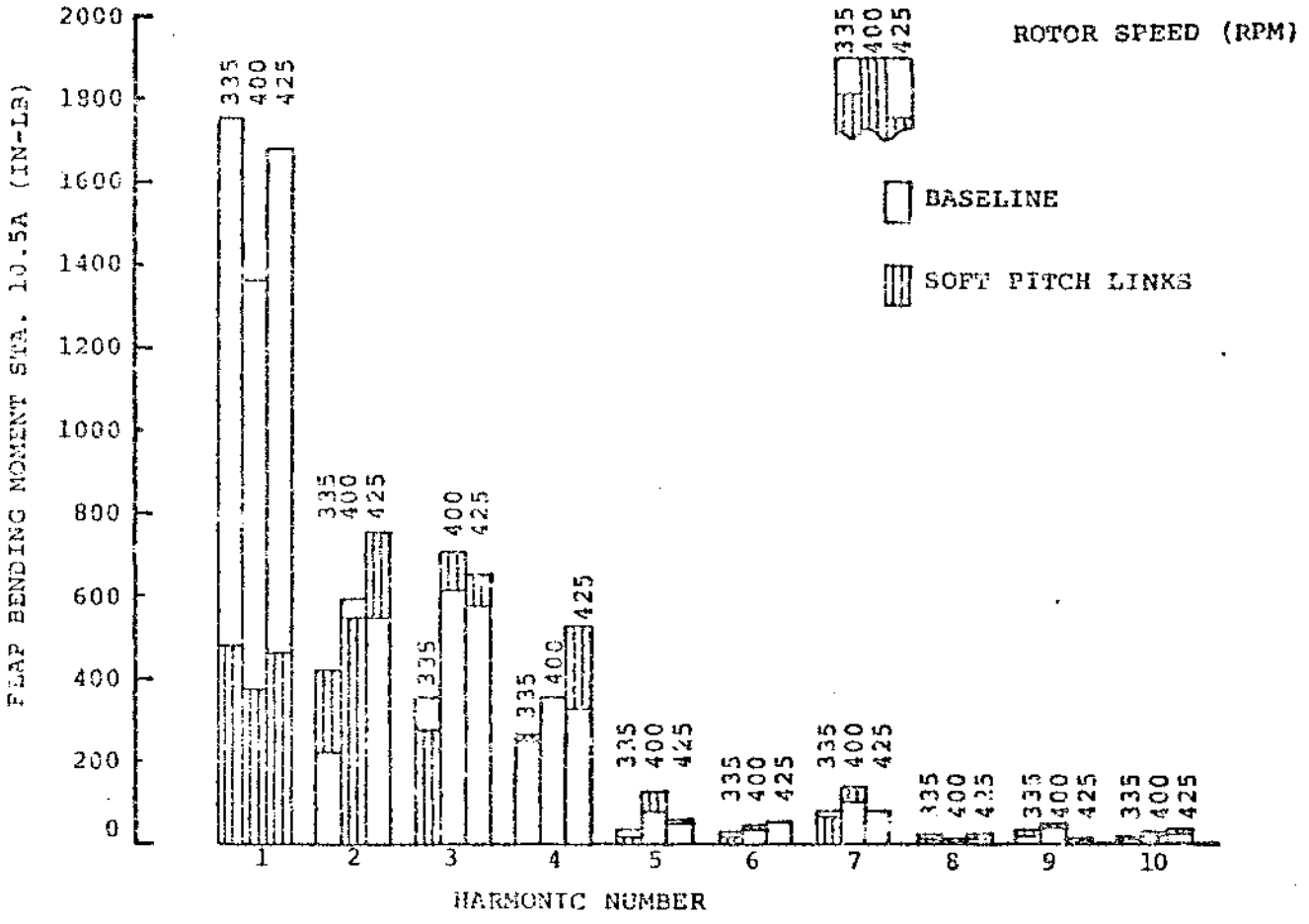

FIGURE 8.173 FLAP BENDING STATION 10.5 BEAM A - HARMONIC CONTENT FOR BASELINE & SOFT PITCH LINKS

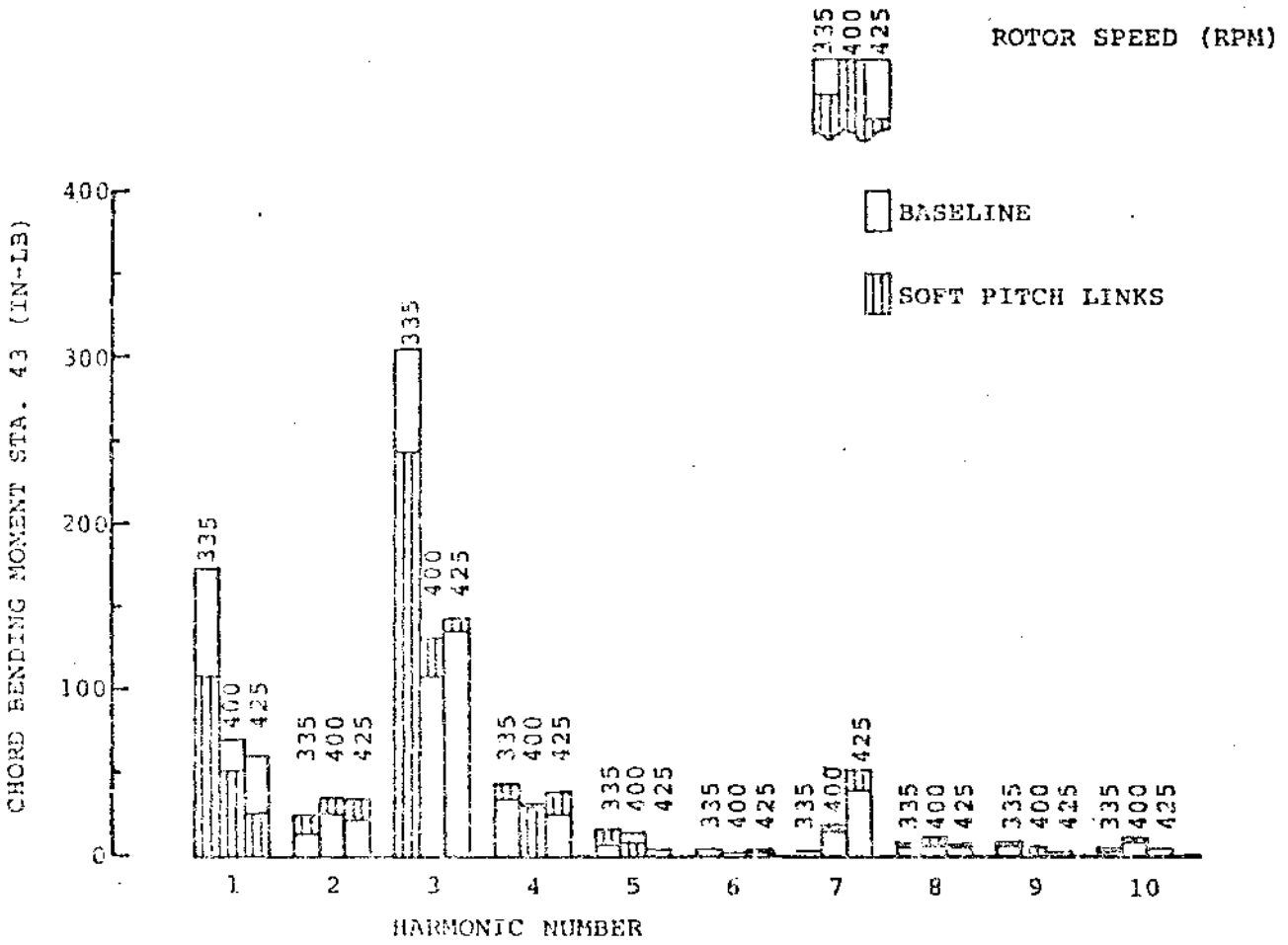

FIGURE 8.174 CHORD BENDING STATION 43 BEAM A - HARMONIC CONTENT FOR BASELINE & SOFT PITCH LINKS

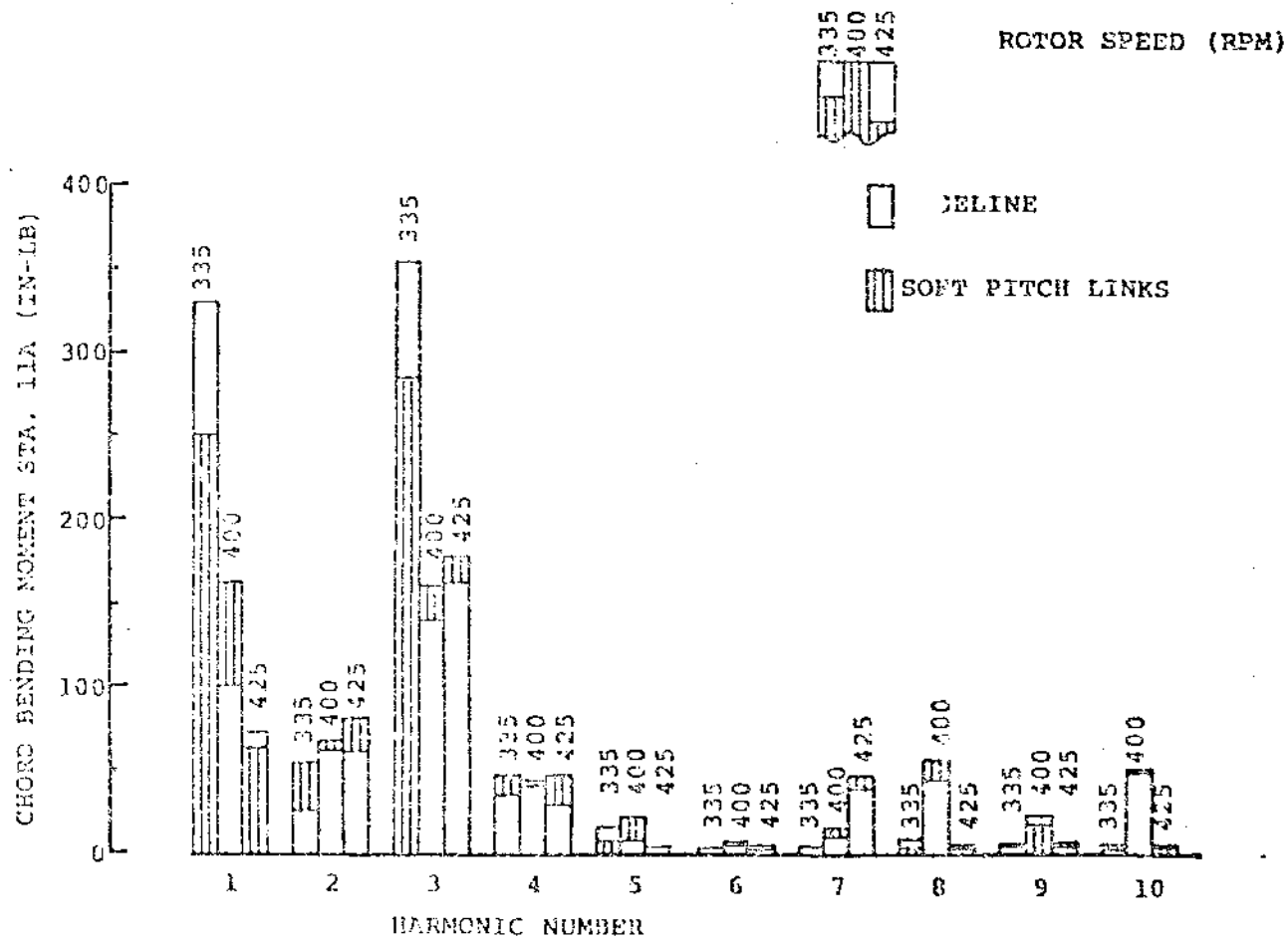

FIGURE 8.175 CHORD BENDING STATION 11 BEAM A - HARMONIC CONTENT FOR BASELINE & SOFT PITCH LINKS

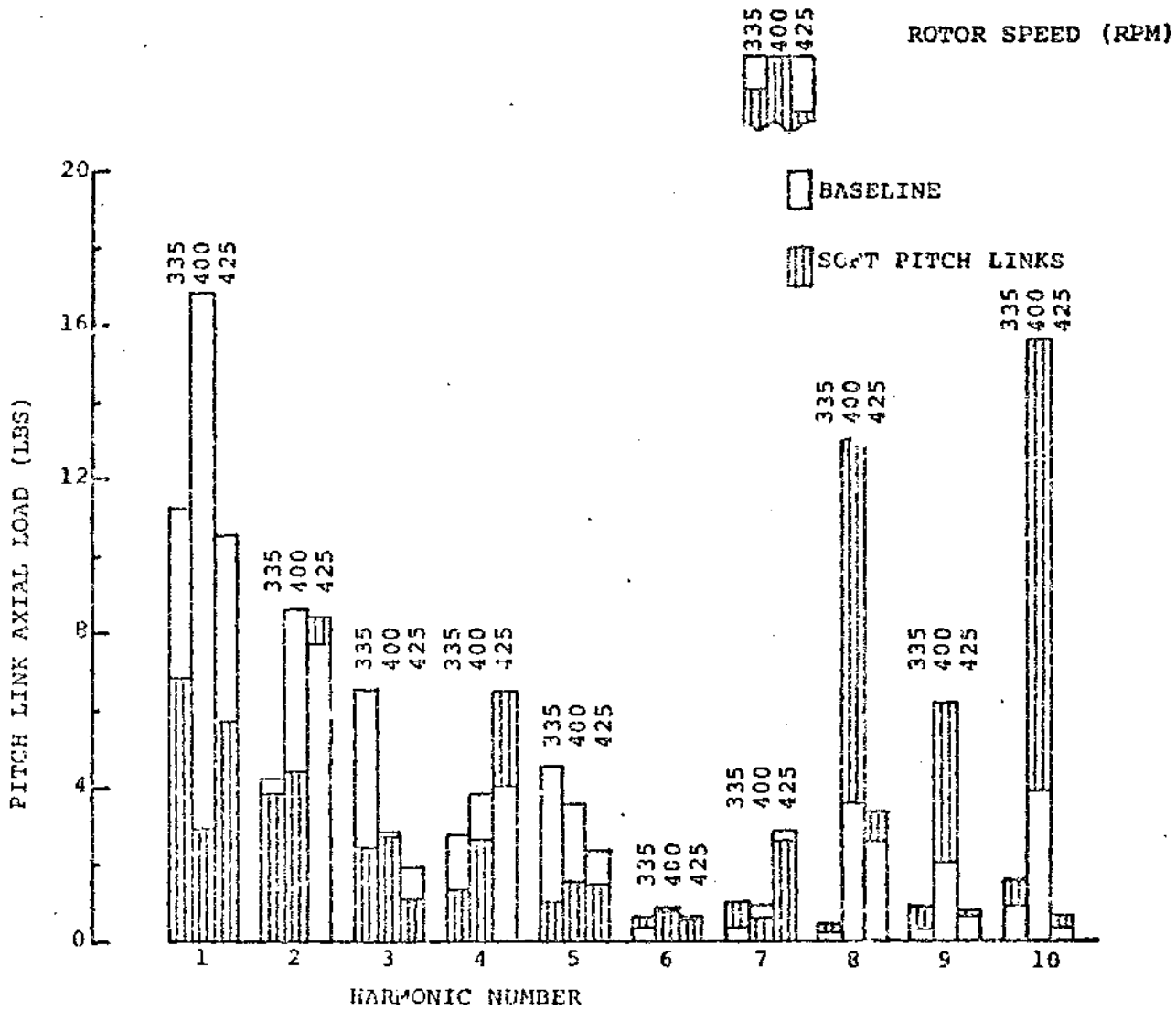

FIGURE 8.176 PITCH LINK AXIAL LOAD - HARMONIC CONTENT FOR BASELINE & SOFT PITCH LINKS

FIGURE 8.177 TORQUE TUBE TORSION - HARMONIC CONTENT FOR BASELINE & SOFT PITCH LINKS

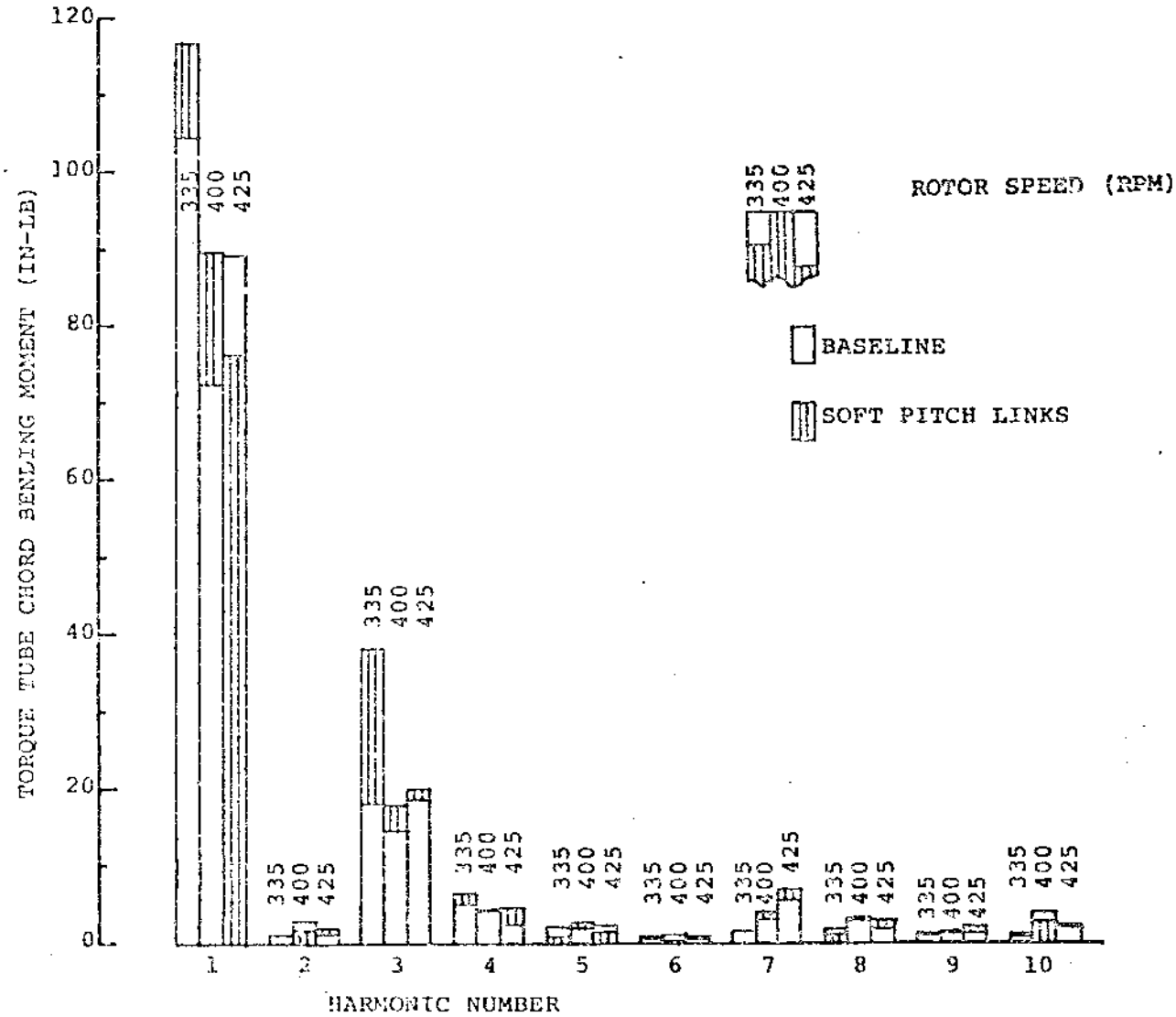

FIGURE 8.178 TORQUE TUBE CHORD BENDING - HARMONIC CONTENT FOR BASELINE & SOFT PITCH LINKS

8.2.2.5.2 Effect of Damper Strips

As noted previously, there are similarities between the soft pitch link configuration and the damper strip configuration. Harmonic content for the effect of damper strips is shown in Figures 8.179 - 8.185. The damper strips also show significant reductions in 1/rev flap bending (station 10.5 and 44), changes in 1/rev and 3/rev chord bending whose direction is dependent upon the operating rotor speed, and the lack of a direct correspondence between vibratory pitch link load and torque tube torsion.

On the other hand, the pitch link vibratory content shows substantially less change relative to the baseline configuration.

For both configurations, the significant torque tube chord bending is limited to 1/rev and 3/rev moments.

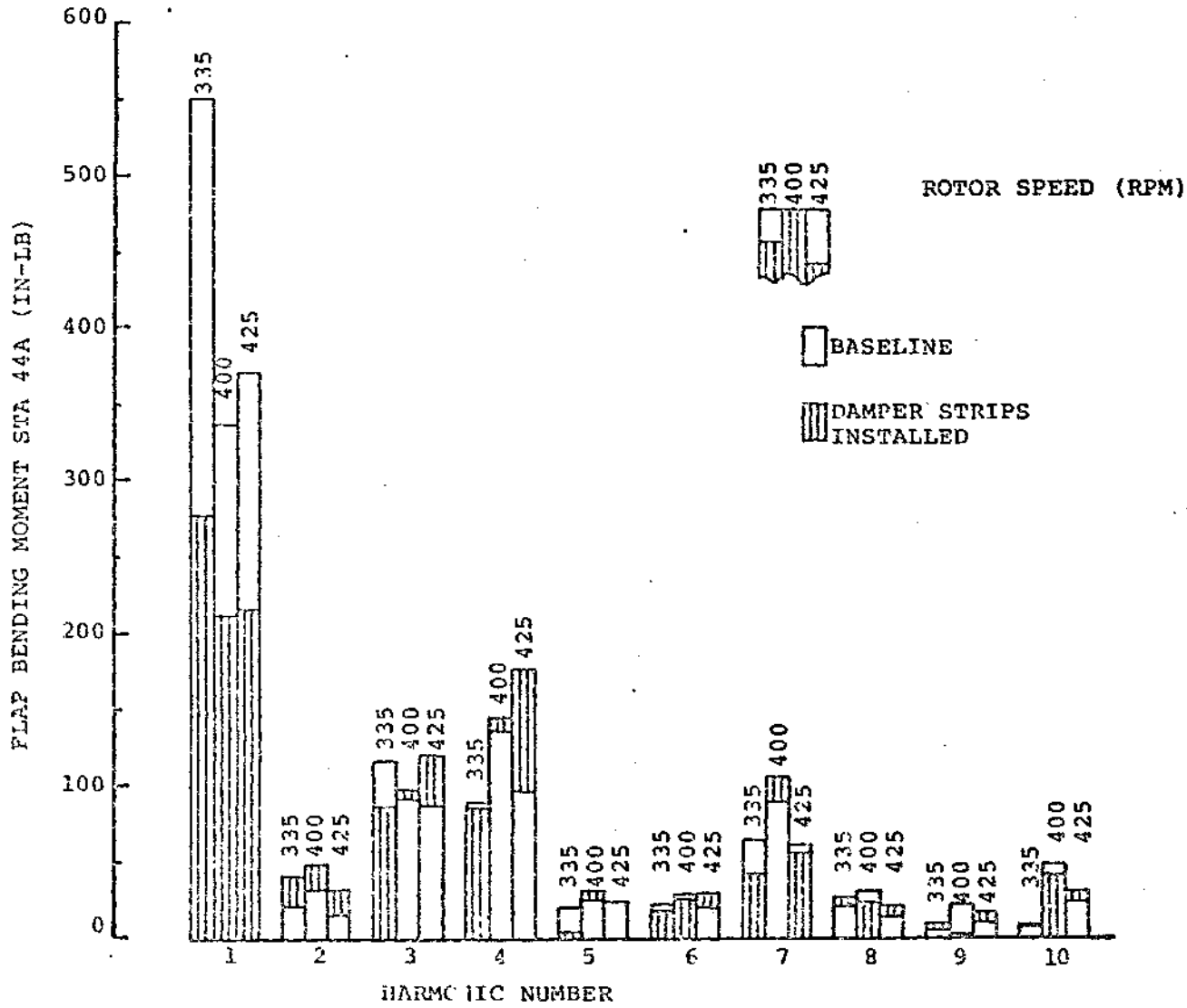

FIGURE 8.179 FLAP BENDING STATION 44 BEAM A - HARMONIC CONTENT FOR BASELINE & DAMPER STRIPS INSTALLED

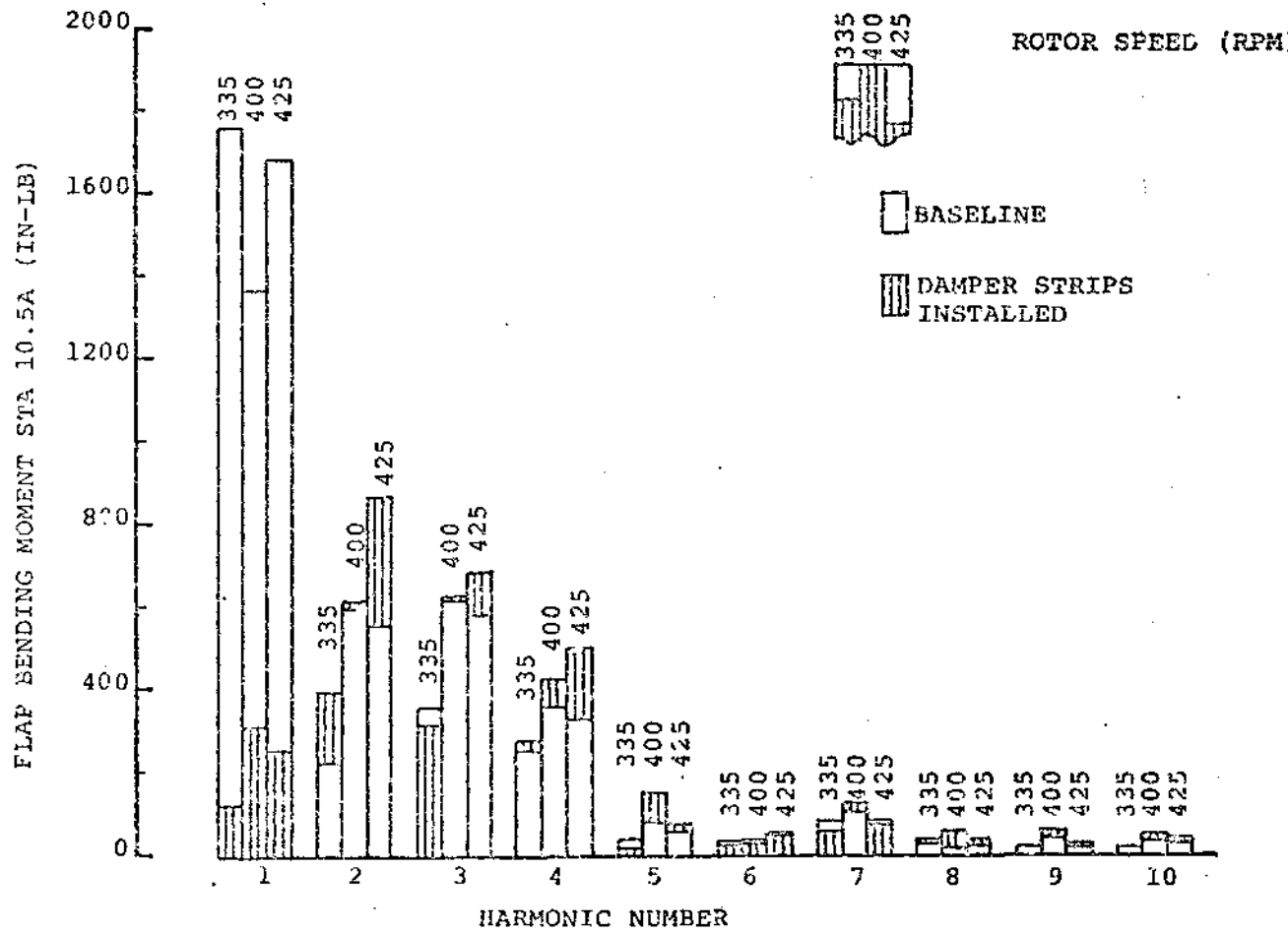

FIGURE 8.180 FLAP BENDING STATION 10.5 BEAM A - HARMONIC CONTENT FOR BASELINE & DAMPER STRIPS INSTALLED

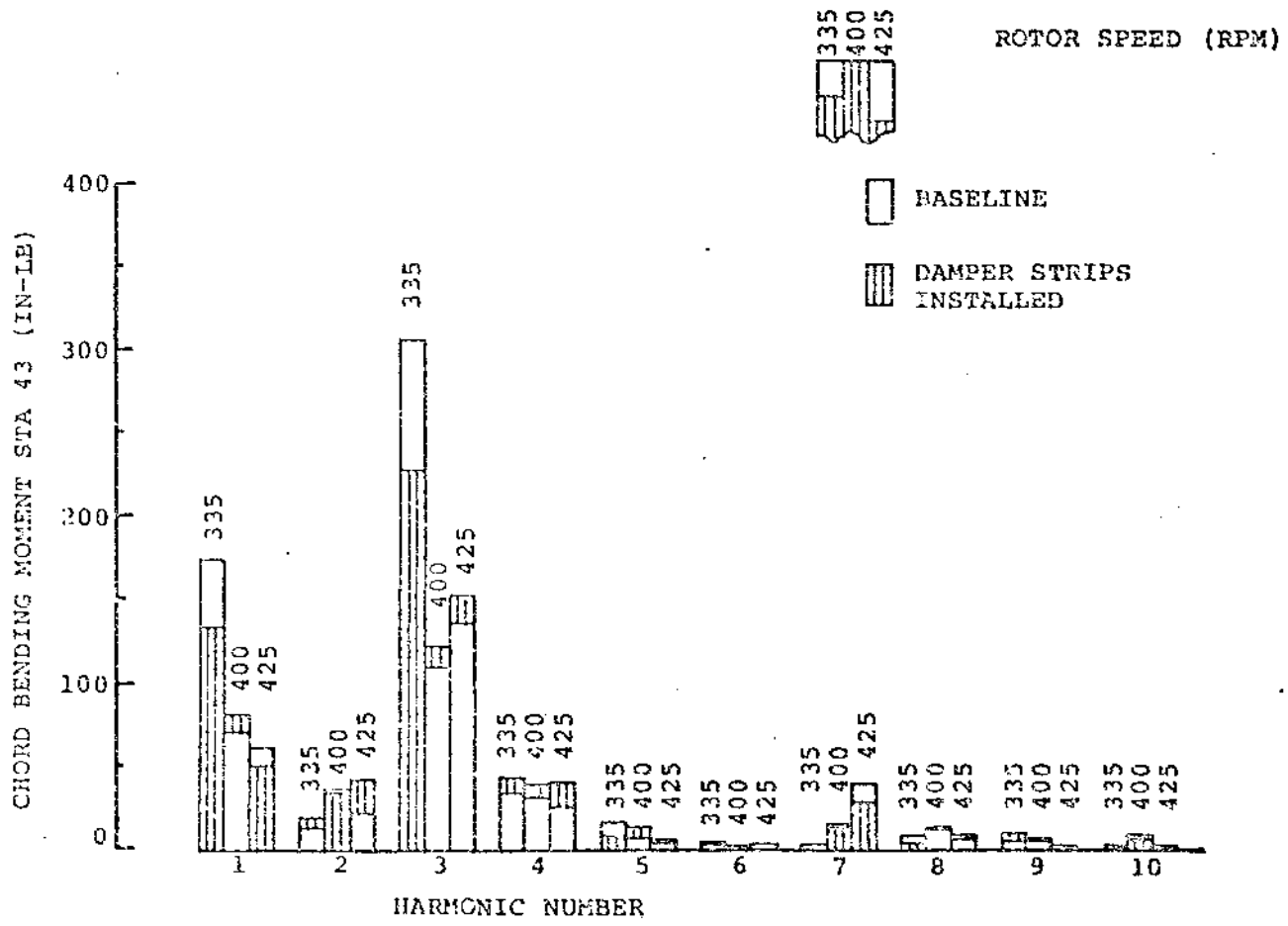

FIGURE 8.181 CHORD BENDING STATION 43 BEAM A - HARMONIC CONTENT FOR BASELINE & DAMPER STRIPS INSTALLED

FIGURE 8.182 CHORD BENDING STATION 11 BEAM A - HARMONIC CONTENT FOR BASELINE & DAMPER STRIPS INSTALLED

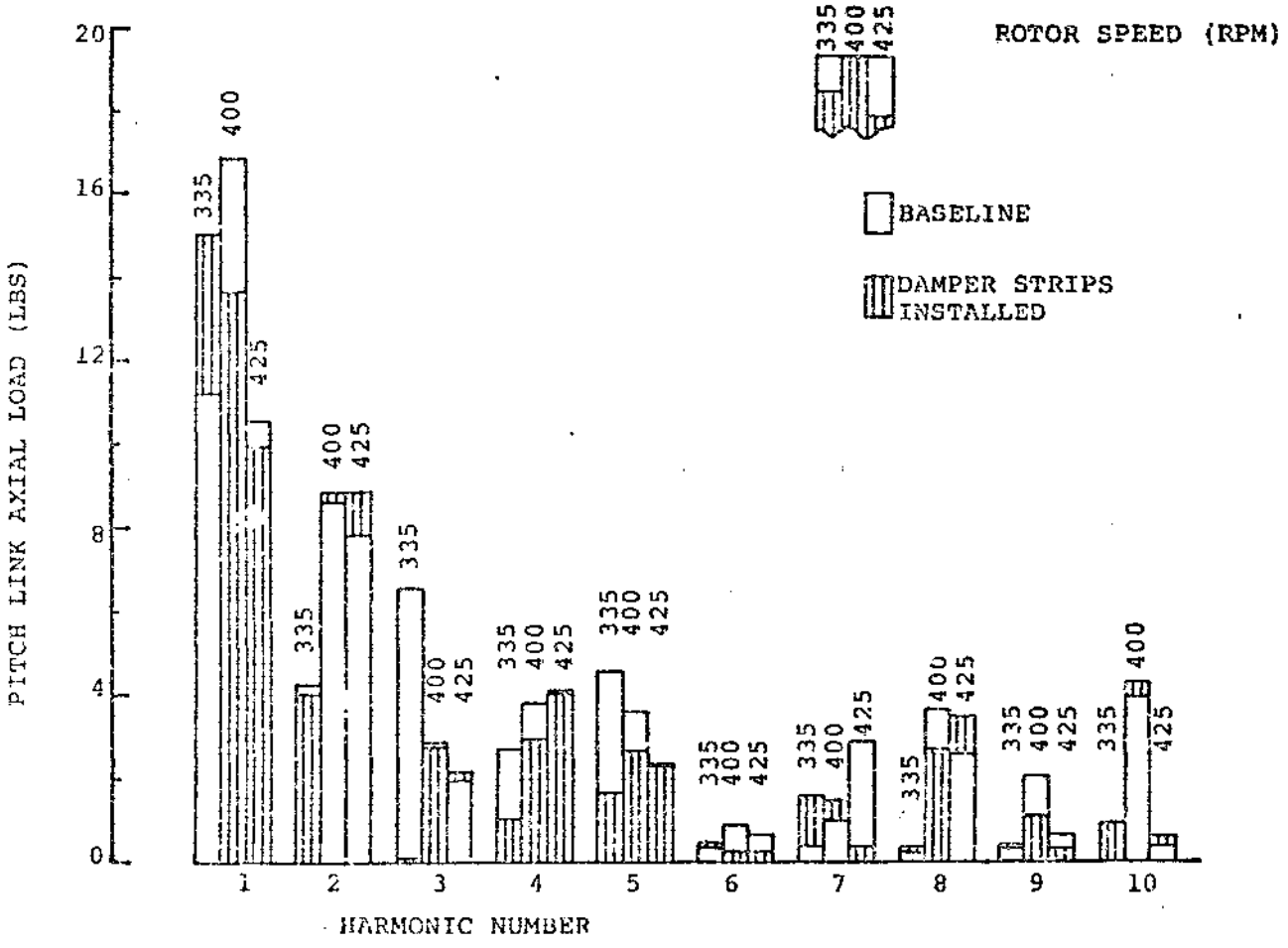

FIGURE 8.183 PITCH LINK AXIAL LOAD - HARMONIC CONTENT FOR BASELINE & DAMPER STRIPS INSTALLED

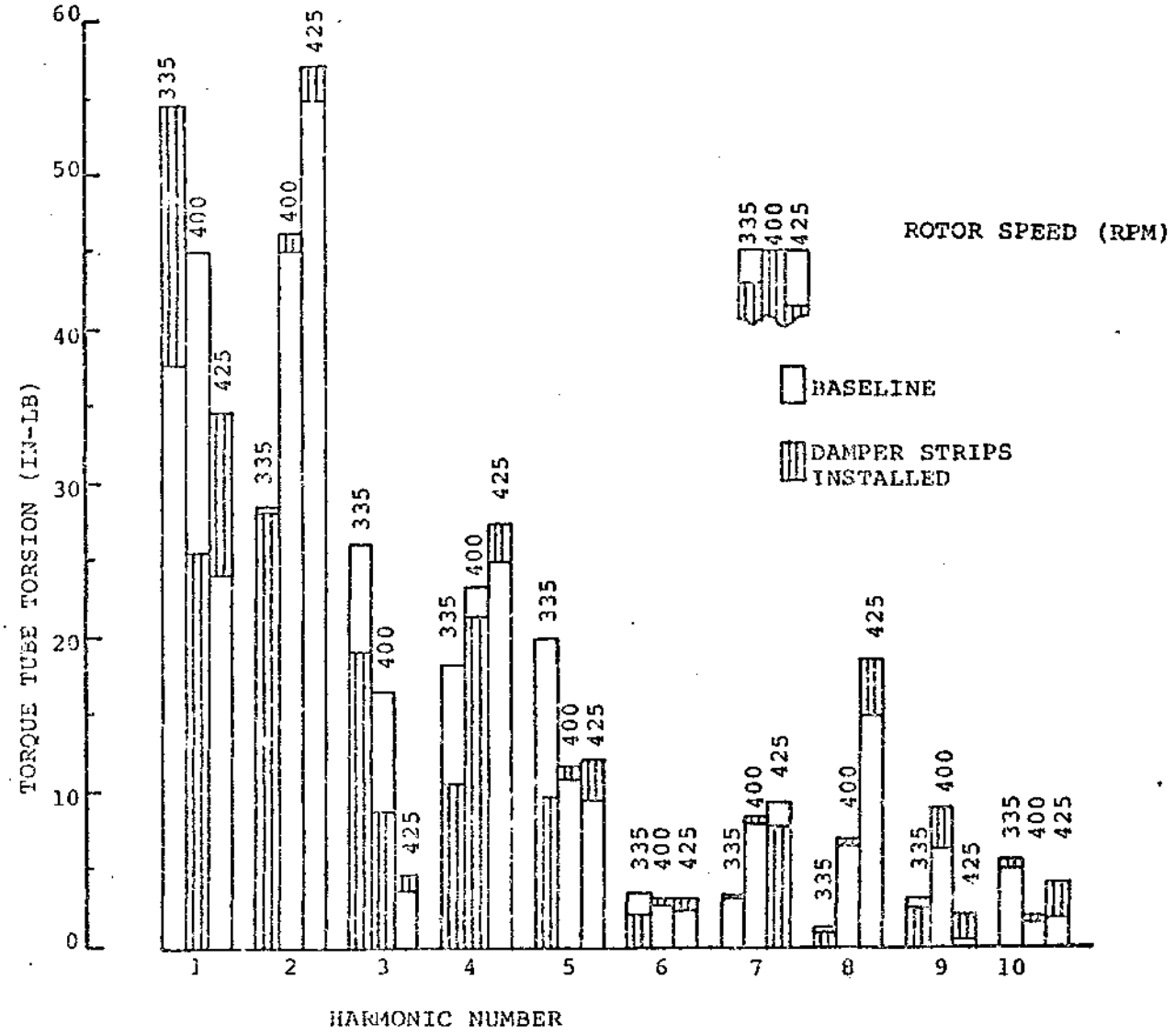

FIGURE 8.184 TORQUE TUBE TORSION - HARMONIC CONTENT FOR BASELINE & DAMPER STRIPS INSTALLED

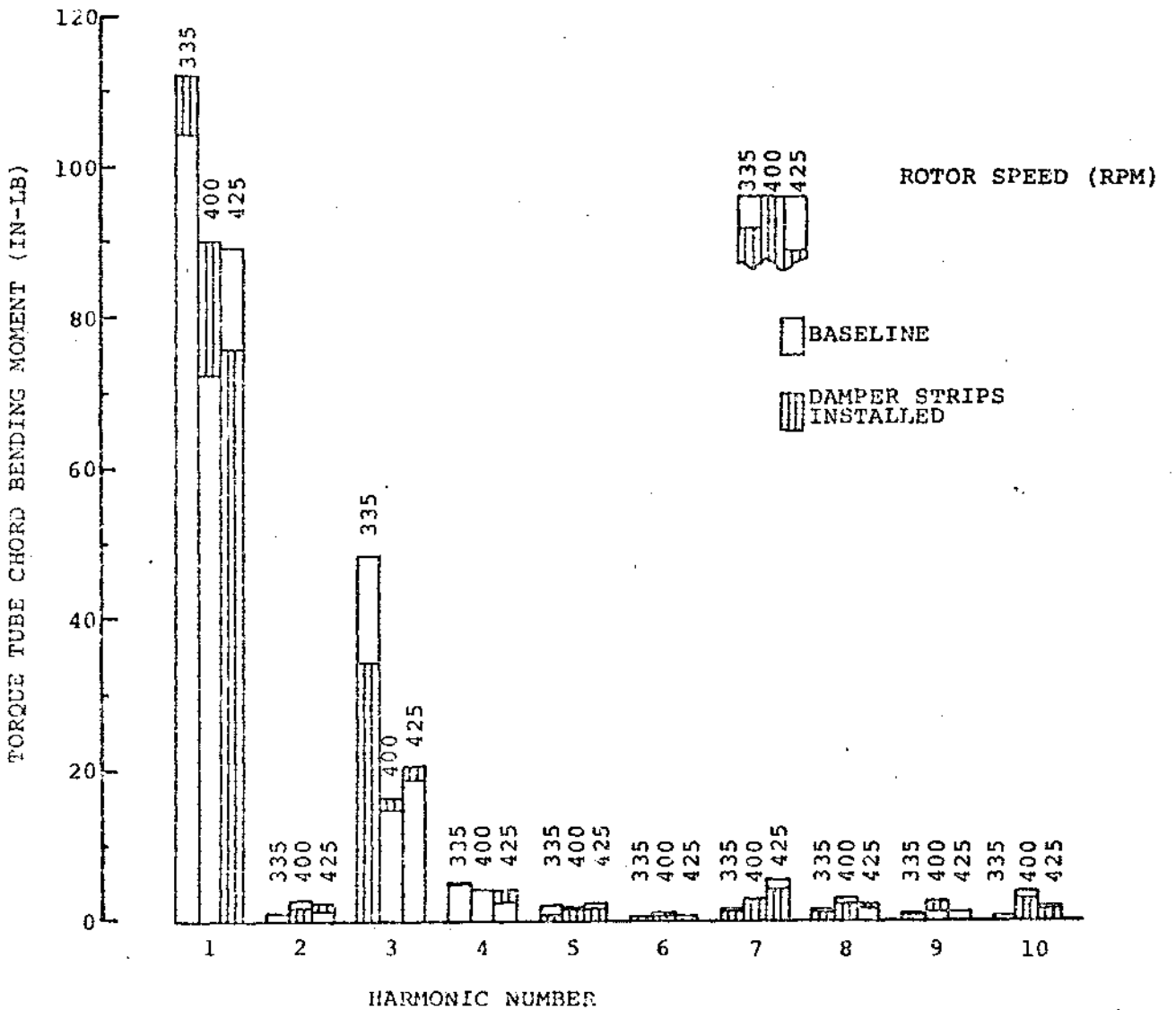

FIGURE 8.185 TORQUE TUBE CHORD BENDING - HARMONIC CONTENT FOR BASELINE & DAMPER STRIPS INSTALLED

8.2.2.5.3 Effect of Balance Dampers

In evaluating the effect of removing the wind tunnel balance dampers on rotor loads as a function of rotor speed, no significant trends were observed. Flap and chord bending moments versus rpm are presented for the inboard and outboard ends of the flexbeams in Figures 8.189 through 8.196.

Figures 8.197 through 8.201 display the effect of removing the balance dampers as a function of collective variation in hover at constant rpm. Only flap bending moments on either side of the blade attachment clevis show significant change. There are two significant effects in vibratory moments. Steady flap bending shows no major change. (Steady FB55 shows no change and is not presented).

One of these changes occurs at the lower end of the collective range (4° with dampers removed versus 4.5° for the baseline). With the dampers removed, there is a substantial increase in flap bending moment at the 4° collective setting. This increase is related to trim as shown in the following table:

Damper Configuration			ON	OFF
Shaft Angle			-10°	-10°
Collective			4.5°	4°
Cyclic	A_1		-0.9°	-0.7°
	B_1		0.1°	0.3°
Fixed System Moments		Pitch	333	-92
(FT-LB)		Roll	-170	-1507

The large discrepancy in roll moments exists only for the 4° collective setting.

The other change is a steeper slope (change in flap bending moment ÷ change in collective) for FB10.5, FB44, and FB55. This change is more pronounced at the stations either side of the blade to flexbeam attachment clevis (FB44 and FB55). It would appear that the balance dampers have an influence on the response of the concentrated mass at the clevis.

Figures 8.202 through 8.206 present steady and vibratory flap bending for stations 7.5 and 44 plus steady flap bending for the blade at station 55 at the 90 knot test condition. Changes in vibratory flapping with balance damper removal are less pronounced than they were in the hover condition. There is a more significant change in steady flap bending moments. Steady flap bending changes in FB7.5 and FB55 would suggest an increase in coning (lift) with the balance dampers removed. Corrected rotor lift values from the static file indicate that higher rotor lifts were obtained for a given collective setting during the testing in which the balance dampers were removed. It appears that there was some shift in the measured actuator position relative to the actual collective setting for this 90 knot collective sweep.

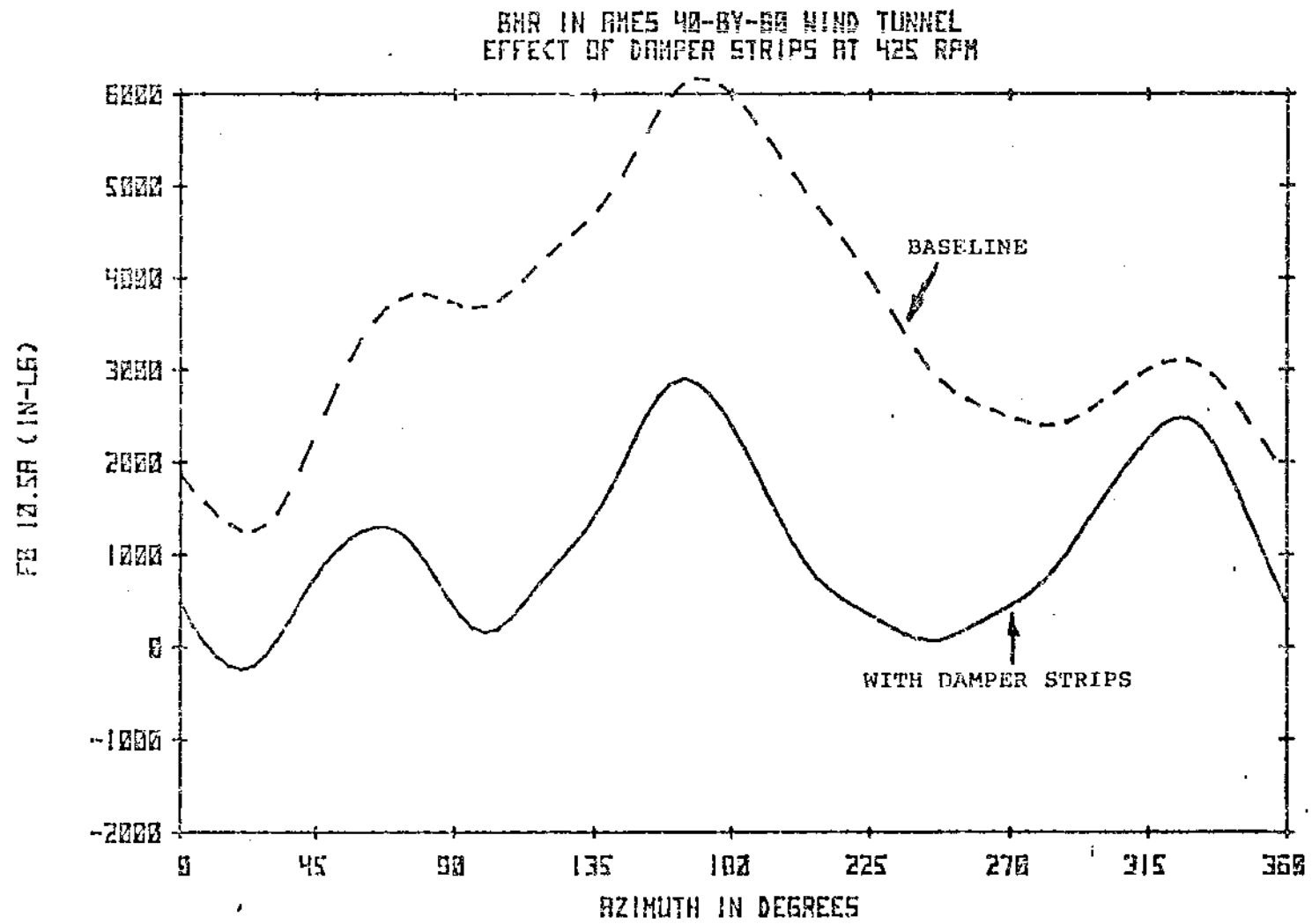

FIGURE 8.186 EFFECT OF DAMPER STRIPS ON FLAP BENDING WAVEFORM AT 425 RPM

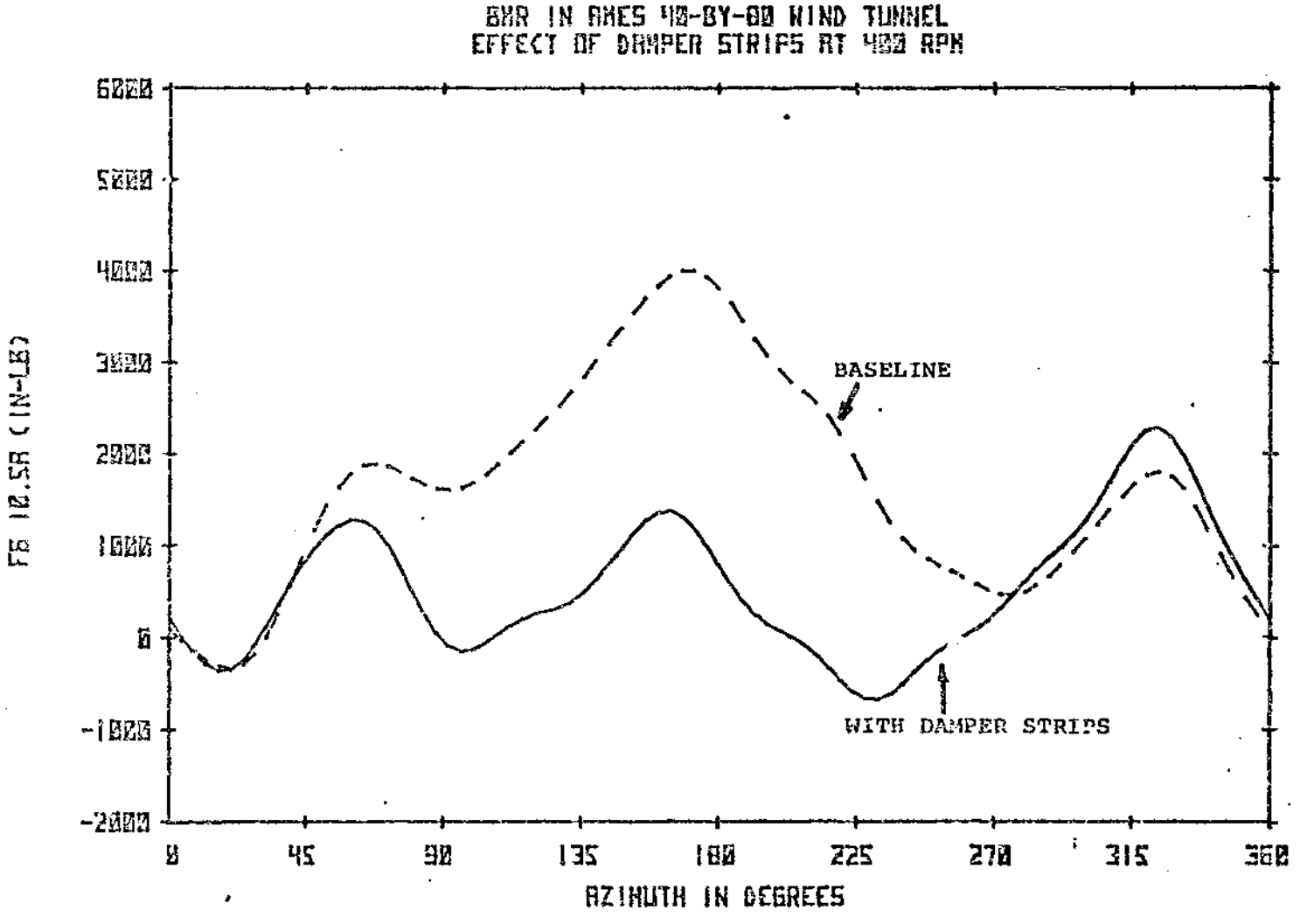

FIGURE 8.187 EFFECT OF DAMPER STRIPS ON FLAP BENDING WAVEFORM AT 400 RPM

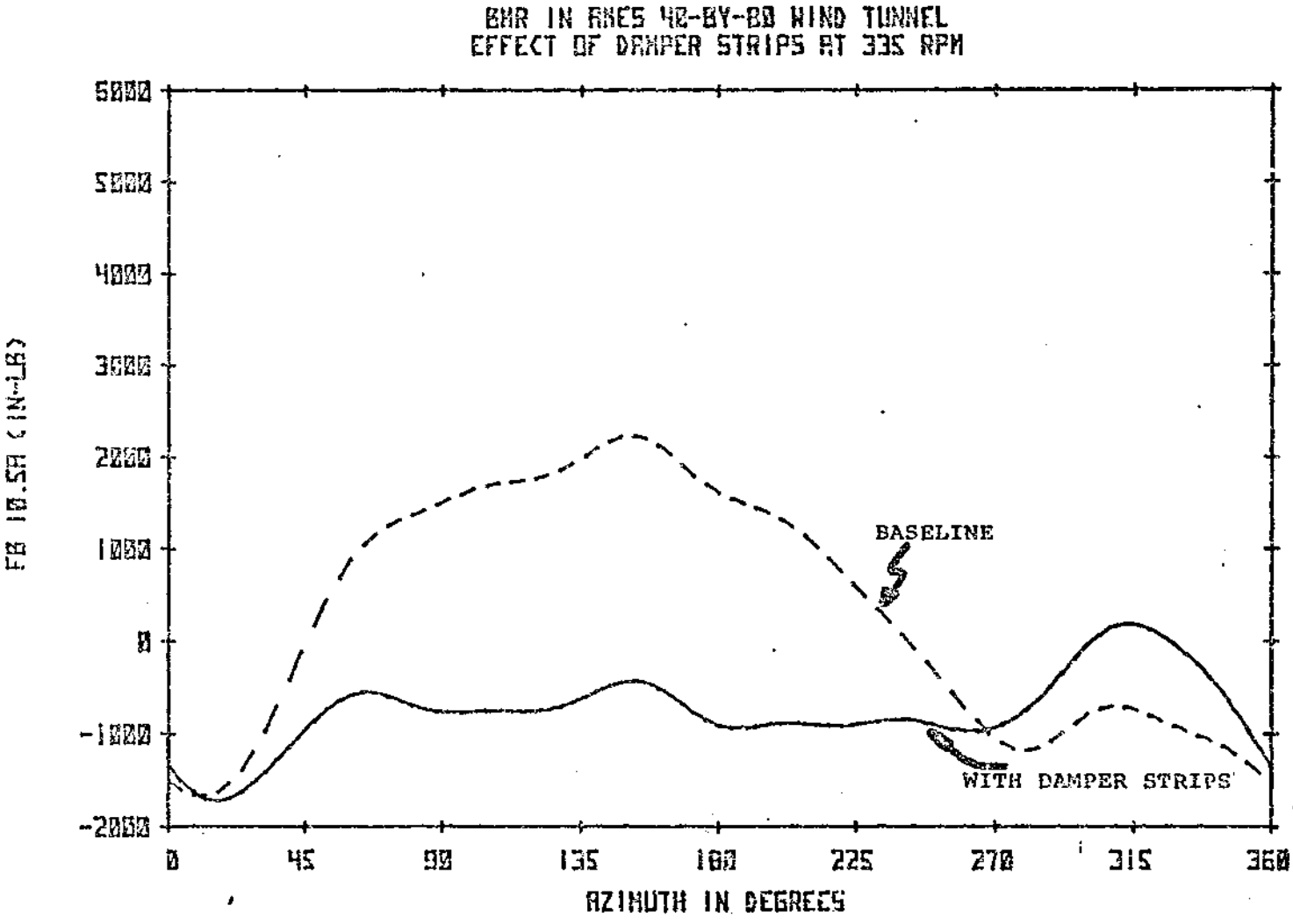

FIGURE 8.180 EFFECT OF DAMPER STRIPS ON FLAP BENDING WAVEFORM AT 335 RPM

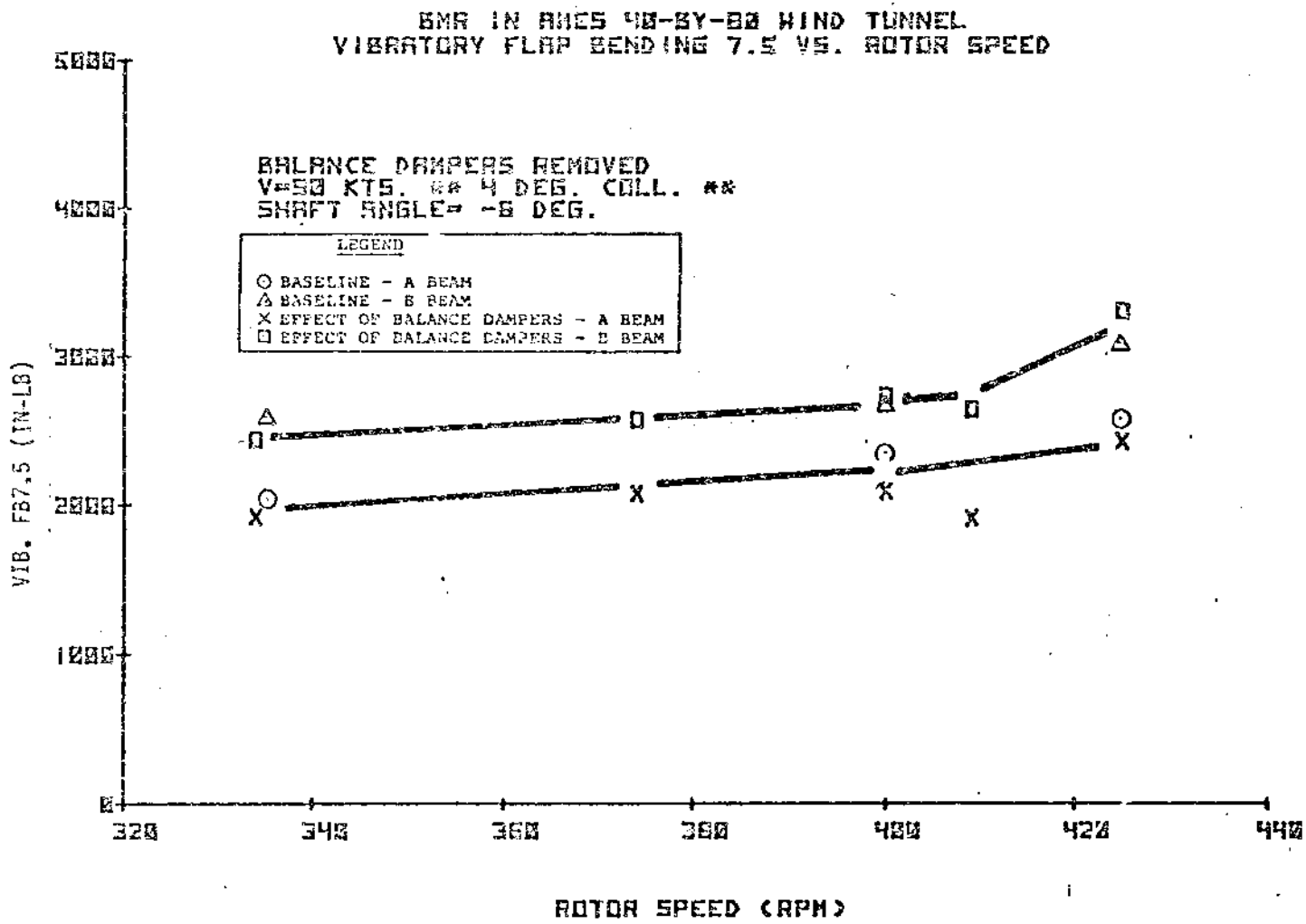

FIGURE 8.189 EFFECT OF BALANCE DAMPERS - VIBRATORY FLAP BENDING 7.5 VERSUS ROTOR SPEED

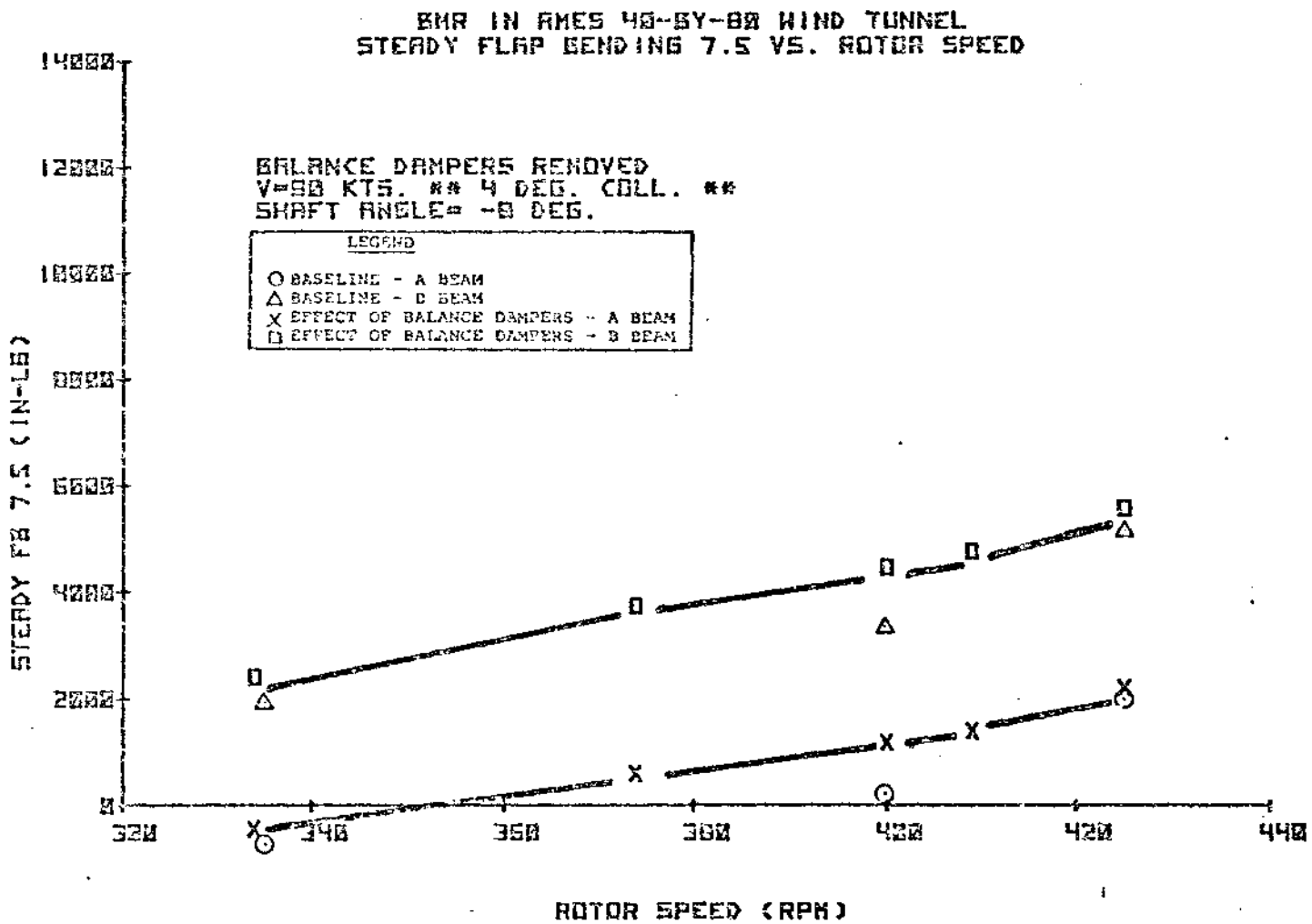

FIGURE 8.190 EFFECT OF BALANCE DAMPERS - STEADY FLAP BENDING 7.5 VERSUS ROTOR SPEED

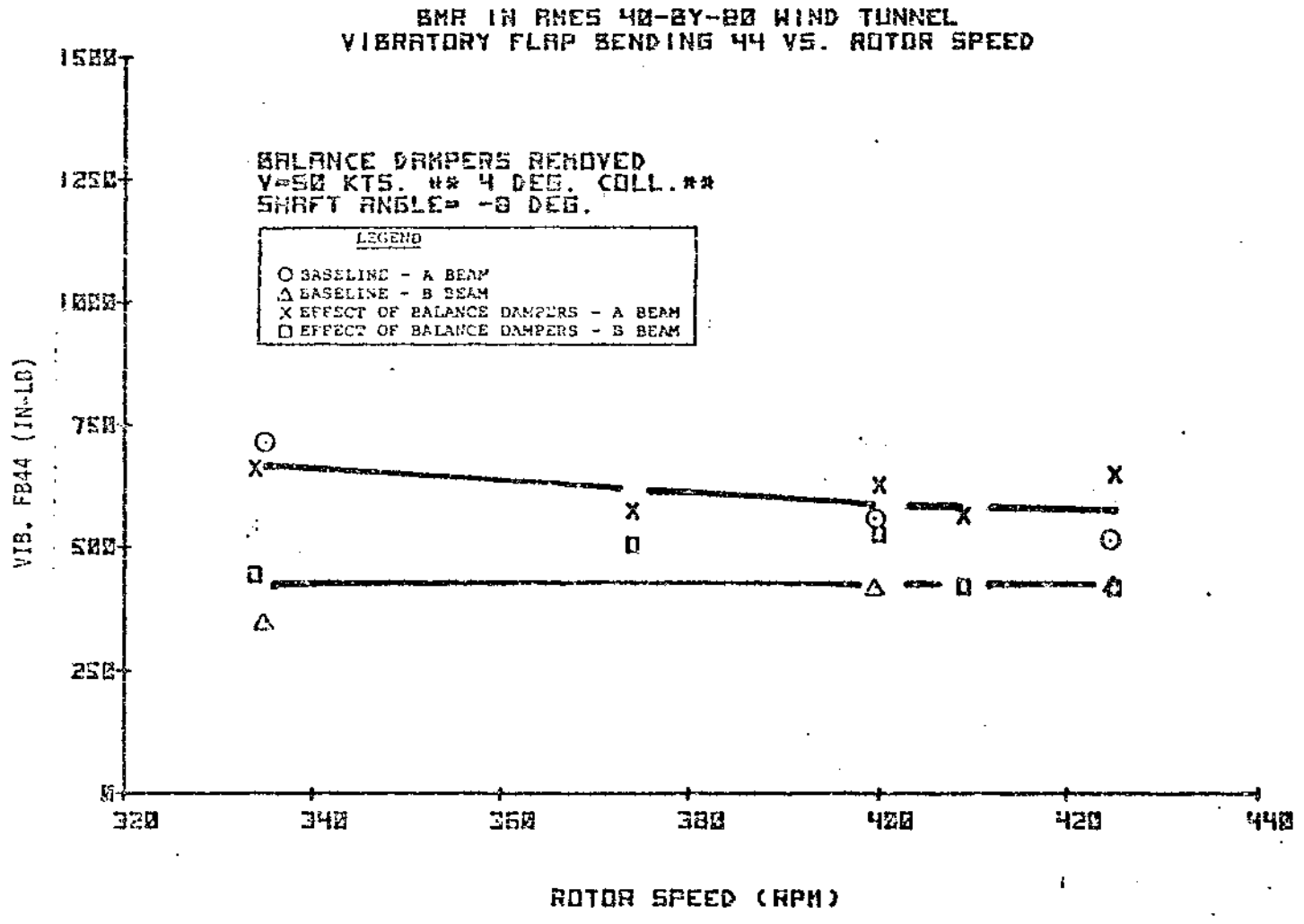

FIGURE 8.191 EFFECT OF BALANCE DAMPERS - VIBRATORY FLAP BENDING 44 VERSUS ROTOR SPEED

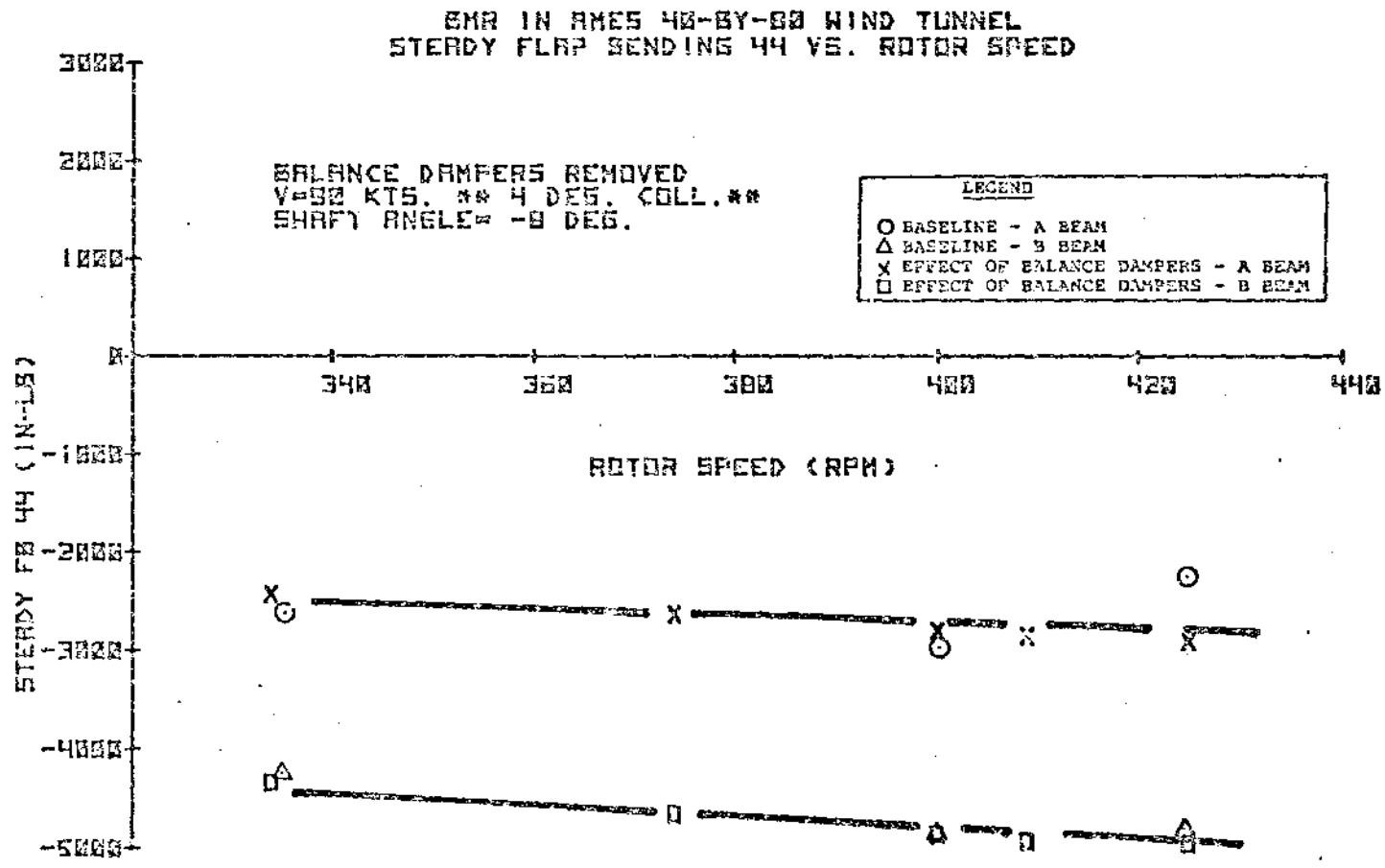

FIGURE 8.192 EFFECT OF BALANCE DAMPERS - STEADY FLAP BENDING 44 VERSUS ROTOR SPEED

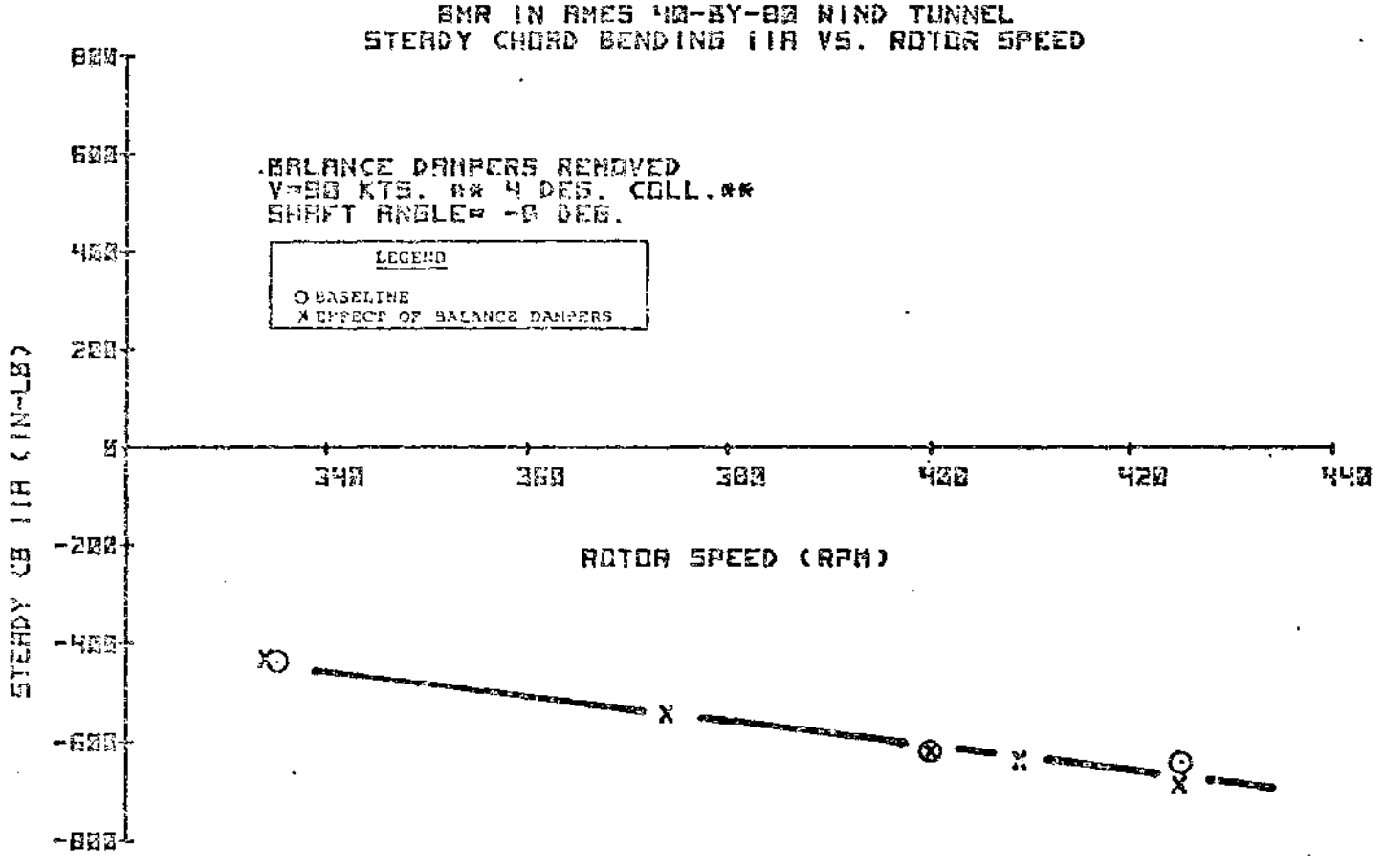

FIGURE 3.193 EFFECT OF BALANCE DAMPERS - STEADY CHORD BENDING 11A VERSUS ROTOR SPEED

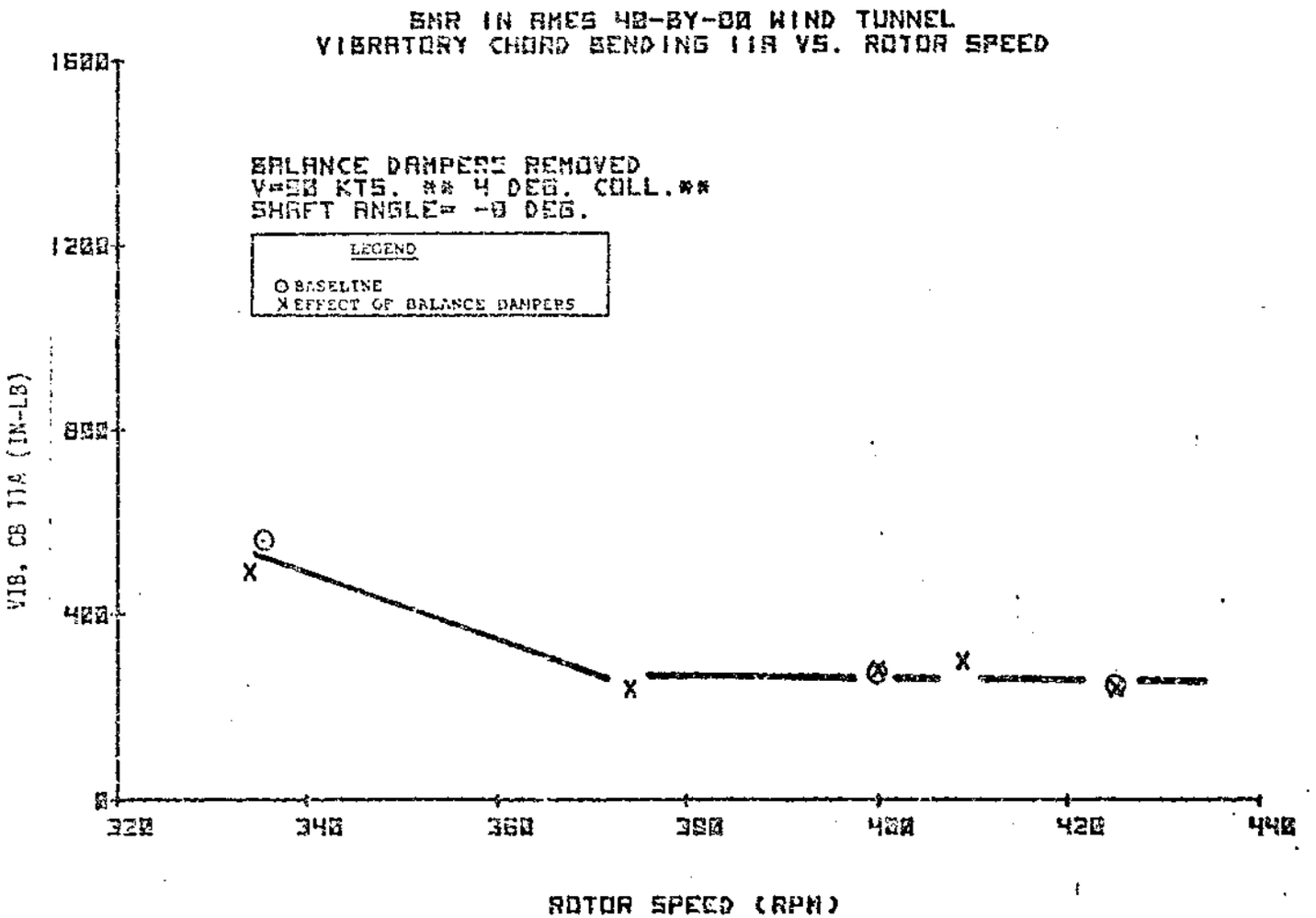

FIGURE 8.194 EFFECT OF BALANCE DAMPERS - VIBRATORY CHORD BENDING 11A VERSUS ROTOR SPEED

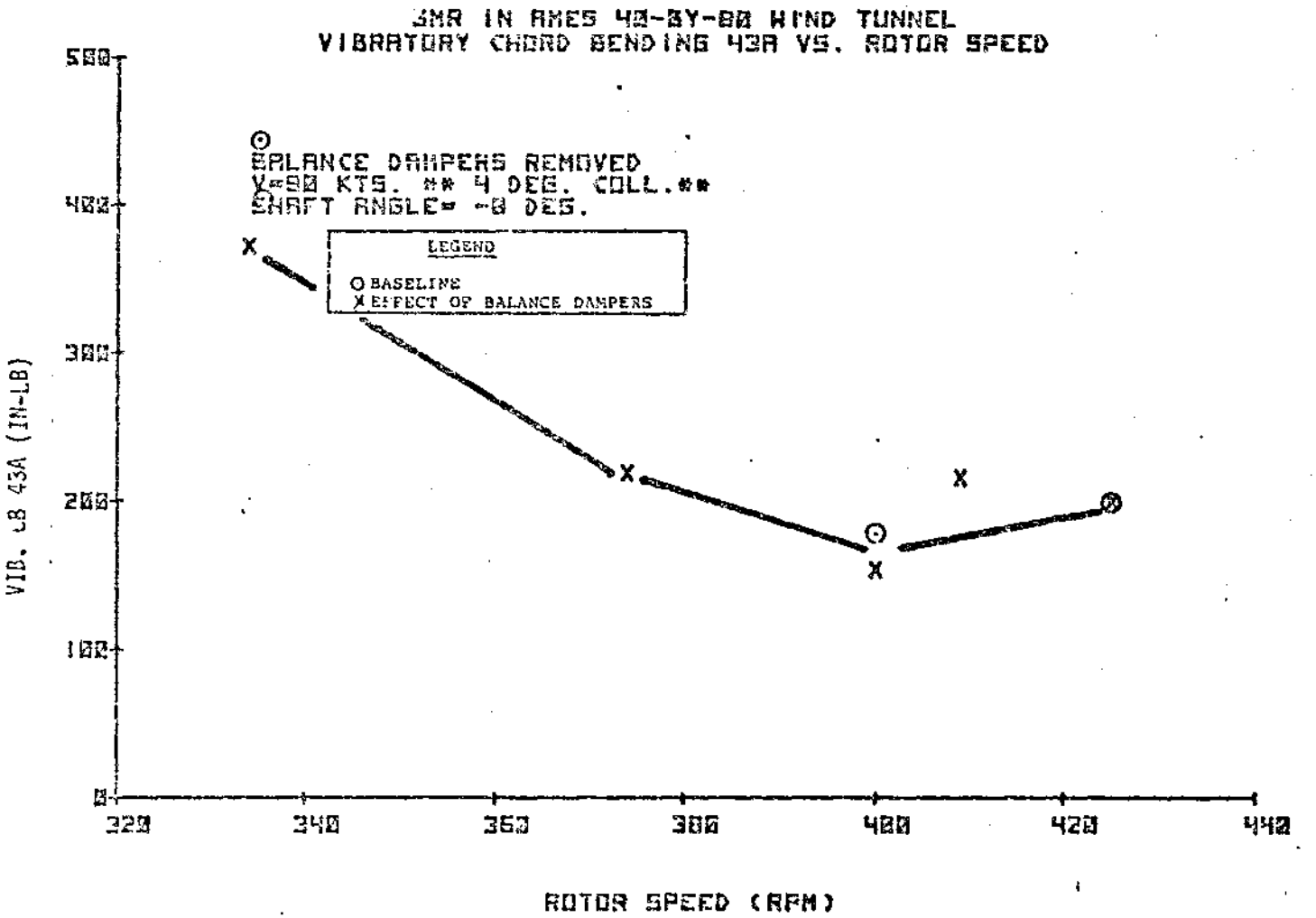

FIGURE 8.195 EFFECT OF BALANCE DAMPERS - VIBRATORY CHORD BENDING 43A VERSUS ROTOR SPEED

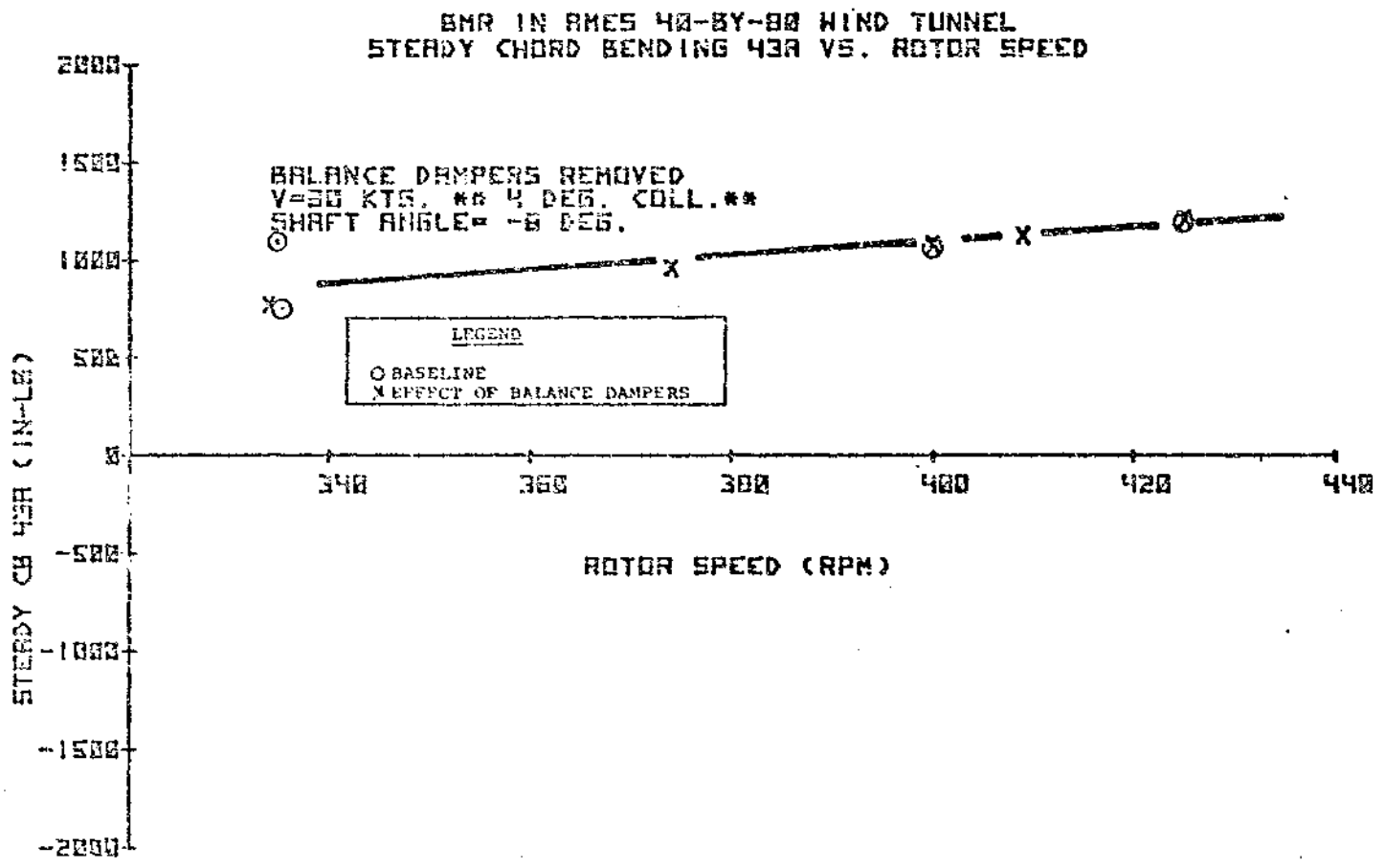

FIGURE 8.196 EFFECT OF BALANCE DAMPERS - STEADY CHORD BENDING 43A VERSUS ROTOR SPEED

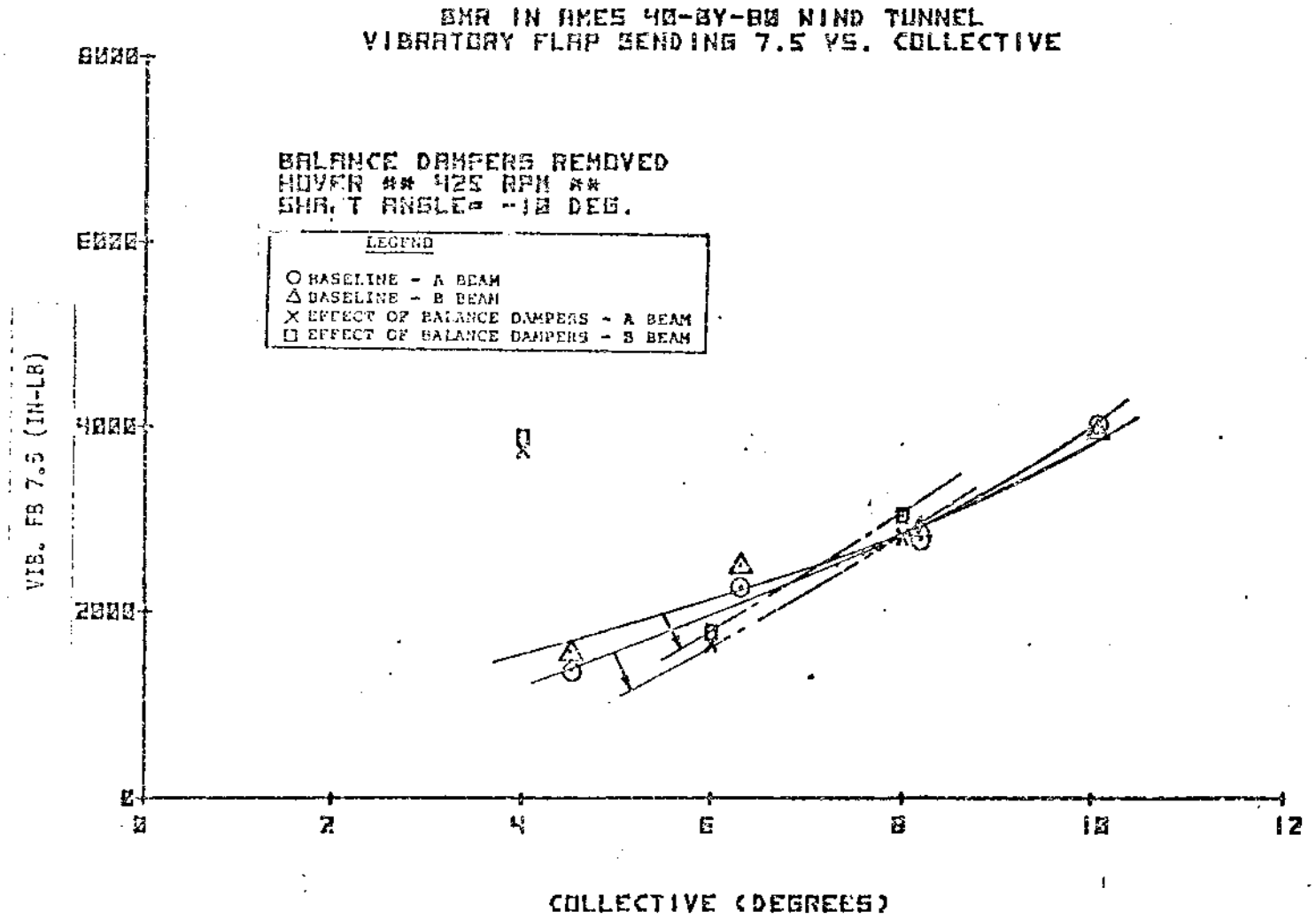

FIGURE 8.197 EFFECT OF BALANCE DAMPERS - VIBRATORY FLAP BENDING 7.5 VERSUS COLLECTIVE

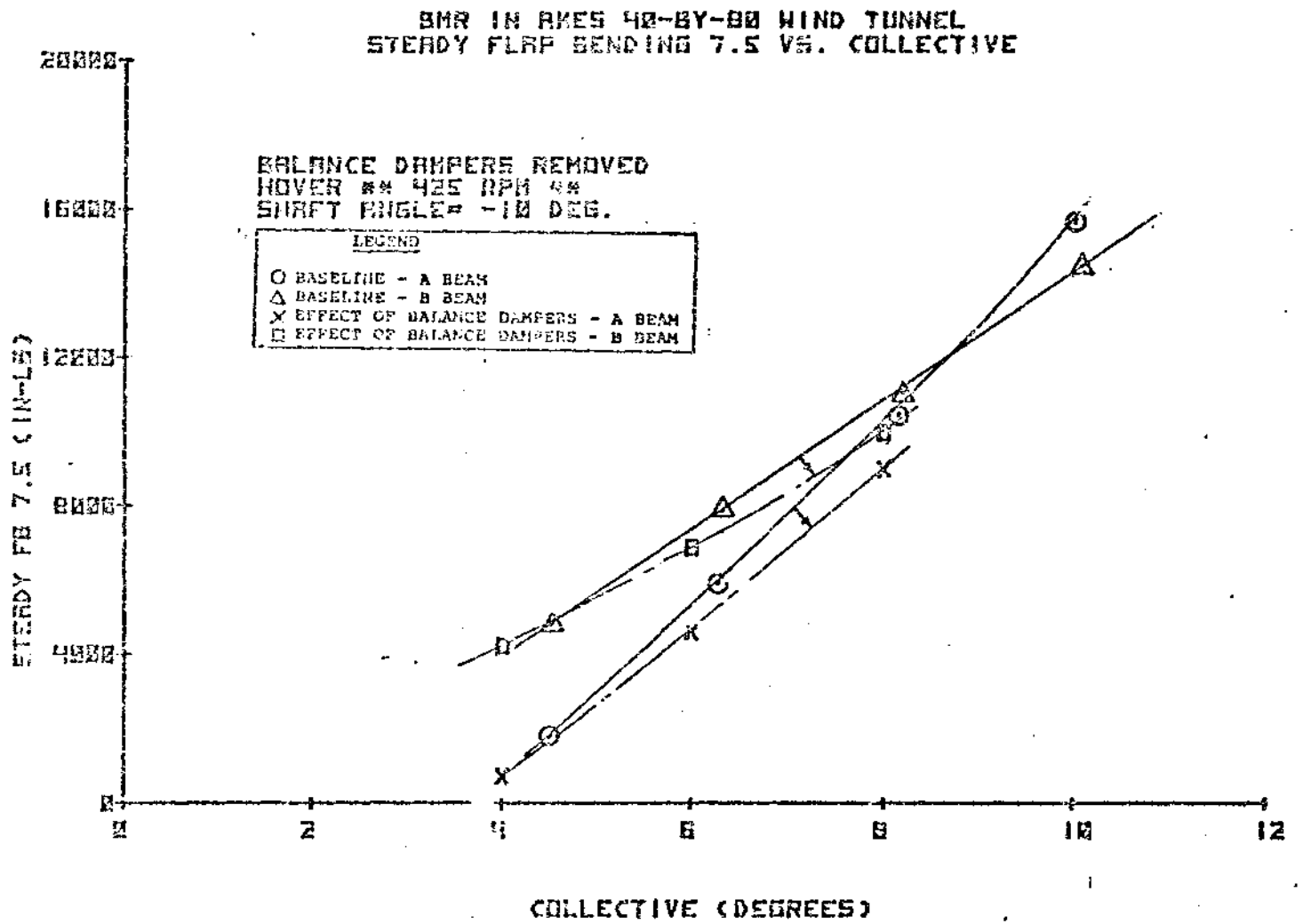

FIGURE 8.198 EFFECT OF BALANCE DAMPERS - STEADY FLAP BENDING 7.5 VERSUS COLLECTIVE

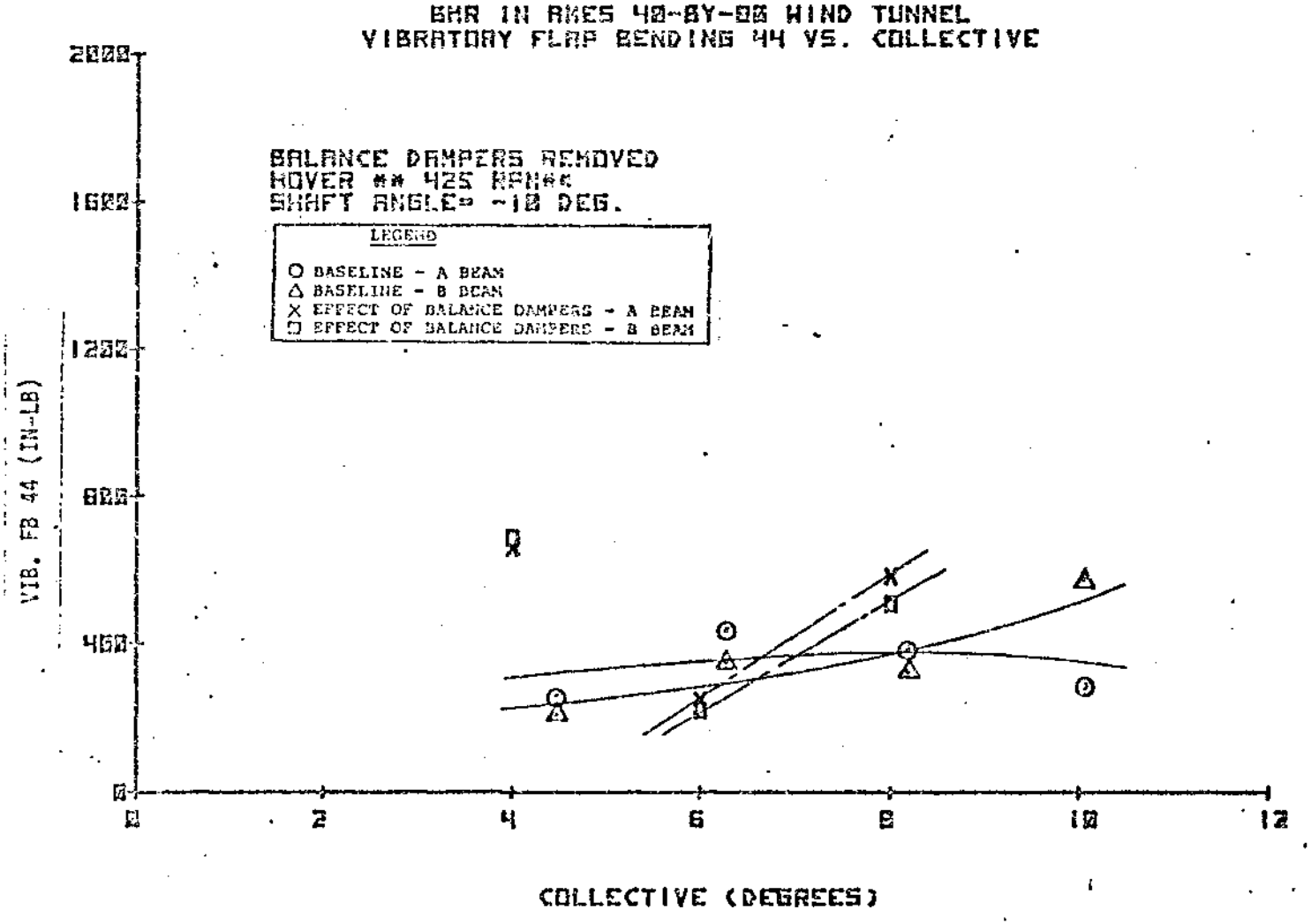

FIGURE 8.199 EFFECT OF BALANCE DAMPERS - VIBRATORY FLAP BENDING 44 VERSUS COLLECTIVE

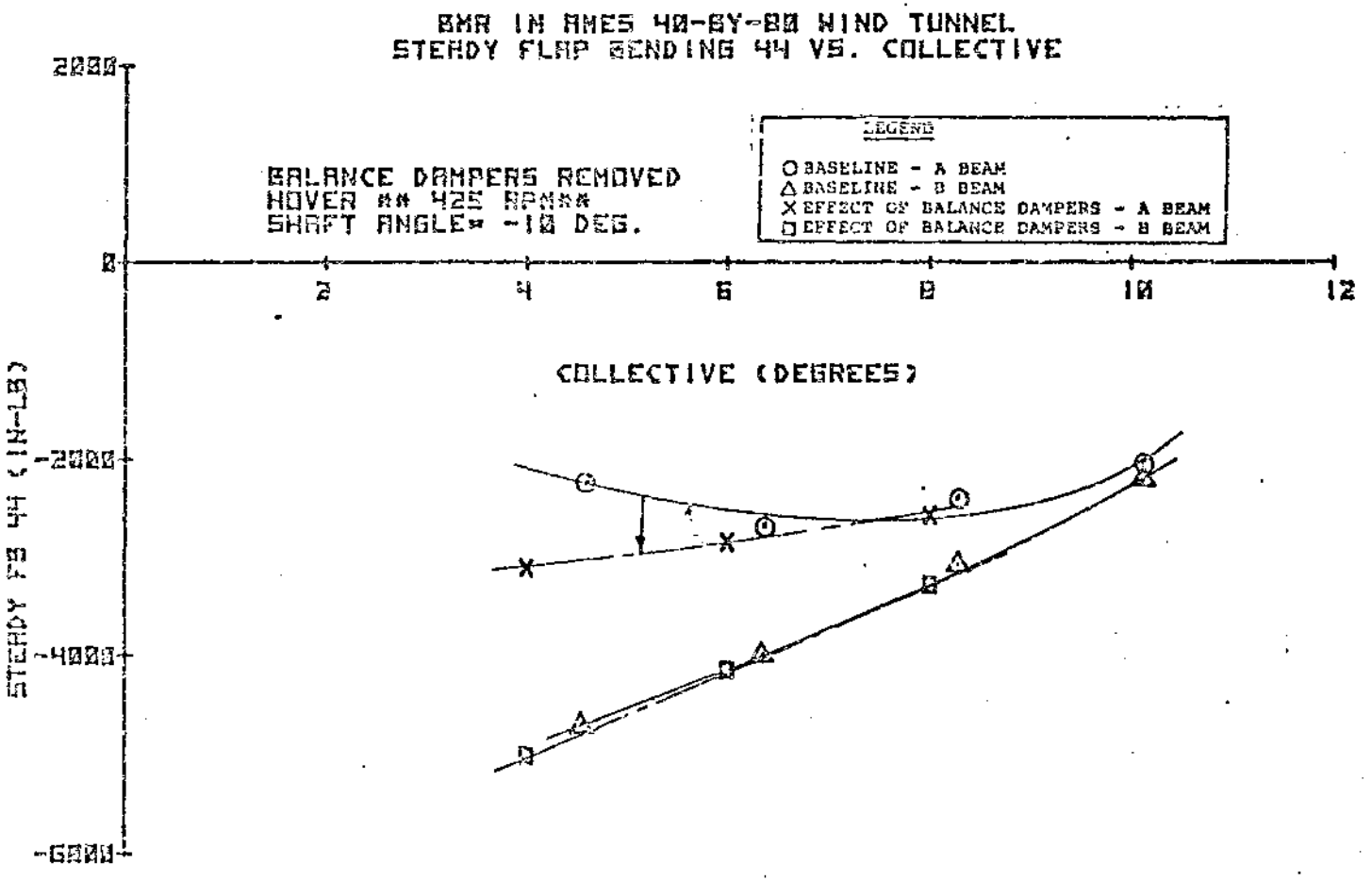

FIGURE 8.200 EFFECT OF BALANCE DAMPERS - STEADY FLAP BENDING 44 VERSUS COLLECTIVE

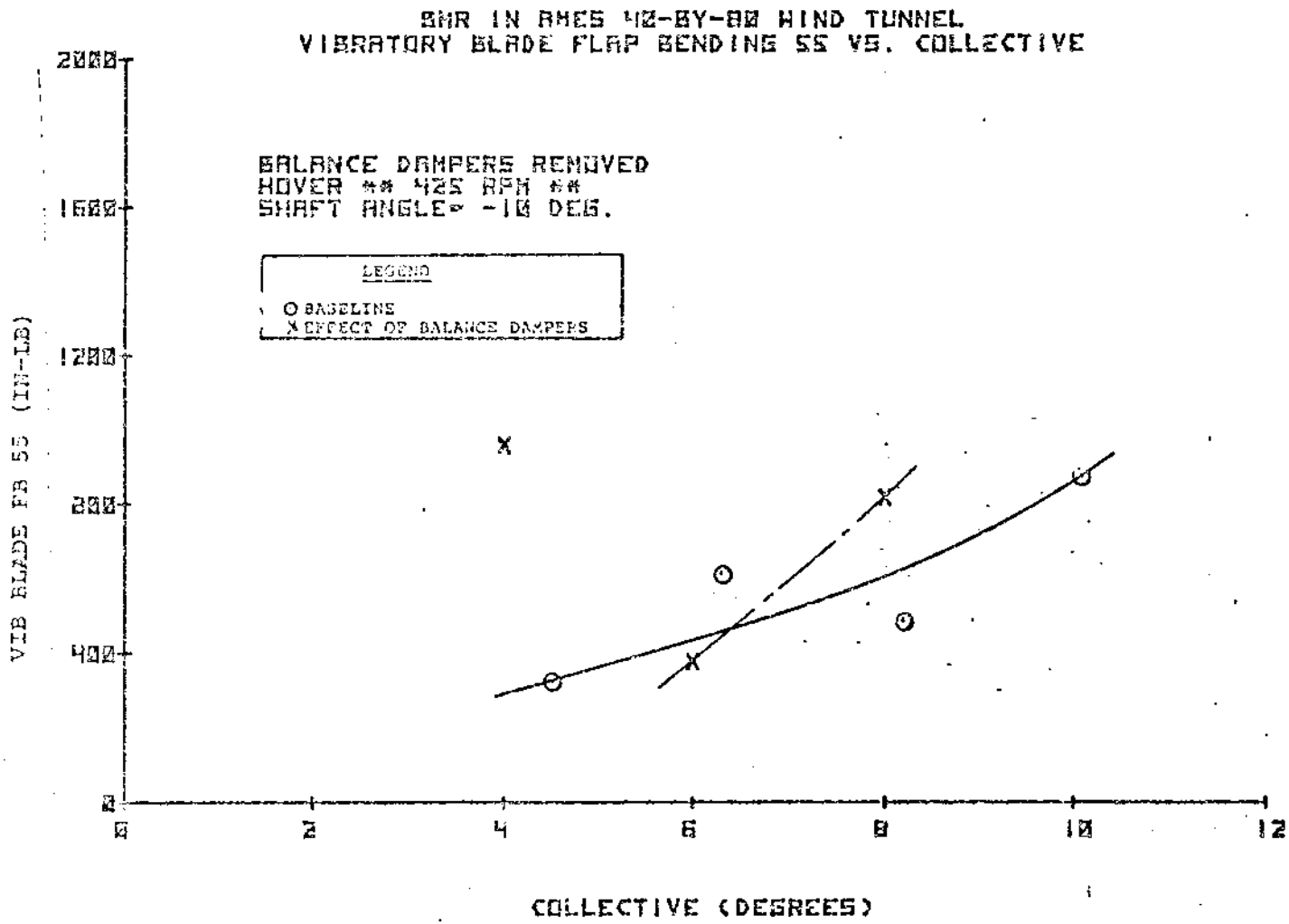

FIGURE 8.201 EFFECT OF BALANCE DAMPERS - VIBRATORY FLAP BENDING 55 VERSUS COLLECTIVE

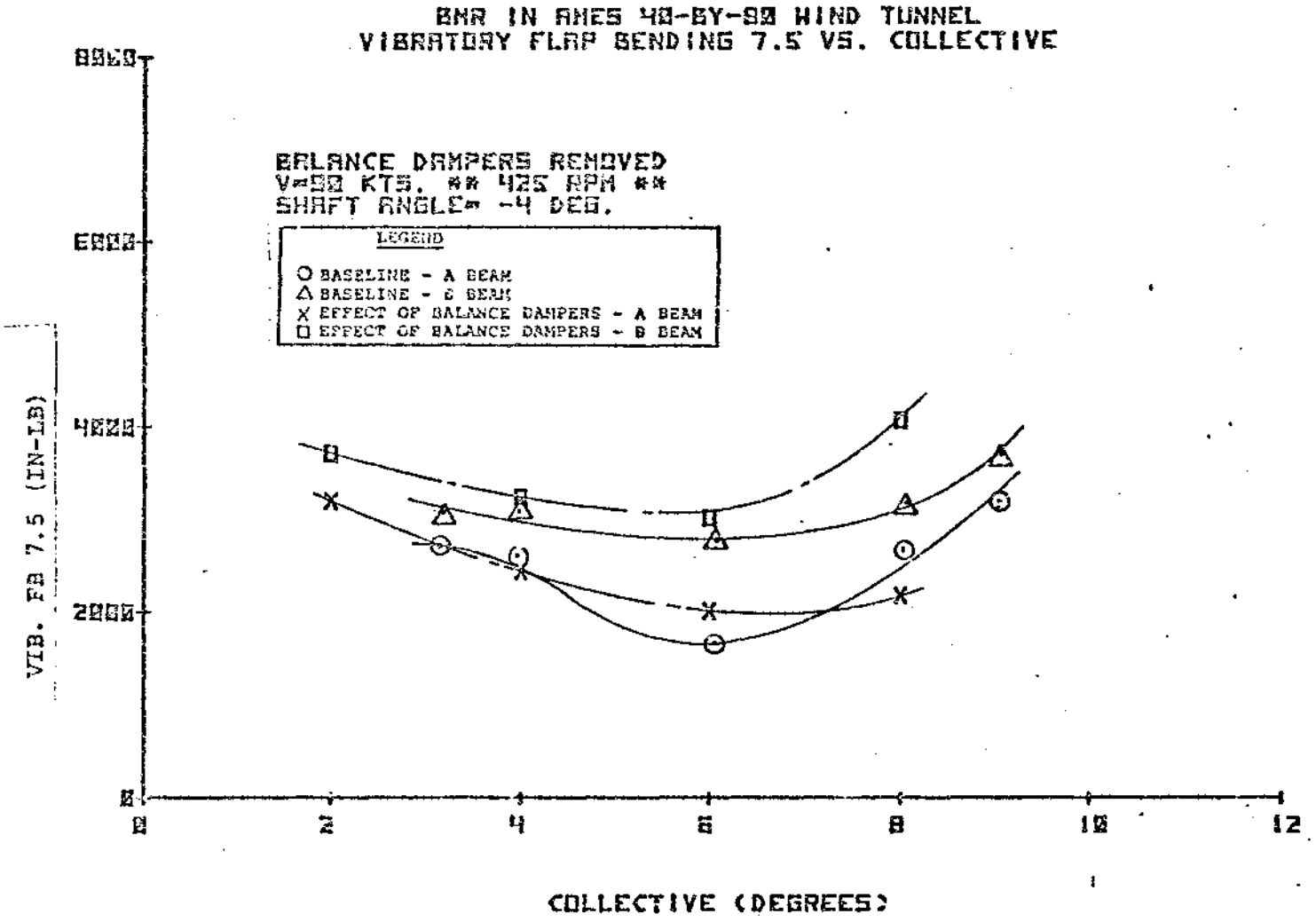

FIGURE 8.202 EFFECT OF BALANCE DAMPERS - VIBRATORY FLAP BENDING 7.5 VERSUS COLLECTIVE

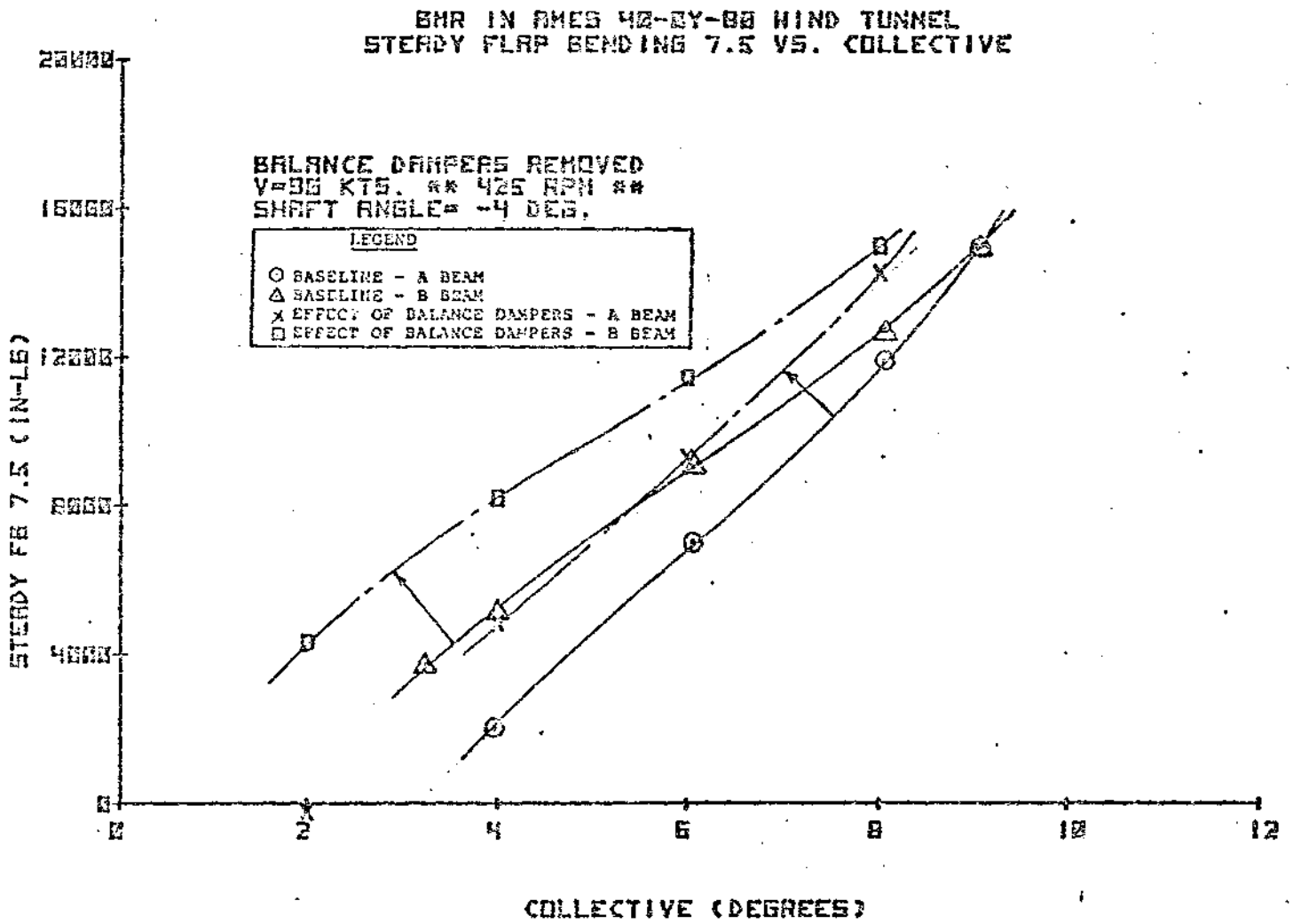

FIGURE 8.203 EFFECT OF BALANCE DAMPERS - STEADY FLAP BENDING 7.5 VERSUS COLLECTIVE

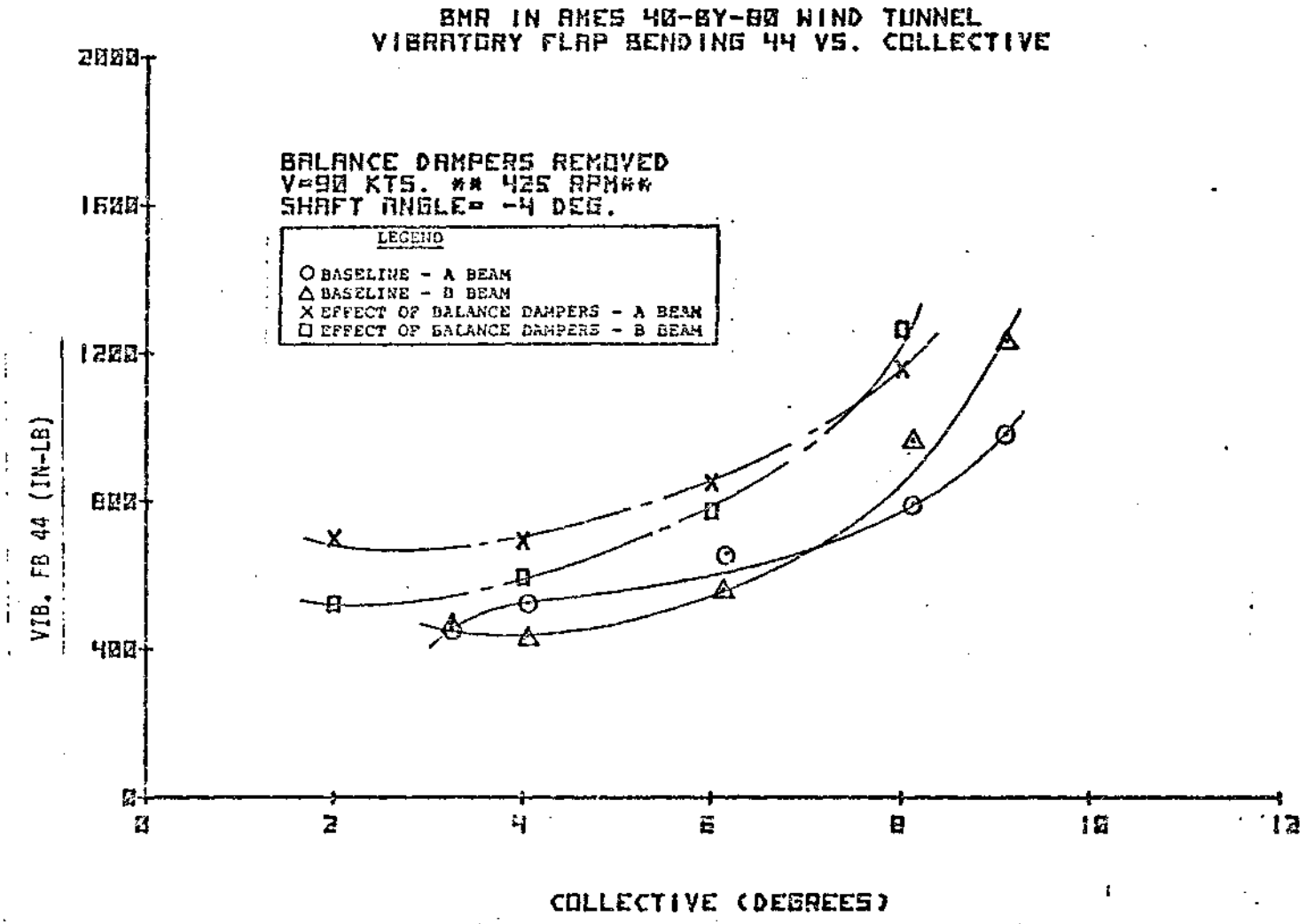

FIGURE 8.204 EFFECT OF BALANCE DAMPERS - VIBRATORY FLAP BENDING 44 VERSUS COLLECTIVE

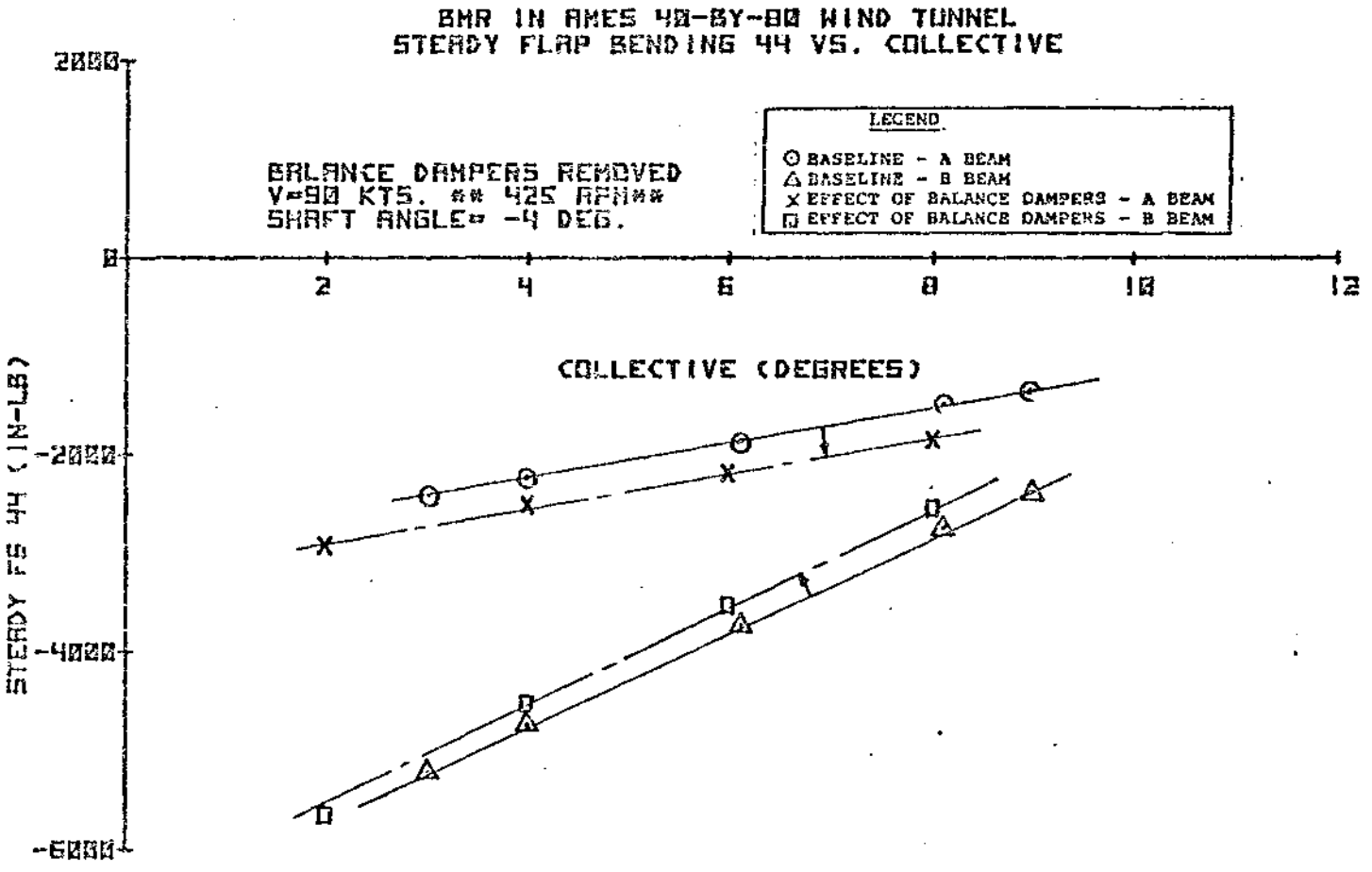

FIGURE 8.205 EFFECT OF BALANCE DAMPERS - STEADY FLAP BENDING 44 VERSUS COLLECTIVE

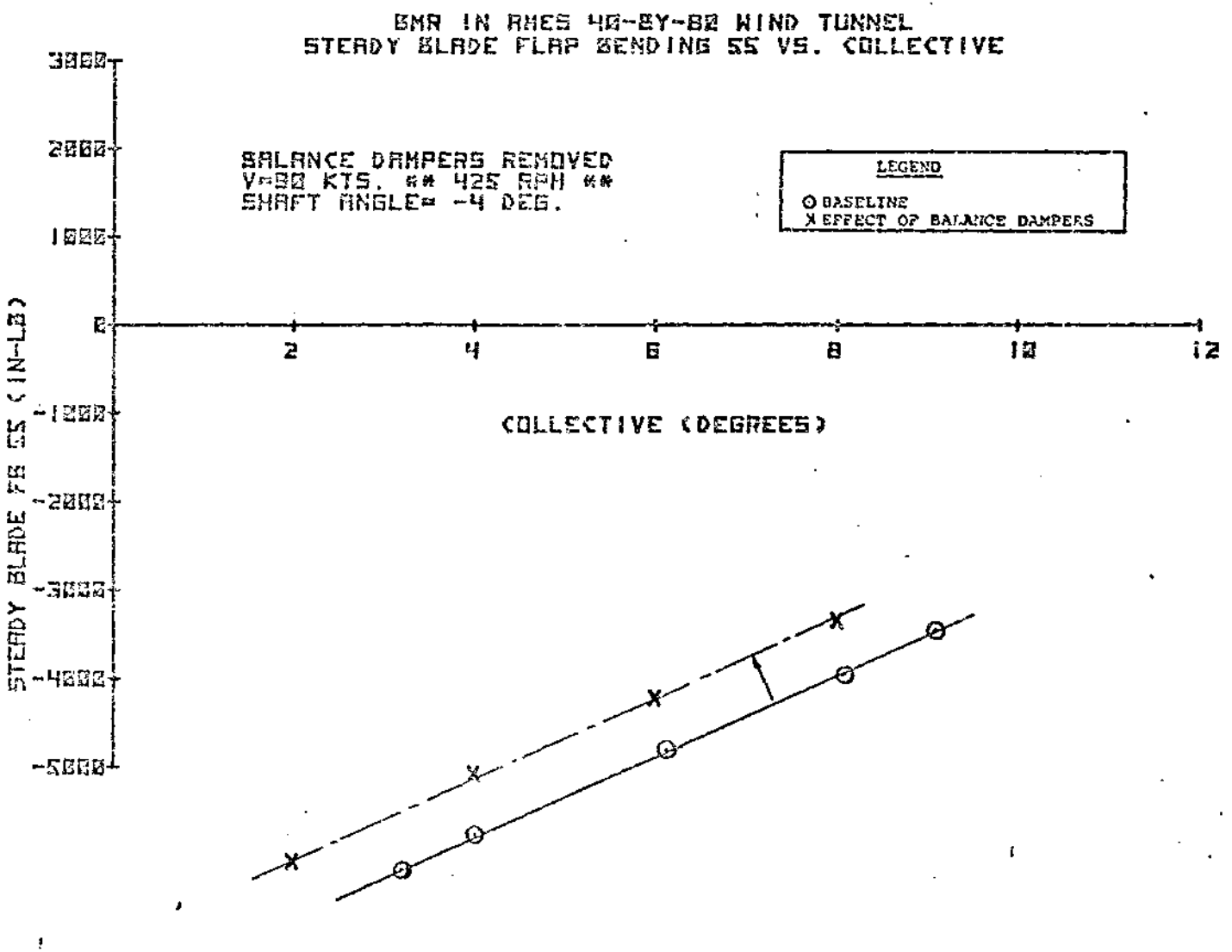

FIGURE 8.206 EFFECT OF BALANCE DAMPERS - STEADY FLAP BENDING 55 VERSUS COLLECTIVE

8.2.3 Correlation With Flight Test Loads

8.2.3.1 Blade Loads

In order to obtain this correlation, control inputs during the test were adjusted to give thrust, propulsive force, and 1/rev flap moments comparable to flight test measurements. The figures in this section present this correlation for a 1G forward flight airspeed sweep.

Blade flapping shows excellent correlation with the exception of steady flap moments at midspan (station 110). The vibratory moment at midspan and moments at the blade root are significantly higher and would be expected to be more reliable. Blade flapping moments are presented in Figures 8.207 through 8.210.

Figures 8.211 through 8.214 present blade chord bending moments. There is relatively good correlation, with the flight test data slightly higher than the wind tunnel data.

Vibratory blade torque shows very good correlation while steady blade torques show somewhat higher nose down pitching for the wind tunnel measurements (Figures 8.215 and 8.216). With the good match in steady blade torque trend with airspeed (neglecting offset), there is a possibility that steady blade torques for flight test are not correctly adjusted for the static 1G strain level.

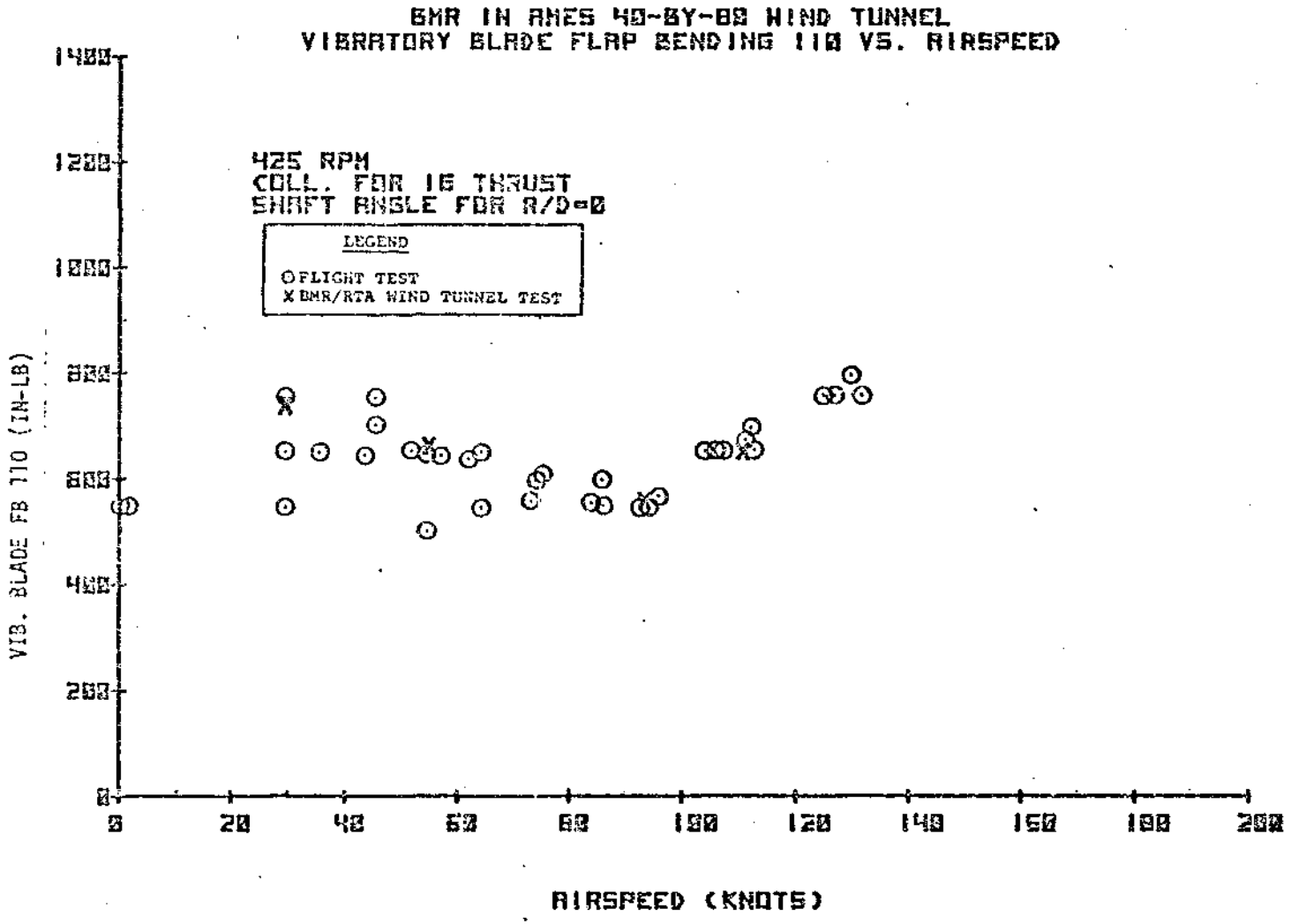

FIGURE 8.207 FLIGHT TEST CORRELATION - VIBRATORY FLAP BENDING 110 VERSUS AIRSPEED

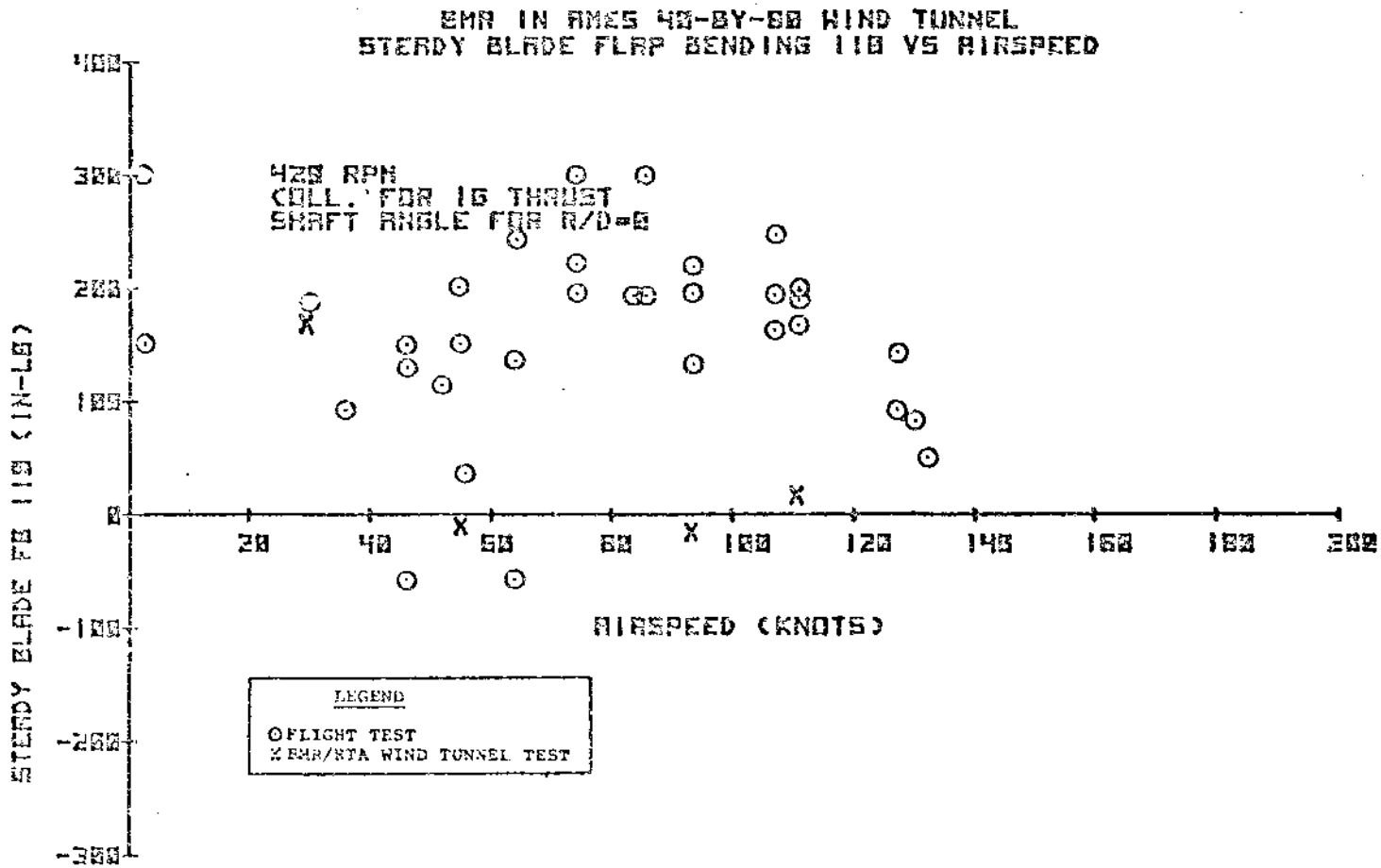

FIGURE 8.208 FLIGHT TEST CORRELATION - STEADY FLAP BENDING 110 VERSUS AIRSPEED

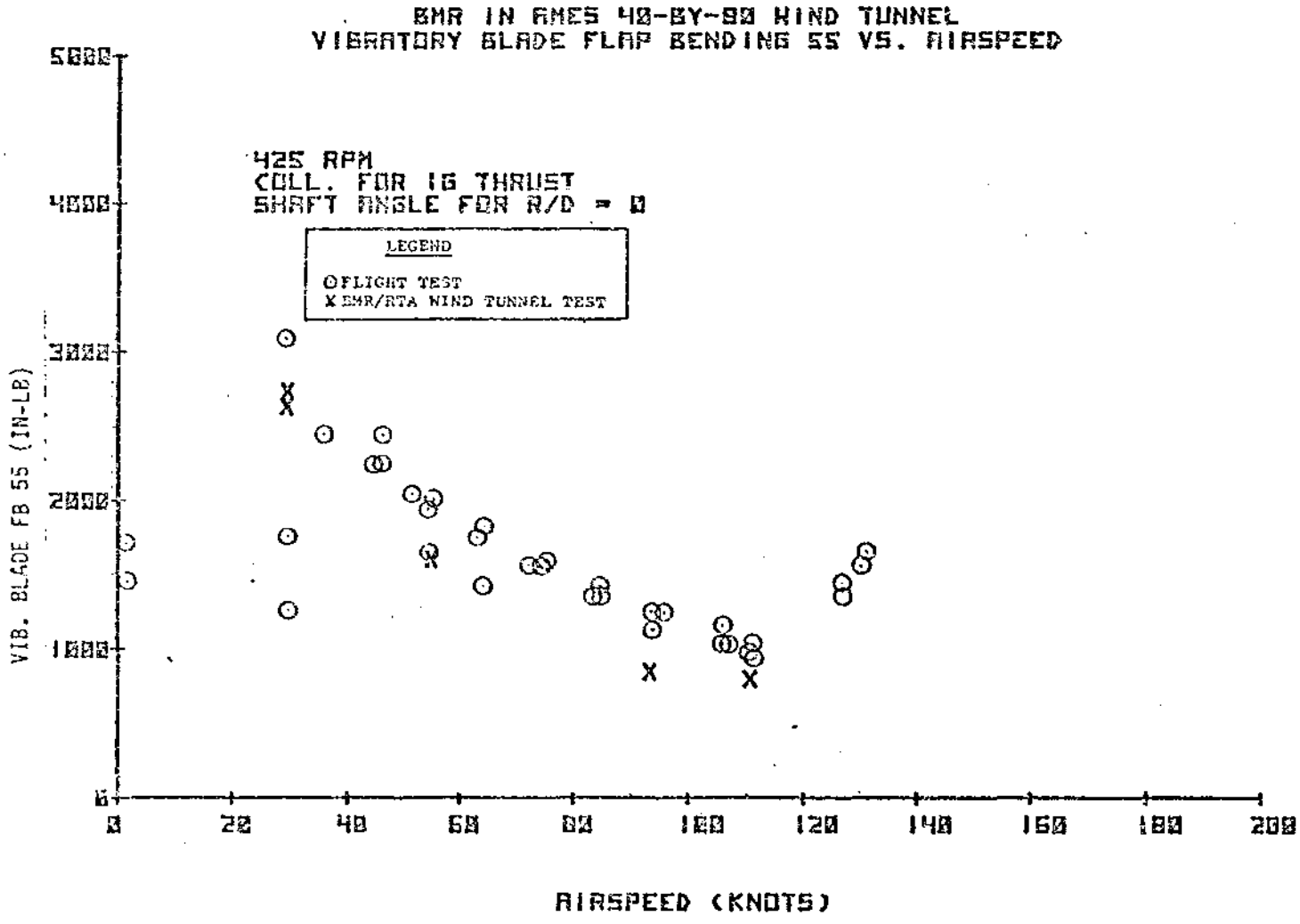

FIGURE 8.209 FLIGHT TEST CORRELATION - VIBRATORY FLAP BENDING 55 VERSUS AIRSPEED

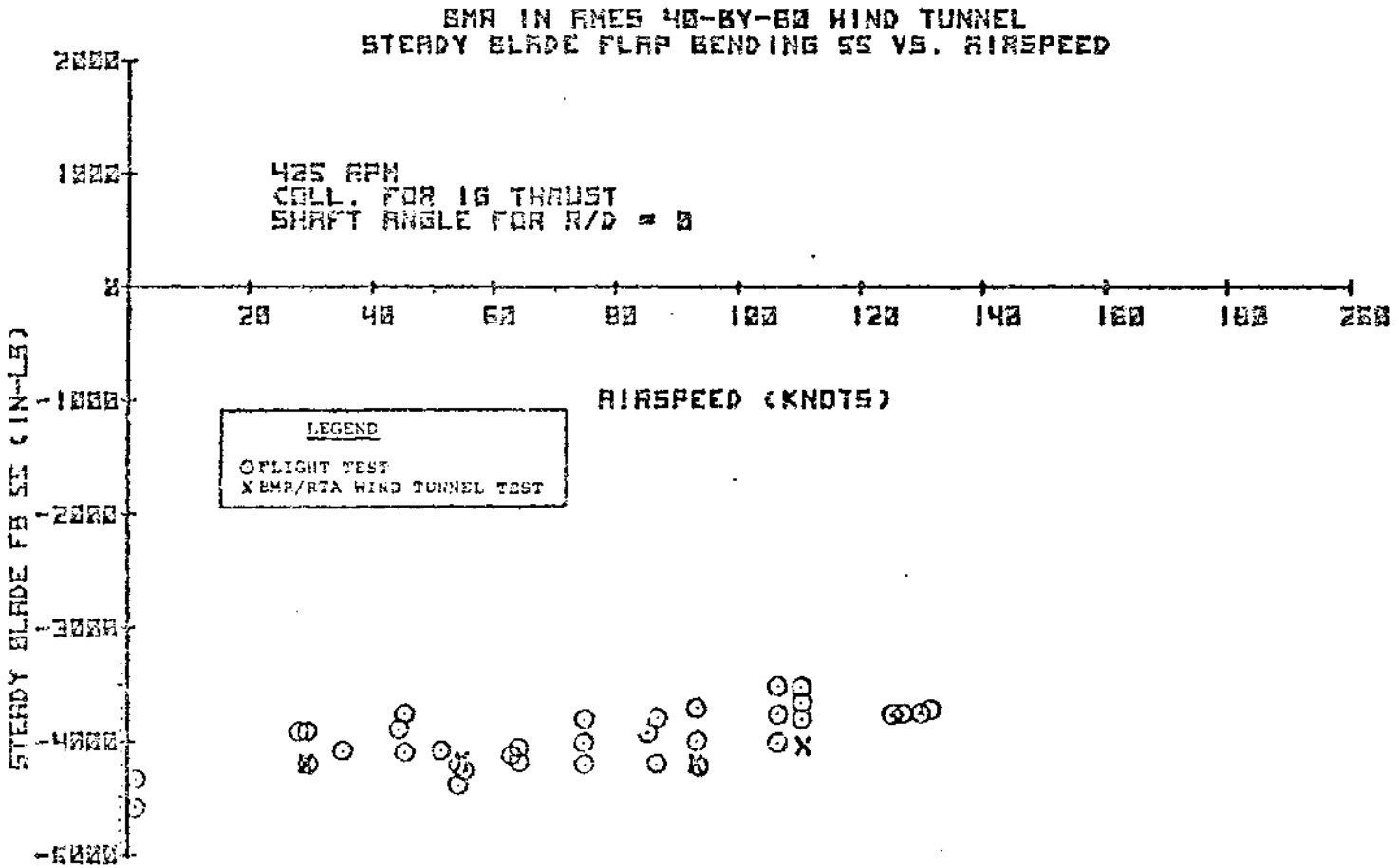

FIGURE 8.210 FLIGHT TEST CORRELATION - STEADY FLAP BENDING 55 VERSUS AIRSPEED

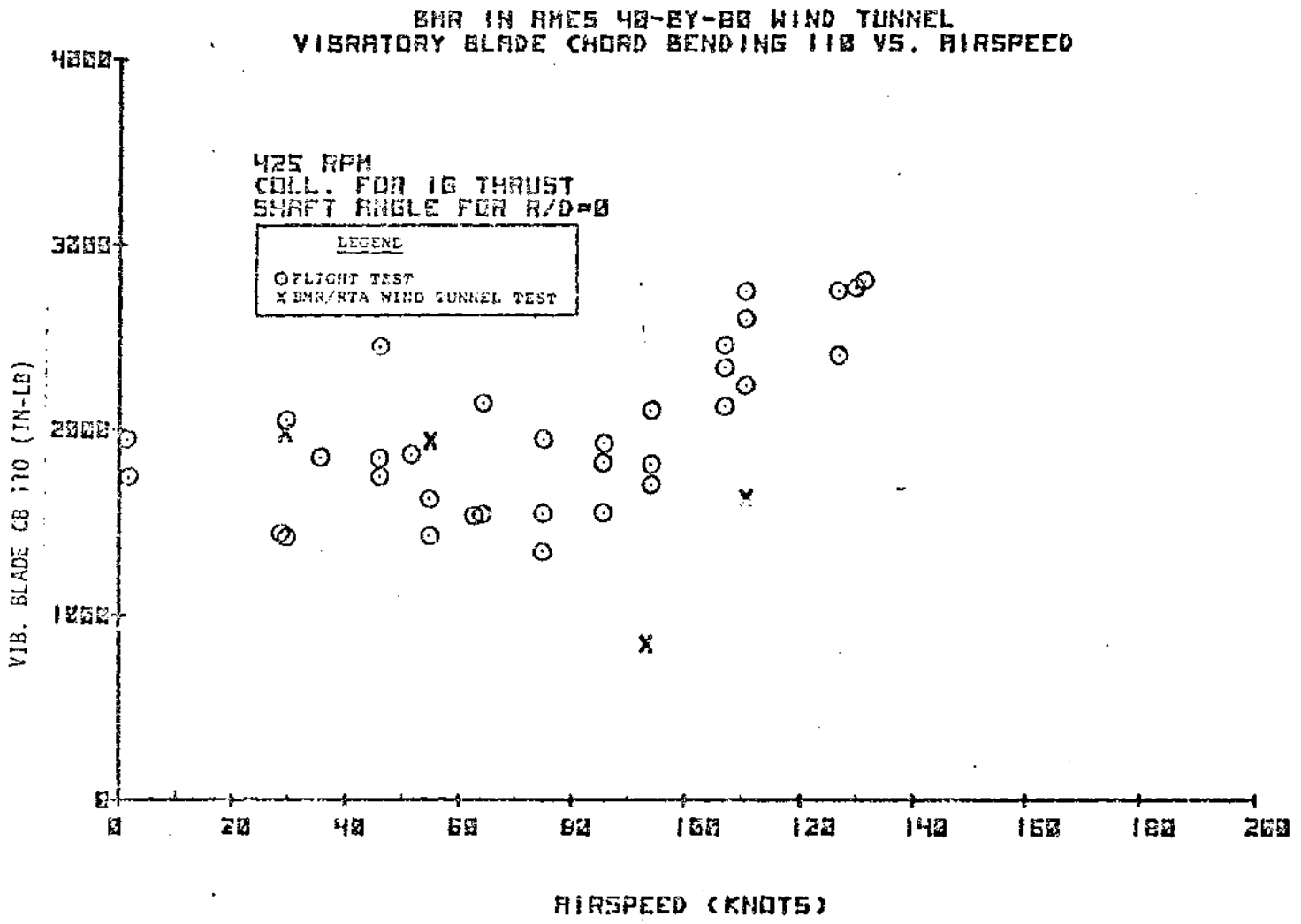

FIGURE 8.211 FLIGHT TEST CORRELATION - VIBRATORY CHORD BENDING 110 VERSUS AIRSPEED

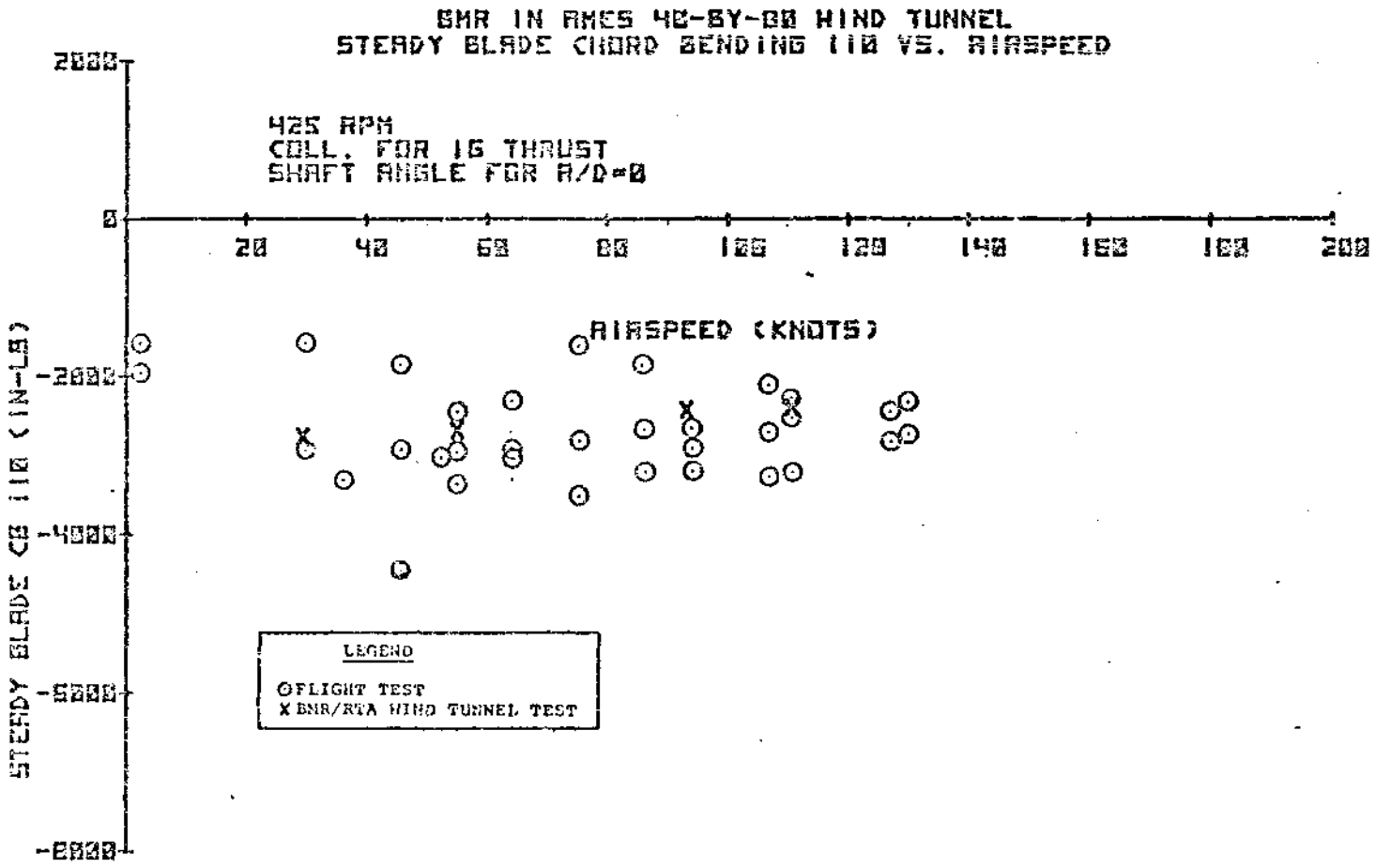

FIGURE 8.212 FLIGHT TEST CORRELATION - STEADY CHORD BENDING 110 VERSUS AIRSPEED

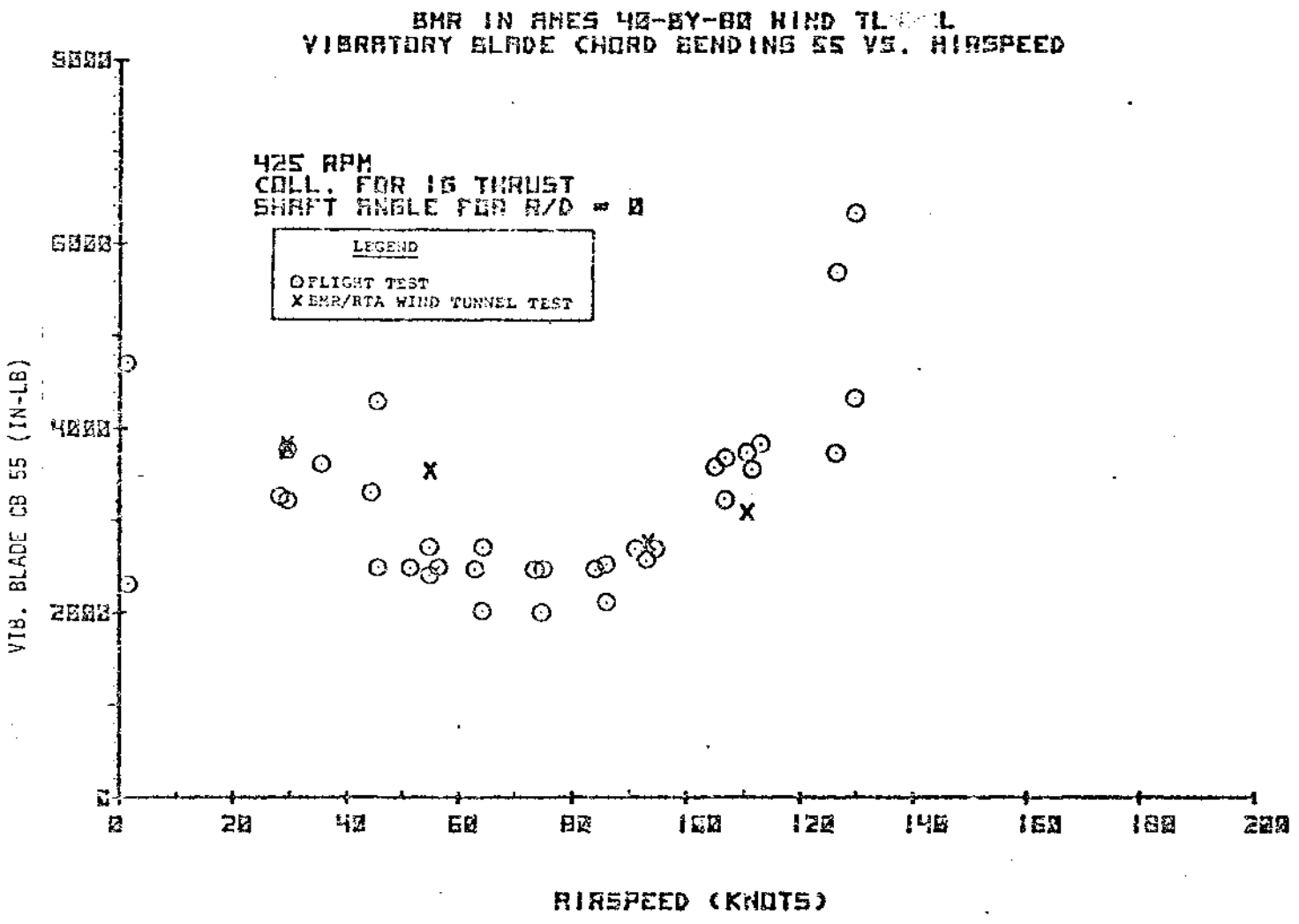

FIGURE 8.213 FLIGHT TEST CORRELATION - VIBRATORY CHORD BENDING 55 VERSUS AIRSPEED

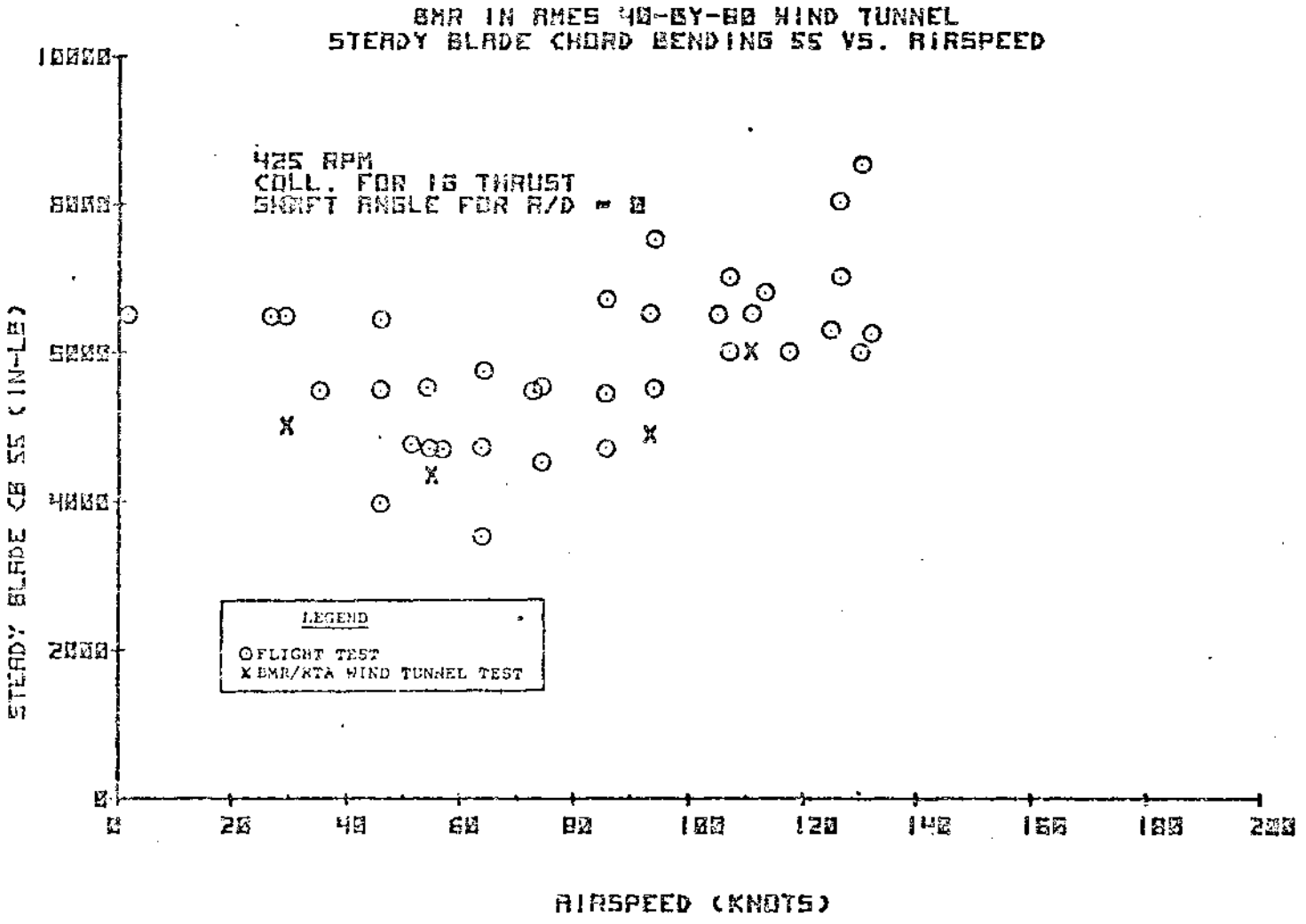

FIGURE 8.214 FLIGHT TEST CORRELATION - STEADY CHORD BENDING 55 VERSUS AIRSPEED

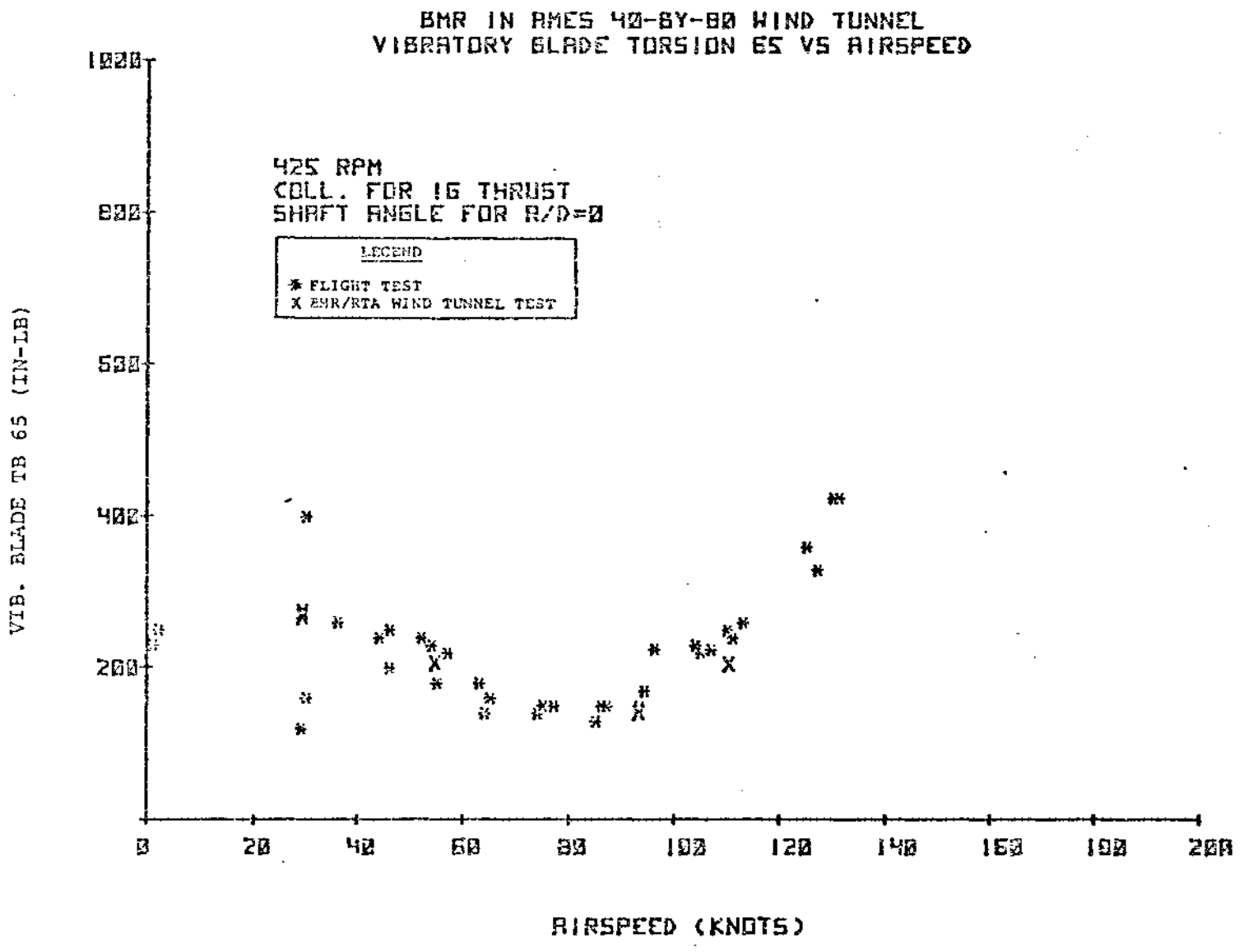

FIGURE 8.215 FLIGHT TEST CORRELATION - VIBRATORY TORSION 65 VERSUS AIRSPEED

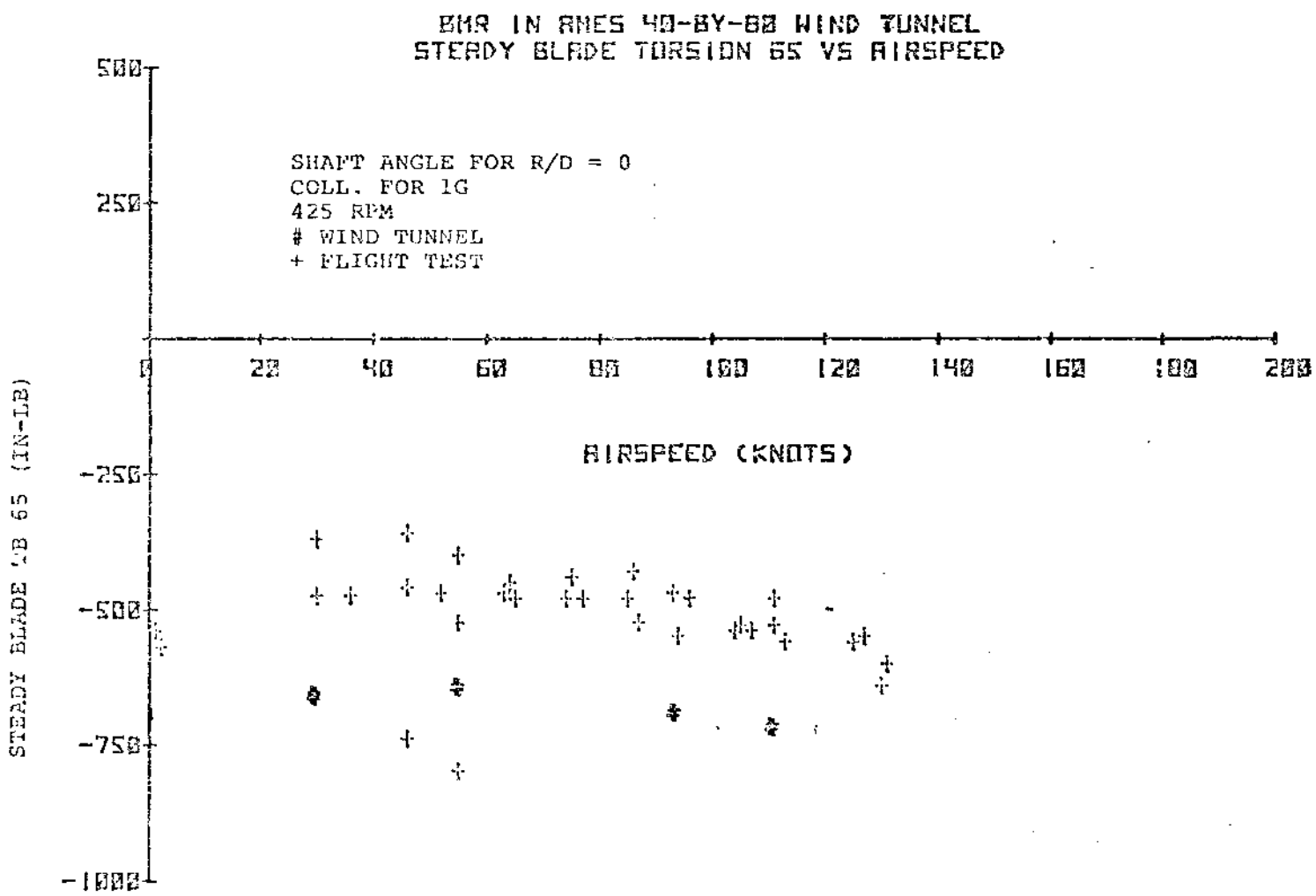

FIGURE 8.216 FLIGHT TEST CORRELATION - STEADY TORSION 65 VERSUS AIRSPEED

8.2.3.2 Flexbeam Loads

Figures 8.217 through 8.226 present flexbeam flap bending correlation. In general, there is relatively good agreement for vibratory flap bending. At 30 knots, there is a substantial 4/rev component of flap bending while at 90 and 110 knots the 4/rev component of flap bending is very small. Combined 1/rev and 4/rev flap bending at 30 knots produces higher total flap bending relative to the higher airspeeds. This build-up is greater in the wind tunnel test data than it is in the flight test data. Since the trim requirements for the RTA model are different than for the BO-105 helicopter, the 1g rotor forces (propulsive force and lift) are matched with different control input and shaft angle settings. As a result of these differences, the 4/rev flap response in the Ames wind tunnel would not be expected to be identical to the 4/rev flap response experienced in flight test. On the other hand, the 1/rev flapping in the wind tunnel was forced to match the 1/rev flapping in flight test as a result of control input and shaft angle changes made to obtain identical 1/rev flapping.

At each of the three flap bending stations, steady flap moments show similar trends with airspeeds but with an offset in magnitude between wind tunnel and flight test data. Differences in steady flap moments probably reflect the more negative shaft angles in the wind tunnel testing. Figure 8.227 presents a comparison of typical flight test shaft angle versus shaft angle required to obtain R/D = 0 in the wind tunnel.

At the fixed ends of the flexbeam, chord bending vibratory moments are in good agreement out to 90 knots. Flight test data shows a rapid build-up at 120 knots which was not experienced in the wind tunnel testing. At the higher airspeeds, the rotor is more sensitive to changes in shaft angle. Steady moments at the outboard section show both differences in magnitude and trend for the leading beam. Leading beam moments are in agreement at the inboard section. Chord bending correlation is presented in Figures 8.220 through 8.231 for beam A only, since the gage on beam B was inoperative.

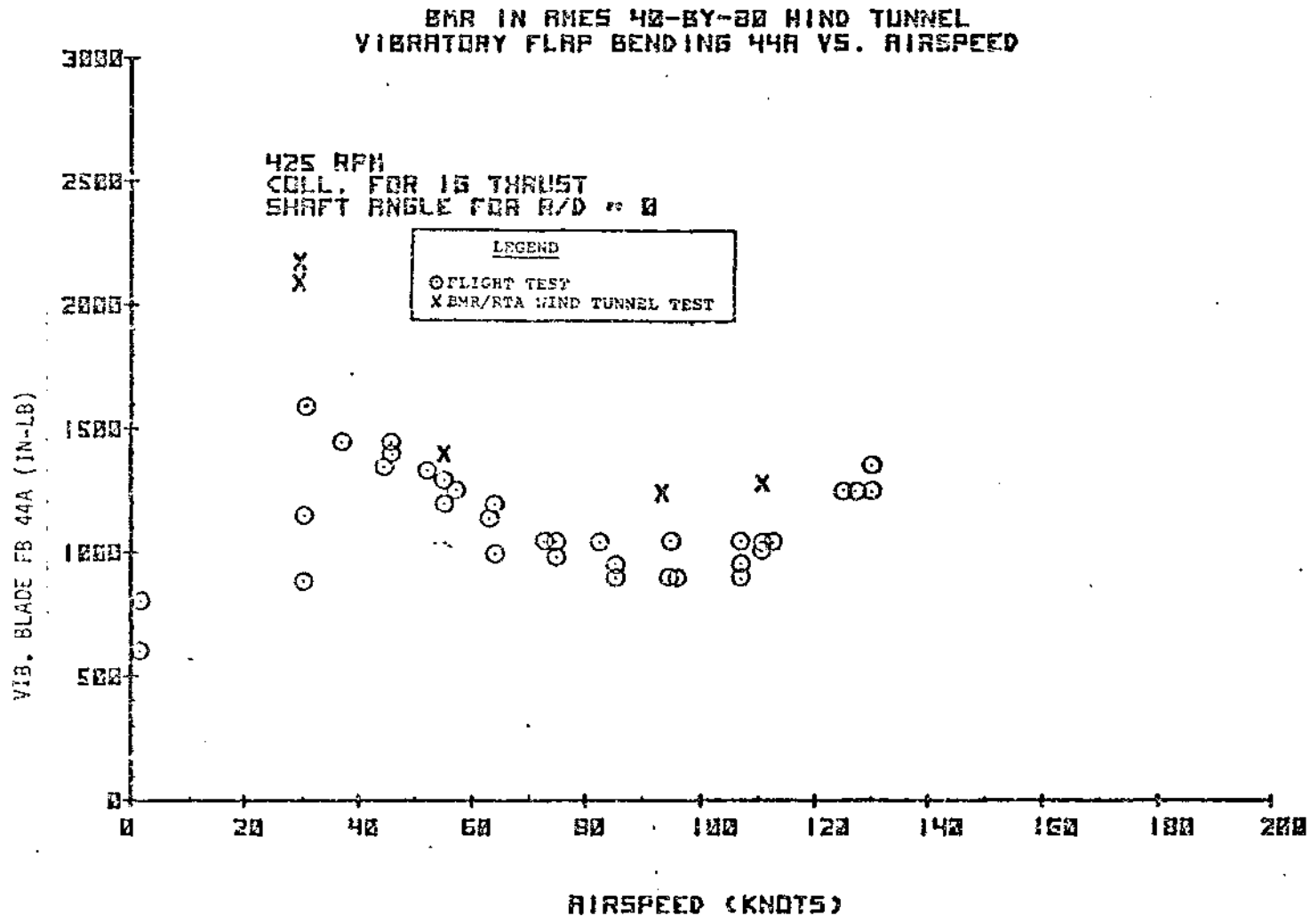

FIGURE 8.217 FLIGHT TEST CORRELATION - VIBRATORY FLAP BENDING 44A VERSUS AIRSPEED

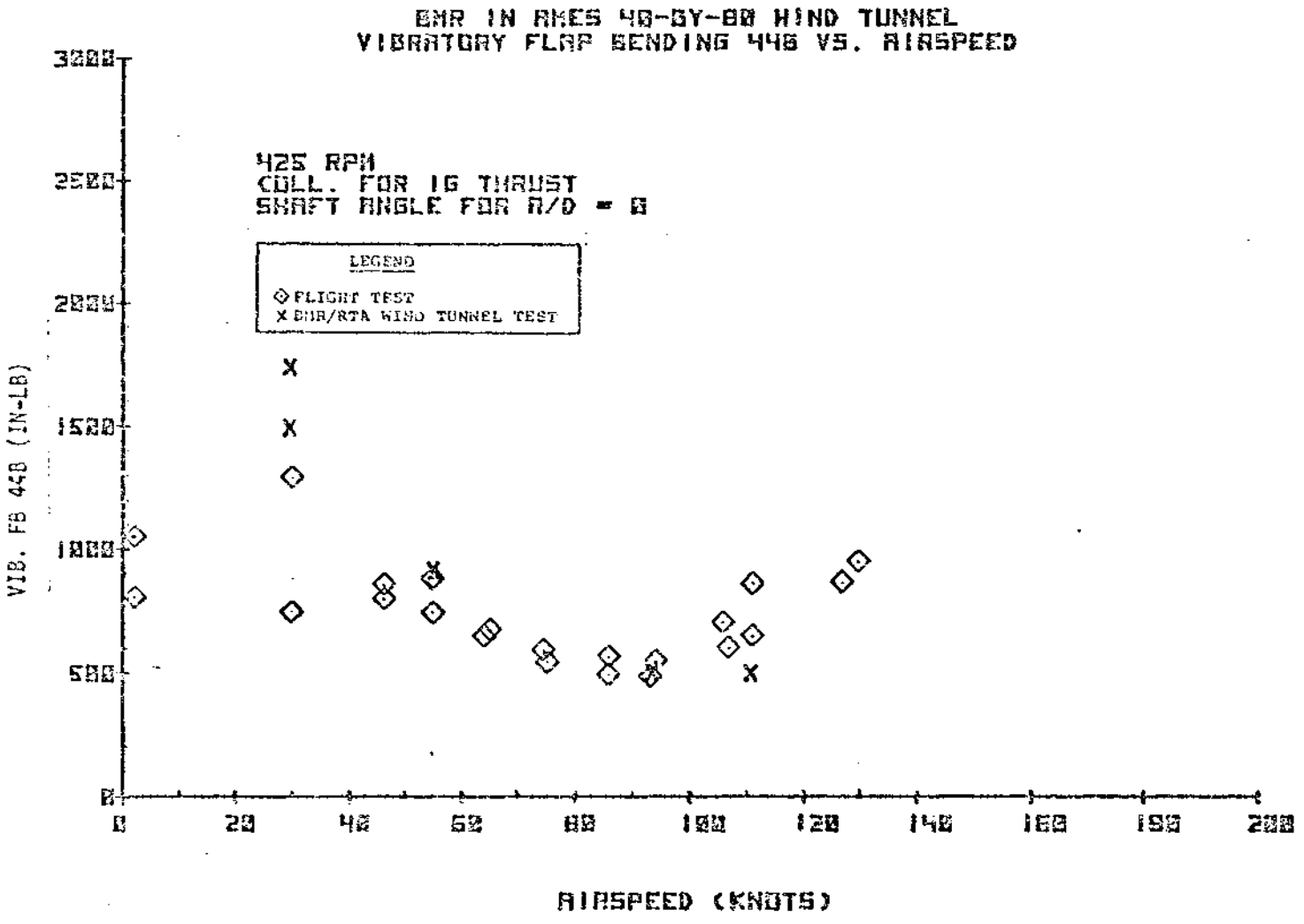

FIGURE 8.218 FLIGHT TEST CORRELATION - VIBRATORY FLAP BENDING 44B VERSUS AIRSPEED

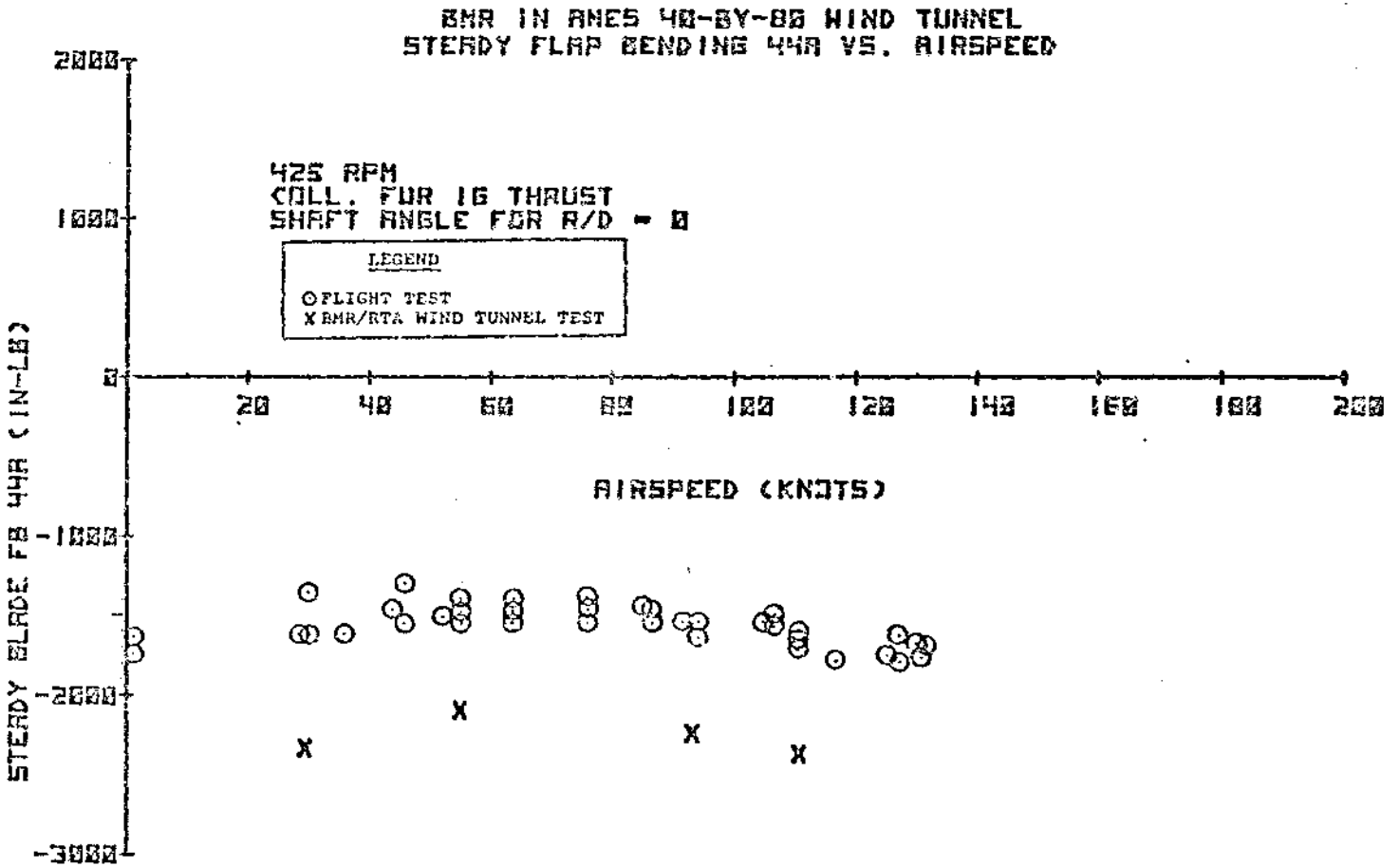

FIGURE 8.219 FLIGHT TEST CORRELATION - STEADY FLAP BENDING 44A VERSUS AIRSPEED

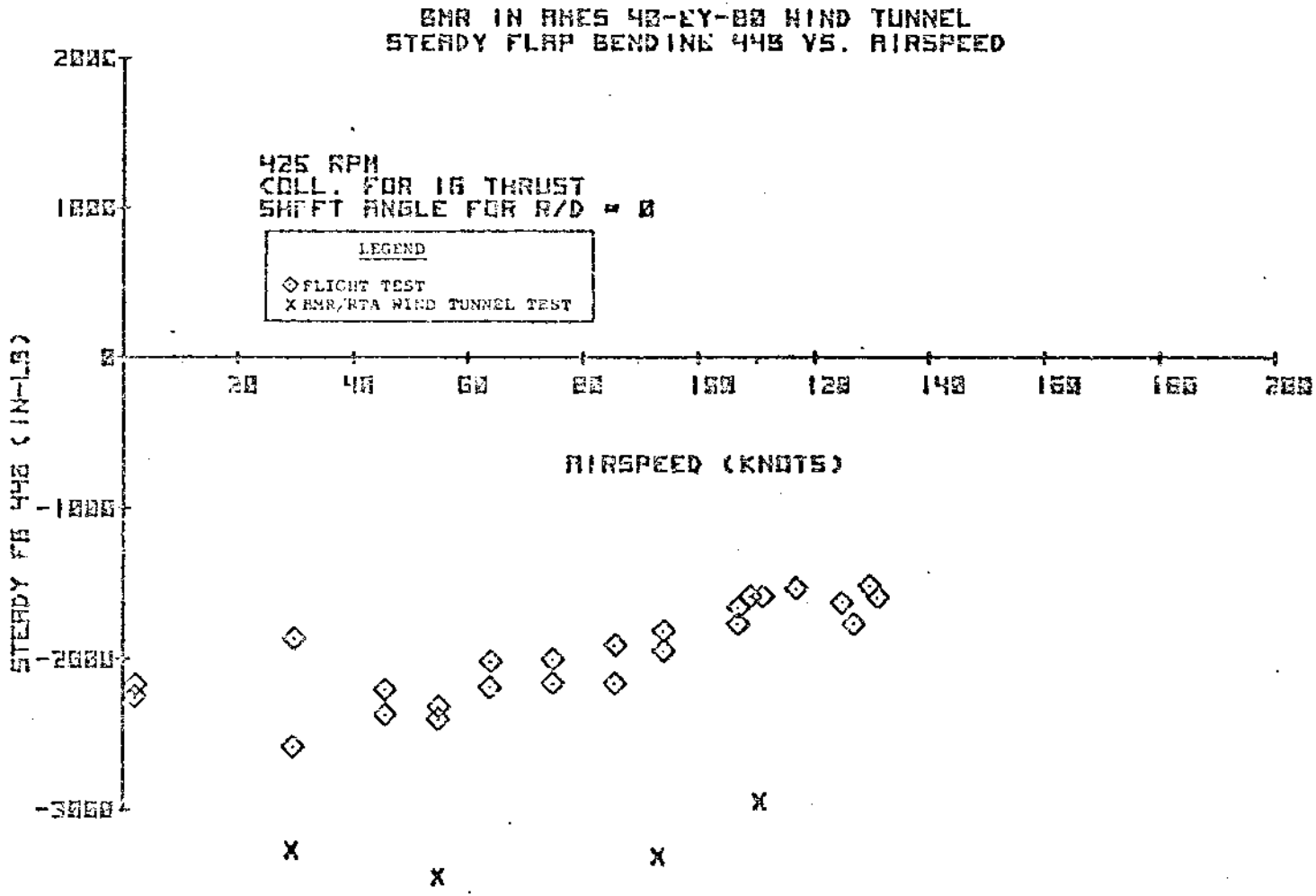

FIGURE 8.220 FLIGHT TEST CORRELATION – STEADY FLAP BENDING 44B VERSUS AIRSPEED

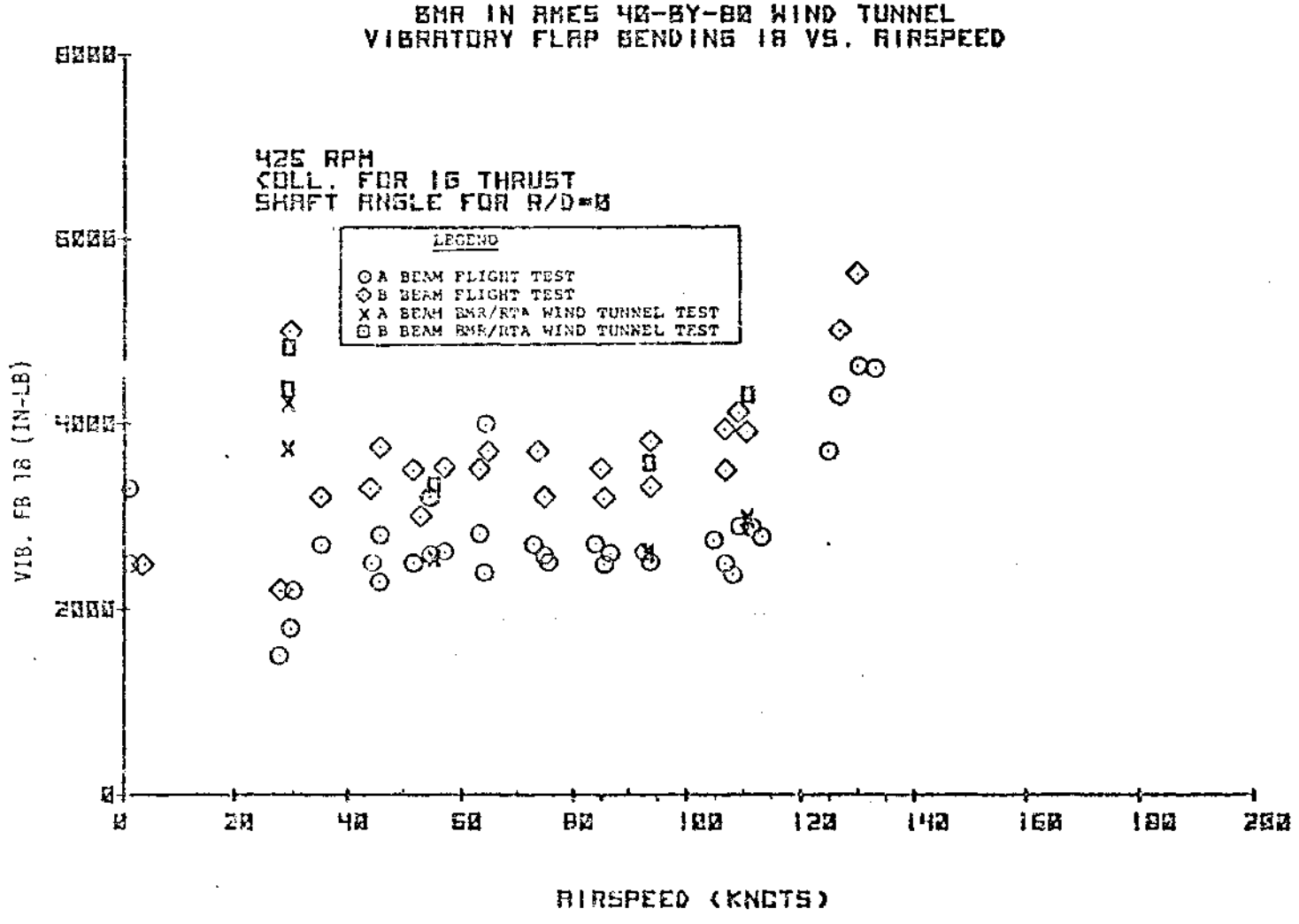

FIGURE 8.221 FLIGHT TEST CORRELATION - VIBRATORY FLAP BENDING 1B VERSUS AIRSPEED

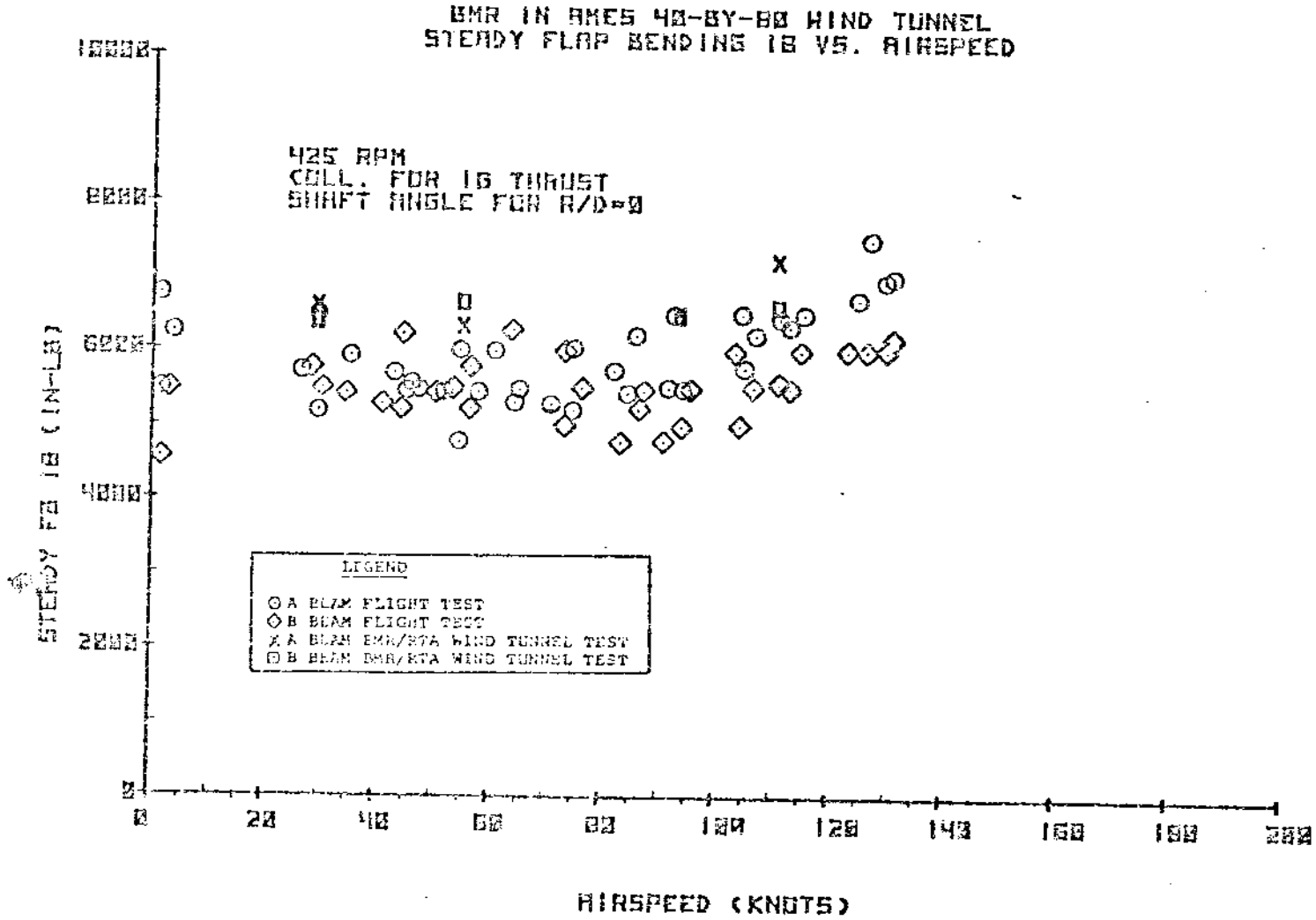

FIGURE 8.222 FLIGHT TEST CORRELATION - STEADY FLAP BENDING 1B VERSUS AIRSPEED

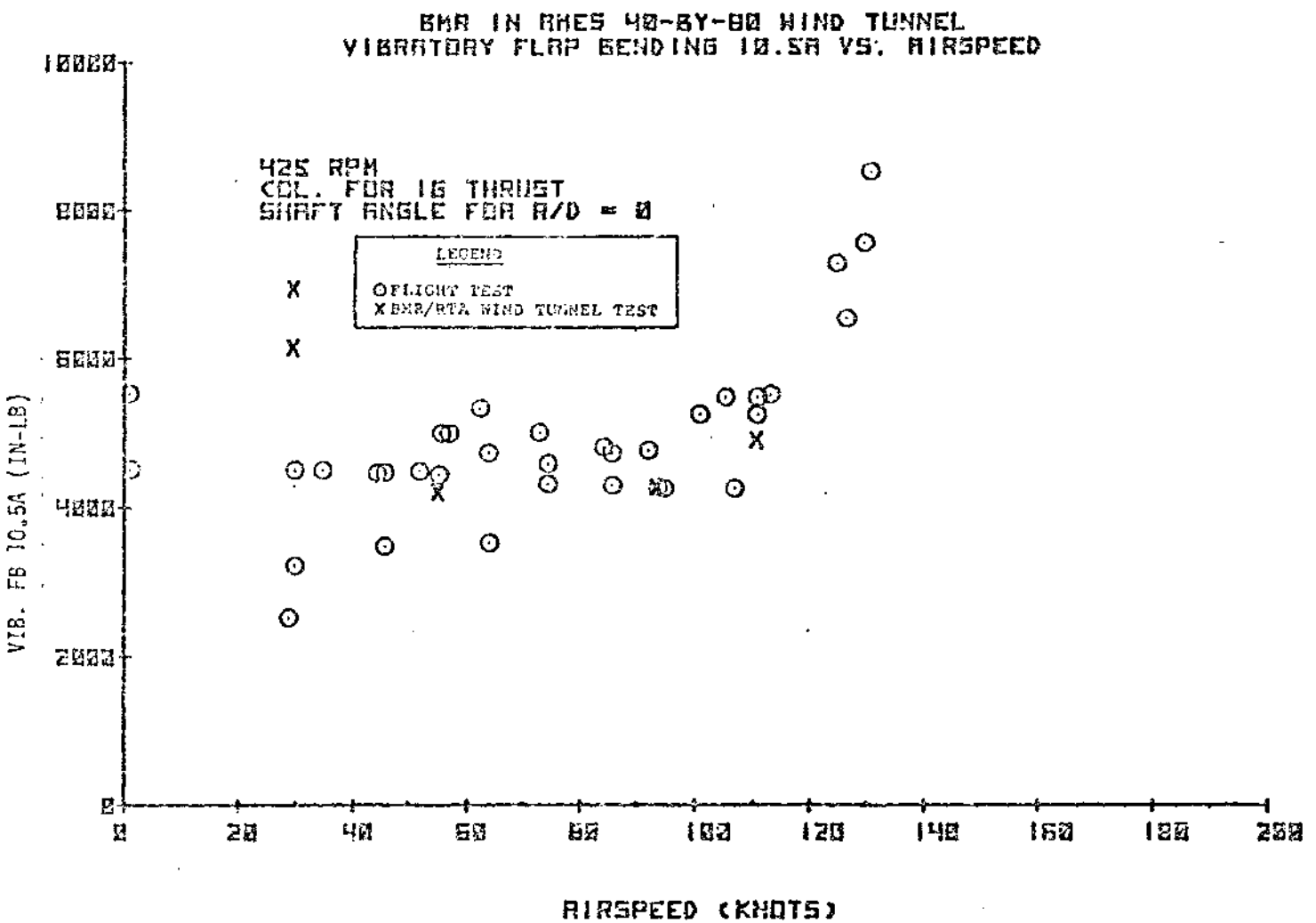

FIGURE 8.223 FLIGHT TEST CORRELATION - VIBRATORY FLAP BENDING 10.5A VERSUS AIRSPEED

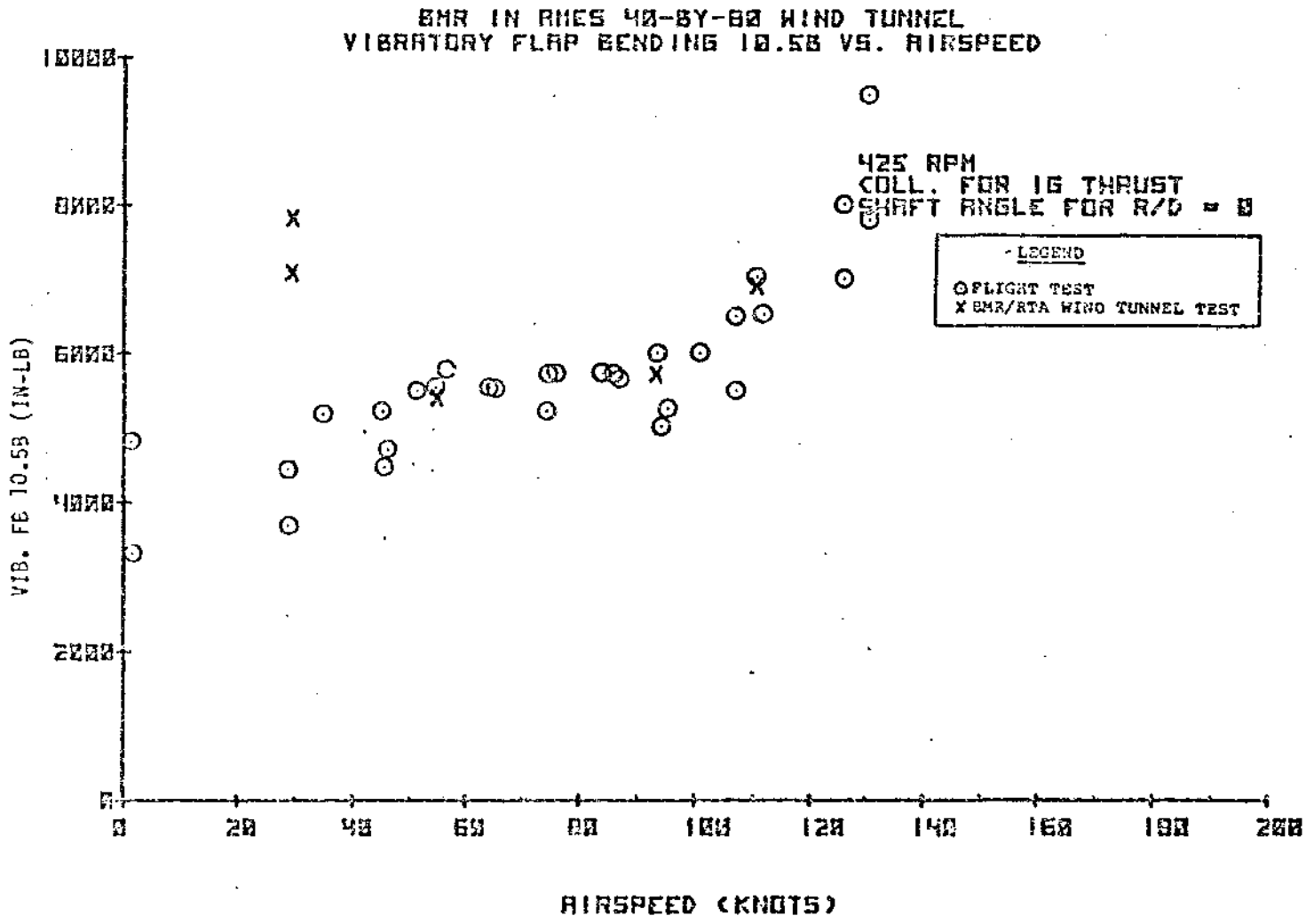

FIGURE 8.224 FLIGHT TEST CORRELATION - VIBRATORY FLAP BENDING 10.5B VERSUS AIRSPEED

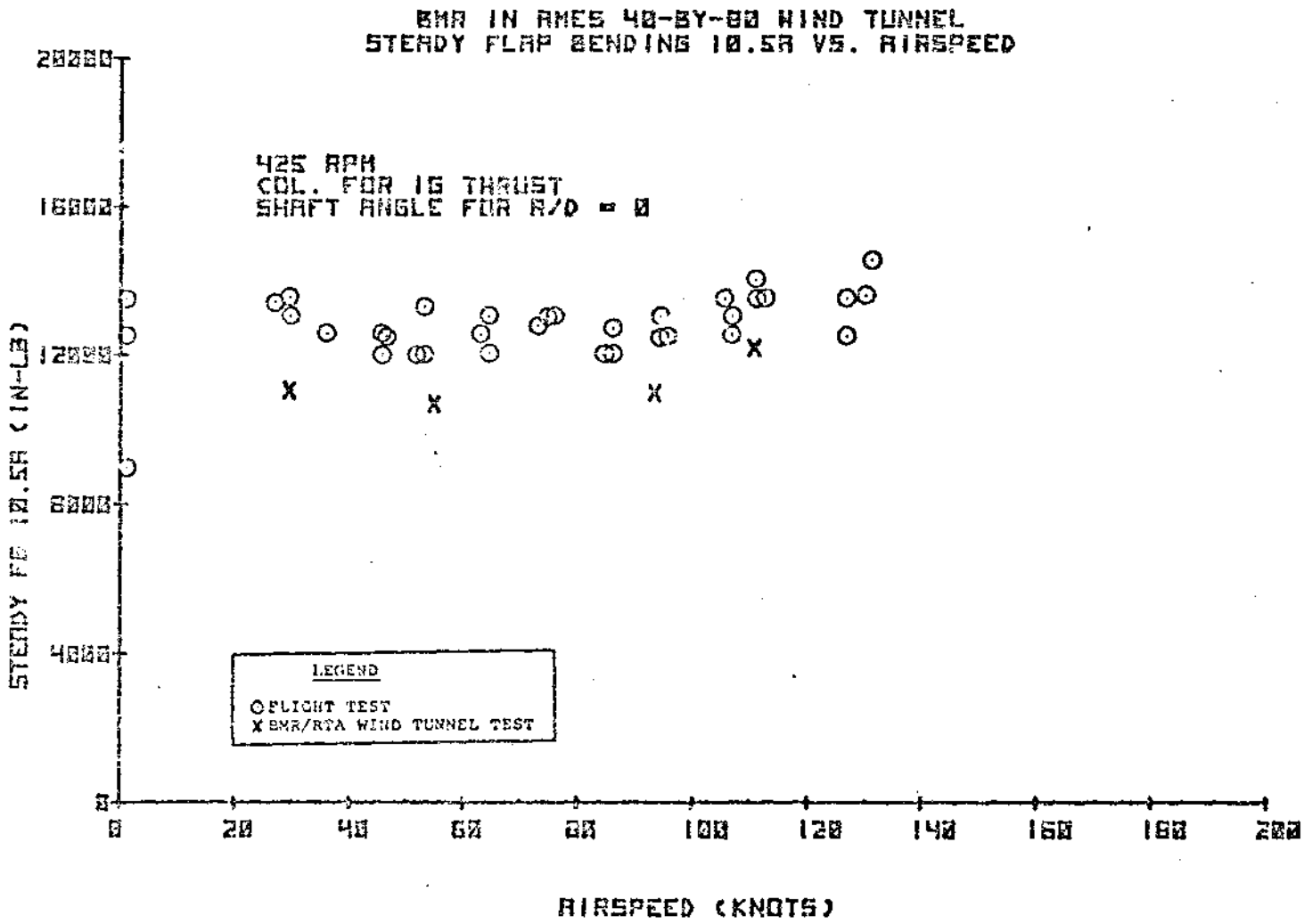

FIGURE 8.225 FLIGHT TEST CORRELATION - STEADY FLAP BENDING 10.5A VERSUS AIRSPEED

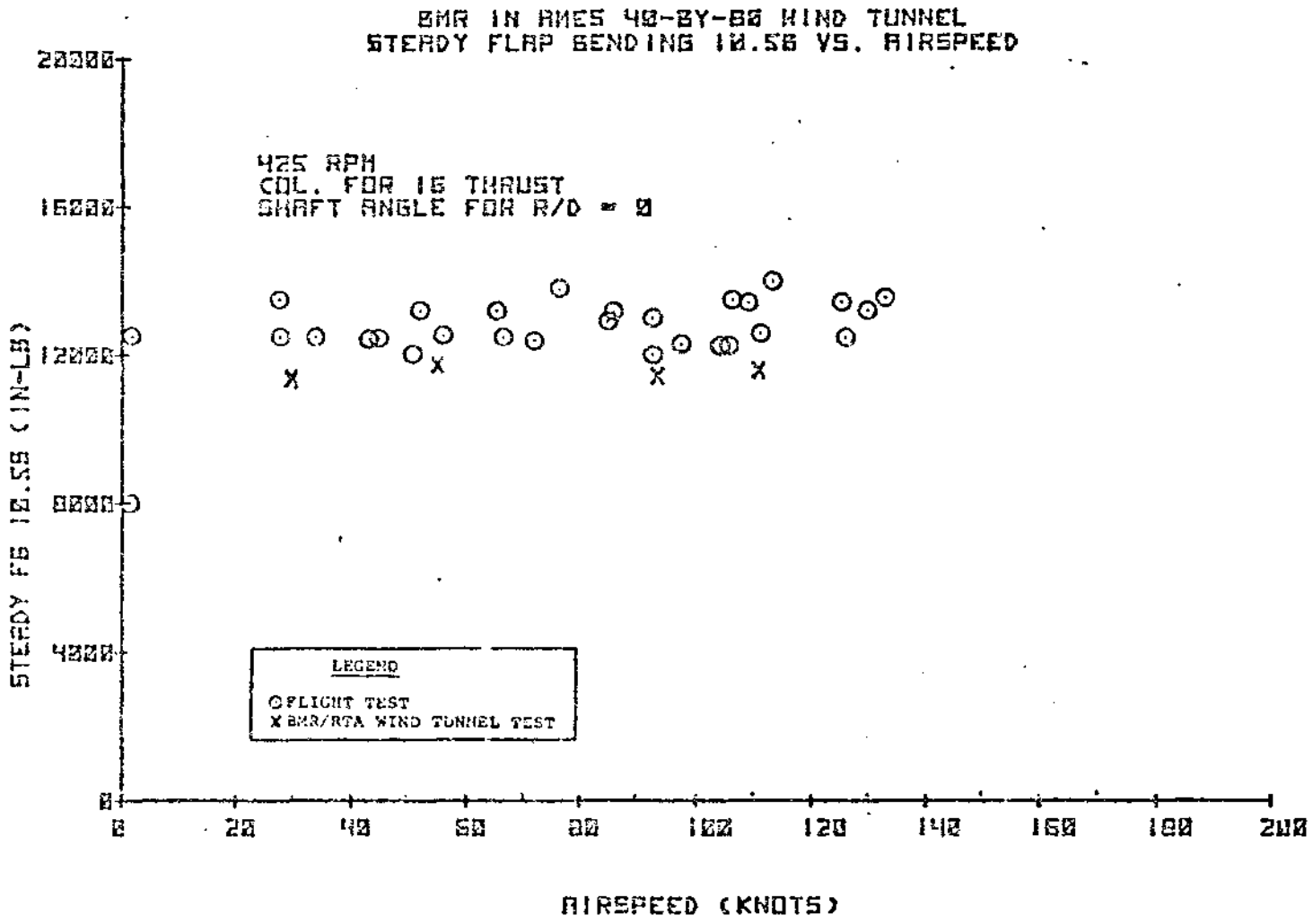

FIGURE 8.226 FLIGHT TEST CORRELATION - STEADY FLAP BENDING 10.5B VERSUS AIRSPEED

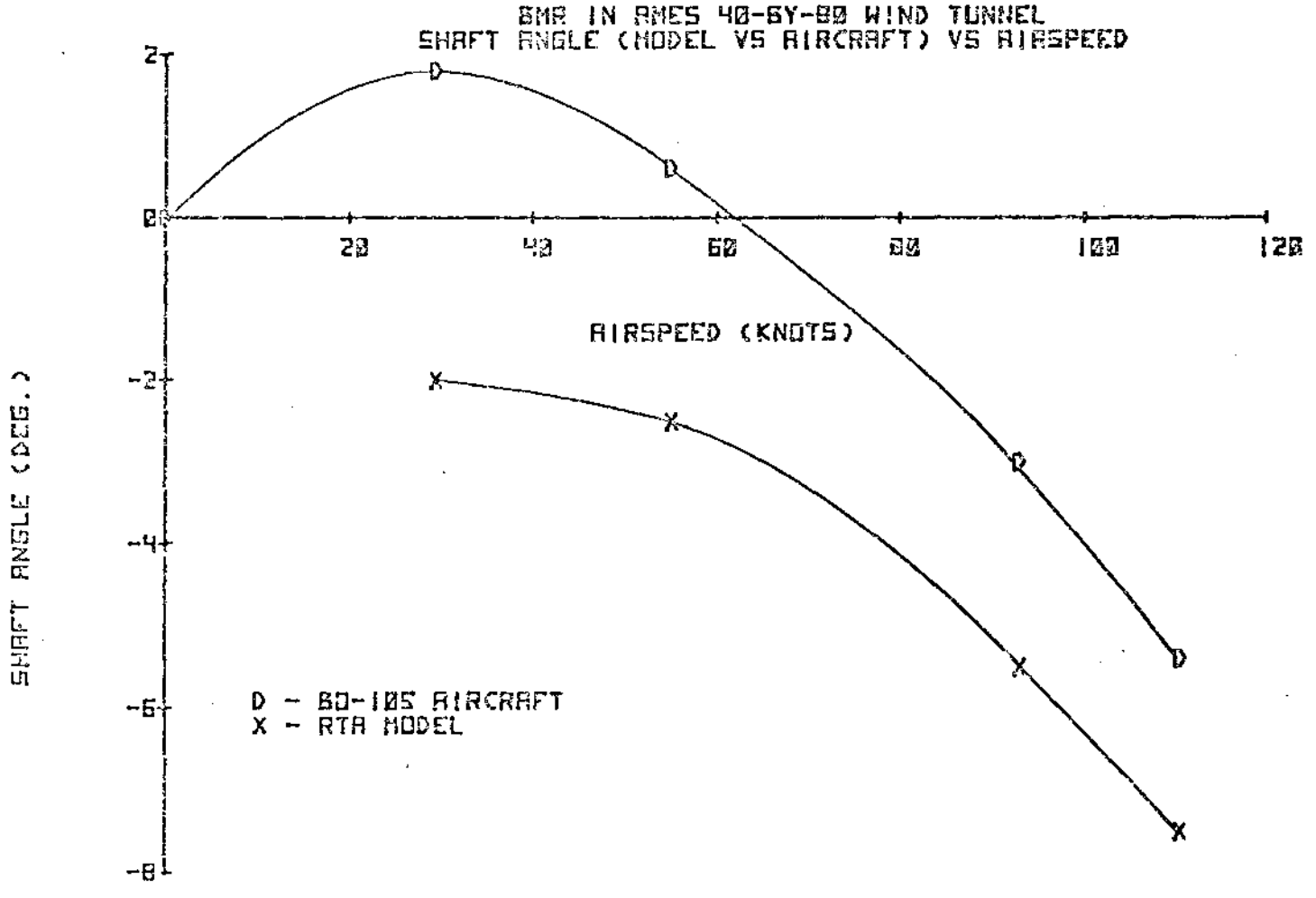

FIGURE 8.227 SHAFT ANGLE VERSUS AIRSPEED - BMR/RTA AND BMR/BO-105

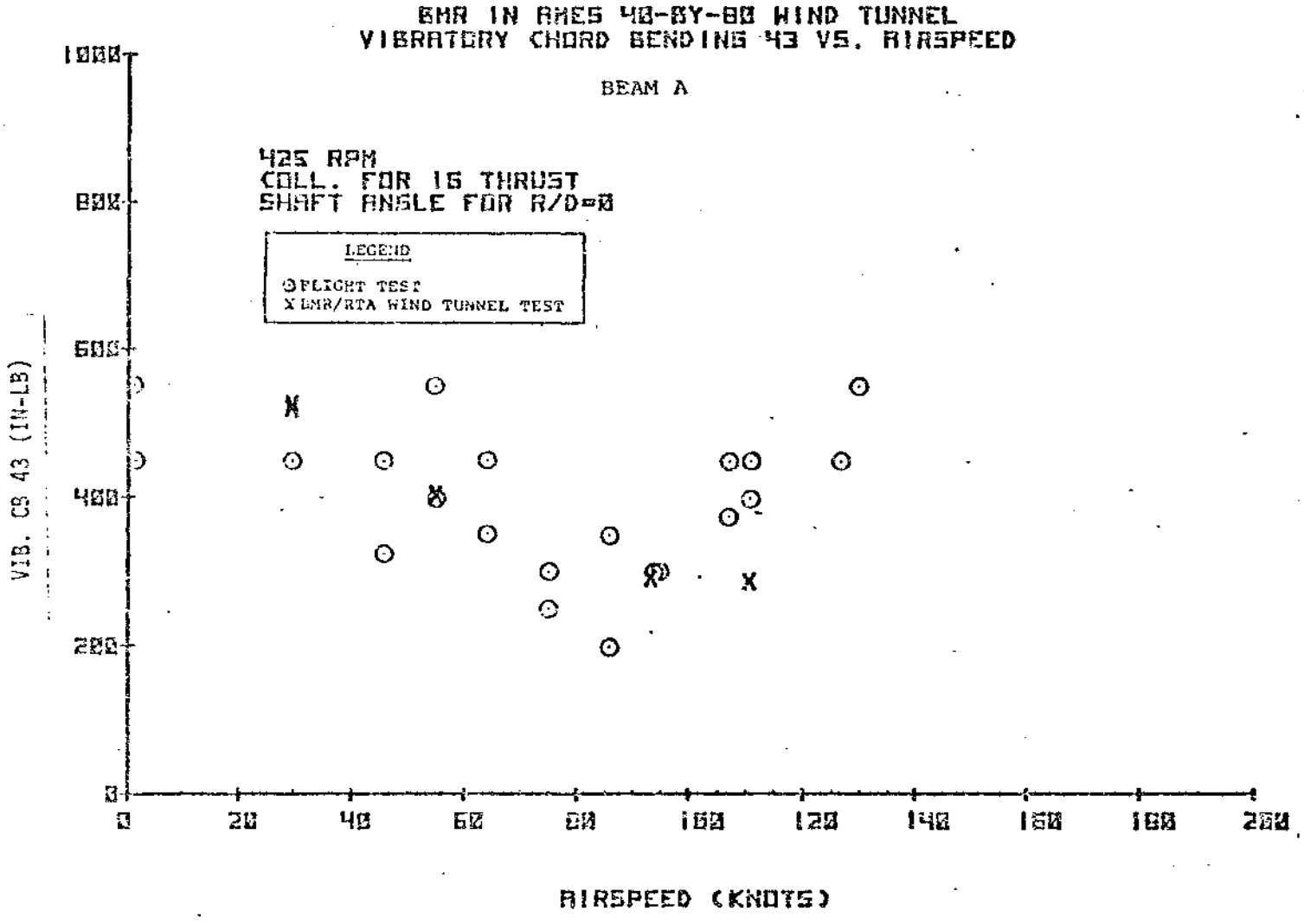

FIGURE 8.228 FLIGHT TEST CORRELATION - VIBRATORY CHORD BENDING 43 VERSUS AIRSPEED

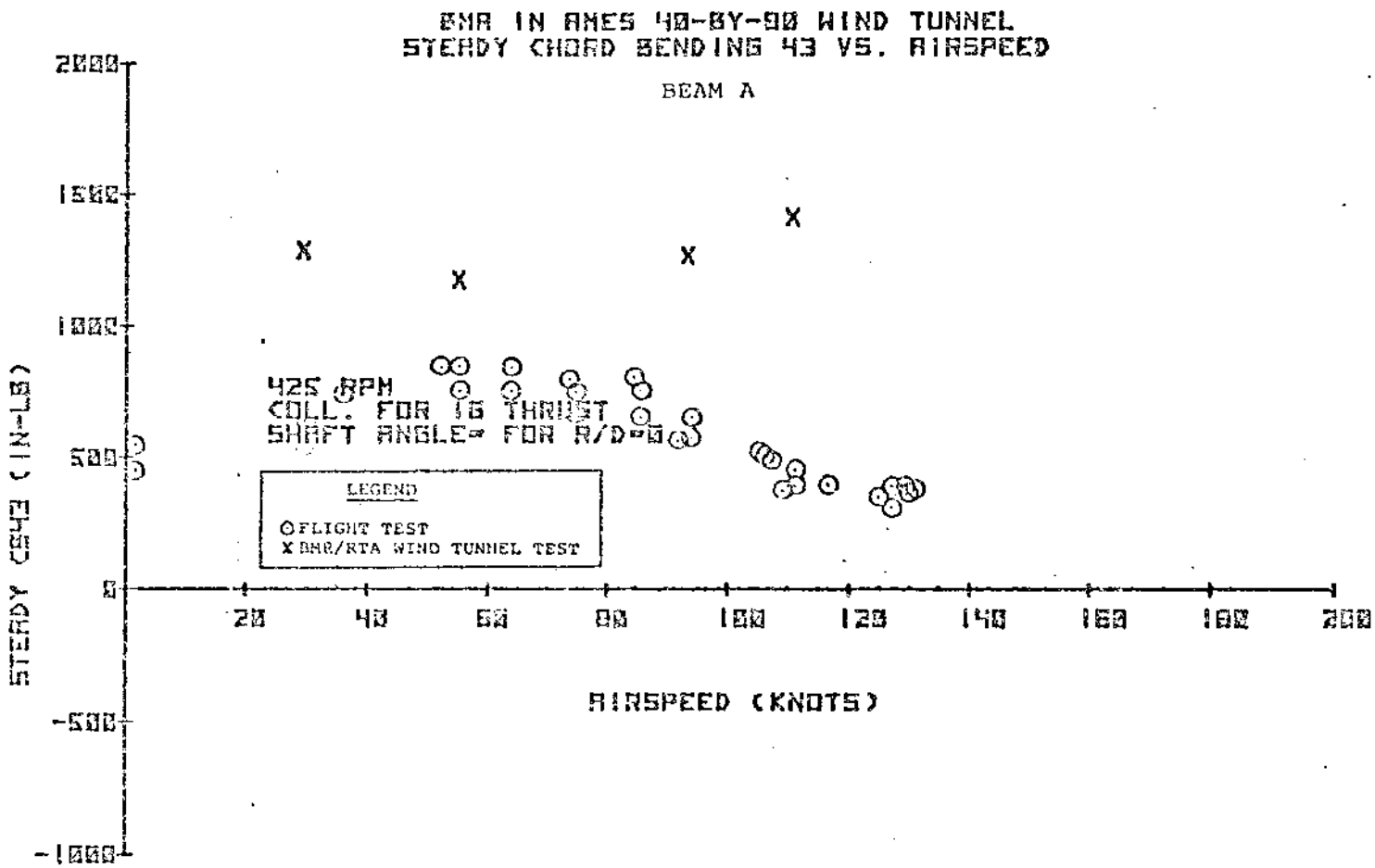

FIGURE 8.229 FLIGHT TEST CORRELATION - STEADY CHORD BENDING 43 VERSUS AIRSPEED

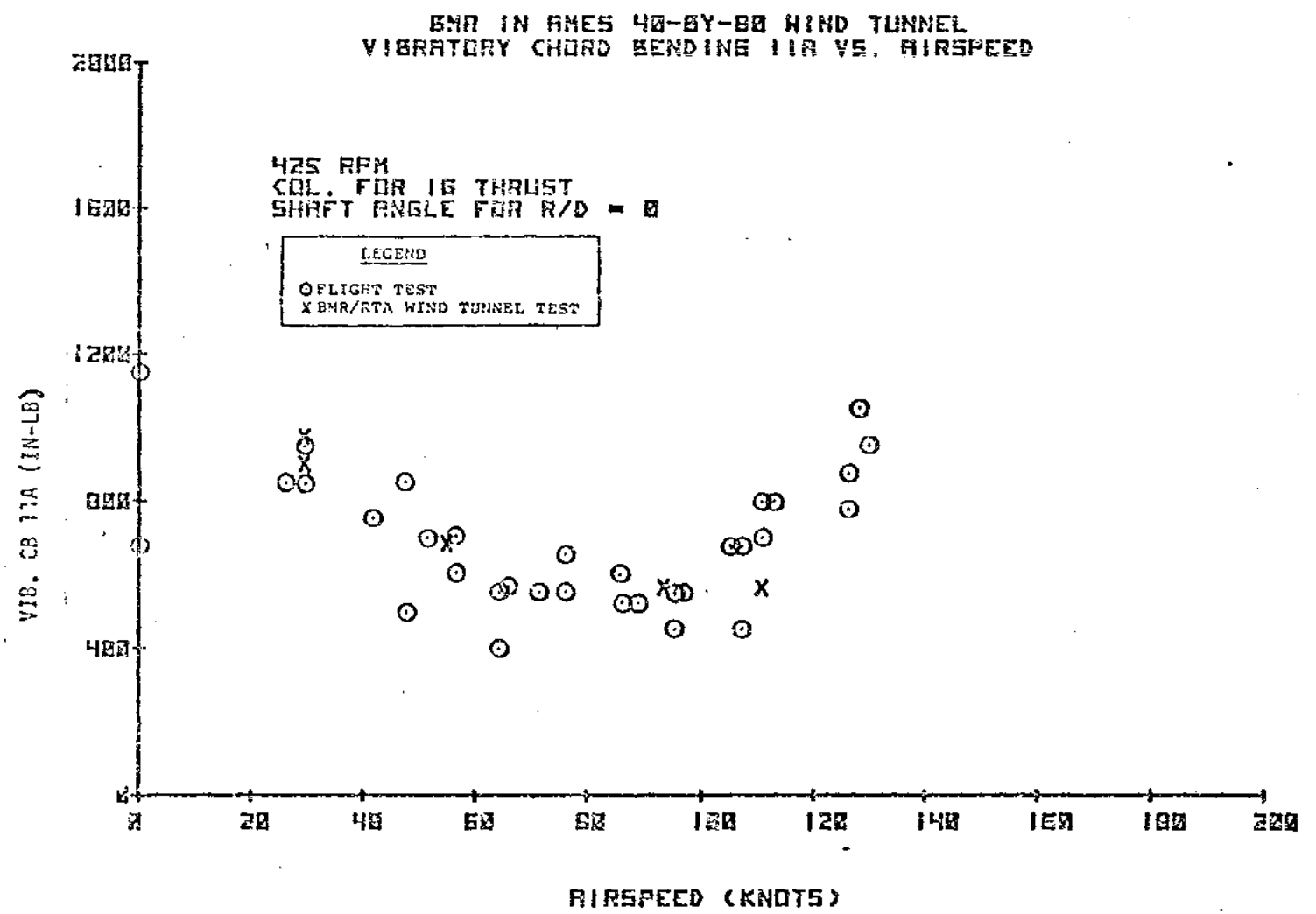

FIGURE 8.230 FLIGHT TEST CORRELATION - VIBRATORY CHORD BENDING 11A VERSUS AIRSPEED

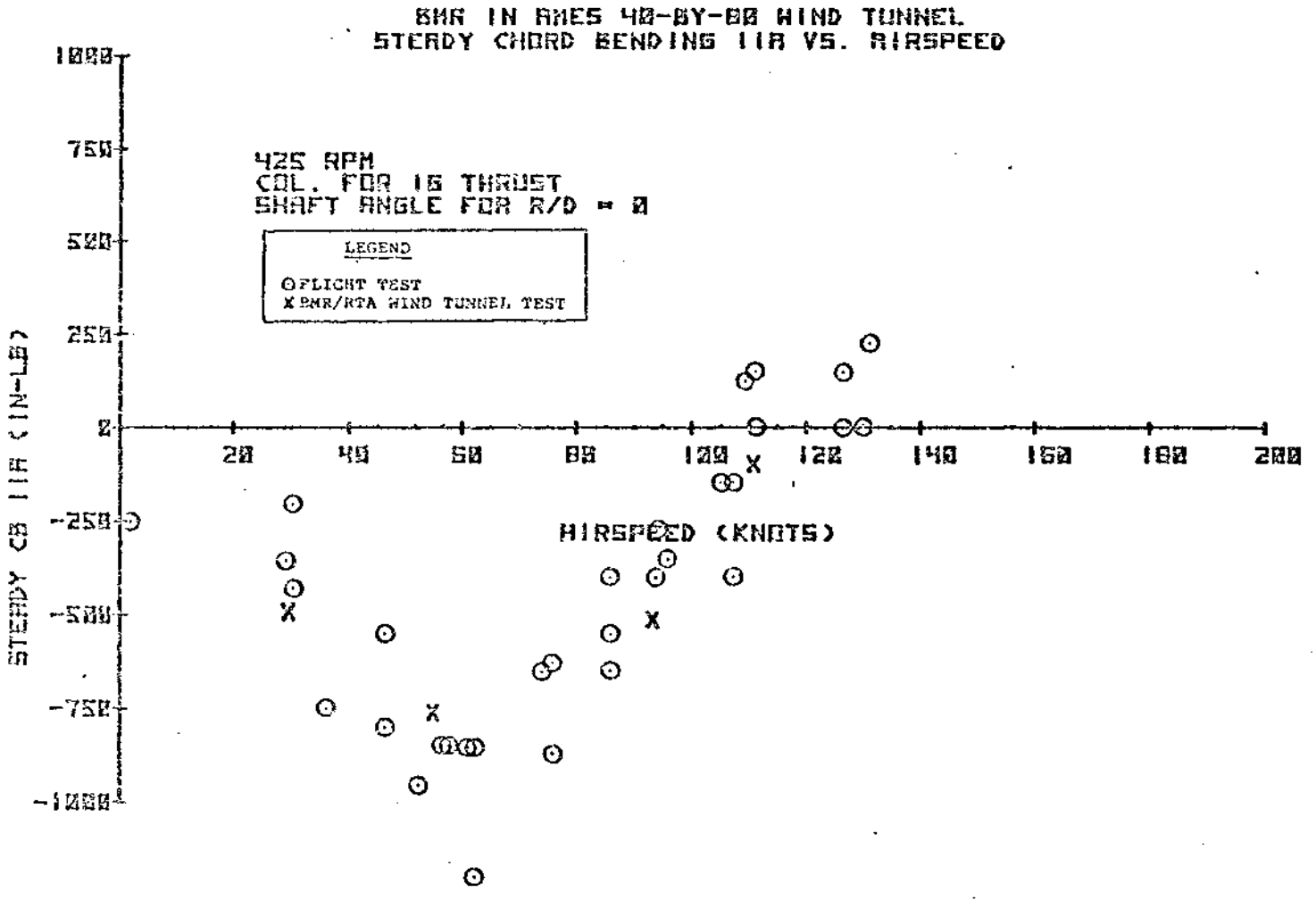

FIGURE 8.231 FLIGHT TEST CORRELATION - STEADY CHORD BENDING 11A VERSUS AIRSPEED

8.2.3.3 Torque Tube and Pitch Link Loads

Figures 8.232 through 8.235 present torque tube chord bending and pitch link load correlation. Vibratory chord bending moments show good agreement between wind tunnel and flight test. By contrast, steady chord bending shows very little correlation. Steady chord bending does vary inversely with collective which is the relationship demonstrated for all wind tunnel testing.

Both vibratory and steady pitch link load trends are consistent with flight test data. Magnitudes are consistently greater for flight test data over the airspeed test range reflecting the higher collective as shown in Figure 8.236.

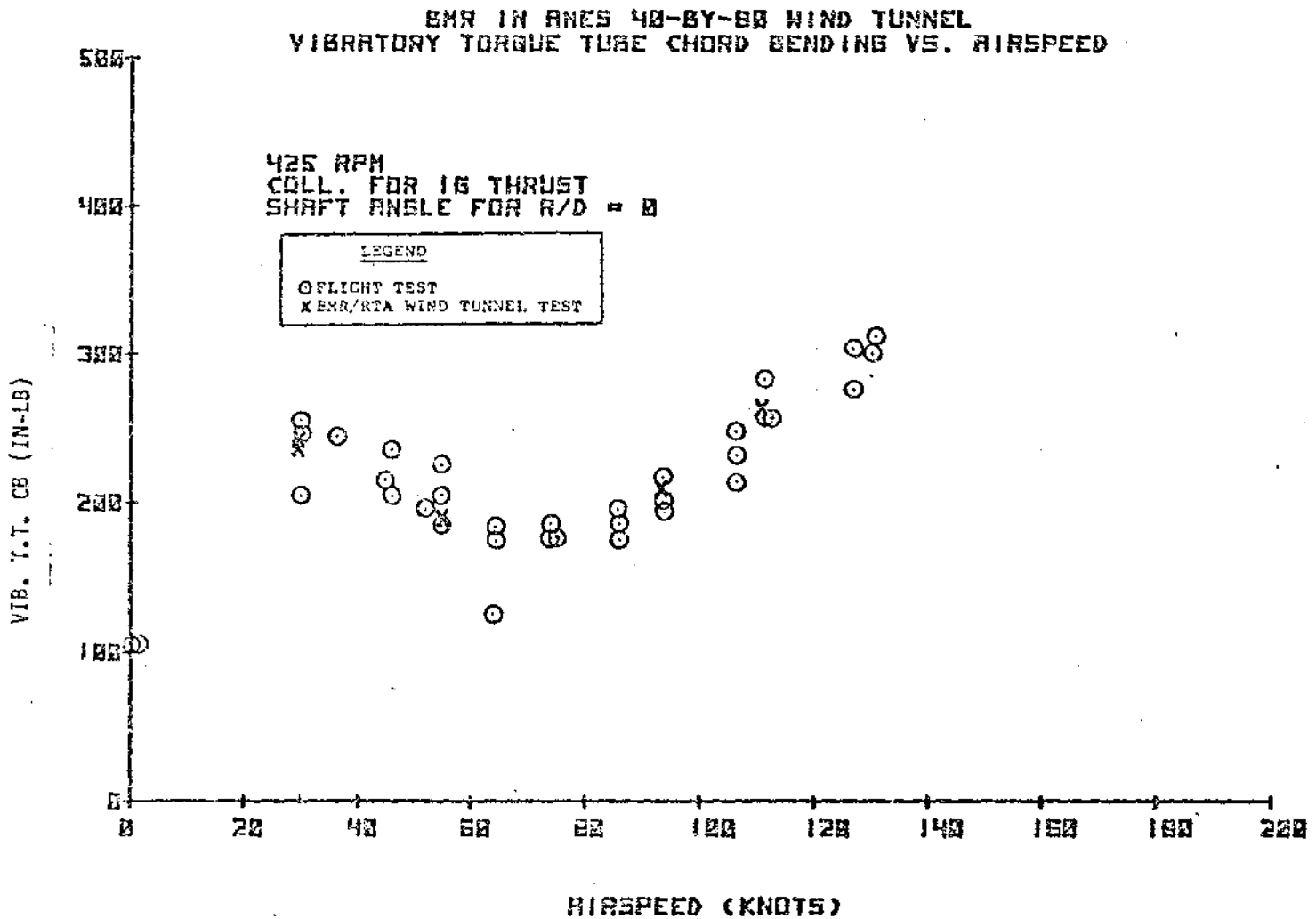

FIGURE 8.232 FLIGHT TEST CORRELATION - VIBRATORY TORQUE TUBE CHORD BENDING VERSUS AIRSPEED

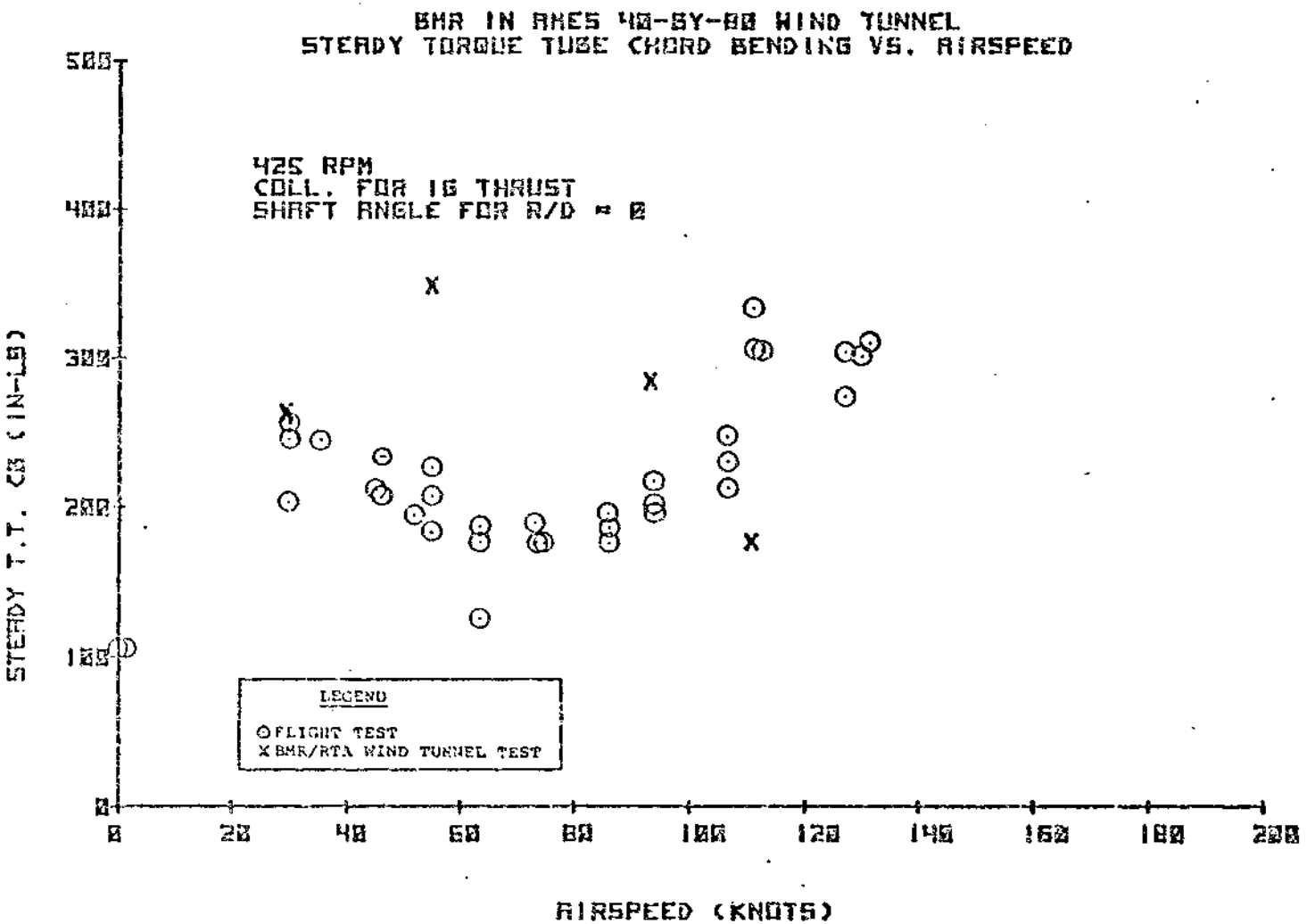

FIGURE 8.233 FLIGHT TEST CORRELATION - STEADY TORQUE TUBE CHORD BENDING VERSUS AIRSPEED

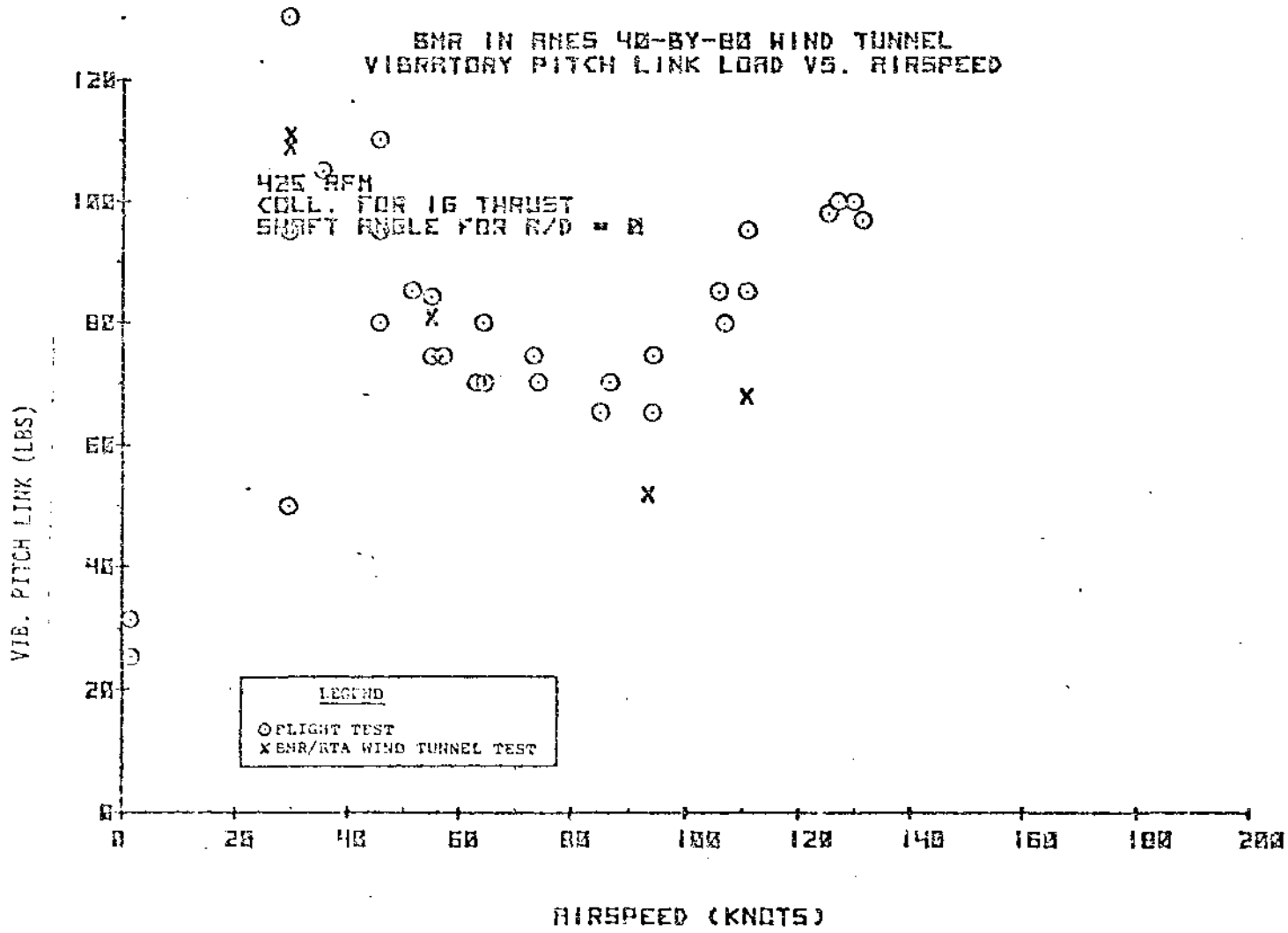

FIGURE 8.234 FLIGHT TEST CORRELATION - VIBRATORY PITCH LINK LOAD VERSUS AIRSPEED

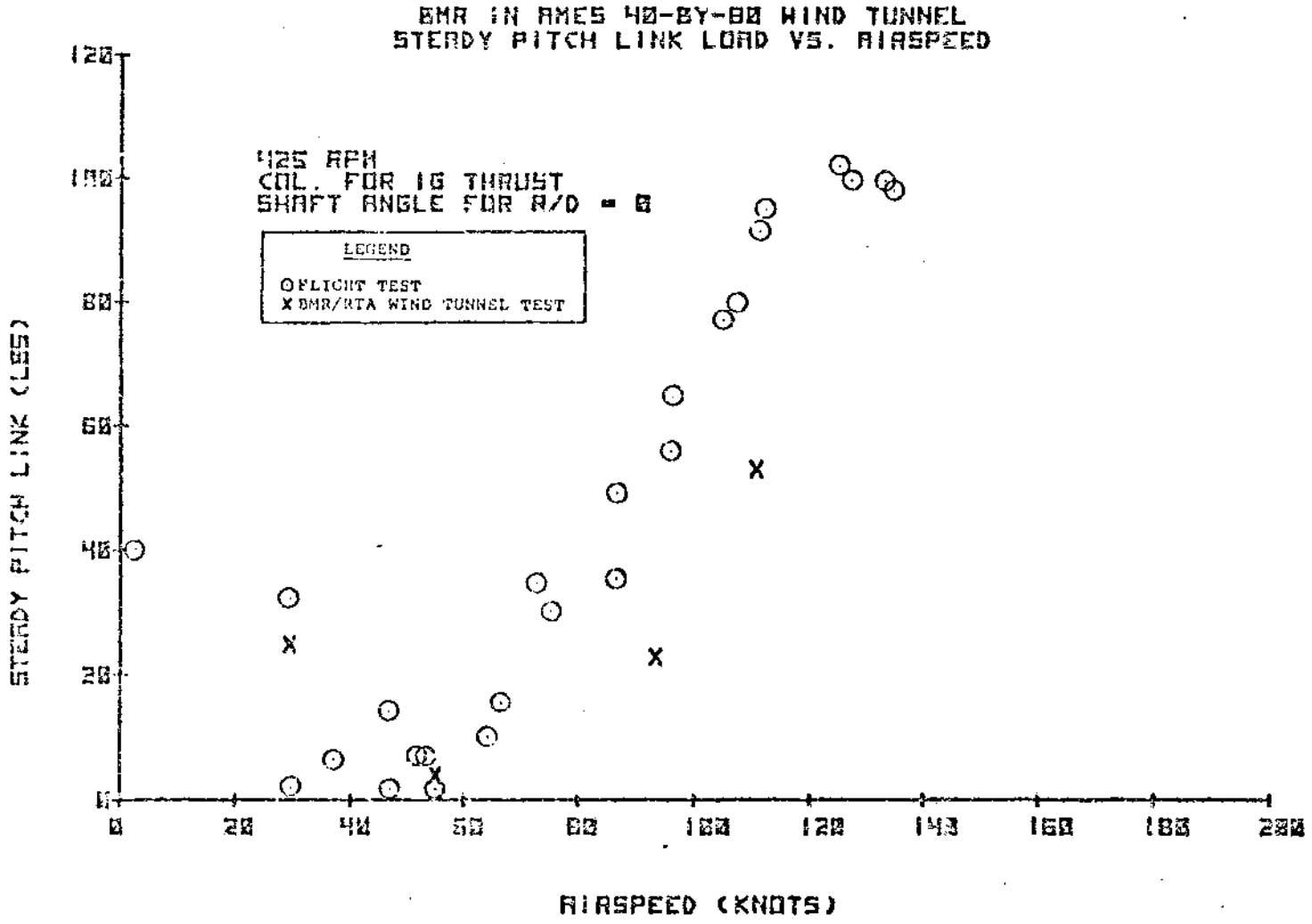

FIGURE 8.235 FLIGHT TEST CORRELATION - STEADY PITCH LINK LOAD VERSUS AIRSPEED

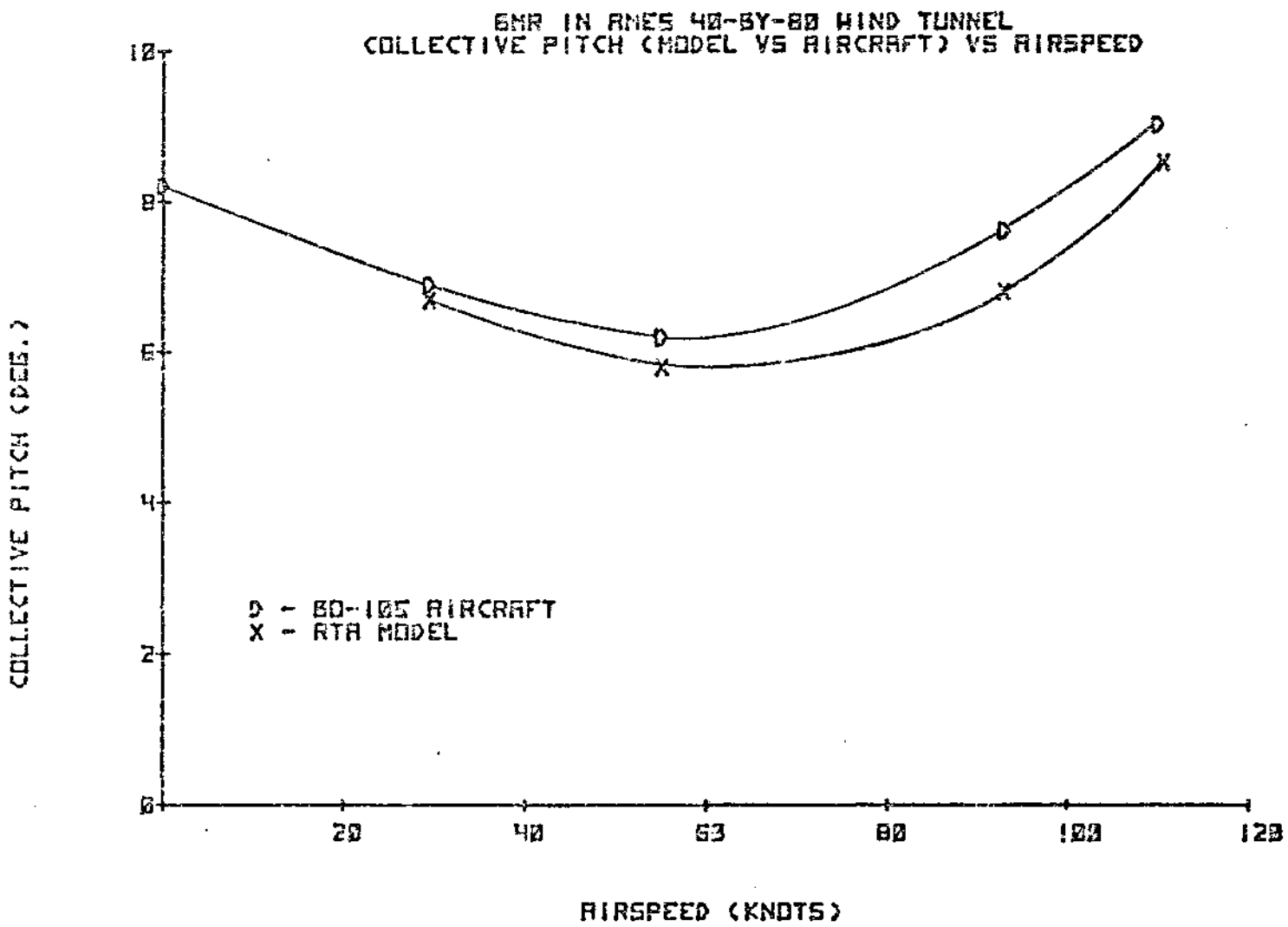

FIGURE 8.236 COLLECTIVE PITCH VERSUS AIRPSEED - BMR/RTA AND BO-105/BMR

8.2.4 Correlation With Analysis

The 1G speed sweep was selected for correlation of the BMR/RTA loads data with the flap and chord moments predicted by the Boeing Vertol computer program C-60. Flap moments were calculated along the span for both the flexbeam and the blade. For chord bending, loads were calculated using equivalent single beam properties in C-60. In addition, a separate program was used to evaluate local chord bending for the dual beam configuration using boundary conditions consistent with the C-60 analysis.

Figures 8.237 and 8.238 present correlation of flap moments. Very good agreement was obtained for both the steady and vibratory flap moment distribution. In the chord bending mode, the correlation with measured blade moments is shown in Figures 8.239 and 8.240. The corresponding correlation for the dual beam computer analysis is presented in Figures 8.241 and 8.242. Both the dual beam and the full blade program (C-60) significantly underpredict the measured chord bending moments along the span. These figures suggest the dual beam local chord moment is dependent on the C-60 moments at the flexbeam-to-blade attachment point. In comparing the deflection and slopes for the dual beam with applied moments and shears from C-60, it is indicated that an incompatibility with deflections and slopes in the full blade program exists. Thus, the dual beam local moment distribution is dependent on the blade mode shape as well as the shear and moment distributions. Additional

effort is required to develop a good chord bending analysis with compatible boundary conditions. Local beam correlation at the 110 knot condition is presented in Figures 8.243 and 8.244 to give an indication of the degree of correlation at the higher airspeeds as well as at 30 knots.

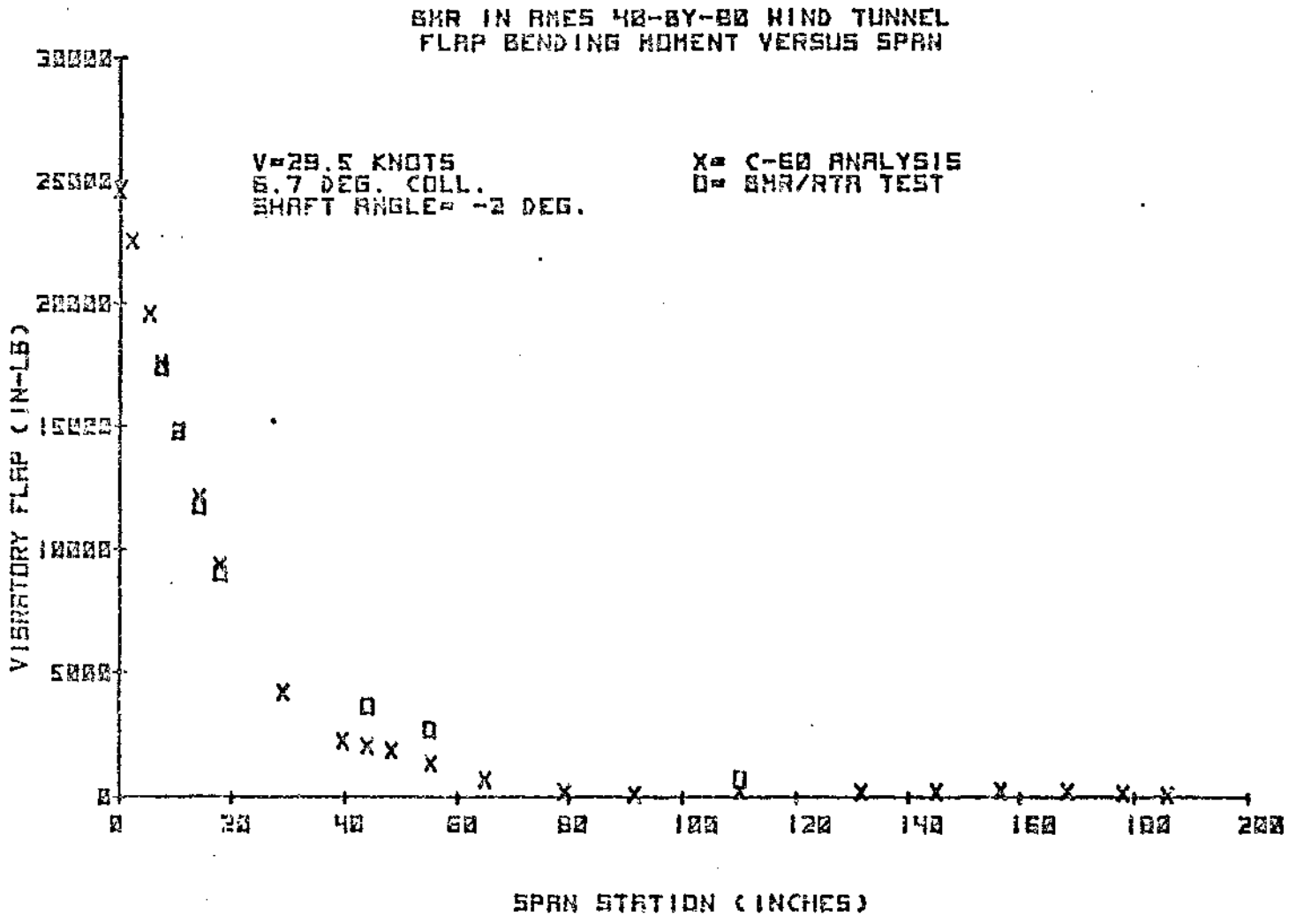

FIGURE 8.237 CORRELATION WITH ANALYSIS - 1G VIBRATORY FLAP MOMENTS AT 29.5 KNOTS

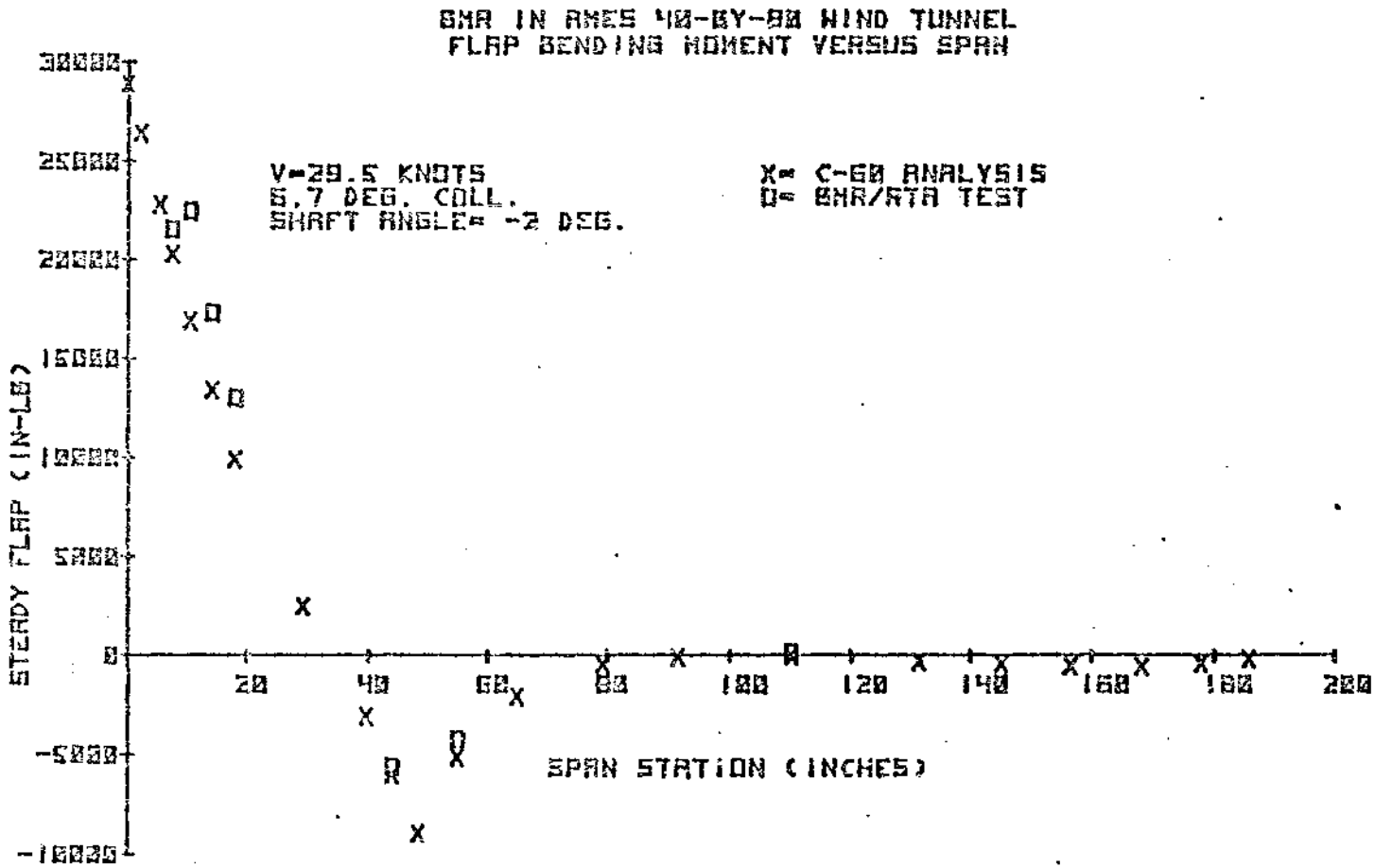

FIGURE 8.238 CORRELATION WITH ANALYSIS - 1G STEADY FLAP MOMENTS AT 29.5 KNOTS

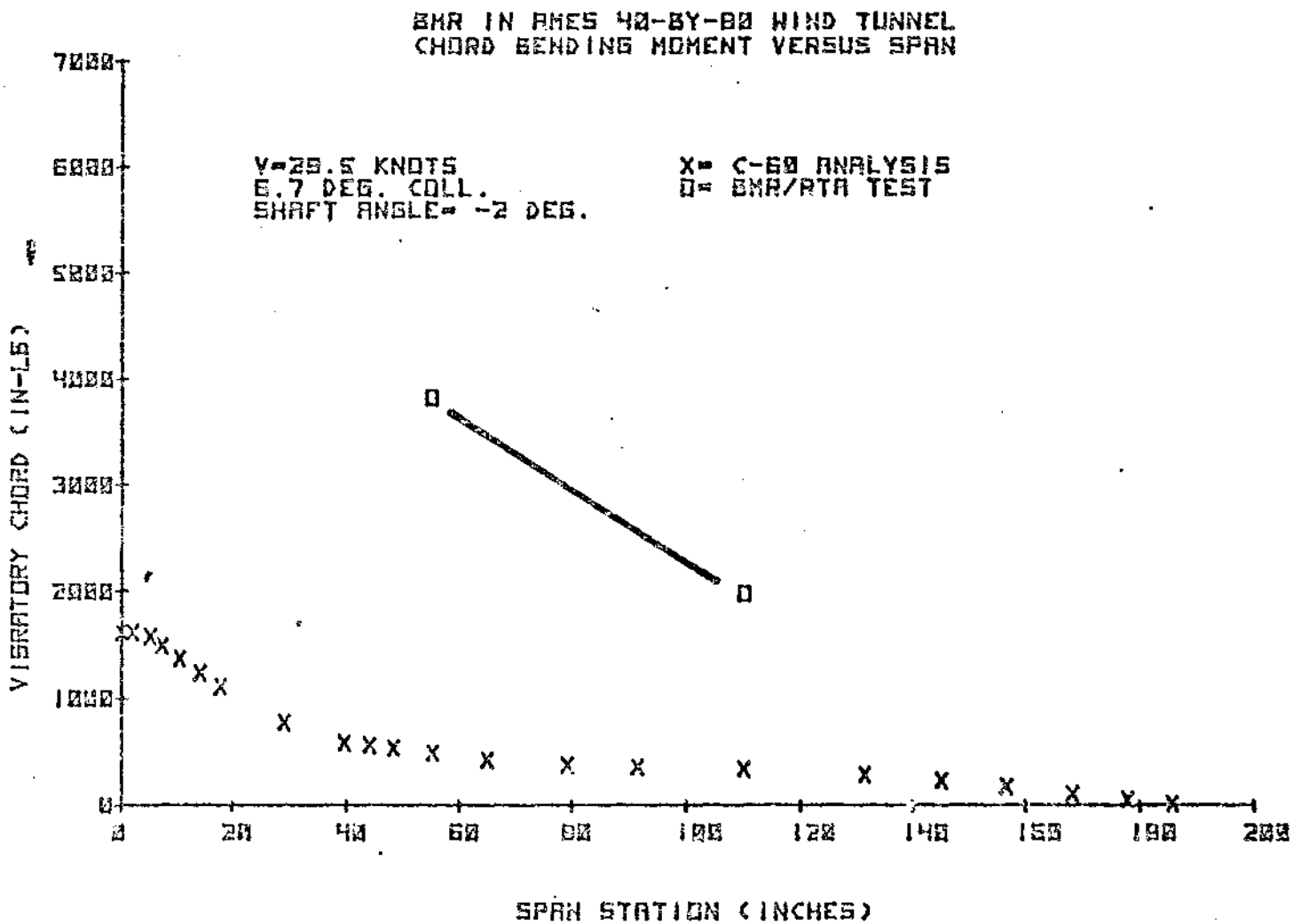

FIGURE 8.239 CORRELATION WITH ANALYSIS - 1G VIBRATORY CHORD MOMENTS AT 29.5 KNOTS

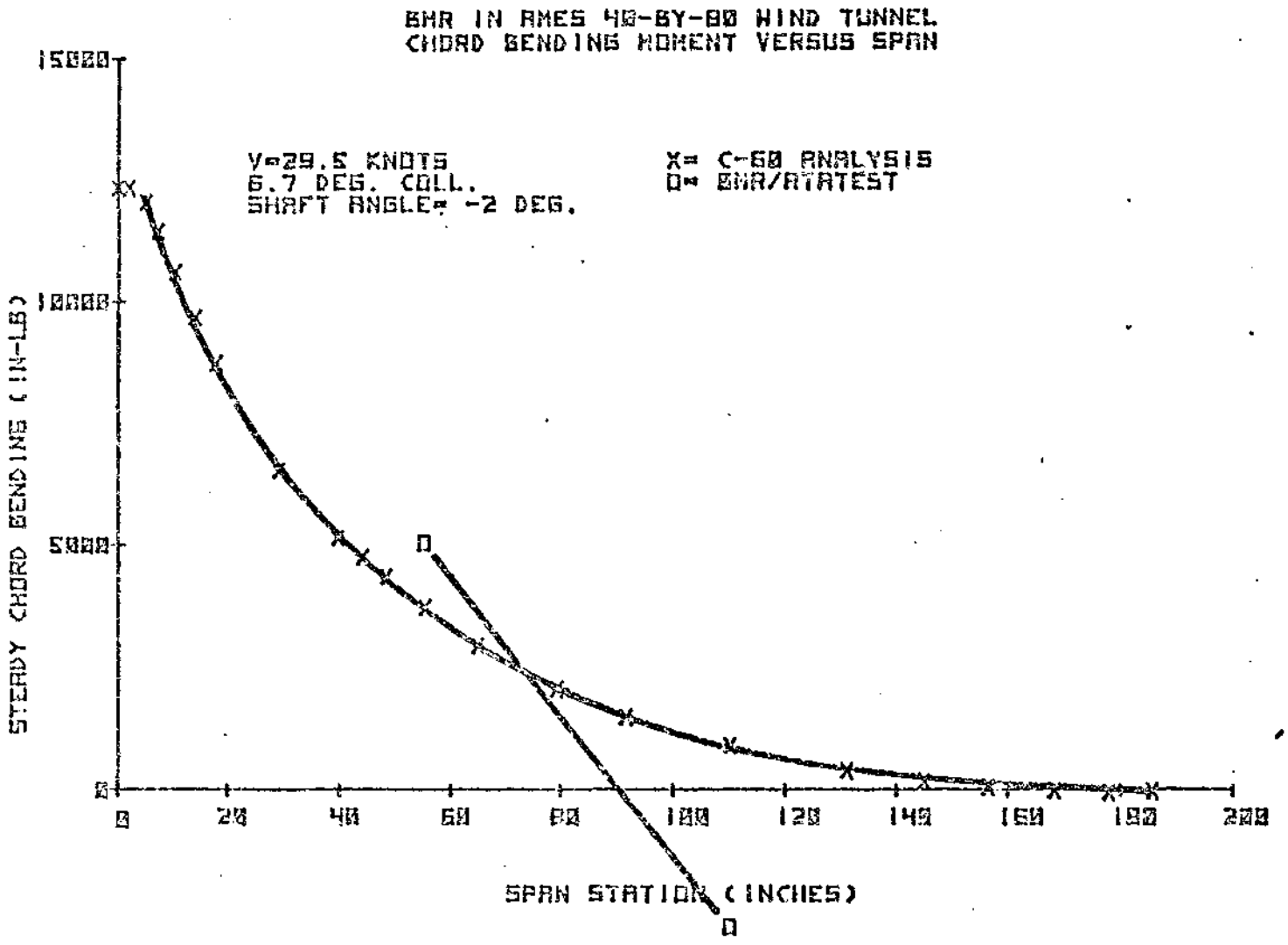

FIGURE 8.240 CORRELATION WITH ANALYSIS - 1G STEADY CHORD MOMENTS AT 29.5 KNOTS

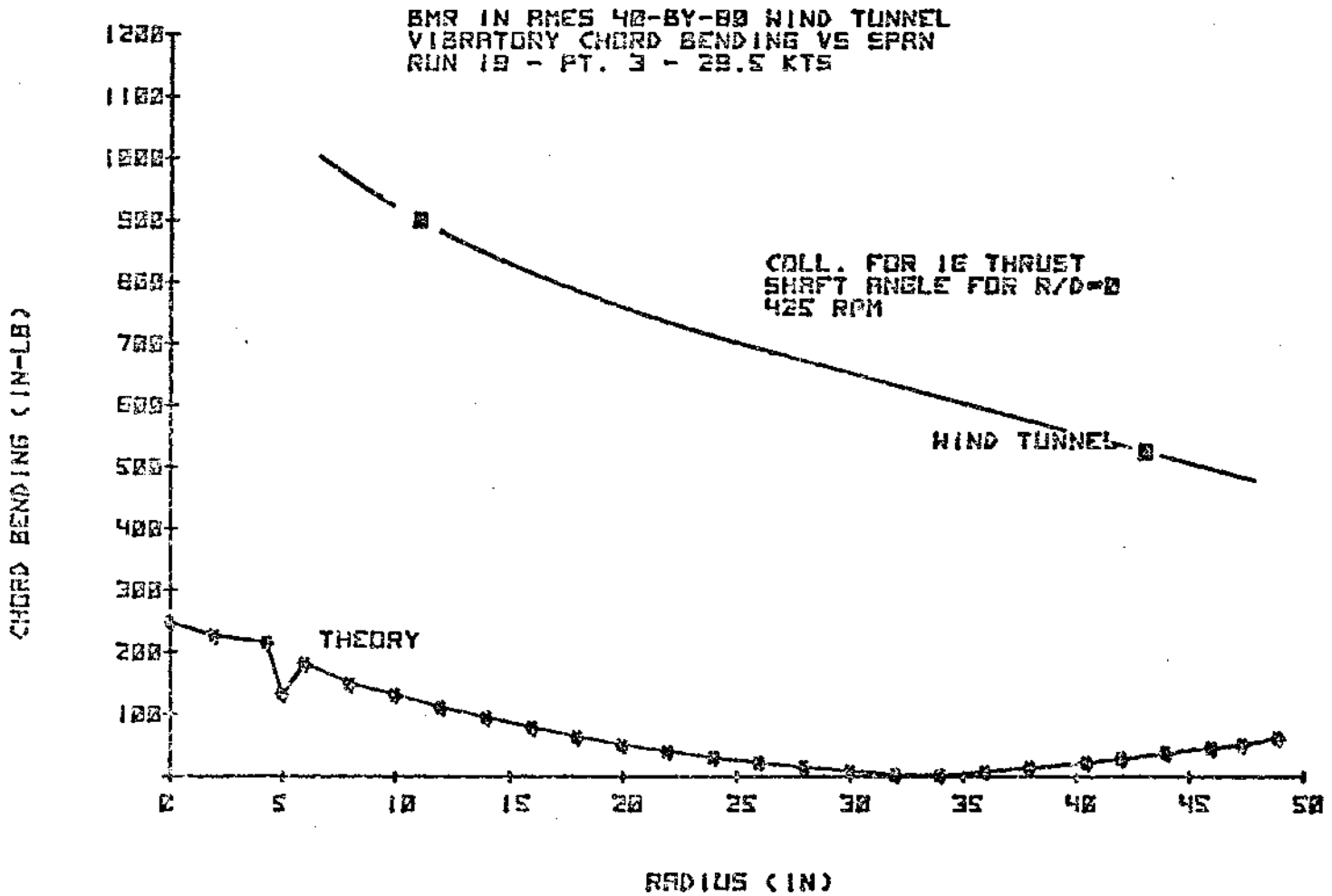

FIGURE 8.241 CORRELATION WITH ANALYSIS - VIBRATORY CHORD MOMENT AT 29.5 KNOTS

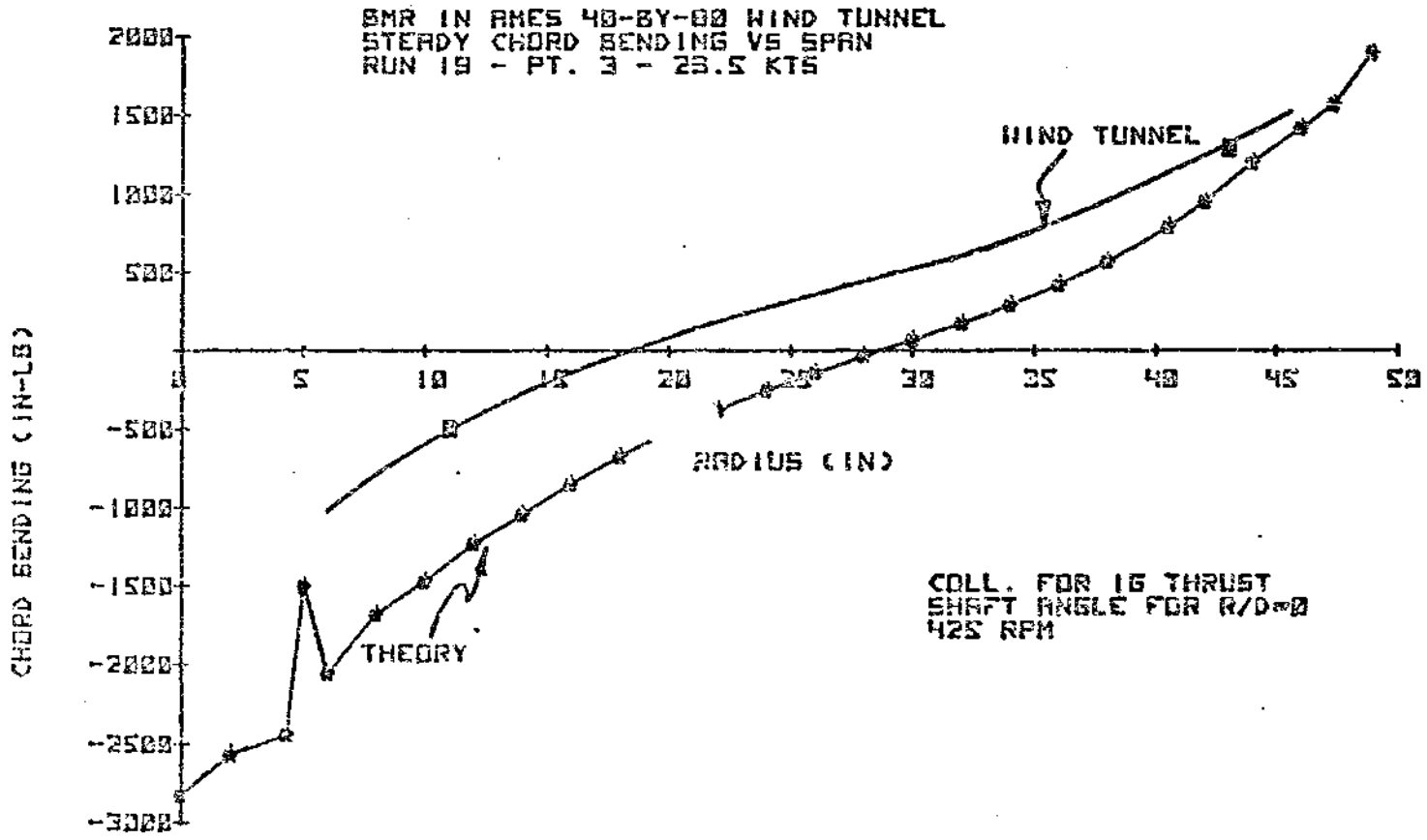

FIGURE 8.242 CORRELATION WITH ANALYSIS - STEADY CHORD MOMENT AT 29.5 KNOTS

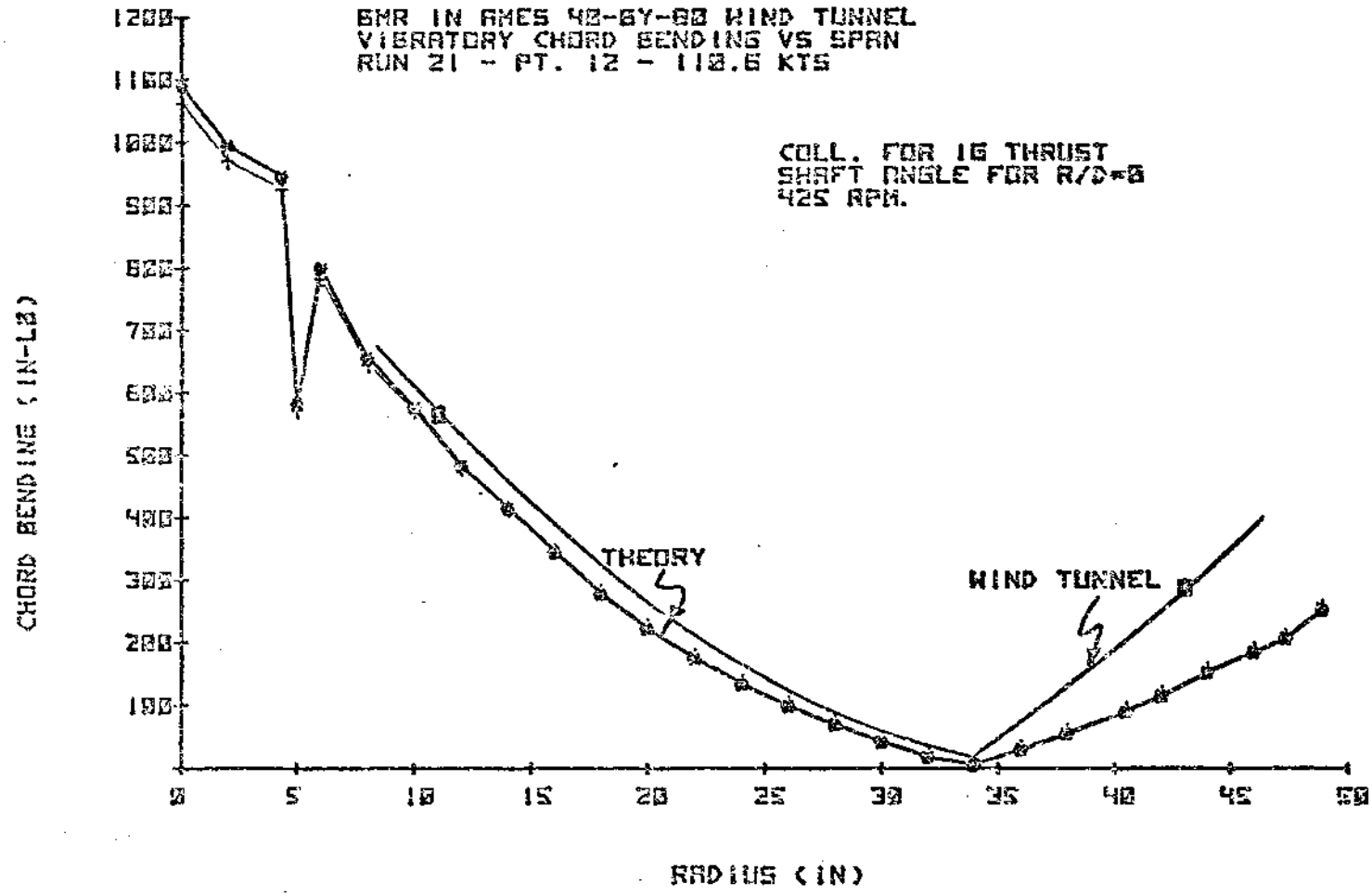

FIGURE 8.243 CORRELATION WITH ANALYSIS - VIBRATORY CHORD MOMENT AT 110.6 KNOTS

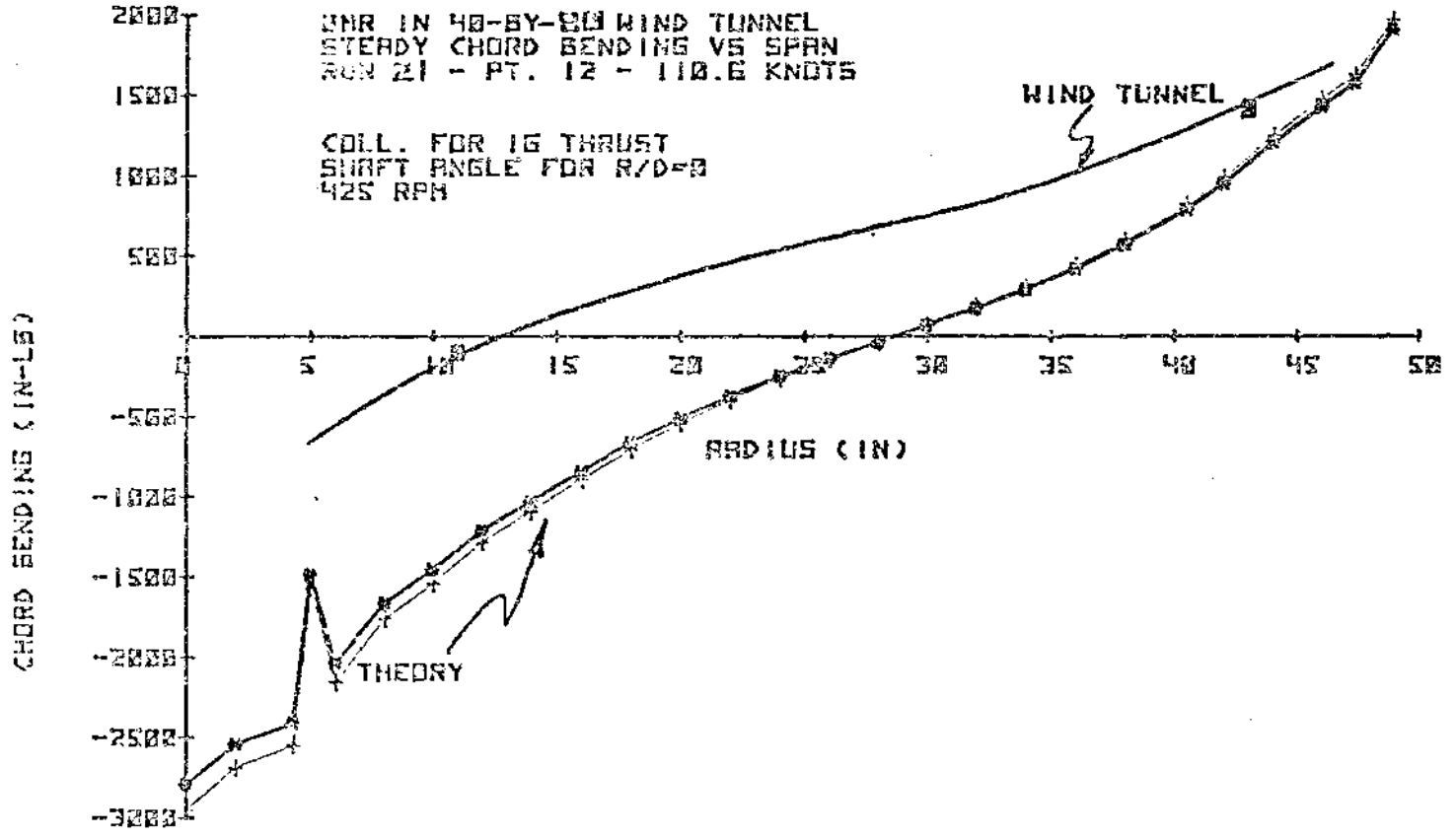

FIGURE 8.244 CORRELATION WITH ANALYSIS - STEADY CHORD MOMENT AT 110.6 KNOTS

8.3 PERFORMANCE

Hub Tares

Data for the hub tares was taken with the flexbeams on and the blades removed. Speeds of 60, 120 and 180 knots were evaluated with the shaft angle ranging from -10 degrees to +10 degrees. Presented in Figure 8.245 are the drag results along with an estimate made of the BMR/BO-105 hub drag using the BO-105 baseline test data at 120 knots (μ = .20). The pretest estimate of 4.41 ft.^{2} at a shaft angle of -2.3 degrees (theoretical trim value) is lower than the measured value of 4.75 ft.^{2}. It is also evident that, at higher speeds, the lift is not very sensitive to variations in shaft angle as indicated in Figure 8.245.

Hover

Hover testing was conducted at a shaft angle of -10° to minimize the effects of the tunnel floor and walls on the flow environment around the rotor. This, however, eventually produced recirculation in the tunnel test section. Referencing FAA Report 8110.32, "Engineering Flight Test Guide For Transport Category Helicopters", acceptable wind speeds for hover testing are between 0 and 3 knots for OGE, IGE and tie-down conditions. For this test, the rotor was 26 ft. above the tunnel floor which puts the rotor in ground effect (h/D = .807).

Only the low speed test points (V ≤ 3.5 kts) were selected for analysis. Figure 8.246 displays Cp/σ as a function of C_T/σ

with a smooth curve drawn through the data. Also shown on the plot is the theoretical prediction which shows the measured power 4.3% higher than the predicted power at 5000 pounds thrust, which corresponds to the takeoff gross weight of the BO-105/BMR.

Forward Flight

Since the objective of the test was primarily to obtain stability data, most of the testing was performed at the minimum collectives where aeroelastic stability is lowest. In addition, shaft angles selected for testing were not based on matching the aircraft flat plate drag area. Therefore, there is a very limited amount of test points which match both aircraft lift and propulsive force values simultaneously. Because of this, no correlation with flight test data is possible.

The data was analyzed at four (4) different forward flight speeds, 60, 90, 120 and 144 knots and a constant tip speed of 717 ft/sec. A theoretical prediction was then made using the Rotor Analysis program B-67 and the results were compared with the test results. The measured values of velocity, shaft angle, thrust, temperature, lateral and longitudinal cyclics were taken from the test data and used as program inputs.

During the test, the rotor was trimmed to zero flapping (lateral and longitudinal flapping coefficients equal to zero) using a flap bending gage located at station 14.25 inches radius. Another indication that the rotor is trimmed to zero flapping is that the pitching moments are near zero. An examination of the equation for pitching moment shows that when the flapping coefficients are zero there is still a small moment due to coning and cyclic pitch, therefore pitching moment will not be equal to zero. Figures 8.247 - 8.250 present the plots of lift coefficient (C_{LR}/σ) versus pitching moment coefficient (C_{PM}/σ) used to analyze the trim of each test point. At all speeds the rotor was trimmed to near zero flapping and the theory and the test data show good agreement.

Performance of the rotor is examined in Figures 8.251 - 8.254 in the form of lift coefficient (C_{LR}/σ) versus lift-to-effective drag ratio (L/De) plots. At low speeds, the trends appear as expected and the predictions agree very well with test data. As speed increases, the theory begins to overpredict the measured L/D_e.

The drag polars appear in Figures 8.255 - 8.258. There is a good correlation between theory and test data for all but the 144 knots condition as shown in the plots of lift coefficient (C_{LR}/σ) versus effective drag coefficient (C_{De}/σ).

Plots of lift coefficient (C_{LR}/σ) versus propulsive force coefficient (C_{XR}/σ) and power coefficient (C_p/σ) versus propulsive force coefficient are shown in Figures 8.259 - 8.266. The trends appear to be as expected, following the theoretical data but with a magnitude shift in propulsive force. Plots of lift coefficient (C_{LR}/σ) versus power coefficient (C_p/σ) (Figures 8.267 - 8.270) show the test data and theory to be almost identical.

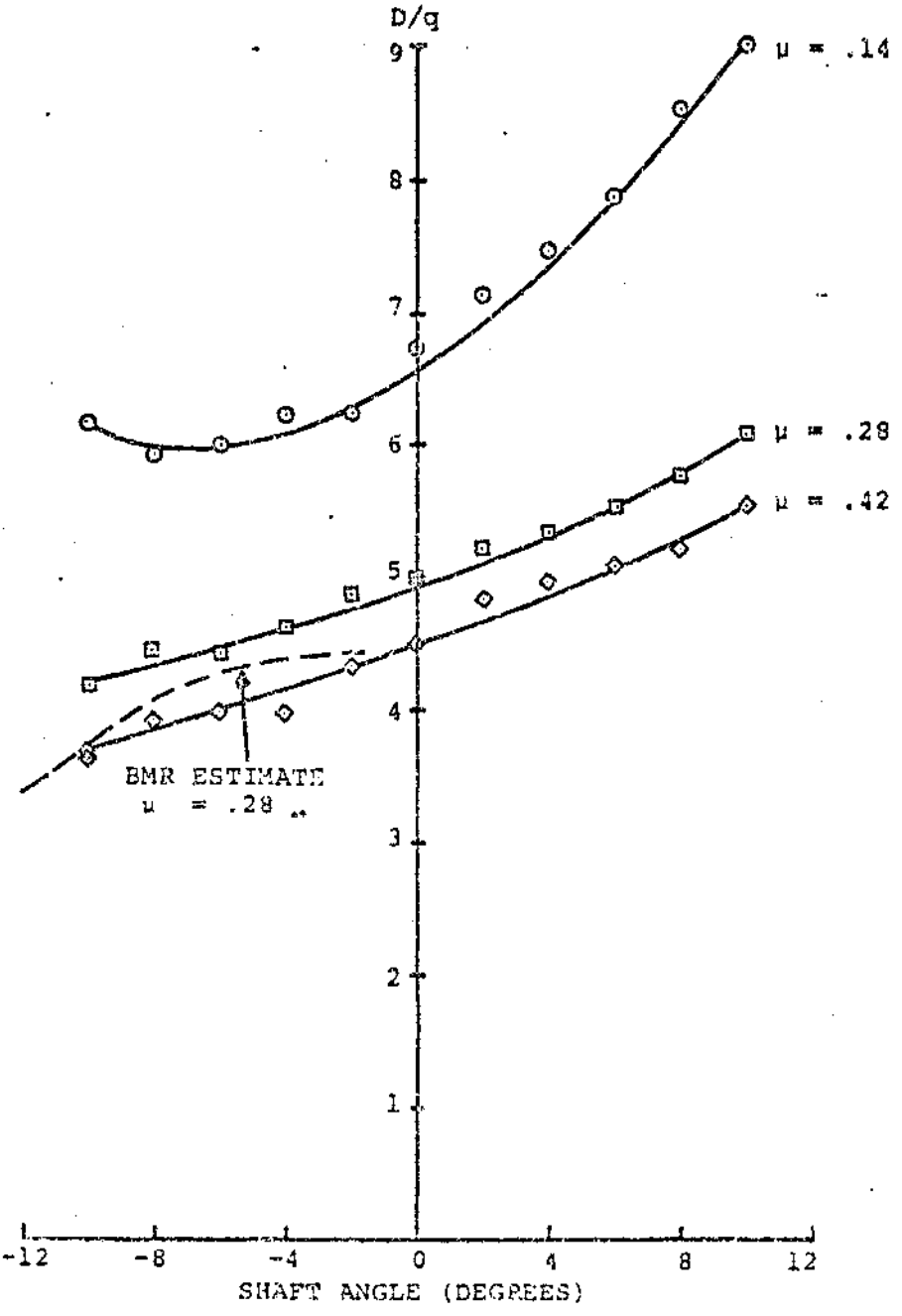

Fig. 8.245 BMR HUB TARES - DRAG/q
VERSUS SHAFT ANGLE (SHEET 1 OF 2)

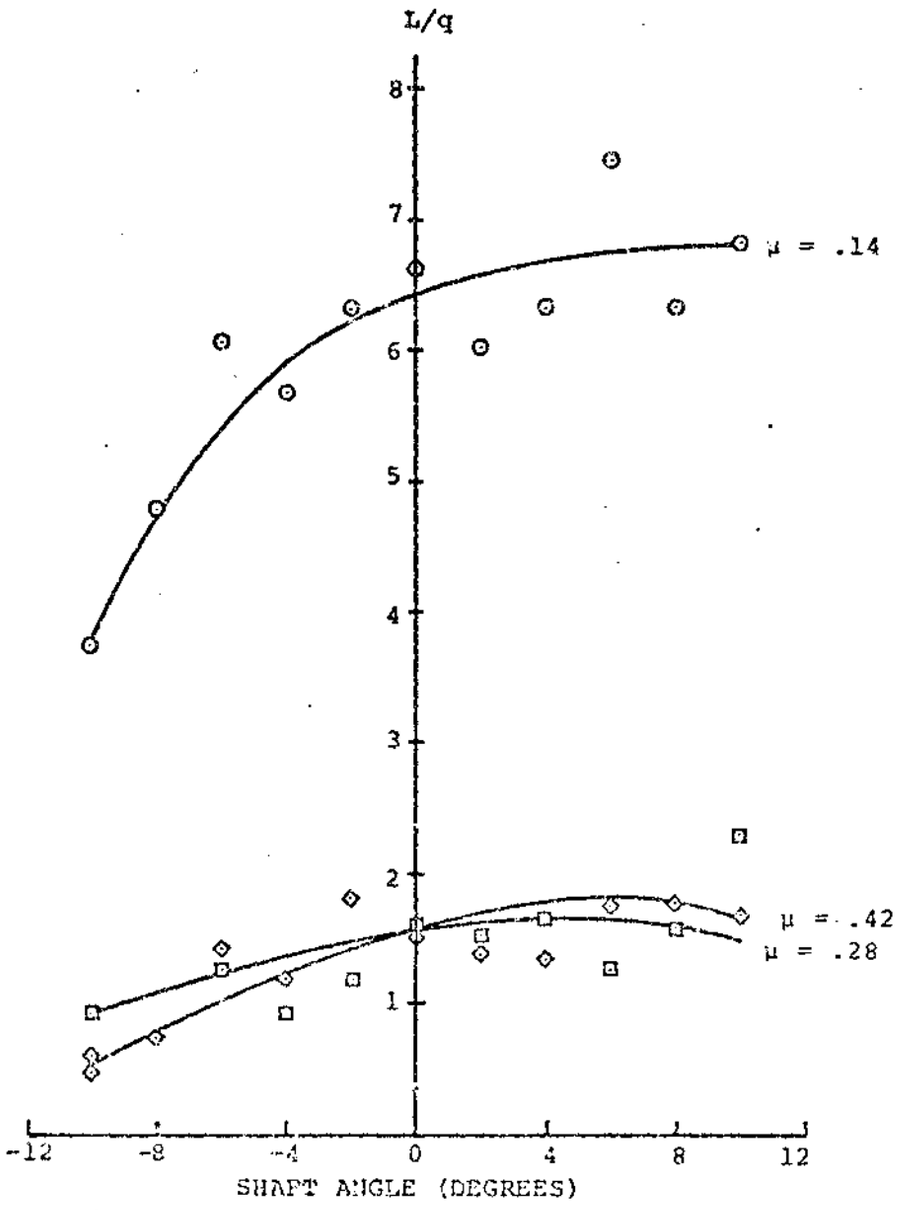

Fig. 8.245 BMR HUB TARES - LIFT/q
VERSUS SHAFT ANGLE (SHEET 2 OF 2)

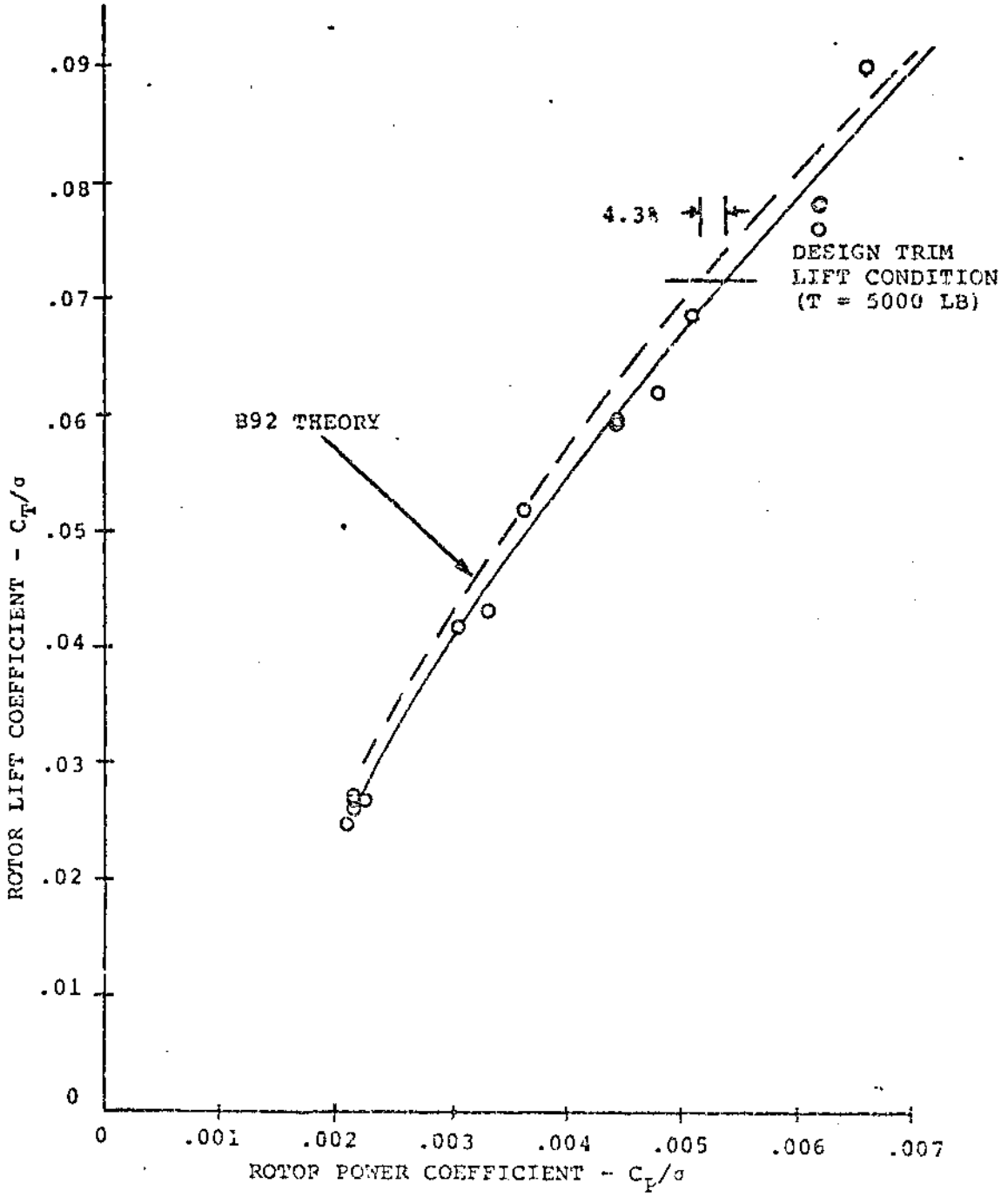

FIGURE 8.246 HOVER PERFORMANCE

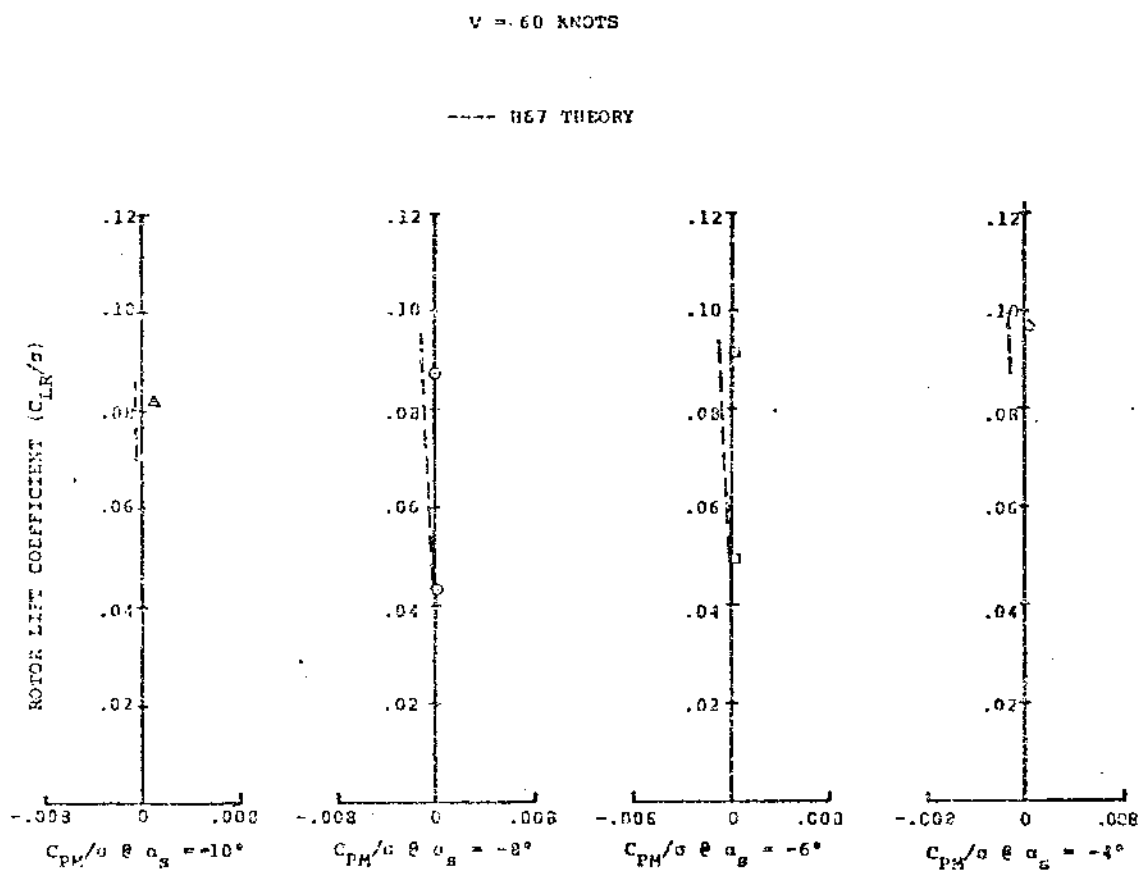

FIGURE 8.247 LIFT COEFFICIENT VERSUS PITCHING MOMENT COEFFICIENT AT 60 KNOTS

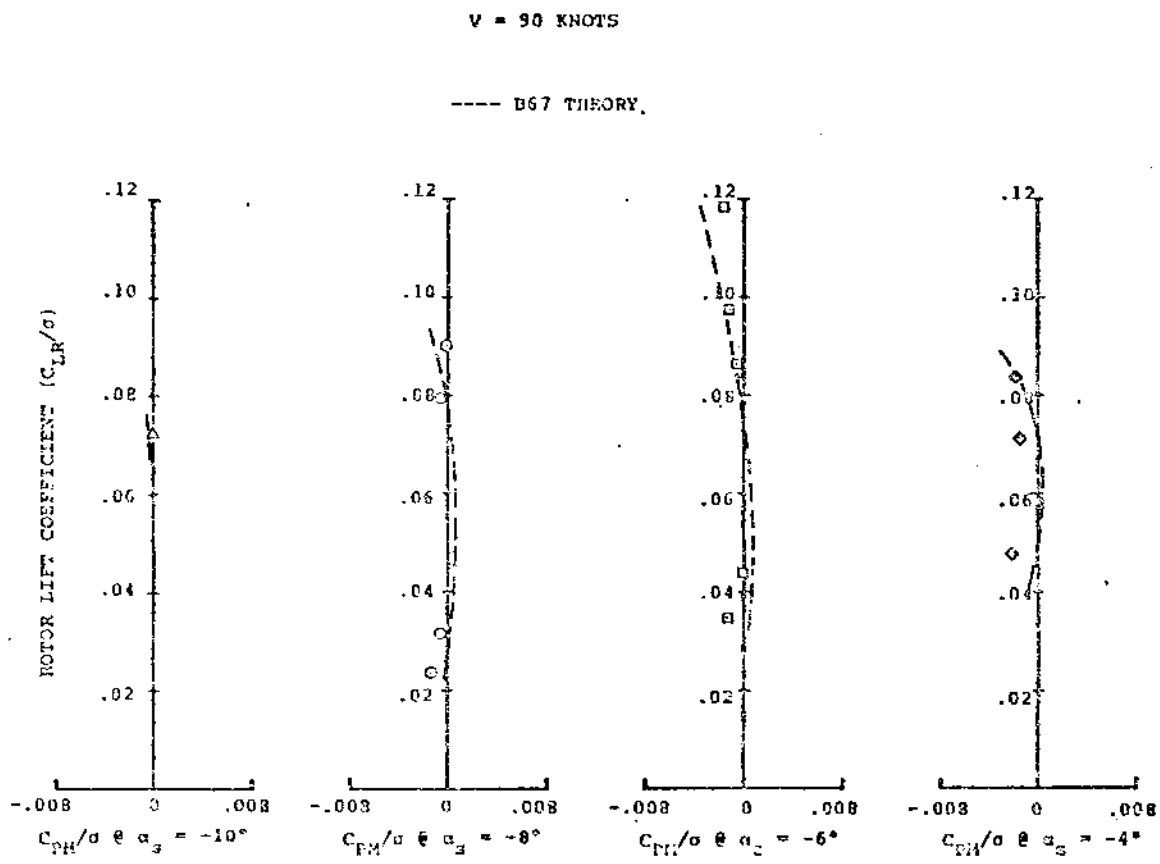

FIGURE 8.248 LIFT COEFFICIENT VERSUS PITCHING MOMENT COEFFICIENT AT 90 KNOTS

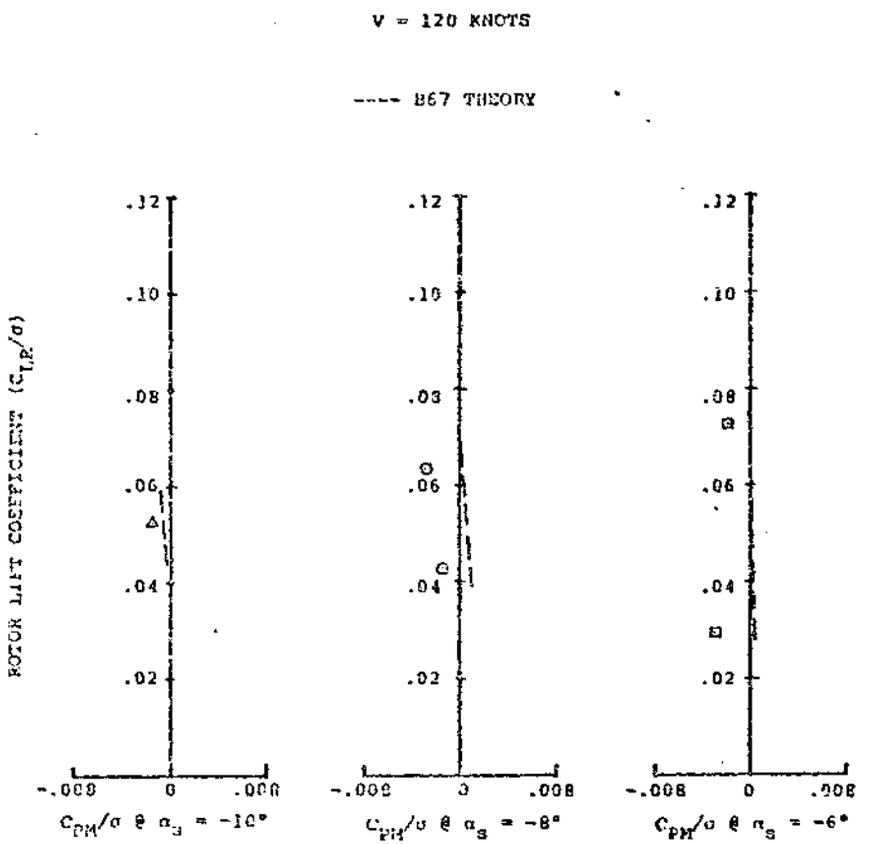

FIGURE 8.249 . LIFT COEFFICIENT VERSUS PITCHING MOMENT COEFFICIENT AT 120 KNOTS

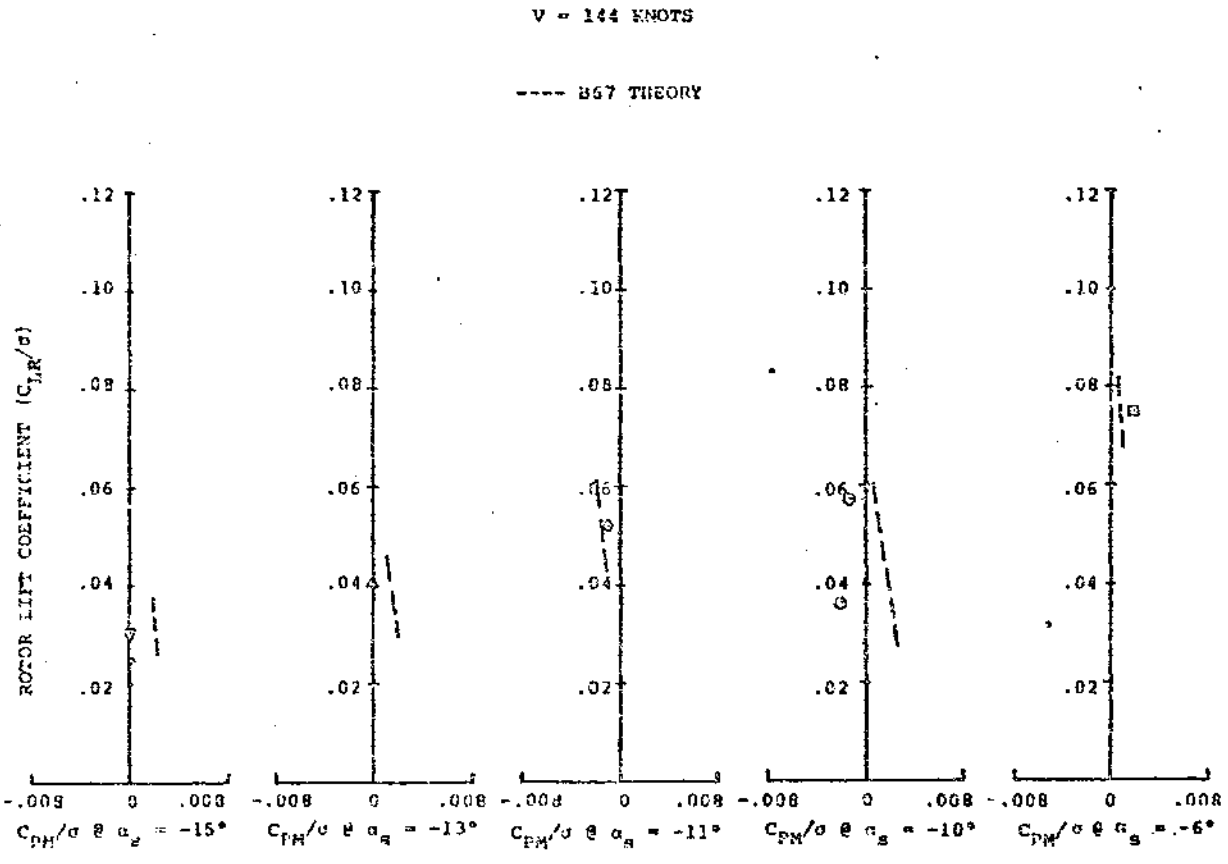

FIGURE 8.250 LIFT COEFFICIENT VERSUS PITCHING MOMENT COEFFICIENT AT 144 KNOTS

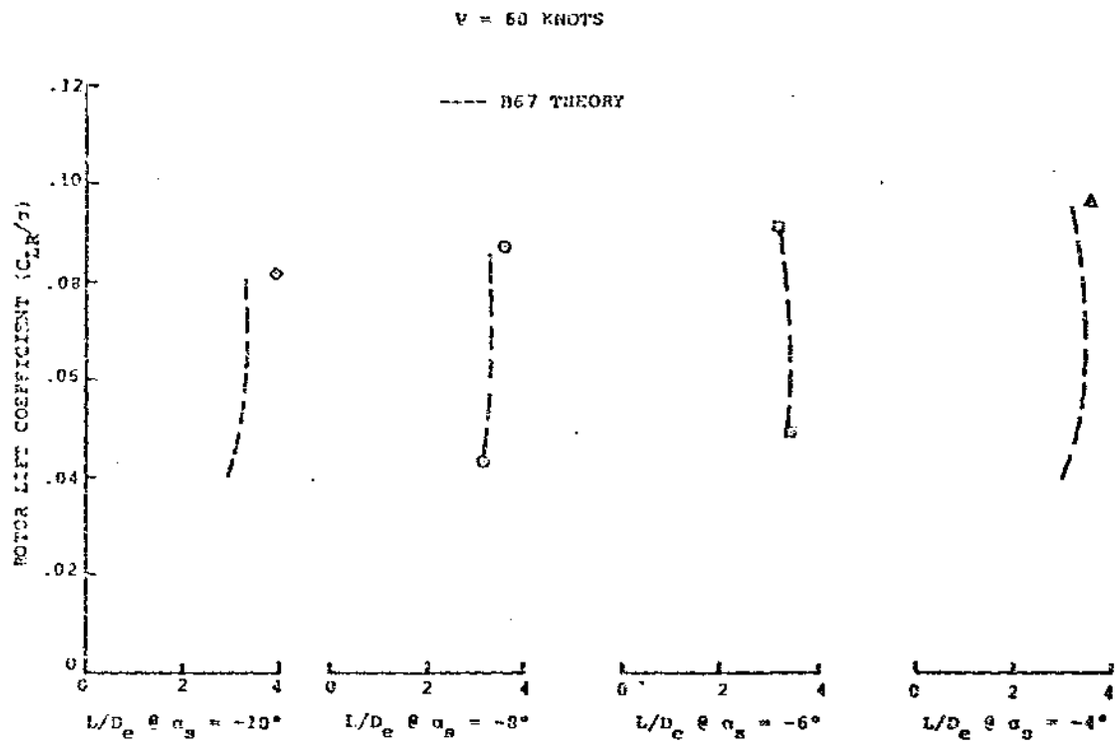

FIGURE 8.251 LIFT COEFFICIENT VERSUS L/D_e AT 60 KNOTS

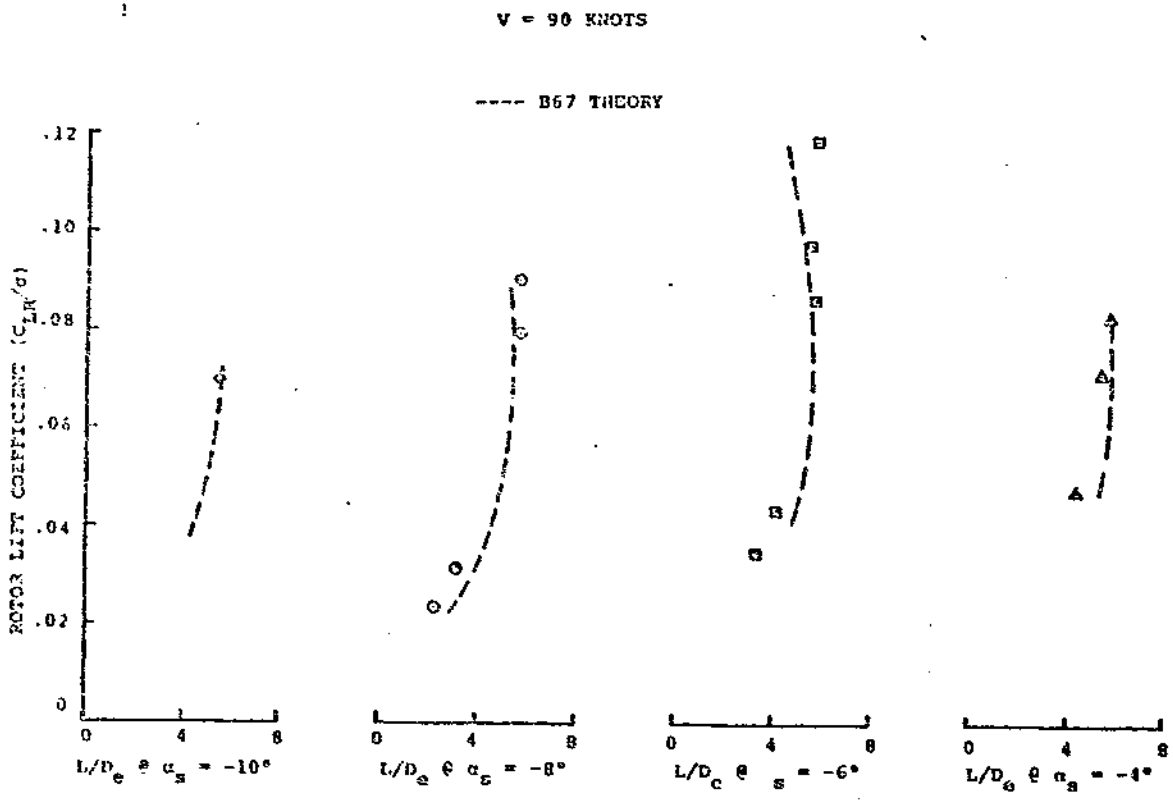

FIGURE 8.252 LIFT COEFFICIENT VERSUS L/D_e AT 90 KNOTS

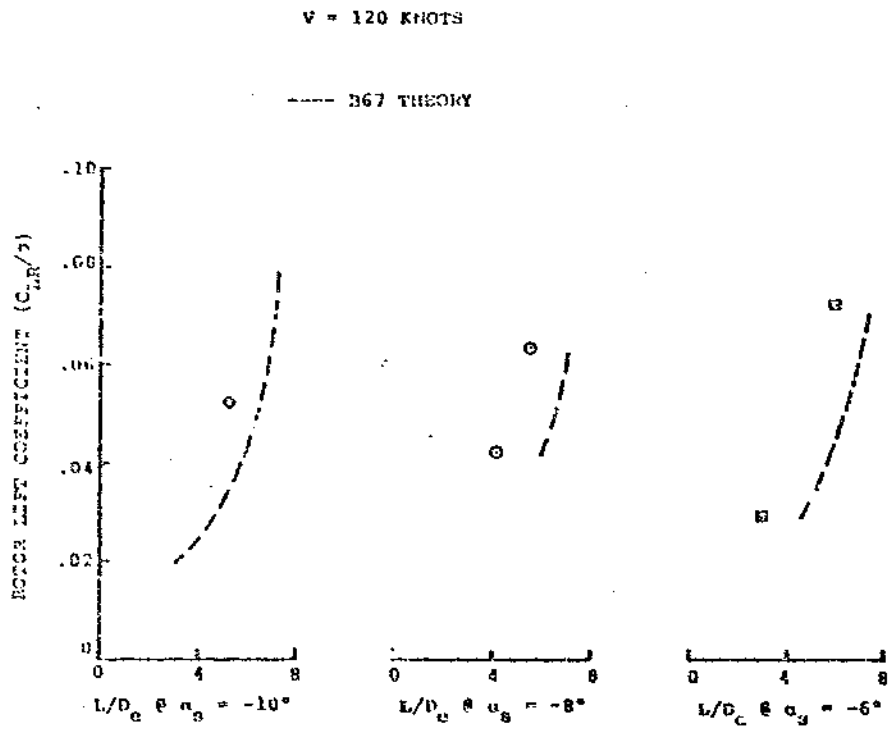

FIGURE 8.253 LIFT COEFFICIENT VERSUS L/D_e AT 120 KNOTS

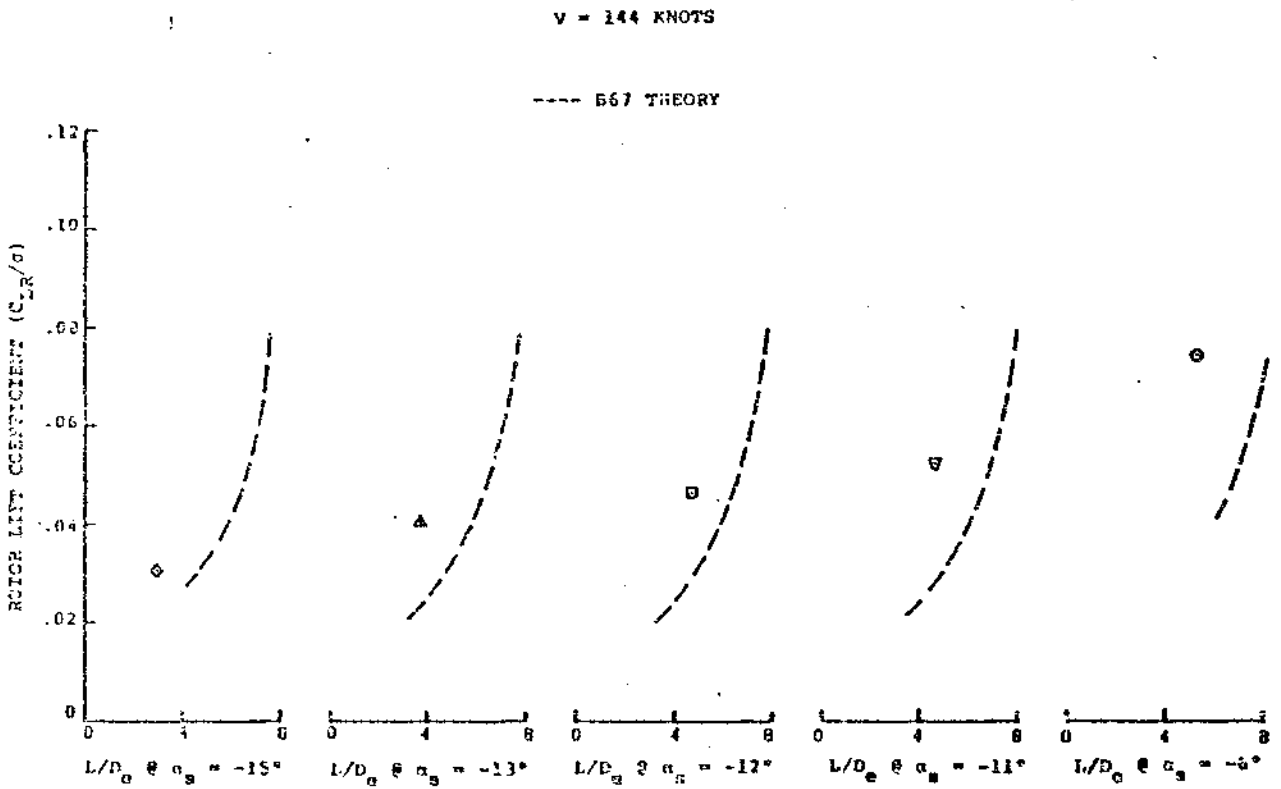

FIGURE 8.254 LIFT COEFFICIENT VERSUS L/D_e AT 144 KNOTS

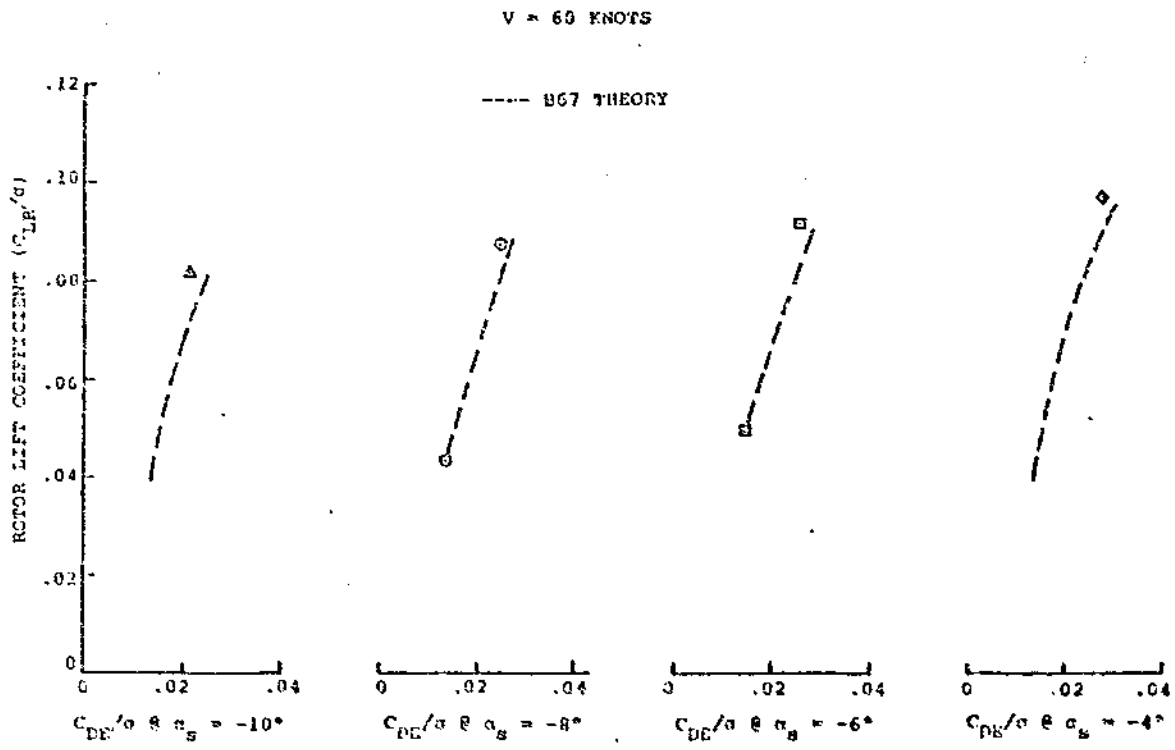

FIGURE 8.255 LIFT COEFFICIENT VERSUS DRAG COEFFICIENT AT 60 KNOTS

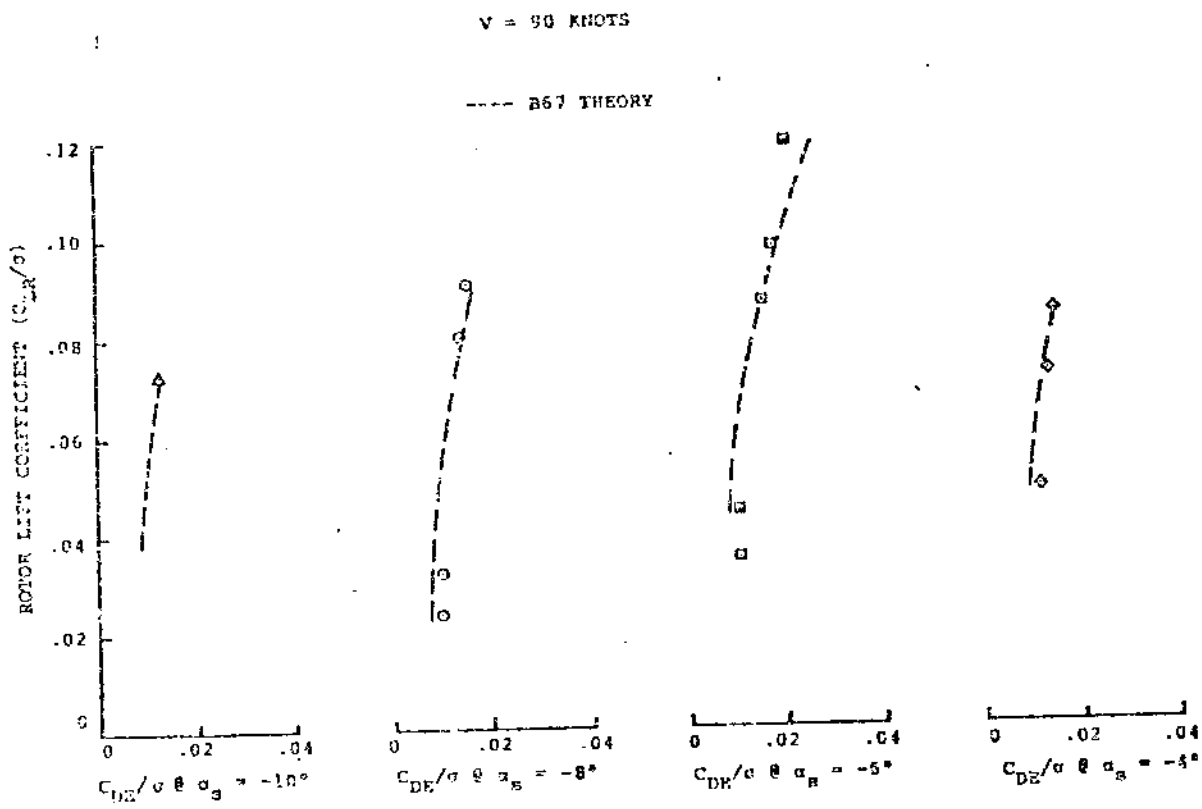

FIGURE 8.256 LIFT COEFFICIENT VERSUS DRAG COEFFICIENT AT 90 KNOTS

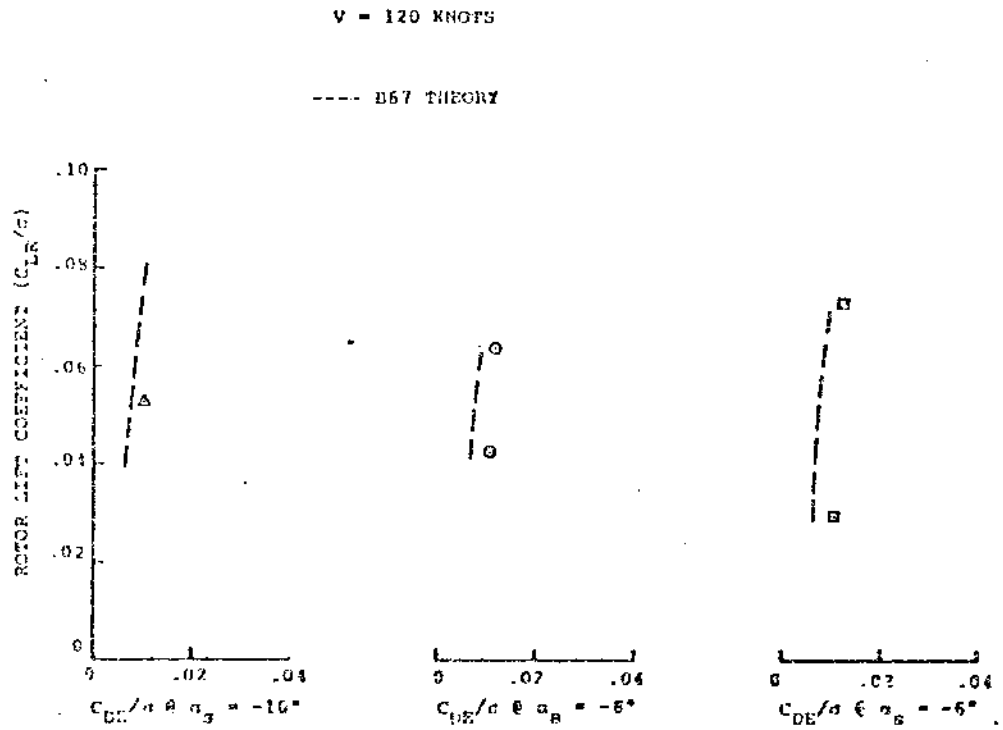

FIGURE 8.257 LIFT COEFFICIENT VERSUS DRAG COEFFICIENT AT 120 KNOTS

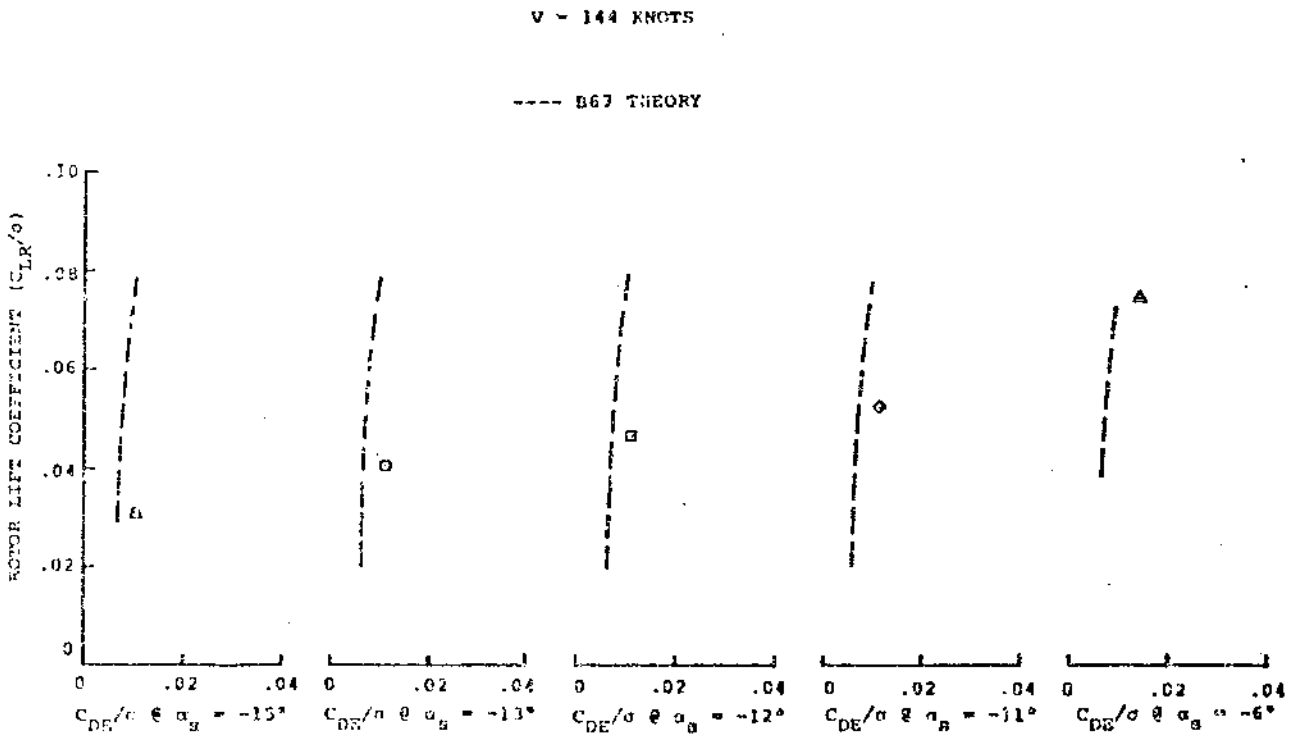

FIGURE 8.258 LIFT COEFFICIENT VERSUS DRAG COEFFICIENT AT 144 KNOTS

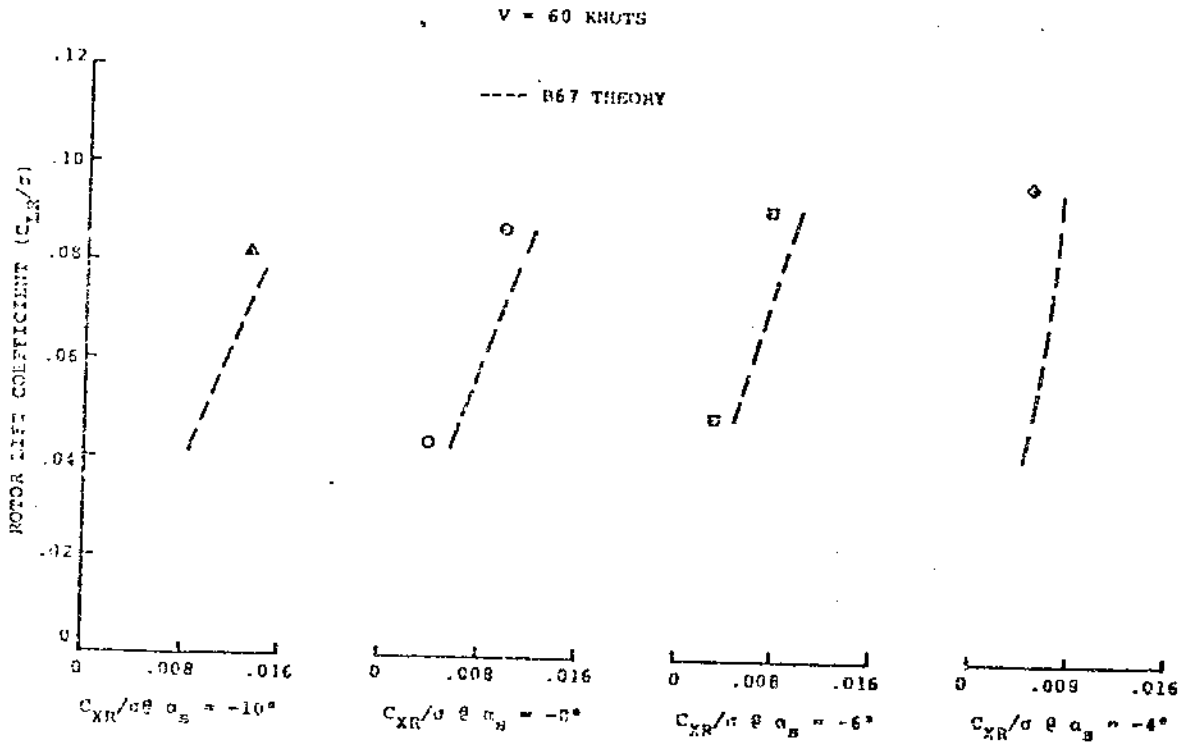

FIGURE 8.259 LIFT COEFFICIENT VERSUS PROPULSIVE FORCE COEFFICIENT AT 60 KNOTS

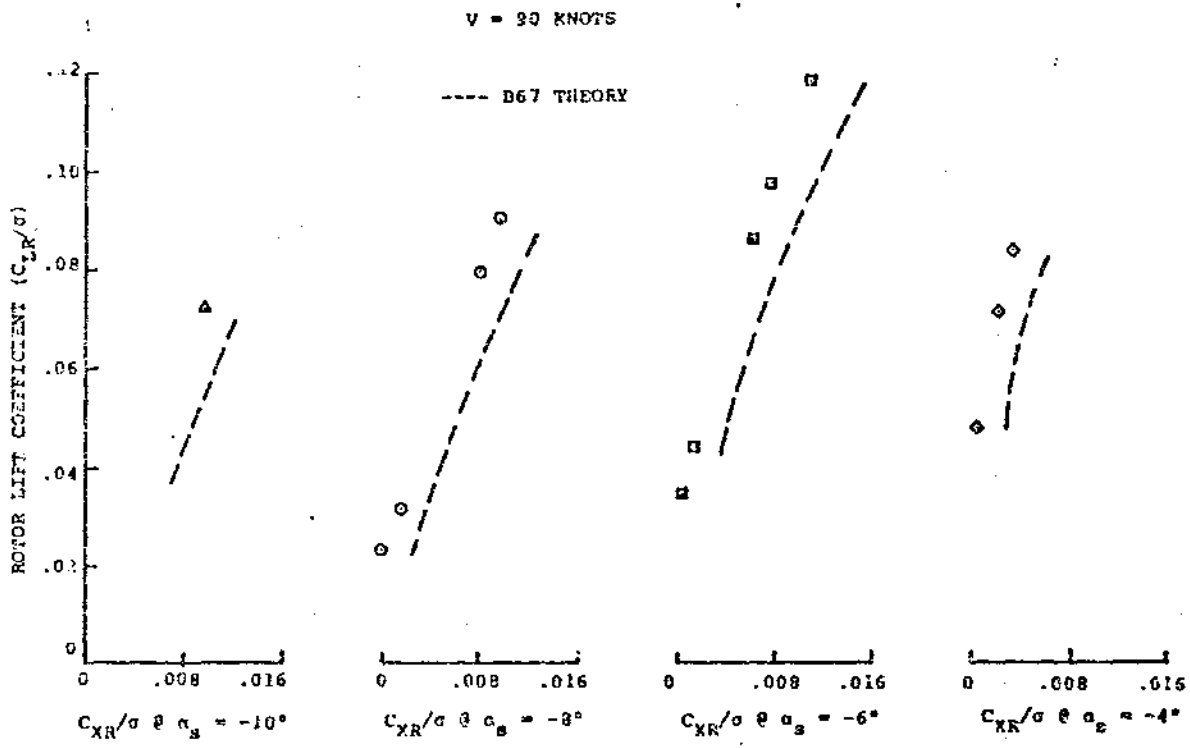

FIGURE 8.260 LIFT COEFFICIENT VERSUS PROPULSIVE FORCE COEFFICIENT AT 90 KNOTS

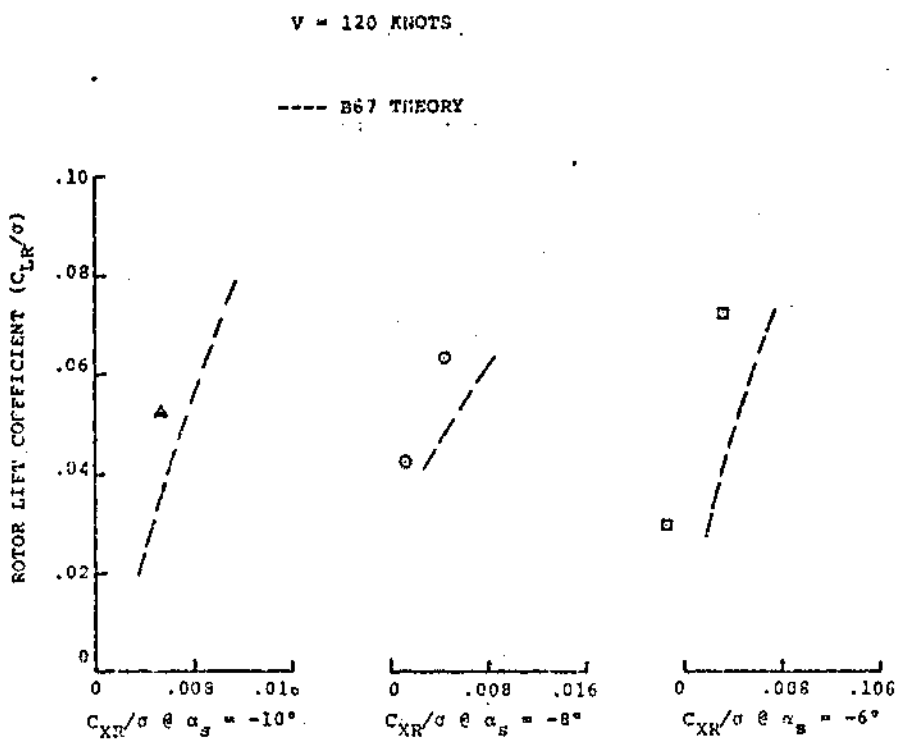

FIGURE 8.261 LIFT COEFFICIENT VERSUS PROPULSIVE FORCE COEFFICIENT AT 120 KNOTS

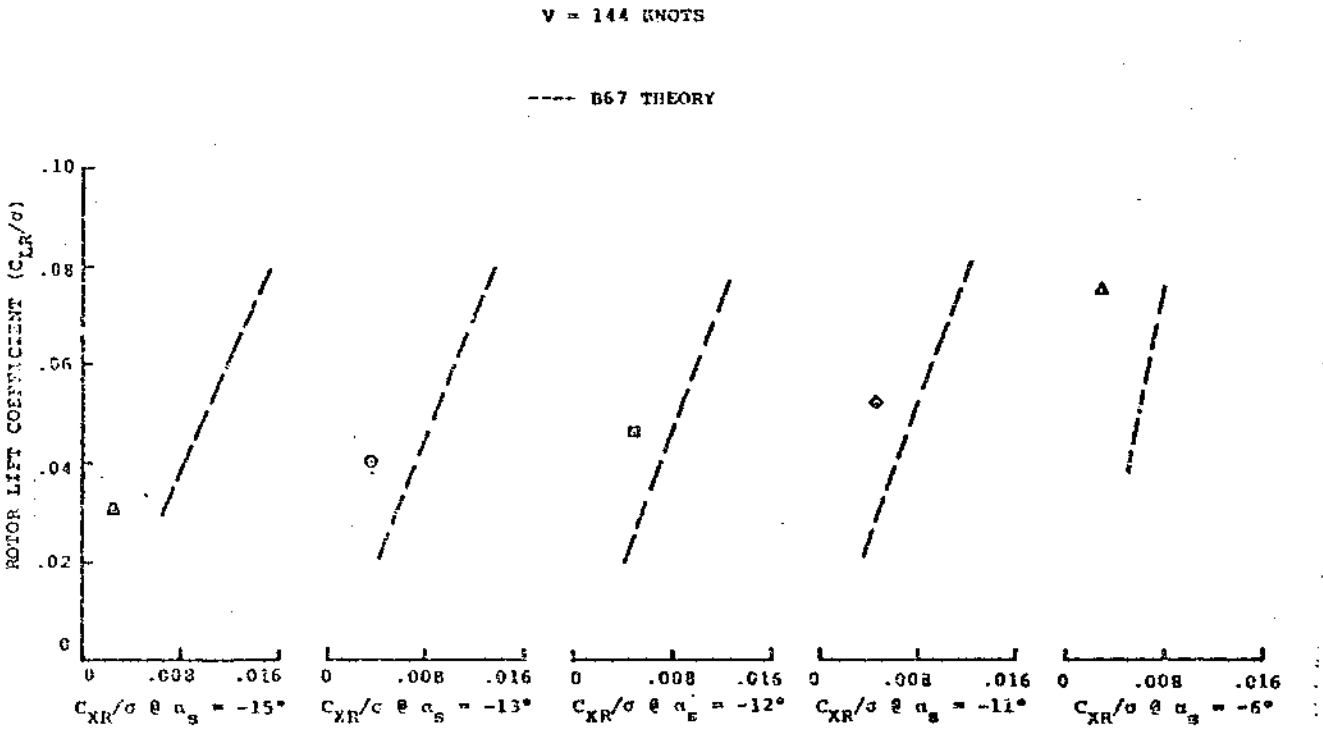

FIGURE 8.262 LIFT COEFFICIENT VERSUS PROPULSIVE FORCE COEFFICIENT AT 144 KNOTS

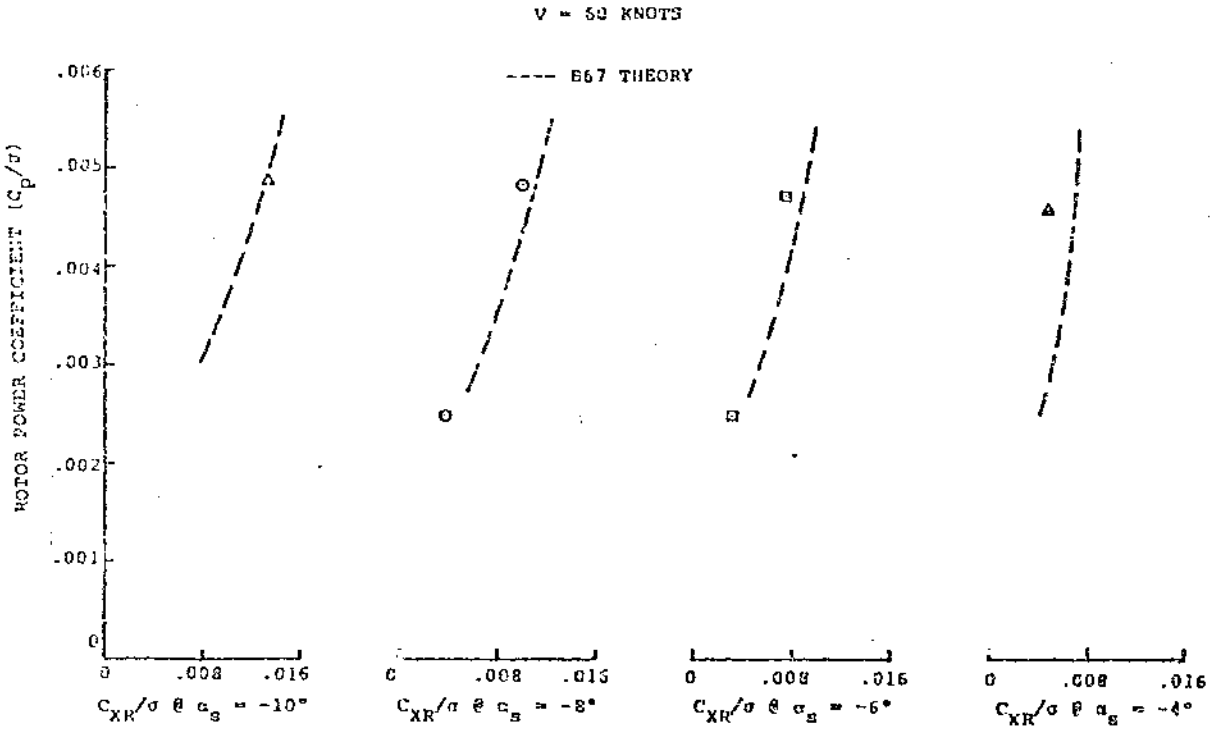

FIGURE 8.263 POWER COEFFICIENT VERSUS PROPULSIVE FORCE COEFFICIENT AT 60 KNOTS

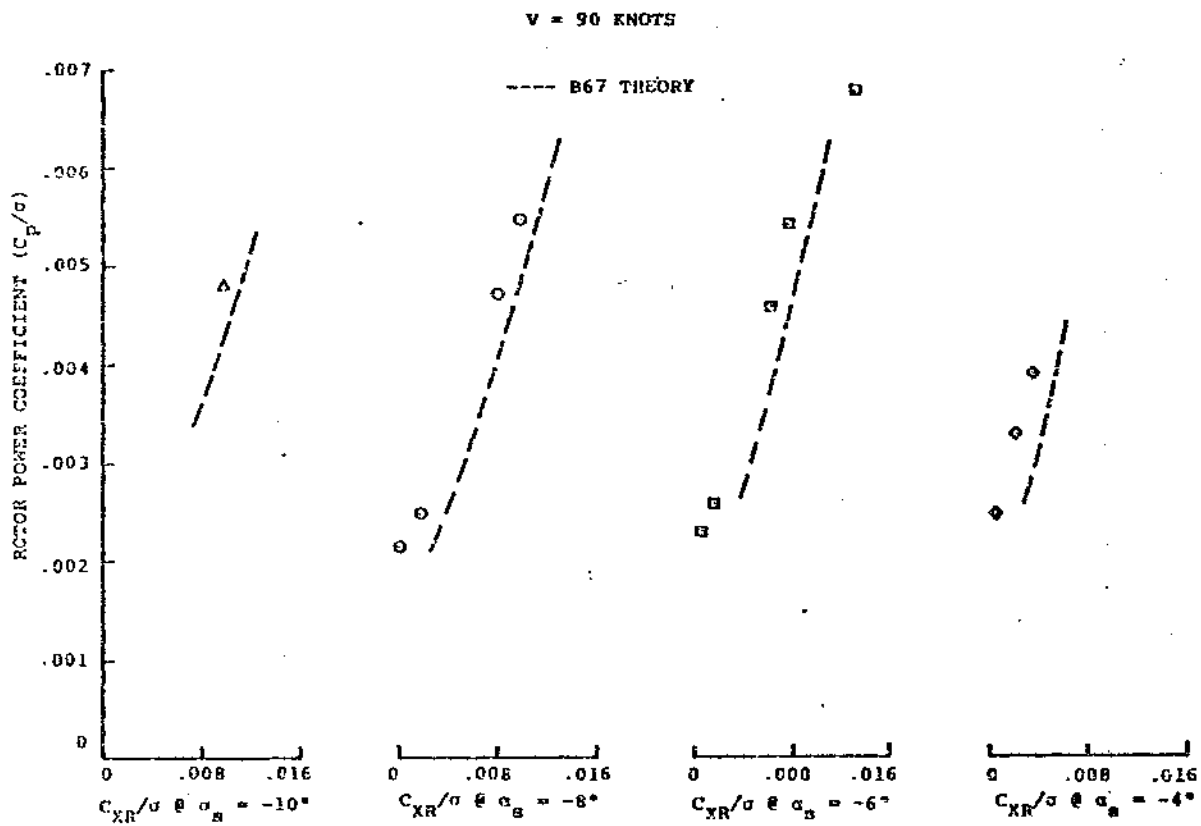

FIGURE 8.264 POWER COEFFICIENT VERSUS PROPULSIVE FORCE COEFFICIENT AT 90 KNOTS

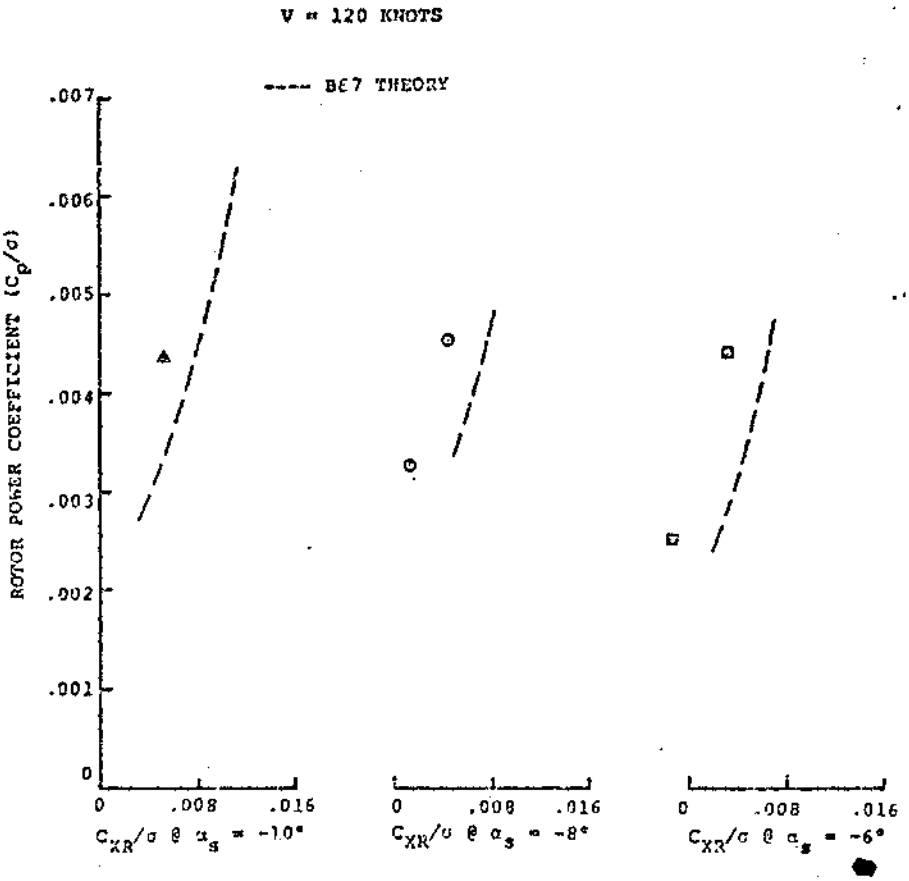

FIGURE 8.265 POWER COEFFICIENT VERSUS PROPULSIVE FORCE COEFFICIENT AT 120 KNOTS

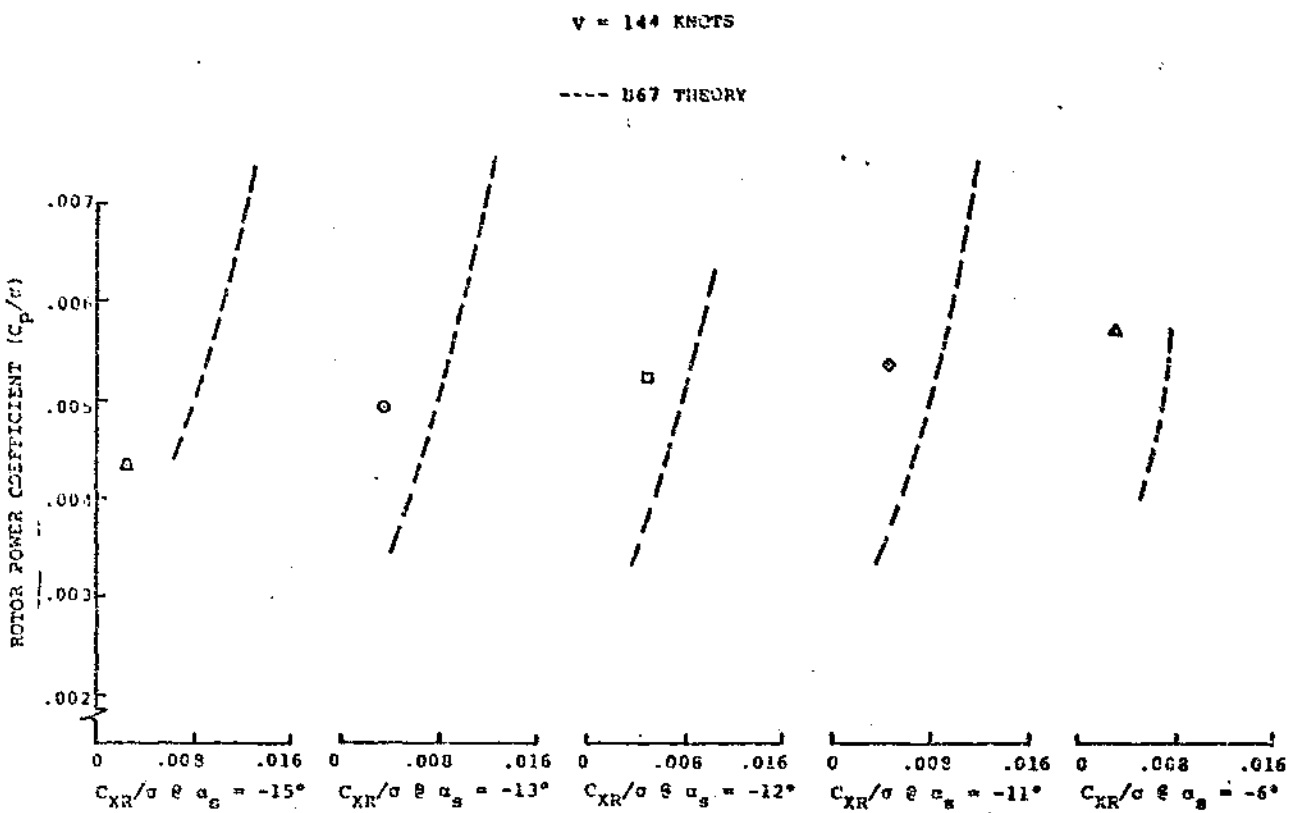

FIGURE 8.266 POWER COEFFICIENT VERSUS PROPULSIVE FORCE COEFFICIENT AT 144 KNOTS

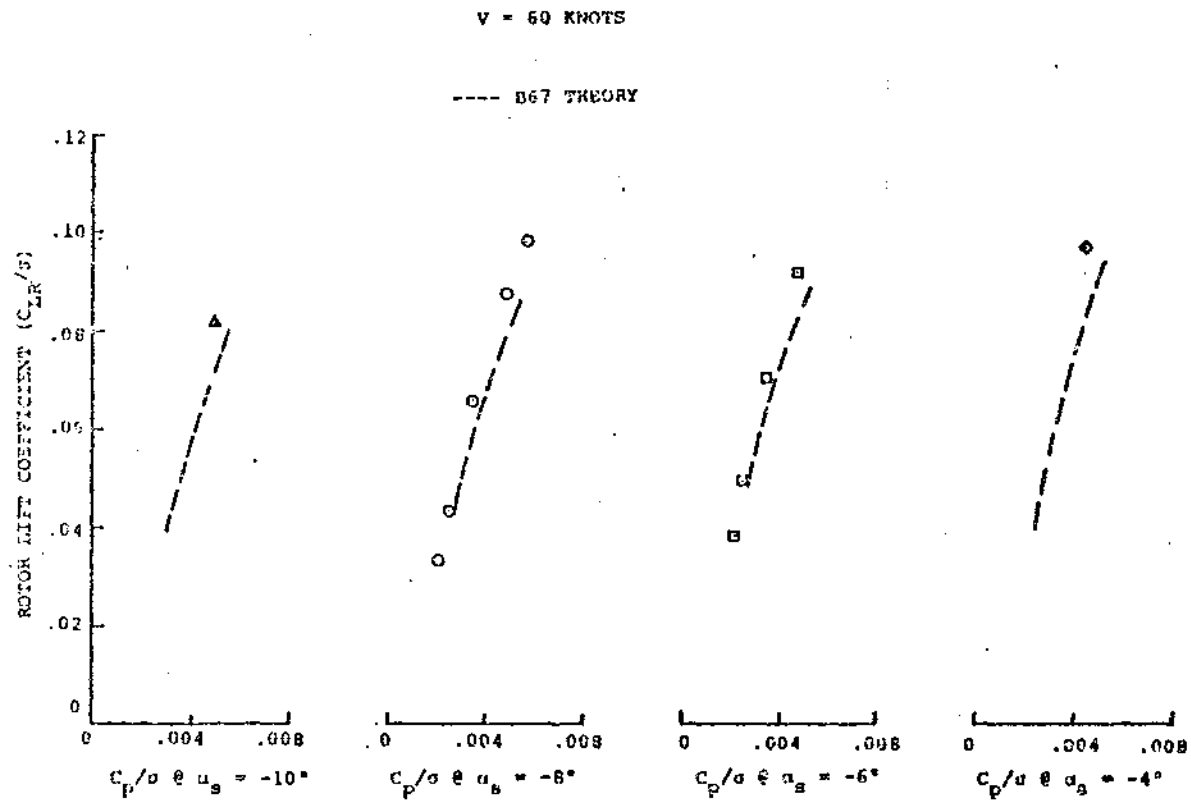

FIGURE 8.267 LIFT COEFFICIENT VERSUS POWER COEFFICIENT AT 60 KNOTS

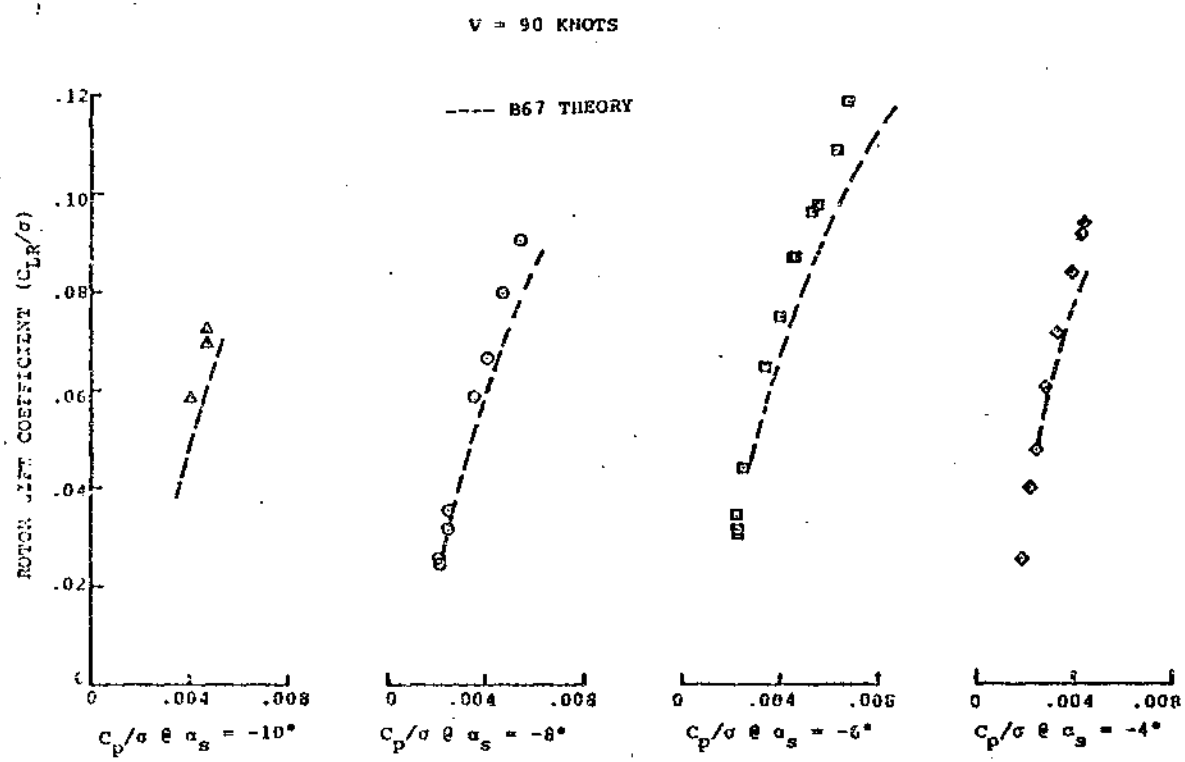

FIGURE 8.268 LIFT COEFFICIENT VERSUS POWER COEFFICIENT AT 90 KNOTS

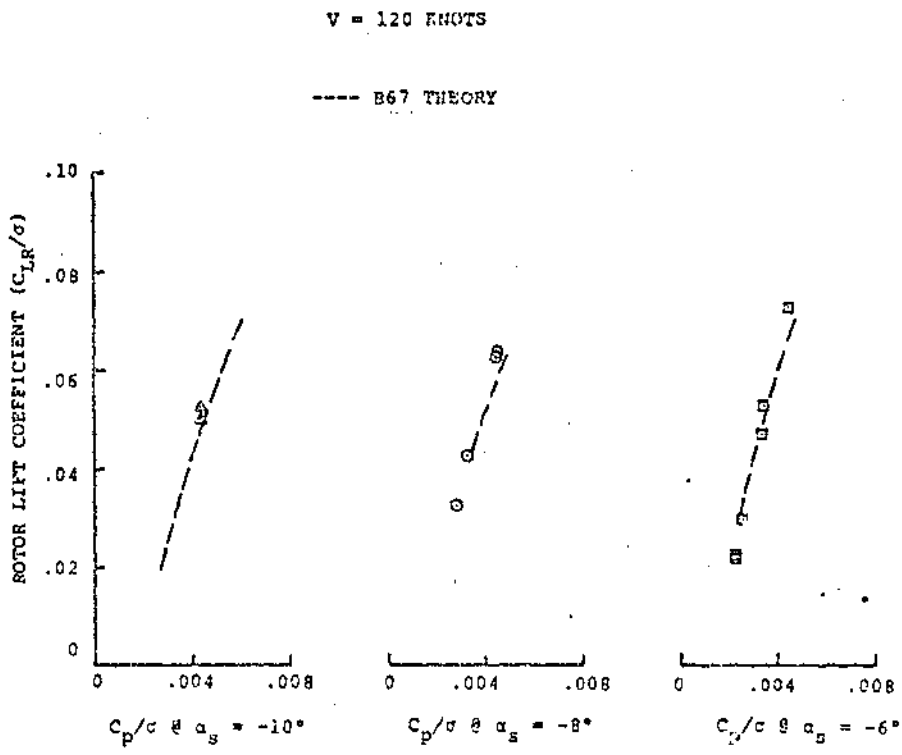

FIGURE 8.269 LIFT COEFFICIENT VERSUS POWER COEFFICIENT AT 120 KNOTS

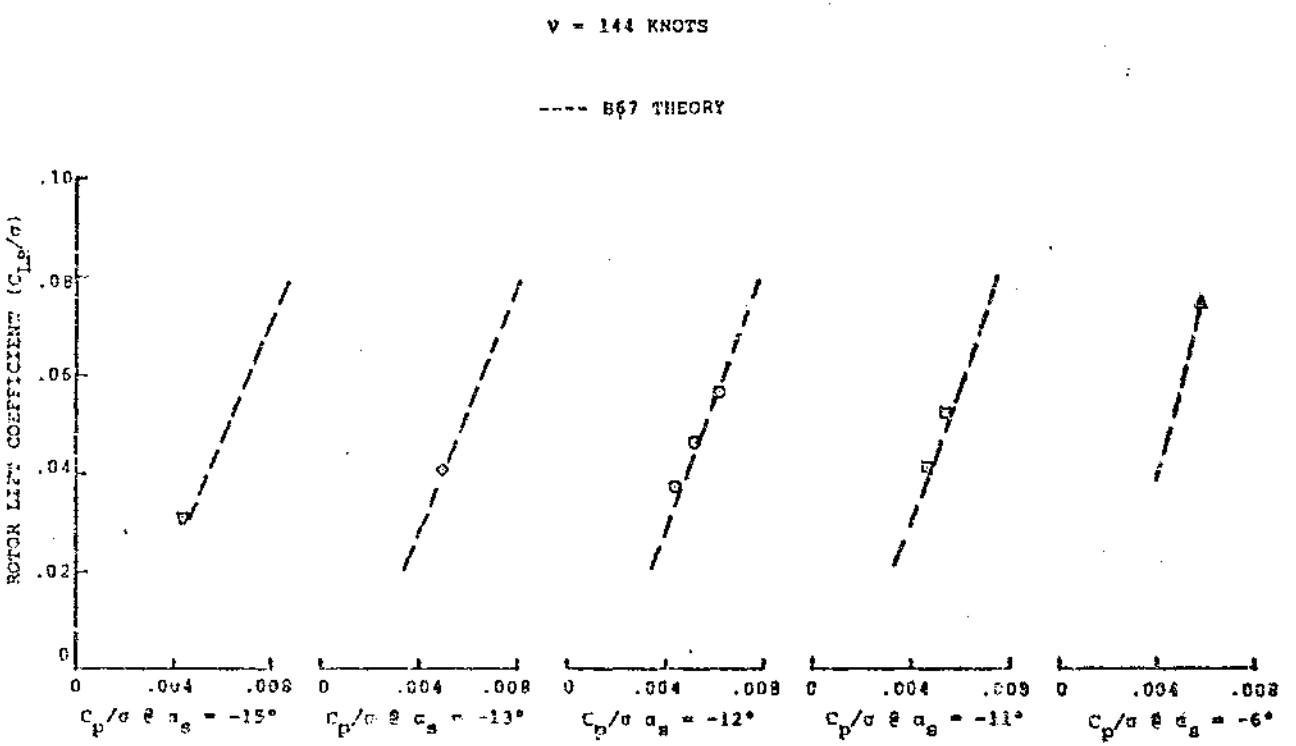

FIGURE 8.270 LIFT COEFFICIENT VERSUS POWER COEFFICIENT AT 144 KNOTS

8.4 FLYING QUALITIES

In order to better understand the nature of cross-axis coupling during maneuvers, it is helpful to know how the rotor behaves during a rapid change in control settings. Because this deals with rotor transients, it is necessary to know the rotor system activity as a function of azimuth at each instant in time. Specifically, it is desirable to know the flap and chord bending moment for each individual blade versus time during a control input. For an articulated rotor, the position of the tip path plane would be of primary interest. For a hingeless rotor, the interest centers on the projection of these bending moments onto the fixed (non-rotating) shaft axis system.

A flying qualities transient time history run was performed during the BMR/RTA full scale wind tunnel test. The test points and conditions are shown in Table 8.1. The flap and chord bending moments at span station 14.25 inches were recorded for each blade during excitations of lateral and longitudinal cyclic pitch introduced through the Dynamic Control System. The strain gage measuring flap bending on blade two failed prior to this run.

One of the first things to consider when transforming data from rotating to non-rotating parameters is the consistency of the data between the blades. The procedure normally requires the use of a state estimator program to evaluate states, sensor biases and scale factors. The technique used here was to first

assess the consistency of the data qualitatively by comparing the waveforms of the rotating data of each blade in trim. Figures 8.271 and 8.272 show a typical comparison of flap bending and chord bending data for two of the four blades in trim. The waveforms are very similar, indicating the blade behavior is consistent from one blade to the next.

Next the data were harmonically analyzed both before the cyclic perturbation and after the transient response had time to settle. Figures 8.273 and 8.274 show the effect of a lateral cyclic perturbation on the rotating flap and chord bending moments for a typical test condition. It was determined that changes in the first harmonic bending moments were comparable for each blade. Therefore, by weighting the data from each blade, resolving the moments into the fixed system reference frame, and using a zero-phase low band-pass filter, the results shown in Figures 8.275 through 8.283 are obtained.

Figures 8.275 and 8.276 represent the results from a negative lateral cyclic perturbation at 55 knots. The time history of the cyclic disturbance from trim is seen in the upper half of Figure 8.275. Figures 8.275 and 8.276 show the first harmonic flap and chord bending moments at station 14.25 versus time. The amount of cross-coupling can be seen by comparing the longitudinal (cosine) and lateral (sine) components of flap bending. The off axis response shows an initial response indicating a pitch up moment followed by a crossover, with a final steady

state roll left/pitch down coupling. It can be seen that there is a rapid change in lateral flap bending, within .3 seconds or 2 rotor revolutions. The response shows little overshoot and quick settling time, characteristics of a good commanded response. It appears that the time history could be modeled by a first order response with a short time constant. Figure 8.276 demonstrates the lightly damped in-plane mode which was excited by the cyclic input. The mode does demonstrate sufficient damping.

Similar results are shown in Figures 8.277 through 8.283 for positive and negative lateral and longitudinal cyclic pitch disturbances at 55 and 111 knots. The analysis procedure was as described earlier to obtain the plots of first harmonic non-rotating flap bending at station 14.25 versus time. For example, Figure 8.277 shows the flap response for a right roll. The response, when compared to Figure 8.275, shows symmetry about the trim point. Figure 8.278 is the non-rotating system flap bending response to a pitch up longitudinal cyclic input. Again the commanded response is rapid, but when compared to Figure 8.277 has a slighly longer rise time. The cross-axis response does not show any long term coupling. Similar conclusions can be drawn from the remaining figures.

TABLE 8.1

FLIGHT CONDITIONS FOR TRANSIENT TIME HISTORIES

RUN NUMBER	TEST POINT	TUNNEL SPEED ∿KNOTS	SHAFT ANGLE ∿.DEG	COLLECTIVE ∿ DEG	LONG. CYCLIC (TRIM) ∿ DEG	LAT. CYCLIC (TRIM) ∿ DEG	CYCLIC PERTURBATION ∿ DEG
21 ↓	3 4 5 6	55	-2.5	5.8	-2.75	2.3	-0.3 (LAT.) +0.3 (LAT.) -0.3 (LONG.) +0.3 (LONG.)
	8 9 10 11	93.	-5.5	6.8	-2.0	3.4	-0.3 (LAT.) +0.3 (LAT.) -0.3 (LONG.) +0.3 (LONG.)
	13 15 16 17	111.	-7.5	8.5	-1.8	4.5	-0.3 (LAT.) +0.3 (LAT.) -0.3 (LONG.) +0.3 (LONG.)

RUN 21 TP 3
V = 55 KNOTS
θ = 5.8°
a_s = -2.5°

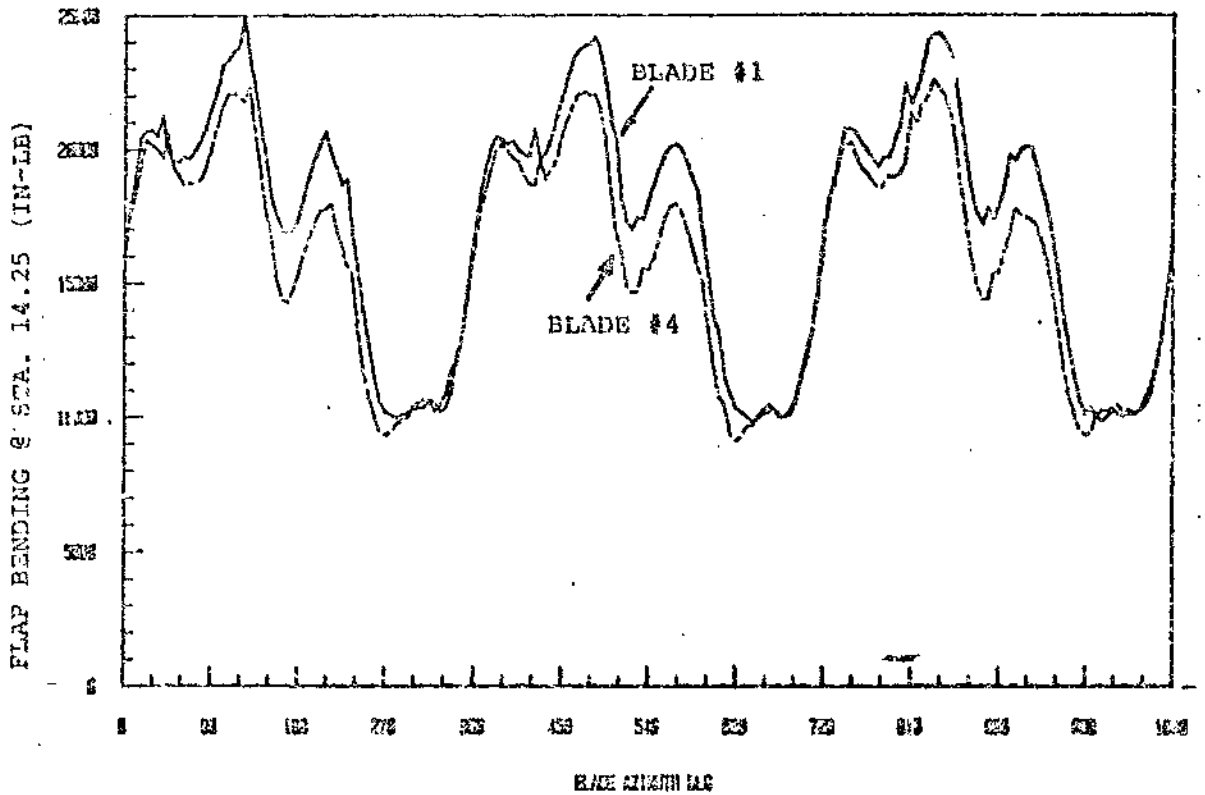

FIGURE 8.271 COMPARISON OF FLAP BENDING BETWEEN BLADES #1 AND #4 IN TRIMMED FLIGHT AT 55 KNOTS

RUN 21 TP 3
V = 55 KNOTS
θ = 5.8°
a_s = -2.5°

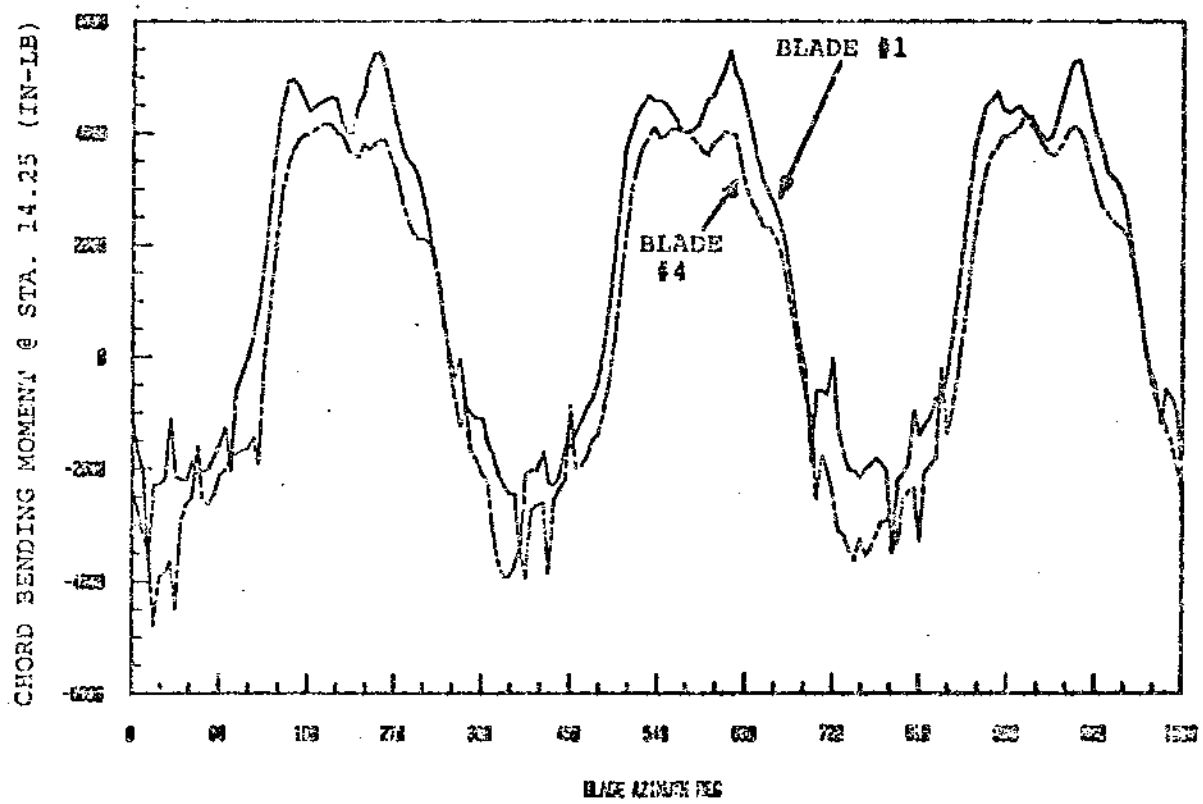

FIGURE 8.272 COMPARISON OF CHORD BENDING BETWEEN BLADES #1 AND #4 IN TRIMMED FLIGHT AT 55 KNOTS

RUN 21 TP 3
V = 55 KNOTS
θ = 5.8°
α_s = -2.5°

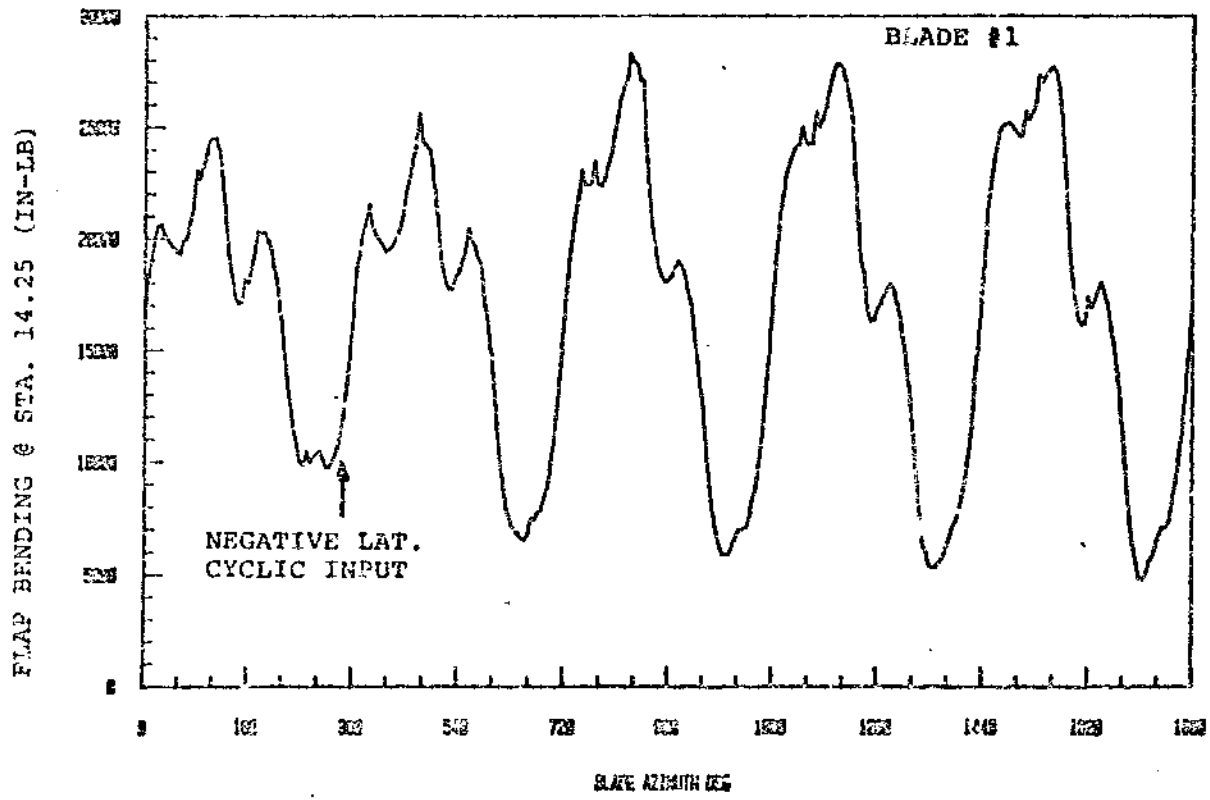

FIGURE 8.273 TRANSIENT BEHAVIOR OF BLADE #1 FLAP BENDING AT 55 KNOTS

RUN 21 TP 3
V = 55 KNOTS
θ = 5.8°
α_s = -2.5°

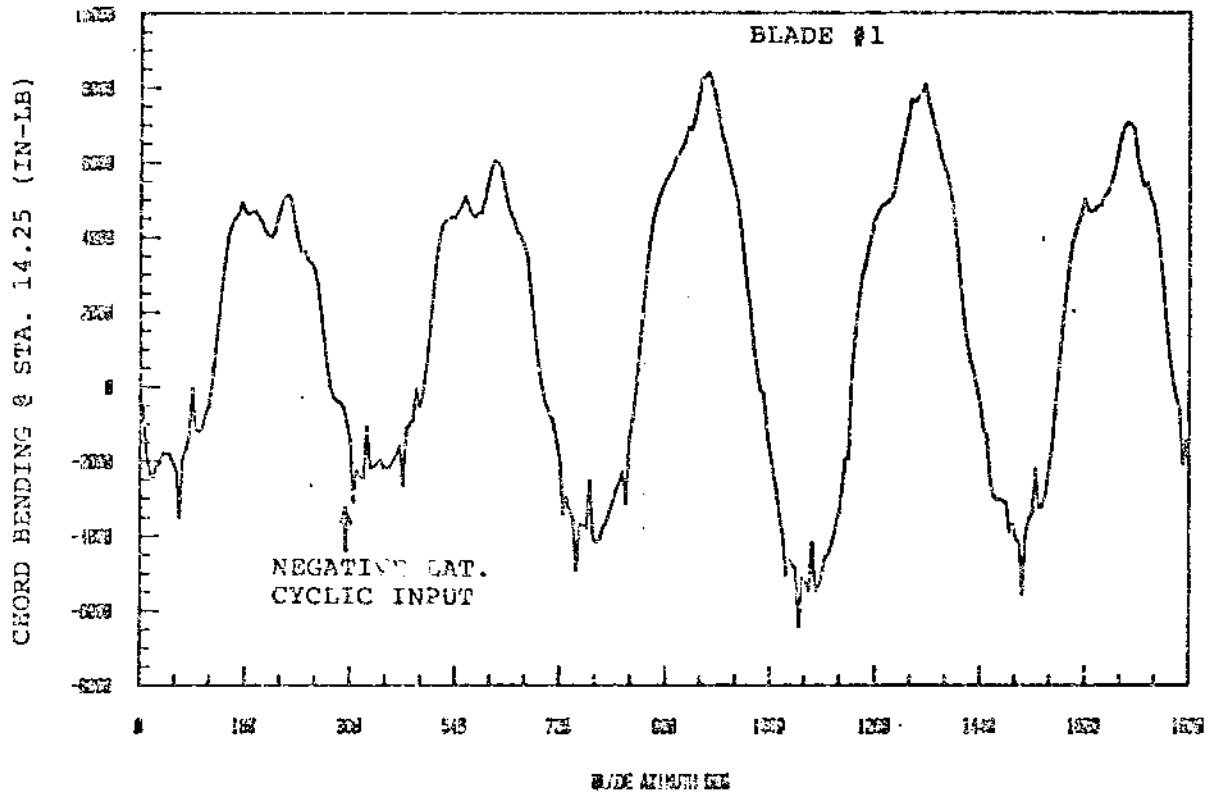

FIGURE 8.274 TRANSIENT BEHAVIOR OF BLADE #1 CHORD BENDING AT 55 KNOTS

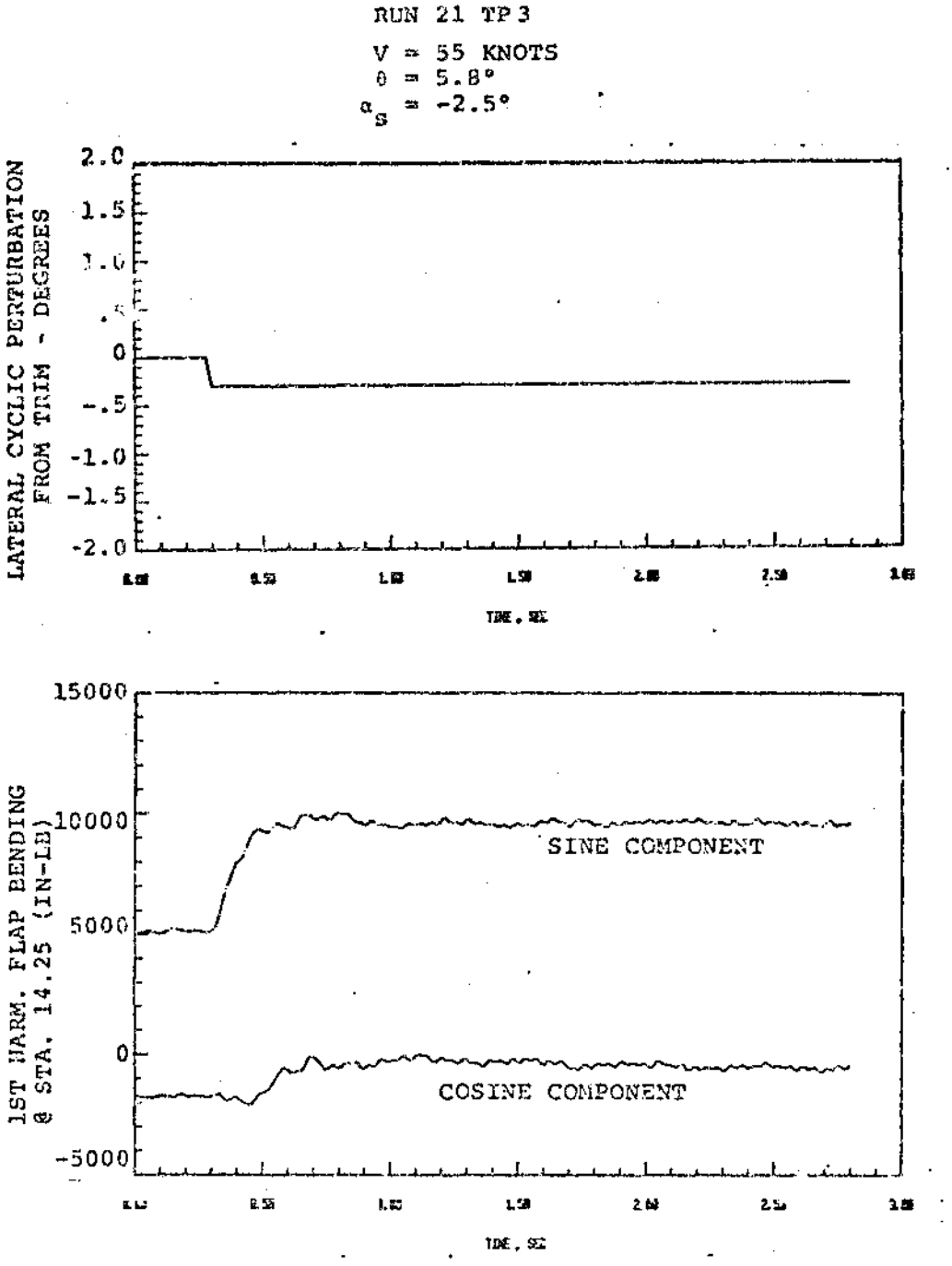

FIGURE 8.275 FIRST HARMONIC FLAP BENDING RESPONSE TO A NEGATIVE LATERAL CYCLIC INPUT AT 55 KNOTS

RUN 21 TP 3
V = 55 KNOTS
θ = 5.8°
α_s = -2.5°

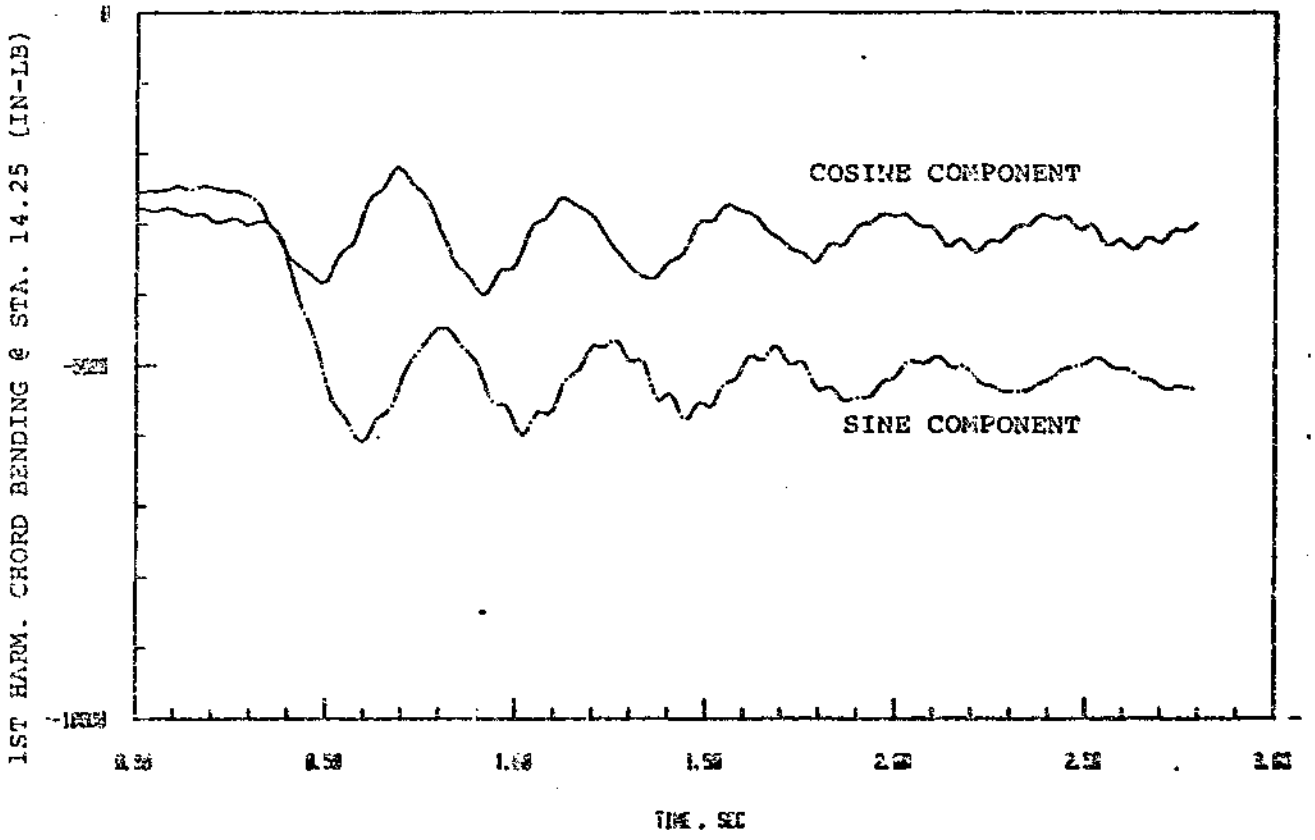

FIGURE 8.276 FIRST HARMONIC CHORD BENDING RESPONSE TO A NEGATIVE LATERAL CYCLIC INPUT AT 55 KNOTS

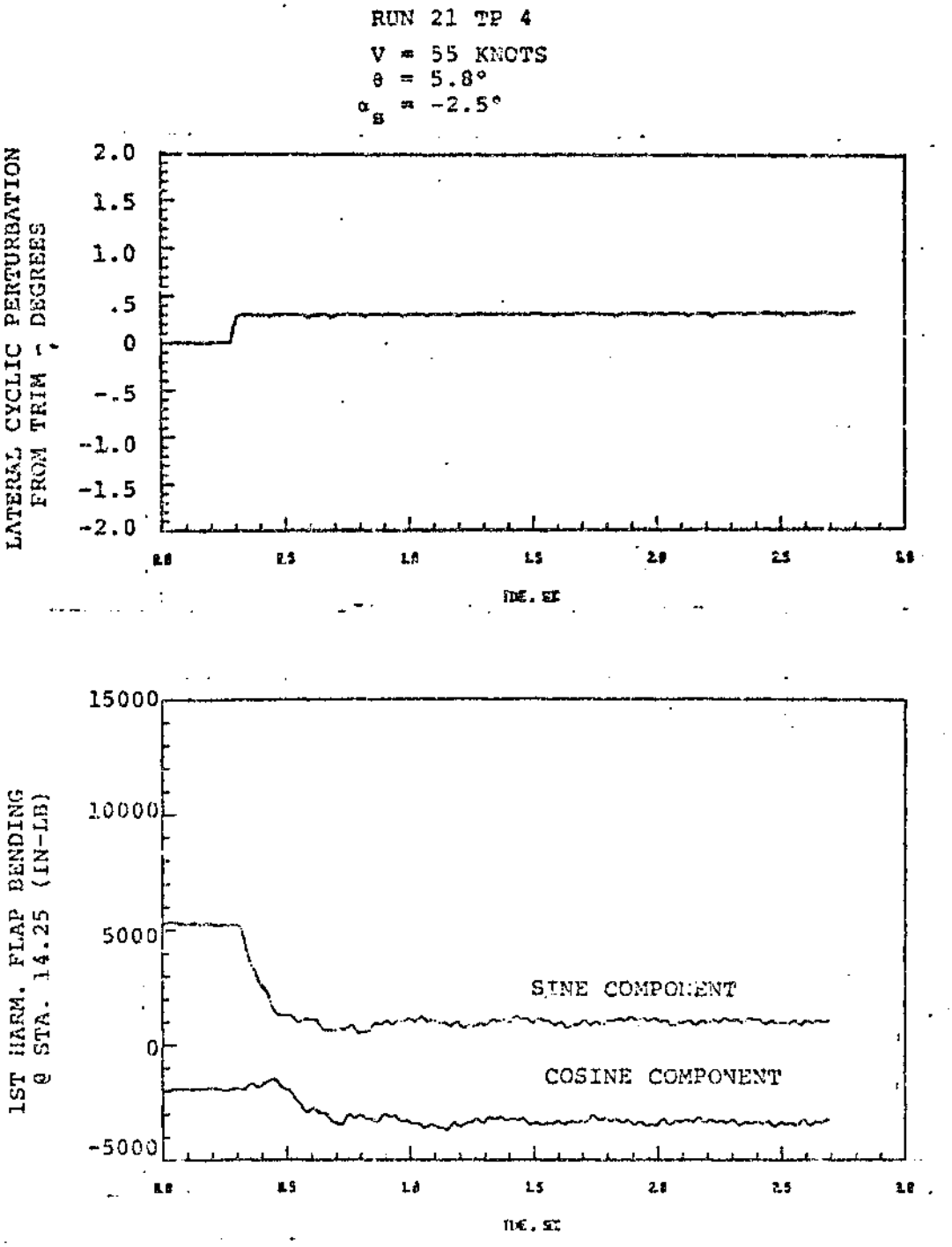

FIGURE 8.277 FIRST HARMONIC FLAP BENDING RESPONSE TO A POSITIVE LATERAL CYCLIC INPUT AT 55 KNOTS

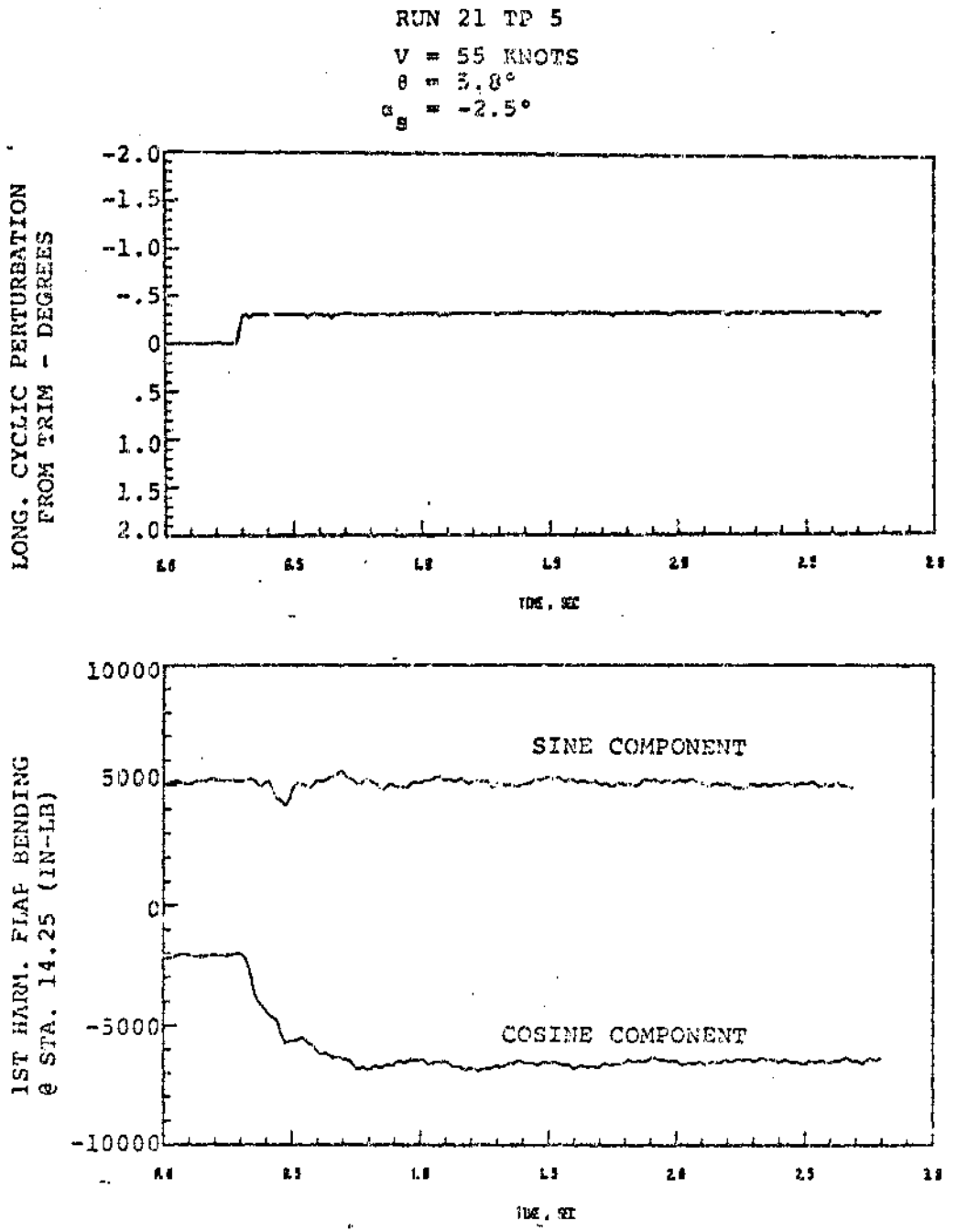

FIGURE 8.278 FIRST HARMONIC FLAP BENDING RESPONSE TO A NEGATIVE LONGITUDINAL CYCLIC INPUT AT 55 KNOTS

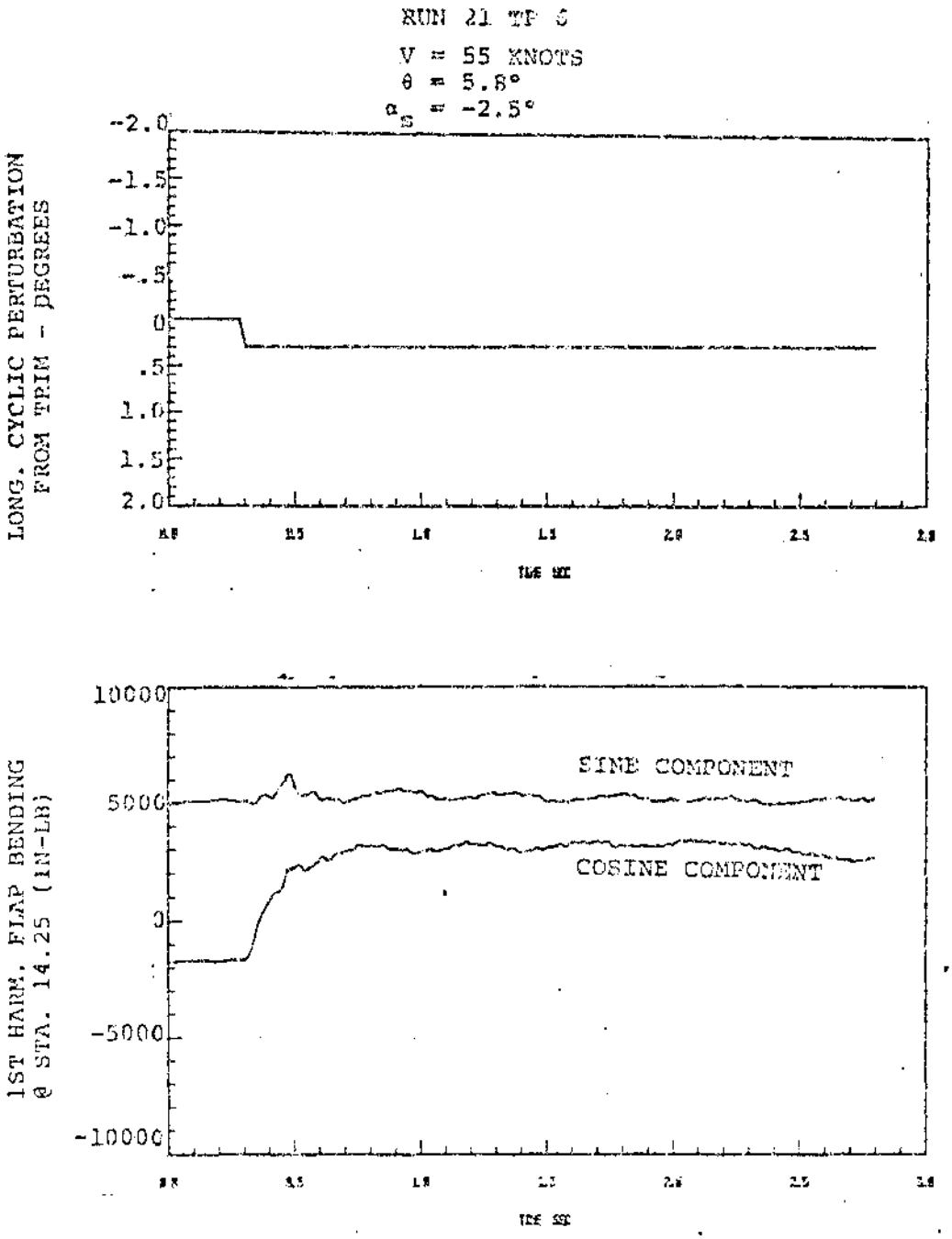

FIGURE 8.279 FIRST HARMONIC FLAP BENDING RESPONSE TO A POSITIVE LONGITUDINAL CYCLIC INPUT

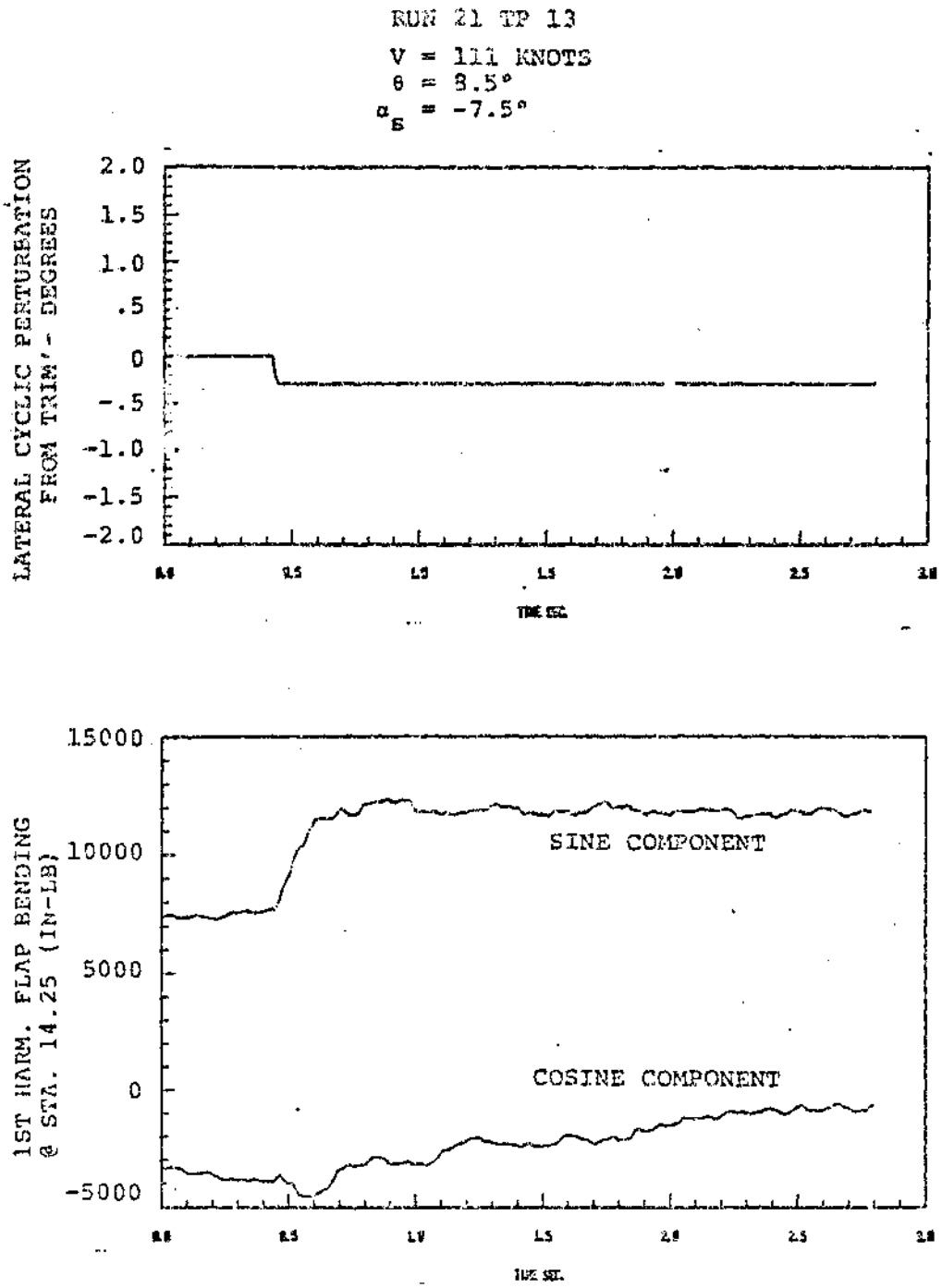

FIGURE 8.280 FIRST HARMONIC FLAP BENDING RESPONSE TO A NEGATIVE LATERAL CYCLIC INPUT AT 111 KNOTS

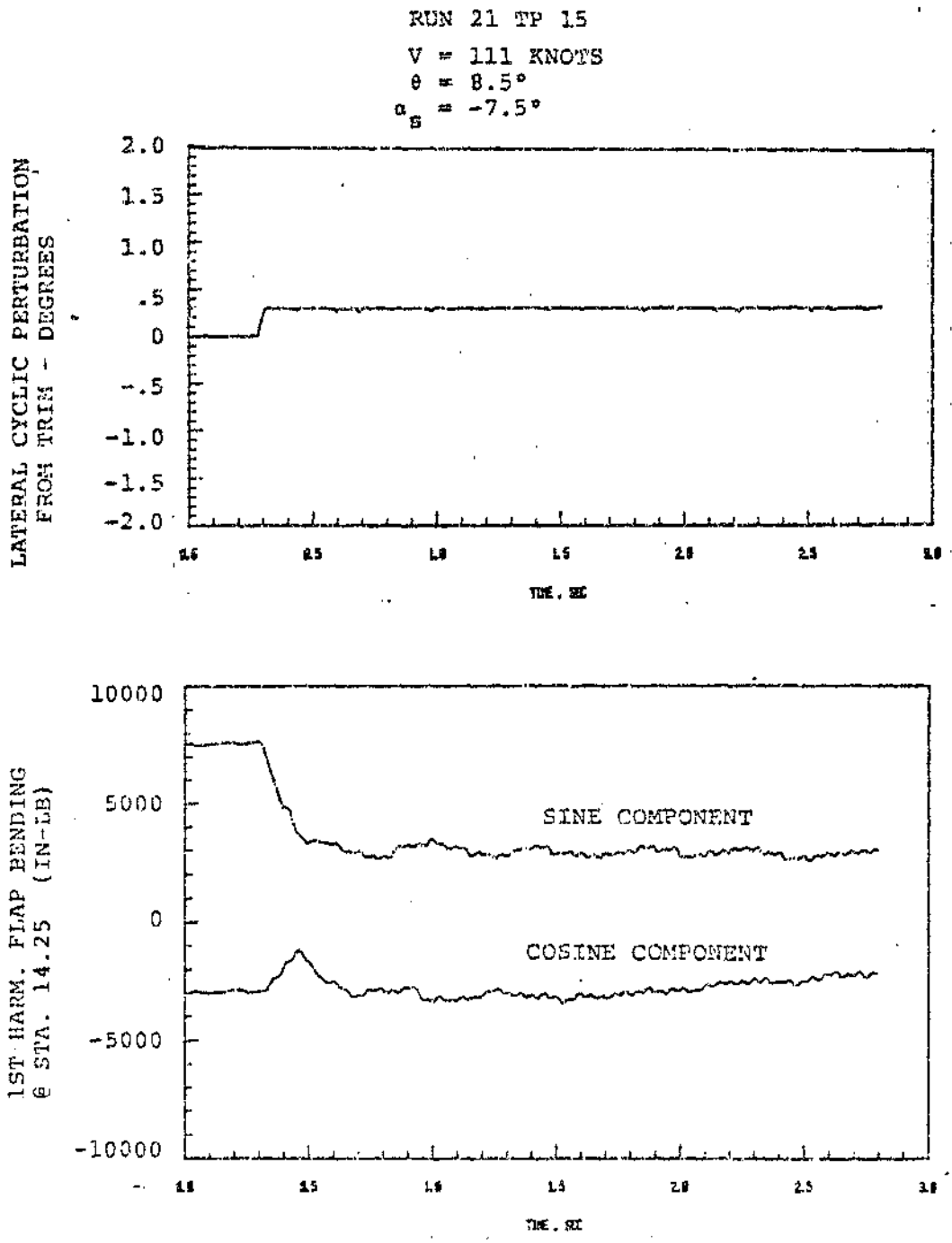

FIGURE 8.281 FIRST HARMONIC FLAP BENDING RESPONSE TO A POSITIVE LATERAL CYCLIC INPUT AT 111 KNOTS

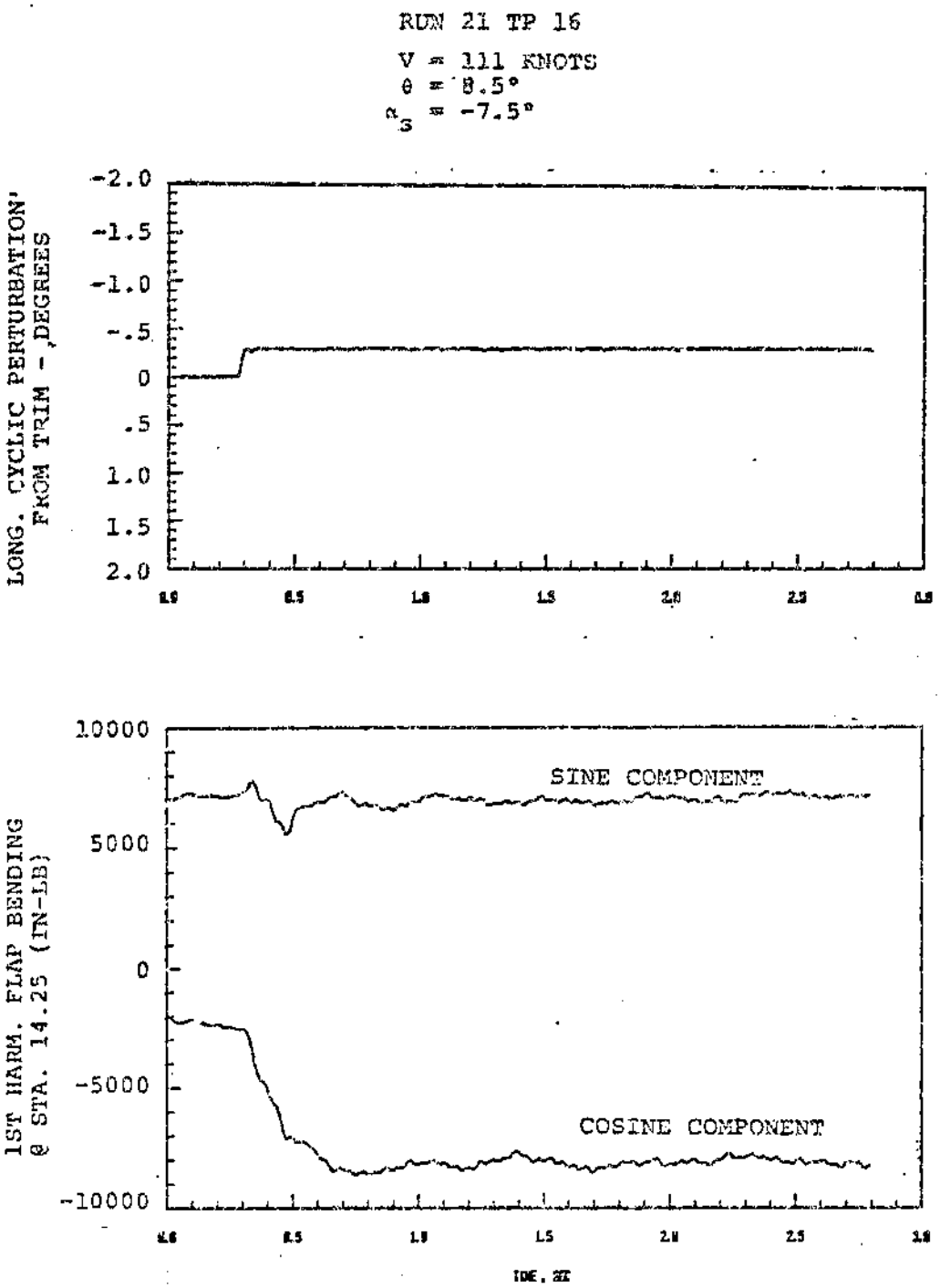

FIGURE 8.282 FIRST HARMONIC FLAP BENDING RESPONSE TO A NEGATIVE LONGITUDINAL CYCLIC INPUT AT 111 KNOTS

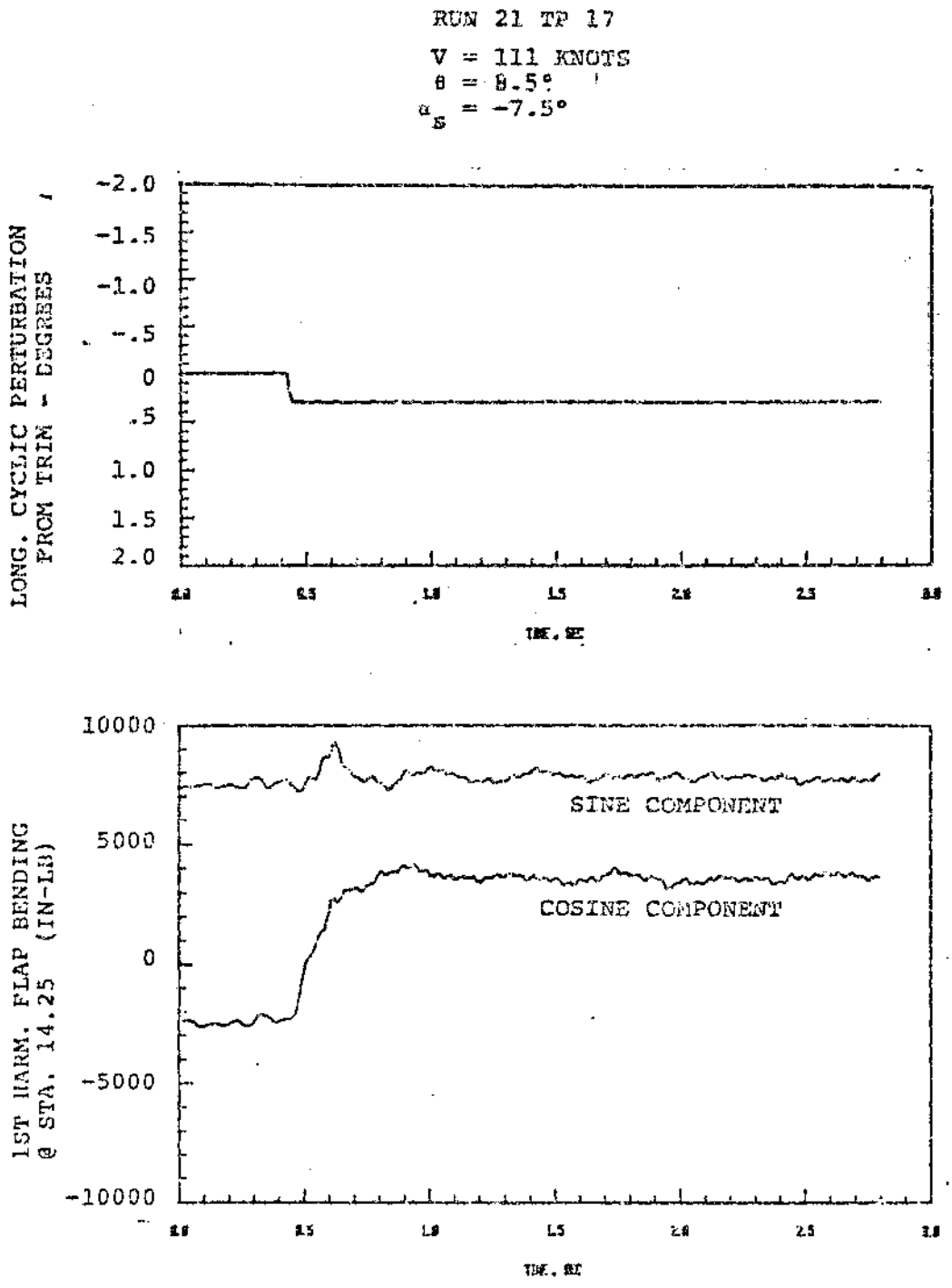

FIGURE 8.283 FIRST HARMONIC FLAP BENDING RESPONSE TO A POSITIVE LONGITUDINAL CYCLIC INPUT AT 111 KNOTS

9.0 CONCLUSIONS

9.1 BMR/RTA IN THE 40-BY-80 WIND TUNNEL

9.1.1 Stability

The BMR is stable at all conditions tested on the RTA. The fixed system damping of the BMR/RTA essentially increases with airspeed at constant collective pitch, shaft angle and rotor speed between hover and 60 knots. Beyond 90 knots the damping decreases. Further testing is desirable to investigate the trend of damping beyond 90 knots. For 1G level flight the fixed system damping decreases from hover to 60 knots, then increases from 60 knots to 120 knots. This trend is verified by analysis, model scale and flight test data.

For both hover and forward flight, the fixed system damping increases with increasing collective pitch at fixed airspeed, rotor speed and shaft angle. Likewise, damping decreases with increasing rotor speed at fixed collective pitch, airspeed and shaft angle. The damping is determined solely by the inherent air mode damping of the rotor system. The effect of potential coupled RTA/rotor instabilities is negligible.

The effect of shaft angle variation on fixed system damping at constant airspeed, collective pitch and rotor speed is very small. There appears to be a tendency towards decreased damping with increasing forward shaft tilt, but the change is within the scatter of the data.

The BMR/RTA full scale wind tunnel test proved to be an effective means of identifying the inherent damping of the rotor system. The full scale testing can be used to determine the air mode damping characteristics of a rotor configuration, and to compare the inherent damping levels of several configuration variations. The one aspect of stability which can not be evaluated in the 40-by-80 wind tunnel using the RTA is ground resonance type of instabilities. Since the RTA does not duplicate the masses and inertias of an actual fuselage, those instabilities induced by the coalescence of body modes with rotor modes will not be present.

9.1.2 Loads

Load trends in hover were difficult to assess due to the sensitivity of loads to change in cyclic pitch and to recirculation effects.

Vibratory flap bending and torsion loads generally show a trend versus airspeed of a a build-up in loads with increasing airspeed. In some cases higher loads are seen in the 30 Knot transition regime. Steady blade and flexbeam flapping are increasingly flap down as airspeed increases. Both vibratory and steady flap bending and torsion loads for all components increase directly as collective pitch is increased. For the blade, flexbeam, and torque tube vibratory flap bending and torsion loads, the effect of increasing positive shaft angles is a gradual increase in loads. The respective steady values are essentially independent of shaft angle.

Chord bending vibratory loads are greatest in the intermediate speed regime (40-80 knots), are lower in hover and decrease with airspeed above 80 knots. The steady blade and flexbeam chord moments are invariant with airspeed. Vibratory chord moments increase with collective pitch above 2000 pounds thrust. At thrust levels below 2000 pounds there is some trend of gradual increasing load with decreasing collective. The midspan and outboard flexbeam steady chord banding gages showed no effect of collective while both the blade and flexbeam root chord moments increased with higher collective angles.

Most noticeable in the steady chord bending moments on the flexbeam was the opposing bending demonstrated for the leading and trailing beams. This seems to indicate opposite rotation of the outboard ends, with a bowing effect at the blade clevis. This could be attributed to an assymmetric line of action of the centrifugal force causing different mode shapes in each beam.

The vibratory chord moments increased proportionately with increasing positive shaft angles. The vibratory flexbeam chord loads were distributed equally between leading and trailing beams. Generally, the steady loads are insensitive to shaft angle.

It was noted that the differences in flapping and chord load distributions between leading and trailing beam could be attri-

buted to some extent to the wind-up in the beams due to steady collective pitch inputs.

Torque tube torsion and pitch link loads are closely related.

9.1.3 Performance

The hover performance data where recirculation effects did not produce tunnel flow above 3.5 knots agrees well with theoretical predictions. The forward flight data looks reasonable and correlates well with analysis. It was difficult to compare to flight data due to the nature of the test. For stability testing the goal was to test at the lowest damping levels, hence collective pitch angles, possible. Also shaft angles were varied without regard to the resulting flat plate drag area. For this reason, most of the test data was at lift and F_e values not representative of BO-105 flight conditions.

9.1.4 Flying Qualities

The rotor responded to both lateral and longitudinal cyclic control inputs within two rotor revolutions after the input was initiated. The response was precise and of the first order,

with little or no overshoot. The cross axis response showed no long term coupling. Responses to positive and negative cyclic inputs for lateral or longitudinal perturbations showed symmetry about trim.

9.2 CONCLUSIONS FROM THE BMR/RTA TEST VERSUS CONCLUSIONS FROM OTHER TESTS

9.2.1 Whirl Tower

The stability results from the whirl tower and the BMR/RTA test were nearly identical. Both tests showed increasing stability with increasing collective pitch, and decreasing damping with increasing rotor speed. The magnitude of the fixed system damping from both tests were the same.

9.2.2 Flight Test

The fixed system damping data versus airspeed for 1G level flight are nearly the same for the BMR/BO-105 and the BMR/RTA. Both tests showed stability dropping from hover to a minimum at 60 knots, then increasing damping beyond 60 knots airspeed. All the test results agree in concluding that the BMR rotor system is stable throughout the flight spectrum.

The ground resonance tests on the BMR/BO-105 were compared to hover results from the BMR/RTA test. The inherent rotor stability levels are the same in both cases, but for those collective pitch values where a body mode of the BO-105 coalesces with a rotor in-plane mode of the BMR, a destabilizing effect is seen which can not occur in the wind tunnel due to the characteristics of the RTA compared to the BO-105. Therefore the wind tunnel BMR/RTA configuration cannot be used to determine the classical ground resonance type of instability.

The flight test loads and those from the BMR/RTA test are in close agreement for most components. Most differences can be attributed to slightly different trim settings between flight test and the wind tunnel. The two major differences are steady chord bending at 44, and steady torque tube chord bending. The torque tube change is probably due to the higher collective settings used in flight test trim.

9.2.3 Small-Scale Wind Tunnel Tests

The 1/5.86 froude-scaled model of the BMR/BO-105 had both pitch and roll degrees of freedom. The mass and inertias of the BMR/BO-105 were modeled to identify the coupled rotor/fuselage instabilities. Many of the conclusions from the test relate to these body mode/rotor mode interactions. However, some general trends from that test can be compared to the BMR/RTA results.

Both tests demonstrate increasing fixed system damping as collective pitch is increased. Free from the effects of body mode coupling, both the BMR/RTA and the 1/5.86 scale BMR/BO-105 model show a trend of reduced stability as rotor speed is increased. The trend of decreasing damping from hover to 60 knots, and increasing damping at airspeeds greater than 60 knots for 1G level flight is seen in both tests. The overall conclusion from both the BMR/RTA and the BMR/BO-105 model tests was that the BMR is stable for the entire flight regime.

9.3 BMR/RTA Results Versus Analysis

The C-90 computer program predicts both the trends and magnitude of fixed system damping in hover. The decrease in stability with rotor speed and the increase in stability with collective pitch are predicted by the analysis. In forward flight the trends are also predicted quite well by C-90, but the correlation of damping levels is increasingly worse with higher collective pitch values (greater damping). The predicted damping increases more rapidly than the test data with increasing collective pitch. It is significant that the correlation is best at the lowest collective pitch levels where damping is a minimum. In this region experimental damping results are determined more accurately with less data scatter, and it is also at these conditions that the prediction of stability is most critical.

The analysis correlates with the 1G level flight results versus airspeed, and also correlates well with the damping versus airspeed at constant rotor speed, collective pitch and shaft angle up to 90 knots. However, at airspeeds above 90 knots the analytical and test results diverge. This difference in trends with airspeed above 90 knots requires further investigation.

Flap bending steady and vibratory moments are predicted by C-60 for both hover and forward flight conditions. C-60 generally underpredicts steady chord bending moments. The degree of correlation for vibratory chord bending moments varies widely, with

excellent correlation for some conditions and poor at other times. This is directly a function of the convergence capability of the analytical iteration procedure. An improved iteration technique or a closed form solution is required to attain better correlation.

The correlation of lift, drag, power and pitching moment coefficients with the B-67 analysis was good at all airspeeds, with the biggest deviations at 144 knots. At the higher airspeeds, there is also some deviation between predicted and measured propulsive force, probably due to some differences in rotor flapping.

9.4 Configuration Changes

The addition of elastomeric damper strips to the BMR flexbeams increased the structural damping by approximately 1.2% and the first chord mode natural frequency by approximately .04/Rev. The combined effect was to increase the fixed system damping ratio by 1.5 to 2.0% at low collectives in hover and by as much as 4.0% at high collectives. In forward flight at 90 knots the increase is 1.5% at 425 rpm and 4.5% at 335 rpm. This increase was anticipated from results of the C-90 program analysis.

The total control system springrate was reduced to 89% of the baseline value by the installation of axially flexible pitch links. In hover at rotor speeds below 425 rpm, the

softer control stiffness produced decreased damping levels. At 425 rpm the baseline and softer control stiffness configurations showed identical values of damping. In forward flight, the effect of control system stiffness was small, with perhaps a decrease in damping for the softer control spring configuration. These results are not compatible with the present understanding of the system, and further analysis and testing are required to clarify these results.

Similar loads results were obtained for the soft pitch links and damper strips. This was attributed to the change in the relative stiffness between the flexbeams and the torque tube load paths. The effect was to produce a different blade pitch angle for the same control input. This is evident in the steady and vibratory flap bending moments, and the torque tube torsion and pitch link load.

10.0 RECOMMENDATIONS

It is felt that further testing of the BMR/RTA system in the Ames 40-by-80 wind tunnel is warranted in order to:

- Investigate stability trends versus airspeed at speeds greater than 90 knots. Stability testing should be performed as thoroughly at 120 knots as it was at 90 knots. This testing would also contribute to the understanding of why the C-90 analysis is apparently not as effective at high speeds and less effective as collective pitch is increased.

- Quantify the effects of a softer control system stiffness by testing pitch links which reduce the total control system springrate to 75% and 60% of the baseline value. Test each configuration thoroughly in hover and at both 60 and 90 knots. It is hoped that this would reduce the discrepancies found in the results of this BMR/RTA test.

- Test additional configuration variations, such as aft sweep. The capability to determine the effects of sweep was present in this BMR/RTA test, but this configuration was not tested due to time constraints. Other possible parameter variations are the location of the 2.5 degree pre-droop angle and the beam-to-hub pre-pitch angle.

- Further study the effects of excitation amplitude and trim values of cycle pitch on stability, since no conclusive results were found from the limited data related to this problem obtained in the BMR/RTA wind tunnel test.

- Test the BMR over a substantial range of test conditions at values of lift and F_e representative of the BMR/BO-105 aircraft.

11.0 APPENDICES

11.1 RUN LOG

The run log for the BMR test at NASA-Ames is presented on the following pages.

THE BOEING COMPANY

NUMBER
REV LTR

RUN NO. 1 TEST 550

TEST PT.	RUN DESCRIPTION	V (KTS)	RPM	SHAFT ANGLE	THETA .7R	NOTES
1	STATIC TARE RUN	—	—	0	—	△
2	↓	—	—	-10	—	↓
3		—	—	-8	—	
4		—	—	-4	—	
5		—	—	0	—	
6		—	—	4	—	
7		—	—	8	—	
8	↓	—	—	10	—	↓

DATE / TIME: 2/4/80

△ BLADES OFF

		REVISED	DATE
PREP.			
CHK.			
APPR			

FORM 48510 (3/70)

516
SHEET

RUN NO. 2 TEST 550

TEST PT.	RUN DESCRIPTION	V (KTS)	RPM	SHAFT ANGLE	THETA .7R	NOTES	DATE / TIME
1	WIND OFF ZERO	—	—	0	0	A	3/4/80
2	WIND OFF ZERO	—	—	0	0	A	
3	HUB TARES	60	425	-10	9.6	—	
4				-10	8.2		
5				-10	15.8		
6				-8	9.6		
7				-6	—		
8				-4			
9				-2			
10	"	"	"	0	"	"	

PREP | CHK. | APPR | REVISED | DATE

FORM 8810 5/70

SHEET 5 OF 7

THE BOEING COMPANY

MODEL 347 A3

THE BOEING COMPANY

NUMBER
REV LTR

TEST 550

RUN NO. 2 (CONT.)

TEST PT.	RUN DESCRIPTION	V (KTS)	RPM	SHAFT ANGLE	THETA .7R	NOTES	DATE / TIME
11	HUB TARES	60	425	2	96	2	2/4/80
12	"	"	"	4	"	"	
13	"	"	"	6	"	"	
14	"	"	"	8	"	"	
15	"	120	"	10	"	"	
16	"	"	"	-10	"	"	
17	"	"	"	-8	"	"	
18	"	"	"	-6	"	"	
19	"	"	"	-4	"	"	
20	"	"	"	-2	"	"	

2 BLADES OFF

PREP.			REVISED	DATE
CHK.				
APPR				

FORM 49519 (3/70)

RUN NO. 2 (CONT.) TEST 550

TEST PT.	RUN DESCRIPTION	V (KTS)	RPM	SHAFT ANGLE	THETA .7R	NOTES								DATE / TIME
21	HUB TARES	120	425	0	9.6	⚠A								2/11/80
22	↓	120	425	2	9.6	↓								

⚠A BLADES OFF

PREP. | CHK. | APPR. | REVISED | DATE

FORM 4-5010 (3/70)

SHEET 519

THE BOEING COMPANY

NUMBER

REV LTR

RUN NO. 3/4 TEST 550

TEST PT.	RUN DESCRIPTION	V (KTS)	RPM	SHAFT ANGLE	THETA .7R	NOTES	DATE / TIME
1	STATIC CHECK	–	–	0	9.6	⚠1	
2	↓	–	–	0	9.6	↓	
3	↓	–	–	0	15.8	↓	
4	↓	–	–	0	-.2	↓	
	RUN 4						
1	WIND OFF ZERO	–	–	0	9.6		2/7/80
2	WIND OFF ZERO	–	–	-10	9.6		
3-12	STATIC CALIBRATION	–	–	⚠2	9.6		

⚠1 BLADES ON INSTRUMENTATION STATIC CHECK

⚠2 TEST PT. 3 4 5 6 7 8 9 10 11 12
α_s -8 -6 -4 -2 0 2 4 6 8 10

PREP. CHK. APPR. REVISED DATE

FORM 4910 (3/70)

SHEET 520

THE BOEING COMPANY

NUMBER

REV LTR

RUN NO. 5 TEST 550

TEST PT.	RUN DESCRIPTION	V (KTS)	RPM	SHAFT ANGLE	THETA .7R	NOTES							DATE / TIME
1,2	WIND OFF ZERO	–	–	0	9.6								17/00
3	BLADE TRACK	0	351	-10	4.								
4	QUAL. STABILITY CHECK	0	350	-10	4.	⚠1							
5	BLADE TRACK	0	375	↓	↓								
6,7	BLADE TRACK & STABILITY CHECK	0	400			⚠2							
8	BLADE TRACK	0	425										
9,10	BLADE TRACK & STABILITY CHECK	0	415			⚠3							
11,12	BLADE TRACK	0	437		↓								
13	BLADE TRACK	0	475		8.								
14	BLADE TRACK	0	405	↓	12.								

⚠1 500 COUNTS LATERAL CYCLIC ON DCS TO EVALUATE STABILITY.

⚠2 TEST PT. 6 [illegible] 500 COUNTS LATERAL CYCLIC ON DCS.

⚠3 SAME AS NOTE 2 FOR POINTS 9 AND 10, RESPECTIVELY.

FORM 4851 (6/70)

PREP. CHK. APPR. REVISED DATE

THE BOEING COMPANY

SHEET 521

NUMBER

REV LTR

RUN NO. 6 TEST 550

THE BOEING COMPANY

NUMBER
REV LTR

TEST PT.	RUN DESCRIPTION	V (KTS)	RPM	SHAFT ANGLE	THETA .7R	NOTES	DATE / TIME
1	WIND OFF ZERO	1	1	0	9.6		2/3/80
2	HOVER STABILITY, LOADS	0	350	-10	4.		
3					11.2		
4					10.		
5					8.		
6					6.		
7					4.		
8					2.		
9					2.	⚠1	
10	↓	↓	↓	↓	0.		

⚠1 500 COUNTS ENTERED CYCLE 0 OF 3 A

PREP | CHK | APPR | REVISED | DATE

FORM 488-0 (3/79)

522
SHEET

RUN NO. 7 TEST 550

TEST PT.	RUN DESCRIPTION	V (KTS)	RPM	SHAFT ANGLE	THETA .7R	NOTES								DATE / TIME
1	WIND OFF ZERO	1	1	0	9.6									2/8/80
2	HOVER STABILITY, LOADS	0	375	-10	4									
3	↓	0	375	-10	8									
4	V	0	375	-10	6									

PREP. CHK. APPR. REVISED DATE

FORM 68510 (3/70)

THE BOEING COMPANY

NUMBER REV LTR

523 SHEET

THE BOEING COMPANY

NUMBER
REV LTR

RUN NO. 8 Test 550

TEST PT.	RUN DESCRIPTION	V (KTS)	RPM	SHAFT ANGLE	THETA, TR	NOTES	DATE / TIME
1	WING ON ZERO	—	—	0	9.6		2/14/80
2-5	HOVER STABILITY LOOPS	0	400	-10	A1		
6-9		0	415	-10	A2		
10-13	↓	0	415	-12	A3		

TEST PT 1 THETA A1
TEST PT 2 THETA A2
TEST PT 3 THETA A3

PREP.			REVISED	DATE
CHK.				
APPR.				

FORM 49510 (3/70)

RUN NO. 9/10 TEST 550

TEST PT.	RUN DESCRIPTION	V (KTS)	RPM	SHAFT ANGLE	THETA .7R	NOTES								DATE / TIME
1	STATIC CALIBRATION	--	0	0	9.6	⚠1								2/14/80
2	↓	–	↓	↓	↓	↓								
3	↓	--	↓	↓	↓	↓								
4	↓	--	↓	↓	↓	↓								
5	↓	–	↓	↓	↓	↓								
	RUN 10													2/15/80
1,2	WIND OFF ZERO	--	--	0	9.6									
3-6	STATIC CALIBRATION	–	0	0	9.6	⚠1								

⚠1 WEIGHT ADDED TO EACH BLADE INDIVIDUALLY TO CHECK INSTRUMENTATION

PREP. | CHK. | APPR. | REVISED | DATE

FORM 4850-(3/72)

THE BOEING COMPANY

SHEET 525

NUMBER

REV LTR

RUN NO. 11 TEST 550

TEST PT	RUN DESCRIPTION	V (KTS)	RPM	SHAFT ANGLE	THETA .7R	NOTES	DATE / TIME
1	WIND OFF	-	7	0	7.6		2/19/80
2,3	HOVER STABILITY, LOADS	0	HIGH	-10	8	1	
4-11	HOVER CHECK OF POWER TRIM	0	HIGH	-10	8	2	
12	"	0	HIGH	"	8	3	
13	"	0	"	"	9	4	
14	"	0	"	"	10	5	
15-21	"	0	"	"	9	6	

1. INSTRUMENTATION
2. TEST POINT
3. [illegible]
4. [illegible]
5. [illegible]
6. [illegible]

PREP | CHK | APPD | REVISED | DATE

ORIGINAL PAGE IS OF POOR QUALITY

SHEET

FORM 4810 (8/78)

THE BOEING COMPANY

NUMBER REV LTR

RUN NO. 12 Test 55D

TEST PT.	RUN DESCRIPTION	V (KTS)	RPM	SHAFT ANGLE	THETA .7R	NOTES	DATE / TIME
1	STATIC ZERO	—	—	0	9.6		2/20/80
2-6	HOVER STABILITY, LOADS	0	2[illegible]	-10	⚠1		
7-10	↓	↓	2[illegible]05	↓	⚠2		
11-13			2[illegible]25		⚠3		
14-17			2[illegible]17		⚠4		

⚠1 TEST THETA 9.6 10.6 11.6 12.6

⚠2 TEST THETA 9.6 10.6 11.6 12.6

⚠3 TEST THETA 9.6 10.6 11.6 12.6

⚠4 TEST THETA 9.6 10.6 11.6 12.6

527 SHEET

NUMBER REV LTR

RUN NO. 13 TEST 550

TEST PT.	RUN DESCRIPTION	V (KTS)	RPM	SHAFT ANGLE	THETA .7R	NOTES	DATE / TIME
1	STATIC ZERO	--	—	0	9.6		2/20/80
2,3	HOVER STABILITY, LOADS	0	400	-10	1		
4,5	↓	↓	415	↓	2		
6-8	↓	↓	430	↓	3		
9	↓	↓	435	↓	4		
10	↓	↓	400	↓	10		
11	↓	↓	440	↓	6		
12	INITIAL FORWARD FLIGHT RUN	90	430	↓	8		

TEST PT. 1 THETA

TEST PT. 2 THETA

TEST PT. 3 THETA

PREP | CHK. | APPD | REVISED | DATE

THE BOEING COMPANY

NUMBER REV LTR

FORM 8910-01 (10/01)

528 SHEET

THE BOEING COMPANY

NUMBER
REV LTR

RUN NO. 14 Test 550

TEST PT.	RUN DESCRIPTION	V (KTS)	RPM	SHAFT ANGLE	THETA .7R	NOTES	DATE / TIME
1		-	-	0	14		2/20/80
2	Start 2100	70	400	-10	3		
3	90 KT. Stability Loads		425	-10	5		
4			423	-6	8		
5			421	-4	8		
6-10			425	-6	V		
11			424	-8	6		
12		4	421	-8	4		

PREP.
CHK.
APPR.
REVISED
DATE

FORM AB610 (3-70)

RUN NO. 15 TEST 550

TEST PT.	RUN DESCRIPTION	V (KTS)	RPM	SHAFT ANGLE	THETA .7R	NOTES	DATE / TIME
1	STATIC ZERO	—	—	0	7.6		2/21/80
2-4	90 KT. STABILITY, LOADS	90	425	-8	①		
5-7	60 KT. STABILITY, LOADS	60	425	-8	②	6	
8-10	↓ ↓	↓	↓	-6	③		
11-15	↓ ↓	↓	↓	-9	④		

① TEST PT 2-4 TEST THETA = 7.6 + 1.0 = 8.6

② TEST PTS 5-7 TEST THETA = 7.6 + 1.0 = 8.6

③ TEST PT 8-10 TEST THETA = 7.6 + 1.0 = 8.6

④ TEST PT 11-15 TEST THETA = 7.6 + 1.0 = 8.6

PREP | CHK. | APPR | REVISED | DATE

THE BOEING COMPANY

NUMBER REV LTR

FORM 4810 (8/70)

530 SHEET

RUN NO. 16 TEST 550

TEST PT.	RUN DESCRIPTION	V (KTS)	RPM	SHAFT ANGLE	THETA .7R	NOTES								DATE / TIME
1	STATIC ZERO	-	-	0	4.6									2/21/80
2	120 KT. STABILITY, LOADS	120	405	-10	8									
3	↓	↓	↓	-8	8									
4				-6	8									
5				-6	6									
6				-6	4									
7				-8	8									
8				-8	6									
9	↓	↓	↓	-8	5									

FORM 4801C (3/70)

APPD | CHK. | PREP. | REVISED | DATE

SHEET 531

THE BOEING COMPANY

NUMBER

REV LTR

RUN NO. 17 TEST 550

TEST PT.	RUN DESCRIPTION	V (KTS)	RPM	SHAFT ANGLE	THETA .7R	NOTES	DATE / TIME
1	STATIS ZERO	-	-	0	9.6		2/22/85
2	127 KT. STABILITY, LOADS	127	425	-10	8	1	
3	113 KT. STABILITY, LOADS	113			9	2	
4	" " "	"	"	"	8		
5	" " "	"	"	"	7		
6	" " "	"	"	"	10		

1 LOW SIDE OF ROUGH ZONE

2 HIGH SIDE OF ROUGH ZONE

PREP. CHK. APPD. REVISED DATE

THE BOEING COMPANY

NUMBER REV LTR

532 SHEET

FORM 4931 D (5/70)

RUN NO. 18 TEST 550

TEST PT.	RUN DESCRIPTION	V (KTS)	RPM	SHAFT ANGLE	THETA .7R	NOTES	DATE / TIME
1	STATIC ZERO	—	—	0	9.6		2/22/80
2	144 KT. LOADS, STABILITY	144	435	-11.2	9		
3	↓	↓	↓	-12	9		
4-7	↓	↓	↓	↓	10		
8	↓	↓	↓	-12	11		
9	↓	↓	↓	-11	10		
10	↓	↓	↓	-10	10		
11	150 KTS. LOADS	150	↓	-12	11		
12	↓	↓	↓	-13	12		
13	↓	↓	↓	-13	10		

TEST POINT

PREP | CHK | APPD | REVISED DATE

533 SHEET

THE BOEING COMPANY

NUMBER
REV LTR

RUN NO. 19 TEST 550

TEST PT.	RUN DESCRIPTION	V (KTS)	RPM	SHAFT ANGLE	THETA .7R	NOTES								DATE / TIME
1	STATIC ZERO	—	—	0	9.6									2/23/80
2,3	ONE G FLIGHT	30	425	-3	6.6									
4	30 KTS., ZERO HUB MOM.	[illegible]		-10	8									
5	ONE G FLIGHT	60		-11.5	6.2	1								
6	ONE G FLIGHT	75		-15	6.3									
7		93		-11	9.4									
8		93		-11	9.4									
9		110		-14	12.4									
10		110		-14	12.4									
11		110		-14	12.2									

1 TEETH SET INCORRECTLY DUE TO ERRATIC A/D DISPLAY

PREP. | CHK. | APPD | REVISED | DATE

THE BOEING COMPANY

NUMBER REV LTR

FORM 4515 D 7/70

534 SHEET

RUN NO. 19 (CONT.) TEST 550

TEST PT.	RUN DESCRIPTION	V (KTS)	RPM	SHAFT ANGLE	THETA .7R	NOTES								DATE / TIME
12-15	90 KT. STABILITY, LOADS	90	335	1	7.9									2/23/90
16-21	↓	↓	↓	-6	2									
22-24			↓	-8	3									
25-28	↓	↓	1100	4	8									

1 TEST PT. 12-15 | 90 | 335 | -6 | 7.9

2 TEST PT. THETA 16-21 | 90 | 335 | -6 | 2

3 TEST PT. THETA 22-24 | 90 | 335 | -8 | 3

4 TEST PT. 25-28 | 90 | 1100 | 4 | 8

		DSIGN	
		CHK.	REVISED
		APPR.	DATE

FORM 4881D (2/70)

535 SHEET

THE BOEING COMPANY

NUMBER REV LTR

RUN NO. 20 TEST 550

THE BOEING COMPANY

NUMBER
REV LTR

TEST PT.	RUN DESCRIPTION	V (KTS)	RPM	SHAFT ANGLE	THETA .7R	NOTES	DATE / TIME
1	STATIC ZERO	—	—	0	9.6		2/23/80
2-7	90 KT. STABILITY, LOADS	90	400	-6	①		
8-12	↓ ↓	90	403	-8	②		
13	RESUM ONE G FLIGHT	93	425	-5.5	7.5		
14	↓ ↓	93	425	-5.5	7.5		

① TEST PT 2 THETA 9.0
② TEST PT 12 THETA 10.0

PREP. CHK. APPR. REVISED DATE

FORM 48510 (1/70)

ORIGINAL PAGE IS OF POOR QUALITY

SHEET 536

RUN NO. 21 TEST 550

TEST PT.	RUN DESCRIPTION	V (KTS)	RPM	SHAFT ANGLE	THETA .7R	NOTES								DATE / TIME
1	STATIC ZERO	—	—	0	9.6									2/24/80
2	ONE G. FLIGHT	55	425	-2.5	6									
3-6	FLYING QUALITIES	55	↓	-2.5	6	△1								
7	ONE G FLIGHT	93		-5.5	6.8									
8-11	FLYING QUALITIES	93		-5.5	6.8	△1								
12	ONE G FLIGHT	111		-7.5	8.5									
13-17	FLYING QUALITIES	111	↓	-7.5	8.5	△1								
18-20	HOVER OVERSPEED STABILITY	0	437	-10	△2									
21-24	CYCLIC TRIM EXCURSIONS	0	375	-10	6	△3								

△1

TEST POINTS	RAMP INPUT ON DCS
3, 8, 13	+ 250 COUNTS LATERAL CYCLIC
4, 9, 14, 15	- 250 COUNTS LATERAL CYCLIC
5, 10, 16	+ 250 COUNTS LONG. CYCLIC
6, 11, 17	- 250 COUNTS LONG. CYCLIC

△2

TEST POINT	18	19	20
THETA	11	10	8

△3

TEST POINT	CYCLIC EXCURSION FROM TRIM
21	+ 1° LONG.
22	- 1° LONG
23	+ 1° LAT.
24	- 1° LAT

FORM 48510 (3/70)

PREP. | CHK. | APPR. | REVISED | DATE

ORIGINAL PAGE IS OF POOR QUALITY

THE BOEING COMPANY

NUMBER

REV LTR

RUN NO. 22 TEST 550

TEST PT.	RUN DESCRIPTION	V (KTS)	RPH	SHAFT ANGLE	THETA .7R	NOTES	DATE / TIME
1	STATIC ZERO	1	1	0	9.6		2/24/80
2-5	BALANCE DAMPERS OFF	0	1	-10	8		
6-9	↓ ↓	0	2	↓	6		
10-13		0	3		8		
14-17		0	4		4		

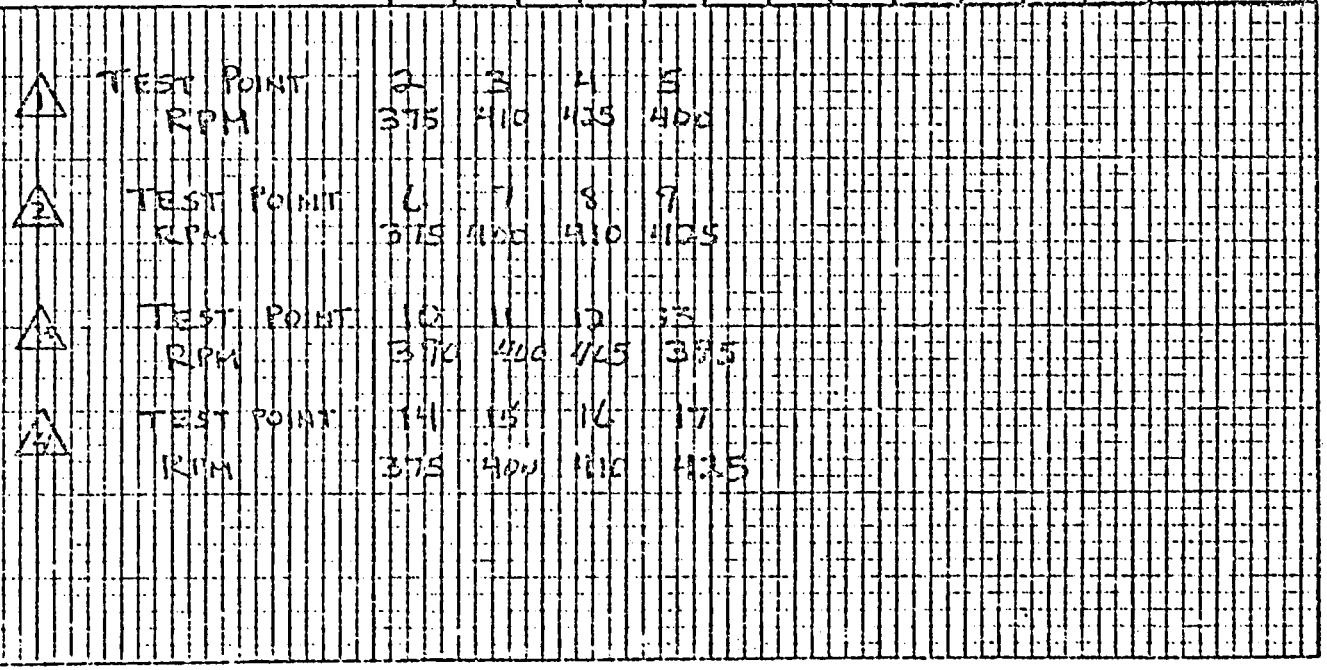

PREP. CHK. APPR. REVISED DATE

THE BOEING COMPANY

NUMBER REV LTR

FORM 48810 (3/70)

52B SHEET

RUN NO. 23 Test 550

TEST PT.	RUN DESCRIPTION	V (KTS)	RPM	SHAFT ANGLE	THETA 7R	NOTES	DATE / TIME
1	STATIC ZERO	–	–	0	7.6		2/26/80
2-6	BALANCE · DAMPERS OFF	90	(1)	-8	4		
7-10	↓	90	425	-4	(2)		
11	↓	120	↓	-6	6		
12	↓	120	↓	-10	8		
13	↓	143	↓	-6	10		
14	↓	159	↓	-6	10		
15	↓	165	↓	-6	10		

	1	2	3	4	5	6
(1) TEST PT.						
RPM	035	375	400	410	425	
(2) TEST PT.	7	9	9	10		
THETA	2	4	6	8		

PREP. | DATE
REVISED
CHK.
APPR.

NUMBER
REV LTR

THE BOEING COMPANY

FORM 49510 (3/70)

539
SHEET

RUN NO. 24/25 TEST 550

TEST PT.	RUN DESCRIPTION	V (KTS)	RPM	SHAFT ANGLE	THETA .7R	NOTES	DATE / TIME
1	STATIC CALIBRATION	--	--	0	9.6		2/24/80
	RUN 25						
1	STATIC ZERO	-	-	0	9.6		
2	TRACK AND BALANCE	0	400	-10	6		
3	↓ ↓	0	0	0	9.6		

PREP | CHK. | APPR | DATE | REVISED

FORM 4513 (8/70)

THE BOEING COMPANY

NUMBER
REV LTR

SHEET 550

RUN NO. 26 TEST 550

TEST PT.	RUN DESCRIPTION	V (KTS)	RPM	SHAFT ANGLE	THETA .7R	NOTES								DATE / TIME
1	STATIC ZERO	--	-	0	9.6									2/26/80
2-5	HOVER - SOFT PITCH LINKS	0	375	-10	⚠1									
6-9	↓	↓	400	↓	⚠1									
10	↓	↓	425	↓	8									
11	↓	↓	425	↓	6									
12	↓	↓	425	↓	4									
13	↓	↓	375	↓	8									

⚠1 TEST PT 2,6 3,7 4,8 5,9
THETA 8 6 4 2

PREP. CHK. APPR. REVISED DATE

SHEET 541

NUMBER
REV LTR

THE BOEING COMPANY

FORM 4810 (3/70)

RUN NO. 27 TEST 550

TEST PT.	RUN DESCRIPTION	V (KTS)	RPM	SHAFT ANGLE	THETA .7R	NOTES	DATE / TIME
1	STATIC ZERO	"	-	0	7.6		2/27/80
2	90 KTS. SOFT PITCH LINKS	90	460	-8	5		
3-7	↓	↓	⚠1	-8	4		
8			425	-6	4		
9-11			425	-4	⚠2		
12			400	-8	6		
13			400	-5	8		
14			375	-6	8		
15	↓		375	-5	6		
16	BALANCE HUB INVEST.	0	375	-10	8		

TEST POINT	3	4	5	6	7
RPM	335	375	406	410	425
TEST POINT	9	10	11		
THETA	7	8	6		

PREP. | CHK. | APPR. | REVISED | DATE

THE BOEING COMPANY

NUMBER REV LTR

FORM 4510 (8/78)

SHEET 543

RUN NO. 28 TEST 550

TEST PT.	RUN DESCRIPTION	V (KTS)	RPM	SHAFT ANGLE	THETA .7R	NOTES	DATE / TIME
1	STATIC ZERO	–	–	0	4.6		2/28/50
2-5	DAMPER STRIPS INSTALLED	0	1	-10	4		
6-8		0	1425	-10	2		
9		90	1425	-10	8		
10-11			1425	-8	3		
12-13			1	-8	4		
14-15			1	-6	4		
16-21	↓	↓	1425	-6	3		

TEST POINT	1	2	3	4	5
RPM	3715	1860	415	4105	
TEST POINT THETA	6	7	8	9	
TEST POINT THETA	6	6	8	10	
TEST POINT RPM	3715	1860	415	4105	
TEST POINT THETA	6	7	8	9	

THE BOEING COMPANY

NUMBER
REV LTR

DESIGN
APPR.
CHK.
REVISED
DATE

543
SHEET

RUN NO. 29 TEST 550

TEST PT.	RUN DESCRIPTION	V (KTS)	RPM	SHAFT ANGLE	THETA .7R	NOTES		DATE / TIME
1	STATIC ZERO	—	—	0	9.6		2	2/20/80
2	DAMPER STRIPS INSTALLED	120	425	-6	4			
3		120				1		
4		90						
5		90		↓		1		
6		0		-10				
7		0		↓				
8	↓	0	↓	↓	↓	1	↓	

1 125 COUNTS CYCLIC AT 2.0 HZ

2 BALANCE DAMPERS ON

PREP. | CHK. | APPR. | REVISED DATE

THE BOEING COMPANY

NUMBER REV LTR

FORM 88510 D/770

544 SHEET

RUN NO. 30 TEST 550

TEST PT.	RUN DESCRIPTION	V (KTS)	RPM	SHAFT ANGLE	THETA .7R	NOTES	DATE / TIME
1	STATIC ZERO	—	—	0	9.6	1	2/29/80
2-13	BLADES OFF TARE	60	1125	2	9.6		
14-24	↓	120	↓	↓	4	↓	
25-27		152					
28-116		180					

1 BLADES OFF

2 TEST POINTS

PREP. CHK. APPR. REVISED DATE

THE BOEING COMPANY

REV LTR NUMBER

FORM 4P510 03/701

545 SHEET

RUN NO. 31 TEST 650

TEST PT.	RUN DESCRIPTION	V (KTS)	RPH	SHAFT ANGLE	THETA .7R	NOTES	DATE / TIME
1	STATIC ZERO	-	-	0	-	1	2/29/80
2-10	BARE HUB TARES	60	375	2	-	-	
11		60	0		-		
12-18		60	0		-		
19-26		90	0		-		
27-37		120	0		-		
38-45		150	0		-		

1 BLADES AND ELASTOMERS OFF

2 TEST POINT SHAFT ANGLE

PREP. CHK. APPR. REVISED DATE

THE BOEING COMPANY

NUMBER REV LTR

SHEET 546

FORM 4881-0 07/70

11.2 INSTRUMENTATION LIST

The following pages contain a compilation of the instrumentation data for the test of the RMR in the Ames 40-by-80 wind tunnel.

GUIDE FOR PRELIMINARY INSTRUMENTATION REQUIREMENTS

Meas #, Item Description: Parameter name, number, general description & location; also include measurement number if any (the number should be unique).

Cat; Category: All parameters must be categorized in priority. The priorities are: A - signal loss - test shut down - signal to be restored or substituted before test continues; B - signal loss - test may continue or shut down at option of test engineer - must be repaired or substituted before restart of test; C - signal loss - test may continue - signal should be restored during next run break; D - signal loss - test to continue - to be repaired as oportunity becomes available.

Input TSP; Input Twisted Shielded Pair for each measurement from wire list

Refer to the Guide for Planning Investigations in the Ames 40- by 80-ft Wind Tunnel for description of the following acronyms. Put a channel assignment in the appropriate box. On the TCS/HS, DAS, DRS & OBS select priority of importance, ie: 1 = high priority,..., 30 = lower priority. On the OGR, CRO, DPM, & PDS select the channel assignment in accordance with your grouping requirements.

HS - High Speed Data Acquisition System
TCS - Transducer Conditioning System
DAS - Dynamic Analysis System
DRS - Dynamic Recording System
BFI - Band Pass Filter
OGR - Visicorder (Oscillograph Recorder)
CRO - Oscilloscope (Cathode Ray Oscilloscope)
OBS - On-Board System
DPM - Digital Panel meters (CTR - Counter)
SI - Special Instrumentation Interface
PDS - Peak to Peak Display (Peak Detector System)

Test BMR (550) Date 1-10-80 Page A

	Meas #	Item STA	Description	Cat	Input TSP	HS	TCS	DAS	DRS	BFI	OGR	CRO	OBS	DPM	SI	PDS	Other
1	4546	11.0	Flex Chord Bend 1A R	A	T 081, 82, 83	1	1	14	1	3, 30, 7	1-13	* 3				3, 30	*Bound Jitter on CRO
2	5502	14.25	Flex Flap Bend #1 Aux R	A	Historian GI 101 102 103	2	2	8	2	19, 46	2-14					19, 46	Parallel input to H.S. 59
3	4542	10.5	Flex Flap Bend 1A R	A	T 84 85 86	3	3	12	3	1, 28	1-11	1				1, 28	
4	4558	46.0	Flex Flap Bend 1A R	A	T 87 88 89	4	4		4	8, 35	2-5	5				8, 35	
5	4570	Axial	Pitch Link #1 R	A	T 91 92 93	5	—		5	5, 32	1-5	8				5, 32	
6	4520	38.1	Torque Tube Flap Bell #1 R	A	T 94 95 96	6	6	16	6	12, 39	1-6	7				12, 39	
7	4522	38.1	Torque Tube Chord Bell 1 R	A	T 97 98 99	7	7	17	7	13, 40	1-7	6				13, 40	
8	4532	55.4	BCD Chord Bend #1 R	A	T 155 156 157	8	8	19	8	17, 44	2-10	2				17, 44	
9	9	RST	Rotor Shaft Torque E	A	T 158 159 160	9	9	22	9					1	1		
10	10	DC I	Dynamic Control Input	B	GI 14	10	—	1	10		1-15, 2-15						
11	5504	15.25	Flex Torsion #1 Hub R	B	Historian GI 104 105 106	11	11		11	21	2-12					21	Parallel input to H.S 60
12	5500	14.25	Flex Chord Bend #1 Hub R	B	T 161 162 163	12	12	4	12	20, 47	2-13					20, 47	

ORIGINAL PAGE IS OF POOR QUALITY

Page A 2 Rev 2-7-80

Test BMR (550) Date 1-10-80 Page B

	Node #	Item	Description	Cat	Input TSP	HS	TCS	DAS	DRS	BFI	OCR	CRO	ORS	DPM	SI	PDS	Other
1	5506	14.25	FLEX CHORD BEND #2 R	B	T1L4 165 166	13	13	5	13								
2	5512	14.25	FLEX CHORD BEND #3 R	B		14	14	6	14								
3	5518	14.25	FLEX CHORD BEND #4 R	B		15	15	7	15								
4	4590	551	STA SWASHPLATE #1 (Ring)	C		16	16		16	25							Gage not good 2-5-80
5	4595	552	STA SWASHPLATE #2 (Ring)	C		17	17		17	26	1-9					26	
6	4593	553	STA SWASHPLATE #3 (Ring)	C		18	18		18		1-10						
7	15418	11.0	FLEX CHORD BEND 1B R	C		19	19	15	19	41, 31	1-14	4				41, 31	
8	15444	10.5	FLEX FLAP BEND 1B F	C		20	20	13	20	2, 29	1-12					2, 29	
9	15460	15.0	FLEX FLAP BEND 1B R	C		21	21		21	9, 36	2-6					9, 36	
10	15430	55.4	BLD FLAP BEND #1 F	C		22	22	20	22	16, 43	2-9					16, 43	
11	15434	110.0	BLD FLAP BEND #1 F	C		23	23		23		1-8					25	
12	15436	110.0	BLD CHORD BEND #1 F	C		24	24		24								

559

ORIGINAL PAGE IS OF POOR QUALITY

Page B

Rev 2-7-80 2-12-80

3

Test BMR (550) Date 1-10-80 Page C

	Meas #	Item	Description	Cat	Input TSP	HS	TCS	DAS	DRS	BFI	OGR	CRO	OBS	DPM	SI	PDS	Other
1	1572	Minimum	Torque Tube Torsion #1 R	C		25	25	18	25	15						15	
2	5508	14.25	Flex Flap Bend #2 R	C		26	26	9	26								
3	5514	14.25	Flex Flap Bend #3 R	C		27	27	10	27								
4	5520	14.25	Flex Flap Bend #4 R	C		28	28	11	28								
5	5524		STA Control Rod #3	D		29	29		29								
6	5526		STA Control Rod #1	D		30	30		30								
7	5528		STA Control Rod #2	D		31	31		31								
8	1528	65.0	Bld Torsion #1 R	D		32	32	21	32	18, 45	2-11					18, 45	
9	5510	15.25	Flex Torsion #2 R	D		33	33		33								
10	5516	15.25	Flex Torsion #3 R	D		34	34		34								
11	5522	15.25	Flex Torsion #4 R	D		35	35		35								
12	1538	7.5	Flex Flap Bend 1A R	D		36	36		36								

550

Page (C) 4

Rev 2-7-80

Test BMR (550) Date 1-10-80 Page D

	Meas #	Item	Description	Cat	Input TSP	HS	TCS	DAS	DRS	BFI	GGR	CRO	OBS	DPM	SI	PDS	Other
1	1540	7.5	FLEX FLAP BEND 1B L	D		37	37		37								
2	1550	18.0	FLEX FLAP BEND 1A L	D		38	38		38	6, 33						9, 33	
3	1552	16.0	FLEX FLAP BEND 1B R	D		39	39		39								
4	1553	43.0	FLEX CHORD BEND 1A L	D		40	40		40	10, 37	2-7					10, 37	
5	1556	43.0	FLEX CHORD BEND 1B L	D		41	41		41	11, 38	2-8					11, 38	
6	12		ACCEL #1 Trans Long	D		42	42	23	42								
7	13		ACCEL #2 Trans Lat	D		43	43	24	43								
8	14		ACCEL #3 Norm Vert	D		44	44	25	44								
9	15		ACCEL #4 Tail Long	D		45	45	26	45								
10	16		ACCEL #5 Tail Lat	D		46	46	27	46								
11	17		ACCEL # 6 Left Side Long	D		47	47	28	47								
12	18		ACCEL # 7 Left Side Lat	D		48	48	29	48								

558

Page D 5

Rev 2-5-80

Test BIIIR (550) Data 1-10-80 Page E

	Meas #	Item	Description	Cat	Input TSP	HS	TCS	DAS	DRS	BFI	OGR	CRO	OBS	DPM	SI	PDS	Other
1	49		ACCEL # 8 Long Right Side	D		49	49	30	49								
2	50		ACCEL # 9 LAT RIGHT SIDE	D		50	50	Spare 30	50								
3	4591	4591	STAT RING ABSOLUTE #4	D		51	51		51								
4	9594	4594	STAT RING ABSOLUTE #5	D		52	52		52								
5	4592	4592	STAT RING ABSOLUTE #6	D		53	53		53								
550	54		#1 Actuator Pos	B		54	—								2	5	
7	55		#2 Actuator Pos	B		55	—								3	6	
8	56		#3 Actuator Pos	B		56	—								4	7	
9						57											
10						58											
11	5502	14.25	RTA Coning (½ lap)	A	GJ102	59	—										RTA Control Comm 229 GJ 107
12	5504	15.25	RTA Orbit Rate (Pitch)	A	GJ105	60	—										RTA Control Comm 231 GJ 108

ORIGINAL PAGE IS OF POOR QUALITY

Page E 16

Rev 2-5-80
2-7-80

Test BMR (550) Date 1-10-80 Page F

	Meas #	Item	Description	Cat	Input TSP	HS	TCS	DAS	DRS	DFI	OGR	CRO	OBS	DPM	SI	PDS	Other
1	61	RPM	RPM, 256 PR REV PHOTO TACH	A				/						CTR 1	4		ACOUSTIC RECORDER STROBE (4TH TRACK)
2	62	AZ	AZIMUTH, 1 PER REV PHOTO TACH	A				/			1-3 2-3						ACOUSTIC RECORDER
3	63	APRB	APR B SYSTEM 72 PER REV	A	BNC						1-16 2-16						RESOLVER CONSOLE
4	64	DANG	DANSCEOMETER	C											2		
5	65	BAR	BAROMETER	C											3		
6	66	COS	COS Ψ (DYN CONT)	B				2									
7	67	SIN	SIN Ψ (DYN CONT)	B				3									
8	68	DASSG	DAS SIGNAL GENERATOR		BNC												DCS BNC
9	69	TT	TUNNEL TEMP	A													FACTOR TABLE
10	70	IRIGB	IRIG B Time Code	C							1-9 2-9						
11																	
12																	

584

Page F Rev 7

Test PMIR (550) Date 1-10-80 Page 6

	Meas #	Item	Description	Cat	Input TSP	HS	TCS	DAS	DRS	BFI	OGR	CRO	OBS	DFM	SI	PDS	Other
1	73		Coning		RIA [illegible] Conn'l 12P37 5108												BNC 1
2	74		Long flap		5109												BNC 2
3	75		Lat flap		5101												BNC 3
4	76		Collective Pitch		5102												BNC 4
5	78		Lat Pitch		5103												BNC 5
6	79		Long Pitch		5104												BNC 6
7																	
8																	
9																	
10																	
11																	
12																	

Page 6

Rev 8

GUIDE FOR INSTRUMENTATION PRETEST DATA

Item Description & Location: Parameter name, number, general location.

Trans Type, Transducer Type & Resistance: SG - Strain Gage; Press - Pressure; Res Pot - Resistance Potentiometer; B - Bridge; A - Accellerometer; ect... ie: 2SG B 350 - double strain gage bridge 350 ohm 4 active legs; SG Press 120 - 120 ohm strain gage type pressure transducer 4 active legs; ½SG B 120 - 120 ohm strain gage 1 active leg; e.t...

Eng Units, Engineering Units: List the engineering units which will be used during the test for each parameter, ie in-lbs.

Ex V, Excitation Voltage: Ranges available; 0-20V & 20-40V. Refer to Transducer Conditioning System in the Guide for Planning Investigations in the Ames 40- by 80ft Wind Tunnel, for further information.

RC K~, K Cal Resistor value: Resistors available are: 50K, 75K, 100K, 125K, 150K, 200K, 250K, & 500K.

Eng U Equiv, Engineering Units Equivalence: Equivalent load in engineering units to corresponding R Cal resistor.

Load/MV Cal, Load per Millivolt or Volt Calibration: The Calibration of the respective transducer. Specify /MV or /V.

Eng U Tare, Engineering Units Tare: Tare load at rest or "parking" position.

Pos Sig Direct, Positve Signal Direction: Positive signal direction relative to physical direction of parameter being measured.

Filter Freq, Filter Frequency: The frequency of the low pass filter on the high speed data acquisition system. Frequencies available are; 1, 10, 30, 100, 300, 1K, 10K, 100K Hz.

Expected Sig Freq, Expected Signal Frequency: The band width of the expected frequency of each parameter.

Expected Sig Eng U, Expected Signal Engineering Units: The expected operating range in engineering units.

D ?, Diagram ?: Wiring diagram of related parameter should be supplied. Insert a yes or no if the diagram has been submitted and is complete.

Define any acronyms used on a separate sheet.

H

Test BHR Date 1-8-80 Page

	TC	HS	Meas ID	Eng Units	Ex V	RC K-Ω /Sw	Eng Limit	R Cal Equiv Load	Cal Load/MV	R Cal MV	Filter Freq	Max MV	Gain	Δ Off Set	R Cal Level /+Δ	+Sig Mode	Tare	Load/V	HS CH
1	1	1	4506 Flex Chord #1 11.0A	IN-lb	10	50K	12,800 "#	12,058 "#	250.4 "#/MV	48.155	100 Hz	52	100	Ø	4.815	tension lead Edge	Ø	2,504.0 "#/V	1
2	2	2	4535 Flex Flap #1 14.25	IN-lb	10	75K	103,100 "# / 27.3 deg	25,333 "# / 17.27 deg	763.6 "#/MV / 0.526 deg/MV	33.175	↓	154	50	7.470V / -.3381	1.659V / 1.205V	flap up	-5,703 "#	15,272.0 "#/V	2
3	3	3	4542 Flex Flap #1 18.5A	IN-lb	10	75K	51,000 "#	19,832	598.9	33.120		86	100	2.992 MV / -.4994	3.312V / 2.81V	flap up	-2,983 "#	5988.0	3
4	4	4	4558 Flex Flap #1 14.0A	IN-lb	10	250K	12,000 "#	2,777	277.7	10.000		44	200	6.596 MV / -1.319	2.000V / 0.621	flap up	-1,915 "#	13985	4
5	5	5	Pitch Link #1	lbs.	10	250K	900 lbs.	2,749.4	800.185 lbs/MV	3.436		2	1,000	Ø	3.436	tension in link	Ø	800.185 lbs/V	5
6	6	6	4520 Torque Tube Flap #1 38.1	In-lb	10	50K	4,750	2,848.1	57.50	49.532		83	100	Ø	11.953	flap up	Ø	575.0	6
7	7	7	4522 Torque Tube #1 Chord 14.1	In-lb	10	125K	1,800 "#	853.03	42.64 "#/MV	20.005		29	200	Ø	4.001	tension lead edge	Ø	213.2	7
8	8	8	4552 #1 BSL Chord 55.4	In-lb	10	500K	32,310	8,199.5	1,626.23	5.042		20	500	Ø	2.521	tension lead edge	Ø	3,252.96	8
9	9	9	7 Rotor Shaft Torque	In-lb	10	100K	200,000	265,920	30,756 "#/MV	8.646		7	1000	Ø	8.646	Driving rotor	Ø	30,756.0	9
10	—	10	10 Open Control Input	V	—	—	±10V	—	1 V/V	—		10V	1	Ø	—	—	Ø	1V/V	10
11	11	11	4504 #1 Flex Tension 15.25	In-lb	10	250K	3,0400 / 58.9 deg	693.0 "# / 13.43 deg	68.81 "#/MV / 1.333 deg/MV	10.071		45	200	Ø	2.014	Lead Edge up	Ø	344.05 "#/V / 6.666 deg/V	11
12	12	12	5510 #1 Flex Chord 14.25	In-lb	10	75K	90,000 "#	19,761	591.9	33.386	↓	154	50	Ø	1.669	Tension lead edge	Ø	11,838.0	12

Page A 9

Rev 2-22-80 2-25-80

Test BMR Date 1-8-80 Page

	TC	HS	Hose ID	Eng Units	Ex V	RC K-m /Sw	Eng Limit	R Cal Equiv Load	Cal Load/MV	R Cal MV	Filter Freq	Max HV	Gain	Δ Off Set	R Cal Level /+Δ	+Sig Mode	Tare	Load/V	HS Ch
1	13	13	5506 #2 Blue Cloud #2 1425	IN-LB	10	75K	99,000 "H	19,431 "H	526.9	33.421	100 HZ	155	50	ø	1.661	tension load edge	ø	11,728.0 "H/V	13
2	14	14	5513 #3 Blue Cloud 1425	IN-LB	10	75K	99,000 "H	19,121 "H	538.4	33.059	100HZ	157	50	-	1.653	tension load edge	ø	11,[illegible] "H/V	14
3	15	15	5518 #4 Blue Cloud 1425	IN-LB	10	75K	99,000 "H	17,861 "H	537.6	33.224	100HZ	167	150	ø	1.661	tension load edge	ø	19,752.0 "H/V	15
4	16	16	16 #1 Stat Quad	psi	10	250K	7,000 PSI	6890.6 psi	1974	3.491	30HZ	4	1,000 #	ø	3.491	tension	ø	19740	16
5	17	17	17 #2 Stat Quad	psi	10	250K	7,000 PSI	6890.6 psi	1974	3.491	300HZ	4	1,000 #	ø	3.491	tension	ø	1974.0	17
6	18	18	18 #3 Stat Quad	psi	10	250K	7,000 PSI	6890.6 psi	1974	3.491	300HZ	4	1,000 #	ø	3.491	tension	"	1974.0	18
7	19	19	5545 #10 Blue Cloud 110	IN-LB	10	50K	12,800 "H	11,724 "H	242.6	48.446	100HZ	53	100	ø	4.845	tension load edge	ø	24200	19
8	20	20	5594 #8 Blue Flap 10.5 4560	IN-LB	15	75K	51,000	18,441 "H	526.5	33.137		92	100	-5.36 V -.516 V	3.314 V 2.775 V	flap up	-2983 "H	5565.0	20
9	21	21	5618 Blue Flap 450	IN-LB	10	250K	12,000 "H	3,035 "H	298.3	10.174		41	200	-6.391 V -1.477 V	2.035 V 0.7566	flap up	-1908 "H	1491.5	21
10	22	22	5550 #1 Blue Flap 555.4	IN-LB	10	200	15,000 "H	5,345.3 "H	485.57	12.562		36	200	-7.443 V -1.461 V	2.512 V 1.024 V	flap up	-3167	2127.35	22
11	23	23	5539 #1 Blue Flap 110.0	IN-LB	10	125	10,000 "H	3,752.5 "H	188.82	20.032		53	100	-6.212 V -0.631 V	2.031 V 1.312 V	flap up	-1173 "	1898.2	23
12	24	24	5534 #1 Blue Cloud 110.0	IN-LB	10	50K	20,000 "H	17,466 "H	3,458.7	5.050		6	1,000	ø	5.050	Tension load edge	ø	3458.7	24

Page B 10

Rev 2-22-

3

Test B W R

Date 1-8-80

Page C

	TC	HS	Meas ID	Eng Units	Ex V	RC K~ /Sv	Eng Limit	R Cal Equiv Load	Cal Load/MV	R Cal MV	Filter Freq	Max	Gain	Δ Off Set	R Cal Level /+σ	+Sig Mode	Tare	Load/V	HS CH
1	25	25	4572 #1 Torque Tube Torsion	in-lb	10	200K	5,600 in	2,7191	216.10	12.583	100 Hz	26	200	Ø	2.517 V	Read edge up	Ø	1080.5	25
2	26	26	5508 #2 Strut Bend 14.25	in-lb	10	15K	100,000 in	24,593	775.0	31.733	100Hz	319	50	-7.357 -.365	1.507V 1.219V	Step up	-5703	15,530.0	26
3	27	27	5514 #3 Strut Bend 14.25	in-lb	10	15K	100,000 in	25,217	763.7	33.016	100Hz	135	50	-7.881 -.325	1.651V 1.277V	Step up	-5703	15,270.0	27
4	28	28	5520 #4 Strut Bend 14.25	in-lb	10	15K	100,000 in	23,210	699.0	33.205	100Hz	145	50	-8.159 -.408	1.660V 1.252V	Step up	-5703	13,980.0	28
5	29	29	5524 #1 Strut Cent Rod	Lbs	10	500K	1,000 4,000	1106.2	634.0	1.745	300Hz	7	1000 in	Ø	1.745V	tension limit	Ø	634.0	29
6	30	30	5516 #2 Strut Cent Rod	Lbs	10	500K	1,000 4,000	1059.6	605.9	1.749	300Hz	7	1000 in	Ø	1.749	tension limit	Ø	605.9	30
7	31	31	5528 #3 Strut Cent Rod	Lbs	10	500K	1,000 4,000	1075.9	614.1	1.752	300Hz	7	1,000 in	Ø	1.752	tension limit	Ø	614.1	31
8	32	32	4528 #1 BSI Torsion 650	in-lb	10	500K	4,500	1588.	314.13	5.064	300Hz	15	500	Ø	2.522	Read edge up	Ø	629.66	32
9	33	33	5510 #2 BSI Torsion 15.25	in-lb	10	350K	4,200	664.6	65.88	10.088	300Hz	64	100	Ø	1.009	Read edge up	Ø	658.50	33
10	34	34	5512 #3 BSI Torsion 15.25	in-lb	10	350K	4,200	677.9	67.20	10.018	300Hz	63	100	Ø	1.009	Read edge up	Ø	672.10	34
11	35	35	5522 #4 BSI Torsion 15.25	in-lb	10	350K	4,200	661.6	65.61	10.053	300Hz	64	100	Ø	1.005	Read edge up	Ø	656.1	35
12	36	36	4536 #4 Strut Bend 7.5	in-lb	10	200K	60000	11754	1178.	12.525	100 Hz	51	100	-2.557 -.255	1.252V 0.994	Step up	-5044	11750.	36

ORIGINAL PAGE IS OF POOR QUALITY

Rev 2-22-80

Page C 11

2-26-80

Test B VA R Date 1-9-90 Page

	TC	HS	Meas ID	Eng Units	Ex V	RC K-/Sw	Eng Limit	R Cal Equiv Load	Cal Load/MV	R Cal MV	Filter Freq	Max	Gain	Off Set	R Cal Level +/-	+Sig Mode	Tare	Load/V	HS CH
1	37	37	4549 #1B Sled Stop 1.5	lb-lb	10	200K	60,000	13,900.	1,114.	12.478	100HZ	54	100	-2.732 V -.2734 V	1.248 V .975 V	Stop up	-3044	11,140.0	37
2	38	39	4550 #1B Sled Stop 12.0	lb-lb	10	75K	31,000	12,655.	382.0	33.128	100HZ	82	100	-7.134 V -.713 V	3.313 V 1.599 V	Stop up	-2725	3,820	38
3	39	39	4552 #1B Sled Stop 12.5	lb-lb	10	75K	31,000	12,249.	370.2	33.088	100HZ	84	100	-7.361 V -.7361 V	3.349 V 2.573 V	Stop up	-2725	3,702.0	39
4	40	40	4554 #1B Sled Clock 430	lb-lb	10	150K	4,000	2,2052	140.9	16.290	100HZ	39	200	0	3.1582 V	Tension Load Cell	0	764.5	40
5	41	41	4556 #1B Sled Clock 420	lb-lb	10	150K	4,000	2,271.5	138.5	16.380	100HZ	89	200	0	3.276V	Tension Load Cell	0	694.0	41
6	42	42	42 Accel #1 Trans Long	g's	5	50K	50 g's	1.4939	0.1822 S/N 15573	8.21	100HZ	28	200	0	1.642		0	0.9110	42
7	43	43	43 Accel #2 Trans Lat	g's	5	50K	50 g's	1.1011 g's	0.1087 g's/mv S/N 11132	10.120		46	200	0	2.024		0	0.5440	43
8	44	44	44 Accel #3 Vert	g's	5	50K	50 g's	1.4901 g's	0.1178 g's/mv S/N 3565	12.647		43	200	0	2.530		0	0.5890	44
9	45	45	45 Accel #4 Tail Long	g's	5	50K	50 g's	.9987 g's	0.1040 g's/mv S/N 11184	9.600		49	200	0	1.920		0	0.5260	45
10	46	46	46 Accel #5 Head Lat	g's	5	50K	50 g's	1.3525 g's	0.1158 g's/mv S/N 10387	11.680		44	200	0	2.336		0	0.5770	46
11	47	47	47 Accel #6 Left Knee	g's	5	50K	50 g's	.9704 g's	0.1169 g's/mv S/N 3644	8.620		44	200	0	1.724		0	0.5745	47
12	48	48	Accel #7 Left Ankle	g's	5	50K	50 g's	.9167 g's	0.1051 g's/mv S/N 3511	8.48		47	200	0	1.696		0	0.5405	48

Rev 2-5-90 2-22-90

Test: B M R Date: 1-9-80 Page: E

	TC	MS	Meas ID	Eng Units	Ex V	RC K~ /Sw	Eng Limit	R Cal Equiv Load	Cal Load/MV	R Cal MV	Filter Freq	Max	Gain	Δ Off Set	R Cal Level /+φ	+Sig Mode	Tare	Load/V	MS CH
1	49	49	49 Accel #9 Rigid Pedlay	g's	5V	50K	5 g's	1.0346 g's	0.1205 g's/mV S/N 3435	8.560	180Hz	42	200	Ø	1.712		Ø	0.6040	49
2	50	50	Accel #9 R Rigid Ped	g's	5V	50K	5 g's	0.9980 g's	0.6995 g's/mV S/N 11133	10.03	100Hz	51	100	Ø	1.003		Ø	0.9950 g's/V	50
3	51	51	51 Strut Ring abs #4	PSI	10	250	7,000 / 14,000	6890.6	1974.	3.491	300Hz	8	1,000	Ø	3.491	Tension	Ø	1974.0	51
4	52	52	Strut Ring abs #5	PSI	10	250	7,000 / 14,000	6890.6	1974.	3.491	300Hz	8	1,000	Ø	3.491	Tension	Ø	1974.0	52
5	53	53	Strut Ring abs #6	PSI	10	250	7,000 / 14,000	6890.6	1974.	3.491	300Hz	8	1,000	Ø	3.491	Tension	Ø	1974.0	53
6	—	54	Accel #1 Position		—	—		—	1 V/V	—	30Hz		1	—				—	1 V/V	54
7	—	55	Accel #3 Position		—	—		—	1 V/V	—	30Hz		1	—				—	1 V/V	55
8	—	56	Accel #5 Position		—	—		—	1 V/V	—	30Hz		1	—				—	1 V/V	56
9		57																	
10		58																	
11	—	59	59 RTA Coupling Shaft	deg	—	—							100						
12	—	60	60 RTA Collective Patch	deg	—	—							200						

Rev 2-5-80

Page E 13

COUNTERS

#	Measurement	HS Ch	Item Index	Input Sig	D	C#	Rate/ Batch	X10 Auto	SI	Comments
1	61 RPM 256 PER REV	—	F-1	Pick Tach	2	2344	M Rate	auto	4	
2										
3										
4										
5										
6										

DIGITAL PANEL METERS

#	Measurement	HS Ch	Item Index	Range	Offset Tare Eng	V	Scaling 1 V	Max @	R Cal Eng	V	SI
1	9 ROCK SHFT TOR	9	A-9	40V	0	0	2,543	2	23,160	8.646	1
2	54 ACTUATOR #1	54	E 6	4V	0	0	1.0V	10V	—	—	5
3	55 ACTUATOR #2	55	E 7	4V	0	0	1.0V	10V	—	—	6
4	56 ACTUATOR #3	56	E 8	4V	0	0	1.0V	10V	—	—	7
5											
6											
7											
8											
9											
10											

Special Instrument Interface

#	Measurement	HS Ch	Item Index	From	Scaling	Comments
1	9 ROCK SHFT TOR	9	A-9	DPM-1	-1 FULL/count	
2	DAUGHTER	—	F 4	DAUG	.001 /count	
3	ENRICHMETER	—	F 5	ENR	.001 PSI/count	
4	61 RPM 256 PER REV	—	F-1	CTR-1	1 RPM/count	
5	54 ACTUATOR #1	54	E-6	DPM-2	.0001 V/count	
6	55 ACTUATOR #2	55	E-7	DPM-3	.0001 V/count	
7	56 ACTUATOR #3	56	E-8	DPM-4	.0001 V/count	

ORIGINAL PAGE IS
OF POOR QUALITY

CATHODE RAY OSCILLOSCOPE

CRO

Test BMR

Date 1-29-80

Page 16

Rev

#	Measurement	HS CH	Item Index	BPF #	BPF Freq	Scale Eng/CH	Input Load/V	Tare offset Eng	Tare offset V	Pos CH	Scale CH/V	"Peaking" R Cal Eng	"Peaking" R Cal V	"Peaking" R Cal CH	Comments	V/CM
1	41542 1A	3	A-3	22	100HZ	4,000	5988.0	Ø	Ø	17.0	1.497	14,814	2.81	4.21		.668
	FLEX FCAP 10.5				BP	"#/CM	"#/V			CM						
2	41532 #1	B	A-B	41		4,000	3,252.46	Ø	Ø	17.5	Ø.813	8,199	2.521	3.05		1.230
	BED CB 55.4					#/CM	"#/V			CM						
3	41546 1A	1	A-1	7		2,000	2,504.8	Ø	Ø	12.0	1.252	12,058	4.815	6.03		.799
	FLEX CB 11.0					#/CM	"#/V			CM						
4	41548 1B	19	B-7	45		2,000	2,420	0	0	12.0	1.210	11,724	4.845	5.86		.826
	FLEX CB 11.0					"#/CM	"#/V			CM						
5	41558 1A	4	A-4	23		1,000	1388.5	0	0	7.5	1.389	862	.621	.862		.720
	FLEX FCAP 45.0					"#/CM	"#/V			CM						
6	41522	7	A-7	34		200	213.2	0	0	7.5	1.066	853	4.001	4.265		.938
	TOR TUBE CB 38.1					#/CM				CM						
7	41520 #1	6	A-6	27		1,000	575	0	0	2.5	.515	2,848	4.953	2.745		1.739
	TOR TUBE FCAP 38.1					"#/CM				CM						
8	41548 #1	5	A-5	24	↓	100	600.125	0	0	2.5	8.002					0.125
	PITCH LINK					#/CM				CM						

Oscillitgraph Recorder
Visicorder

OGR CH	Measurement	HS CH	Item Index	HGD MPD	∅	HS. F Off Freq	Scale Eng/In	Input Load/V	Tare Offset Eng	Tare Offset V	Pos In	Scale In/V	R Cal Eng	R Cal V	R Cal IN	Range	V/In
1-1	Border	—	—	HGD	—	—	—	—	—	—	0.25	—	—	—	—	—	
1-2				↓													
1-3	62 Aft Hyd Tach	—	F-2	MPD	—	—	5V/2"	—	∅	∅	∅.4	.2"/5V	—	—	—	—	25.0
1-4	75 IRIG B Time Code	—	F-10	↓	—	—	5V/5"	—	∅	∅	0.9	.5"/5V	—	—	—	OFF	16.67
1-5	#1 Tach Link	5	A-5	MPD	HS	300Hz LP	300 Lb/In	800.185 Lb/V	∅	∅	0.9	1.0001					1.000
1-6	1520 #1 Tac Tube Flap 38.1	6	A-6				3,000	575.0	∅	∅	2.1	.192	2,878	4.95	.95		5.217
1-7	1522 Tac Tube Ch 38.1	7	A-7				1,000	213.2	∅	∅	3.0	.213	553	4.00	.85		4.690
1-8	1534 #1 BIU Flap 11.0	23	B 11			300Hz LP	10,000 Lb/In	1888.2	∅	∅	5.8	.189	3703	2.903	0.378		5.296
1-9	17 #2 Stn Sumsh	17	B 5			300Hz LP	3150 PSI/In	1974.0	∅	∅	5.7	.627	6,891	3.99	2.187		1.596
1-10	18 #3 Stn Sumsh	18	B 6			300Hz LP	3150 PSI/In	1974.0	∅	∅	5.5	.627	6,891	3.99	2.187		1.596
1-11	1542 1A Flex Flap 10.5	3	A-3			100 LP	20,000 Lb/In	5988.6	∅	∅	5.3	.299	19,852	3.312	.99		3.340
1-12	1544 1B Flex Flap 10.5	20	B 8				29,000	5,565.0	∅	∅	5.9	.278	18,491	3.319	.92	055	3.594
1-13	1546 1A Flex Ch 11.0	1	A-1			Bessel 5.1Hz	5,000	2,504.3	∅	∅	3.8	.50	12,058	4.82	2.42		2.000
1-14	1548 1B Flex Ch 11.0	19	B 7		↓	300Hz LP	10,000	2,420.0	∅	∅	6.7	.242	11,724	4.85	1.17		4.132
1-15	10 Vib Calib In	10	A-10		—	—	4 Lb/In		∅	∅	7.3		—	—	—		
1-16	63 MPR B Stg #2 Inc Rev	—	F-3	↓	—	—			∅	∅	7.8	.2"/5V	—	—	—	055	
1-17				HGD													
1-18				↓													

OGR 1 Test 8 MR Date 1-29-70 Page 17

2-24-70 2-25-70 2-27-70 2-28-70 Rev

Oscilligraph Recorder
Visicorder

OGR 2 Test BM2 Date 1-29-90

OGR Ch	Measurement	HS Ch	Item Index	HGD MFD	H.S. F Off Ø	H.S. F Off Freq	Scale Eng/In	Input Load/V	Tare Offset Eng	Tare Offset V	Pos In	Scale In/V	R Cal Eng	R Cal V	R Cal IN	Range	V/In
2-1				HGD													
2-2				V													
2-3	62 AZ PHOTO TACH 1 PER REV	—	F-2	MPD	LL	LL	5V/.2"	—	Ø	Ø	Ø.4		—	—	—		
2-4	15 I RIG B TIME CODE	—	F-10		LL	LL	5V/.3"		Ø	Ø	0.9		—	—	—	05 S	
2-5	4558 1A FLEX FEMP 45.0	4	A-4		HS	300 LP	5,000	1388.5	Ø	Ø	1.0	.278	2,771	2.000	0.56		3.601
2-6	4560 1B FLEX FEMP 45.0	21	B 9				5,000	1,491.5	Ø	Ø	1.6	.295	3,035	2.015	Ø.61		3.352
2-7	4554 1F FLEX CHORD 43.0	40	D 4				3,000	704.5	Ø	Ø	3.3	.235	2,295	3.158	Ø.765		4.255
2-8	4556 1B FLEX CH 43.0	41	D 5				3,000	694.0	Ø	Ø	2.9	.231	2,279	3.472	Ø.758	05 S	4.323
2-9	4530 #1 PED FEMP 55.4	22	B 10				10,000	2127.55	Ø	Ø	3.7	.213	6,343	2.572	0.53		4.700
2-10	4532 #1 PED CHORD 55.4	8	A 8				20,000	3,252.96	Ø	Ø	5.0	.163	8,199	2.521	Ø.410		6.149
2-11	4528 #1 PED TOE 65.0	32	C 8			300 HZ LP	2,000	629.66	Ø	Ø	5.0	.315	1,588	5.044	1.330		3.175
2-12	5004 #1 FLEX TOE 15.25	11	A 11			150 HZ LP	3,000	344.05	Ø	Ø	6.7	.115	693	2.014	Ø.231	05 S	8.728
2-13	5000 #1 FLEX CH 14.25	12	A 12				30,000	15,838.0	Ø	Ø	6.5	.395	19,761	1.669	Ø.659	05 S	2.531
2-14	5002 #1 FLEX FEMP 14.25	2	A2				30,000	15,272.0	Ø	Ø	6.8	.509	25,335	1.659	Ø.84		1.964
2-15	10 IDYN COUT IN	10	A-10				4V/1		Ø	Ø	7.3		—	—	—		
2-16	63 MPR B SYS 32 PER REV	—	F-3						Ø	Ø	7.8		—	—	—	05 S	
2-17				HGD													
2-18				V													

Page 1 of 1

Rev 2-21-90 2-12-90 2-11-90

Band Pass Filters
Peak Detector System

#	Measurement	MS CH	Item Index	Band Pass Filters Gain	Mode	Freq	Out	AC DC	Load @ Limit	Load @ 100% Alarm	Alarm %	%/V	P. Cal Eng	V	%	Eng/%	Book
1	1542 1A Flex Temp 10.5	3	A-3	1	BP	100Hz		AC	15,000	7,500	50	39.9	16,849	2.81	112.2	150	5985.0
2	1541 1B Flex Temp 10.5	20	B-8						15,000	7,500	50	37.1	15,458	2.778	103.06	150	5,565.0
3	1546 1A Flex CH 11.0	1	A-1						4,400	2,200	50	56.9	12058	4.815	321.03	44	2,504.0
4	1548 1B Flex CH 11.0	19	B-7						4,400	2,200	50	55.0	11721	1.845	266.46	44	2,420.0
5	#1 Pitch Link	5	A-5						460	230.	50	175.0				4.6	800.105
6	1550 1A Flex Temp 18.0	38	D-2	↓	↓	↓		↓	19,000	5,[illegible]	50	38.2	9930	2.591	99.3	100	3,820.0
7	1A FEB 11.0	1	A-1	1	BP	100Hz	1									→	cR03
8	1558 1A Flex Temp 15.0	4	A-4	1				Ac	2,580	1,290	50	53.8	862	.0621	33.91	25.8	1,338.5
9	1560 1B Flex Temp 15.0	21	B-9						2,580	1,290	50	57.8	1127	.756	43.68	25.8	1,491.5
10	1554 1A Flex CH 43.0	40	D-4						1,720	860	50	41.0	2,215.4	3.258	133.99	17.2	704.5
11	1556 1B Flex CH 43.0	41	D-5						1,720	860	50	40.3	2293.5	3.276	132.18	17.2	694.0
12	1520 #1 Top Turb Temp 28.1	6	A-6			↓			2,200	1,100	50	26.1	2018.1	1.95	129.46	22.0	575.0
13	1522 Top Turb Comp 28.1	7	A-7	↓	↓	100Hz		↓	440	220	50	48.5	853.03	9.001	193.87	4.4	213.2
14																	—
15	4572 #1 Top Turb Temp 36.1	25	C-1	1	BP	300Hz		AC	3,040	1,520	50	35.5	2749.1	2.517	81.44	30.4	1490.5
16	1530 #1 Bck Temp 55.1	22	B-10			100Hz			6,100	3,050	50	34.88	21783	1.024	35.71	61.0	2,127.55
17	1532 #1 Bck CH 55.4	8	A-8			300Hz			18,800	9,400	50	17.3	8199	2.521	45.1	188.0	3,252.00
18	1528 #1 Bck Tor 165.0	32	C-8			300Hz			1,760	880	50	17.9	1688	5.021	90.3	17.6	314.83
19	5502 #1 Flex Temp 14.25	2	A-2			100Hz			24,400	12,200	50	62.57	19572	1265	60.2	244.0	15,272.0
20	5500 #1 Flex CH 14.25	12	A-12			100Hz			25,120	13,560	50	47.8	19761	1.665	78.7	251.2	11,838.0
21	5504 #1 Flex Tor 15.25	11	A-11	↓	↓	300Hz		↓	3,040	1,520	50	11.3	693	2.014	22.8	30.4	[illegible]
22	4502 1A FEB 10.5	3	A3	1	BP	100Hz	1									→	cR01
23	4551 1A FEB	4	A4	1	BP	100Hz	1									→	cR05
24	4578 #1 PL	5	A5	1	BP	100Hz	1									→	cR08
25	4534 #1 Bck FB 110.0	33	B-11	1	BP	100Hz		AC	2,800	1,400	50	67.4	26095	1.382	93.2	28.0	1,888.2

BPF - PDS Test BMR Date 11-29-80 Page 19 Rev 2-7-1

Band Pass Filters
Peak Detector System

#	Measurement	HS CH	Item Index	Band Pass Filters Gain	Mode	Freq	Out	AC DC	Load @ Limit	Load @ Alarm	Alarm %	%/V	"Parking" R Cal Eng	V	%	Eng/%	Load/V
26	17 #2 Stn South 552	17	B-5	1	BP	300Hz		AC	1,460	730	50	135.2				14.6	1974.0
27	4520. Torque F	6	A6	1	BP	100Hz	1	—	limit 500.1								CR07
28	1542 1A Flex Flap 10.5	3	A-3	1	LP			DC	51,000	40,800	40	5.87	16,849	2.31	14.5	1,020	5988.6
29	1544 1B Flex Flap 10.5	20	B-8						51,000	40,800	40	5.46		2.78	15.2	1,020	5,565.0
30	1546 1A Flex Ch 11.0	1	A-1						12,800	10,240	40	9.78	13,051	4.82	47.2	256	2,504.0
31	1548 1B Flex Ch 11.0	19	B-7						12,800	10,240	40	9.45	11,329	4.75	45.9	256	2,420.0
32	#1 Pitch Govr	5	A-5						860	690	40	46.52		---		17.2	800.185
33	1550 1A Flap Trim 18.0	38	D-2	↓	↓	↓		↓	31,600	24,500	40	6.16	9,930	2.599	15.0	620	3,820.0
34	4549 1B F CB 11.0	7	A7	1	BP	100Hz	1	—								→	CR06
35	1558 1A Flex Flap 15.0	4	A-4	1	LP			DC	9,000	7,200	40	7.71	962	.621	4.9	180	1,388.5
36	1560 1B Flex Flap 15.0	21	B-9						9,000	7,200	40	8.29	1,125	.756	6.3	180	1,494.5
37	1554 1A Flex Ch 13.0	40	D-4						3,000	2,400	40	11.74	2295	3.258	38.3	60	704.5
38	1556 1B Flex Ch 13.0	41	D-5						3,000	2,400	40	11.57	2274	3.276	37.9	60	694.0
39	1520 #1 [illegible] 18.1	6	A-6						4700	3,800	40	6.05	2,546	4.95	39.0	95	575.0
40	1522 [illegible] 18.1	7	A-7	↓	↓	↓		↓	865	690	40	12.32	851	4.01	49.31	17.3	213.2
41	4532 #1 Bld CB	8	A8	1	BP	100Hz	1	—								→	CR02
42																	
43	1520 #1 Ld Trim 55.4	22	B-10	1	LP	100Hz		DC	15,000	12,000	40	7.09	2178	1.027	7.26	300	2,127.55
44	1532 #1 Bld Ch 55.4	8	A-8			300Hz			32,310	22,610	35	5.03	8,199	2.521	12.7	646	3,252.46
45	1528 #1 Bld Tor 65.0	32	C-8			300Hz			4,180	3,345	40	7.53	1,559	2.322	17.6	83.60	629.66
46	5502 #1 Flex Flap 11.25	2	A-2			100Hz			76,800	60,800	40	10.047	19,634	1.215	12.91	1520.9	15,272
47	5500 #1 Flex Ch 11.25	12	A-12	↓	↓	100Hz		↓	68,520	54,520	40	8.635	19,761	1.669	14.42	1,370.4	11,838.0
48	4546 #3 F CB	19	B7	1	BP	100Hz	1	—								→	CR04
49																	
50																	

BPF - PDS Test: B H L Date: 1-24-80 Page 20 Rev 4-25-80 2-22-80 2-7-80

Eng/V
Eng/%

DAS Setup | Test: BMK | Date 12/13/19 | Tape 21

(TO BE FILLED OUT BY ANALOG ENGINEER)

CH	DS	Measure	R Cal Engr	R Cal Volts	Load/V	
1	10	DAS Control Current				
2		Cos ψ (Dynamic Control)				
3		Sin ψ (Dynamic Control)				
4	12	FB Chord @ M.25 #1	19761.			
5	13	FB Chord @ M.5T #2	19481.			
6	14	FB Chord @ M.3T #3	19121.			
7	15	FB Chord @ 19.3T #4	17861.			
8	2	FB Flap @ M.7T #1	25335.			
9	16	FB Flap @ M.5T #2	24593.			
10	17	FB Flap @ 19.2T #3	25214.			
11	28	FB Flap @ 14.5T #4	23210.			
12	3	FB Flap @ 10.5A #1	19832.			
13	20	FB Flap @ 10.5B #2	13041.			
14	1	FB Chord @ 11.0A #1	12058.			
15	19	FB Chord @ 11.0B #2	11724.			
16	6	TT Flap @ 20.1	2848.1			
17	17	TT Chord @ 20.1	853.03			
18	25	TT Torsion @ 20.1	2719.1			
19	8	Blade Chord @ 15.0 #1	8199.3			
20	22	Blade Flap @ 15.0 #1	5345.3			
21	32	Blade Torsion @ 15.0 #1	1538.0			
22	9	Rotor Shaft Torque				
23	42	RTP Accel Nose Vert				
24	43	RTP Acc Trans Lat				
25	44	RTP Acc Tail Long				
26	45	RTP Acc LHS Long				
27	46	RTP Acc RHS Long				
28	47	RTP Acc Trans Lat				
29	48	RTP Acc Tail Vert				
30	M/SC	RTP Acc LHS/RHS Vert				Will determine which are recorded at beginning of test

DRS Set Up	Test BYR	Date 1-31-80	Page 22 Rev

Ch In	H.S.	Measure	Index
1-1	1	4546 1A FCB 11.0	A-1
1-2	2	5502 1 F FB 14.45	A 1
1-3	3	45462 1A FFP 10.5	A 2
1-4	4	4545 1A FF 8	A 3
1-5	5	4577 1 PHL	A 4
1-6	6	4520 1 TT FB	A 5
1-7	7	4520 1 TT CB	A 6
2-1	8	4539 1 BM CB	A 7
2-2	9	9 RST	A 8
2-3	10	10 DCI	A 9
2-4	11	5504 1 FTB	A 10
2-5	12	5500 1 FCB	A 11
2-6	13	5506 2 FCB	A 12
2-7	14	5512 3 FCB	B 1
3-1	15	5518 4 FCB	B 2
3-2	16	4502 #1 Std Rec	B 3
3-3	17	4505 #2 Std Rec	B 4
3-4	18	4507 #3 Std Rec	B 5
3-5	19	4548 1B FCB	B 6
3-6	20	4546 1B FFB	B 7
3-7	21	4540 1B F FB	B 8
4-1	22	4530 1BM FB	B 9
4-2	23	4534 1BM FB	B 10
4-3	24	4536 1 BM CB	B 11
4-4	25	4572 1 TTT	B 12
4-5	26	5507 2 F FB	C 1
4-6	27	5514 3 F FB	C 2
4-7	28	5520 4 F FB	C 3

Ch In	H.S.	Measure	Index
5-1	29	4524 #3 Std CR	C 4
5-2	30	5526 #4 Std CR	C 5
5-3	31	5528 #5 Std CR	C 6
5-4	32	4528 1 BM TB	C 7
5-5	33	5510 2 F TB	C 8
5-6	34	5516 3 F TB	C 9
5-7	35	5522 4 F TB	C 10
6-1	36	4538 1A FFB	C 11
6-2	37	4540 1B FFB	C 12
6-3	38	4550 1A FFB	D 1
6-4	39	4552 1B FFB	D 2
6-5	40	4554 1A FCB	D 3
6-6	41	4556 1B FCB	D 4
6-7	42	42 #1 Aud	D 5
7-1	43	43 #2	D 6
7-2	44	44 #3	D 7
7-3	45	45 #4	D 8
7-4	46	46 #5	D 9
7-5	47	47 #6	D 10
7-6	48	48 #7	D 11
7-7	49	49 #8	D 12
8-1	50	50 #9 V	E 1
8-2	51	4501 #11 Std Rec	E 2
8-3	52	4504 #5	E 3
8-4	53	4502 #L	E 4
8-5			
8-6			
8-7			

Track	Mode	VCO	Disc	Source
1	Dir	1		
2	"	2		
3	"	3		
4	"	4		
5	"	5		
6	"	6		
7	"	7		
8	"	8		
9	"			Sync
10	PCM			
11	"			
12	FM			NPR
13	"			AZ
14	Dir			TC

Tape Speed	15 IPS

Sync	Tach	Tape

BNC Locations | BNR | Date 11-24-80 | 23

#	Parameter	STEN Loc'n	From	To
1	Coming	A1	12P37 ST 09 U32/P11	BNC 1 available
2	Lone Dup	C2	ST 09 U33/P14	1 2
3	Lat Dup	C3	ST 01 U25/P5/6	3
4	Collective Pitch	A4	ST 02 U26/P7/8	4
5	Lateral Pitch	C5	ST 03 U27/P9/10	5
6	Long Patch	C6	ST 04 U28/P11/12	6
7	Sin Ψ	F6		
8	Cos Ψ	F7		
9				
10				
11				
12				
13				
14				
15				
16				
17				
18				
19	AZ	F	Patch Panel BNC 19	Acex Recorder
20	AZ	F	Patch Panel BNC 20	DAS
21	NPR 2 ω 1	F		
22	2 ω 2	F	Patch Panel BNC 22	DAS
23	2 ω 3	F	Patch Panel BNC 23	Acex Recorder
24				
25				
26				
27				
28				
29				
30				
31				
32				
33	T2/rev	F3	RTA Control Console	exp Patch - OGR
34	I.R.I.G. D	F10	Time Code Generator	CGR 1-4, 2-4
35	4546 IAFIm 23 11.0	A-1	output gdm HS 1	Boeing filter input
36	4546	A-1	Boeing filter output	CRO ch # 3

11.3 TABULATION OF BMR/RTA AEROELASTIC STABILITY TEST RESULTS

Table 11.1 is a compilation of aeroelastic stability data for the BMR/RTA. The table shows run numbers and corresponding test point number if trim data was taken of the test condition just prior to obtaining stability data. Test conditions, type of excitation, magnitude of excitation and the parameter used for determining stability data are shown. Stability data are shown in terms of rotating and fixed system damping and time to half amplitude. The test configuration is also indicated. Definitions of configuration, table headings, etc. are given at the end of Table 11.1.

TABLE 11.1 COMPILATION OF BHR/RTA AEROELASTIC STABILITY DATA
(SHEET 1 OF 33)

CONFIG ALPHA (DEG) OM*ZET (HZ) THALF (SEC)	RUN RPM ETA ROT (%)	TEST POINT THRUST (LB) ETA FIX (%)	V (KNOTS) TYPE EXCIT GAGE	THETA (DEG) MAG EX (DT) D CYCLIC	COMMENT
1.00	5.00	4.00	0.00	4.00	INITIAL HOVER DATA
-10.00	350.00	1430.00	1.00	500.00	
****	1.10	4.05	1.00	0.00	
2.19					
1.00	5.00	5.00	0.00	4.00	
-10.00	375.00	1550.00	1.00	500.00	
-100.00	1.20	3.55	1.00	0.00	
****					
1.00	5.00	6.00	0.00	4.00	
-10.00	400.00	1790.00	1.00	500.00	
****	1.30	3.23	1.00	0.00	
1.79					
1.00	5.00	8.00	0.00	4.00	
-10.00	425.00	1985.00	1.00	500.00	
****	1.00	2.15	1.00	0.00	
2.28					
1.00	5.00	9.00	0.00	4.00	
-10.00	415.00	1870.00	1.00	500.00	
****	0.80	1.82	1.00	0.00	
2.87					
1.00	5.00	11.00	0.00	4.00	
-10.00	436.00	2060.00	1.00	500.00	
****	1.30	2.64	1.00	0.00	
1.74					

TABLE 11.1 COMPILATION OF BMR/RTA AEROELASTIC STABILITY DATA (SHEET 2 OF 33)

CONFIG ALPHA (DEG) OM ZET (HZ) THALF (SEC)	RUN RPM ETA ROT (%)	TEST POINT THRUST (LB) ETA FIX (%)	V (KNOTS) TYPE EXCIT GAGE	THETA (DEG) MAG EX (CT) D CYCLIC	COMMENT
1.00 -10.00 4.63 1.72	6.00 350.00 1.40	2.00 1550.00 5.15	0.00 1.00 1.00	4.00 500.00 0.00	
1.00 -10.00 4.75 0.93	6.00 350.00 2.60	5.00 3275.00 9.19	0.00 1.00 1.00	6.00 500.00 0.00	
1.00 -10.00 4.50 0.92	6.00 350.00 2.60	6.00 2345.00 9.57	0.00 3.00 1.00	4.00 125.00 0.00	
1.00 -10.00 4.63 1.34	6.00 350.00 1.80	7.00 1605.00 6.63	0.00 3.00 1.00	4.00 125.00 0.00	
1.00 -10.00 4.63 2.65	6.00 349.00 0.90	9.00 850.00 3.49	0.00 3.00 1.00	2.00 125.00 0.00	
1.00 -10.00 4.63 2.06	6.00 349.00 1.16	9.00 850.00 4.50	0.00 1.00 1.00	2.00 500.00 0.00	

TABLE 11.1 COMPILATION OF BHR/RTA AEROELASTIC STABILITY DATA
(SHEET 3 OF 33)

CONFIG ALPHA (DEG) OM ZET (HZ) THALF (SEC)	RUN RPM ETA ROT (%)	TEST POINT THRUST (LB) ETA FIX (%)	V (KNOTS) TYPE EXCIT GAGE	THETA (DEG) MAG EX (CT) D CYCLIC	COMMENT
1.00 -10.00 4.75 2.95	6.00 350.00 0.80	10.00 315.00 3.20	0.00 3.00 1.00	0.00 125.00 0.00	
1.00 -10.00 4.63 4.73	6.00 350.00 0.50	10.00 315.00 2.00	0.00 1.00 1.00	0.00 500.00 0.00	
1.00 -10.00 4.50 0.84	7.00 375.00 2.87	3.00 3785.00 7.94	0.00 3.00 1.00	8.00 125.00 0.00	
1.00 -10.00 4.75 0.96	7.00 375.00 2.49	4.00 2745.00 7.12	0.00 3.00 1.00	6.00 125.00 0.00	
1.00 -10.00 4.75 1.02	7.00 375.00 2.34	4.00 2745.00 6.69	0.00 2.00 1.00	6.00 500.00 0.00	
1.00 -10.00 4.75 1.04	7.00 375.00 2.30	4.00 2745.00 6.57	0.00 2.00 1.00	8.00 500.00 0.00	

TABLE 11.1 COMPILATION OF BMR/RTA AEROELASTIC STABILITY DATA
(SHEET 4 OF 33)

CONFIG ALPHA (DEG) OM ZET (HZ) THALF (SEC)	RUN RPM ETA ROT (%)	TEST POINT THRUST (LB) ETA FIX (%)	V (KNOTS) TYPE EXCIT GAGE	THETA (DEG) MAG EX (CT) D CYCLIC	COMMENT
1.00 -10.00 4.75 1.30	7.00 375.00 1.82	2.00 1045.00 5.38	0.00 2.00 1.00	4.00 490.00 0.00	
1.00 -10.00 4.50 0.53	8.00 400.00 4.50	4.00 6217.00 10.11	0.00 2.00 1.00	11.00 300.00 0.00	
1.00 -10.00 4.63 0.55	8.00 400.00 4.30	3.00 5620.00 9.79	0.00 2.00 1.00	10.00 350.00 0.00	
1.00 -10.00 4.75 0.81	8.00 400.00 2.90	2.00 4425.00 6.80	0.00 2.00 1.00	8.00 175.00 0.00	
1.00 -10.00 4.75 1.02	8.00 400.00 2.30	5.00 3090.00 5.55	0.00 2.00 1.00	6.00 200.00 0.00	
1.00 -10.00 4.76 0.45	8.00 425.00 5.20	8.00 6306.00 10.35	0.00 2.00 1.00	10.00 250.00 0.00	

TABLE 11.1 COMPILATION OF BMR/RTA AEROELASTIC STABILITY DATA
(SHEET 5 OF 33)

CONFIG ALPHA (DEG) OM ZET (HZ) THALF (SEC)	RUN RPM ETA ROT (%)	TEST POINT THRUST (LB) ETA FIX (%)	V (KNOTS) TYPE EXCIT GAGE	THETA (DEG) MAG EX (CT) D CYCLIC	COMMENT
1.00 -10.00 4.75 0.72	8.00 425.00 3.20	9.00 4790.00 6.54	0.00 2.00 1.00	8.00 275.00 0.00	
1.00 -10.00 4.75 0.38	8.00 414.00 6.20	11.00 6901.00 12.89	0.00 2.00 1.00	11.00 250.00 0.00	
1.00 -10.00 **** 0.55	8.00 415.00 4.30	12.00 5780.00 9.01	0.00 2.00 1.00	10.00 200.00 0.00	
1.00 -10.00 4.75 0.90	8.00 415.00 2.60	13.00 4580.00 5.60	0.00 2.00 1.00	8.00 200.00 0.00	
1.00 -10.00 4.75 0.85	8.00 415.00 2.75	14.00 3995.00 6.00	0.00 2.00 1.00	7.00 150.00 0.00	
1.00 -10.00 **** 1.00	12.00 375.00 2.38	2.00 2775.00 6.79	0.00 2.00 1.00	0.10 300.00 0.00	NONZERO CYCLIC TRIM

TABLE 11.1 COMPILATION OF BMR/RTA AEROELASTIC STABILITY DATA
(SHEET 6 OF 33)

CONFIG ALPHA (DEG) OM ZET (HZ) THALF (SEC)	RUN RPM ETA ROT (%)	TEST POINT THRUST (LB) ETA FIX (%)	V (KNOTS) TYPE EXCIT GAGE	THETA (DEG) MAG EX (CT) D CYCLIC	COMMENT
1.00 -10.00 4.25 0.61	12.00 375.00 3.95	5.00 3700.00 10.90	0.00 2.00 1.00	8.10 300.00 0.00	
1.00 -10.00 **** 0.58	12.00 375.00 4.16	5.00 3700.00 11.50	0.00 2.00 2.00	8.00 300.00 0.00	
1.00 -10.00 4.75 1.61	12.00 375.00 1.47	6.00 1925.00 4.33	0.00 2.00 1.00	4.20 250.00 0.00	
1.00 -10.00 4.75 1.64	12.00 375.00 1.44	6.00 1925.00 4.24	0.00 2.00 2.00	4.20 250.00 0.00	
1.00 -10.00 4.63 0.51	12.00 405.00 4.67	8.00 5755.00 10.29	0.00 2.00 1.00	10.30 250.00 0.00	
1.00 -10.00 4.68 0.55	12.00 406.00 4.26	9.00 4415.00 9.60	0.00 2.00 1.00	8.30 350.00 0.00	

TABLE 11.1 COMPILATION OF BMR/RTA AEROELASTIC STABILITY DATA
(SHEET 7 OF 33)

CONFIG ALPHA (DEG) OM ZET (HZ) THALF (SEC)	RUN RPM ETA ROT (%)	TEST POINT THRUST (LB) ETA FIX (%)	V (KNOTS) TYPE EXCIT GAGE	THETA (DEG) MAG EX (CT) D CYCLIC	COMMENTS
1.00 -10.00 4.75 1.16	12.00 404.00 2.02	10.00 3200.00 4.74	0.00 2.00 1.00	6.30 300.00 0.00	
1.00 -10.00 4.75 1.62	12.00 405.00 1.43	**** **** 3.44	0.00 2.00 1.00	4.00 300.00 0.00	
1.00 -10.00 **** 0.42	12.00 425.00 5.62	11.00 6290.00 11.19	0.00 2.00 1.00	10.00 200.00 0.00	
1.00 -10.00 **** 0.36	12.00 424.00 6.50	12.00 4775.00 13.31	0.00 2.00 1.00	8.20 250.00 0.00	*
1.00 -10.00 **** 0.78	12.00 424.00 2.96	12.00 4775.00 6.06	0.00 2.00 1.00	8.20 250.00 0.00	
1.00 -10.00 4.80 1.33	12.00 425.00 1.88	13.00 3615.00 3.92	0.00 2.00 1.00	8.30 250.00 0.00	

TABLE 11.1 COMPILATION OF BMR/RTA AEROELASTIC STABILITY DATA
(SHEET 8 OF 33)

CONFIG ALPHA (DEG) OM ZET (HZ) THALF (SEC)	RUN RPM ETA ROT (%)	TEST POINT THRUST (LB) ETA FIX (%)	V (KNOTS) TYPE EXCIT GAGE	THETA (DEG) MAG EX (CT) D CYCLIC	COMMENT
1.00 -10.00 **** 0.52	12.00 410.00 4.53	14.00 5605.00 9.74	0.00 2.00 1.00	10.10 325.00 0.00	
1.00 -10.00 **** 0.64	12.00 410.00 3.64	15.00 4520.00 8.02	0.00 2.00 1.00	8.30 400.00 0.00	
1.00 -10.00 **** 1.09	12.00 410.00 2.13	16.00 3380.00 4.82	0.00 2.00 1.00	6.30 350.00 0.00	
1.00 -10.00 4.75 1.57	12.00 410.00 1.47	17.00 2180.00 3.42	0.00 2.00 1.00	4.30 300.00 0.00	
1.00 -10.00 **** 1.33	13.00 400.00 1.76	2.00 2966.00 4.21	0.00 3.00 1.00	6.50 175.00 0.00	
1.00 -10.00 ****, 1.50	13.00 399.60 1.55	3.00 2056.00 3.84	0.00 3.00 1.00	4.60 150.00 0.00	

TABLE 11.1 COMPILATION OF BMR/RTA AEROELASTIC STABILITY DATA
(SHEET 9 OF 33)

CONFIG ALPHA (DEG) OM ZET (HZ) THALF (SEC)	RUN RPM ETA ROT (%)	TEST POINT THRUST (LB) ETA FIX (%)	V (KNOTS) TYPE EXCIT GAGE	THETA (DEG) MAG EX (CT) D CYCLIC	COMMENT
1.00 -10.00 **** 1.11	13.00 416.00 2.09	4.00 3230.00 4.57	0.00 3.00 1.00	6.40 150.00 0.00	
1.00 -10.00 4.88 1.50	13.00 415.00 1.54	5.00 2161.00 3.47	0.00 3.00 1.00	4.60 150.00 0.00	
1.00 -10.00 **** 0.65	13.00 420.00 3.60	6.00 6046.00 7.30	0.00 3.00 1.00	10.50 125.00 0.00	
1.00 -10.00 **** 0.71	13.00 420.00 3.27	7.00 4601.00 6.82	0.00 3.00 1.00	8.40 150.00 0.00	
1.00 -10.00 **** 1.04	13.00 421.00 2.22	8.00 5755.00 4.72	0.00 3.00 1.00	6.50 150.00 0.00	
1.00 -10.00 **** 1.62	13.00 420.00 1.41	-100.00 -100.00 3.12	0.00 3.00 1.00	4.00 150.00 0.00	

TABLE 11.1 COMPILATION OF BMR/RTA AEROELASTIC STABILITY DATA
(SHEET 10 OF 33)

CONFIG ALPHA (DEG) OM ZET (HZ) THALF (SEC)	RUN RPM ETA ROT (%)	TEST POINT THRUST (LB) ETA FIX (%)	V (KNOTS) TYPE EXCIT GAGE	THETA (DEG) MAG EX (CT) D CYCLIC	COMMENT
1.00	13.00	9.00	0.00	4.50	
-10.00	425.00	2261.00	3.00	125.00	
4.88	1.42	3.03	1.00	0.00	
1.61					
1.00	13.00	10.00	0.00	10.30	
-10.00	400.00	5231.00	3.00	150.00	
****	6.25	14.17	1.00	0.00	
0.38					
1.00	13.00	11.00	0.00	8.40	
-10.00	399.00	4260.00	3.00	150.00	
4.63	3.94	9.24	1.00	0.00	
0.60					
1.00	14.00	6.00	90.00	8.80	
-6.00	424.00	6474.00	3.00	125.00	
****	3.67	7.46	1.00	0.00	
0.63					
1.00	14.00	7.00	89.70	7.90	
-6.00	426.00	5895.00	3.00	150.00	
4.75	3.37	6.86	1.00	0.00	
0.69					
1.00	14.00	8.00	89.80	5.90	
-6.00	424.00	4360.00	3.00	150.00	
****	2.26	4.77	1.00	0.00	
1.02					

TABLE 11.1 COMPILATION OF BMR/RTA AEROELASTIC STABILITY DATA
(SHEET 11 OF 33)

CONFIG ALPHA (DEG) OM ZET (HZ) THALF (SEC)	RUN RPM ETA ROT (%)	TEST POINT THRUST (LB) ETA FIX (%)	V (KNOTS) TYPE EXCIT GAGE	THETA (DEG) MAG EX (CT) D CYCLIC	COMMENT
1.00 -6.00 **** 1.72	14.00 424.00 1.33	9.00 2970.00 2.88	90.00 3.00 1.00	4.00 150.00 0.00	
1.00 -6.00 **** 2.16	14.00 424.00 1.05	10.00 2095.00 2.30	90.00 3.00 1.00	2.90 125.00 0.00	
1.00 -8.00 **** 1.05	14.00 424.00 2.19	11.00 3942.00 4.61	90.10 3.00 1.00	6.10 125.00 0.00	
1.00 -8.00 4.88 1.92	14.00 425.00 1.19	12.00 2392.00 2.56	89.50 3.00 1.00	4.00 125.00 0.00	
1.00 -8.00 **** 0.62	15.00 426.00 3.73	2.00 6228.00 7.48	90.30 2.00 1.00	9.10 250.00 0.00	
1.00 -8.00 **** 0.78	15.00 425.00 2.97	3.00 5468.00 6.06	90.20 2.00 1.00	8.10 250.00 0.00	

TABLE 11.1 COMPILATION OF BHR/RTA AEROELASTIC STABILITY DATA
(SHEET 12 OF 33)

CONFIG ALPHA (DEG) OM ZET (HZ) THALF (SEC)	RUN PCT ETA ROT (%)	TEST POINT THRUST (LB) ETA FIX (%)	V (KNOTS) TYPE EXCIT GAGE	THETA (DEG) MAG EX (CT) D CYCLIC	COMMENT
1.00	15.00	4.00	89.90	3.20	
-8.00	425.00	1773.00	2.00	200.00	
****	0.82	1.78	1.00	0.00	
2.77					
1.00	15.00	6.00	59.80	8.00	
-6.00	435.00	6296.00	2.00	150.00	
****	3.80	7.76	1.00	0.00	
0.61					
1.00	15.00	8.00	59.80	6.10	
-6.00	425.00	4846.00	2.00	250.00	
****	2.24	4.69	1.00	0.00	
1.03					
1.00	15.00	9.00	59.70	4.10	
-6.00	425.00	3386.00	2.00	300.00	
****	1.31	2.81	1.00	0.00	
1.74					
1.00	15.00	10.00	59.80	3.10	
-6.00	435.00	2616.00	2.00	325.00	
****	0.94	2.05	1.00	0.00	
2.42					
1.00	15.00	11.00	59.50	9.10	
-8.00	425.00	6752.00	2.00	150.00	
****	4.07	8.20	1.00	0.00	
0.57					

TABLE 11.1 COMPILATION OF BMR/RTA AEROELASTIC STABILITY DATA
(SHEET 13 OF 33)

CONFIG ALPHA (DEG) OM ZET (HZ) THALF (SEC)	RUN RPM ETA ROT (%)	TEST POINT THRUST (LB) ETA FIX (%)	V (KNOTS) TYPE EXCIT GAGE	THETA (DEG) MAG EX (CT) D CYCLIC	COMMENT
1.00 -8.00 **** 0.73	15.00 425.00 3.20	12.00 5988.00 6.53	59.80 2.00 1.00	8.10 150.00 0.00	
1.00 -8.00 **** 1.15	15.00 425.00 2.01	13.00 4508.00 4.20	59.70 2.00 1.00	6.20 350.00 0.00	
1.00 -8.00 **** 1.87	15.00 426.00 1.22	14.00 3003.00 2.61	59.70 2.00 1.00	4.10 300.00 0.00	
1.00 -8.00 -100.00 2.64	15.00 425.00 0.86	15.00 2268.00 1.87	60.10 2.00 1.00	3.10 225.00 0.00	
1.00 -6.00 **** 1.05	16.00 425.00 2.21	4.00 4822.00 4.50	120.00 2.00 1.00	8.20 150.00 0.00	
1.00 -6.00 **** 1.62	16.00 425.00 1.42	5.00 3502.00 2.97	120.00 2.00 1.00	6.20 175.00 0.00	

TABLE 11.1 COMPILATION OF BHP/RTA AEROELASTIC STABILITY DATA
(SHEET 14 OF 33)

CONFIG ALPHA (DEG) OM ZET (HZ) THALF (SEC)	RUN PPH ETA POT (%)	TEST POINT THRUST (LB) ETA FIX (%)	V (KNOTS) TYPE EXCIT GAGE	THETA (DEG) MAG EX (CT) D CYCLIC	COMMENT
1.00 -6.00 **** 2.54	16.00 425.00 0.90	6.00 1958.00 1.93	119.70 2.00 1.00	4.20 150.00 0.00	
1.00 -8.00 **** 0.98	16.00 425.00 2.38	7.00 4226.00 4.84	120.00 2.00 1.00	8.30 175.00 0.00	
1.00 -8.00 **** 1.86	16.00 425.00 1.24	8.00 2826.00 2.59	119.70 2.00 1.00	6.20 175.00 0.00	
1.00 -8.00 **** 2.03	16.00 424.00 1.13	9.00 2161.00 2.41	119.60 2.00 1.00	5.20 150.00 0.00	
1.00 -10.00 4.75 1.05	17.00 425.00 2.20	2.00 3272.00 1.49	127.20 2.00 1.00	8.10 200.00 0.00	
1.00 -10.00 4.75 1.02	17.00 425.00 2.29	**** **** 4.62	143.00 2.00 1.00	9.00 200.00 0.00	

TABLE 11.1 COMPILATION OF BHR/RTA AEROELASTIC STABILITY DATA
(SHEET 15 OF 33)

CONFIG ALPHA (DEG) OM ZET (HZ) THALF (SEC)	RUN RPM ETA ROT (%)	TEST POINT THRUST (LB) ETA FIX (%)	V (KNOTS) TYPE EXCIT GAGE	THETA (DEG) MAG EX (CT) D CYCLIC	COMMENT
1.00 -10.00 4.75 1.13	17.00 425.00 2.05	4.00 2420.00 4.18	143.40 2.00 1.00	8.10 175.00 0.00	
1.00 -10.00 4.88 1.51	17.00 424.00 1.53	5.00 1947.00 3.18	143.30 2.00 1.00	7.10 150.00 0.00	
1.00 -10.00 4.75 0.94	17.00 425.00 2.48	6.00 3829.00 4.94	144.10 2.00 1.00	10.00 150.00 0.00	
1.00 -12.00 4.75 0.56	18.00 425.00 2.45	8.00 3720.00 4.80	143.60 3.00 1.00	11.30 100.00 0.00	
1.00 -12.00 4.75 0.88	18.00 425.00 2.06	4.00 3071.00 5.28	143.40 3.00 1.00	10.30 100.00 0.00	
1.00 -12.00 4.75 1.16	18.00 424.00 2.01	3.00 2445.00 4.06	143.20 3.00 1.00	9.30 100.00 0.00	

TABLE 11.1 COMPILATION OF BMR/RTA AEROELASTIC STABILITY DATA
(SHEET 16 OF 33)

CONFIG ALPHA (DEG) OM ZET (HZ) THALF (SEC)	RUN RPM ETH ROT (%)	TEST POINT THRUST (LB) ETA FIX (%)	V (KNOTS) TYPE EXCIT GAGE	THETA (DEG) MAG EX (CT) D CYCLIC	COMMENT
1.00 -6.00 4.38 0.72	19.00 335.00 3.47	18.00 3644.00 13.41	89.80 3.00 1.00	9.10 150.00 0.00	
1.00 -6.00 4.50 0.84	19.00 335.00 2.94	14.00 3144.00 11.67	90.10 3.00 1.00	7.90 200.00 0.00	
1.00 -6.00 4.50 1.07	19.00 335.00 2.29	19.00 2324.00 9.49	89.80 3.00 1.00	6.00 200.00 0.00	
1.00 -6.00 4.63 1.90	19.00 335.00 1.28	20.00 1479.00 5.55	90.00 3.00 1.00	4.00 125.00 0.00	
1.00 -6.00 4.63 2.71	19.00 335.00 0.89	21.00 615.00 4.05	89.70 3.00 1.00	2.00 100.00 0.00	
1.00 -8.00 4.50 0.88	19.00 335.00 2.82	13.00 2788.00 11.17	90.00 3.00 1.00	8.00 100.00 0.00	

TABLE 11.1 COMPILATION OF BMR/RTA AEROELASTIC STABILITY DATA
(SHEET 17 OF 33)

CONFIG ALPHA (DEG) ON SET (HZ) THALF (SEC)	RUN RPM ETA POT (%)	TEST POINT THRUST (LB) ETA FIX (%)	-V (KNOTS) TYPE EXCIT GAGE	THETA (DEG) MAG EX (CT) D CYCLIC	COMMENT
1.00 -8.00 4.63 1.30	19.00 335.00 1.09	22.00 1943.00 7.83	90.30 3.00 1.00	6.00 125.00 0.00	
1.00 -8.00 4.63 1.98	19.00 335.00 1.23	23.00 1162.00 5.34	89.90 3.00 1.00	4.00 100.00 0.00	
1.00 -8.00 4.63 3.39	19.00 335.00 0.71	24.00 125.00 3.23	89.60 3.00 1.00	2.00 100.00 0.00	
1.00 -6.00 4.63 0.52	20.00 400.00 4.57	3.00 6075.00 10.39	89.80 3.00 1.00	10.10 125.00 0.00	
1.00 -6.00 4.63 0.72	20.00 400.00 3.38	4.00 4830.00 7.69	89.80 3.00 1.00	8.00 125.00 0.00	
1.00 -6.00 4.75 1.24	20.00 400.00 1.88	5.00 3530.00 4.53	89.70 3.00 1.00	6.00 125.00 0.00	

TABLE 11.1 COMPILATION OF BMR/RTA AEROELASTIC STABILITY DATA
(SHEET 18 OF 33)

CONFIG ALPHA (DEG) OM ZET (HZ) THALF (SEC)	RUN MPH ETH POT (%)	TEST POINT THRUST (LB) ETH FIX (%)	V (KNOTS) TYPE EXCIT GAGE	THETH (DEG) MAG EX (IN) D CYCLE	COMMENT
1.00 -6.00 4.75 2.00	20.00 400.00 1.16	6.00 2256.00 2.88	89.30 3.00 1.00	4.00 125.00 0.00	
1.00 -6.00 4.75 2.74	20.00 399.00 0.84	7.00 860.00 2.16	89.90 3.00 1.00	2.00 125.00 0.00	
1.00 -8.00 4.63 0.68	20.00 400.00 3.52	8.00 5608.00 8.81	90.70 3.00 1.00	10.16 125.00 0.00	
1.00 -8.00 4.75 0.91	20.00 400.00 2.58	9.00 4347.00 6.85	89.89 3.00 1.00	8.00 125.00 0.00	
1.00 -8.00 4.75 1.44	20.00 400.00 1.62	10.00 3007.00 3.91	90.00 3.00 1.00	6.00 125.00 0.00	
1.00 -8.00 4.79 2.19	20.00 400.00 1.08	11.00 1727.00 2.88	89.90 3.00 1.00	4.00 125.00 0.00	

TABLE 11.1 COMPILATION OF BHR/RTA AEROELASTIC STABILITY DATA
(SHEET 19 OF 33)

CONFIG ALPHA (DEG) OM ZET (HZ) THALF (SEC)	RUN RPM ETA ROT (%)	TEST POINT THRUST (LB) ETA FIX (%)	V (KNOTS) TYPE EXCIT GAGE	THETA (DEG) MAG EX (CT) D CYCLIC	COMMENT
1.00 -8.00 4.75 3.11	20.00 399.00 0.74	12.00 347.00 1.90	90.00 3.00 1.00	2.00 125.00 0.00	
1.00 -10.00 4.63 0.51	21.00 437.00 4.55	19.00 3086.00 8.56	0.00 3.00 1.00	10.00 125.00 0.00	
1.00 -10.00 4.75 0.64	21.00 438.00 3.61	20.00 4976.00 6.92	0.00 3.00 1.00	8.00 125.00 0.00	
1.00 -10.00 4.63 1.09	21.00 375.00 2.18	21.00 2616.00 6.23	0.00 2.00 1.00	6.00 250.00 1.00	CYCLIC TRIM VAR.
1.00 -10.00 4.63 0.86	21.00 376.00 2.77	22.00 2570.00 7.86	0.00 2.00 1.00	6.00 250.00 2.00	
1.00 -10.00 4.63 1.08	21.00 375.00 2.20	22.00 2510.00 6.20	0.00 2.00 1.00	6.10 250.00 3.00	

TABLE 11.1 COMPILATION OF BHR/RTA AEROELASTIC STABILITY DATA
(SHEET 20 OF 33)

CONFIG ALPHA (DEG) OM ZET (HZ) THALF (SEC)	RUN RPM ETA ROT (%)	TEST POINT THRUST (LB) ETA FIX (%)	V (KNOTS) TYPE EXCIT GAGE	THETA (DEG) MAG EX (%) D CYCLE	COMMENTS
1.00 -10.00 4.63 1.24	21.00 375.00 1.92	24.00 2525.00 5.49	0.00 2.00 1.00	6.00 250.00 4.00	CYCLIC TRIM VAR.
1.00 -10.00 4.75 1.05	21.00 375.00 2.27	**** **** 6.49	0.00 2.00 1.00	6.00 50.00 0.00	EXCIT. AMPLITUDE VAR.
1.00 -10.00 4.75 1.19	21.00 375.00 2.01	**** **** 5.74	0.00 2.00 1.00	6.00 100.00 0.00	
1.00 -10.00 4.63 1.20	21.00 375.00 1.99	**** **** 5.69	0.00 2.00 1.00	6.00 200.00 0.00	
1.00 -10.00 4.63 1.11	21.00 375.00 2.15	**** **** 6.14	0.00 2.00 1.00	6.00 400.00 0.00	
2.00 -10.00 4.50 0.57	22.00 375.00 4.25	2.00 3436.00 11.75	0.00 2.00 1.00	8.00 200.00 0.00	

TABLE 11.1 COMPILATION OF BMR/RTA AEROELASTIC STABILITY DATA
(SHEET 21 OF 33)

CONFIG ALPHA (DEG) ON ZET (HZ) THALF (SEC)	RUN RPM ETA ROT (%)	TEST POINT THRUST (LB) ETA FIX (%)	V (KNOTS) TYPE EXCIT GAGE	THETA (DEG) MAG EX (CT) D CYCLIC	COMMENT
2.00 -10.00 4.75 0.95	22.00 400.00 2.48	5.00 3825.00 5.81	0.00 2.00 1.00	8.00 300.00 0.00	
2.00 -10.00 4.75 0.70	22.00 410.00 3.35	3.00 4115.00 7.41	0.00 2.00 1.00	00 2[illegible].00 0.00	
2.00 -10.00 4.75 0.71	22.00 425.00 3.29	4.00 [illegible]80.00 6.72	0.00 2.00 1.00	8.00 225.00 0.00	
2.00 -10.00 4.63 0.99	22.00 375.00 2.41	6.00 2[illegible]0.00 6.89	0.00 2.00 1.00	6.00 400.00 0.00	
2.00 -10.00 4.75 1.05	22.00 400.00 2.22	7.00 2675.00 5.35	0.00 2.00 1.00	6.00 200.00 0.00	
2.00 -10.00 4.75 1.29	22.00 410.00 1.80	8.00 2795.00 4.09	0.00 2.00 1.00	5.00 250.00 0.00	

TABLE 11.1 COMPILATION OF BMR/RTA AEROELASTIC STABILITY DATA
(SHEET 22 OF 33)

CONFIG ALPHA (DEG) OM ZET (HZ) THALF (SEC)	RUN RPM ETA ROT (%)	TEST POINT THRUST (LB) ETA FIX (%)	V (KNOTS) TYPE EXCIT CAGE	THETA (DEG) MAG EX (CT) D CYCLIC	COMMENT
2.00 -10.00 4.88 1.28	22.00 424.00 1.00	9.00 2975.00 3.79	0.00 2.00 1.00	6.00 250.00 0.00	
2.00 -10.00 4.63 0.86	22.00 390.00 2.77	10.00 3585.00 6.90	0.00 2.00 1.00	8.10 250.00 0.00	
2.00 -10.00 4.75 0.79	22.00 400.00 2.97	11.00 3816.00 6.96	0.00 2.00 1.00	8.00 350.00 0.00	
2.00 -10.00 4.75 0.86	22.00 405.00 2.73	12.00 3905.00 6.21	0.00 2.00 1.00	0.00 350.00 0.00	
2.00 -10.00 4.63 0.82	22.00 395.00 2.09	13.00 3745.00 6.98	0.00 2.00 1.00	8.00 300.00 0.00	
2.00 -10.00 4.75 1.79	22.00 374.00 1.32	14.00 1540.00 3.93	0.00 2.00 1.00	4.00 300.00 0.00	

TABLE 11.1 COMPILATION OF BHR/RTA AEROELASTIC STABILITY DATA
(SHEET 23 OF 33)

CONFIG ALPHA (DEG) OM ZET (HZ) THALF (SEC)	RUN RPM ETA ROT (%)	TEST POINT THRUST (LB) ETA FIX (%)	V (KNOTS) TYPE EXCIT GAGE	THETA (DEG) MAG EX (CT) D CYCLIC	COMMENT
2.00	22.00	15.00	0.00	4.00	
-10.00	400.00	1675.00	2.00	275.00	
4.75	1.32	3.20	1.00	0.00	
1.76					
2.00	22.00	16.00	0.00	4.00	
-10.00	409.00	1695.00	2.00	300.00	
4.88	1.19	2.80	1.00	0.00	
1.94					
2.00	22.00	17.00	0.00	4.00	
-10.00	425.00	1845.00	2.00	250.00	
4.80	1.06	2.28	1.00	0.00	
2.15					
2.00	23.00	2.00	90.10	4.00	
-8.00	334.00	1268.00	3.00	125.00	
4.63	1.36	5.97	1.00	0.00	
1.79					
2.00	23.00	3.00	90.10	3.90	
-8.00	374.00	1633.00	3.00	125.00	
4.75	1.08	3.32	1.00	0.00	
2.19					
2.00	23.00	4.00	90.30	3.90	
-8.00	400.00	1803.00	3.00	125.00	
4.75	1.31	3.01	1.00	0.00	
1.92					

TABLE 11.1 COMPILATION OF BMR/RTA AEROELASTIC STABILITY DATA
(SHEET 24 OF 33)

CONFIG ALPHA (DEG) ON ZET (HZ) THALF (SEC)	RUN RPM ETA ROT (%)	TEST POINT THRUST (LB) ETA FIX (%)	V (KNOTS) TYPE EXCIT GAGE	THETA (DEG) MAG EX (CT) D CYCLIC	COMMENT
2.00 -8.00 4.75 1.91	23.00 409.00 1.21	5.00 1983.00 2.85	90.30 3.00 1.00	3.90 125.00 0.00	
2.00 -8.00 4.80 1.92	23.00 425.00 1.19	6.00 2183.00 2.56	90.00 3.00 1.00	4.00 125.00 0.00	
2.00 -4.00 4.88 2.33	23.00 425.00 0.97	7.00 1741.00 2.14	90.10 3.00 1.00	2.00 125.00 0.00	
2.00 -4.00 4.88 1.70	23.00 425.00 1.34	8.00 3291.00 2.98	90.20 3.00 1.00	4.00 125.00 0.00	
2.00 -4.00 4.75 1.12	23.00 424.00 2.06	9.00 4856.00 4.34	90.30 3.00 1.00	6.00 125.00 0.00	
2.00 -4.00 4.75 0.70	23.00 425.00 3.32	10.00 6260.00 6.78	90.50 3.00 1.00	8.00 125.00 0.00	

TABLE 11.1 COMPILATION OF BHR/RTA AEROELASTIC STABILITY DATA
(SHEET 25 OF 33)

CONFIG ALPHA (DEG) OM ZET (HZ) THALF (SEC)	RUN PPM ETA ROT (%)	TEST POINT THRUST (LB) ETA FIX (%)	V (KNOTS) TYPE EXCIT GAGE	THETA (DEG) MAG EX (CI) D CYCLIC	COMMENT
3.00	26.00	2.00	0.00	8.00	
-10.00	375.00	3195.00	3.00	125.00	
4.63	2.39	6.61	1.00	0.00	
1.01					
3.00	26.00	3.00	0.00	5.90	
-10.00	375.00	2215.00	3.00	125.00	
4.63	1.92	5.50	1.00	0.00	
1.24					
3.00	26.00	4.00	0.00	3.90	
-10.00	375.00	1350.00	3.00	125.00	
4.75	1.08	3.20	1.00	0.00	
2.19					
3.00	26.00	5.00	0.00	3.10	
-10.00	373.00	1030.00	3.00	125.00	
-100.00	0.92	2.76	1.00	0.00	
2.56					
3.00	26.00	6.00	0.00	8.10	
-10.00	400.00	3681.00	3.00	125.00	
4.75	2.50	5.85	1.00	0.00	
0.94					
3.00	26.00	7.00	0.00	6.10	
-10.00	399.00	2501.00	3.00	125.00	
4.75	1.56	3.78	1.00	0.00	
1.50					

TABLE 11.1 COMPILATION OF BNR/RTA AEROELASTIC STABILITY DATA
(SHEET 26 OF 33)

CONFIG ALPHA (DEG) OM ZET (HZ) THALF (SEC)	RUN RPM ETA ROT (%)	TEST POINT THRUST (LB) ETA FIX (%)	V (KNOTS) TYPE EXCIT GAGE	THETA (DEG) MAG EX (CT) D CYCLIC	COMMENT
3.00 -10.00 4.75 2.15	26.00 400.00 1.08	8.00 1555.00 2.68	0.00 3.00 1.00	4.10 125.00 0.00	
3.00 -10.00 -100.00 2.60	26.00 400.00 0.39	9.00 1071.00 3.24	0.00 3.00 1.00	3.00 125.00 0.00	
3.00 -10.00 4.75 0.80	26.00 425.00 2.69	10.00 4035.00 5.90	0.00 3.00 1.00	8.00 125.00 0.00	
3.00 -10.00 4.75 1.36	26.00 424.00 1.69	11.00 2741.00 3.56	0.00 3.00 1.00	6.00 125.00 0.00	
3.00 -10.00 4.89 1.95	26.00 425.00 1.17	12.00 1725.00 2.52	0.00 3.00 1.00	4.00 125.00 0.00	
3.00 -10.00 4.89 1.84	26.00 425.00 1.24	12.00 1725.00 2.67	0.00 2.00 1.00	4.00 50.00 0.00	

TABLE 11.1 COMPILATION OF BHR/RTA AEROELASTIC STABILITY DATA
(SHEET 27 OF 33)

CONFIG ALPHA (DEG) OM ZET (HZ) THALF (SEC)	RUN RPM ETA ROT (%)	TEST POINT THRUST (LB) ETA FIX (%)	V (KNOTS) TYPE EXCIT. GAGE	THETA (DEG) MAG EX (CT) D CYCLIC	COMMENT
3.00 -10.00 4.88 2.30	26.00 425.00 0.99	12.00 1725.00 2.13	0.00 2.00 1.00	4.00 100.00 0.00	EXCIT. AMPLITUDE VAR.
3.00 -10.00 4.88 2.00	26.00 425.00 1.14	12.00 1725.00 2.45	0.00 2.00 1.00	4.00 200.00 0.00	
3.00 -10.00 4.88 1.90	26.00 425.00 1.15	12.00 1725.00 2.47	0.00 2.00 1.00	4.00 300.00 0.00	
3.00 -10.00 4.88 1.92	26.00 425.00 1.19	12.00 1725.00 2.56	0.00 2.00 1.00	4.00 400.00 0.00	
3.00 -10.00 4.88 2.00	26.00 425.00 1.14	12.00 1725.00 2.45	0.00 2.00 1.00	4.00 500.00 0.00	
3.00 -8.00 4.63 1.80	27.00 335.00 1.35	3.00 802.00 5.86	89.90 3.00 1.00	4.00 125.00 0.00	

TABLE 11.1 COMPILATION OF BHR/RTA AEROELASTIC STABILITY DATA
(SHEET 28 OF 33)

CONFIG ALPHA (DEG) OH ZET (HZ) THALF (SEC)	RUN RPM ETA POT (%)	TEST POINT THRUST (LB) ETA FIX (%)	V (KNOTS) TYPE EXCIT GAGE	THETA (DEG) MAG EX (CT) D CYCLIC	COMMENT
3.00 -8.00 4.75 2.36	27.00 375.00 1.00	4.00 1152.00 2.96	90.00 3.00 1.00	4.00 125.00 0.00	
3.00 -8.00 4.75 2.23	27.00 400.00 1.04	5.00 1370.00 2.58	90.10 3.00 1.00	4.00 125.00 0.00	
3.00 -8.00 4.88 2.48	27.00 410.00 0.93	6.00 1522.00 2.17	90.00 3.00 1.00	4.00 125.00 0.00	
3.00 -8.00 4.88 1.83	27.00 425.00 1.25	7.00 1652.00 2.69	89.80 3.00 1.00	4.10 125.00 0.00	
3.00 -4.00 4.75 0.93	27.00 426.00 2.49	10.00 5663.00 5.05	90.30 3.00 1.00	8.10 125.00 0.00	
3.00 -4.00 4.75 1.31	27.00 425.00 1.75	11.00 4055.00 3.67	89.70 3.00 1.00	6.00 125.00 0.00	

TABLE 11.1 COMPILATION OF BHR/RTA AEROELASTIC STABILITY DATA
(SHEET 29 OF 33)

CONFIG ALPHA (DEG) OM ZET (HZ) THALF (SEC)	RUN ETA ROT (%)	TEST POINT THRUST (LB) ETA FIX (%)	V (KNOTS) TYPE EXCIT GAGE	THETA (DEG) MAG EX (CT) D CYCLIC	COMMENT
3.00 -4.00 4.88 2.07	27.00 425.00 1.10	9.00 2704.00 2.36	90.00 3.00 1.00	4.10 125.00 0.00	
4.00 -10.00 5.00 1.42	28.00 375.00 1.55	2.00 1440.00 6.20	0.00 3.00 1.00	4.00 200.00 0.00	
4.00 -10.00 5.13 1.45	28.00 400.00 1.48	3.00 1585.00 4.94	0.00 3.00 1.00	4.10 125.00 0.00	
4.00 -10.00 5.13 1.37	28.00 415.00 1.57	4.00 1670.00 4.51	0.00 3.00 1.00	4.10 125.00 0.00	
4.00 -10.00 5.13 1.26	28.00 435.00 1.71	5.00 1720.00 4.49	0.00 3.00 1.00	4.10 125.00 0.00	
4.00 -10.00 5.13 0.95	28.00 425.00 2.27	6.00 2890.00 5.96	0.00 3.00 1.00	6.10 125.00 0.00	

TABLE 11.1 COMPILATION OF BHR/RTA AEROELASTIC STABILITY DATA
(SHEET 30 OF 33)

CONFIG ALPHA (DEG) OR ZET (HZ) THALF (SEC)	RUN RPM ETA ROT (%)	TEST POINT THRUST (LB) ETA FIX (%)	V (KNOTS) TYPE EXCIT GAGE	THETA (DEG) MAG EX (CT) D CYCLIC	COMMENT
4.00 -10.00 5.00 0.53	28.00 425.00 4.18	7.00 4125.00 10.03	0.00 3.00 1.00	8.10 125.00 0.00	
4.00 -10.00 4.88 0.64	28.00 425.00 3.54	8.00 5430.00 7.84	0.00 3.00 1.00	10.00 125.00 0.00	
4.00 -8.00 5.13 1.34	28.00 424.00 1.61	11.00 1587.00 4.26	89.70 3.00 1.00	4.10 125.00 0.00	
4.00 -8.00 5.00 1.41	28.00 400.00 1.56	12.00 1377.00 4.68	90.10 3.00 1.00	4.10 125.00 0.00	
4.00 -8.00 -100.00 -0.05	28.00 335.00 2.22	13.00 867.00 -2.10	90.10 3.00 1.00	4.10 125.00 0.00	
4.00 -6.00 4.75 1.06	28.00 335.00 2.19	14.00 1239.00 12.48	90.60 3.00 1.00	4.00 125.00 0.00	

TABLE 11.1 COMPILATION OF BMR/RTA AEROELASTIC STABILITY DATA
(SHEET 31 OF 33)

CONFIG ALPHA (DEG) OM ZET (HZ) THALF (SEC)	RUN RPM ETA ROT (%)	TEST POINT THRUST (LB) ETA FIX (%)	V (KNOTS) TYPE EXCIT GAGE	THETA (DEG) MAG EX (CT) D CYCLIC	COMMENT
4.00 -6.00 5.00 1.42	28.00 400.00 1.55	15.00 1819.00 4.65	90.30 3.00 1.00	4.10 125.00 0.00	
4.00 -6.00 5.13 1.44	28.00 424.00 1.49	16.00 2124.00 3.95	90.30 3.00 1.00	4.10 125.00 0.00	
5.00 -6.00 5.00 1.43	29.00 425.00 1.54	3.00 1461.00 3.70	120.20 3.00 -100.00	4.00 **** 0.00	
5.00 -6.00 5.00 1.28	29.00 425.00 1.73	5.00 2321.00 4.15	89.40 3.00 -100.00	4.00 **** 0.00	

TABLE 11.1 COMPILATION OF BMR/RTA AEROELASTIC STABILITY DATA
(SHEET 32 OF 33)

TABLE NOTES

CONFIG = CONFIGURATION

1 = BASELINE BMR/RTA
2 = BASELINE BMR/RTA, BALANCE DAMPERS OFF
3 = BASELINE BMR/RTA, BALANCE DAMPERS OFF, SOFT PITCH LINK
4 = BASELINE BMR/RTA, PLUS FLEXBEAM DAMPER STRIPS
5 = BASELINE BMR/RTA, PLUS FLEXBEAM DAMPER STRIPS, BALANCE DAMPERS OFF

RUN = WIND TUNNEL RUN NUMBER

TEST POINT = TEST POINT NUMBER FOR TEST CONDITION DATA, I.E., SHAFT ANGLE, TUNNEL SPEED, ETC., WHEN THESE DATA WERE RECORDED JUST PRIOR TO ACQUIRING STABILITY DATA.

V = WIND TUNNEL SPEED

THETA = INDICATED NOMINAL COLLECTIVE PITCH AT 70 PERCENT BLADE RADIUS

ALPHA = ROTOR SHAFT ANGLE (PLUS NOSE UP)

RPM = ROTOR SPEED

TYPE EXCIT: 1 = LATERAL CYCLIC STEP
2 = LATERAL CYCLIC SINUSOID
3 = NUTATION

MAG EX = MAGNITUDE OF EXCITATION IN COUNTS, 500 COUNTS APPROXIMATELY = .75 DEGREES

1M ZET = FIRST CHORD MODE ROTATING FREQUENCY, Hz

TABLE 11.1 COMPILATION OF BMR/RTA AEROELASTIC STABILITY DATA
(SHEET 33 OF 33)

ETA ROT = ROTATING SYSTEM DAMPING AT FIRST CHORD MODE FREQUENCY, PERCENT CRITICAL

ETA FIX = FIXED SYSTEM DAMPING AT THE LEAD-LAG REGRESSING MODE FREQUENCY (BASED ON ETA ROT), PERCENT CRITICAL (SEE NOTE 1 BELOW)

GAGE = MEASUREMENT USED TO DETERMINE DAMPING

1 = BEAM CHORD BENDING AT STA 11 (CB 11A)
2 = BLADE CHORD BENDING AT STA 14.25(CB 14.25, BLADE #1)

D CYCLIC = CYCLIC TRIM VARIATION

0: CYCLIC FOR MINIMUM HUB PITCH AND ROLL MOMENTS
1: A1 = -1.$^{\circ}$ B1 = 1.5°
2: A1 = - .7° B1 = -.5°
3: A1 = .6° B1 = .3°
4: A1 = -1.3° B1 = 0°
(REFERENCE A1 = -.0°, B1 = .5°)

THALF = TIME TO HALF AMPLITUDE, BASED ON ETA ROT AND ON ZET, SECONDS (SEE NOTE 1 BELOW)

* = DATA MAY NOT BE VALID
***** = DATA NOT AVAILABLE

NOTE 1: FOR COMPUTING ETA FIX AND THALF:

A) FOR CONFIG = 4 OR 5, THE MOVING BLOCK VALUE FOR ETA ROT WAS USED (MOVING BLOCK VALUES FOR ETA ROT ARE PRINTED IN THIS TABLE)

B) FOR CONFIG = 1,2, OR 3, A VALUE FOR ETA ROT BASED ON VERTOL WHIRL TOWER TESTS = 4.75 + 1.24((Ω/375)-1)-.02$\theta_{.7}$ HZ, Ω IN RPM, $\theta_{.7}$ IN DEGREES, WAS USED TO COMPUTE ETA FIX AND THALF FROM ETA ROT.

12.0 REFERENCES

1. "Proposal for an Improved Rotor Hub Concept", Boeing Vertol Company Document D210-10860-1, October 1974.

2. "Proposal for Flight Evaluation of Loads and Stability Characteristics of a Bearingless Main Rotor (BMR)", Boeing Vertol Company Document D210-11001-1, November 1975.

3. Chen, C., Staley, J.A., Miao, W., and Harris, F.D., "Aeroelastic Stability Test Results for a 1/5.86 Scale Model of a Bearingless Main Rotor System on the BC-105 Helicopter", Boeing Vertol Company Report D210-11245-1, June 1977.

4. Bishop, H., "Summary Report of BMR Component Fatigue Tests", Boeing Vertol Company Report D210-11427-1, To be released.

5. Bishop, H., "BMR Main Rotor Whirl Test Report", Boeing Vertol Company Report D210-11428-1, To be released.

6. Dixon, P.G.C., "Design, Development and Flight Demonstration of the Loads and Stability Characteristics of a Bearingless Main Helicopter Rotor (BMR) - Final Report", Boeing Vertol Company Report D210-11542-1, August 1979.

7. Staley, J.A., and Reed, D.A., "Aeroelastic Stability and Vibration Characteristics of a Bearingless Main Rotor", Boeing Vertol Company Report D210-11498-1, June 1979.

8. Bishop, H., and Dixon, P.G.C., "Loads Characteristics of a Bearingless Main Rotor", Boeing Vertol Company Report D210-11417-1, August 1979.

9. "Proposal for Investigation of Bearingless Main Helicopter Rotors", Boeing Vertol Company Document D210-11519-1, June 1979.

10. "Guide for Planning Investigations in the Ames 40-by-80 ft. Wind Tunnel Operated by the Large-Scale Aerodynamics Branch", NASA Report, June 1978.

11. Sheffler, M.W., and Shaw, J., "Investigation of a Bearingless Main Helicopter Rotor - Final Test Plan", Boeing Vertol Company Report D210-11553-1, September 1979.

12. Huber, H.B., "Effect of Torsion-Flap-Lag Coupling on Hingeless Rotor Stability", 29th Annual National Forum of the American Helicopter Society, Preprint No. 731, May 1973.

13. Hammond, Charles E., and Doggett, Robert, V., Jr., "Demonstration of Subcritical Damping by Moving-Block/ Randomdec Applications", NASA SP-415, Flutter Testing Techniques Conference Proceedings, 1976, pp. 59-76.

14. Johnson, W., and Gupta, N.K., "Transfer Function and Parameter Identification Methods for Dynamic Stability Measurement", 33rd Annual National Forum of the American Helicopter Society, No. 77.33-35, May 1977.

15. Gabel, R., and Capurso, V., "Exact Mechanical Instability Boundaries as Determined from the Coleman Equation", Journal of the American Helicopter Society, January 1962.

16. Lytwyn, R.T., "Aeroelastic Stability Analysis of Hingeless Rotor Helicopters in Forward Flight Using Blade and Airframe Normal Modes", 36th Annual National Forum of the American Helicopter Society, May 1980.

17. Lytwyn, R.T., "Aeroelastic Stability Analysis Computer Program Documentation (C-90 User's Manual)", Boeing Vertol Company Report D210-11468-1 (to be released).

18. Staley, J.A., Gabel, R., and MacDonald, H.I., "Full Scale Ground and Air Resonance Testing of the Army/ Boeing Vertol Bearingless Main Rotor", 35th Annual National Forum of the American Helicopter Society, No. 79-23, May 1979.

END

DATE

FILMED

JAN 9 1981